GEOEXPO/86

Exploration in the North American Cordillera

Proceedings of a symposium jointly sponsored by The Association of Exploration Geochemists and The Cordilleran Section, Geological Association of Canada, University of British Columbia, Vancouver, B.C., Canada, May 12th - 14th, 1986

Edited by

I. L. ELLIOTT

Chief Geochemist, Cominco Ltd., Vancouver, B.C.

and

B. W. SMEE

Exploration Supervisor, Abermin Corporation, Vancouver, B.C.

Published by
THE ASSOCIATION OF EXPLORATION GEOCHEMISTS

Copies of this book may be purchased from the publisher at the above address at a cost of $Can. 45.00 including postage and packing.

Photo composed and printed in Canada by Ronalds Printing, Calgary and Vancouver.

ISBN: 0-9691014-3-0

SYMPOSIUM COMMITTEE

Chairman (AEG):	Stan Hoffman, BP-Selco
Co-Chairman (GAC):	John Hamilton, Cominco Ltd.
Secretary:	Ian Thomson, Placer Development Ltd.
Treasurer:	David Jenkins, Metamin Enterprises
Technical Program:	Ivor Elliott, Cominco Ltd.
Facilities:	John Kowalchuk, Orequest Consultants Ltd.
Workshops:	Barry Smee, Abermin Corporation
Field Trips:	Ian Sutherland
Publicity:	Paul Matysek, B.C. Ministry of Energy Mines and Petroleum Resources
Publications:	Robert Hewton, Cassiar Mining Corporation
Registration:	Joan Carne, Cordilleran Section, GAC
Display and Advertising:	Bruce Downing, Newmont Exploration of Canada
UBC Liaison:	Al Sinclair, Department of Geological Sciences, UBC
General Duties:	John Gravel, GHS Geochemical Services Ltd.
Guest Program:	Ann Kowalchuk Vicky Troup Irma Muntainian
Ex Officio:	Jack Armstrong, GAC

Acknowledgements

Grateful acknowledgement is made by the members of the Meeting Committee to their respective employers for the use of their time and facilities, to those organizations who made financial contributions and to all those individuals who gave so freely of their advice and practical assistance.

FOREWORD

About 400 delegates from five countries gathered at the University of British Columbia in Vancouver from May 12-14, 1986 to attend GEOEXPO/86. This symposium addressed exploration in the North American Cordillera; it was jointly sponsored by the Association of Exploration Geochemists and the Cordilleran Section of the Geological Association of Canada.

Three two-day workshops, held at the Department of Geological Sciences immediately preceeded the symposium. They addressed the topics of heavy mineral techniques in geochemical prospecting, exploration techniques in desert environments and lithogeochemistry. Twenty two speakers presented results from current and past research, numerous case histories, and encouraged an open exchange of ideas with nearly 100 participants.

The main meeting comprised 49 presented papers, in either the general session during the first two days or in two simultaneous sessions on the third day. In addition to oral presentations, eleven papers were presented in poster sessions. A measure of the quality of these presentations can be gleaned from the fact that most attendees stayed until the very end of the program despite the beckoning of Vancouver's highly successful Expo 86 located a few kilometres from the campus.

The technical presentation was complemented by relevant commercial exhibits and an attractive social program which included a B.C. salmon barbeque to the accompaniment of a steel band; delegates were afforded ample opportunity to interact technically and socially.

Four field trips; Montana, Vancouver Island, Nevada and Washington immediately followed the meeting. Those delegates who chose a field trip instead of lingering at Expo 86 had an excellent opportunity to view mineral deposits in areas of current exploration activity.

Delegates to the symposium were offered an opportunity to purchase this volume at a pre-publication price. The fact that many people did so even though the exact nature of its contents was not known again attests to the overall quality of the science presented at the meeting. We hope you find that this volume contains material of use and benefit to you in your work.

We take this opportunity to thank our Organizing Committee members and the many volunteers who made this symposium a success. Our most sincere thanks are extended to those who contributed technically during the workshops, oral and poster sessions, displays and field trips. Without their extra efforts the meeting would not have been the stimulating experience it was. Finally, our warmest thanks go to Ivor Elliott, who not only organized the technical program but who, in conjunction with Barry Smee has gone on to edit this record of the symposium.

STANLEY J. HOFFMAN
General Chairman (AEG)
Selco Div BP Resources
Canada Ltd.

JOHN M. HAMILTON
General Co-Chairman (GAC)
Cominco Ltd.

EDITORS' ACKNOWLEDGEMENTS

The editors sincerely thank the authors and reviewers of the papers for their cooperation and help in bringing this volume to fruition. In particular we owe a special debt of thanks to Dr. A. A. Levinson who gave so generously and enthusiastically of his expert knowledge of scientific publishing. Finally, we thank our respective employers Cominco Ltd. and Abermin Corporation for giving us the opportunity to make this contribution to our profession.

CONTENTS

	Page
Symposium Committee	v
Foreword	vii
Mineral Deposits in British Columbia; A Review of their Tectonic Settings W. J. McMILLAN, A. PANTALEYEV and T. HÖY	1
Distribution of Mineral Deposits in the Pacific Border Ranges and Coast Mountains of the Alaskan Cordillera R. J. GOLDFARB, S. W. NELSON, H. C. BERG and T. D. LIGHT	19
Geology of Newmont Gold Company's Gold Quarry Deposit, Eureka County, Nevada J. C. ROTA	42
Geochemistry and Geology of the Wind River Gold Prospect, A Cascade Epithermal Precious Metal System K. I. McGOWAN	51
Geology and Soil Geochemistry of the Quesnel River Gold Deposit, British Columbia P. E. FOX, R. S. CAMERON and S. J. HOFFMAN	61
A Multidisciplinary Exploration Case History of the Shasta Epithermal Gold-Silver Deposit, British Columbia, Canada B. W. DOWNING and S. J. HOFFMAN	72
Soil and Plant Geochemical Orientation Surveys on the Congress Property, Bridge River District, B.C. B. J. COOKE and J. J. BARAKSO	77
Comparison of Rock Geochemistry and Mineralogical Alteration Guides for Cordilleran Epithermal Precious and Base Metal Vein-Type Deposits in Bolivia and Peru J. D. APPLETON, J. CLAROS and W. RODRIGUEZ	83
Application of R-Mode Factor Analysis to Geochemical Studies in the Eureka Mining District and Vicinity, Eureka and White Pine Counties, Nevada M. A. CHAFFEE	94
Variation of Trace Elements in Hydrothermal Tourmalines Associated with Mineralization: El Correo, Sonora, Mexico S. M. SMITH, L. G. CLOSS and P. K. THEOBALD	109
Geochemical Characterization of Two Mineral Provinces in the Healy Quadrangle, Alaska T. D. LIGHT, R. B. TRIPP and H. D. KING	126
Pb-Isotope Signatures of Devonian-Mississipian Massive Sulphide Deposits in Alaska and their Significance to Mineral Exploration S. E. CHURCH, J. E. GRAY, M. H. DELAVAUX and A. P. LEHURAY	132
Analysis of Fluid Inclusion Gases in Jasperoid as an Exploration Method for Micron Gold Deposits P. S. HAYNES and S. E. KESLER	142
Fluid Inclusion Constraints on the Genesis of the Alaska-Juneau Gold Deposit D. L. LEACH, R. J. GOLDFARB and T. D. LIGHT	150
Nature of Ore Fluids in the Coquihalla Gold Belt, B.C. J. B. MUROWCHICK, K. MUEHLENBACHS and B. E. NESBITT	160
Diamond Exploration in the North American Cordillera H. T. DUMMETT, C. E. FIPKE and S. L. BLUSSON	168
Behaviour of Scheelite in a Cordilleran Stream D. SAXBY and W. K. FLETCHER	177
Current Atomic Absorption and Inductively Coupled Plasma Optical Emission Methods for Geochemical Investigations J. S. KANE and A. F. DORRZAPF, JR.	184
Comparison of Some Multielement Analytical Techniques Applied to Massive Sulfides from the Juan de Fuca Ridge and to Sulfide Standards J. A. PHILPOTTS, J. S. KANE, R. G. JOHNSON, A. F. DORRZAPF, JR., Z. A. BROWN, J. S. MEE, H. KIRSCHENBAUM, N. RAIT, C. SKEEN, W. CRANDELL, C. PALMER, J. MARINENKO and F. BROWN	189
Classical Chemical Analysis of Forms of Bound Sulfur in Massive Sulfides with an Application to Chimney Samples from the Juan de Fuca Ridge H. KIRSCHENBAUM and J. A. PHILPOTTS	198

Determination of Anions by Ion Chromatography — Application to Pedogeochemical Exploration for Metallic Mineralization 202
P. J. LECHLER and M. O. DESILETS

Gallium: An Overview, Markets, Supplies and Occurrence 209
R. W. TEKVERK and J. E. FAY

Workshop Report. Exploration in Desert Environments 213
P. K. THEOBALD

Workshop Report. Heavy Mineral Sampling 214
W. K. FLETCHER

Workshop Report. Lithogeochemical Sampling 215
A. DAVIDSON

Other Papers Presented 217

List of Contributors 220

Mineral Deposits in British Columbia: A Review of Their Tectonic Settings

W. J. McMillan, A. Panteleyev and T. Höy
Geological Survey Branch, B.C. Ministry of Energy, Mines and Petroleum Resources
Victoria, B.C. V8V 1X4

Abstract — This paper describes the main genetic types of deposits from the wide spectrum of mineral deposits found in British Columbia in terms of their tectonic settings, ages and geological settings. Rapid advances in the understanding of the settings of the deposits came with the realization that much of the Cordillera is allochthonous (Monger et al., 1982). Comparison of various classes of mineral deposits from around the world to the province's deposits has revolutionized mineral exploration methodology in British Columbia.

INTRODUCTION

Advances in the understanding of the genesis of mineral deposits in the Cordillera are founded on sound geological and mineral deposit research and data — data gathered through many years of effort. Information from geology, geochronology, paleomagnetism, paleontology, geochemistry and many other facets of earth science had to be gathered and evaluated before a defensible interpretation of the geological history of the Cordillera was possible. Our present views are still evolving and our understanding will be expanded as new facts come to light.

Development of mineral deposit databases and metallogenic modelling in British Columbia has accelerated rapidly during the last decade due to new genetic deposit models, direct observations of mineralizing processes in submarine and hot spring settings, and plate tectonic research. Key factors in our current understanding are new or improved methods of geochemical analyses, age dating, and isotopic analyses, and studies of alteration, fracturing and fluid inclusions in ore deposits. Together, these factors have contributed to the construction of powerful models that are applicable to a wide range of important mineral deposits. These models have been applied in the search for porphyry copper, volcanogenic massive sulphide, and epithermal vein deposits.

A BRIEF PLATE TECTONIC OVERVIEW

The Cordillera consists of a collage of allochthonous terranes accreted to the North American craton (Fig. 1). We now have a good working hypothesis for the timing of amalgamations of major terranes, and their accretion to North America (Monger et al., 1982; Monger and Berg, 1984; Armstrong, 1987). Metallogenic patterns can play a role in testing the validity of these terrane analyses and in refining terrane boundaries.

Recognition that the Cordillera contains allochthonous elements began to appear in published works in the early 1970's (Monger and Ross, 1971; Monger et al., 1972). Since then supporting evidence from paleontology, paleomagnetism, geology and tectonic interpretations have brought general acceptance to the concept. The terranes that comprise the Cordillera are discrete crustal fragments with distinctive, laterally persistent stratigraphic records; but these records differ from coeval records in adjacent terranes, and the terranes are tectonically separated (Monger et al., 1982). The interpretation is still evolving but it seems clear that the Cordillera consists of two "superterranes", each consisting of several smaller terranes (Monger et al., 1982).

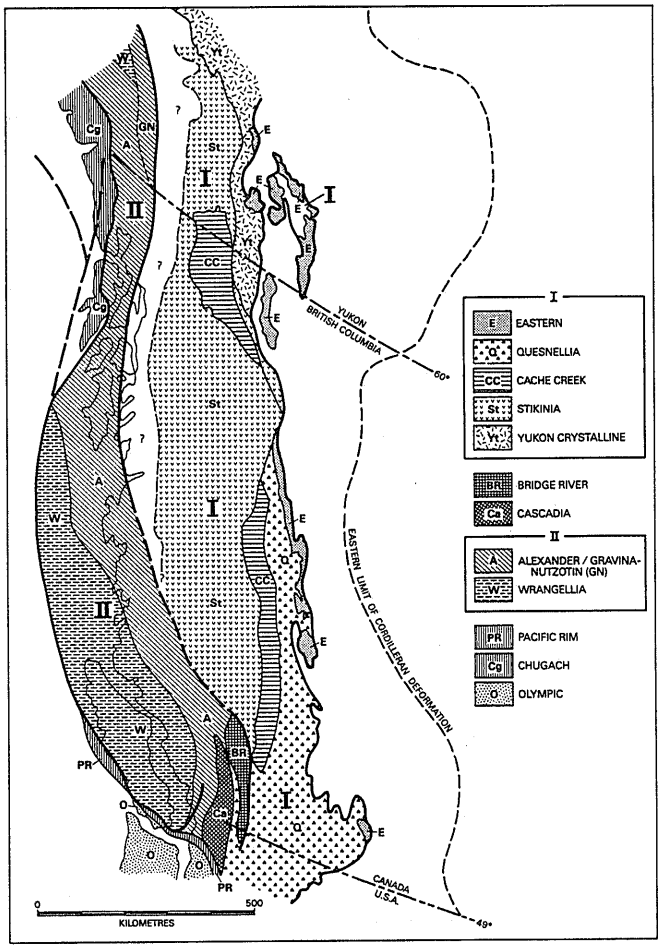

Fig. 1. Allochthonous terranes in the Cordillera (simplified after Monger et al., 1982).

Major events in the tectonic history of the Cordillera are illustrated in Figs. 2 and 3; these figures are derived from Monger et al. (1982), Armstrong (1987), and a host of others. Fossils (Tipper, 1984) and paleomagnetic data (Irving et al., 1980) indicate that the major allochthonous terranes originated far to the south of their present positions, and amalgamated into "superterranes" I and II in latest Triassic to middle Jurassic time respectively prior to docking with North America. Superterrane I was attached to the North American plate about 190 million years ago, in early Jurassic time, and superterrane II was attached about 100 million years ago, in mid-Cretaceous time (Monger et al., 1982). Amalgamation and docking events resulted in volcanism, metamorphism and plutonism. The older, eastern "suture zone", the Omineca Crystalline Belt, was created during docking of superterrane I, and reactivated during docking of superterrane II, which created the younger, western suture zone, the Coast Crystalline Belt (Armstrong, 1987). Later modification of the patterns took place during major Eocene strike slip faulting, which was accompanied by extension and voluminous continental magmatism (Ewing, 1981).

Each of the superterranes (Fig. 3), are composites of oceanic (ophiolitic), and island arc volcanic and sedimentary rocks. Some plutonic and volcanic rocks within the superterranes reflect their oceanic or volcanic arc origins; others are derived from tectonism during amalgamation, collision with the North American plate, or subsequent events. Similarly, mineral deposit patterns within the superterranes are composite, and include pre-amalgamation, amalgamation, accretionary and post-accretionary events. A clear knowledge of the timing of mineralization, first within a plate tectonic setting, and then following accretion, is a critical element in mineral deposit modelling.

MINERAL DEPOSITS AND PLATE TECTONICS

Introduction

Even before the advent of plate tectonic models, deposits could be placed in a tectonic framework. On the basis of regional geology, Sutherland Brown et al. (1971) placed Cordilleran mineral deposits into five tectonic belts that are almost coincident with Monger et al.'s divisions. From east to west they include the deformed cratonic margin of the North American Plate, the Omineca suture zone, superterrane I, the Coast Crystalline suture zone, and superterrane II.

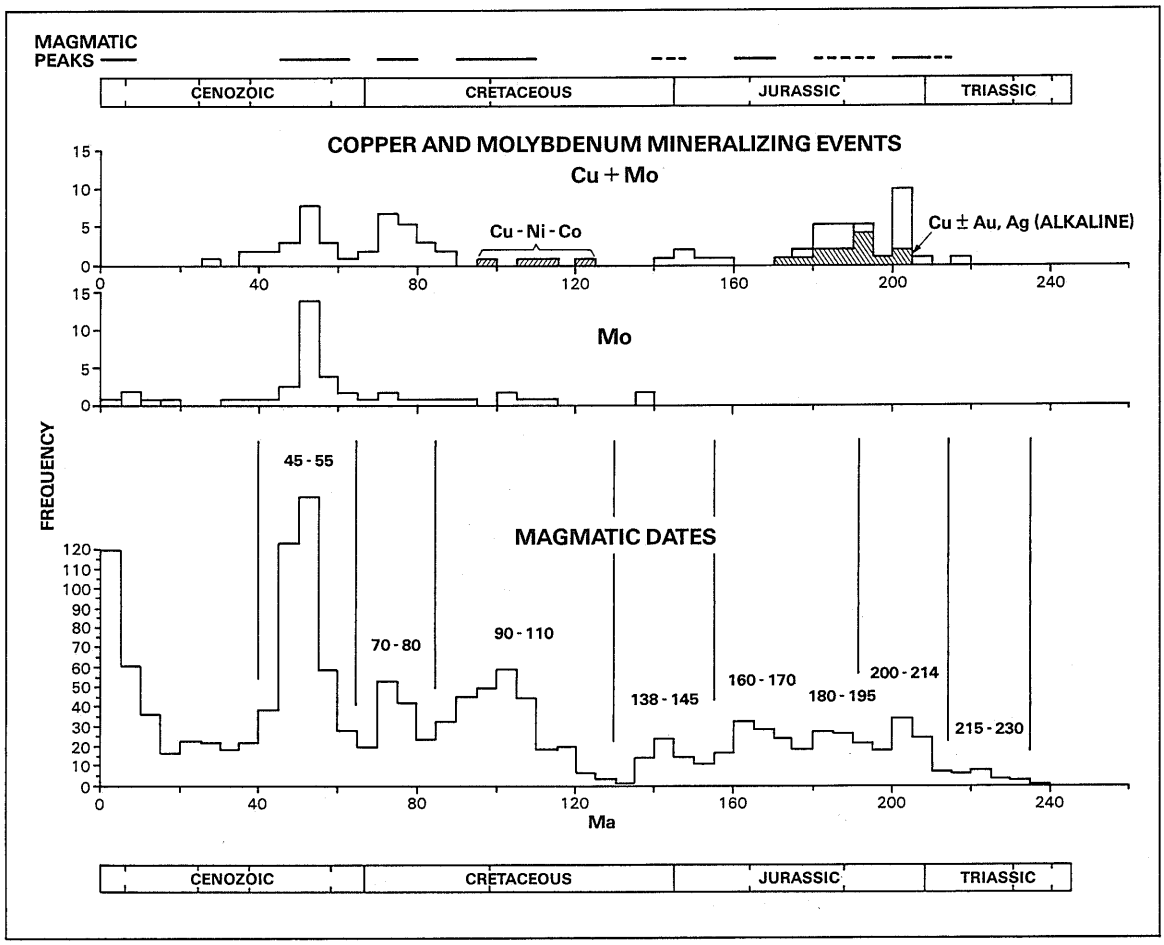

Fig. 2. Major tectonic and magmatic events in the Cordillera (partly after Armstrong, 1987).

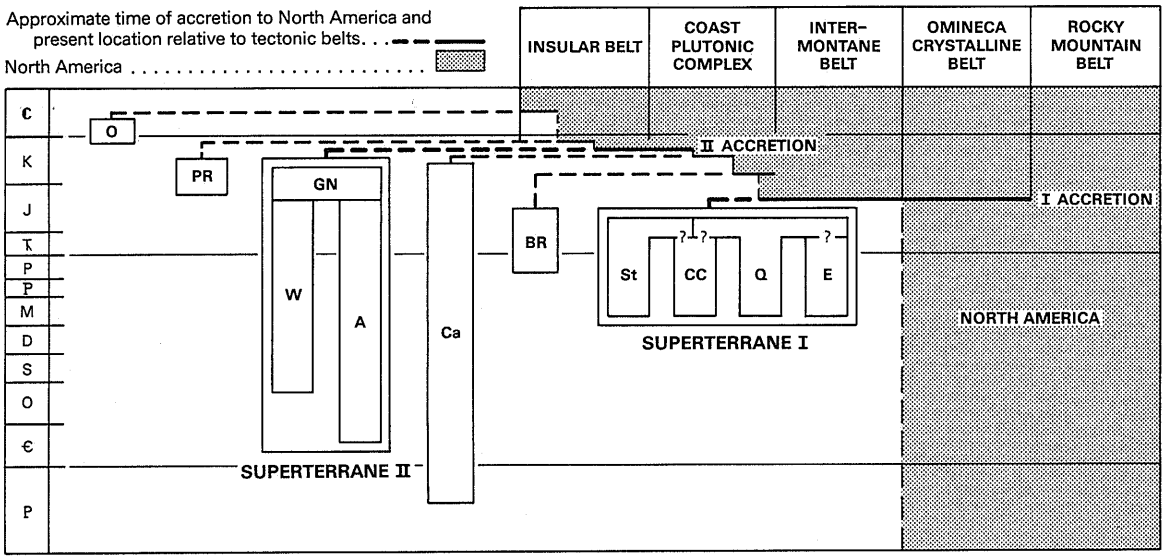

Fig. 3. Stratigraphic sections showing docking of allochthonous terranes with North America (after Monger et al., 1982).

As Sawkins (1984) clearly pointed out, classes of mineral deposits characteristically occur in specific plate tectonic settings. It should, therefore, be possible to classify Cordilleran mineral deposit types according to their plate tectonic settings within the autochthonous and allochthonous terranes. Timing of mineralization is critical to understanding metallogenic patterns; some deposits originated in allochthonous terranes prior to accretion, some probably formed during accretion and some were later. Observed metal or deposit patterns in adjacent terranes may be completely unrelated.

Mineral Deposits in Passive Continental Margin Settings

Passive trailing edge or Atlantic-type margins develop where spreading centres underlie continental lithosphere. Early rifting is followed by local sedimentation and possibly emplacement of oceanic crust; then subsidence occurs which leads to deposition of thick prograding clastic wedges (Bally and Oldow, 1986). In the Canadian Cordillera the oldest rocks of the Rocky Mountain Fold and Thrust Belt are derived predominantly from North America and were deposited in this type of passive margin setting. Episodes of mineralization are related to rifting events that provided structural controls for igneous activity and localized areas of high geothermal heat flow in which convective hydrothermal cells formed. Deposits in these settings in British Columbia include the large Proterozoic turbidite-hosted, Sullivan silver-lead-zinc deposit, as well as the smaller Devonian shale-hosted lead-zinc-barite-silver deposits of the Gataga area of northeastern British Columbia.

The Sullivan deposit occurs within Middle Proterozoic sedimentary rocks near the junction between a major east-trending tectonic zone, the Kanasewich "rift", that can be traced eastward into Hudsonian cratonic basement, and a more northerly trending zone parallel to the Rocky Mountain Trench that may represent an ancient rifted continental margin (Fig. 4a). Faults in the east-trending zone have been active intermittently since Proterozoic time and have modified the regional depositional patterns of Proterozoic flysch deposits and younger miogeoclinal rocks. The Kanasewich zone contains localized granitic intrusions. Stratabound lead-zinc deposits, some vein-type silver-lead-zinc deposits, the Cambrian age lead-zinc deposits in the Kootenay Arc to the west, and younger gold deposits may also be related to the rift zone (Höy, 1982a).

Sullivan is one of the world's largest silver-lead-zinc massive sulphide deposits. Its central portion comprises a thick zone of massive to indistinctly bedded pyrrhotite, galena and sphalerite, whereas distal portions comprise interbedded thinly laminated sulphides and clastic rocks (Fig. 4b). The sulphides were deposited on or close to the sediment-seawater interface. In more distal, bedded sections of the orebody, sulphide deposition was interrupted frequently by turbidites sweeping across the deposit. The central part of the orebody is underlain by a footwall feeder zone characterized by intense chlorite and tourmaline alteration. Hydrothermal alteration continued after sulphide deposition; hangingwall rocks are altered to chlorite and albite and local zones of chlorite alteration occur in the footwall (Hamilton et al., 1982). Diorite sills within the host turbidite succession appear to be partly contemporaneous with sedimentation (Höy, 1984). The presence of the sills supports the interpretation that the basin developed in response to rifting and had an elevated geothermal gradient. Convective hydrothermal systems evolved within the turbidite succession and penecontemporaneous faults channeled hydrothermal fluids to the sea floor. A modern analogue of the Sullivan environment may be the spreading Guaymas Basin in the Gulf of California, where unconsolidated sediments are intruded by basic sills (Höy, 1984). One point of exploration significance is that sulphide mounds in the Guaymas Basin correlate closely with gabbroic sills. The sills are not the heat source; they act as impermeable cap rocks that channel or pond the hydrothermal fluids (Peter et al., 1986).

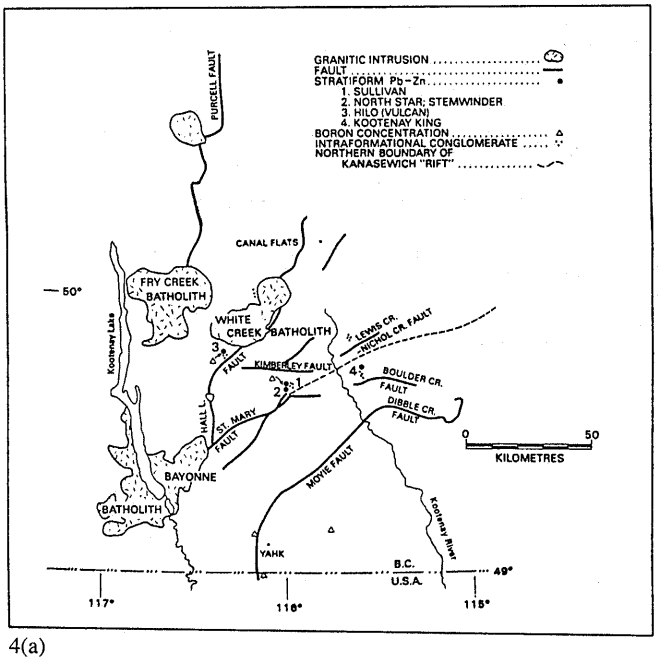

4(a)

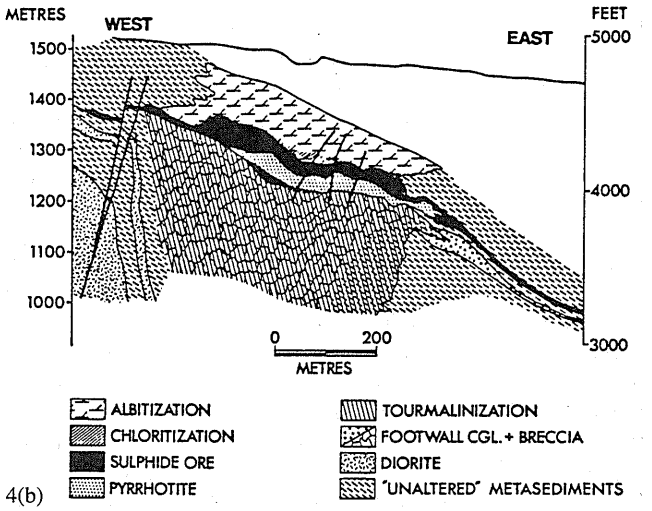

4(b)

Fig. 4. Regional setting (4a) and general geology (4b) of the Sullivan massive sulphide deposit (after Höy, 1984 and Hamilton et al., 1982).

Other stratabound massive sulphide deposits in passive margin settings in the Cordillera include thin but extensive sulphide-rich horizons in well layered but highly metamorphosed and deformed platformal rocks in the Shuswap Metamorphic Complex. The deposits consist largely of pyrrhotite and sphalerite with minor galena and pyrite (Höy, 1982b). The age of the mineralization is not known but, based on comparisons with deposits in other tectonostratigraphic settings, may be Lower Paleozoic.

Stratabound lead-zinc deposits in Lower Cambrian rocks of the Kootenay Arc are restricted to a shallow marine shelf carbonate unit (Höy, 1982b). The deposits consist of lenticular masses of pyrite, sphalerite and galena in dolomite or chert zones within highly deformed limestone (Fyles, 1970). The larger deposits range in size from 6 to 10 million tonnes and contain 1-2 percent lead, 3-4 percent zinc, and minor amounts of silver. Different studies concluded that the deposits are either structurally controlled and of replacement origin (Fyles and Hewlett, 1959) or are synsedimentary (Sangster, 1970). A genetic model that accommodates the conflicting evidence includes diagenetic karst development and contemporaneous deposition of sulphides both in the dissolved zones and on the seafloor, where they formed stratiform layers (Höy, 1982b).

Other, younger, examples of passive margin deposits are found in the Gataga area of northeastern British Columbia, a southern extension of the Selwyn Basin (Fig. 5). Base metal deposition occurred during a Late Devonian to Early Mississippian rifting event that opened the Anvil Ocean (Tempelman-Kluit, 1979) and may be correlative with the Antler orogeny to the south (Gabrielse, 1986). Gabrielse noted that barite deposits in the Elko area of southeastern British Columbia are identical in stratigraphic setting to the lead-zinc-barite deposits in northeastern British Columbia and the Selwyn Basin. The geological setting of the Gataga area is characterized by starved basin sedimentation at a time when there was active uplift and volcanic activity to the west (Fig. 5). The sediments accumulated in a series of structurally bound basins flanked by carbonate banks. Deposits consist of stratabound lead-zinc-silver-barite lenses that are commonly zoned from galena-sphalerite at the base to pyritic beds above and grade laterally into barite layers. Locally the sulphides are also overlain by barite layers (McIntyre, 1982). Mineralization was episodic (McClay and Insley, 1986), with sulphide layers separated by layers of siliceous exhalite. The deposits occur where hydrothermal fluids were channeled by syn-depositional, deep-seated faults (Carne and Cathro, 1982) that bound second and third order basins within the Kechika Trough (Fig. 5).

Mineral Deposits in Oceanic Settings

The allochthonous western two-thirds of the Canadian Cordillera consists largely of island arc volcanic and sedimentary rocks and remnant slices of oceanic material (Fig. 6). The oceanic slices are variably thrust over other allochthons or autochthonous miogeoclinal or metamorphic rocks, or are separated from them by subduction-related melange complexes. Mineralization within the oceanic slices includes lode and placer gold and platinum, chromite, and volcanogenic massive sulphide deposits.

Clusters of lode and placer gold deposits in the province spatially correlate with oceanic assemblages (Hodgson et al., 1982), although gold-bearing massive sulphide, porphyry copper, and epithermal and "micron" gold deposits also occur in island arc and other rock assemblages (compare Figs. 6 and 7). Many important gold deposits also are related to major northwest trending transcurrent and northeast trending transverse structural zones that can be traced from the Canadian shield westward into the Cordillera (Hodgson et al., 1982). Particularly important among these major structures are the northeasterly-trending Stikine and Skeena Arches, the Quesnel lineament, and the St. Mary and Moyie-Dibble Creek fault zones (Fig. 4a).

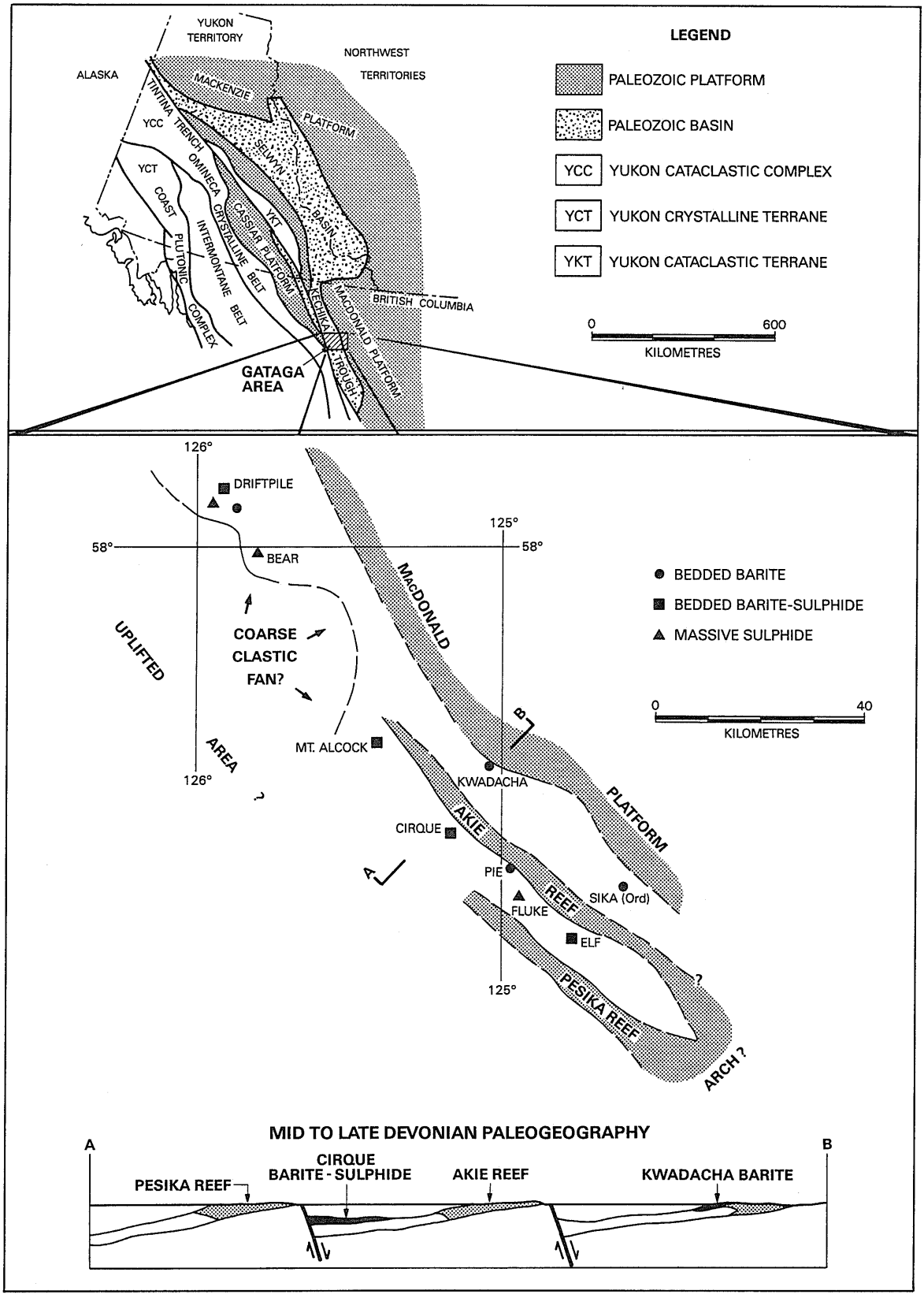

Fig. 5. General setting of lead-zinc deposits in Gataga area (after MacIntyre, 1984).

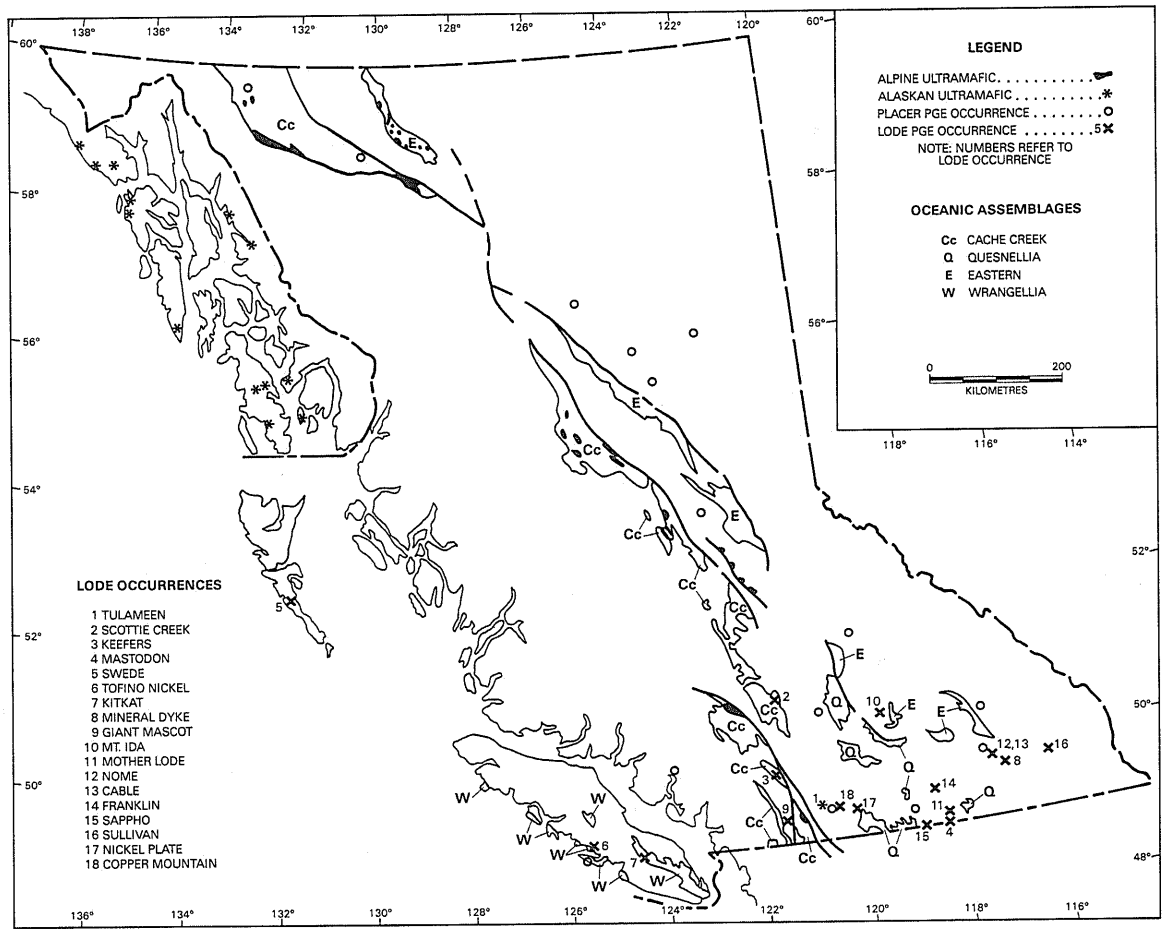

Fig. 6. Distribution of oceanic rocks and platinum occurrences in the Canadian Cordillera (after Rublee, 1986).

Gold deposits in oceanic terranes, such as those in the Bridge River, Coquihalla, Cassiar and Atlin camps, have common characteristics. Many occur within disrupted ophiolitic assemblages — serpentinite, greenstone and argillite-greywacke. Deposits typically occur near intrusive bodies but genetic relationships between them and the intrusions are generally unclear. The deposits are structurally controlled. Gold/silver ratios tend to be high and zoning is common, from gold at depth to antimony and mercury near surface. Alteration assemblages mainly include calcium-magnesium-iron carbonate, albite and fuchsite (mariposite) — the "listwanite" assemblage. Other alteration minerals are chlorite, talc and graphite. Lead isotopic analyses suggest that the country rock supplied lead. By analogy, gold may also be derived from the country rock.

The Coquihalla and Bridge River gold camps are faulted segments of the same belt (Fig. 8b); both segments contain oceanic gold deposits (Ray et al., 1983). The Coquihalla belt gold deposits are in Ladner Group wackes, siltstones and argillites near Spider Peak greenstone contacts. The zone containing gold deposits lies next to the Hozameen fault, adjacent to the Coquihalla serpentine belt, and near the Needle Peak pluton (Fig. 8a). The deposits are in quartz "reefs" and have associated sodic alteration. Sodic dykes are also associated with the Needle Peak pluton, but the relative ages of the pluton and the mineralization are uncertain.

The Bralorne deposits produced 4.1 million ounces of gold. Cumulatively, the Bridge River camp has been the largest lode gold producer in the Canadian Cordillera. The deposits are within the Hozameen-correlative Bridge River Terrane (Fig. 8b), which consists of basalts, ribbon cherts and argillites of Permian to Triassic age. In order of decreasing age the intrusive rocks in the Bralorne area are serpentinite, diorite, soda granite, and albitite dykes (Barr, 1980). Mineralization has a strike length of more than 6 kilometres. In this case the deposits are hosted mainly by the Bralorne intrusives and Pioneer greenstones, and mineralization is apparently cut by dykes dated at 85 million years. (C. Leitch, pers. comm., 1986). Native gold occurs with pyrite and arsenopyrite in sulphide septae in ribbon quartz-carbonate veins. Associated minerals are sphalerite, galena, tetrahedrite, scheelite and chalcopyrite. Mariposite occurs locally.

Another area with oceanic gold deposits is Cassiar where gold mineralization occurs in small shoots in quartz veins and in locally derived placers. The lode deposits consist of gold in quartz vein systems that either follow persistent fracture zones in Mississippian to Triassic greenstones or occur in greenstone-argillite contact zones of the Slide Mountain Terrane (Panteleyev, 1979). The host rock is altered to serpentinite, talc, magnesite, and fuchsite — the listwanite assemblage (Sketchley, 1986). Some veins at the Erickson properties are highly graphitic. The

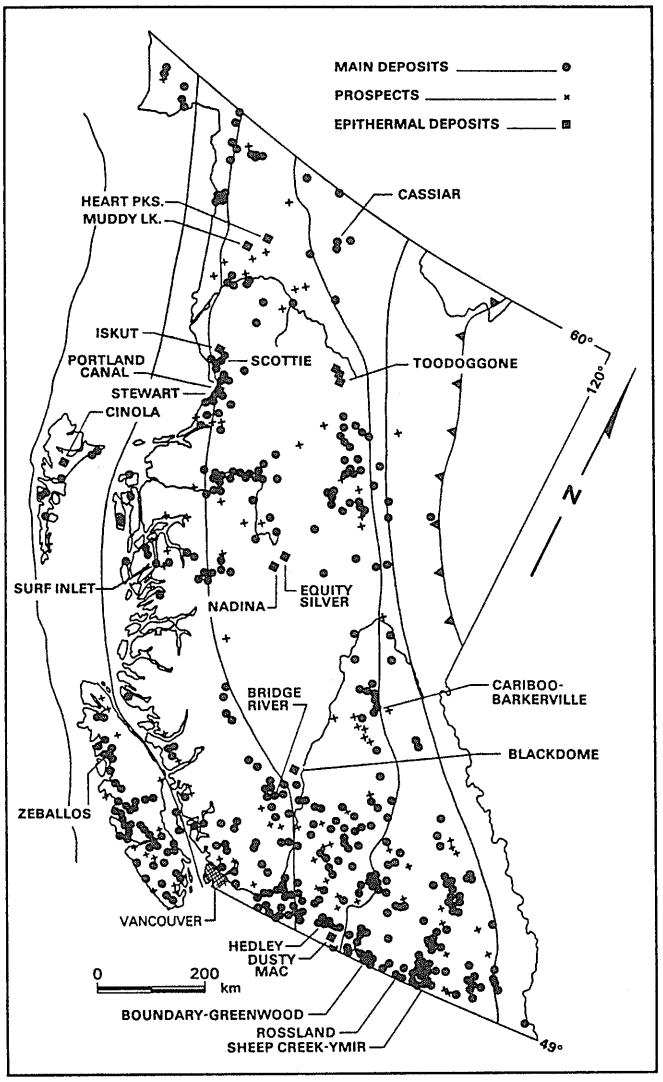

Fig. 7. Lode gold deposits in British Columbia (after Panteleyev, 1986).

native gold mineralization is associated with pyrite, sphalerite and tetrahedrite. Isotopic dates of 129 million years were obtained for the mineralizing event (Sketchley et al., 1986). The nearby Cassiar batholith, at 100 million years, and the Cassiar stock, at 72 million years, are clearly post-ore. Mineralization in oceanic rocks in the Atlin area is similar to that near Cassiar.

At the Muddy Lake gold deposit (Fig. 9), mineralization occurs as disseminations and fracture fillings of extremely fine grained pyrite in silicified and dolomitized or brecciated limestone, or in fuchsite-altered tuff, adjacent to a persistent, intense fault zone (Schroeter, 1986; Wober and Shannon, 1986). The host rocks are a pre-Upper Triassic age assemblage of limestone and mafic tuffs and flows and/or sills. The tuffs contain iron carbonate alteration and are cut by foliated diorite of Late Triassic to Early Jurassic age. Local Alpine serpentinites were emplaced tectonically along the major north-south trending faults (Wober and Shannon, 1986). Mineralization consists of gold with lesser silver. Other metallic minerals include pyrite with trace amounts of arsenopyrite, scorodite, pyrrhotite and chalcopyrite (in amygdules in fuchsite altered tuff), and rare tetrahedrite and hessite (Schroeter, 1986). Drilling to date has indicated reserves of 1.02 million tonnes, containing about 10 grammes/tonne (0.38 ounce/ton) gold, along a strike length of three kilometres.

Lode and placer platinum group elements (PGE) also occur in oceanic terranes. In British Columbia, PGE deposits (Rublee, 1986) have not been significant producers, but they are more numerous than is generally realized. In a number of areas placer PGE deposits are known that have no located bedrock sources (Fig. 6).

Most PGE deposits in British Columbia occur in alpine-type ultrabasic rocks within oceanic terranes. In other settings they can occur: as components of nickel or nickel-copper sulphide deposits in zoned ultramafic-mafic suites (the so-called Alaskan-type intrusions); as hydrothermal quartz veins, usually in a granitic host; in skarn deposits, such as those at Hedley; in alkalic porphyry copper deposits, like those at Copper Mountain; in alkalic copper gold deposits as in the Franklin camp; and in and near dykes, usually of dioritic composition. They may also occur in base metal deposits, such as the Sullivan, where small amounts were noted in smelter products. The PGE's are uncommon and recent studies on Sullivan (Hamilton, pers. comm., 1986) found neither platinum nor palladium concentrations above the 50 ppb detection limits.

Alpine ultramafic bodies are poorly zoned and extensively serpentinized. In British Columbia, they are widespread in dismembered ophiolite terranes within oceanic slices in both the Cache Creek Terrane and Quesnellia. PGE's occur with chromite (Cabri, 1982) which forms nodules, lenses and tabular sheets as well as irregularly spaced massive pods in the faulted serpentinites. PGE placer deposits are known throughout the province (Fig. 6) from areas with serpentinized ultramafic rocks but none has had significant production.

Alaskan-type ultramafics are generally zoned: dunite cores are enclosed by successive layers of peridotite followed by olivine and hornblende clinopyroxenite, and then hornblendite which is commonly pegmatitic. Osmium, iridium, rhenium and platinum are associated with the refractory phases, dunite and peridotite. Palladium is generally partitioned into the hornblende-rich border phases (Cabri, 1982). The highest PGE values are in chromite-rich dunites, peridotites and serpentinites. The Tulameen complex 24 kilometres west of Princeton is an example of this type of ultramafic; it is within Quesnellia near the Methow Terrane boundary. Findlay (1969) has described the geology, and St. Louis (1984), the distribution of PGE's in this complex. Placers in creeks draining the ultramafic body are reported to have produced 20,000 ounces of PGE's — the only known production in British Columbia to date.

Volcanogenic massive sulphide deposits occur in rift environments in a variety of tectonic settings, including rifted continental margins, back arcs, island arcs, and oceanic ridges (Hutchinson and Searle, 1971). These environments are characteristically associated with volcanic sequences that are distinctive in their chemistry, mineralogy, and association with sedimentary rocks (Table 1). Massive sulphide deposits in each environment are generally distinctive in tenor, form, alteration and mineralogy (Lydon, 1984). Pyritic copper-zinc deposits, like the Besshi deposits in Japan, formed in back arcs, or in

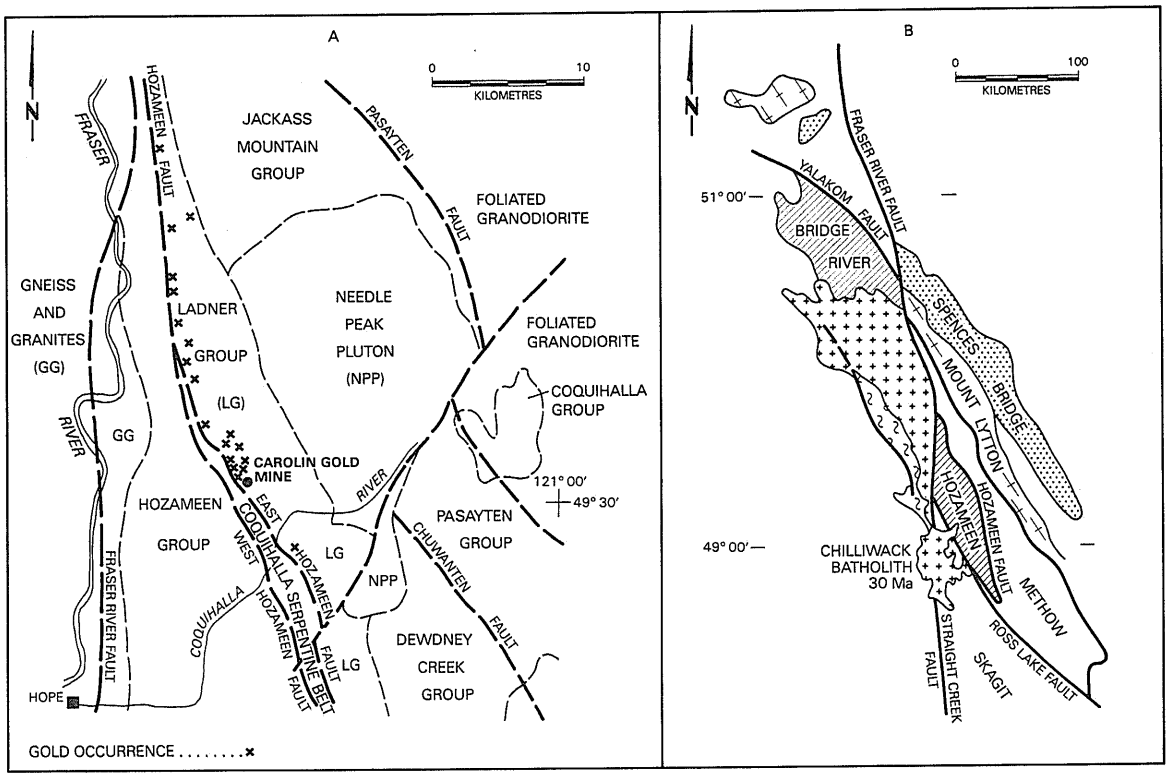

Fig. 8. Gold deposits (8a) in the Coquihalla serpentine belt (after Ray et al., 1983) and inferred relationships (8b) between the Bridge River and Hozameen Groups (after Monger, 1984).

rifted continental margin settings, such as the Guaymas Basin, and are commonly associated with calc-alkaline to tholeiitic basalts. They are thin, but laterally persistent, and without a well-developed footwall alteration zone. Polymetallic lead-zinc-copper-silver-gold deposits, such as the Kuroko deposits in Japan, formed in rifts within island arcs, and are associated with bimodal calc-alkaline volcanism. They are generally lensoid with fragmented sulphides above a well-developed footwall stockwork feeder zone and may be capped by sulphate or silica. Pyritic copper-zinc deposits, similar to those in the Troodos ophiolite complex, formed on or close to spreading oceanic ridges. They occur in tholeiitic basalts within ultramafic, gabbro, sheeted dyke and pillow lava complexes. Most are small and lensoid; few are more than one million tonnes. Most have a pronounced footwall stringer zone, siliceous ore in the footwall, and a capping zone of Fe and Mn-rich ochre.

Volcanogenic massive sulphides are not restricted to specific terranes in British Columbia (Fig. 10). Oceanic ridge and island arc-type deposits occur in the Alexander Terrane, Wrangellia and Stikinia; continental margin or back arc deposits occur in Wrangellia, Stikinia and Quesnellia.

Volcanogenic massive sulphide deposits that may have formed in rifted marginal basins include Goldstream in southeastern B.C., and perhaps Windy Craggy in the Tatshenshini area of northwestern B.C.. Goldstream (Fig. 11) comprises a sheet of massive sulphides that occurs within a thick accumulation of highly metamorphosed terrigenous clastic rocks deposited in an unstable rifted continental margin setting (Höy, 1979; Höy et al., 1984). Other, similar, copper-zinc deposits in the area are hosted by calc-alkaline pillow basalts and tuffs. Another possible example is the arsenical J & L lead-zinc deposit which is located north of Revelstoke (Höy, 1985). This deposit, which occurs within a Cambrian quartzite, limestone, schist sequence, contains silver and gold values; reserves are 3.5 million tonnes.

Deposits in the remote Tatshenshini area of northwest British Columbia, particularly the huge Windy Craggy massive sulphide deposit, may also be similar to the Besshi-type deposits. Host rocks are folded and altered, calc-alkaline to alkaline, Late Triassic pillow basalts with limy and cherty sedimentary interbeds (MacIntyre, 1984, 1986). The deposits are gold-bearing copper-cobalt massive sulphides that occur above thick sills injected into a volcano-sedimentary succession. The deposits may have formed in an immature island arc or a back arc basin setting, or perhaps in a rifted continental margin setting (MacIntyre, 1986).

Volcanogenic deposits formed in island arc environments similar to the Kuroko-type deposits are important producers or past-producers in B.C., and are major targets of present exploration programs. The Westmin deposits on Vancouver Island are hosted by bimodal calc-alkaline volcanic rocks of the Paleozoic Sicker Group. Sicker rocks were deposited in an immature island arc setting in Lower Silurian to Devonian time. The deposits occur along a strike length of more than 6 000 metres and persist down dip for 150 to 1 000 metres. To date, production has come from the Price, Myra, Lynx and H-W orebodies. Composite reserves are about 20 million tonnes of gold-silver-copper-zinc-lead-cadmium ore. Although intense post-ore deformation and alteration hindered exploration efforts and delayed

Table 1. Volcanogenic Massive Sulphide Deposits of British Columbia

	NAME	LOCATION	AGE	HOST LITHOLOGY	SHAPE	SIZE* (mill. tonnes)	Fe SULPHIDE	Cu	GRADE % Zn	Pb	GRADE g/t Ag	Au	SULPHATE
CYPRUS	SUNRO	92C-8	Tertiary	Metchosin Fm - basalt, gabbro		2.8	po,py	1.3			2	0.7	
	ANYOX	103P-12	Jurassic?	Salmon River Fm - basalt	lenses, stringer	25.1	py,po	1.4			9.5	0.17	
	CHU CHUA	92P-5	Permian	Fennel Fm - basalt	3 lenses	3	py	2	0.5		8	0.5	
BESSHI	GRANDUC	104B-8	Jurassic	Hazelton Fm - andesite, "schist"	lenses, stringer	32.5	py,po	1.93	(Co)		7	0.13	
	WINDY-CRAGGY	114P-11	Triassic	- basalt	folded mass. stringer	300	po,py	1.5	(0.08% Co)			2-3	
	GOLDSTREAM	82M-8	L Paleozoic	Lardeau Gp - phyllite	sheet	3.2	po	4.5	3.1		20		
KUROKO	BRITANNIA	92G-11	Jurassic (Cretaceous?)	Gambler Gp - andesite - dacite	lenses, stringer	47.8	py	2.8	0.26		3.8	0.3	Ba,Ah, Gy
	SENECA	92H-5	Jurassic	Harrison L. Fm - andes. - rhyodac.	lenses/diss.	0.8	py	0.8	6.6	0.3	58	1	Ba,Gy
	TULSEQUAH CHIEF	104K-12E	Paleozoic (Penn/Perm)	Stikine - felsic volc.	2 lenses	1.6(?)	py	1.3	8	1.6	93	3	Ba
	KUTCHO CREEK	104I-2E	U Triassic	"Kutcho" Fm - schist - felsic volc.	lenses, diss.	17 10	py py	1.7 1.0	2.3 1.2	0.06	36	0.9	
	ECSTALL	103H-13E	Permian	- schist - felsic volc.	2 lenses	4.5	py	0.8	2.3				
	WESTMIN (LYNX, MYRA, H-W)	92F-12	Devonian	Sicker Gp - basalt - rhyolite	lenses, stringer	20	py	2.2	5.3	0.3	35	2.2	Ba
	TWIN J	92B-13	Devonian	Sicker Gp - basalt - rhyolite	lenses, stringer	0.6	py	3	0.9	0.08	~100	~2	Ba,Ah
	LARA	92B-13	Devonian	Sicker Gp - basalt - rhyolite	2 lenses	1	py	0.8	6.2	1.3	113	5	
	HOMESTAKE	82M-4W	Devono-Mississippian	Eagle Bay Fm - schist, felsic volc.	lenses	~1	py	0.55	4	2.5	224		Ba
	REA	82M-4W	Devono-Mississippian	Eagle Bay Fm - sericitic phyllite	2 lenses	0.12	py	0.85	4.11	3.67	141	18.2	Ba

*size includes production and reserve estimates

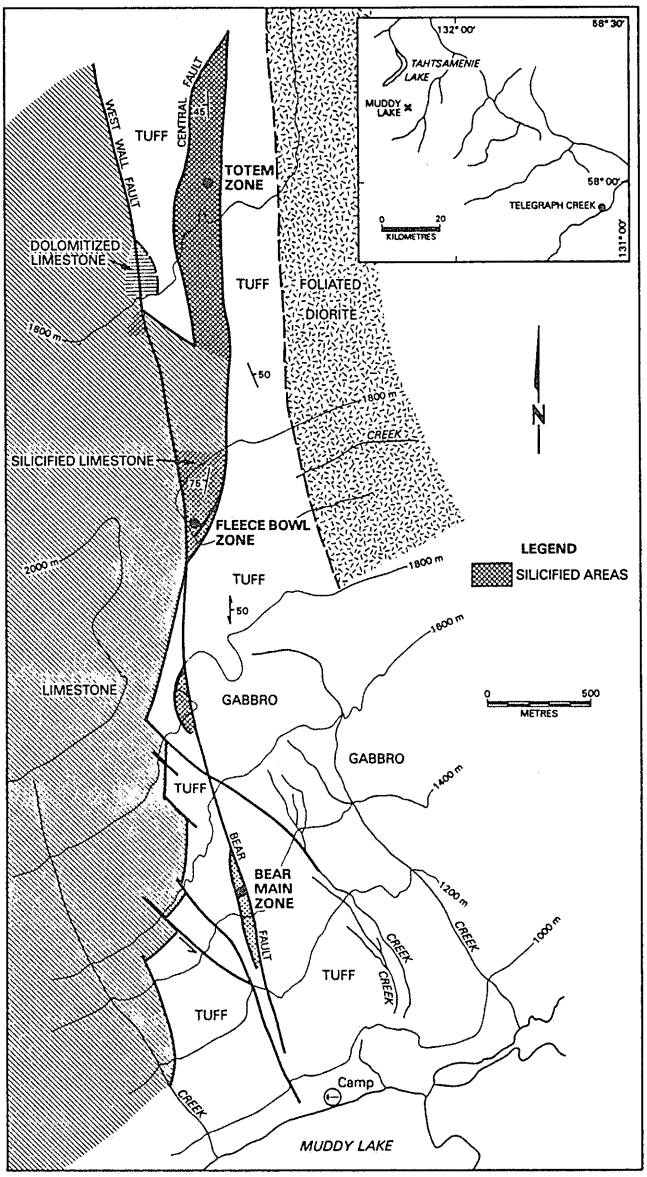

Fig. 9. General geologic setting of the Muddy Lake gold deposits (after Schroeter, 1986).

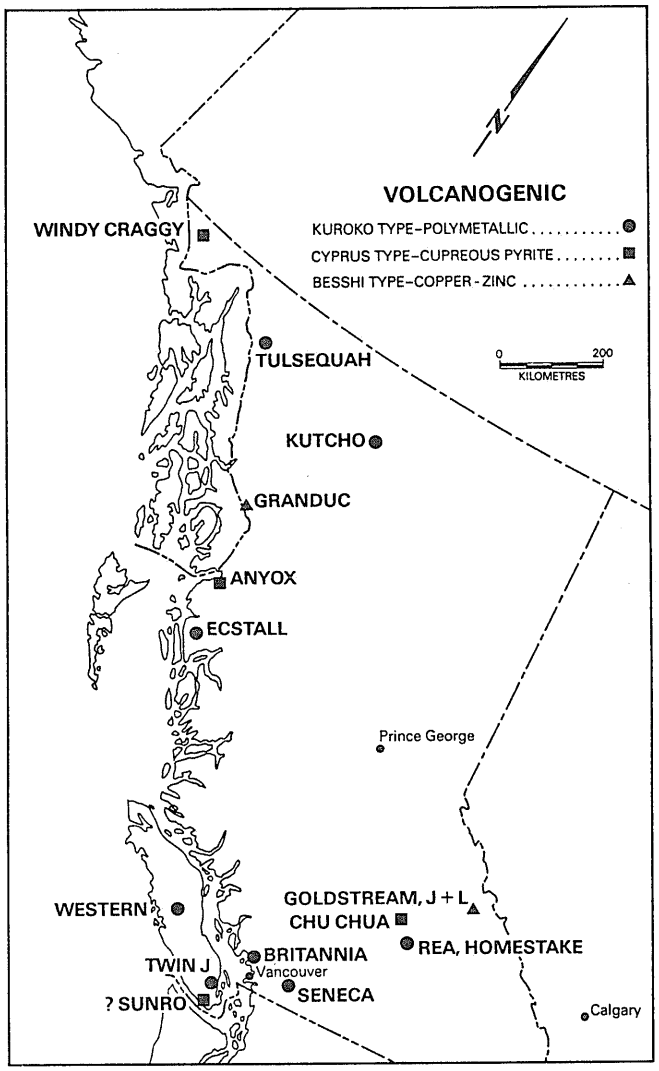

Fig. 10. Distribution of volcanogenic massive sulphide deposits in British Columbia.

recognition of the genesis of the deposits, recent work (Walker, 1983), has shown that all the orebodies were deposited near the ends of volcanic cycles. The host rocks are rhyolitic rocks at several stratigraphic levels within a 500-metre thick volcanic section (Fig. 12). The lowest mineralized volcanic unit consists of calc-alkaline andesite containing pyritic stringer zones and is overlain successively by the H-W rhyolite, calc alkalic andesite flows, a sodic dacite dome, volcaniclastic rocks with local massive sulphide clasts, the Myra rhyolite, and finally, mafic wacke and chert.

The Britannia deposit, north of Vancouver, was virtually mined out before the volcanogenic nature of the deposit was recognized (Sutherland Brown, 1975). The Britannia ore deposits are within strongly deformed Jurassic-Cretaceous Gambier Group rocks that form a roof pendant in the Coast Plutonic Complex. Kuroko-type black and yellow ore deposits formed within epiclastic and pyroclastic dacitic rocks near dacitic eruptive centres (Stone and Payne, 1982). Ore zones consisted dominantly of pyrite, chalcopyrite, and minor amounts of galena and tetrahedrite in schistose and altered host rocks. Ore lenses were stratabound and occurred at several stratigraphic levels; most had underlying stringer ore from which most of the mine production came. Black, galena-sphalerite-barite ore zones occurred in fine grained andesitic volcaniclastic sediments, tuffs and sericite schists. Yellow, chalcopyrite-pyrite ore occurred near the contact of coarse dacitic tuff with overlying andesitic, tuffaceous and cherty sediments.

Kuroko-type deposits also occur in Jurassic rocks of the Harrison Lake Formation near Harrison Hot Springs, east of Vancouver. Major elements and oxygen isotope zonation typical of many volcanogenic massive sulphide deposits are well displayed (S. Scott, pers. comm., 1986). The iron to iron plus magnesium ratio of chlorites in the country rock decreases toward mineralized zones; that is, chlorites near ore are the most magnesium rich. Even under relatively low levels of heating, distinctive alteration assemblages, which typically consist of a

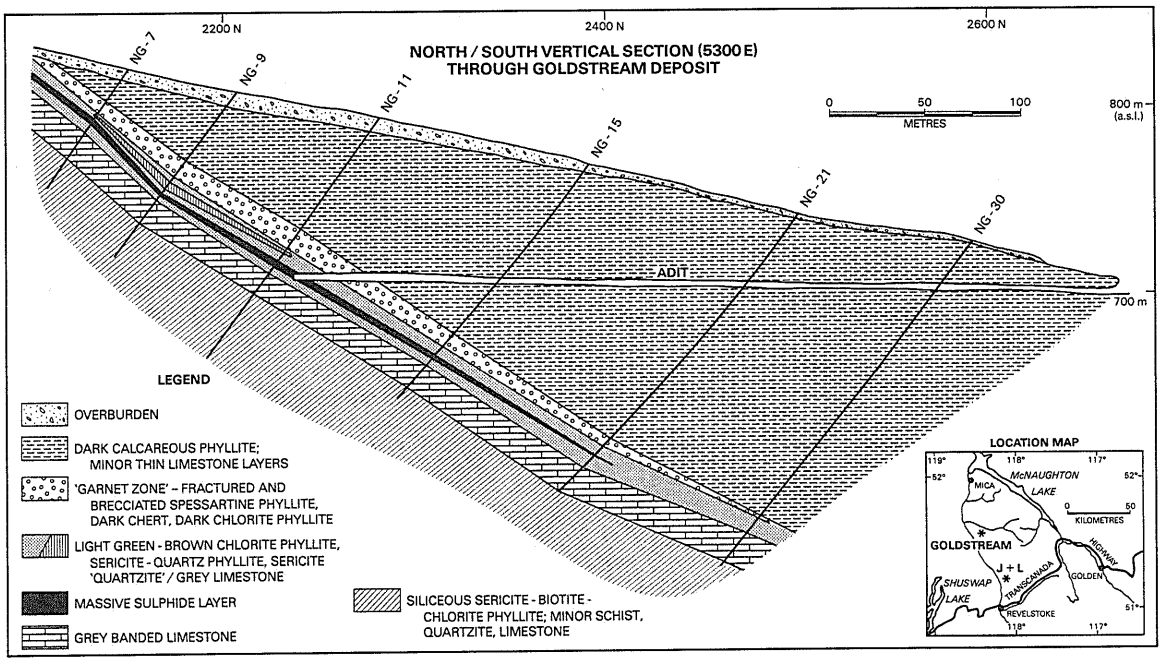

Fig. 11. Geology and setting of the Goldstream volcanogenic copper-zinc deposit (after Höy, 1979).

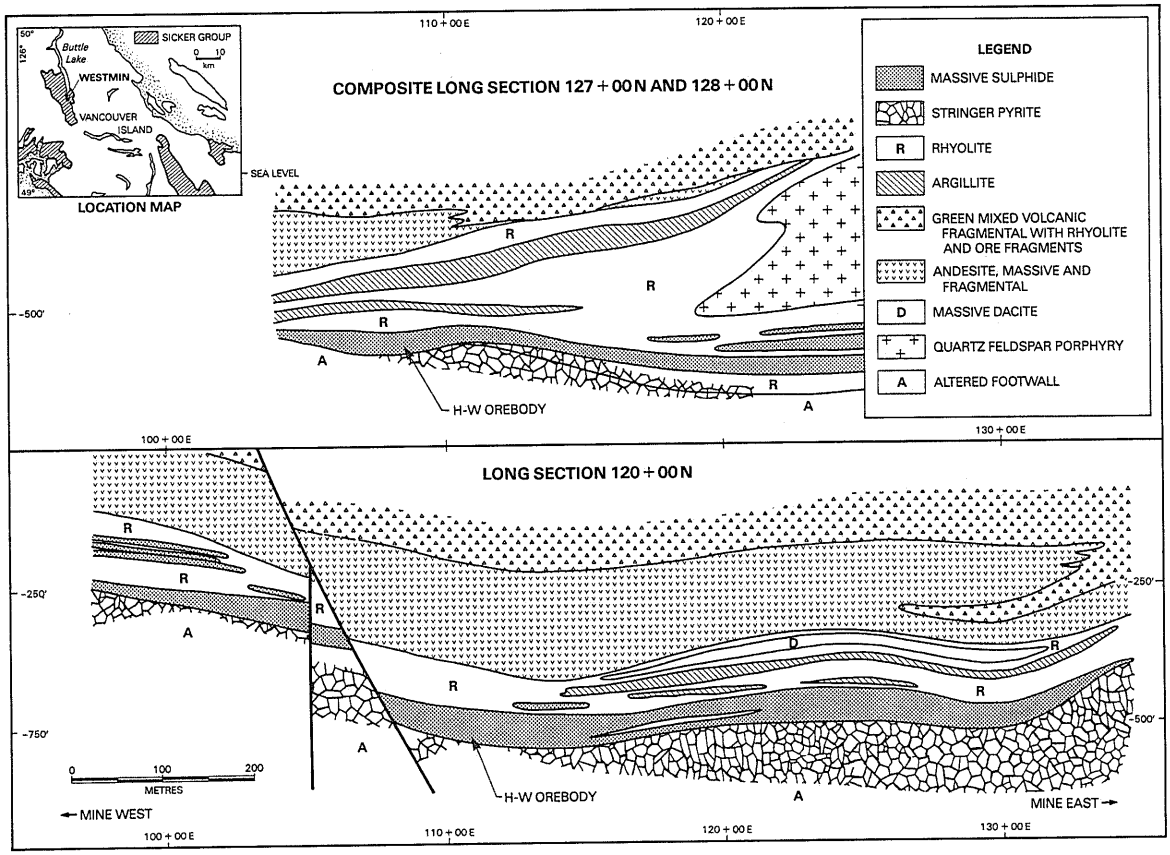

Fig. 12. Geology and setting of the polymetallic Westmin deposits (after Walker, 1983).

core zone of sericite with fringing chloritic and kaolinitic zones, can be destroyed. However, at the Seneca occurrence, hydrothermally induced oxygen isotope patterns survived; near ore δO^{18} values average 6, while in the fringing zone they average 12 (S. Scott, pers. comm., 1986). As oxygen isotope analyses become less expensive and more accessible, they could become another routine exploration tool in low grade metamorphic terranes.

Cyprus-type cupriferous pyrite deposits are related to episodes of oceanic rifting (Constantinou and Govett, 1973). In general, alteration in the underlying pillow lavas is fracture-related and narrow, probably indicative of a shallow heat source above which water moved quickly up and down the proximal fractures. The deposits form during periods of volcanic quiescence and are commonly at basalt-sediment interfaces at the top of or within pillow lava sequences. This interval represents a hiatus during which hydrothermal activity took place in an ongoing volcanic cycle. Synvolcanic block faulting is common. The deposits are often associated with siliceous exhalites which generally have a tuffaceous component. Chert layers and iron or manganese enriched pelagic muds may occur above or along strike from the sulphide lenses. The sulphide lenses tend to be

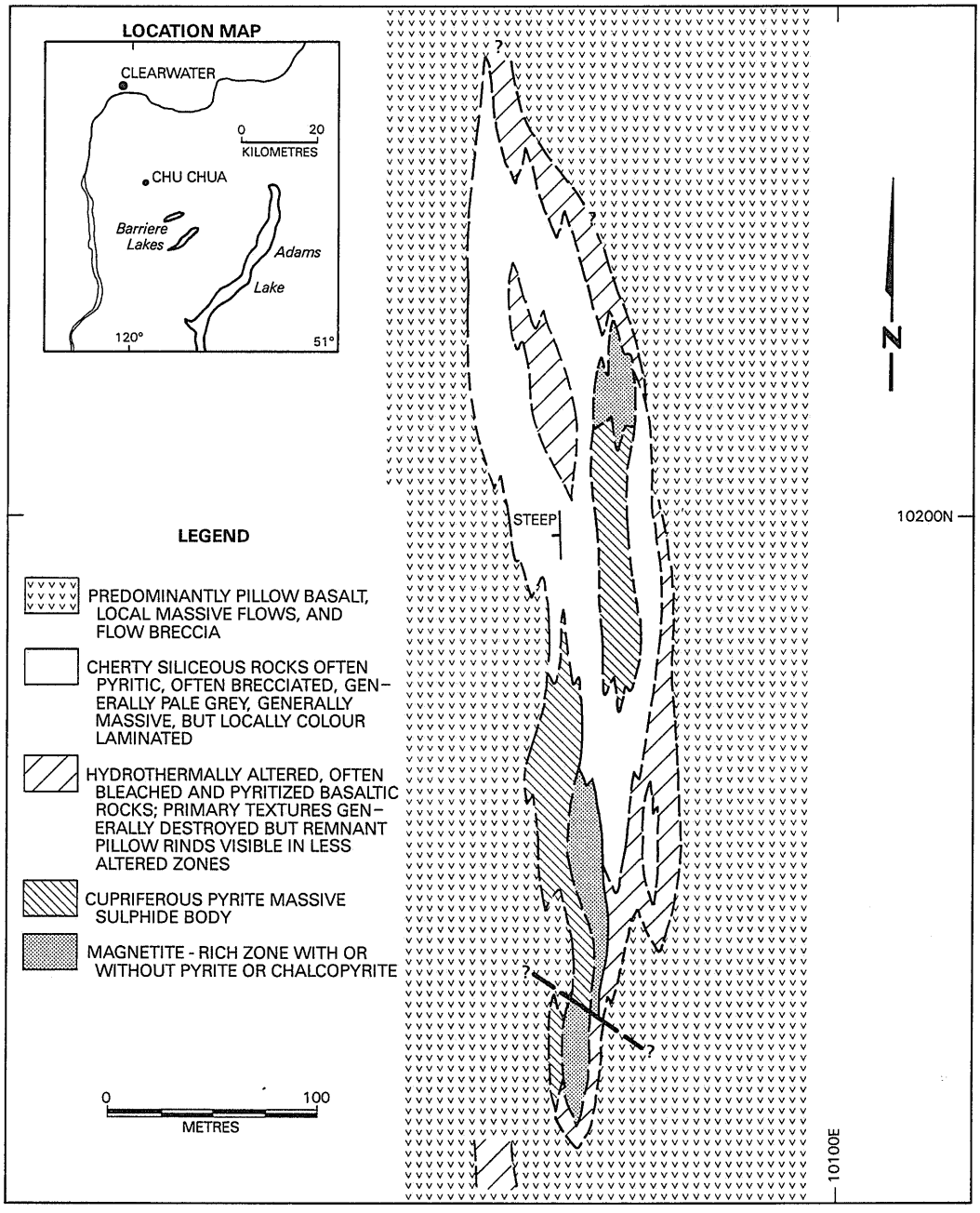

Fig. 13. Generalized geology of the Chu Chua deposit (after McMillan, 1980).

copper-zinc rich with little lead. Gold/silver ratios are relatively high, cobalt is a common minor constituent and relative cobalt/nickel ratios may be high.

The Chu Chua deposit in south-central B.C. consists of cupriferous pyritic massive sulphide lenses in a pillowed basalt sequence (Fig. 13) consisting of low-potassium alkalic tholeiites that apparently formed in an ocean floor, ocean island, or seamount setting (Aggarwal and Nesbitt, 1984). The massive sulphides carry up to 1,000 ppm cobalt and locally, gold values to 3 ppm. No distinct sedimentary unit is present but the sulphide lenses are associated with tuffaceous cherts, commonly pyritic, interpreted to be siliceous exhalites (McMillan, 1980). The mineralized interval contains local massive magnetite and talc layers. Underlying pillow lavas are altered and bleached to a pale green color. Adjacent to mineralization the basalts are anomalous in barium. One sample contained almost 8 percent Ba (M. Chaudhry, pers. comm., 1980). Apparently the barium occurs in silicate minerals such as armenite and cymrite (J. Kwong, pers. comm., 1980).

Another deposit that may have formed in an oceanic ridge environment is Anyox in northern B.C. (Fig. 10) (Alldrick, 1986). The sulphide lenses occur at the tops of mafic volcanic cycles and are generally overlain by argillites that are excellent stratigraphic exploration guides.

Mineral Deposits in Convergent Margin Settings

There are two classes of convergent boundaries: subduction boundaries, in which oceanic material composes the downgoing plate; and collisional boundaries, where continental lithosphere constitutes the downgoing plate. Fold and thrust belts commonly develop in the upper plate but local extensional structures are also important (Bally and Oldow, 1986). The accompanying strike-slip displacement is an important, and often overlooked, component of collisional boundaries. Oblique collision is likely to be the rule, not the exception. Convergent margins create volcanic arcs, which are narrow, well-defined belts of igneous and plutonic activity (Sawkins, 1984). Deposits containing principally copper, iron, molybdenum, gold and silver are related to calc-alkaline magmatism associated with convergent margins.

Many deposit types occur in the rocks of volcanic arcs. Among these are porphyry coppers (Fig. 14), skarns, vein

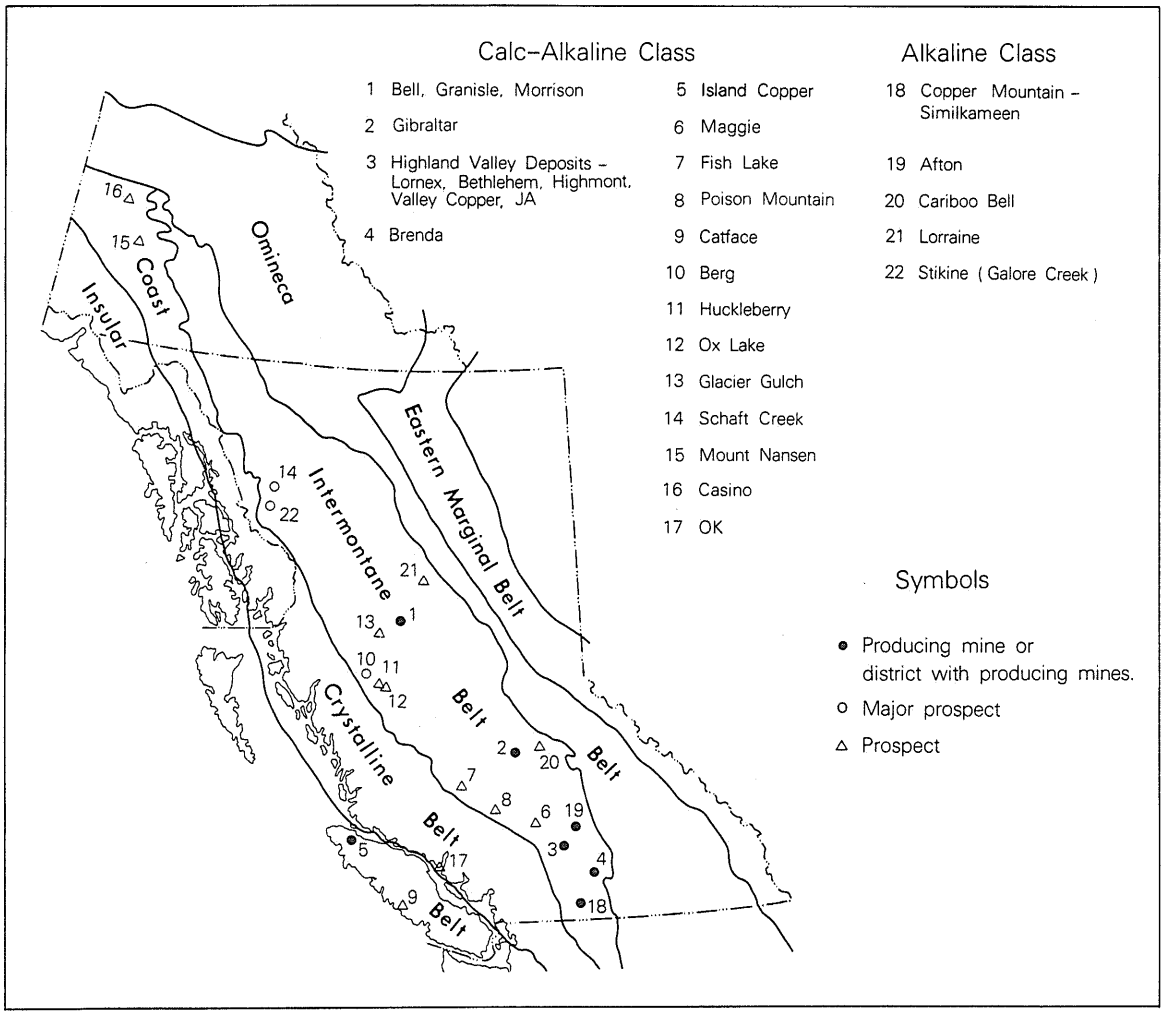

Fig. 14. Distribution of porphyry deposits in British Columbia showing the major gold-bearing alkalic deposits (after McMillan and Panteleyev, 1980).

deposits, some volcanogenic massive sulphide deposits, such as the Kuroko-type deposits already described, and Alaskan-type platinum deposits. This discussion concentrates on those with precious metal or platinum potential.

An epithermal model considers depth zoning and covers the range from deeper porphyry copper, skarn and mesothermal vein deposits, to shallower epithermal vein deposits, to surface-deposited siliceous sinters (Panteleyev, 1986). Generally, in this model, a plutonic heat source at depth energizes the hydrothermal system. A preliminary attempt has been made to position various Cordilleran deposits within this depth zoning scheme (Fig. 15).

Arc-related porphyry copper-molybdenum or copper-gold deposits occur in both alkaline and calc-alkaline host rocks. Gold-bearing porphyry deposits are associated with volcanic rocks, or are subvolcanic whilst plutonic type porphyries, especially those enriched in molybdenum, form a distinct, gold-poor population (Sinclair et al., 1982). At least some of the alkaline porphyries are associated with relatively alkali-rich, shoshonitic country rocks. Among these are the Afton, Cariboo Bell and Galore Creek deposits. Precious metal deposits of epithermal and submarine exhalative origin are also associated with alkaline rocks (Mutschler et al., 1986).

Skarn deposits are typically formed in calcareous rocks adjacent to stocks of intermediate composition. Metals are zoned around the stocks, with inner iron-copper-gold-silver zones grading outward into gold-silver, and then into lead-zinc-silver zones (Myers, 1985). Skarns form in a wide variety of environments, including volcanic arcs and the inner sides of volcanic arcs (Sawkins, 1984). Along the inner sides of volcanic arcs the host rocks are platformal and are cut by intermediate to felsic intrusives. Manto zinc-lead-silver, tin, and tungsten deposits characterize this setting.

Skarn deposits with significant gold values developed as a result of Jurassic plutonic events during Nicola island arc volcanism. At Hedley (Bacon, 1978, Ray et al., 1986) skarn formed in the Triassic age Nickel Plate Formation adjacent to 190 million year old dioritic sills, dykes and plugs (Fig. 16). The Nickel Plate Formation consists of the basal Sunnyside limestone, the Middle unit of limestone and quartzite, and the Upper unit of quartzite and breccia. Skarn alteration forms a hard, green pyroxene-garnet rock. Mineralization replaces skarn and rarely fills fractures in the diorites. It consists of auriferous arsenopyrite, pyrrhotite, and chalcopyrite. Ore zones are localized by folds and faults and form a series of tabular bodies which are virtually confined to the skarn zones. The mine produced 3.6 million tonnes of ore grading almost 15 grams/tonne (0.436 ounces/ton) gold. The property has recently been re-evaluated by Mascot Gold Mines and open pit production is scheduled to begin in 1987.

Vein and replacement lode gold systems formed at both deep and shallow depths in island arc settings in British Columbia. In the Rossland Camp, for example, deposits are mesothermal and consist of lodes and replacements along fractures and faults (Fyles, 1984). Gold occurs in pyrrhotite and chalcopyrite. The country rock is altered to quartz, calcite and other silicates. The 5.5 million tonnes of production from the Rossland camp graded 13 grams/tonne gold, 17 grams/tonne silver, and 1 percent copper. Production from related "bonanza" epithermal veins was only 10,000 tonnes, but it averaged 100 grams/tonne gold. Gold in the camp is multicyclic. Textures indicate that some mineralization is likely of Jurassic age, but some veinlets

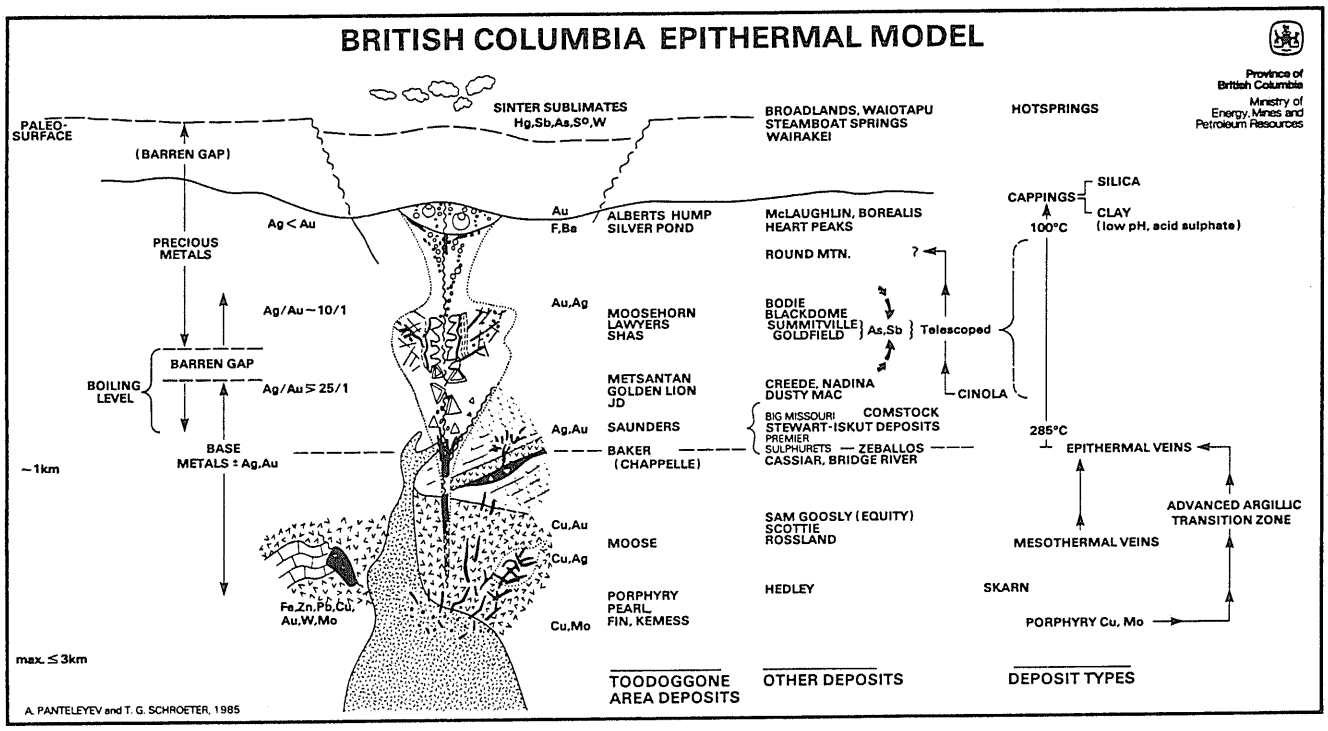

Fig. 15. Depth zoning model for Cordilleran epithermal precious metal deposits (after Panteleyev, 1986).

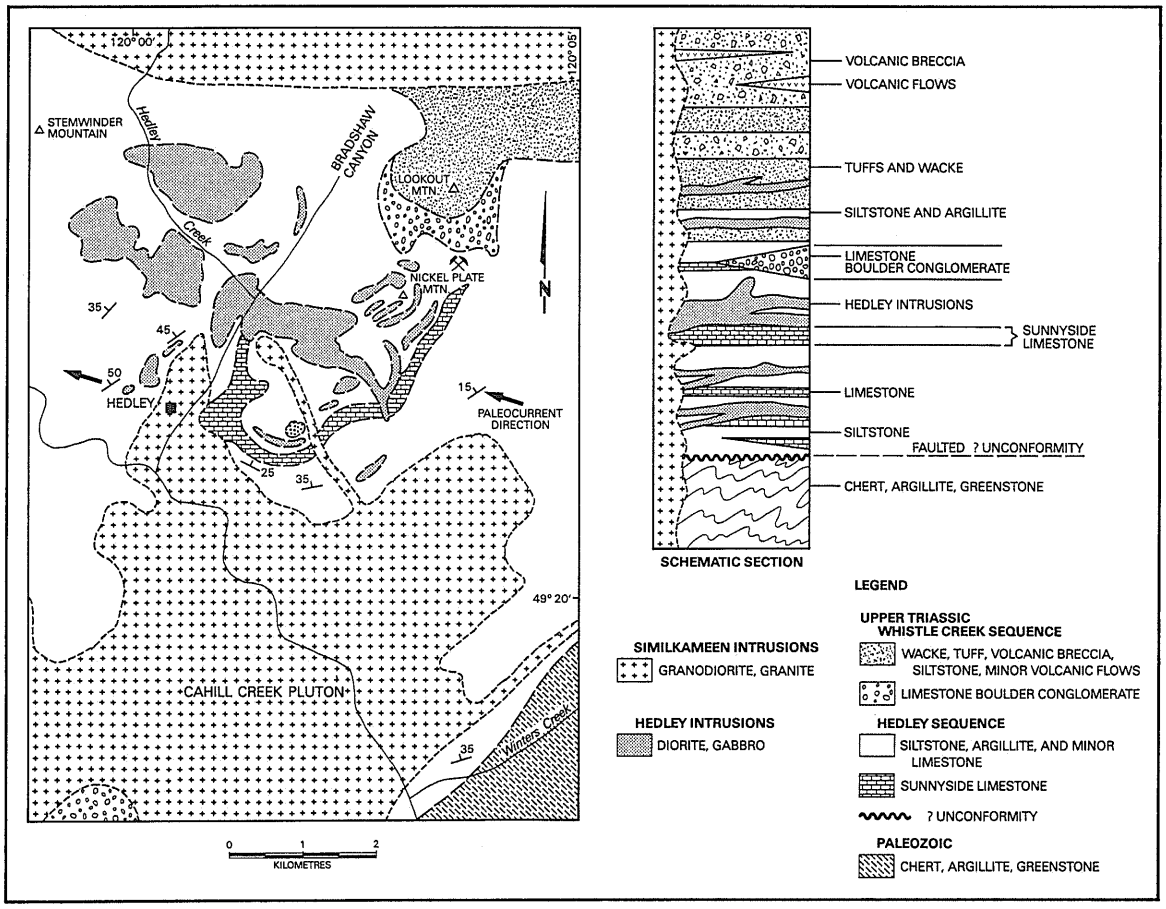

Fig. 16. General geology and setting of the Hedley gold skarn deposits (after Ray et al., 1986).

cut Tertiary lamprophyres. Whether the Tertiary age veinlets represent remobilization and the main mineralizing event is of Jurassic age is not certain.

The deposits are hosted by shoshonitic volcanic rocks (Spence, 1985) of the Jurassic age Rossland Group. Worldwide, shoshonites are geochemically anomalous in gold. According to Spence, before a subduction zone is abandoned, the rate of subduction slows and the dip of the subduction zone steepens. This steepening leads to deep mantle melting in the presence of water and produces shoshonitic melts.

Recent work also indicates the presence of shoshonitic rocks near the Tillicum Mountain gold deposit (Ray and Spence, 1986). As well, rocks forming the roof pendant that hosts the Willa copper-gold breccia deposit near Silverton, are also apparently correlative with the Rossland Group (Wong et al., 1986), and may be shoshonitic in part. Other roof pendants of Rossland volcanic rocks present attractive exploration targets.

Molybdenite mineralization in the Rossland camp is associated with 160 million year old granitic plutons (Fyles, 1984).

OTHER MINERAL DEPOSIT ENVIRONMENTS

Many other deposits within the Canadian Cordillera formed in environments that are not clearly related to passive or convergent margin settings. These deposits include epithermal and mesothermal vein deposits, replacement gold deposits and some skarn deposits. However, all are related to thermal and/or tectonic events.

Epithermal vein and stockwork precious metal deposits are important exploration targets in British Columbia. In the north, for example, deposits in the Stewart and Toodoggone areas are under intensive exploration. Mineralization in both areas is hosted by rocks of Jurassic age (Barr, 1980). In the Stewart area, the multiphase epithermal stockworks, stratabound replacement, and vein deposits are underlain by the 210 million year old Texas Creek granodiorite (Alldrick, 1985). Mineralogical and metal zoning in the deposits is spatially related to the older intrusive but radiometric dates of 180 million years suggest the veins are younger. The deposits might be related to a late cycle of felsic volcanism within the Jurassic arc. Silver rich vein deposits in the Stewart camp are of Eocene age and related to emplacement of the Coast Plutonic Complex. In the Toodoggone area, mineralized quartz veins occur in the continental, possibly back-arc, shoshonitic Toodoggone volcanics. Gold mineralization is found in Jurassic high level veins related to ancient hot spring environments (Panteleyev, 1986).

In the Cariboo district, historically productive auriferous veins, lodes, sheet zones and tabular replacement zones occur mainly in Proterozoic to Paleozoic sedimentary rocks of the Barkerville

terrane. However, potassium-argon dates from alteration minerals associated with the mineralization cluster around a 140 million year age (R. Hall, pers. comm., 1986).

The penetratively deformed host rocks are generally greywackes, although the replacement lodes occur in calcareous rocks (Alldrick, 1983) with silica and carbonate alteration. Talc and fuchsite are also present. Dominant sulphides are pyrite and arsenopyrite. The ore shoots are structurally controlled. Host rocks in the Cariboo area may be correlative with parts of the Eagle Bay and Lardeau groups to the south (Struik, 1985). Gold mineralization also occurs in Paleozoic to Mesozoic black pelite, rhyolite and andesite of the Quesnel Terrane.

Sediment hosted disseminated gold deposits (Romberger, 1986) occur on the Queen Charlotte Islands. The 13 million year old Cinola deposit lies within a zone of silicified rocks with peripheral argillitic alteration adjacent to a Miocene rhyolite intrusion and along a major fault (Sutherland Brown and Schroeter, 1976; Champigny and Sinclair, 1982). Gold in the deposit is in the 5 micron size range. It occurs both in silicified rocks and in narrow quartz veins and in the latter tends to be coarser in size. Gold in mineralization is associated with pyrite and marcasite. The hosting sediments contain abundant carbonized wood and plant debris and away from the mineralized zones are porous and poorly consolidated. Geochemically, mineralization is associated with anomalous concentrations of mercury, arsenic, antimony and tungsten (Champigny and Sinclair, 1982).

Manto deposits are epigenetic, replacement bodies with characteristic pipe-like or blanket shapes that generally form at moderately high temperatures. The plunge of the "pipes" can vary from horizontal to vertical. Ore controls may include structural traps and sedimentary or structurally induced porosity. Recent evidence (Wood, 1985) indicates that solution openings and caves can form in aquifers at great depth. The Midway pyritic silver-zinc-lead deposit consists of mineralized pipes that occur in Devonian carbonates of the Cassiar Platform. The pipes are shallow-plunging, and developed preferentially below the McDame limestone-Earn shale contact, but also occur within the limestone away from the contact (W. Jacubowski, pers. comm., 1985). Sedimentary exhalative deposits were the initial target in the area (MacIntyre, 1982), but as a result of further exploration and supported by lead isotope analyses (C. Godwin, 1985, pers. comm.), there is now some question whether any of the showings are of exhalative origin. Although no intrusions are exposed on the property, it is possible that the mineralization is of Tertiary age and is related to granitic intrusive rocks.

Basin and range style extensional tectonics in the Slocan area are related to a large scale "slide" or detachment zone. The upper plate of the slide, where horst and graben structures are developed, contains Tertiary age volcanic rocks and their Mesozoic age basement (Tempelman-Kluit, 1984), including the Nelson granites of Jurassic age (Parrish, 1985). The lower plate consists of a metamorphic core complex.

Epithermal gold mineralization, such as occurs in the Dusty Mac deposit near Okanagan Falls (Church, 1973) occurs in silicified Eocene age volcanic rocks in a similar setting. In California, as described by W. Rehrig to a Mining Exploration Group meeting in December, 1986 in Vancouver, precious metal mineralization in this type of setting seems to occur on the east side of the metamorphic complexes, east of the surface zone that marks the ancestral continental margin. Mineralization can occur in chloritic breccia zones, disseminated in the detachment zone, or in association with listric normal faults in rocks above it. Characteristic associated features include early albitic alteration, chloritic hematitic breccias, alkalic rhyolites, and late, strongly oxidized, breccia zones with orthoclase and carbonate alteration in rocks above the detachment zone.

Paleoplacer deposits of gold and platinum should not be overlooked. For instance, basins that drain areas with gold mineralization, like the Toodoggone, have placer deposit potential (Eisbacher, 1974). Paleocurrent studies followed by lithogeochemical sampling are logical exploration approaches.

DISCUSSION

At convergent margins the amount of material melted in the downgoing slab depends on the geothermal gradient, the depth, and the source rock type. The melts produced in subduction zones are influenced by the compositions of the underplated rocks and by the amount of water that they introduce. Similarly, metallic mineral deposits related to the melts will reflect the source rock and the amount of melting that takes place. As Anderson (1985) and many others have pointed out, copper and molydenum deposits occur with I-type granites; tin, tungsten and copper, with S-type: and molybdenum, tungsten and tin with A-type. Furthermore, trace element variations in modern subduction-related granitoid suites from circum-Pacific arcs reflect distance from the active trench (Brown et al., 1984), thus, studying the geochemistry of ancient granitoids might give clues about their plate tectonic settings.

Ideas expressed in the preceding discussions relating deposits to oceanic terranes, island arcs, and passive margins are generalized. Specific types of mineral deposits can occur in several plate tectonic settings if conditions favorable for ore formation are duplicated. In a general way, however, copper, iron and gold deposits favor settings with little influence of continental crust, whereas lead, zinc, molybdenum, tin and tungsten are concentrated in areas underlain by continental crust.

CONCLUSIONS

Plate tectonic setting can be used to formulate an exploration strategy but is not an effective exploration model at deposit scale. Plate tectonic interpretations distinguish terranes that are favorable hosts for specific deposits. In British Columbia, where allochthonous terranes are incompletely defined, there remains scope for finding favorable areas that have been overlooked or mis-identified.

Petrology, geochemistry and isotopic analyses support geological and structural mapping as tools for defining plate tectonic settings. Geochemical and isotopic signatures of igneous rocks reflect the source rocks from which the magma was derived and also reflect the tectonic setting — whether it was compres-

sive or extensional. The types of granitic rocks present also relate to plate tectonic setting and their nature can be determined from their mineralogy and chemistry. Isotopic dating and paleontology provide critical data for correlating units within and between terranes. But the importance of field mapping cannot be overlooked!

Modern exploration programs frequently apply genetic deposit modelling in the search for specific deposit types, whether the search is for gold skarns or polymetallic massive sulphide deposits. A significant pool of data on modern deposits that occur in specific settings, like seafloor polymetallic sulphide deposits (Scott, 1986) or hot spring deposits, is now available and expanding rapidly. These data can be applied to analogous, but older, mineral deposits.

Acknowledgements — This report draws heavily on papers written about mineral deposits and plate tectonics in the Canadian Cordillera; compilation of the report would not have been possible without them. We wish to extend our thanks to all our colleagues at the Ministry, particularly Gerry Ray, Don MacIntyre and Dani Alldrick; to Jim Monger, Howard Tipper, Ted Irving and Ken Dawson of Energy, Mines and Resources Canada; and Colin Godwin and Dick Armstrong of the University of British Columbia. Figures were drafted by Pierino Chicorelli. This report is published with the permission of the Chief Geologist, Geological Survey Branch, B.C. Ministry of Energy, Mines and Petroleum Resources.

REFERENCES

Aggarwal, P. K. and Nesbitt, B. E., 1984, Geology and geochemistry of the Chu Chua massive sulphide deposit, British Columbia: Econ. Geol., v. 79, p. 815-825.

Alldrick, D. J., 1983, The Mosquito Creek Mine: B.C. Min. Energy, Mines and Pet. Res., Pap. 1985-1, p. 99-112.

Alldrick, D. J., 1985, Stratigraphy and petrology of the Stewart Mining Camp (104B/1): B.C. Min. Energy, Mines and Pet. Res., Pap. 1985-1, p. 316-342.

Alldrick, D. J., 1986, Stratigraphy and structure in the Anyox area: B.C. Min. Energy, Mines and Pet. Res., Pap. 1986-1, p. 211-216.

Anderson, R. G., 1985, Variation of Mesozoic to Tertiary plutonic style with tectonic setting in the northern Canadian Cordillera; Geol. Soc. Amer., Abst., Cordilleran Section Meeting, Vancouver, May, 1985.

Armstrong, R. L., 1987, Mesozoic and early Cenozoic magmatic evolution of the Canadian Cordillera: Rodgers Symposium Volume, in press.

Bacon, W. R., 1978, Lode gold deposits in Western Canada: Can. Inst. Mining Metall., Bull., v. 71, July, p. 96-104.

Bally, A. W. and Oldow, J. S., 1986, Plate tectonics, structural styles and the evolution of sedimentary basins: Geol. Assn. Canada, Cordilleran Section, Short Course No. 7, 238 pp.

Barr, D. A., 1980, Gold in the Canadian Cordillera: Can. Inst. Mining Metall., Bull., v. 73, June, p. 59-68.

Brown, G. C., Thorpe, R. S. and Webb, P. C., 1984, The geochemical characteristics of granitoids in contrasting arcs and comments on magma sources: J. Geol. Soc. London, v. 141, p. 413-426.

Cabri, L. J., 1982, Classification of platinum group deposits with reference to the Canadian Cordillera: *in* Precious Metals in the Northern Cordillera, A. A. Levinson, ed., Association of Exploration Geochemists, p. 21-32.

Carne, R. C. and Cathro, R. J., 1982, Sedimentary exhalative (Sedex) zinc-lead-silver deposits, northern Canadian Cordillera: Can. Inst. Mining Metall., Bull., v. 75, p. 66-78.

Champigny, N. and Sinclair, A. J., 1982, Cinola gold deposit, Queen Charlotte Islands, B.C. — a geochemical case history: *in* Precious Metals in the Northern Cordillera, A. A. Levinson, ed., Association of Exploration Geochemists, p. 121-138.

Church, B. N., 1973, Geology of the White Lake basin: B.C. Min. Energy, Mines and Pet. Res., Bull. 61, 120 pp.

Constantinou, B. and Govett, G. J. S., 1973, Geology, geochemistry and genesis of Cyprus sulphide deposits: Econ. Geol. v. 68, p. 843-858.

Eisbacher, G. H., 1974, Sedimentary history and tectonic evolution of the Sustut and Sifton basins, north-central British Columbia: Geol. Surv. Can., Pap. 73-31, 45 pp.

Ewing, T. E., 1981, Regional stratigraphy and structural setting of the Kamloops Group volcanics, British Columbia: Can. J. Earth Sciences, v. 18, p. 1478-1498.

Findlay, D. C., 1969, Origin of the Tulameen ultramafic-gabbro complex, southern British Columbia: Can. . Earth Sciences, v. 6, p. 399-425.

Fyles, J. T., 1984, Geological setting of the Rossland Mining Camp: B.C. Min. Energy, mines and Pet. Res., Bull. 74, 61 pp.

Fyles, J. T., 1970, Geological setting of lead-zinc deposits in the Kootenay Lake and Salmo areas of B.C., *in* Lead-zinc deposits of the Kootenay Arc, northeast Washington and adjacent British Columbia: Department of Natural Resources, State of Washington, Bull. 61, p. 41-53.

Fyles, J. T. and Hewlett, C. G., 1959, Stratigraphy and Structure of the Salmo lead-zinc area: B.C. Min. Mines, Bull. 41, 162 pp.

Gabrielse, H., 1986, The Gangue, No. 23, p. 10.

Hamilton, J. M., Bishop, D. T., Morris, H. C. and Owens, O. E., 1982, Geology of the Sullivan orebody, Kimberley, B.C., Canada: *in* Precambrian Sulphide Deposits, H. S. Robinson Memorial Volume, R. W. Hutchinson, C. D. Spence and J. M. Franklin, eds., Geol. Assoc. Can., Spec. Pap. 25, p. 597-666.

Hodgson, C. J., Chapman, R. S. G. and MacGeehan, P. J., 1982, Application of exploration criteria for gold deposits in the Superior Province of the Canadian Shield to gold exploration in the Cordillera: *in* Precious Metals in the Northern Cordillera, A. A. Levinson, ed., Association of Exploration Geochemists, p. 173-206.

Höy, T., 1985, J&L, A stratabound gold-arsenic deposit, southeastern British Columbia: B.C. Min. Energy, Mines and Pet. Res., Pap. 1986-1, p. 101-104.

Höy, T., 1984, Structural setting, mineral deposits, and associated alteration and magmatism, Sullivan Camp, southeastern British Columbia: B.C. Min. Energy, Mines and Pet. Res., Pap. 1984-1, p. 24-35.

Höy, T., 1982a, The Purcell supergroup in southeastern British Columbia; Sedimentation, tectonics and stratiform lead-zinc deposits: *in* Precambrian Sulphide Deposits, H. S. Robinson Memorial Volume, R. W. Hutchinson, C. D. Spence and J. M. Franklin, eds., Geol. Assoc. Can., Spec. Pap. 25, . 91-126.

Höy, T., 1982b, Stratigraphic and structural setting of stratabound lead-zinc deposits in southeastern B.C.: Can. Inst. Mining Metall., Bull., v. 75, April, 1982, p. 114-134.

Höy, T, 1979, Geology of the Goldstream area: B.C. Min. Energy, Mines and Pet. Res., Bull. 71, 49 pp.

Höy, T., Gibson, G. and Berg, N. W., 1984, Copper-zinc deposits associated with basic volcanism, Goldstream area, southeastern B.C.: Econ. Geol., v. 79, p. 789-814.

Hutchinson, R. W. and Searle, D. L., 1971, Stratabound pyrite deposits in Cyprus and relations to other sulphide ores: Soc. Mining Geologists, Japan, Spec. Issue 3, p. 198-205.

Irving, E., Monger, J. W. H. and Yole, R. W., 1980, New paleomagnetic evidence for displaced terranes in British Columbia, *in* Strangway, D. W., Ed., The continental crust and its mineral deposits: Geol. Assoc. Can., Spec. Pap. 20, p. 441-456.

Lydon, J. W., 1984, Ore deposits models - 8. Volcanogenic massive sulphide deposits Part 1; A descriptive model: Geoscience Canada, v. 11, p. 195-202.

McClay, K. R. and Insley, M. W., 1986, Structure and Mineralization of the Driftpile Creek area, northeastern British Columbia: B.C. Min. Energy, Mines and Pet. Res., Pap. 1986-1, p. 343-350.

MacIntyre, D. G., 1982, Midway occurrence (104O/16W): B.C. Min. Energy, Mines and Pet. Res., Pap. 1982-1, p. 162-166.

MacIntyre, D. G., 1984, Geology of the Alsek-Tatshenshini Rivers area (114P): B.C. Min. Energy, Mines and Pet. Res., Pap. 1984-1, p. 173-184.

MacIntyre, D. G., 1986, The geochemistry of basalts hosting massive sulphide deposits, Alexander Terrane, northwest British Columbia: B.C. Min. Energy, Mines and Pet. Res., Pap. 1986-1, p. 197-210.

McMillan, W. J., 1980, CC prospect, Chu Chua Mountain: B.C. Min. Energy, Mines and Pet. Res., Pap. 1980-1, p. 37-48.

McMillan, W. J. and Panteleyev, A., 1980, Deposit models — 1. Porphyry copper deposits: Geoscience Canada, v. 7, p. 52-63.

Monger, J. W. H., 1984, Structural evolution of the southwestern Intermontane Belt, Ashcroft and Hope map-areas, British Columbia: *in* Current Research, Part A, Geol. Surv. Can., Pap. 85-1A, p. 349-358.

Monger, J. W. H. and Ross, J. V., 1971, Distribution of fusilinaceans in the Canadian Cordillera: Can. J. Earth Sciences, v. 8, p. 259-278.

Monger, J. W. H., Souther, J.G. and Gabrielse, H., 1972, Evolution of the Canadian Cordillera: A plate tectonic model: Amer. J. Sci., v. 272, p. 577-602.

Monger, J. W. H., Price, R. A. and Tempelman-Kluit, D. J., 1982, Tectonic accretion and the origin of the two major metamorphic and plutonic welts in the Canadian Cordillera: Geology, v. 10, p. 70-75.

Monger, J. W. H., and Berg, H. C., 1984, Lithotectonic terrane map of Western Canada and southeastern Alaska: U.S. Geol. Surv., Open File Rept., p. 84-523.

Mutschler, F. E., Griffin, M. E., Stevens, D. S. and Shannon, S. S., Jr., 1986, Precious metal deposits related to alkaline rocks in the North American Cordillera: Geol. Soc. South Africa, Trans., in press.

Myers, G. L., 1985, Gold distribution in the Fe-Cu-Au skarns of Kasaan Penninsula, southeast Alaska: Geol. Soc. Amer., Abst., Cordilleran Section Meeting, Vancouver, May, 1985.

Panteleyev, A., 1986, Ore Deposits #10. A Canadian Cordilleran model for epithermal gold-silver deposits: Geoscience Canada, v. 13, p. 101-112.

Panteleyev, A., 1979, Cassiar map-area: B.C. Min Energy, Mines and Pet. Res., Pap. 1983-1. p. 142-148.

Parrish, R., 1985, Metamorphic core complexes of southern B.C.: Distinctions between extensional or compressional origins: Geol. Soc. Amer., Abst., Cordilleran Section Meeting, Vancouver, May, 1985.

Peter, J. M., Scott, S. D., Shanks, W. C. III, and Kadko, D., 1986, Geochemical, mineralogical, fluid inclusion, and stable isotope studies of hydrothermal vent precipitates, Guaymas Basin, Gulf of California: *in* The genesis of stratiform sediment-hosted lead and zinc deposits, Conference Proceedings, R. J. W. Turner and M. T. Einaudi, eds. Stanford University Publications, Geol. Soc., v. XX, 1986.

Ray, G. E., Simpson, R., Wilkinson, W. and Thomas, P., 1986, Preliminary report on the Hedley mapping project: B.C. Min. Energy, Mines and Pet. Res., Pap. 1986-1, p. 45-50.

Ray, G. E. and Spence, A. 1986, The potassium-rich volcanic rocks at Tillicum Mountain — Their geochemistry, origin, and regional significance: B.C. Min. Energy, Mines and Pet. Res. Pap. 1986-1, p. 45-50.

Ray, G. E., Shearer, J. T. and Niels, R. J. E., 1983, Carolin gold mine: *in* Some gold deposits in the Western Canadian Cordillera, GAC-MAC-CGU, Field Trip Guidebook No. 4, p. 40-64.

Romberger, S. B., 1986, Ore deposits #9. Disseminated gold deposits: Geoscience Canada, v. 13, p. 23-32.

Rublee, J., 1986, Platinum group occurrences in the Canadian Cordillera: B.C. Min. Energy, Mines and Pet. Res., Open File 1986-7.

Sangster, D., 1970, Metallogenesis for some Canadian lead-zinc deposits in carbonate rocks: Geol. Assn. Can., v. 22, p. 27-36.

Sawkins, F. J., 1984, Metal deposits in relation to plate tectonics: Springer Verlag, New York, 325 pp.

Scott, S. D., 1986, Seafloor polymetallic sulphides: Scientific curiosities or mines of the future: P. Teleki et al., eds. 1986, Proceedings NATO Advanced Research workshop on "Marine minerals: Resource Assessment Strategies", D. Reidel Publishing Company.

Schroeter, T. G., 1986, Muddy Lake prospect (104K/1): B.C. Min. Energy, Mines and Pet. Res., Pap. 1986-1, p. 175-184.

Sinclair, A. J., Drummond, A. D., Carter, N. C. and Dawson, K. M., 1982, A preliminary analysis of gold and silver grades of porphyry-type deposits in Western Canada: *in* Precious Metals in the Northern Cordiller, A. A. Levinson, ed., Association of Exploration Geochemists, p. 157-172.

Sketchley, D. A., 1986, The nature of carbonate alteration of basalt at Erickson Gold Mine, Cassiar, British Columbia: Unpub. MSc Thesis, The University of B.C., Vancouver.

Sketchley, D. A., Sinclair, A. J. and Godwin, C. I., 1986, Early Cretaceous mineralization in the Sylvester allochthon, near Cassiar, north-central British Columbia: Can. J. Earth Sci., v. 23, p. 1455-1458.

Spence, A., 1985, Shoshonites and associated rocks of central British Columbia: B.C. Min. Energy, Mines and Pet. Res., Pap. 1985-1, p. 426-442.

St. Louis, R. M., 1984, Geochemistry of the platinum group elements in the Tulameen ultramafic complex, British Columbia: Unpub. M.Sc. Thesis, University of Edmonton, 127 pp.

Stone, B. G. and Payne, J. G., 1982, Deformed Mesozoic volcanogenic Cu-Zn sulphide deposits in the Britannia district, British Columbia: Econ, Geol., v. 77, p. 712-714.

Struik, L. C., 1985, Thrust and strike-slip faults bounding tectono-stratigraphic terranes, central British Columbia: Geol. Soc. Amer., Cordilleran Section Meeting, Vancouver, 1985, Field Trip No. 14, p. 14-1 to 14-8.

Sutherland Brown, A. S., 1975, Britannia Mine: B.C. Min. Energy, Mines and Pet. Res., Geology Exploration and Mining in B.C., 1974, p. 190-197.

Sutherland Brown, A. S., Cathro, R. J., Panteleyev, A. and Ney, C. S., 1971, Metallogeny of the Canadian Cordillera: Can. Inst. Mining Metall. Bull., v. 64, p. 37-61.

Sutherland Brown, A. S., and Schroeter, T. G., 1976, Report on the Babe gold prospect: B.C. Min. Energy, Mines and Pet. Res., Pap. 1976-1, p. 71-75.

Tempelman-Kluit, D. J., 1979, Transported cataclasite, ophiolite and granodiorite in Yukon: Evidence of arc-continent collision: Geol. Surv. Can., Pap. 79-14.

Tempelman-Kluit, D. J., 1984, Meteoric water model for gold veins in a detached terrane: Geol. Soc. Amer., Abst., 1984, p. 674.

Tipper, H. W., 1984, The allochthonous Jurassic-Lower Cretaceous terranes of the Canadian Cordillera and their relation to correlative strata of the North American craton: *in* Jurassic-Cretaceous paleogeography of North America, G.E.G. Westerman, ed., Geol. Assoc. Can., Spec. Pap. 27, p. 113-120.

Walker, R. K., 1983, Westmin Resources massive sulphide deposits: *in* Fleming, J. Walker, R. and Wilton, P., Mineral deposits of Vancouver Island: Westmin Resources (Au-Ag-Cu-Pb-Zn), Island Copper (Cu-Au-Mo), Argonaut (Fe), GAC-MAC-CGU, Field Trip Guidebook, May, 1983, p. 5-19.

Wober, H. H. and Shannon, K. R., 1986, The discovery of the Bear-Totem Au-Ag deposit, Muddy Lake, northern B.C.: *in* Exploration in the North American Cordillera, Geoexpo/86, Vancouver, May 12-14, 1986. Programme with Abstracts p. 83.

Wong, R. H., Spence, C. D., Mustard, D. K. and Werner, L. J., 1986, Geology and exploration of the Willa prospect — a breccia hosted Au-Cu-Ag deposit, southeastern B.C.: *in* Exploration in the North American Cordillera, Geoexpo/86, Vancouver, May 12-14, 1986. Programme with Abstracts p. 84.

Wood, W. W., 1985, Origin of caves and other solution openings in the undersaturated (vadose) zone of carbonate rocks: A model for CO_2 generation, Geology, v. 13, p. 822-824.

Distribution of Mineral Deposits in the Pacific Border Ranges and Coast Mountains of the Alaskan Cordillera

R. J. GOLDFARB
U.S. Geological Survey, Box 25046, MS 973, Denver Federal Centre, Denver, Colorado 80226

S. W. NELSON
U.S. Geological Survey, 4200 University Avenue, Anchorage, Alaska 99508

H. C. BERG
115 Malvern Avenue, Fullerton, California 92632

and

T. D. LIGHT
U.S. Geological Survey, Box 25046, MS 973, Denver Federal Centre, Denver, Colorado 80226

Abstract — The allochthonous tectonostratigraphic terranes comprising the Pacific Border Ranges and Coast Mountains stretch across much of southern Alaska and host many of Alaska's largest mineral deposits formed before, during, and after Late Mesozoic and Early Cenozoic accretion of the terranes to North America. Gold-bearing quartz veins in shear zones, faults, and joints, largely within metamorphosed turbidite sequences, have produced about 95% of Alaska's total lode gold. In southeastern Alaska, 3 groups of polymetallic volcanogenic massive sulfide (VMS) deposits are associated with felsic through mafic volcanic units. Both productive Besshi-type and nonproductive Cyprus-type Fe-Cu-Zn VMS deposits form an arcuate belt through Prince William Sound in south-central Alaska. Further north, the Kennecott copper ore bodies are localized in the dolomitic sabkha facies of the Chitistone Limestone. Mesozoic porphyry Mo and Cu mineralization is generally widespread but subeconomic within calc-alkaline subduction-related plutons; however, the Tertiary, rift-related Quartz Hill stock may be the world's largest known porphyry Mo deposit. Calcic Fe-Cu-Au-rich skarns, developed during preaccretionary island-arc magmatism, occur throughout much of the Pacific Border Ranges. Important Fe, Ti, Cu, Ni, Co, and (or) Cr resources are associated with the Border Ranges ultramafic-mafic complex, the Klukwan-Duke belt of zoned ultramafics, and the gabbros and norites within the Fairweather-Baranof belt of layered mafic-ultramafic intrusions. This diversity of mineral deposits reflects the long and complex pre-, syn-, and post-accretionary history of the Pacific Border Ranges and Coast Mountains.

INTRODUCTION

THE SOUTHERN Alaskan Cordillera, consisting of the Pacific Border Ranges, Coastal Trough, and Coast Mountains physiographic provinces (Wahrhaftig, 1965), contain many of Alaska's most significant mineral deposits. The complex tectonic history of this region rimming the Gulf of Alaska has led to the formation of economically significant gold vein, molybdenum porphyry, and copper and polymetallic volcanogenic massive sulfide ore bodies. Distal island-arc magmatism and oceanic ridge volcanism, subduction and(or) accretion of allochthonous terranes, regional uplift and magmatic-arc plutonism, and finally transcurrent movement in southeastern Alaska, have all combined to produce a relatively high concentration of many metals in this portion of the crust.

The portion of the northern Cordillera described in this report contains Alaska's three largest lode gold producers (AJ-Treadwell, Chichagof, and Willow Creek), two largest copper producers (Kennecott and Beatson), and the only past barite (Castle Island), chromium (Red Mountain), and uranium (Bokan Mountain) producers. Within the last 25 years, possibly the world's largest known molybdenum porphyry system (Quartz Hill), one of the United States' largest nickel resources (Brady Glacier), and a major stratiform polymetallic volcanogenic massive sulfide deposit (Greens Creek) have been discovered in southeastern Alaska. Recent advances in the understanding of accretionary tectonics, and the application of those concepts to the geological evolution of south-central and southeastern Alaska (Jones et al., 1981; Coney and Jones, 1985), have led to a new understanding of the genesis of many of the mineral deposits. Many of these relatively new ideas that relate environment of formation of mineral deposits to tectonic settings are summarized throughout this paper, and are currently being applied to exploration for metals in the southern Alaskan Cordillera.

REGIONAL GEOLOGY AND TECTONICS

The south-central (Fig. 1) and southeastern (Fig. 2) coastal regions of Alaska consist of all or parts of at least eleven reportedly fault-bounded tectonostratigraphic terranes (Silberling and Jones, 1984), most of which were accreted to the North American craton since mid-Cretaceous time. Many of the boundaries between terranes are crustal sutures (Coney et al., 1980), reactivated in mid-Tertiary time by transcurrent motion within southeastern Alaska. The terranes consist of thick sequences of turbidite flysch, fragments of oceanic crust, oceanic arcs, rift-related mafic bodies, and slices of distal continental margins. Major thrusting played a dominant role during the various accretionary episodes (Coney et al., 1980). Regional metamorphism, usually defining a Barrovian metamorphic field gradient, has converted many of the pelitic sequences to greenschist and amphibolite facies. Subsequent to accretion, Late Cretaceous through mid-Tertiary plutonism was widespread within the tectonically deformed rocks.

Stikinia is the innermost of the accreted terranes within the southern Alaskan Cordillera. It includes Mississippian to Per-

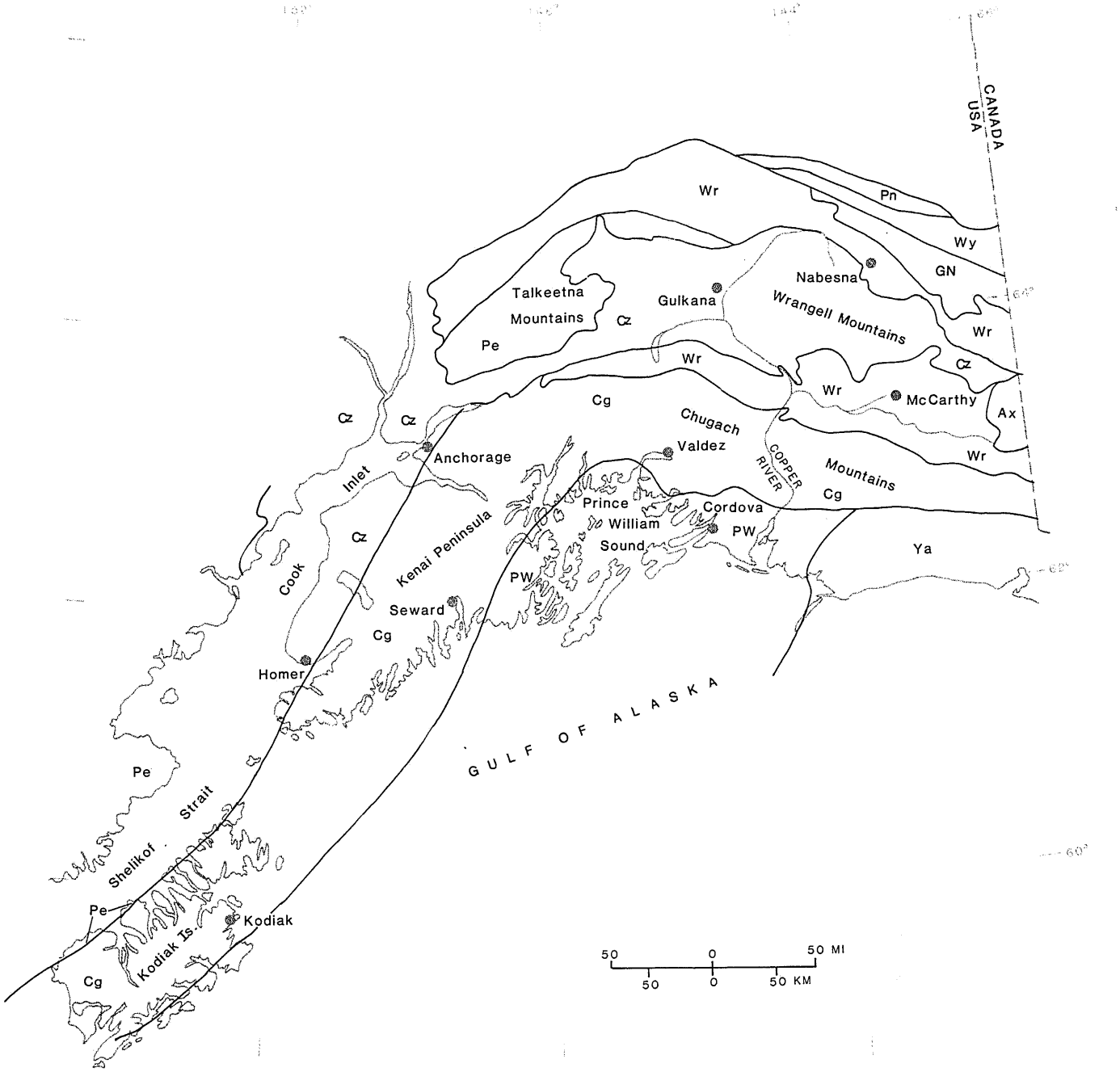

Fig. 1. Generalized tectonostratigraphic terrane map of south-central Alaska. Terranes as follows: Ax-Alexander, Cg-Chugach, Cz-Cenozoic cover, GN-Gravina-Nutzotin, Pe-Peninsular, Pn-Pingston, PW-Prince William, Wr-Wrangellia, Wy-Windy, Ya-Yakutat. Generalized from Silberling and Jones (1984).

mian bimodal volcanic rocks and carbonates and Lower Mesozoic carbonates in British Columbia, and Lower Jurassic granodiorite in southeastern Alaska. Stikinia was amalgamated with the Quesnellia, Eastern, and Cache Creek terranes by Late Triassic-Early Jurassic time and was then accreted to the craton in the Jurassic as composite terrane I of Monger et al. (1982).

Greater Wrangellia (Coney and Jones, 1985), or composite terrane II (Monger et al., 1982), was accreted to Stikinia in southeastern Alaska and the Yukon-Tanana region of south-central Alaska by mid-Cretaceous (Hillhouse and Gromme, 1984) or earliest Tertiary time (Panuska, 1985). This superterrane, with northward translations exceeding 3000 km (Hillhouse and Gromme, 1984), formed by pre-accretionary amalgamation of the Wrangellia, Peninsular, and Alexander terranes. The Peninsular terrane of south-central Alaska is dominantly composed of Triassic bedded rocks and Lower Jurassic plutons. Mid-Jurassic and younger sedimentary rocks link the Peninsular terrane with Wrangellia. Upper Paleozoic submarine arc complexes and overlying bedded rocks and the lower Mesozoic basalts and bedded rocks of Wrangellia extend throughout south-

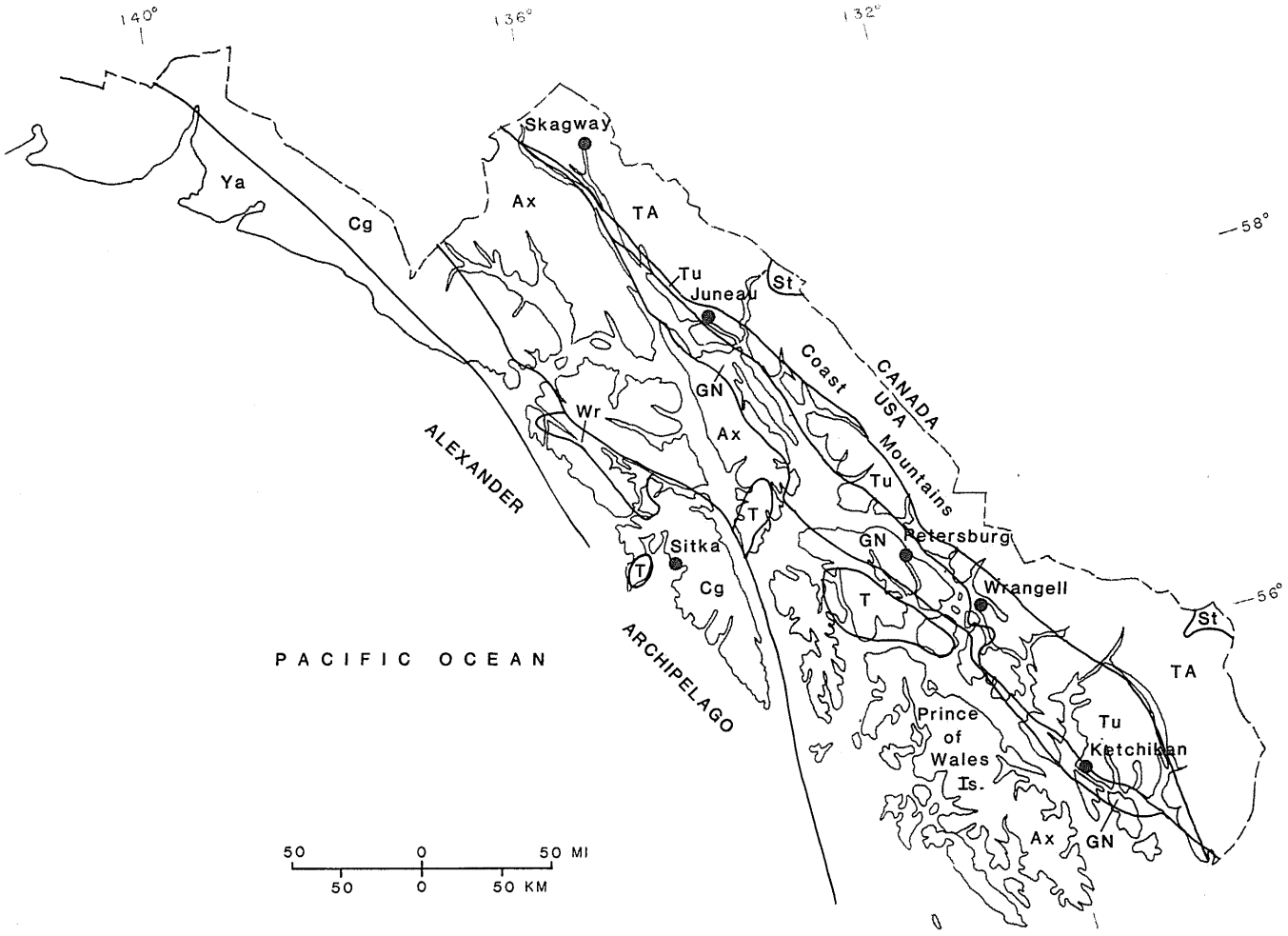

Fig. 2. Generalized tectonostratigraphic terrane map of southeastern Alaska. Terranes as follows: Ax-Alexander, Cg-Chugach, GN-Gravina-Nutzotin, St-Stikinia, T-Tertiary cover, TA-Tracy Arm, Tu-Taku, Wr-Wrangellia, Ya-Yakutat. Generalized from Silberling and Jones (1984).

ern Alaska. The Upper Jurassic to mid-Cretaceous flysch and subordinate submarine volcanic rocks of the Gravina-Nutzotin belt link Wrangellia to the Alexander terrane in southeastern Alaska. The Alexander terrane is composed of Precambrian(?) through Paleozoic volcanic and bedded rocks and Mesozoic volcanosedimentary units.

The Taku and Tracy Arm terranes are believed by many workers to lie between Stikinia and Greater Wrangellia within southeastern Alaska. The Taku terrane mainly consists of Upper Jurassic to mid-Cretaceous flysch that filled the suture zone between the two larger composite terranes (Berg et al., 1978). Brew and Ford (1985), on the other hand, believe that the Taku terrane may instead be a metamorphosed section of the Alexander terrane. Crawford and Crawford (1986) report the suture between Greater Wrangellia and Taku to be a thrust fault.

The similarly problematic Tracy Arm terrane, of schist and paragneiss between Stikinia and the Taku terrane, may represent a discrete tectonostratigraphic packet or just the deeper crustal levels of Stikinia (Coney and Jones, 1985). Brew and Ford (1985) argue instead that the Tracy Arm terrane may be part of the Alexander terrane and not a discrete tectonostratigraphic assemblage. The Cretaceous through Eocene Coast Range batholith, intruding the Tracy Arm terrane and forming a continental margin or Andean-type magmatic arc (Barker and Arth, 1984), consists of orthogneiss and plutonic rocks separated in some places from the Taku terrane to the west by a vertical shear zone (Crawford and Crawford, 1986). Brew and Ford (1984) have termed these granitic and gneissic rocks, as well as adjacent metamorphic units, the northern Coast plutonic-metamorphic complex.

The Upper Jurassic-Lower Cretaceous melange and Upper Cretaceous flysch plus lesser pillow basalt of the Chugach terrane are thrust below Greater Wrangellia, and form the most seaward terrane in southeastern Alaska. This largely well-preserved, trenchfill turbidite sequence was accreted onto the southern Alaska continental margin by the end of the Cretaceous (Plafker et al., 1977) or by the early Tertiary (Tysdal and Case, 1979). The Paleocene-Eocene deep sea fan deposits, pelagic sediments, and pillow basalts of the Prince William terrane (Plafker et al., 1977), and the Mesozoic flysch and melange and Cenozoic sediments of the Yakutat terrane (Bruns, 1985) have been thrust below the south-central Alaskan margin, respectively, during Paleogene and Neogene time.

Table 1. Major gold districts within the southern Alaskan Cordillera

District	Major Gold Mines	Estimated Total Production (oz Au)	Associated Metals[1]	Host Terrane	Host Lithology	References
Admiralty Island	Funter Bay, Hawk Inlet	>10-15,000	py, po, sl, gn, cp, spec hem	Gravina-Nutzotin	schists and phyllites; especially associated with black graphitic layers; aplite dike forms part of footwall at Funter Bay mine	Buddington (1926)
Berners Bay	Jualin, Comet, Kensington, Ivanhoe, Northern Belle, Bear Creek, Horrible	>75,000	py ±, cp, sl, gn	Taku	Jualin diorite	Knopf (1911)
Chichagof	Chichagoff, Hirst-Chichagof, Apex, El Nido	800,000	py, aspy ± cp, sl, gn, tt; sch (at El Nido)	Chugach, Wrangellia	graphitic units within graywacke at Chichagoff and Hirst-Chichagof; felsic dike forms footwall of main H-C vein; diorite or amphibolite within diorite at Apex and El Nido	Reed and Coats (1941); Rossman (1959b)
Dolomi Bay	Golden Fleece, Valparaiso	a few thousand	tt, gn, sl, py, cp	Alexander	marble	Herreid (1967)
Eagle River	Eagle River	23,000	aspy ± py, po, gn, sl	Gravina-Nutzotin	slate and graywacke	Knopf (1912)
Endicott Peninsula	Sumdum Chief, Holkham Bay, Windham Bay	25,000 (plus 2,000 placer Au)	gn, sl	Taku	schist, phyllite, and graphitic limestone	Buddington (1925); Brew et al (1977)
Girdwood	Monarch, Jewel	5,000 (plus 42,500 placer Au)	aspy, py, mar, sl, gn, cp, mo	Chugach	argillite, graywacke, and felsic dikes	Park (1933)
Helm Bay (Ketchikan)	Gold Standard, Gold Mountain, Melville, Rainy Day, Keystone, Old Glory, Goldstream	>1,000	py, cp, sl, gn, ± aspy	Gravina-Nutzotin, Taku	schist, slate, and felsic dikes	Wright and Wright (1908)
Hollis	Crackerjack, Dawson, Harris River, Puyallup, Cascade	10,000	py, cp, gn, sl ± tt, aspy	Alexander	black slates and argillites within graywacke sequence; some veins within felsic dikes	Twenhofel et al (1949); Herreid and Rose (1966)
Hyder (Portland Canal)	Riverside; Silbak Premier and Big Missouri in British Columbia	2,450 (plus 1.9 million ounces of Au from Canadian mines)	gn, py, sch, cp, bar, sl, po, tt	Stikinia	granodiorite and schist roof pendants	Thorne et al (1948); Byers and Sainsbury (1956)

Table 1. Major gold districts within the southern Alaskan Cordillera (continued)

District	Major Gold Mines	Estimated Total Production (oz Au)	Associated Metals[1]	Host Terrane	Host Lithology	References
Juneau	Alaska-Juneau (AJ), Treadwell, Silver Queen	6,800,000 (plus 66,000 placer Au)	po, gn, sl, aspy, py	Taku, Gravina-Nutzotin	slate and diorite sill	Spencer (1906); Wayland (1939); Twenhofel (1952)
Moose Pass-Hope-Sunrise	Hirshey-Lucky Strike, Primrose, Gilpatrick, Crown Point	40,000 (plus 90,000 placer Au)	aspy ± gn, sl, cp, py, po ± sb	Chugach	slate, graywacke, and felsic dikes	Tuck (1933); Mitchell (1979)
Nuka Bay	Nukalaska, Golden Horn, Beauty Bay, Sonny Fox	6,000	aspy ± cp, py, gn, sl	Chugach	graywacke and felsic dikes; often associated with graphitic layers in graywacke	Richter (1970)
Nizina	Dan and Chititu Creek placers	143,500 placer Au only	cp, sb, gn	Wrangellia	from drainages underlain by felsic-intermediate plutons and clastic sediments both hosting small quartz veins carrying gold and sulfides	Cobb (1973); MacKevett (1976)
Porcupine Creek	Porcupine, Glacier and Nugget Creek placers	>30,000 placer Au only	gn, mt, cp, py, aspy	Alexander	from drainages underlain by phyllite, slate, marble, and diorites cut by quartz stringers containing gold and sulfides	Cobb (1973)
Port Valdez	Cliff, Ramsey-Rutherford, Gold King, Big Four	62,000	py, gn, cp, aspy, sl, po, sb	Chugach	graywacke, slate, and quartz diorite	Brooks (1912); Johnson (1915); Pickthorn (1982)
Port Wells	Granite, Mineral King, Portage Bay	28,000	py, gn, sl, aspy, sb, cp ± tt	Chugach	graywacke, slate, argillite, and tonalite	Johnson (1914); Stuwe (1984)
Reid Inlet	LeRoy, Rainbow, Sentinel, Monarch #1 and #2, Incas	7-8,000	aspy, py, gn, sl, cp	Alexander	pelite, marble, greenstone, amphibolite, granodiorite, quartz diorite	Twenhofel et al (1949); Rossman (1959a); MacKevett et al (1971); Brew et al (1978)
Snettisham	Crystal, Friday	>2,000	py, mt	Taku	amphibolite and slate	Berg (1984)
Willow Creek	Gold Cord, Independence, Fern, Lonesome, Snowbird	448,000 (plus 204,000 placer Au)	aspy, py ± gn, sl, tt, cp, sch, tl	Peninsular	quartz and diorite	Ray (1933); Ray (1954); Silberman et al (1978b)

[1]aspy = arsenopyrite, bar = barite, cp = chalcopyrite, gn = galena, mar = marcasite, mo = molybdenite, mt = magnetite, po = pyrrhotite, py = pyrite, sb = stibnite, sch = scheelite, sl = sphalerite, spec hem = specular hematite, tl = tellurides, and tt = tetrahedrite.

GOLD DEPOSITS

Approximately 95 percent of Alaska's lode gold production has come from the Pacific Border Ranges and Coast Mountains within the south-central (Fig. 3) and southeastern (Fig. 4) portions of the state. Total lode gold production from these areas is between 8.2 and 8.5 million ounces, with associated placer occurrences responsible for about an additional 600,000 ounces. Most of the lode production has come from Alaska's three largest gold districts: Juneau (6.8 million ounces) along the western flank of the Coast Mountains, Chichagof (800,000 ounces) within the Alexander Archipelago of southeastern Alaska, and Willow Creek (448,000 ounces) along the southern edge of the Talkeetna Mountains northeast of Anchorage. However, smaller, gold-bearing, quartz-filled fissures and shear zones are widespread throughout the uplifted southern Alaska Cordillera. Most of the gold systems described in Table 1, with the possible exception of Willow Creek, exhibit similar characteristics.

The gold-bearing quartz veins of the southern Alaska Cordillera are structurally controlled by shear and tensile fractures believed to have been generated during periods of regional uplift (Goldfarb et al., 1987). Gold-bearing quartz veins generally cross-cut the metamorphic foliation and therefore postdate the regional Barrovian metamorphism of the accreted terranes. Characteristic wallrock ribbons within the veins at many deposits indicate repeated episodes of syntectonic dilation. An exception might be the world-class Alaska-Juneau deposit (Juneau district), where a dense and unique array of thousands of irregularly spaced, discontinuous, massive quartz veins yielded 3.5 million ounces of gold from ore averaging less than 0.1 oz. gold per ton (Light et al., 1987).

Although many of the gold-bearing quartz veins are hosted by metagraywacke-slate turbidite sequences, they are often found in close spatial association with dikes, sills, or small stocks ranging in composition from diorite to granite. The mines at Berners Bay, the El Nido mine in the Chichagof district, the Riverside mine in the Hyder district, and the Rough and Tough mine in the Port Valdez district are hosted by small stocks. More commonly, quartz or quartz-carbonate veining occurs within thin sills or dikes, or along the contacts between these intrusives and the metasedimentary country rocks.

The Treadwell deposit in the Juneau district produced over 3 million ounces of gold and is virtually confined to a diorite sill that lies along the contact between black slate and greenstone (Spencer, 1905). Most of the gold in the Treadwell system occurs in calcite and quartz stringers and veinlets that cut the 3 km long sill. Mineralized dikes also occur in the Helm Bay, Hollis, Hope-Sunrise, Moose Pass, and Nuka Bay districts. Veinlets occur in the fractured and brecciated portions of the igneous bodies, and rarely extend out into the less brittle and less fractured metasedimentary rocks. Commonly the mineralized dikes contain abundant disseminated arsenopyrite, extending beyond the zones of visible silicification. Dikes or sills make up part or all of the hanging wall or footwall of gold-bearing veins within some mines in the Admiralty Island, Chichagof, Girdwood, Hollis, Moose Pass, Nuka Bay, and Port Wells districts.

In many cases both the gold-bearing quartz veins and the adjacent dikes or sills appear to follow the same pre-existing faults or bedding contacts. Hollister and Crawford (1986) suggest that deformation within convergent tectonic blocks, including the propagation of major shear zones, is focused along zones of anatectic and/or mantle-derived melts. These shear zones then may later serve as the main fluid conduits for gold-bearing quartz vein formation. This might help to explain the common spatial association between the veins and dikes.

Pyrite, pyrrhotite, or arsenopyrite are the most abundant sulfide minerals within the gold-bearing quartz veins; sphalerite, galena, and chalcopyrite are also abundant. Traces of scheelite, stibnite, and tetrahedrite are not uncommon, and tungsten production from scheelite-rich quartz veins occurred at the Riverside mine (Hyder district) and El Nido mine (Chichagof district). Sulfide minerals rarely comprise more than 1 to 3 percent of the vein material, but massive arsenopyrite or galena and sphalerite occur in some of the veins. Gold occurs either as small, wiry segregations in the vein quartz, as blebs or veinlets within the sulfides, or concentrated along carbonaceous ribbon structures.

Wallrock alteration halos extend up to several meters beyond most of the gold-bearing quartz veins. Alteration is much more intense in igneous- and metavolcanic-hosted deposits than in metasedimentary-hosted systems, reflecting greater fluid-rock disequilibrium in the former. Evidence for sulfidization, silicification, and carbonatization is usually visible in outcrop, with an abundance of quartz stringers, pyrite, arsenopyrite, calcite, dolomite, and ankerite gradually decreasing away from the veins. Some degree of albitization, biotitization, and sericitization is commonly seen in thin sections adjacent to many veins and alteration of Fe-Mg silicates to epidote and chlorite often defines the outermost portions of the halos.

Fluid inclusion studies have been used to determine the nature of the ore fluids and the environment of ore deposition in the Hope-Sunrise, Moose Pass, Port Wells, and Port Valdez districts of south-central Alaska (Goldfarb et al., 1987), and in the Juneau (Goldfarb et al., 1986; Leach et al., this volume) and Chichagof districts of southeastern Alaska. Gold-bearing quartz veins within the south-central districts contained small (<5 microns), liquid-dominant, low salinity (<5 equivalent wt. percent NaCl) fluid inclusions adjacent to gold and sulfide grains. Uncorrected homogenization temperatures generally ranged from 210°C to 280°C with minimum estimated trapping depths of 3.5 km to 5 km. Microthermometry indicated a CO_2-N_2-CH_4 volatile phase of approximately 10 mole percent, trapped within a one-phase field. Preliminary fluid inclusion work on samples from the Chichagoff mine (Chichagof district) indicates similar gas contents of ore-related fluid inclusions, with slightly lower homogenization temperatures of 190°C to 220°C.

Fluid inclusion studies at the Alaska-Juneau deposit (Juneau district) show that ore-forming fluids may also be defined by a H_2O-CO_2-CH_4-N_2-NaCl system (Leach et al., this volume). But, whereas the volatile components within both the previously discussed veins and the Alaska-Juneau lodes are similar, other fluid inclusion characteristics are markedly different. The Alaska-Juneau gold-bearing quartz contains relatively large fluid inclusions (up to 50 microns), a relatively low density of secondary inclusions trapped along healed fracture planes, conclusive evidence of heterogeneous trapping of immiscible fluids, and an extremely high bulk CO_2/H_2O ratio. Despite the similar fluid components and minimum trapping temperatures (230°C)

and depths (5.5 km), the other unique fluid inclusion features indicate that the Alaska-Juneau deposit, and perhaps the entire Juneau district, reflect a spectacular and more extensive fluid flow regime within the southern Alaska Cordillera. Leach et al. (this volume) suggest the possible tapping of a deeper, more CO_2-rich reservoir in the Juneau region relative to the other gold-quartz lodes of southern Alaska.

Most of the gold districts within the Pacific Border Ranges and Coast Mountains are hosted in prehnite-pumpellyite through amphibolite facies metamorphic rocks. Oxygen isotope data from gold-bearing quartz from districts within the Chugach terrane show a range in $\delta^{18}O$ values from +13.9 per mil to +17.0 per mil (Pickthorn et al., 1985; Goldfarb et al., 1987) and those from the further inboard Alaska-Juneau system range from +17.1 per mil to +18.1 per mil (Light et al., 1987). Calculated $\delta^{18}O$ for vein-forming fluids coincide with both the magmatic and metamorphic water compositional fields of Taylor (1979). If some of the igneous activity in and near known gold districts is anatectic in origin, little chemical or isotopic differences are expected between the two fluids produced during plutonism and regional metamorphism.

Fluid inclusion waters from quartz veins from many of the southern Alaska gold systems, upon initial crushings, yield isotopically light fluids with δD values between −120 per mil to −110 per mil. Continued crushing of the gold-bearing quartz produces continually heavier fluids, leveling off at −80 per mil to −60 per mil (Goldfarb et al., 1987), values that still may reflect contamination from secondary fluid inclusions unrelated to the ore-forming fluids. Hydrogen isotope analysis of hydrothermal micas adjacent to gold-bearing quartz veins in the Port Valdez district and the Alaska-Juneau deposit indicate ore-forming solutions with δD values of −12 per mil and −20 per mil, respectively (Pickthorn et al., 1987). These relatively heavy δD values are believed to be representative of the gold-bearing solutions and support either a deep-seated magmatic fluid or fluids produced during prograde metamorphic reactions associated with tectonic underplating.

The Willow Creek district, in the Peninsular terrane along the southern margin of the Talkeetna Mountains batholith, ranked third in lode gold production in Alaska. Gold-bearing veins occur within shear zones in quartz diorite, and intense sericitization, chloritization, silicification, carbonatization, and sulfidization occur within 0.5 m of most veins. Metallic minerals in gold-bearing quartz veins include pyrite, arsenopyrite, sphalerite, chalcopyrite, galena, tetrahedrite, scheelite, and tellurides. The latter are commonly intergrown with gold grains (Ray, 1954).

A number of features distinguish the Willow Creek district from the other gold systems of southern Alaska. Tellurides are unique to Willow Creek; there is little documentation of tellurides in other gold districts. The abundant chalcopyrite-molybdenite-bearing quartz veins, as well as sericitic and propylitic alteration in the quartz diorite and the presence of pegmatite dikes, led Silberman and O'Leary (1976) to suggest that the gold-bearing quartz veins could represent an upper level system peripheral to a porphyry system. However, Silberman et al. (1978b) point out that K-Ar dates from muscovite gave ages roughly 20 million years younger than emplacement of the main intrusive mass and its relationship to a porphyry system is thus uncertain.

The districts in Table 1, with the possible exception of Willow Creek, show many similar geochemical and geological characteristics. The characteristics also closely resemble those of the Mother Lode-type gold vein systems in the Canadian Cordillera further to the south (Murowchick et al., 1985; Nesbitt et al., 1985). However, there are two obvious differences: the Canadian gold lodes commonly contain tellurides and they are almost always associated with serpentinite. Additional isotopic data and fluid inclusion study is necessary to assess the significance of these differences.

VOLCANOGENIC MASSIVE SULFIDE DEPOSITS

Volcanogenic massive sulfide (VMS) deposits in south-central Alaska largely form an arcuate belt hosted by flyschoid strata of the Late Cretaceous Valdez Group and Early Tertiary Orca Group in Prince William Sound. These occurrences can be classified as both Cyprus-type and Besshi-type; only the latter has been productive. VMS deposits in southeastern Alaska, hosted by Precambrian(?) through Mesozoic metasedimentary and metavolcanic rocks, include some almost certainly of Kuroko-type and others that have been too deformed, disrupted, or metamorphosed to accurately classify. The VMS bodies throughout the entire southern Alaska Cordillera (Table 2) contain significant gold and silver. These metals, along with silica, have been locally remobilized into shear zones and breccia pipes during post-accretionary metamorphism.

Fe-Cu occurrences at Rua Cove on Knight Island in Prince William Sound are the most significant Cyprus-type bodies known in south-central Alaska. These tabular pyrrhotite- and chalcopyrite-rich deposits occur in tholeiitic ophiolite sequences, most probably formed at an oceanic spreading center near a continental margin. Complete alteration of volcanic wallrock to chlorite-talc-quartz occurs within the feeder zones (Koski et al., 1985). Low tonnage of massive Cu ore has discouraged development of these Fe-Cu bodies.

Almost 100,000 metric tons of Cu, in addition to significant Au and Ag, have been produced from the turbidite-hosted massive sulfide mines within the Prince William Sound region. The Beatson mine on LaTouche Island was Alaska's second largest copper producer and also yielded approximately 1.5 million oz of Ag. Dominant sulfide minerals within the sediment-hosted occurrences consist of pyrrhotite, pyrite, chalcopyrite, sphalerite and occasional galena. Gold and silver are free or are within a sulfide phase, probably pyrite. These deposits may represent distal portions of the mineralized ophiolite sequences within Prince William Sound. The Beatson mine is stratigraphically adjacent to the Knight Island ophiolite sequence, and the Ellamar, Midas, and Schlosser mines are spatially related to thick sequences of pillow basalt. If these are classified as Besshi-type deposits, as indicated by most of their characteristics, they may be the only Tertiary examples known of such type. However, their probable origin within an extensional tectonic setting contrasts with the more commonly observed island arc origin for this type of VMS.

Numerous massive sulfide lenses and layers within interbedded volcanic and sedimentary units occur throughout the Alexander terrane. Most of these loosely form a Permian-Triassic volcanogenic Ag-Au-Cu-Pb-Zn-rich belt of deposits stretching the

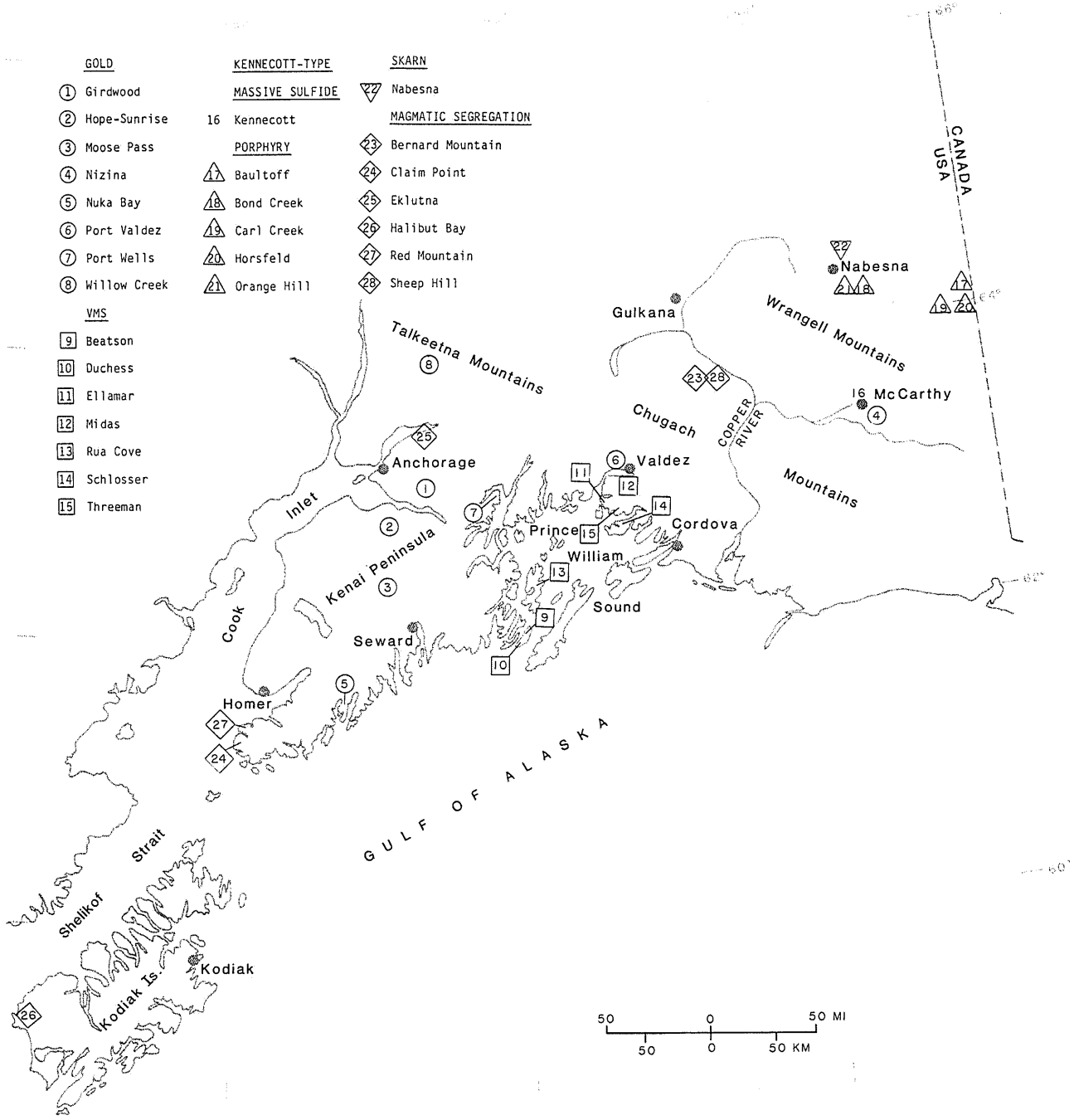

Fig. 3. Distribution of mineral deposits within south-central Alaska.

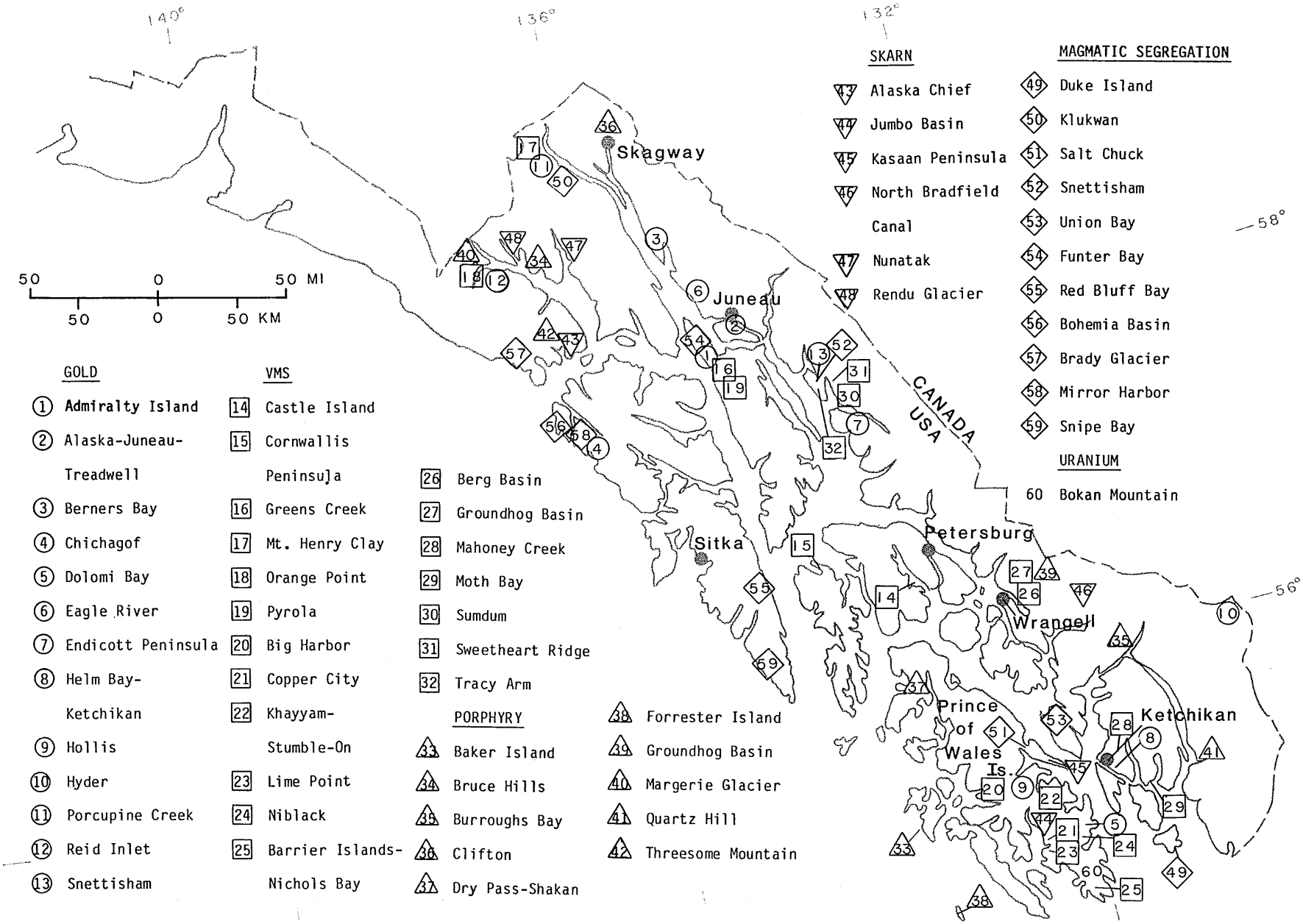

Fig. 4. Distribution of mineral deposits within southeastern Alaska.

Table 2. Volcanogenic massive sulfide deposits within the southern Alaskan Cordillera

Terrane	Age	Deposit	Mineralogy	Reserves	Past Production	Host Lithology	Alteration	References
Alexander	Permian-Triassic	Greens Creek	sl-gn-Ag-Au ± bar, cp, py, po	3.5-4 m.t. of 6.4% Zn, 2.1% Pb, 10.3 oz/t Ag, .09 oz/t Au	--	between felsic tuff and carbonaceous shale	--	Dressler and Dunbire (1981); Eakins et al (1985)
		Orange Point	py-po-sl-cp ± Ag, Au, bar, gn	.27 m.t. of 2.7% Cu, 5.2% Zn, .03 oz/t Au, 1 oz/t Ag; .53 m.t. of .4% Cu, .3% Zn, .006 oz/t Au, .35 oz/t Ag	--	andesite flow and tuff	--	Brew et al (1978)
		Mt. Henry Clay area (Glacier Creek, Jarvis Glacier)	sl-py-cp-gn-bar ± Ag, Au	.75 m.t. of 60% barite, 1.7% Zn, 60 ppm Ag at Glacier Creek	--	andesite, slate, and limestone; capped by unmineralized pillow basalt	chloritic	Still (1984a); MacIntyre (1986)
		Pyrola	py-sl-gn-bar ± Ag, Au	--	--	at contact between tholeiitic volcanics, and fine-grained clastics and carbonates	chlorite-carbonate-epidote-albite overprinted by sericite-quartz-talc	Van Nieuwenhuyse (1984)
		Castle Island	bar ± py, sl, gn, mar, cp, bn, tt	--	850,000 tons of 90% barite	basalt, metarhyolite, and phyllite	--	Berg and Grybeck (1980); Eakins et al (1985)
		Cornwallis Peninsula	bar-sl ± Cu, Pb, Ag	--	--	felsic volcanics and carbonaceous limestone	--	Twenhofel et al (1949); Eakins et al (1985)
Alexander	pre-Mid Ordovician	Niblack	py-cp-sl ± gn, cc, cov, Ag, Au	--	1.95 million lbs Cu 1,341 oz Au, and 20,687 oz Ag from ore averaging 3.2% Cu, .68 oz/t Ag, and .044 oz/t Au	rhyolite to dacite siliceous tuffs	--	Peek (1975)
		Khayyam and Stumble-On	py-cp-sl-po-mt ± po, Au, Ag	--	7.05 million lbs Cu, 1,290 oz Au, and 1,711 oz Ag from ore averaging 1.7% Cu, .06 oz/t Au and .3 oz/t Ag at Khayyam	mafic and felsic volcanic rocks, and chemical sediments	chloritic; Na enrichment and K depletion of wallrocks	Barrie (1984)

Table 2. Volcanogenic massive sulfide deposits within the southern Alaskan Cordillera (continued)

Terrane	Age	Deposit	Mineralogy	Reserves	Past Production	Host Lithology	Alteration	References
		Lime Point	bar	5,000 tons 91% barite	--	limestone	--	Twenhofel et al (1949)
		Big Harbor	cp-py ± sl, Au, Ag	--	minor Cu	schist	--	Twenhofel et al (1949)
		Copper City	cp-py-sl ± Au, Ag	--	minor Zn, Ag, Au	slate and schist	--	Wright and Wright (1908); Berg (1984)
Alexander	Ordovician-Silurian	Barrier Islands-Nichols Bay	py ± sl, gn, aspy, Ag, Au	--	--	silicic to intermediate volcanic rocks and graywacke		Gehrels et al (1983)
Taku	Permian-Triassic	Moth Bay	py-po-sl-cp ± bn, cov, mt, gn, Ag, Au	100,000 tons of 7.5% Zr and 1% Cu	--	schist and quartzite roof pendant	--	Robinson and Twenhofel (1953)
		Groundhog Basin	po-sl ± gn, py, cp, mt, Ag	240,000 tons of 8% Zn, 1.5% Pb, and 1.5 oz/t Ag	--	metasediments	--	Gault et al (1953)
		Sweetheart Ridge	py±cp-sl	--	--	schist	--	Stowell (1981)
		Sumdum	py-po-cp-sl ± bn, cc, mal, az, gn, hm, Au	26.7 m.t. of .6% Cu, .4% Zn, and .3 oz/t Ag	--	gneiss	--	USGS and USBM (1984); MacKevett and Blake (1964)
		Tracy Arm	py-po ± cp, sl, mt, Ag, Au	187,000 tons of 3.4% Zn, 1.4% Cu, .4 oz/t Ag, and .008 oz/t Au	--	phyllite and schist	--	Gault and Fellows (1953); USGS and USBM (1977)
Prince William	Tertiary	Beatson	py-cp-po ± sl, Ag, Au	--	91,300 tons from 1.65% Cu, plus 1,467,000 oz of Ag and unrecorded Au	graywacke	--	Bateman (1924); Jansons et al (1984)
		Ellamar	cp-py-po-sl ± gn, Ag, Au	536,000 tons of 0.6% Cu	7,881 tons from 2.46% Cu, plus 51,305 oz Au and 191,615 oz Ag	slate and graywacke	--	Capps and Johnson (1915); Jansons et al (1984)
		Schlosser	cp-py-po-sl ± Ag, Au	224,000 tons of 3.2% Cu	2,080 tons from 8.70% Cu, plus minor Ag	slate and graywacke	--	Capps and Johnson (1915); Jansons et al (1984)

Table 2. Volcanogenic massive sulfide deposits within the southern Alaskan Cordillera (continued)

Terrane	Age	Deposit	Mineralogy	Reserves	Past Production	Host Lithology	Alteration	References
		Threeman	cp-po-sl-py ± Ag, Au	1.9 m.t. of 1% Cu	580 tons from 8.63% Cu, plus minor Au and Ag	greenstone	--	Capps and Johnson (1915); Jansons et al (1984)
		Rua Cove	py-po-cp-sl	1.3 m.t. of 1.2% Cu	--	pillow basalt	chlorite-talc-quartz	Jansons et al (1984); Koski et al (1985)
		Duchess	py-po-cp	2.7 m.t. of 1.2% Cu	107 tons from 5.8% Cu	slate and graywacke	--	Moffit and Fellows (1950); Jansons et al (1984)
Chugach	Cretaceous	Midas	py-cp-sl-po ± Au, Ag	62,000 tons of 1.6% Cu	1,693 tons from 3.32% Cu, plus 15,157 oz Ag and 2,569 oz Au	graywacke and slate	--	Jansons et al (1984); Moffit and Fellows (1950)

length of southeastern Alaska (Berg and Grybeck, 1980), from Mt. Henry Clay and Orange Point in the north to small occurrences near Ketchikan in the south. Some of the sulfide bodies are intercalated with massive barite and are spatially associated with both rhyolitic and basaltic volcanism, suggesting that they are Kuroko-type deposits. Geologic data suggest that the deposits and their volcanosedimentary host rocks formed in a tensional environment during back arc spreading or strike-slip faulting between 300 and 200 m.y. ago. The only one of these deposits mined to date is on Castle Island, where 850,000 tons of 90% barite were produced between 1963 and 1980 (Eakins et al., 1985).

Greens Creek, on northern Admiralty Island, is the largest high-grade polymetallic VMS known within the Permian-Triassic belt. Estimates of proven and indicated reserves are 3.5 to 4 million tons of ore with 6.4% Zn, 2.1% Pb, 10.3 oz/ton Ag, and 0.09 oz/ton Au (Eakins et al., 1985). The ore is located between a tuffaceous hanging wall and a black carbonaceous clastic footwall in the limb of an overturned anticline. Dressler and Dunbire (1981) described 4 main ore types at Greens Creek; massive, black, white, and vein stockwork. The white ore consists of Fe-Mg carbonates, phyllosilicates, and chert, whereas the black ore represents the final settling out of organic material and sulfides suspended in seawater. They interpret the massive sulfide mounds as having formed over vents and in brine pools.

Alteration assemblages generally have not been documented in association with many of the Permian-Triassic VMS bodies. This may reflect the distal character of many of the ore horizons and thus the general lack of recognition of stratigraphically lower stringer zones and volcanic vents. Van Nieuwenhuyse (1984), however, studying the Pyrola polymetallic deposit just 15 km south of Greens Creek describes in detail the zonal alteration around one of the VMS systems. Pyrola consists of massive pyrite-sphalerite-galena-barite (± chalcopyrite) between mafic volcanic rocks and calcareous clastic sediments. A siliceous stockwork zone is enriched in pyrite and precious metals. Van Nieuwenhuyse reported a large, semi-conformable chlorite-carbonate-epidote-albite halo surrounding the mineralized stockwork. A later sericite-quartz-pyrite alteration assemblage overprints this earlier assemblage in the vicinity of the deposit footwall. Hawley (1976) noted sericite-quartz-talc alteration of pillowed mafic volcanic rocks containing polymetallic sulfide layers at Glacier Creek near Haines.

Polymetallic VMS deposits also occur in the southern Alexander terrane (Gehrels et al., 1983) in the Precambrian(?) Wales Group and in an Ordovician-Silurian volcano-plutonic complex. The Wales Group consists of arc-related mafic through felsic volcanic rocks and chemical and clastic sediments. Between 1901 and 1908, the Khayyam and Niblack polymetallic deposits in the Wales Group on Prince of Wales Island produced the only Cu, Ag, and Au recorded to date from VMS occurrences in southeastern Alaska (Table 2). Pyrite, chalcopyrite, sphalerite, pyrrhotite, and magnetite comprise most of the ore horizons within the Wales Group-hosted bodies; at Lime Point, however, massive barite lies within a limestone lens. Barrie (1984) described strong chloritic alteration, Na enrichment, K depletion, and silicification surrounding the ore at Khayyam. Ordovician-Silurian graywacke and silicic to intermediate volcanic rocks also host VMS deposits on Prince of Wales Island. Known massive sulfide layers are similar to, but generally less extensive than, those hosted by the older Wales Group.

A third group of polymetallic VMS deposits in southeastern Alaska occurs on the mainland south of Juneau and on southern Revillagigedo Island within metasedimentary rocks flanking the Coast Range batholith. Fossiliferous Permian and Triassic slates, phyllites, and marbles are associated with both felsic and mafic volcanic rocks of the tectonically poorly understood Taku terrane. Massive sulfide lenses at Groundhog Basin, Sumdum, Tracy Arm, Sweetheart Ridge, and Moth Bay, believed to have formed in an island-arc environment (Stowell, 1981), are dominated by pyrite, pyrrhotite, chalcopyrite, sphalerite, and(or) magnetite. Precious metals and minor galena are also associated with many of the ore pods. Iron- and Cu-minerals hosted in discordant quartz veins and breccia may indicate some metamorphic remobilization of these VMS occurrences at Sumdum, Mahoney Creek (Robinson and Twenhofel, 1953), and Berg Basin (Gault et al., 1953).

KENNECOTT-TYPE MASSIVE SULFIDE DEPOSITS

The Kennecott sabkha-type copper deposits, on the southern flank of the Wrangell Mountains, have been Alaska's largest producer of copper, yielding 1.2 billion pounds of copper plus 9 million ounces of silver between 1913 and 1938 (MacKevett, 1976). The Kennecott-type ores are the only significant sediment-hosted massive sulfides not directly related to volcanic exhalative activity known in the southern Alaskan Cordillera. The massive, dominantly chalcocite bodies are hosted by the Upper Triassic Chitistone Limestone, generally within 100 m of the underlying tholeiitic Nikolai Greenstone. The greenstone contains an abnormally high background level of Cu (160 ppm) (Armstrong and MacKevett, 1976) and is believed by many workers to be the source of the Kennecott copper.

The Kennecott ore bodies are localized within the more dolomitized and highly fractured portions of the lower part of the Chitistone Limestone. Most of the copper mineralization forms irregular, massive bodies, though copper-rich stockworks and fissure veins also occur. Bateman and McLaughlin (1920) report that the ore averages 92-97% chalcocite, 2-5% covellite, and less than 1% enargite, bornite, chalcopyrite, luzonite, tennantite, pyrite, sphalerite, and galena. They also recognized that the chalcocite and covellite had largely replaced pre-existing bornite.

Armstrong and MacKevett (1977) hypothesize that the initial, bornite-rich ore was deposited by oxygenated groundwater, that leached copper from the Nikolai greenstone and deposited it in an overlying, reducing sabkha environment. Silberman and others (1978a) have suggested that the modification of the copper ores to chalcocite and covellite occurred in late Cenozoic time. Fluid inclusions within calcite intergrown with the chalcocite have yielded pressure-corrected temperatures of about 90°C and have shown average salinities of 15 equivalent wt. percent NaCl (Silberman and others, 1978a). They interpreted this moderately high salt content to represent a significant "non-meteoric component" within the ore remobilizing fluid. A 6.5 million year old hypabyssal rhyolitic porphyry, approximately 2 km south of the main Kennecott deposits, is the most likely source for such a component.

PORPHYRY DEPOSITS

Many intrusive rocks of the southern Alaskan Cordillera contain traces of disseminated molybdenite, but Quartz Hill presently is the only deposit of economic significance. The stockwork deposit is located approximately 70 km southeast of Ketchikan and has been estimated to contain more than 1.5 billion tons of 0.136% molybdenite, with core zones exceeding 0.2% Mo (Bundtzen et al., 1984), making it perhaps the world's largest known porphyry molybdenum deposit. Quartz Hill largely consists of an epizonal to hypabyssal felsic stock, 2 km in outcrop diameter, that intrudes high-grade metamorphic rocks of the Coast plutonic-metamorphic complex (Hudson et al., 1979).

The porphyritic host stock was emplaced in Late Oligocene or Early Miocene time and contains roughly equivalent amounts of quartz, K-feldspar, and albite, with less than 2.5 percent biotite plus other accessory minerals. The Quartz Hill stock is granitic in composition, averaging 74 - 77% SiO_2, 3.6 - 3.8% Na_2O, 4.2 - 4.6% K_2O, and 0.5 - 1.1% CaO. Fluorine concentrations are less than .05% and no fluorite has been identified. Concentrations of B, Pb, Sn, Li, and rare earth elements are all relatively low for a high SiO_2, low Ca granitic system (Hudson et al., 1981).

Hudson et al. (1979) have described the dominantly fracture-controlled alteration and mineralization of the Quartz Hill stock. Development of secondary quartz, pyrite, K-feldspar, biotite, white mica, chlorite, and zeolite characterizes the most intensely altered rocks. They are cut by dense vein and fracture stockworks with molybdenite occurring within the quartz veins and as fracture coatings. Pyrite is disseminated throughout the altered rocks, as well as in adjacent, unaltered porphyritic granite.

As first suggested by Hudson et al. (1979, 1981), the classification of the Quartz Hill deposit is uncertain. Sillitoe (1980) divided the world's major stockwork molybdenum deposits into two types; those hosted by quartz monzonite in subduction-related (compressive) geotectonic settings and those hosted by alkali granite in rift-related environments (Climax-type). Despite the granite host rock at Quartz Hill, many characteristics of the deposit resemble those of the compressive continental margin porphyry types.

Unlike the typical alkali-calcic Climax-type porphyry molybdenum systems (White et al., 1981), Quartz Hill is fluorine deficient and lacks intense silicification and multiple ore shells. The minor element geochemistry at Quartz Hill, reported by Hudson et al. (1981), is very similar to that of many of the major calc-alkaline molybdenum stockwork deposits in adjacent British Columbia (T. Theodore, oral communication, 1986). Theodore and Menzie (1984) report that fluid inclusions at Quartz Hill, and at other fluorine deficient molybdenum deposits, contain about 4 - 16 equivalent weight percent NaCl and 4 - 8 mole percent CO_2. This represents more gas-rich, less-saline fluids than within main stage quartz-molybdenite veins from Climax-type deposits, where salinities may range from 30 - 65 weight percent NaCl equivalent.

In addition to the granitic host for the molybdenite stockworks other aspects of Quartz Hill prevent classification of the deposit within the quartz monzonite category of White et al. (1981) or the plutonic calc-alkaline category of Westra and Keith (1981). For example, topaz reported within a quartz vein at Quartz Hill (Hudson et al., 1979) is more characteristic of Climax-type rather than compressive type porphyries. More significantly, as pointed out by Hudson et al. (1981), the much younger age, the low $^{87}Sr/^{86}Sr$ (0.7049 to 0.7051), and possibly Tertiary

Table 3A. Porphyry molybdenum deposits within the southern Alaskan Cordillera

Occurrence	Porphyritic Host Stock	Ore Body Type	Percent Molybdenum	Tonnage	Age	Associated Ore Minerals[1]	Reported Alteration	References
Quartz Hill	granite	stockwork	.136	>1.5 billion	late Oligocene-early Miocene	py	potassic	Hudson et al (1979, 1981)
Burroughs Bay	granite	stockwork	--	--	late Oligocene-early Miocene	py, mt	potassic	Hudson et al (1981)
Groundhog Basin	granite sill	stockwork	<.05	--	Cretaceous(?)	--	--	Twenhofel et al (1946)
Clifton	granite	disseminated	1	--	--	--	--	Smith (1942)
Forrester Island	quartz monzonite to granodiorite	stockwork	<.07	--	Cretaceous(?)	py, cp, po, mt	pyritization, propylitic	Clark et al (1971)
Threesome Mountain	granodiorite	stockwork	>.02	--	--	sch	--	Berg (1984)
Baker Island	quartz diorite	stockwork	<.10	--	Late Jurassic-Early Cretaceous	py, aspy, po(?)	intense silicification	Twenhofel et al(1946)
Dry Pass-Shakan	diorite	in veinlets and disseminated in brecciated fault zone	1.5	10-20,000	Late Jurassic-Early Cretaceous	py, cp, sl, mt	--	Twenhofel et al (1946); Herreid and Kaufman (1964)

bimodal volcanism indicate that the Quartz Hill stock could not be derived by fractional crystallization of earlier intrusions within the region. It is, therefore, not a part of the calc-alkaline suite of subduction-related magmas associated with other molybdenum deposits in British Columbia. Hudson et al. (1981) believe that the Quartz Hill deposit is a simple initial melt of the lower crust or mantle, or rapidly recycled mantle-derived material, and that the mineralized stock was emplaced during extensional tectonics during or following regional uplift and erosion of the Coast plutonic-metamorphic complex.

A number of other poorly explored, granite-hosted porphyry molybdenum occurrences are known within southeastern Alaska (Table 3A). At Burroughs Bay, approximately 85 km northwest of Quartz Hill, molybdenite-quartz veins and molybdenite-coated fractures occur within a stockwork system hosted by an intrusive similar in age and composition to Quartz Hill (Hudson et al., 1981). Molybdenite stockworks and(or) disseminated blebs occur in a granite sill in Groundhog Basin east of Wrangell (Twenhofel et al., 1946), in a small granite stock at Clifton about 12 km north of Skagway (Smith, 1942), and in granite bodies on a ridge west of Rendu Inlet in Glacier Bay (MacKevett et al., 1971). Geological and geochronological data for these occurrences are rare and prevent assessment of their regional tectonic association.

A few molybdenite occurrences within southeastern Alaska are associated with quartz monzonite plutons most likely derived from subduction-related magmatism. The most significant of these is the Nunatak deposit in Muir Inlet west of Juneau; however the porphyritic stock is essentially barren and most of the molybdenite occurs within adjacent skarn (see next section). Stockwork quartz-pyrite-molybdenite veinlets and disseminated molybdenite and chalcopyrite occur within porphyritic quartz monzonite to granodiorite on Forrester Island, southwest of Craig (Clark et al., 1971). The mineralized stocks are strongly pyritized and propylitized. More mafic granodioritic to dioritic stocks at Threesome Mountain (Berg, 1984), on Baker Island (Twenhofel et al., 1946), and at Dry Pass and Shakan on Kosciusco Island (Twenhofel et al., 1946) host other molybdenum-rich stockworks and disseminations. At Shakan, the greatest molybdenum concentrations are near mafic pegmatite dykes and quartz-adularia veins within a narrow, brecciated fault zone in hornblende diorite. Twenhofel et al. (1946) estimated the fault zone to contain approximately 10,000 to 20,000 tons of mineralization averaging 1.5% molybdenum.

Porphyry copper deposits within the southeast Alaskan Cordillera are relatively small and mainly hosted by quartz monzonite, granodiorite and diorite bodies (Table 3B). The Margerie Glacier prospect near Skagway is probably the most significant of these copper occurrences. It is hosted within a Tertiary porphyritic quartz monzonite stock intruding Permian (?) volcanic and sedimentary rocks. Chalcopyrite occurs in quartz stockworks and as disseminated crystals along with pyrite, pyrrohotite, scheelite and powellite. Within the mineralized zones, plagioclase is partly altered to sericite and K-feldspar and biotite is chloritized. Inferred resources at the prospect consist of 160 metric tons of mineralization containing 0.2% Cu, 0.008 oz Au/ton, 0.013 oz Ag/ton, and 0.01% W (Brew et al., 1978). Chalcopyrite, along with molybdenite and pyrite, also occurs in shear zones,

Table 3B. Porphyry copper deposits within the southern Alaskan Cordillera

Occurrence	Porphyritic Host Stock	Ore Body Type	Percent Copper	Tonnage	Age	Associated Ore Minerals[1]	Reported Alteration	References
Margerie Glacier	quartz monzonite	stockwork and disseminated	.20	160 million	Tertiary	py, po, pw, sch	sericitization, propylitic	Brew et al (1978)
Bruce Hills	granodiorite to quartz diorite	stockworks, shear zones, disseminated	.30	--	--	py, po, mo, hem, gn, sl	potassic, propylitic	MacKevett et al (1971); Brew et al (1978)
Orange Hill	quartz diorite	stockwork	.35	320 million	Cretaceous	mo	potassic-phyllic-argillic-propylitic	Richter et al (1975); Hollister et al (1975); Linn (1973)
Bond Creek	granodiorite	stockwork	.30	500 million	Cretaceous	mo	potassic-phyllic-argillic-propylitic	Richter et al (1975); Hollister et al (1975)
Baultoff	diorite	stockwork	.20	160 million	Cretaceous	--	potassic-propylitic	Richter et al (1975); Hollister et al (1975)
Horsfeld	quartz monzonite	breccia	.20	60 million	Cretaceous	--	argillic-propylitic	Richter et al (1975); Hollister et al (1975)
Carl Creek	quartz monzonite	stockwork	.20	16 million	Cretaceous	--	--	Richter et al (1975); Hollister et al (1975)

[1]aspy = arsenopyrite, cp = chalcopyrite, gn = galena, hem = hematite, mo = molybdenite, mt = magnetite, po = pyrrhotite, pw = powellite, py = pyrite, sl = sphalerite, sch = scheelite

stockworks, and as disseminations in granodiorite and quartz diorite within the Bruce Hills of northern Glacier Bay.

A number of porphyry copper deposits occur near Nabesna on the north side of the Wrangell Mountains in south-central Alaska. Richter et al. (1975) identified 8 porphyry copper deposits hosted by Cretaceous quartz monzonite through diorite stocks. Cumulative indicated and inferred resources for the 8 deposits are roughly 1 billion metric tons averaging 0.20 - 0.35% Cu. Ore minerals in stockworks and as disseminations mainly include pyrite, pyrrhotite, chalcopyrite and molybdenite within potassically altered rocks. Approximately 80% of the copper is hosted by quartz diorite porphyry at Orange Hill and by granodiorite porphyry at Bond Creek. These two large deposits also contain about 0.02% molybdenum and Orange Hill averages 0.005 oz Au/ton and 0.01 oz Ag/ton. Hollister et al. (1975) report a potassic-phyllic-argillic-propylitic zoning pattern (Lowell and Guilbert, 1970) for alteration assemblages at both the Orange Hill and Bond Creek deposits. This alteration model was shown to be inapplicable for dioritic porphyry hosts (Hollister, 1978), such as at the Baultoff porphyry copper deposit located about 65 km east of Orange Hill. Both the phyllic and argillic zones are absent at Baultoff and the copper ore occurs within stockworks cutting both the potassic and propylitic zones.

SKARN DEPOSITS

Southern Alaska contains both primitive island arc-associated Fe-Cu-Au skarns, and more evolved calcic Cu-Mo skarns generated within a post-accretionary continental margin magmatic arc (Table 4). The former are more numerous, and among them, the Kasaan Peninsula, Jumbo Basin, and Nabesna district contain the only metal producers from skarns within southern Alaska. Newberry (1985) noted almost 100 gold-rich skarns associated with porphyritic gabbro-diorite-tonalite or diorite-quartz monzodiorite intrusive suites in Wrangellia superterrane adjoining the Gulf of Alaska. These plutons are invariably low in Si and K, and contain higher Na_2O/K_2O ratios than those associated with other types of skarns (Meinert, 1984).

The calcic Fe-Cu-Au skarns are spatially associated with basaltic and andesitic submarine volcanic rocks, as well as with their intrusive equivalents. Thin, lenticular limestone horizons and other shallow marine pelites represent products of back-arc sedimentation coeval with island arc magmatism. Economic mineralization usually consists of massive magnetite containing disseminated chalcopyrite and pyrite localized at limestone-igneous rock contacts. Garnet-pyroxene-epidote calc-silicate assembalges are common both as endoskarn and exoskarn, with widespread Na metasomatism characteristic of the former. These gold-bearing skarns are often enriched in Ni, Co, As, V, Mo, Sb, and Bi, and are relatively depleted in Zn, Pb, F, Sn, Be, W, and Ba (Newberry, 1985). Fluid inclusion data from similar skarns in the Wrangellia terrane of British Columbia show ore-forming fluids of moderate to high salinity (10 - 50 equivalent weight percent NaCl ± KCl), with homogenization temperatures between 370°C and 460°C (Meinert, 1984). Meinert believes that the higher salinities correlate with increased Fe, and possibly Au concentrations, reflecting the dominance of chloride complexing for metal transport.

The Mount Andrew, Mamie and Stevenstown mines on the Kasaan Peninsula, eastern Prince of Wales Island, produced approximately 12.8 million pounds of copper, 7,000 oz of Au, and 56,000 oz of Ag, from dominantly garnet-pyroxene-epidote-hornblende skarn, and have resources of 4 million tons containing 50% Fe. Most of the ore bodies on the Kasaan Peninsula consist of massive magnetite within skarn in mid-Paleozoic calcareous sandstone and siltstone, and less commonly in fault zones in metavolcanic rocks (Warner et al., 1961). Highest gold and silver concentrations correlate with highest Cu/Fe ratios, usually localized in more oxidized skarn containing abundant quartz, calcite, and hematite, in addition to the calc-silicate minerals (Myers, 1985).

The Jumbo mine on southeastern Prince of Wales Island yielded about 10 million lbs of Cu, 7,000 oz of Au and 88,000 oz of Ag. Endoskarn, dominantly scapolite-sericite-albite within gabbro, and epidote-calcite-quartz-garnet exoskarn host chalcopyrite with subordinate pyrite, pyrrhotite, and sphalerite, and traces of molybdenite. The lack of magnetite distinguishes the Jumbo mine ore body from all the other nonproductive magnetite-diopside-garnet ± chalcopyrite skarn occurrences within the mid-Paleozoic sedimentary rocks of Jumbo Basin. These latter, more-reduced skarns, however, contain resources of 370,000 tons averaging 45% Fe (Kennedy, 1953).

Similar Fe-Cu-Au skarns occur within Upper Triassic limestones on both the north (Richter et al., 1975) and south (MacKevett, 1976) sides of the Wrangell Mountains. The most productive of these deposits has been the Nabesna mine, with approximately 60,000 oz of Au recovered from pyrite lenses in fractured limestone largely beyond zones of exoskarn containing garnet-pyroxene ± epidote, serpentine, chlorite, wollastonite, quartz, and specularite. The veins also contain pyrrhotite, calcite, chalcopyrite, sphalerite, and galena, and rare stibnite and arsenopyrite have been reported. Pyrrhotite veins and bodies, and magnetite bodies, also just beyond exoskarn zones, contain much less gold than do the pyrite veins (Wayland, 1943). The facts that the pyrite-gold veins are mainly in post-metasomatic fractures (Wayland, 1943), and that the sulfide assemblage is similar to that of the epigenetic gold lodes of southern Alaska, discussed previously, suggest that several mineralizing events may be superimposed at the Nabesna mine.

MacKevett and Blake (1963) described magnetite-rich skarn, with 0.1 - 0.5% Cu, hosted by a Paleozoic(?) marble roof pendant along the north Bradfield River about 65 km southeast of Wrangell. The skarn consists of garnet-pyroxene ± scapolite, quartz, and epidote in contact with quartz diorite(?) of the Coast Range batholith. The deposit apparently represents a relatively rare association in the Alaska Cordillera of Fe-rich skarn (50 - 65% Fe) with continental margin magmatism.

None of the more evolved Cu-Mo skarns has yet yielded any ore. The largest known occurrence of this type is in northeastern Glacier Bay, where the Nunatak deposit contains 7.4 million tons of indicated resources averaging 0.06% Mo and 0.02% Cu, and 124 million tons averaging 0.04% Mo and 0.02% Cu (Brew et al., 1978). Most of the mineralization consists of molybdenite-chalcopyrite stockworks in zoisite-diopside ± actinolite skarn, although molybdenite in epidotized fault zones reaches grades of 0.102% Mo (Twenhofel et al., 1946). The skarn and mineralized stockworks occur at the contact between

Table 4. Skarn deposits within the southern Alaskan Cordillera

District	Mines	Associated Intrusives	Age	Tectonic Setting	Skarn Morphology[1]	Ore Minerals[1]	Reserves and Production	References
Kasaan Peninsula	Mt. Andrew, Mamie, Stevenstown, Poor Man, It, Rich Hill	diorite, gabbro, subordinate granodiorite	mid-Paleozoic	island arc	gar-px-mt-hb	mt ± cp, py	produced 12.8 million lbs Cu, 6,939 oz Au, and 55,933 oz Ag; reserves of 4 m.t. of 50% Fe and 1.5 m.t. <2% Cu	Myers (1984, 1985); Warner et al (1961)
Jumbo Basin	Jumbo, prospects	gabbro	Late Triassic-Early Cretaceous	island arc	gar-dp-scp-ser-alb-epi-cc-qtz	cp ± py, po, sl	produced 10 million lbs Cu, 7,076 oz Au, and 87,778 oz Ag	Kennedy (1953)
Nabesna	Nabesna, Ramble	quartz diorite	Cretaceous(?)	island arc	gar-id-dp-mt-epi-serp-wl-chl-cc	py, Au ± cp, po, sl, gn	produced about 60,000 oz Au	Wayland (1943); Richter et al (1975)
Muir Province	Nunatak prospect	quartz monzonite porphyry	Cretaceous or Tertiary	magmatic arc	qtz-orth-hb-dp-act	mo, cp, py, mt ± po, tt, bn	indicated reserves of 7.4 m.t. of .06% Mo and 124 m.t. .04% Mo	Twenhofel et al (1946); Brew et al (1978)
North Geikie Province	Rendu Glacier prospect	diorite	Cretaceous or Tertiary	magmatic arc	gar-epi-dp-act-mt-chl-tc	cp-po-sch-sl	4,300 tons of inferred resources averaging 5% Cu, .5% W, 7 oz/t Ag and .15 oz/t Au	Brew et al (1978)
South Chilkat sub-province	Alaska Chief prospect	diorite	Cretaceous or Tertiary	magmatic arc	--	py-po-cp-bn-sl(?)	27,000 tons of indicated reserves averaging 1% Cu, 2 oz/t Ag and .1 oz/t Au	MacKevett et al (1971); Brew et al (1978)
--	North Bradfield Canal prospect	quartz monzonite	Cretaceous	magmatic arc	gar-dp-hb ± qtz, kf, plag, epi, scp, sph, ap, zeo	mt ± cp, po	--	MacKevett and Blake (1963)

[1] act = actinolite, alb = albite, ap = apatite, bn = bornite, cc = calcite, chl = chlorite, cp = chalcopyrite, dp = diopside, epi = epidote, gar = garnet, gn = galena, hb = hornblende, id = idocrase, kf = feldspar, mo = molybdenite, mt = magnetite, orth = orthoclase, plag = plagioclase, po = pyrrhotite, px = pyroxene, py = pyrite, qtz = quartz, sch = scheelite, scp = scapolite, ser = sericite, serp = serpentinite, sl = sphalerite, sph = sphene, tc = talc, tt = tetrahedrite, wl = wollastanite, zeo = zeolite

Devonian(?) limestone and calcareous metapelites and barren, porphyritic Cretaceous and Tertiary stocks and dikes. The stockworks and calc-silicate zones are separated from the quartz monzonite bodies by a barren, completely silicified inner alteration zone. Brew et al. (1978) report pyrrhotite, pyrite, tetrahedrite, and bornite associated with the quartz-molybdenite-chalcopyrite stockworks.

The Rendu Glacier and Alaska Chief occurrences, also within the Glacier Bay region, contain Cu-Au-Ag±Zn mineralization within skarn zones in discontinuous carbonate lenses in Devonian or Silurian clastic sediments (Brew et al., 1978). The Rendu Glacier deposit also carries a 0.5% W as scheelite veins within skarn. The association of the prospects with dioritic phases of Cretaceous to Tertiary plutonic complexes contrasts with the more common granodiorite to granite compositional range for calcic Cu skarns (Einaudi et al., 1981).

MAGMATIC SEGREGATION DEPOSITS

Mafic-ultramafic deposits (Table 5) largely form three major metallogenic belts within the southern Alaskan Cordillera. Chromite resources are scattered throughout the Jurassic Border Ranges ultramafic-mafic complex, stretching for more than 1000 km across south-central Alaska. Small lenses of chromite are also abundant within Mesozoic(?) ultramafic bodies on central Baranof Island near Sitka. Large Fe and Ti resources are contained within the Cretaceous Klukwan-Duke mafic-ultramafic belt, consisting of more than 30 small zoned intrusive complexes extending in a narrow belt for the length of southeastern Alaska and into the Yukon. The Tertiary gabbro-norite bodies of the Fairweather-Baranof intrusive belt host important Ni-Cu-Co occurrences.

The Border Ranges ultramafic-mafic complex (Burns, 1985), forms a narrow, discontinuous belt across south-central Alaska. Gabbroic bodies and cumulate ultramafic rocks consisting of dunite, wehrlite, and clinopyroxenite are situated along the Border Ranges fault system, which separates the Chugach terrane from the Peninsular terrane. A composite section of the complex includes basal harzburgite, 2 - 3 km of dunite, peridotite and pyroxenite, and 4 - 7 km of gabbroic bodies. Overlying andesites of the Talkeetna Formation, coeval quartz diorite bodies, and the lack of mid-oceanic ridge pillow basalts, led Burns to conclude that the complex is the basement of an Early to middle Jurassic island arc system.

The stratigraphically lowest dunite bodies, generally intensely serpentinized, host pods, wisps, bands, and disseminations of relatively high chromium (average Cr:Fe = 2.5 - 2.7) chromite. Some of the largest chromite pods reach 100 m in length and 15 m in thickness. Most of the deposits average 5 - 10 percent chromite. A total resource of 2.8 million tons of Cr_2O_3 occurs within 42 deposits in the Border Ranges ultramafic-mafic complex, representing about two-thirds of Alaska's total chromite resources (Foley et al., 1985). A large portion of the resources are located at Red Mountain near Seldovia, which contains 1,487,000 tons in material averaging 5 - 6% Cr_2O_3, and 95,000 tons in material averaging more than 20% Cr_2O_3; the adjacent Windy River placer contains 556,000 tons of material averaging 1.33% Cr_2O_3 (Foley et al., 1985). The only chromite mined to date in Alaska has come from the Red Mountain and nearby Claim Point deposits. Claim Point produced slightly more than 2,000 short tons, averaging 40 - 49% Cr_2O_3, in 1917 and 1918. Red Mountain yielded 28,849 tons averaging 40% Cr_2O_3 during intermittent mining activity between 1943 and 1958 (Foley and Barker, 1985).

The Klukwan-Duke belt of Cretaceous mafic-ultramafic complexes extends for over 500 km, within a roughly 40 km wide belt, through southeastern Alaska generally parallel to and slightly west of the Coast Range batholith. The complexes within the belt are usually distinguished by at least portions of a unique zonal sequence, which consists of a dunite core and grades outward through peridotite to olivine pyroxenite and hornblende pyroxenite. The common association of these bodies with nearby extrusive basalts of the Gravina-Nutzotin belt suggests a genesis of both intrusive and extrusive bodies from the same crystallization sequence. These zoned complexes are distinguished by highly calcic clinopyroxene, absence of orthopyroxene and plagioclase, abundant hornblende, and Fe-rich chromite (Irvine, 1974).

Two hypotheses have been offered to explain emplacement of the zoned complexes. Taylor and Noble (1969) believe that the bodies formed by multiple injections of crystallizing ultramafic magmas. Irvine (1974), however, feels that each complex formed during a single crystal-settling and fractional-crystallization episode. The complexes were subsequently diapirically emplaced as a mixture of crystals and intercumulus fluid in a tectonic environment of lateral compression and recumbent folding.

The outer hornblende pyroxenite zone of many of the complexes consists of diopsidic augite, hornblende, and up to 15 - 20% by volume magnetite. Toward the core, the magnetite decreases abruptly with an increase of olivine (Taylor and Noble, 1969). The complexes at Klukwan, Snettisham, Union Bay, and Duke Island are the largest, and economically most important, of the known complexes. Klukwan has been estimated to contain 3.5 billion tons of rock averaging 16.8% Fe; an adjacent alluvial fan contains another 1 billion tons averaging 10.8% Fe. The deposit also contains 500 million tons of titaniferous magnetite averaging 0.0027 oz PGM/ton (Still, 1984b). Snettisham has been estimated to contain about 500 million tons of 14 - 22% Fe and Union Bay approximately 1 billion tons of 18% Fe. Titanium oxide generally ranges from 2 - 3% in most of the complexes but at Klukwan and Snettisham occasionally reaches 4 - 5% within more massive magnetite zones.

The only ultramafic body in southeastern Alaska with any recorded mineral production is at Salt Chuck on Prince of Wales Island, which produced over 20,000 oz of PGM prior to 1940 (Bundtzen et al., 1984). Despite its position along the belt of zoned ultramafic complexes, the Salt Chuck may not be such a concentrically zoned mass (Page et al., 1977). The Salt Chuck ore body is a pipe-like replacement deposit in pyroxenite and gabbro, and consists of bornite, with subordinate chalcopyrite, precious metals, and secondary copper minerals. The concentration of ore minerals may reflect supergene enrichment, rather than primary segregations of metals during igneous body emplacement (Berg, 1984).

To the west of the Klukwan-Duke belt, small, serpentinized bodies of olivine-rich and olivine-poor peridotite crop out at Red Bluff Bay on central Baranof Island. The peridotite contains

Table 5. Magmatic segregation deposits within the southern Alaskan Cordillera

Type	Age	Ore Host	Deposit	Reserves	References
Border Ranges ultramafic-mafic complex	Jurassic	dunite	Sheep Hill	26,000 tons of Cr_2O_3 from rock averaging 5% chromite	Foley et al (1985); Foley and Barker (1985)
			Bernard Mountain	343,000 tons of Cr_2O_3 from 5% chromite	--do--
			Eklutna	1,000 tons of Cr_2O_3 from 19% chromite	--do--
			Red Mountain	1.58 m.t. of Cr_2O_3 from 5-6% chromite (minor production)	--do--
			Claim Point	90,000 tons of Cr_2O_3 from up to 30% chromite (minor production)	--do--
			Halibut Bay	201,000 tons of Cr_2O_3 from 5-20% chromite	--do--
Klukwan-Duke belt of zoned complexes	Cretaceous	hornblende pyroxenite	Klukwan	3.5 b.t. of 16.8% Fe and 1.0 b.t. of 10% Fe; significant Ti and PGM concentrations	Still (1984b)
			Union Bay	1 b.t. of 18-20% Fe plus anomalous amounts of PGM Ti, Cr, and V	Berg (1984)
			Snettisham	500 m.t. averaging 18.9% Fe, 2.6% Ti, 0.7% V_2O_5, and .0027 oz/t PGM	Berg (1984); Bundtzen et al
			Duke Island	unknown amount of 8-17% Fe	Irvine (1959)
Zoned (?) intrusive	Mesozoic (?)	peridotite	Red Bluff Bay	29,000 tons of 12% Cr_2O_3	Guild and Balsley (1942); Loney et al (1975)
Pipe	Mesozoic (?)	gabbro and norite	Funter Bay (Admiralty-Alaska)	>560,000 tons of .34% Ni, .35% Cu, and .15% Co	Reed (1942); Barker (1963)
Layered intrusive	Tertiary	gabbro and peridotite	Brady Glacier	100 m.t. of .5% Ni and .3% Cu; 54 million lbs proven Co	MacKevett et al (1971); Brew et al (1978); Bundtzen et al (1984)
		norite	Mirror Harbor	8,000 tons 1.57% Ni and .88% Cu; several m.t. .2% Ni, and .1% Cu	Pecora (1942); Bundtzen et al (1984)
		norite	Bohemia Basin	22 m.t. of .33-.51%, .21-.27% Cu, and .04% Co	Reed and Dorr (1942); Bundtzen et al (1984)
		altered gabbro or norite	Snipe Bay	430,000 tons of .3% Ni, .3% Cu, and .13 oz/t Ag	Reed and Gates (1942); Bundtzen et al (1984)

small lenses, thin layers, and disseminations of Fe-rich chromite. Magnetite, a probable product of this serpentinization, occurs in veinlets and also commonly rims the chromite grains (Loney et al., 1975). Guild and Balsley (1942) estimated chromite resources of 29,000 tons averaging 12% Cr_2O_3. This is the only potentially significant chromite occurrence known in southeastern Alaska. Loney et al. (1975) suggest that the periodotite at Red Bluff was an intrusion similar to the zoned bodies in the Klukwan-Duke belt that subsequently was tectonically displaced.

Cu-Ni-sulfide deposits are associated with gabbroic and noritic bodies within the Fairweather-Baranof belt along the Alexander Archipelago north of Sitka. These massive sulfide deposits most likely formed by early separation and gravity settling of immiscible sulfide fluids from a silicate-rich magma. Pyrrohotite, pentlandite, and chalcopyrite were concentrated near the base of the gabbros and norites, usually in lenticular masses, veinlets, and as disseminations.

The Brady Glacier deposit, 20 km north of Dixon Harbor and on the eastern edge of the Crillon-La Perouse gabbro, represents one of the United States' largest nickel resources. It is known to contain 100 million tons averaging 0.5% Ni and 0.3% Cu, plus 50,000 tons of proven or inferred Co (Bundtzen et al., 1984). The more massive sulfide bodies also average about 1.30 ppm PGM (Brew et al., 1978). Only a couple of small nunataks of mineralized gabbro are exposed above Brady Glacier, hindering study of the deposit except by deep drilling. Some layers within the Crillon-La Perouse stock, as well as the adjacent Astrolabe-DeLangle stock, also contain up to 25% ilmenite with 47 - 52% TiO_2 (Rossman, 1963).

Bohemia Basin on Yakobi Island, just off the northwest corner of Chichagof Island, has been estimated to contain resources of 22 million tons averaging 0.33 - 0.51% Ni, 0.21 - 0.27% Cu, and 0.04% Co within an olivine gabbronorite host. Pyrrhotite, pentlandite, and chalcopyrite are the major sulfide minerals and Jirik (1982) identified minor cobaltite intergrown with these sulfides. Norite or gabbro at Snipe Bay, on the outer coast of Baranof Island, contains 430,000 tons averaging 0.3% Ni, 0.3% Cu, and 0.013 oz Ag/ton (Bundtzen et al., 1984). The mafic host rock, which also carries 10 - 25% magnetite, consists of pyroxene altered to hornblende and calcic plagioclase altered to albite (Reed and Gates, 1942). Norite near Mirror Harbor, on the west coast of Chichagof Island, contains an estimated 8,000 tons averaging 1.57% Ni and 0.88% Cu, and several million tons averaging 0.2% Ni and 0.1% Cu (Bundtzen et al., 1984).

URANIUM DEPOSITS

The Upper Jurassic Bokan Mountain peralkaline granite stock on southern Prince of Wales Island has been the only producing uranium deposit in Alaska. A total of 120,000 tons of uranium ore with an average grade exceeding 1% U_3O_8 was recovered in 1957, 1969 and 1971 from the Ross-Adams mine (Thompson et al., 1980). This highly fractionated igneous body intrudes Ordovician-Silurian slates and igneous rocks, and is a compositionally unique intrusive system within the southern Alaskan Cordillera.

The petrogenesis of the uranium-bearing stock was described in detail by MacKevett (1963) and by Thompson et al. (1982). The outer edge of the complex consists of a discontinuous border zone of pegmatite and aplite. This zone grades inward to a 180 m thick zone of aegirine granite porphyry. The core of Bokan Mountain consists of riebeckite granite porphyry 5 km in outcrop diameter, some of which formed as ring dykes during magma roof collapse. Thompson et al. (1980) felt that the final phase of intrusion, which consisted of injection of fine-grained riebeckite granite porphyry during a second episode of roof collapse, coincided with release of a separate volatile phase containing H_2O, CO_2, F, Na, U, Th, REE, and Be.

The characteristics of the uranium-bearing pipes and veins, emplaced along faults and intrusive contacts during retrograde boiling, were discussed by Thompson et al. (1980). Many of these structures developed during collapse of the magma roof and ring dike emplacement. Uranothorite is the dominant ore mineral, with less significant uraninite and rare brannerite. The ore bodies contain less than two volume percent sulfide minerals, largely pyrrhotite, pyrite, chalcopyrite, sphalerite, galena, and bornite; ilmenite and fluorite are also present. Adjacent to the pipes and veins, Thompson et al. (1980) noted K-feldspar completely altered to albite, riebeckite partially to totally replaced by aegirine, and aegirine replaced by calcite, chlorite, fluorite, sulfides, quartz, tourmaline, and sericite; hematite occurs beyond the zone of albite and chlorite. The alteration halos often exceed 15 m in width. Fluid inclusions in cogenetic quartz and fluorite indicate that the uranium ores were deposited at temperatures of at least 320°C - 360°C from low salinity H_2O-CO_2-rich fluids. Sulfur and carbon isotopes suggested moderately reducing ore fluids with a pH of roughly 4.5.

FUTURE OF EXPLORATION IN THE SOUTHERN ALASKAN CORDILLERA

The southern Alaskan Cordillera appears to contain abundant favorable ground for future discovery of metallic mineral deposits (Berg, 1984; MacKevett, 1976; Nelson et al., 1984; Richter et al., 1975). Improvements in our understanding of the accretion tectonics of southern Alaska have helped to fit known mineralization into a more systematic geological framework and classification, leading to improved mineral resource assessments. Relatively recent discoveries, such as the major ore deposits at Quartz Hill and Greens Creek, suggest that exploration efforts within this portion of North America can still be quite fruitful. New ore bodies may remain to be discovered, and numerous known deposits remain to be studied and exploited.

Whereas many metallic deposits in southern Alaska are of economically acceptable size and grade, other factors, in addition to current metal prices, probably will continue to hinder mining activity. Despite relatively accessible coastlines, the rugged topography and extensive glacial cover, mainly from the Copper River southeast to Glacier Bay, discourage relatively costly exploration in the more mountainous terrain. Closure to mineral entry of much of the public domain has further impaired exploration activity. This is especially evident with respect to exploration for critical and strategic minerals. Almost 50% of the PGM, 90% of the cobalt, and 92% of the nickel

reserves known in Alaska are on withdrawn lands within southeastern Alaska (U.S. Geological Survey, 1983). Therefore, while tracts geologically favorable for significant undiscovered mineral resources certainly exist throughout southern Alaska, many of these tracts are not of current interest to industry.

REFERENCES

Armstrong, A. K., and MacKevett, E. M., Jr., 1976, Relations between Triassic carbonate sabkhas and Kennecott-type copper deposits, *in* Cobb, E. H., ed., The U.S. Geological Survey in Alaska — Accomplishments during 1975: U.S. Geol. Surv. Circ. 733, p. 50-51.

Armstrong, A. K. and MacKevett, E. M., Jr., 1977, The Triassic Chitistone Limestone, Wrangell Mountains, Alaska — stressing detailed descriptions of sabkha facies and other rocks in lower parts of the Chitistone and their relations to Kennecott-type copper deposits: U.S. Geol. Surv. OF Rep. 77-217, 23 p.

Barker, F., 1963, The Funter Bay nickel-copper deposit, Admiralty Island, Alaska: U.S. Geol. Surv. Bull 1155, p. 1-10.

Barker, F., and Arth, J. G., 1984, Preliminary results, Central Gneiss Complex of the Coast Range batholith, southeastern Alaska — the roots of a high-K, calc-alkaline arc?: Phys. Earth Planet. Int., v. 35, p. 191-198.

Barrie, C. P., 1984, The geology of the Khayyam and Stumble-On deposits, southeastern Alaska: Unpub. M.A. thesis, U. Texas at Austin, 171 p.

Bateman, A. M., 1924, Geology of the Beatson copper mine, Alaska: Econ. Geol., v. 19, p. 338-368.

Bateman, A. M., and McLaughlin, D. H., 1920, Geology of the ore deposits of Kennecott, Alaska: Econ, Geol., v. 15, p. 1-80.

Berg, H. C., 1984, Regional geologic summary, metallogenesis, and mineral resources of southeastern Alaska: U.S. Geol. Surv., OF Rep. 84-572, 298 p.

Berg, H. C., and Grybeck, D., 1980, Upper Triassic volcanogenic Zn-Pb-Ag (-Cu-Au) -barite mineral deposits near Petersburg, Alaska: U.S. Geol. Surv. OF Rep. 80-527, 9 p.

Berg, H. C., Jones, D. L., and Coney, P. J., 1978, Map showing pre-Cenozoic tectonostratigraphic terranes of southeastern Alaska and adjacent areas: U.S. Geol. Surv., OF Rep. 78-1085, scale 1:100,000, 2 sheets.

Brew, D. A., and Ford, A. B., 1984, The northern Coast plutonic-metamorphic complex, *in* Coonrad, W. L., and Elliott, R. L., eds., The U.S. Geological Survey in Alaska — Accomplishments during 1981: U.S. Geol. Surv. Circ. 868, p. 120-124.

Brew, D. A., and Ford, A. B., 1985, Southeastern Alaska tectonostratigraphic terranes revisited: Program and Abstracts, 60th Annual Meeting, AAPG-SEPM-SEG, Pac. Sec., Anchorage, p. 57.

Brew, D. A., Johnson, B. R., Grybeck, D., Griscom, A., and Barnes, D. F., 1978, Mineral resources of the Glacier Bay National Monument Wilderness Study Area, Alaska: U.S. Geol. Surv. OF Rep. 78-494, 670 p.

Brooks, A. H., 1912, Gold deposits near Valdez: U.S. Geol. Surv. Bull. 520, p. 108-131.

Bruns, T. R., 1985, Tectonics of the Yakutat block, an allochthonous terrane in the northern Gulf of Alaska: U.S. Geol. Surv. OF Rep. 85-13, 112 p.

Buddington, A. F., 1925, Mineral investigations in southeastern Alaska: U.S. Geol. Surv. Bull. 773, p. 71-139.

Buddington, A. F., 1926, Mineral investigations in southeastern Alaska: U.S. Geol. Surv. Bull. 783, p. 41-62.

Bundtzen, T. K., Eakins, G. R., Clough, J. G., Lueck, L. L., Green, C. B., Robinson, M. S., and Coleman, D. A., 1984, Alaska's mineral industry 1983: Alaska Div. Geol. Geophys, Surv. Spec. Rep. 33, 56 p.

Burns, L. E., 1985, The Border Ranges ultramafic and mafic complex, south-central Alaska — cumulate fractionates of island-arc volcanics: Can. J. Earth Sci., v. 22, p. 1020-1038.

Byers, F. M., Jr., and Sainsbury, C. L., 1956, Tungsten deposits of the Hyder district, Alaska: U.S. Geol. Surv. Bull. 1024-F, p. 123-140.

Capps, S. R., and Johnson, B. L., 1915, The Ellamar district, Alaska: U.S. Geol. Surv. Bull. 605, 125 p.

Clark, A. L., Berg, H. C., Grybeck, D., and Ovenshine, A. T., 1971, Reconnaissance geology and geochemistry of Forrester Island National Wildlife Refuge, Alaska: U.S. Geol. Surv. OF Rep. 71-67, 8 p.

Cobb, E. H., 1973, Placer deposits of Alaska: U.S. Geol. Surv. Bull. 1374, 213 p.

Coney, P. J., and Jones, D. L., 1985, Accretion tectonics and crustal structure in Alaska: Tectonophysics, v. 119, p. 265-283.

Coney, P. J., Jones, D. L., and Monger, J. W. H., 1980, Cordilleran suspect terranes: Nature, v. 188, p. 329-333.

Crawford, M. L., and Crawford, W. A., 1986, Formation of tectonic sutures southeasternmost Alaska: Geol. Soc. Am., Cord. Sec., Abstr, p. 97.

Dressler, J. S., Jr., and Dunbire, J. C., 1981, The Greens Creek ore deposit, Admirality Island, Alaska: Can. Inst. Min. Metall. Bull. 74 (no. 833), p. 57.

Eakins, G. R., Bundtzen, T. K., Lueck, L. L., Green, C. B., Gallagher, J. L., and Robinson, M. S., 1985, Alaska's mineral industry 1984: Alaska Div. Geol. Geophys. Surv., Spec. Rep. 38, 57 p.

Einaudi, M T., Meinert, L. D., and Newberry, R. J., 1981, Skarn deposits, *in* Skinner, B. J., ed., Econ. Geol., 75th Anniv. Vol, p. 317-391.

Foley, J. Y., and Barker, J. C., 1985, Chromite deposits along the Border Ranges fault, southern Alaska — 1. Field investigations and descriptions of chromite deposits: U.S. Bur. Mines., Inf. Circ. 8990, 54 p.

Foley, J. Y., Barker, J. C., and Brown, L. L., 1985, Critical and strategic minerals investigations in Alaska — chromium: U.S. Bur. Mines. OF Rep. 97-85, 44 p.

Gault, H. R. and Fellows, R. E., 1953. Zinc-copper deposit at Tracy Arm, Petersburg district, Alaska: U.S. Geol. Surv. Bull. 998-A, 11 p.

Gault, H. R., Rossman, D. L., Flint, G. M., Jr. and Ray, R. G., 1953, Some zinc-lead deposits of the Wrangell District, Alaska: U.S. Geol. Surv. Bull. 998, 15-58.

Gehrels, G. E., Berg, H. C. and Saleeby, J. B., 1983, Ordovician-Silurian volcanogenic massive sulfide deposits on southern Prince of Wales Island and the Barrier Islands, southeastern Alaska: U.S. Geol. Surv. OF Rep. 83-318, 9 p.

Goldfarb, R. J., Leach, D. L., Miller, M. L. and Pickthorn, W. J., 1987, Geology, metamorphic setting and genetic constraints of epigenetic lode-gold mineralization within the Cretaceous Valdez Group, south-central Alaska, *in* Keppie, J. D., Boyle, R. W. and Haynes, S. J., eds., Turbidite-hosted gold deposits: Geol. Assoc. Can. Spec. Pap. 32 (in press).

Goldfarb, R. J., Light, T. D. and Leach, D. L., 1986, Nature of the ore fluids at the Alaska-Juneau gold deposit, *in* Bartsch-Winkler, Susan, ed., The U.S. Geological Survey in Alaska — Accomplishments during 1985: U.S. Geol. Surv., Circ. 978, p. 92-95.

Guild, P.W. and Balsley, J.R., Jr., 1942, Chromite deposits of Red Bluff Bay and vicinity, Baranof Island, Alaska: U.S. Geol. Surv. Bull. 936-G, p. 171-187.

Hawley, C. C., 1976, Exploration and distribution of stratiform sulfide deposits in Alaska, *in* Miller, T. P., ed., Symposium on recent and ancient sedimentary environments in Alaska: Alaska Geol. Soc. Anchorage, T1-T28.

Herreid, G., 1967, Geology and mineral deposits of the Dolomi area, Prince of Wales Island, Alaska: Alaska Div. Mines Mins. Geol. Rep. 27, 25 p.

Herreid, G. and Kaufman, M. A., 1964, Geology of the Dry Pass area, southeastern Alaska: Alaska Div. Mines Mins. Geol. Rep. 7, 16 p.

Herreid, G. and Rose, A. W., 1966, Geology and geochemistry of the Hollis and Twelvemile Creek areas, Prince of Wales Island, southeastern Alaska: Alaska Div. Mines Mins. Geol. Rep. 17, 32 p.

Hillhouse, J.W . and Gromme, C. S., 1984, Northward displacement and accretion of Wrangellia — New paleomagnetic evidence from Alaska: J. Geophys. Res., v. 89, no. B6, p. 4461-4477.

Hollister, L. S. and Crawford, M. L., 1986, Melt-enhanced deformation — A major tectonic process: Geology, v. 14, p. 558-561.

Hollister, V. F., 1978, Geology of the porphyry copper deposits of the Western Hemisphere: New York, Soc. Min. Eng., AIME, 219 p.

Hollister, V. F., Anzalone, S. A. and Richter, D. H., 1975, Porphyry copper deposits of southern Alaska and contiguous Yukon Territory: Can. Inst. Min. Metall. Bull., v. 68, p. 104-112.

Hudson, T., Smith, J. G. and Elliott, R. L., 1979, Petrology, composition, and age of intrusive rocks associated with the Quartz Hill molybdenum deposit, southeastern Alaska: Can. J. Earth Sci., v. 16, p. 1805-1822.

Hudson, T., Arth, J. G. and Muth, K. G., 1981, Geochemistry of intrusive rocks associated with molybdenite deposits, Ketchikan quadrangle, southeastern Alaska: Econ. Geol., v. 77, p. 1225-1232.

Irvine, T. N., 1959, The ultramafic complex and related rocks of Duke Island, southeastern Alaska: Unpub Ph.D. thesis, Calif. Inst. Tech., 320 p.

Irvine, T. N., 1974, Petrology of the Duke Island ultramafic complex, southeastern Alaska: Geol. Soc. Am. Mem. 138, 240 p.

Jansons, U., Hoekzema, R. B., Kurtak, J. M. and Fechner, S. A., 1984, Mineral occurrences in the Chugach National Forest, south-central Alaska: U.S. Bur. Mines, MLA, p. 5-84.

Jirik, R. S., 1982, Geology of the Takanis copper-nickel-cobalt prospect, Yakobi Island, southeastern Alaska: unpub. M.S. thesis, Washington State U., 182 p.

Johnson, B. L., 1914, The Port Wells gold-lode district: U.S. Geol. Surv. Bull. 592, p. 195-236.

Johnson, B. L., 1915, The gold and copper deposits of the Port Valdez district: U.S. Geol. Surv. Bull. 622, p. 140-188.

Jones, D. L., Silberling, N. J., Berg, H. C. and Plafker, G., 1981, Tectonostratigraphic terrane map of Alaska: U.S. Geol. Surv. OF Rep., p. 81-792.

Kennedy, G. C., 1953, Geology and mineral deposits of Jumbo Basin, southeastern Alaska: U.S. Geol. Surv. Prof. Pap. 251, 46 p.

Koski, R. A., Silberman, M. L., Nelson, S. W. and Dumoulin, J. A., 1985, Rua Cove — Anatomy of volcanogenic Fe-Cu sulfide deposit in ophiolite on Knight Island, Alaska: 60th Annual Meeting, AAPG-SEPM-SEG, Pac. Sec., Prog. and Abs., p. 63.

Knopf, A., 1911, Geology of the Berners Bay region, Alaska: U.S. Geol. Surv. Bull. 446, 58 p.

Knopf, A., 1912, The Eagle River region, southeastern Alaska: U.S. Geol. Surv. Bull. 502, 61 p.

Leach, D. L., Goldfarb, R. J. and Light, T. D., 1987, Fluid-inclusion constraints on the genesis of the Alaska-Juneau gold deposits: (this volume).

Light, T. D., Brew, D. A. and Ashley, R. P., 1987, The Alaska-Juneau and Treadwell lode systems, southeastern Alaska, *in* Shawe, D. (editor), World-class gold deposits: U.S. Geol. Surv. Prof. Pap. (in press).

Linn, G. W., 1973, Geology of Orange Hill, Alaska: Unpub. M.A. thesis, U of California-Berkeley, 76 p.

Loney, R. A., Brew, D. A., Muffler, L. J. P. and Pomeroy, J. S., 1975, Reconnaissance geology of Chichagof, Baranof, and Kruzof Islands, southeastern Alaska: U.S. Geol. Surv. Prof. Pap. 792, 105 p.

Lowell, J. D. and Guilbert, J. M., 1970, Lateral and vertical alteration-mineralization zoning in porphyry ore deposits: Econ. Geol., v. 65, p. 373-408.

MacIntyre, D. G., 1986, The geochemistry of basalts hosting massive sulfide deposits, Alexander Terrane, northwest British Columbia, *in* B.C. Min. of Energy, Mines, and Petrol. Res., Geological Fieldwork, 1985, Pap. 1986-1: 197-210.

MacKevett, E. M., Jr., 1963, Geology and ore deposits of the Bokan Mountain uranium-thorium area, southeastern Alaska: U.S. Geol. Surv. Bull. 1154, 125 p.

MacKevett, E. M., Jr., 1976, Mineral deposits and occurrences in the McCarthy quadrangle, Alaska: U.S. Geol. Surv. Misc. Field Studies Map MF-773B, scale 1:250,000, 2 sheets.

MacKevett, E. M., Jr. and Blake, M. C., Jr., 1963, Geology of the North Bradfield River iron prospect, southeastern Alaska: U.S. Geol. Surv. Bull. 1108-D, p. D1-D21.

MacKevett, E. M., Jr. and Blake, M. C., Jr., 1964, Geology of the Sumdum copper-zinc prospect, southeastern Alaska: U.S. Geol. Surv. Bull. 1108-E, p. E1-E31.

MacKevett, E. M., Jr., Brew, D. A., Hawley, C. C., Huff, L. C. and Smith, J. G., 1971, Mineral resources of Glacier Bay National Monument, Alaska: U.S. Geol. Surv. Prof. Pap. 632, 90 p.

Meinert, L. D., 1984, Mineralogy and petrology of iron skarns in western British Columbia: Can. Geol. Assoc., Prog. with Abs., 9, p. A46.

Mitchell, P. A., 1979, Geology of the Hope-Sunrise (gold) mining district, north-central Kenai Peninsula, Alaska: Unpub. MS thesis, Stanford U., 123 p.

Moffit, F. H. and Fellows, R. E., 1950, Copper deposits of the Prince William Sound district, Alaska: U.S. Geol. Surv. Bull. 963-B, p. 47-80.

Monger, J. W. H., Price, R. A. and Tempelman-Kluit, D. J., 1982, Tectonic accretion and the origin of the two major metamorphic and plutonic welts in the Canadian Cordillera: Geology, v. 10, p. 70-75.

Murowchick, J. B., Nesbitt, B. E. and Muehlenbachs, K., 1985, Multiple origins of Canadian Cordilleran gold deposits — Geochemical characteristics: Geol. Soc. Am., Abs. with Prog., p. 672.

Myers, G. L., 1984, Geology of the Cu-Fe-Au skarns of Kasaan Peninsula, southeastern Alaska: Geol. Soc. Am., Abs. with Prog., 16, no. 5, p. 327.

Myers, G. L., 1985, Gold distribution in the Fe-Cu-Au skarns of Kasaan Peninsula, southeast Alaska: Geol. Soc. Am., Cord. Sec., Abs. with Prog., p. 397.

Nelson, S. W., Miller, M. L., Barnes, D. F., Dumoulin, J. A., Goldfarb, R. J., Koski, R. A., Mull, C. G., Pickthorn, W. J., Jansons, U., Hoekzema, R. B., Kurtak, J. M. and Fechner, S. A., 1984, Mineral resource potential of the Chugach National Forest, Alaska: U.S. Geol. Surv. Misc. Field Studies Map MF-1645-A, scale 1:250,000.

Nesbitt, B. E., Murowchick, J. B. and Muehlenbachs, K., 1985, Multiple origins of Canadian Cordilleran gold deposits — Geologic-tectonic constraints: Geol. Soc. Am., Abs. with Prog., p. 676.

Newberry, R. J., 1985, Overview of gold-bearing skarns of southern Alaska: 60th Annual Meeting, AAPG-SEPM-SEG, Pac. Sec., Prog. and Abs., p. 51.

Page, N. J., Berg, H. C. and Haffty, J., 1977, Platinum, palladium, and rhodium in volcanic and plutonic rocks from the Gravina-Nutzotin belt, Alaska: U.S. Geol. Surv., J. Res., v. 5, p. 629-636.

Panuska, B. C., 1985, Paleomagnetic evidence for a post-Cretaceous accretion of Wrangellia: Geology, v. 13, p. 880-883.

Park, C. F., Jr., 1933, The Girdwood district, Alaska: U.S. Geol. Surv. Bull 849-G, p. 381-424.

Pecora, W. T., 1942, Nickel-copper deposits on the west coast of Chichagof Island, Alaska: U.S. Geol. Surv. Bull. 936-I, p. 221-243.

Peek, B. C., 1975, Geology and mineral deposits of the Niblack Anchorage area, Prince of Wales Island, Alaska: Unpub. M.S. thesis, U. Alaska-Fairbanks, 50 p.

Pickthorn, W. J., 1982, Stable isotope and fluid inclusion study of the Port Valdez gold district, southern Alaska: Unpub. M.S. thesis, U.C.L.A., 66 p.

Pickthorn, W. J., Goldfarb, R. J. and Leach, D. L., 1985, Reconnaissance oxygen isotope study of gold-bearing quartz veins within metasedimentary rocks of Valdez Group, Alaska: 60th Annual Meeting, AAPG-SEPM-SEG, Pac. Sec., Prog. and Abs., p. 49.

Pickthorn, W. J., Goldfarb, R. J. and Leach, D. L., 1987, Response to "Dual origin of lode gold deposits in the Canadian Cordillera": Geology, (in press).

Plafker, G., Jones, D. L. and Pessagno, E. A., Jr., 1977, A Cretaceous accretionary flysch and melange terrane along the Gulf of Alaska margin, *in* Blean, K. M., ed., The U.S. Geological Survey in Alaska — Accomplishments during 1976: U.S. Geol. Surv. Circ. 751-B, p. B41-B43.

Ray, J. C., 1933, The Willow Creek gold-lode district, Alaska: U.S. Geol. Surv. Bull. 849-C, p. 165-229.

Ray, R. G., 1954, Geology and ore deposits of the Willow Creek mining district, Alaska: U.S. Geol. Surv. Bull. 1004.

Reed, J. C., 1942, Nickel-copper deposit at Funter Bay, Admiralty Island, Alaska: U.S. Geol. Surv. Bull. 936-0, p. 349-361.

Reed, J. C. and Coats, R. R., 1941, Geology and ore deposits of the Chichagof mining district, Alaska: U.S. Geol. Surv. Bull. 929, 148 p.

Reed, J. C. and Dorr, J. V. N., II, 1942, Nickel deposits of Bohemia Basin and vicinity, Yakobi Island, Alaska: U.S. Geol. Surv. Bull. 931-F, p. 105-138.

Reed, J. C. and Gates, G. O., 1942, Nickel-copper deposits at Snipe Bay, Baranof Island, Alaska: U.S. Geol. Surv. Bull. 936-M, p. 321-330.

Richter, D. H., 1970, Geology and lode-gold deposits of the Nuka Bay area, Kenai Peninsula, Alaska: U.S. Geol. Surv. Prof. Pap. 625G, 16 p.

Richter, D. H., Singer, D. A. and Cox, D. P., 1975, Mineral resources map of the Nabesna quadrangle, Alaska: U.S. Geol. Surv. Misc. Field Studies Map MF-655K, scale 1:250,000.

Robinson, G. D. and Twenhofel, W. S., 1953, Some lead-zinc and zinc-copper deposits of the Ketchikan and Wales districts, Alaska: U.S. Geol. Surv. Bull. 998-C, p. 59-84.

Rossman, D. L., 1959a, Geology and ore deposits in the Reid Inlet area, Glacier Bay, Alaska: U.S. Geol. Surv. Bull. 1058-B, p. 33-59.

Rossman, D. L., 1959b, Geology and ore deposits of northwestern Chichagof Island, Alaska: U.S. Geol. Surv. Bull. 1058-E, p. 139-216.

Rossman, D. L., 1963, Geology and petrology of two stocks of layered gabbro in the Fairweather Range, Alaska: U.S. Geol. Surv. Bull. 1121-F, p. F1-F50.

Silberling, N. J. and Jones, D. L., eds., 1984, Lithotectonic terrane maps of the North American Cordillera: U.S. Geol. Surv. OF Rep. 84-523.

Silberman, M. L., Mathews, Alan, Potter, R. W., and Nissenbaum, Arie, 1978a, Stable isotope geochemistry, sulfide mineralogy, and potassium-argon ages of the Kennecott massive sulfide deposits, Alaska, *in* Blean, K. M., ed., The U.S. Geological Survey in Alaska — Accomplishments during 1976: U.S. Geol. Surv. Circ. 772-B, p. B56-B58.

Silberman, M. L. and O'Leary, R. M., 1976, Geochemical anomalies in the Willow Creek mining district, Talkeetna Mountains, *in* Cobb, E. H., ed., The U.S. Geological Survey in Alaska — Accomplishments during 1975: U.S. Geol. Surv. Circ. 733, p. 48-49.

Silberman, M. L., O'Leary, R. M., Csejtey, Bela, Jr., Smith, J. G. and Connor, C. L., 1978b, Geochemical anomalies and isotopic ages in the Willow Creek mining district, southwestern Talkeetna Mountains, Alaska: U.S. Geol. Surv. OF Rep. 78-233, 32 p.

Sillitoe, R. H., 1980, Types of porphyry molybdenum deposits: Min. Mag., 142, p. 550-553.

Smith, P. S., 1942, Occurrences of molybdenum minerals in Alaska: U.S. Geol. Surv. Bull. 926-C, p. 161-210.

Spencer, A. C., 1905, The Treadwell ore deposits, Douglas Island: U.S. Geol. Surv. Bull. 259, p. 69-87.

Spencer, A. C., 1906, The Junean gold belt, Alaska: U.S. Geol. Surv. Bull. 287, 161 p.

Still, J. C., 1984a, Stratiform massive sulfide deposits in the Mt. Henry Clay area, southeast Alaska: U.S. Bur. Mines. OF Rep. 118-84, 65 p.

Still, J. C., 1984b, Copper, gold, platinum, and palladium sample results from the Klukwan mafic/ultramafic complex, southeast Alaska: U.S. Bur. Mines. OF Rep. 84-21, 16 p.

Stowell, H. H., 1981, Geology of Sweetheart Ridge and adjacent areas, southeast Alaska: Unpub. M.S. thesis, U. South Carolina, 110 p.

Stuwe, K., 1984, Granitoid intrusions and gold mineralization in the western Port Wells mining district, Prince William Sound, Alaska: Unpub. M.S. thesis, U. Leoben, Austria.

Taylor, H. P., Jr., 1979, Oxygen and hydrogen isotope relationships in hydrothermal mineral deposits, *in* Barnes, H. L., ed., Geochemistry of hydrothermal ore deposits: New York, John Wiley and Sons, p. 236-277.

Taylor, H. P., Jr., and Noble, J. A., 1969, Origin of magnetite in the zoned ultramafic complexes of southeastern Alaska: Econ. Geol., Mon. 4, p. 209-230.

Theodore, T. G. and Menzie, W. D., 1984, Fluorine-deficient porphyry molybdenum deposits in the western North America cordillera: Proc. 6th Quadrennial IAGOD Symp., Stuttgart, Germany, p. 463-470.

Thompson, T. B., Lyttle, T. and Pierson, J. R., 1980, Genesis of the Bokan Mountain, Alaska, uranium-thorium deposit: U.S. DOE, NURE Rep. GJBX-38(80), 232 p.

Thompson, T. B., Pierson, J. R. and Lyttle, T., 1982, Petrology and petrogenesis of the Bokan granite complex, southeastern Alaska: Geol. Soc. Am. Bull. v. 93, p. 898-908.

Thorne, R. L., Muir, N. M., Erickson, A. W., Thomas, B. I., Heide, H. E. and Wright, W. S., 1948, Tungsten deposits in Alaska: U.S. Bur. Mines. Rep. Inv. 4174, 22 p.

Tuck, R., 1933, The Moose Pass-Hope district, Kenai Peninsula, Alaska: U.S. Geol. Surv. Bull. 849-I, p. 469-530.

Twenhofel, W. S., 1952, Geology of the Alaska-Juneau lode system, Alaska: U.S. Geol. Surv. OF Rep. 60, 170 p.

Twenhofel, W. S., Reed, J. C. and Gates, G. O., 1949, Some mineral investigations in southeastern Alaska: U.S. Geol. Surv. Bull. 963-A, p. 1-45.

Twenhofel, W. S., Robinson, G. D. and Gault, H. R., 1946, Molybdenite investigations in southeastern Alaska: U.S. Geol. Surv. Bull. 947-B, p. 7-38.

Tysdal, R. G. and Case, J. E., 1979, Geologic map of the Seward and Blying Sound quadrangles, Alaska: U.S. Geol. Surv. Misc. Inv. Ser. Map I-1150, scale 1:250,000.

United States Geological Survey, 1983, 1983 Annual Report on Alaska's Mineral Resources: U.S. Geol. Surv. Circ. 908, 48 p.

U.S. Geological Survey and U.S. Bureau of Mines, 1984, Mineral resources of the Tracy Arm-Fords Terror Wilderness Study Area and vicinity, Alaska: U.S. Geol. Surv. Bull. 1525, 308 p.

Van Nieuwenhuyse, R. E., 1984, Geology and geochemistry of the Pyrola massive sulfide deposit, Admiralty Island, Alaska: Unpub. M.A. thesis, U. Arizona.

Wahrhaftig, Clyde, 1965, Physiographic divisions of Alaska: U.S. Geol. Surv. Prof. Pap. 482, 52 p.

Warner, L. A., Goddard, E. N. and others, 1961, Iron and copper deposits of Kasaan Peninsula, Prince of Wales Island, southeastern Alaska: U.S. Geol. Surv. Bull. 1090, 136 p.

Wayland, R. G., 1939, Geology of the Juneau region, Alaska, with special reference to the Alaska Juneau ore body: Unpub. Ph.D. thesis, U. Minnesota.

Wayland, R. G., 1943, Gold deposits near Nabesna: U.S. Geol. Surv. Bull., 933-B, 175-199.

Westra, G. and Keith, S. B., 1981, Classification and genesis of stockwork molybdenum deposits: Econ. Geol., v. 76, p. 844-873.

White, W. H., Bookstrom, A. A., Kamilli, R. J., Ganster, M. W., Smith, R. P., Ranta, D. E. and Steininger, R. C., 1981, Character and origin of Climax-type molybdenum deposits, *in* Skinner, B. J., ed., Seventy-Fifth Anniv. Vol., Econ. Geol., 75th Anniv. Vol., p. 270-316.

Wright, F. E., and Wright, C. W., 1908, The Ketchikan and Wrangell mining districts, Alaska: U.S. Geol. Surv. Bull. 347, 210 p.

Geology of Newmont Gold Company's Gold Quarry Deposit, Eureka County, Nevada

J. C. ROTA
Newmont Exploration Ltd., c/o Newmont Gold Company, P.O. Box 669, Carlin, NV 89822

Abstract — The Gold Quarry deposit is the latest bulk-tonnage epithermal gold deposit in northeastern Nevada to be developed by Newmont Gold Company. Gold Quarry is the largest gold deposit of the "Carlin Trend".

The magnitude of Gold Quarry was discovered in 1979 when percussion drilling eventually delineated a deposit containing 130 Mt of ore that averaged 1.68 grams of gold per ton. Mill operations commenced in 1985 and 6.5 t of gold are scheduled for production in 1986.

The spatial distribution of jasperoids, the wallrock alteration suite, and associated geochemistry all suggest a fossil hot-springs genetic model for Gold Quarry.

INTRODUCTION

District history

THE GOLD Quarry deposit occupies the southern half of Section 35 (Township 34 North, Range 51 East) in the Tuscarora Mountains of northeastern Nevada. It is the largest gold deposit in the Maggie Creek (Schroeder Mountain) mining district, located 11 km northwest of the town of Carlin (Fig. 1).

The first prospecting in the district occurred soon after the transcontinental railroad was completed through Carlin in 1869. The first organized mining occurred at the Good Hope mine, located one kilometre northwest of Gold Quarry. A 75 m deep inclined shaft was driven across the Good Hope fault to develop a one metre wide vein of galena, silver, copper carbonates and barite. No significant gold production was reported from this mine.

The Copper King base metal property is located two kilometres northwest of Gold Quarry, along strike of the Good Hope fault. Lode claims were first staked in 1908, with mining occurring a few years later. Ore minerals produced from the small surface and underground workings consisted of chrysocolla, azurite, malachite, and turquoise. Small amounts of gold and silver were also mined. This mine was listed in 1974 as the only North American occurrence of the mineral Faustite, a hydrous zinc-copper aluminum phosphate (Roberts et al., 1974).

The first recorded production at Gold Quarry was from quartz veins located in a highly silicified area of the deposit. In 1936, 54 t of material that averaged 13 grams of gold and 27 grams of silver per ton were shipped to the railhead at Carlin. The ore was reported to be composed of iron-stained quartzite and chert (Roberts et al., 1967).

Total production for the Maggie Creek mining district from 1932 to 1958 was 26 kg gold, 136 kg silver, 297,581 kg copper and 12,520 kg lead.

Recent developments

In 1960, the search for a large, near-surface gold orebody in Nevada was sparked by a paper written by Ralph Roberts entitled "Alinement of mining districts in north-central Nevada" (Ramsey, 1973). Geologist J. Alan Coope was brought in by Robert Fulton (Newmont Mining Corporation) to assist John Livermore in the evaluation of the Gold Acres, Gold Quarry and Lynn Window (Carlin Mine) areas. Exploration drilling centred around the Gold Quarry jasperoid had, by 1970, delineated a deposit of 306 Kt that averaged 4.1 g/t gold.

In 1962, Newmont discovered the Carlin deposit 10 km to the northwest. Interest in Gold Quarry declined until 1972 when Donald M. Hausen (Newmont Exploration Ltd.) recommended renewed exploration due to significant alteration features in drill cuttings. In 1977, Carlin Gold Mining Company (now known as Newmont Gold Company) geologists Larry Noble and Charles Ekburg mapped and sampled a group of claims staked by Mike Barstow. These claims were located

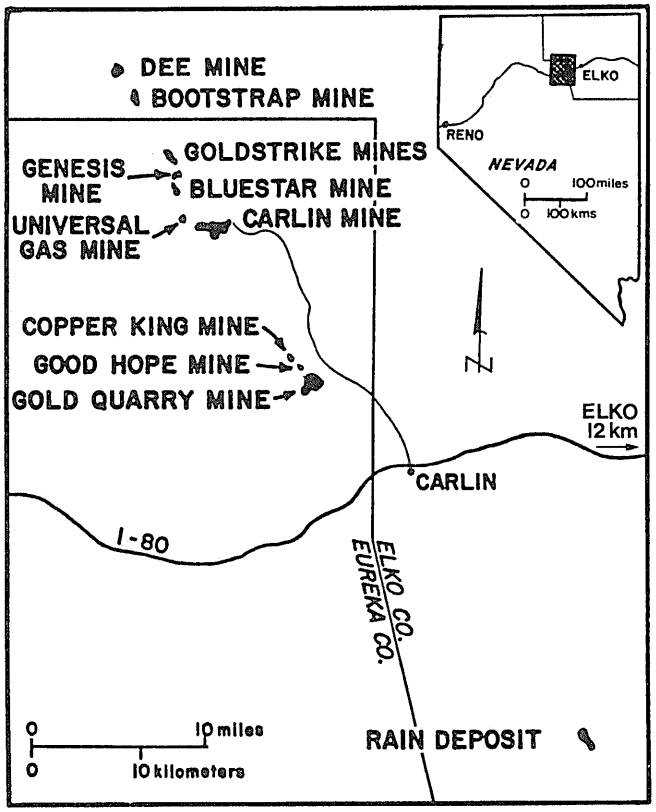

Fig. 1. General location map of the Gold Quarry mine and other gold mines of the Carlin trend, Nevada.

less than one kilometre southwest of Gold Quarry, and were to become a part of the Maggie Creek disseminated gold deposit.

The discovery of Maggie Creek prompted additional drilling and investigation of the Gold Quarry area. Activities were accelerated in 1979 when gold assays of over four grams per ton were reported in samples from a drill hole located 600 m south of the Gold Quarry fault jasperoid. This drilling had encountered a blind ore zone beneath 75 m of Pliocene lacustrine sediments. To define the ore, over 550 fifteen-centimetre conventional circulation holes were drilled from the surface to an average depth of 185 metres. All percussion drilling was vertical and was conducted on a 30 m square grid. Both downhole hammers and tri-cone bits were used throughout the program.

HQ wire-line core drilling was used to collect rock from the central, oxidized portions of the orebody for geological and metallurgical testing. Three inclined and one vertical hole were drilled to average depths of 235 and 105 metres, respectively. Seven vertical PQ-size holes that averaged 177 m in depth were used to collect additional metallurgical test material.

Drilling eventually defined a deposit that contained geologic reserves of over 248 t of gold. Proven and probable reserves, mineable by open pit, are estimated at 130 Mt of ore that averages 1.68 grams of gold per ton. This includes high-grade ore zones of 45 Mt, averaging 2.64 grams of gold per ton, which currently feed the Carlin #2 mill at an average rate of 9,000 tpd. About 10% of the mill grade ore is carbonaceous in nature. The remaining 85 Mt reserves, averaging 1.2 grams of gold per ton, are to be treated by dump leach methods. Total 1986 production from the #2 mill is estimated at 6.5 t of gold.

In 1982, a central area of the near surface portion of the orebody was opened and more than 900 Kt of material removed for heap leach and milling tests. The Carlin #2 mill was built two kilometres east of Gold Quarry by the Bechtel Corporation in 1984 at a cost of U.S. $130 million.

REGIONAL AND DISTRICT STRUCTURE

Regional structure

The complex structural history of Nevada is described in great detail by Stewart (1980). Briefly, the Roberts Mountains Thrust is a product of the Antler orogenic event of the Late Devonian (to possibly earliest Triassic — Ketner, 1982). A subduction-related highland formed immediately west of the North American craton and a thick sequence of deep-water siliceous and volcanic rocks was transported at least 145 km eastward along the Roberts Mountains Thrust Fault over coeval shallow-water miogeoclinal rocks. The upper plate of the Roberts Mountains Thrust is composed of interleaved, broad, thin, thrust plates commonly subparallel to bedding. Differential movement of these plates has caused a juxtapositioning of western siliceous and transitional (mixed carbonate and siliceous) assemblages. The transitional siltstone and silty limestone of the Roberts Mountains allochthon are separated from the western siliceous rocks both stratigraphically and by small thrust and high-angle normal faults. Most of the upper plate lithologies are folded along a northwest axis.

As tectonic regimes changed through the Paleozoic and Mesozoic, major fault trends shifted from west to north, then to northwest. Doming of both allochthonous and autochthonous rocks along a northwest trend began during or shortly after thrusting. Cretaceous and Tertiary intrusive events combined with subsequent erosion to produce a N45W trend of fensters, or windows.

Cenozoic extensional faulting in the area commenced about 17 million years ago. Displacement along these north to northeast striking high-angle faults has formed the mountains and valleys that dominate the present topography of the Basin and Range province.

District structure

The Carlin Window is the principal geologic feature of the Gold Quarry area. It is roughly circular in outline and is about three kilometres in diameter (Fig. 2). The window exposes

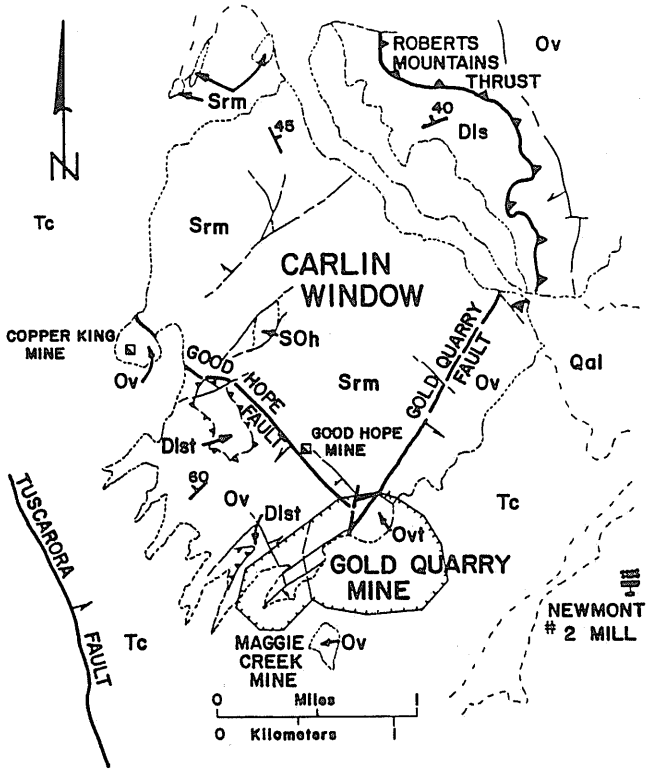

Fig. 2. Maggie Creek Mining District general geology.

Explanation:
- Qal = Quaternary alluvium
- Tc = Tertiary Carlin Formation
- Dls = Devonian unnamed limestone
- Dlst = Devonian Transitional limestone
- Srm = Silurian Roberts Mountains Formation
- SOh = Silurian/Ordovician Hanson Creek Formation
- Ov = Ordovician Vinini Formation
- Ovt = Ordovician Vinini/Transitional siliceous sediments

thin-bedded silty limestone of the Roberts Mountains Formation and an overlying, relatively massive unnamed Devonian limestone. These carbonates are exposed through siltstone, shale, sandstone, chert and impure limestone of the Roberts Mountains allochthon.

The Carlin Window is defined on the northeast by the Roberts Mountains Thrust and on the southwest and southeast by the high-angle Good Hope and Gold Quarry faults, respectively. The northwest boundary is buried by Quaternary alluvium and Tertiary lacustrine sediments.

STRATIGRAPHY

The stratigraphy of the Carlin Window has been described by Evans and Cress, 1972, Roberts, 1967, Stewart, 1980, and West, 1976. A brief summary of their work, and the work of others, is given below.

Western assemblage — Siliceous

A thick sequence of Ordovician strata assigned to the Vinini Formation is exposed in the Tuscarora Mountains. The sequence is primarily composed of medium-bedded black and green chert, thin bedded shale, minor sandstone, quartzite and rare greenstone. Ten to 20 kilometres north of the Gold Quarry area, this formation is greater than 4,300 metres thick. In the vicinity of the Carlin Window, a 765 metre section of the Vinini Formation is composed of carbonaceous shale, siliceous shale, chert, siltstone, quartzite and minor limey siltstone.

Transitional assemblage — Siliceous and carbonates

Roberts et al., 1958, described rocks of mixed siliceous and carbonate facies in northern Nevada as "transitional assemblage". These rocks are primarily siltstone, silty limestone, shale, sandstone and chert. This sequence has been recognized by the author as composing the dominant host lithologies of the Gold Quarry deposit. The transitional section at Gold Quarry is estimated to be over 450 metres thick. These Ordovician siltstones are typically thin-bedded and noncompetent. Bedding generally strikes about N45W and dips between 30 and 80 degrees either southwest or northeast. Isoclinal folding of bedding is common, with chaotic, discordant bedding near large faults. Low-amplitude folding on a northwest trend is also present.

Eastern assemblage — Carbonates

The youngest member of the eastern assemblage is an unnamed Devonian limestone exposed in the northern part of the Carlin Window, the upper portions of which have been cut by the Roberts Mountains Thrust. This formation is a thick to massively bedded sequence of dark grey to black (often fossiliferous) dolomitic limestone. The silt content of this Devonian limestone increases vertically and grades upward into a sandy limestone. Devonian corals and crinoids are common. Estimated thickness of this formation varies from 75 metres in the Carlin Window to 175 metres for the equivalent Popovich limestone at the Carlin mine, 10 kilometres to the northwest.

The Silurian Roberts Mountains Formation makes up the bulk of the exposed rock within the Carlin Window. This formation is a dark grey, platy, fine-grained, silty dolomitic limestone. The basal unit of the Roberts Mountains Formation is a three metre thick section of black chert overlain by a pyritic, carbonaceous silty dolomite that contains some thin chert lenses. A grey, dolomitic, locally sandy limestone with intercalated thin, dark grey, bioclastic limestone beds and lenses of chert overlies the dolomite. These carbonates typically weather to a light grey slope of angular plates and are estimated to be 350 metres thick.

Several fault-bounded exposures of the Silurian-Ordovician Hanson Creek Formation are found on the southern portion of the Carlin Window. This formation consists primarily of grey to black dolomite and chert lenses. Due to limited outcrop, the thickness of this formation within the window is estimated at only 50 metres.

Tertiary sediments

To the south of Gold Quarry, Tertiary volcanic flows dammed major drainages of the area. This created basins where extensive lacustrine deposits accumulated during the Pliocene. These deposits are divided by Regnier, 1960, into several formations. One of these, the Carlin Formation, rests either unconformably on, or in fault contact with, the Paleozoic bedrock of the district. This formation consists of over 200 m of lacustrine tuffaceous siltstone, conglomerate, diatomite, shale, limestone and rhyolite tuffs. The Carlin Formation is considered to be of Pliocene age (Regnier, 1960). The depositional basin deepens to the east to include over 700 m of other Tertiary sediments (all a part of the 2 200 m section of Cenozoic rocks in northeastern Nevada). Within the Gold Quarry mine, the Carlin Formation includes well-defined scour and fill channels, gravel bars that contain siliceous angular to sub-rounded clasts, and bedded vitric tuffs. Adjacent to the orebody, clay and siliceous gravel of the Carlin Formation were derived from the erosion of hydrothermally altered Paleozoic rocks, giving the appearance of mineralized Tertiary sediments (as suggested by Ekburg, 1986). The author believes that the Pliocene age of the Carlin formation postdates the mineralization at Gold Quarry.

Small faults and gentle folds are common; the dip of the Tertiary beds ranges from 10 to 20 degrees to the east. The occurrence of a basal montmorillonitic-hematitic clay layer usually marks the Paleozoic bedrock contact. This layer appears lateritic in nature and is considered by the author to represent a paleosol horizon.

Igneous rocks

The only igneous rock exposed in the immediate area is found in the west pit of the Maggie Creek mine, about 925 m southwest of the centre of Gold Quarry. The dike is classified

as a latite-porphyry, being composed of minute quartz phenocrysts in an argillically altered feldspar groundmass. The dike contains both anomalous gold and arsenic values and is stained by iron oxides. It is exposed along a northwest strike for about 10 m and averages about one metre in width. No age dates are available for the dike.

ALTERATION

Hypogene alteration

Silicification and argillization are the principal alteration processes observed at Gold Quarry. Descriptions of wallrock subjected to either style range from slightly noticeable effects to total erasure of original bedding features. Silicification appears to be more directly associated with gold deposition.

Silicification at Gold Quarry is the most pervasive style of alteration observed and has been superimposed on siliceous siltstone and silty limestone. Silica flooding has produced unique rock characteristics, the most noticeable being a cherty, flint-like rock containing over 97% silica. Roughly one-half of the drilled area is composed of slightly to highly silicified rock (Fig. 3); about 60% of the total contained gold in the deposit is associated with these rocks. The effects of silicification are noted to be concentrated along high-angle faults, particularly in their hanging walls. In general, the intensity and amount of silicified rock decreases with an increase in depth. This decrease results in the deposit appearing to have a "silica cap" that overlies moderately argillized and silicified lithologies.

The first hydrothermal silica to be introduced at Gold Quarry is probably represented by quartz veinlets that contain abundant organic carbon ("black quartz"). Black quartz from the 5540 bench was examined by J. Coe in 1983. She states that, "The black speckled inclusions in the quartz were very minute (about 2 to <0.5 microns) and medium to dark grey in reflected light, similar to organic carbon . . . Microscopic textural evidence suggests that the organic carbon was derived from a form of asphalt bitumen that was mobilized by [hydrothermal] solutions, and became embedded in vein quartz penecontemporaneous with barite and gold . . ." It has been suggested that the carbonaceous material in these veins was derived from carbonate source rocks by fluids that pre-date the formation of the auriferous hydrothermal system (Kuehn, 1986). The pre-existing pyrobitumen reservoir was intersected by the first pulse of hypogene fluids and micron-sized particles of carbonaceous material became included in the quartz.

The exact number of silica introduction events is difficult to estimate. Besides the black quartz, at least one clear quartz and one quartz-barite veining event are observed in the deposit. Three episodes of silica flooding are also recognized, thus three degrees of general wallrock silicification are noted in the mine. The final silica event appears to consist of supergene milky quartz that filled open fractures, cross-cutting all previous veins (Fig. 4).

Alunitization followed the main stages of silicification, with alunite occurring as replacements along fractures and as vertical stockwork veins that transect earlier quartz-barite veins. Hausen et al. (1983) noted that these replacements are more common at Gold Quarry than at other Carlin-type gold deposits. Most of the alunite occurs in siliceous sediments and appears to

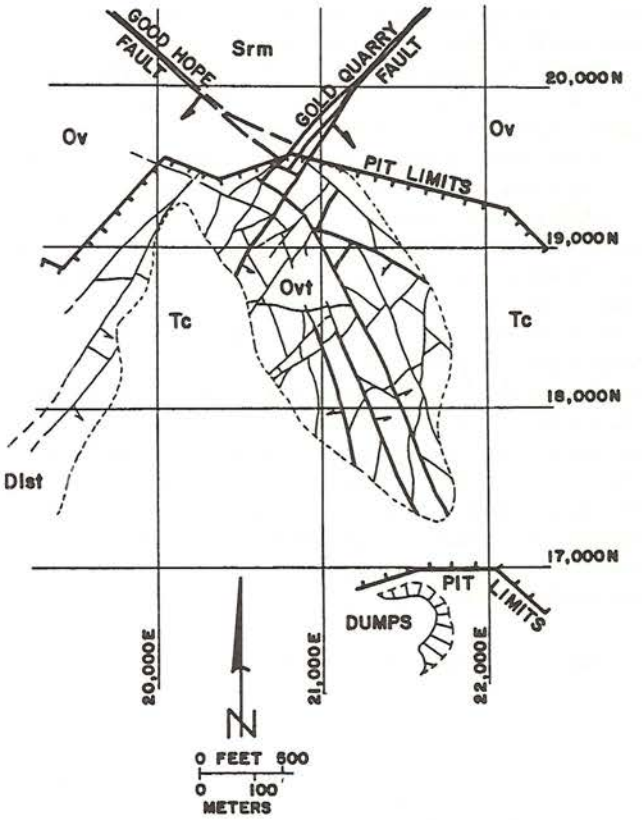

Fig. 3. General geology of the Gold Quarry mine.

Explanation: Tc = Tertiary Carlin Formation
Dlst = Devonian Transitional limestone
Srm = Silurian Roberts Mountains Formation
Ovt = Ordovician Vinini/Transitional siliceous sediments

MINERALS AND TEXTURAL FEATURES	ALLOGENIC	DIAGENIC	EPIGENETIC	SUPERGENE
QUARTZ				
DETRITAL	■			
CHERT		■		
REPLACEMENT			■	■
CALCITE	■	■	■	■
ILLITE	■	■	■	■
MONTMORILLONITE		■		
KAOLINITE			■	■
PYRITE		■	■	■
IRON OXIDES				■
CHALCOPYRITE			■	
SPHALERITE			■	
GALENA			■	
GOLD			■	■
BARITE			■	
ALUNITE			■	■
MICROFRACTURING		■	■	■

Fig. 4. Gold Quarry paragenetic sequence (after D. M. Hausen).

be both lithologically and structurally controlled. Numerous veins, from 1 mm to 10 cm wide, are noted to have assimilated small fragments of country rock, suggesting that most alunite formed under hypogene conditions. Alunite occurring along open fractures may be of supergene origin. The centre of the deposit contains most of the alunite. Late argillic alteration has obscured the alunite veins so that field identification is difficult.

Argillic alteration followed silicification and alunitization. Clay alteration fronts are observed in the mine to encroach upon slightly to highly silicified rock. Argillic alteration has been observed to penetrate two to three centimetres into highly silicified rock from post-silicification fractures, leaving a core of siliceous rock surrounded by a clay rind (that is still composed of about 75 to 80% silica). Argillic alteration of sedimentary lithologies produces a slightly soft rock to a fluffy or greasy clay. Alteration minerals near the top of the deposit consist predominately of illitic clay and kaolinite (Table 1) with traces of montmorillonite. The roots of the deposit are predominately kaolinitic. Deer et al. (1966), note that illitic clays may have a hydrothermal origin and are often found in alteration zones around hot springs and metalliferous veins. The vertical zonation of illite at Gold Quarry suggests that it is hypogene in nature, accentuated by near-surface acid leaching. Because argillic rocks are a product of wallrock-fluid interaction, even the most altered sediments still contain 50 to 60% quartz (as detrital grains).

Table 1. Wallrock alteration features (distribution in wt. %)

	Whole deposit (disseminated values)	Localized concentrations (structural values)
Quartz	40.0 - 60.0%	>90.0%
Alunite	5.0 - 20.0	30.0 - 40.0
Iron Oxides	2.0 - 6.0	10.0 - 18.0
Barite	—	1.0 - 3.0
Illite	4.0 - 5.0	10.0 - 15.0
Kaolinite	—	4.0 - 20.0

Decalcification, the removal of carbonate minerals from limestone through hydrothermal processes, has occurred along many faults and local areas in silty limestone within the deposit. A general decrease in bulk density and increase in porosity of the affected rock is usually associated with this process (Hausen and Kerr, 1968). This left most of the silty limestone very receptive to silica-bearing fluids; the former carbonate units are now highly silicified and contain little to no calcite. No hydrothermal calcite veins have been noted within the siliceous sediments in Gold Quarry, however, the nearby Maggie Creek mine contains abundant calcite veins.

Baritization has occurred throughout Gold Quarry, especially in the vicinity of large faults. Bladed barite crystals up to 5 cm have been taken from the highly iron-stained, open-spaced breccias of a few northwest-trending faults. Barite is also a common feature of the jasperoidal faults and quartz-gold veins within the deposit. Deposition of barite ranges from early through late epigenesis of the orebody (Fig. 4).

Supergene alteration

Late-Tertiary supergene oxidation followed formation of the Gold Quarry orebody. Drill data indicate that primary, unoxidized, pyritic, carbonaceous ore begins between 120 and 200 m below the Paleozoic bedrock surface. The oxidation boundary, in general, reflects the erosional bedrock surface above it. Deep weathering is indicated by the occurrence of pyrite molds in siliceous rock, lateritic soil development and the abundance of hematitic and limonitic clays found on nearly all open fractures of the near-surface portions of the deposit. These iron-rich clays give the Gold Quarry pit a distinctive red hue. Supergene redistribution of some gold is indicated by Hausen (1983), ". . . small amounts of pyrite have been detected in Gold Quarry ores, most of which is assumed to be auriferous, analogous to Carlin, Getchell, Cortez, and other similar deposits. Small amounts of gold are therefore assumed to be liberated during this late period of oxidation of sulfides." Unexpectedly high ore grades encountered in mining immediately beneath the bedrock surface also tend to support some supergene movement of gold.

GOLD MINERALIZATION

Gold Quarry is the largest deposit of the Carlin Trend, a 60 km long northwest alignment of epithermal, sediment-hosted, disseminated gold deposits. Collectively, these deposits contained more than 620 t of gold, with Gold Quarry alone accounting for nearly forty percent of the total.

Primary controls

Detailed pit mapping at Gold Quarry has shown that steeply dipping normal faults, and associated fracturing, are the major controlling features of gold deposition. Mechanically induced permeability was important to the formation of this deposit. Highly pervasive fracture systems produced by faulting provided the ore bearing fluids access to the host rocks. This produced the stockwork distribution pattern of greater gold values along major faults, connected by overlapping, disseminated, lower grade zones. The attitudes of the northwest-trending Good Hope fault and the intersecting, northeast-trending Gold Quarry fault are mirrored by many smaller faults and fractures within the deposit (Figs. 5 and 6). Antithetic and sympathetic fracturing down to a spacing of a few centimetres can be traced through the deposit along these trends.

Nearly all faults within Gold Quarry appear to pre-date gold deposition and most of the large faults show signs of post-ore movement. North-northwest trending faults dominate the current pit geology and ore distribution, with northeasterly-trending faults and fractures in a subordinate role. Silica-filled faults within the Gold Quarry ore zones appear to have been enhanced by hydrothermal dissolution and brecciation, as these faults are less noticeable when away from centres of ore deposition. Seismic, or mechanical, brecciation appears to have provided

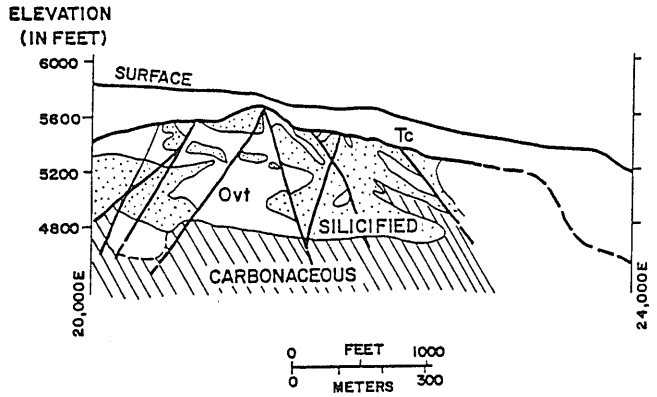

Fig. 5. General cross-section of Gold Quarry deposit.

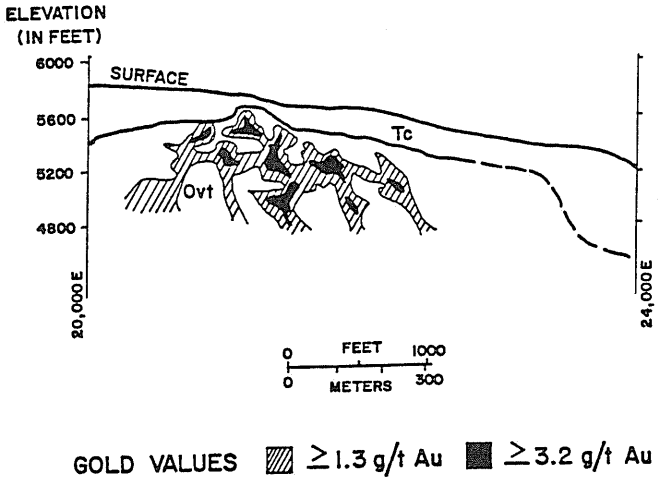

Fig. 6. General cross-section distribution of gold in the Gold Quarry deposit.

hypogene fluids an open access through these structures, allowing additional hydrothermal brecciation and microbrecciation to occur.

Secondary controls

Secondary ore controls are provided by the host rock lithologies. Relatively porous siltstone and silty limestone are noted to localize ore zones away from the main controlling faults. The dense primary chert that occurs within the deposit contains gold on fracture surfaces only and, therefore, tends to be of a lower ore grade than the more permeable lithologies.

Brecciation

Hydrothermal breccias occur as silica-cemented vein and pod-like bodies from 1 cm to 20 cm in width throughout the deposit. These breccias are distinguished by their single lithology, angular to rounded clasts locked within a quartz or quartz-barite matrix, and their ability to be "re-assembled" if the supporting matrix material could be removed. Hydrothermal breccias may occur within a fault, but are often found away from recognized structures. Mechanical breccias will often occur within a recognized fault zone, be composed of several lithologies, contain "rock flour" between clasts and generally be clast-supported.

The combination of large, open space, siliceous to moderately argillic hydrothermal breccias, barite crystals, gypsum crystals and abundant manganese and iron oxides appear to define possible "vent" areas near the top of the deposit. According to Berger (1985), areas such as this may have been formed by predominately gaseous discharges. Aqueous fluids were prevented from flooding these areas because of boiling during late-stage steam dominance in the hydrothermal system. These "vent" features are often isolated at northeast-northwest fault intersections and do not usually display anomalous gold values.

Timing and fracturing

According to Hausen (1983), gold deposition began immediately following initial silicification, and continued until the last silicification events. Through petrographic examinations conducted while studying a large mass of highly silicified rock, Hausen states, "Gold mineralization appears to have occurred over an extended period of time, beginning with the early introduction of quartz-barite veins and continuing during the waning stages of late cherty silicification. The most intense period of gold mineralization appears to be associated with this late stage of silicification, related to low temperature hot springs activity." Gold particles occur mostly as fine, native granules of less than one to ten microns in size, associated with microfractures or a microcrystalline cherty matrix.

In 1983, D. M. Hausen found evidence for several periods of microfracturing relevant to gold deposition. At least three periods were recognized, the first being described as "pattern fracturing". This microfracturing is pervasive, is usually recemented by quartz and often contains gold. Spacing of these fractures ranges down to about 50 microns. A later period of fracturing transgressed the pattern fractures. This second period is commonly filled by vuggy quartz, and also contains some gold. A final period of fracturing is post-mineralization in nature and is related to post-mineral faulting. These latest fractures are generally open in nature, but often contain varying amounts of iron oxide, clay, and alunite. Density of these latest fractures ranges from 3 cm to 10 cm in argillized rock and from 10 cm to one metre in silicified rock, as mapped in the Gold Quarry pit.

Silver is present in highly anomalous amounts at Gold Quarry. Sub-economic silver grades of 0.3 to 3.5 g/t are common within the gold ore zones. Silver deposition may have predated gold; the general background of silver values appear to be overprinted by gold, as indicated by drill sample studies. Limited tests have shown silver to occur at about a 2:1 Au/Ag ratio in mill grade (>1.71 g/t) gold ore, ranging up to 1:3 in leach grade (0.68 to 1.70 g/t) ores. Both gold and silver seem to have been controlled by the same pre-existing faults and fractures.

GEOCHEMISTRY

Surface geochemistry was of limited use as an exploration guide at Gold Quarry due to the thick blanket of post-mineral lacustrine sediments of the Tertiary Carlin Formation. Gold values in the surface jasperoid were found to be highly variable, ranging from nil to over 2 ppm within a few metres. Gold was found to be the best geochemical pathfinder (Fig. 6 and Table 2). In general, sampling of soil, outcrop, and stream sediments all provided surface indications of the gold deposit.

The second best indicator of gold was arsenic (Fig. 7 and Table 2). Anomalous arsenic values were found to be directly associated with gold deposition. This arsenical association is common at other disseminated gold deposits, including the Maggie Creek and Carlin mines. The arsenic distribution appears to be controlled by the same faults, fractures and lithologies that control gold deposition.

Geochemically anomalous antimony, copper, lead, nickel and mercury occur in the Gold Quarry deposit (Table 2). Most of the trace elements are restricted to fault-controlled gold ore zones, so that their distribution mirrors that of gold. Anomalous zinc values usually define the carbonate lithologies and are not closely related to gold deposition.

Table 2. Gold Quarry geochemical values (distribution in parts per million)

	Whole Deposit (disseminated values)	Localized concentrations (structural values)
Gold	0.3 - 3.0 ppm	>6.9 ppm
Silver*	0.1 - 2.0	>6.9
Arsenic	<200.0	>500.0
Antimony	<50.0	200.0 - 2000.0
Mercury	<1.0	>50.0
Lead	<100.0	500.0 - 3000.0
Copper	<50.0	200.0 - 1500.0
Manganese	<200.0	500.0 - 1000.0
Nickel	<100.0	300.0 - 1000.0

* Limited Data

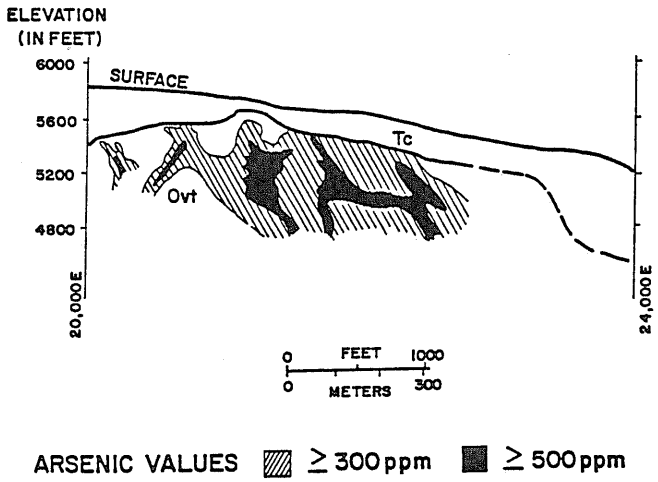

Fig. 7. General cross-section distribution of arsenic in the Gold Quarry deposit.

GENETIC MODEL

Several factors point directly to an eroded fossil epithermal/hot springs genetic model for the Gold Quarry deposit. The spacial relationship between gold deposition, jasperoids, silicified wallrock, argillized wallrock and seismic and hydrothermal brecciation are summarized in this section.

Jasperoids and silica

The concept of a silica cap and the occurrence of large silica-filled faults at Gold Quarry can be compared to the active geothermal system at Waiotapu, New Zealand, as described by Hedenquist and Henley (1985). Briefly, in the present-day system, ascending hydrothermal fluids begin to cool as they near the surface due to a decrease in hydrostatic pressure and resulting boiling and vapor loss. Below a depth of 100 m, silica is usually deposited as quartz; above 100 m silica is more often deposited as chalcedony. Almost no hydrothermal chalcedonic silica has been found in the Paleozoic rocks at Gold Quarry, indicating that any surface sinter, and the upper 100 m of the deposit, have been removed by erosion. Ore and gangue mineral deposition, as a result of boiling, serves to decrease the permeability in the upper portion of the system. Fault conduits to the surface become sealed at different rates depending on the ratio of flow rate to fracture width, temperature-pressure drop, and the periodic occurrence of tectonic activity.

A local interpretation of this concept for the fossil Gold Quarry system is sketched in Fig. 8. A highly fractured hanging wall provides channels accessible to ascending fluids when the main feeder conduit (in this case the Gold Quarry fault) becomes plugged with silica. Repeated tectonic movement and hydraulic fracturing brecciates and opens the silica plug, releas-

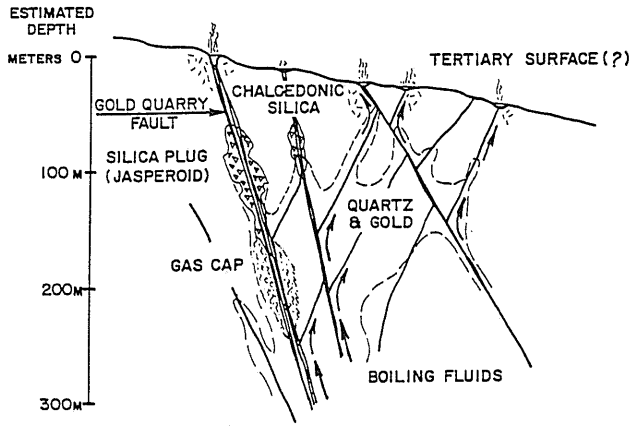

Fig. 8. Sketch section of Gold Quarry deposit during mainstage gold deposition.

ing the backpressure from below. Silicification and gold deposition in the hanging wall rock decreases when the main conduit vents to the surface. Resealing of the conduit begins, possibly lower in the system, due to a decrease in pressure (venting to the surface). The jasperoids presently exposed at the surface have developed at this point.

Jasperoid formation within the large, high-angle normal faults that border the Carlin Window can be directly linked to repeated silicification of the Gold Quarry host rocks. These faults were a part of the pre-existing plumbing system that directed the ascending hydrothermal fluids. Brecciation and silicification appear to have occurred periodically within these faults, indicating a repeated history of seismic and hydrothermal events. As these conduits became sealed near the surface, silica flooded out into the hanging-wall rocks, creating zones of varying intensities of silicification (depending on the spacial overlap of flood events). Jasperoid bodies at Gold Quarry become narrower at depth, existing over a vertical range of 75 m. This may indicate a fluctuation in depth of formation of the silica seal. Areas of "spongy" (porous, vuggy) silicification ore often spacially associated with the large jasperoid bodies, and may be further indications of a near-surface environment of formation (Berger, 1985).

Argillic alteration patterns

The spacial distribution of argillic alteration at Gold Quarry is similarly consistent with a fossil hot springs genetic model. Deer et al., (1966) note that, in laboratory experiments, acidic conditions favor the formation of kaolinite. The clay mineral assemblage at Gold Quarry reflects these conditions.

The nature of hypogene argillic alteration at Gold Quarry was probably intensifed by "acid leaching" processes. This is a supergene process, involving the formation of sulfuric acid through the oxidation of sulfur-bearing minerals or gases, and the effects of these descending acidic waters upon wallrock. Features diagnostic of a surficial alteration are relict rock structures of a siliceous residue and a kaolin-alunite zone immediately beneath (Schoen et al., 1974). The concentrations of kaolinite in the roots of Gold Quarry, beneath the central alunitic zone, are consistent with this model (Fig. 9).

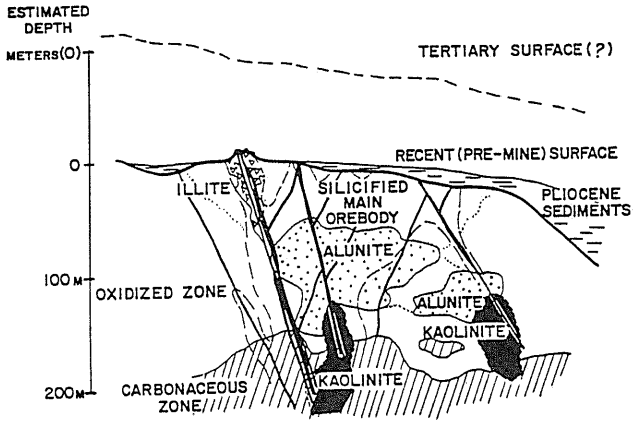

Fig. 9. Sketch section of Gold Quarry deposit before mining.

Evidence of a former hot springs environment can also be indirectly gathered from the pathfinder element assemblage at Gold Quarry. The elemental association of gold, silver, arsenic, antimony, mercury, lead, copper, manganese and nickel at Gold Quarry is similar to the group reported from the active geothermal system at Waiotapu (Hedenquist and Henley, 1985), although the concentrations vary somewhat.

Age

While the age of mineralization at Gold Quarry is still in question; recognized chronologic relationships provide relative age constraints.

The precursor to the present Humboldt River drainage system was dammed by Tertiary volcanic flows between 6 and 17 Ma. This led to sedimentation in the Pliocene basins (1.6 to 5.3 Ma) and deposition of the Tertiary Carlin Formation. Siliceous mineralized material eroded from Gold Quarry is incorporated in this formation both as basal gravels lying immediately above the unconformable bedrock contact and as gravel bars throughout the Pliocene sediments. Since erosion of the deposit occurred after the main stages of mineralization, the incorporation of gravels in the Carlin Formation places the age of mineralization as older than 6 Ma. Stewart, 1980, shows that Cenozoic igneous activity in northeastern Nevada was at its peak between 43 and 34 Ma. Intrusive rocks of this age are mineralized elsewhere, thus, mineralization is probably related to the high heat flow in this area of that time. This dating (between 43 and 6 Ma) places a probable early Oligocene age on the mainstage Gold Quarry mineralization events.

Acknowledgements — The geological evaluation of the Gold Quarry deposit has extended over many years, occupied the time and efforts of many people and is still far from complete. This paper draws upon the extensive works of these people. The author extends thanks to Donald M. Hausen for his many years of research on Gold Quarry, and to Charles Ekburg for his geological input to this paper. Thanks are also extended to Odin Christensen, Gale Knutsen, Deb McFarlane, Tyler Shepherd and Chuck Zimmerman for their review and comments on this paper. The author also extends thanks to Don Hammer, Robert Miller and Newmont Mining Corporation for permitting publication of this paper.

REFERENCES

Berger, B. R., 1985, Geological-geochemical features of hotsprings precious-metal deposits, *in* Tooker, W. E. (editor), Geological characteristics of sediment-hosted disseminated gold deposits — Search for an occurrence model. U.S. Geol. Surv., Bull. 1646, 150 pp.

Coe, J., 1983, Examination of black quartz veins at Gold Quarry: Newmont Exploration Ltd., in-house memorandum.

Deer, W., Howie, R. and Zussman, J., 1966, An Introduction to the Rock Forming Minerals: Halsted Press, p. 255-263.

Ekburg, C., 1986, General Geology of the Maggie Creek Gold Deposit, Eureka County, Nevada, *in* Tingley, J. and Bonham, H. (editors), Sediment-hosted precious metal deposits of northern Nevada. Nev. Bur. Mines Geol., Rep. 40, 103 pp.

Evans, J. and Cress, L., 1972, Preliminary geologic map of the Schroeder Mountain Quadrangle, NV: U.S. Geol. Surv., Map MF-324.

Hausen, D., 1983, Fundamental study of single rock alteration types at Gold Quarry: Newmont Exploration Ltd., Metallurgical Dept., Danbury, CT, in-house report.

Hausen, D., 1982, Early exploration and metallurgical evaluation of the Gold Quarry-Good Hope areas, Maggie Creek Mining District, NV: Newmont Exploration Ltd., in-house report.

Hausen, D., Ekburg, C. and Kula, F., 1983, Geochemical and XRD-Computer Logging for Lithologic Ore Type Classification of Carlin-Type Gold Ores, *in* Hagni, R. D. (editor), Process Mineralogy II, Applications in Metallurgy, Ceramics and Geology. Metallurgical Soc. of A.I.M.E., Warrendale, PA. p. 421-450.

Hausen, D. and Kerr, P., 1968, Fine Gold Occurrence at Carlin, Nevada, *in* Ridge, J. (editor), Ore Deposits of the United States, 1933-1967. A.I.M.E., N.Y., p. 908-940.

Hedenquist, J. and Henley, R., 1985, Hydrothermal eruptions in the Waiotapu geothermal system, New Zealand: Their origin associated breccias and relation to precious metal mineralization: Econ. Geol. v. 80, p. 1640-1668.

Ketner, K. and Smith, F., 1982, Mid-Paleozoic age of the Roberts thrust unsettled by new data from northern Nevada: Geology, v. 10, p. 298-303.

Khuen, C. and Rose, A., 1986, Temporal relationships between hydrocarbon introduction and gold mineralization/alteration at Carlin, Nevada: A tale of two fluids: A.I.M.E. 116th Annual Mtg. Abstr., p. 38.

Ramsey, R., 1973, Men and Mines of Newmont. A Fifty-Year History: Octagon Books, NY, 344pp.

Regnier, J., 1960, Cenozoic geology in the vicinity of Carlin, Nevada: Geol. Soc. Am. Bull., v. 71 8, p. 1189-1210.

Roberts, R., Hotz, P., Gilluly, J. and Ferguson, H., 1958, Paleozoic rocks in north-central Nevada: Am. Assoc. Pet. Geol. Bull., v. 42, p. 2813-2857.

Roberts, R., Montgomery, K. and Lehner, R., 1967, Geology and mineral resources of Eureka County, Nevada: Nev. Bur. Mines, Bull. 64, 167pp.

Roberts, W., Rapp, G. and Weber, J., 1978, Encyclopedia of Minerals: VanNostrand and Reinhold, p. 205-206.

Schoen, R., White, D. and Hemly, J., 1974, Argillization by descending acid at Steamboat Springs, Nevada: Clays Clay Miner, v. 22, p. 1-22.

Stewart, J., 1980, Geology of Nevada: Nev. Bur. Mines, Spec. Pub. #4.

West, P., 1976, Tuscarora survey final report: Newmont Exploration Ltd., in-house report.

Geochemistry and Geology of the Wind River Gold Prospect, A Cascade Epithermal Precious Metal System

K. I. McGowan
Department of Earth Sciences, 253 Science Hall 1, Iowa State University, Ames, IA 50011, U.S.A.

Abstract — The Wind River gold prospect, an epithermal gold-quartz vein system located in the southern Washington Cascade Range, is anomalous in terms of accepted models of Cascade metallogenesis relating ore-forming systems to a porphyry copper model. Hydrothermal alteration and geochemical anomalies associated with the Wind River system, representing expression of the hydrothermal system at different lateral and vertical distances from major fluid channels, affect rocks within a 20 km^2 area surrounding the prospect and may serve as an exploration guide. Au, Ag, As, Sb, Hg, and W are found in veins at the prospect.

INTRODUCTION

The Wind River gold prospect is an epithermal gold-quartz vein system located in the southern Cascade Range of Washington, in an area dominated by Lower Tertiary andesitic volcanic rocks of the Western Cascade Group (Fig. 1). The prospect is located on a minor tributary of the Wind River in section 9, T5N, R7E (Fig. 2) of the Wind River 15′ quadrangle. The prospect does not lie within an organized mining district, but is located approximately 16 km northeast of the Washougal district and to the south of the St. Helens mining district of southern Washington (Fig. 3). The area is 32 km north of the town of Carson, Washington, near the headwaters of the Wind River. The prospect is developed by approximately 146 m of adit driven along the No. 2 vein, and vertical exposure of 270 m is available along an exploratory roadcut zigzagging up the hill above the development adit.

The Wind River prospect differs from other mineralization in the Cascade Range in that it is a gold-quartz vein system with little or no associated base metal mineralization, and does not fit with a porphyry-related model of metallogenesis.

Although the amount of gold produced from the Wind River prospect has been relatively minor, the deposit has produced the most gold of the southwestern Washington districts. Up to 1977, 831 tons of gold ore had been shipped from the mine (Moen, 1977) representing approximately 90% of the total metal production of southwestern Washington during that same period. Poor recovery rates and low gold content of the siliceous ore have forced repeated cessation of activity and the property has changed hands many times. Currently the property is being worked by Youngquist Mining Co.

REGIONAL GEOLOGY

The Cascade Range in the Wind River area of southern Washington is composed of thick and laterally extensive deposits of Tertiary lavas and pyroclastic rocks of calcalkaline chemical affinity (Wise, 1961, 1970). These volcanic rocks have been stratigraphically divided into the informally named pre-Pliocene Western Cascade Group and the Quaternary High Cascade Group (Hammond, 1979; Hammond et al., 1977; Peck et al., 1964).

The Wind River prospect is hosted in rocks of the Ohanapecosh Formation, a Late Eocene to Middle Oligocene unit first described at Mt. Rainier National Park by Fiske and others (1963) consisting of interstratified andesitic and basaltic lava flows, pyroclastic rocks of andesitic to rhyodacitic composition, and volcaniclastic rocks. Where there has been no repetition of units by faulting, the Ohanapecosh Formation in the Wind River area is nearly 5800 m thick, and the base of the section is not exposed (Wise, 1970).

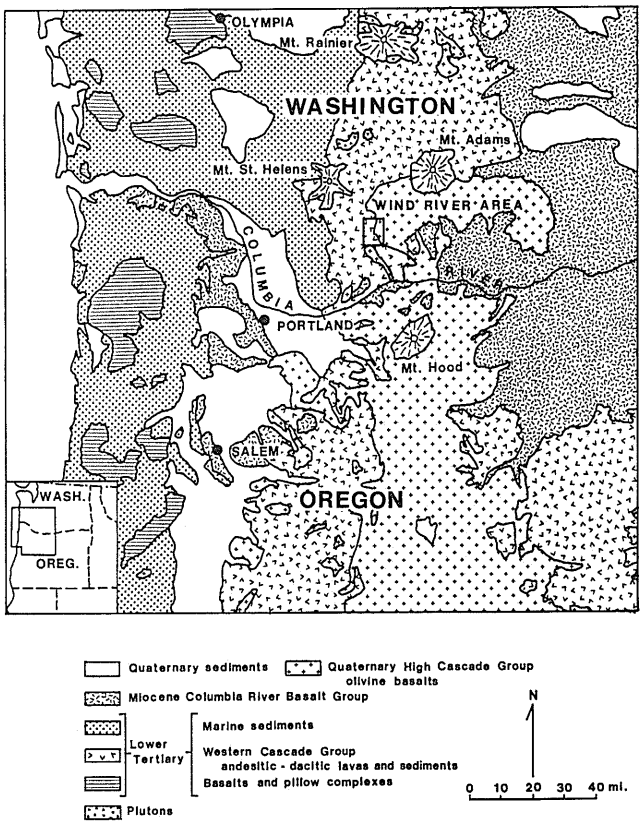

Fig. 1. General geology of the Cascade Range in Washington and Oregon and location of the study area (modified from Wise, 1970).

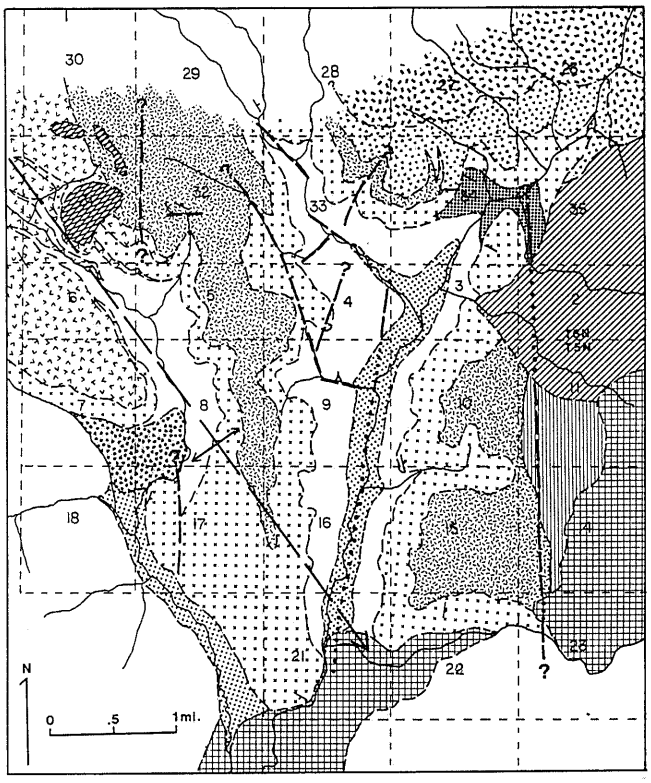

Fig. 2. Geology of the Wind River area.

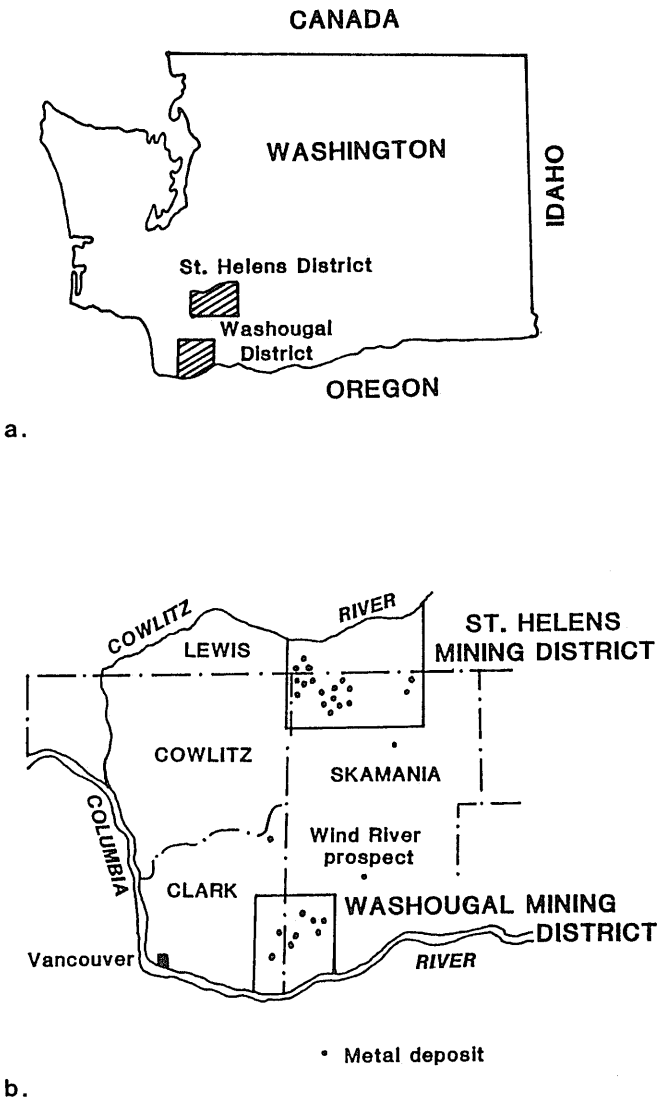

Fig. 3. Location of: (a) the St. Helens and Washougal mining districts and, b) distribution of metal deposits in these districts (modified from Moen, 1977).

The Ohanapecosh Formation is unconformably overlain by the Stevens Ridge Formation, a distinctive unit consisting of light colored, interstratified dacitic to rhyodacitic ash flow tuffs with subordinate lahars, volcaniclastic rocks, and minor porphyritic lava flows (Fiske et al., 1963; Hammond, 1980, 1974; Hammond et al., 1977). South of the study area, the Stevens Ridge Formation is unconformably overlain by the Eagle Creek Formation, a sequence of volcanic conglomerates, sandstones, and tuffs of early Miocene age (Wise, 1970). Also to the south of the study area, flows of the Yakima Basalt Subgroup of the Columbia River Basalt Group overlie the Eagle Creek Formation. Quaternary olivine basalts of the High Cascade Group erupted during the Pleistocene from vents located outside the study area are exposed in the eastern, northeastern, and southern part of the Wind River area (Fig. 2).

Hydrothermal alteration is prevalent in deeper stratigraphic levels of the Western Cascade Group, and coincides with two north-south trending belts of Upper Cretaceous to Tertiary age epizonal plutons extending south from the Canadian border (Fig. 4). The western belt ends near Portland, Oregon, while the eastern belt continues south along the western slope of the Oregon Cascades. Ages of the plutons decrease to the south in both belts, but the western belt is slightly younger than the eastern belt. Plutons of the western belt were emplaced between 35 to 15 Ma, while plutons of the eastern belt in Washington were emplaced between 50 to 25 Ma (Hammond, 1979). The intrusions have a composite magmatic history. Main phase rocks are calcalkaline and predominantly granodioritic to quartz dioritic in bulk composition, but late stage differentiates of quartz monzonite and granite are relatively common. Emplace-

ment of these late intrusive rocks appears to have been partly controlled by development of structures transverse to the regional trend (Grant, 1969).

Regional structural features of Washington are shown in Fig. 4. Major features are the Straight Creek Fault, the Olympic-Wallowa Lineament, and the Yakima folds. The Wind River area is located in a part of the Washington Cascades in which major northwest, north-northeast, and east-west regional structural trends converge, and structures paralleling all three trends are found in the area.

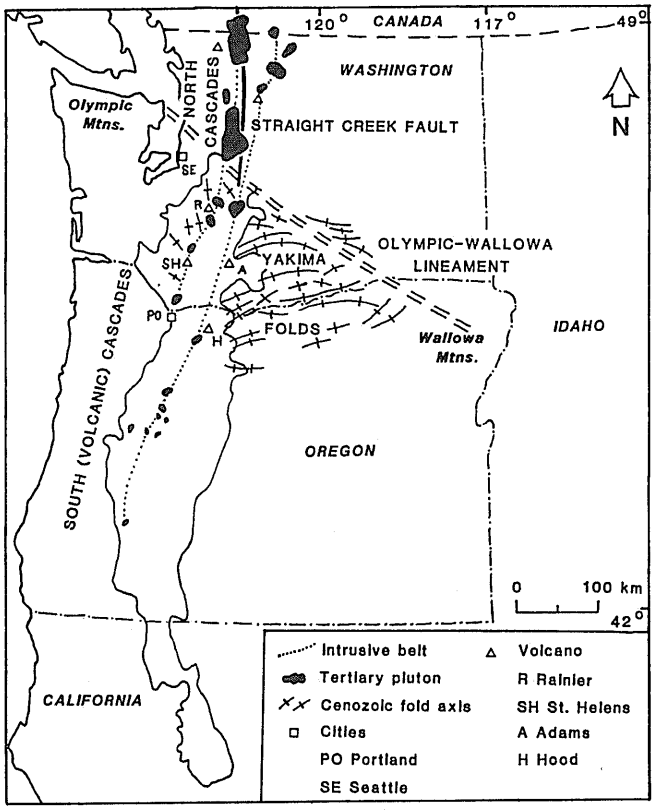

Fig. 4. Regional structural features of the Washington Cascades (modified from Hammond, 1979).

The north-south-trending Straight Creek Fault has been recognized as a major structure with large right-lateral displacement (Davis et al., 1978; Misch, 1977). In central Washington, faults associated with the southern segment of the Straight Creek Fault swing into alignment with the Olympic-Wallowa Lineament. The fundamental structure underlying this lineament is not known.

Two major fold patterns are found in rocks of the Western Cascade Group in Washington. Older, northwest-trending folds parallel the Olympic-Wallowa lineament. A younger fold pattern characteristic of the Yakima fold system of the western Columbia Plateau (Newcomb, 1970) is superimposed on the older northwest fold trend (Hammond, 1979) and has been found to extend into the Cascade Range (Beeson et al., 1982). Deformation of the Yakima folds is considered to have occurred during the period of approximately 12 to 5 Ma (Hammond, 1979).

The principal fault directions in the southern Washington Cascades are northwest and north-south. The northwest fault trend parallels the northwest fold trend and is believed to have developed at the same time (Hammond, 1980, 1979). Prominent north-south faulting in proximity to the Wind River area occurs between Mt. St. Helens and Mt. Rainier, and in the Indian Heaven and King Mt. fissure zones located between Mt. St. Helens and Mt. Adams (Hammond, 1980, 1979).

ECONOMIC GEOLOGY

Mineralization in the southern Cascade Range of Washington is considered to be of the porphyry copper type (Grant, 1969, 1982; Moen, 1977). Work done on Cascade porphyry systems in Washington and Oregon (Field and Power, 1985; Grant, 1982, 1969) indicates a systematic regional progression from south to north of increasing complexity and depth of emplacement of intrusions, Cu and Mo relative to Pb and Zn, and veinlet, disseminated, and breccia pipe mineralization relative to vein mineralization. Fluid inclusions show an increase in salinity (1-30 equiv. wt. % NaCl), homogenization temperatures (160°->385°C), and quantity of daughter minerals. These changes record a change of mineralization style from epithermal (Au-Ag) to mesothermal (Pb-Zn-Cu-Ag) to hypothermal (Cu-Mo). Deposits located in the nearby St. Helens and Washougal districts of southern Washington are porphyry copper systems where Cu is the dominant metal, with Pb, Zn, Mo, Au, and Ag also reported (Moen, 1977). Fluid inclusions contain halite daughter crystals, and salinities are greater than 26.3 equivalent weight % NaCl (Shepard, 1979). Current levels of exposure of these systems fit the mesothermal environment of Field and Power (1985).

WIND RIVER PROSPECT AREA

Wise (1961, 1970) mapped the area surrounding the Wind River prospect as a sequence of massive andesite flows within the Ohanapecosh Formation. More detailed investigation has revealed the presence of other lithologic units in the area. Geology and general stratigraphy of the area are given in Fig. 2.

The Ohanapecosh Formation comprises most of the bedrock geology of the area, and has been divided into eight subunits which are described in greater detail by McGowan (1985). The most important of these subunits are the P_1 pyroclastic sequence in which the mineralization is developed, and the A_1 and A_2 lava flow groups, which acted as a limited permeability barrier on the system.

The P_1 pyroclastics are the stratigraphically lowest subunit and consist of a sequence of crystal-bearing lithic lapilli tuffs and lithic lapilli tuffs with minor intercalated andesite lava flows. P_1 rocks are weakly to moderately altered thoughout the area by regional propylitic alteration, and more strongly altered in proximity to the hydrothermal system.

The P_1 pyroclastic sequence is overlain by lava flows which have been divided into two groups on the basis of primary textures. The sequences of lava flows are thickest in the North Butte-Middle Butte area, where they are up to 415 m thick. Individual flows in both groups are separated by flow breccias and subordinate quantities of intercalated pyroclastic rocks.

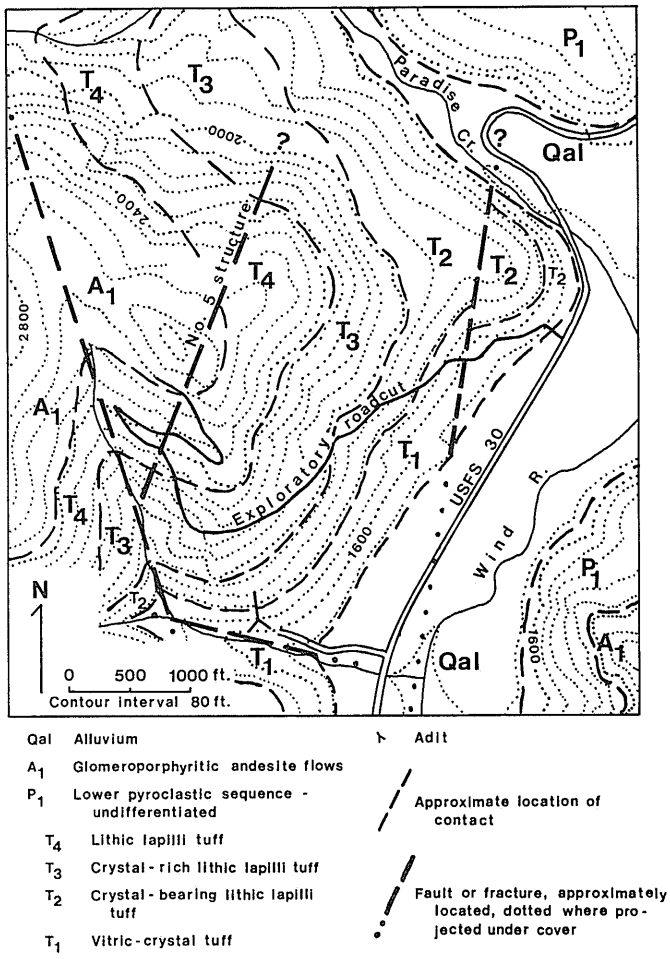

Fig. 5. Geology of the immediate vicinity of the Wind River prospect.

Flows of the lower flow group, A_1, are porphyritic to glomeroporphyritic andesites wherein the majority of the plagioclase phenocrysts occur in glomerocrysts. The upper group of flows, A_2, have finer-grained, more abundant phenocrysts than those of A_1, fewer glomerocrysts, and a groundmass with a high glass content. Away from areas affected by the hydrothermal system, lavas of the flow groups are unaltered to weakly altered.

The flow units cap the ridges and are folded by a southeast-plunging anticlinal warp over the length of Paradise Ridge (Fig. 2). Towards the west, the number of flows in the A_1 and A_2 flow groups decreases and the proportion of intercalated pyroclastic rocks increases, and the section becomes dominated by pyroclastic rocks in the western part of the area.

In the vicinity of the prospect, the P_1 pyroclastic sequence has been further subdivided into four subunits, T_1 to T_4, on the basis of field relations and textural criteria. These units are shown on the geologic map of the area immediately surrounding the prospect (Fig. 5).

Three groups of subvolcanic dikes, D_1, D_2, and D_3, have been recognized in the vicinity of the prospect. These intrusions are distinguished on the basis of degree of alteration, apparent relations to the most intensely altered pyroclastic rocks which they cut, and geochemical characteristics (McGowan, 1986). Alteration of D_1 dikes ranges from weak to strong. D_2 and D_3 dikes are weakly altered. Away from the zones of most intense alteration, it would be difficult to distinguish different groups of dikes.

Topography and stream drainage in the Wind River area are controlled by three major high-angle fracture and fault sets which parallel regional northwest, north-northeast, and east-west trends. Fracture trends along the exploratory roadcut at the prospect are most commonly oriented northwest and north-northeast. East-west-trending fractures are present but less common. The veins exposed along the roadcut also follow these trends, with the north-northeast orientation predominant. Areas of sulfide-rich, quartz-cemented brecciation have been identified associated with both north-northeast and northwest-trending fractures along Paradise Creek and its tributaries.

REGIONAL HYDROTHERMAL ALTERATION

Three associations of hydrothermal alteration and geochemical anomalies are present in the Wind River area, and affect rocks within a 20 km^2 area surrounding the prospect. Distribution of these types is shown in Fig. 6.

Type 1 alteration occurs at the periphery of the hydrothermal system at similar elevations. These zones of least intense alteration or 'rootless zones' lack readily apparent structural controls. Localized breccias found in these zones are cemented by a thin layer of massive white quartz, with coarsely crystalline euhedral quartz grown into the interstices. Calcite is found grown into open spaces in the euhedral quartz in some locations. Some of the massive quartz contains bladed cavities that are thinly coated by Fe and/or Mn oxides. Clasts in these breccias are weakly altered and contain smectites, illite, and some chlorite. Sulfide minerals have not been observed in these zones.

Geochemical anomalies of Sb to 9 ppm in quartz, and to 1 ppm in clasts from Type 1 breccias were detected. Anomalies of Au, As, or Hg were not detected in these zones.

Type 2 alteration zones are located peripheral to the main system at higher elevations. This type is found along the crest of Paradise Ridge to the west and northwest of the prospect. It occurs in larger, more continuous areas than Type 1, but also lacks obvious structural control. The rocks include strongly altered lavas and tuffs which are bleached and/or silicified. Alteration of tuff layers is in general more intense, and appears to be more laterally extensive than alteration of lavas. Silification occurs more frequently in tuffs. Kaolinite, illite, and poorly crystalline or amorphous clays are common alteration products in all rock types. No quartz veins were found in these areas, but rare, quartz-cemented breccias have been noted. The quartz matrix is very fine-grained and may exhibit 'frothy' textures. Breccia clasts are strongly altered to kaolinite, illite, and quartz. Sulfide minerals have not been observed in these zones.

Celadonite alteration has been noted peripheral to both Type 1 and Type 2 alteration zones. Where it occurs, celadonite alteration is more pervasive in tuffs, lahars, and flow breccias than in lava flows.

Geochemical anomalies of As to 10 ppm and Sb to 2 ppm were detected in rocks from Type 2 alteration zones. No Au or Hg were detected.

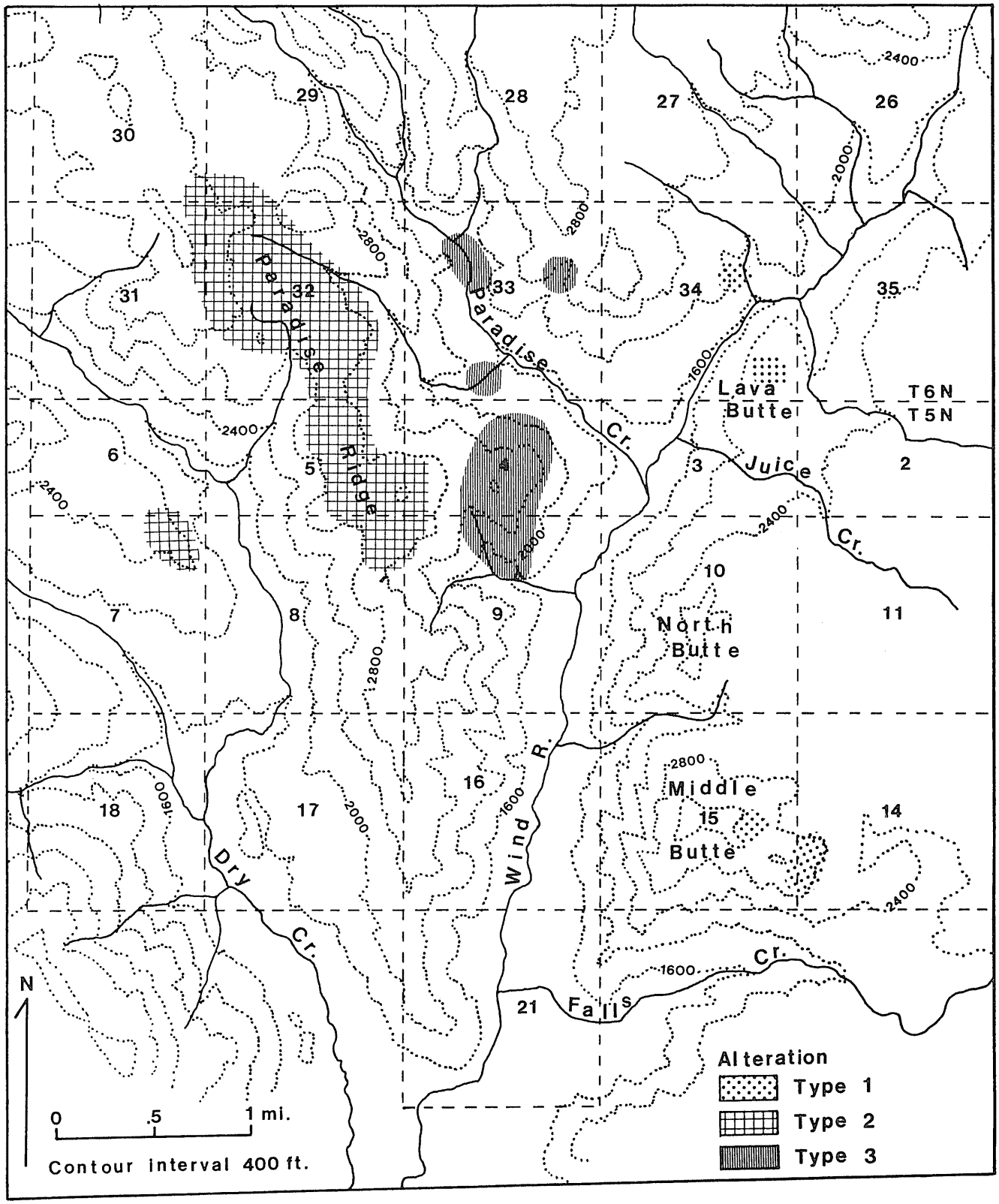

Fig. 6. Distribution of regional hydrothermal alteration types in the Wind River area.

Type 3 alteration is associated with structures, and is found at the Wind River prospect. Zoned alteration at the prospect is distributed relative to the No. 5 structure (Fig. 7) and grades from weak to intense. Large banded quartz veins cut the alteration zones. Breccias at the prospect occur marginal to the large quartz veins. These breccias are quartz-cemented and contain clasts altered to smectites, illite, chlorite, calcite, and quartz. Sulfides are not found in these breccias.

Sulfide-rich breccias are associated with fault and fracture zones along Paradise Creek and its tributaries at moderate distances from the prospect. These breccias do not appear to be vein margin breccias, but may have quartz or quartz-calcite veins crosscutting them. These breccias show evidence of multiple episodes of brecciation and cementation. Cement is fine-grained, sulfide-rich quartz and may contain drusy cavities. Clasts are strongly altered to kaolinite, illite, and quartz.

Gold to 0.4 ppm, As to 53 ppm, Sb to 24 ppm, and Ag and Hg were detected in the Paradise Creek breccias.

HYDROTHERMAL ALTERATION AT THE WIND RIVER PROSPECT

The alteration zones at the Wind River prospect are best exposed within the adit driven along the No. 2 vein, and along the exploratory roadcut which runs from USFS road 30 to the top of the lobe of Paradise Ridge located in sections 4 and 9 (Figs. 5 and 7).

The alteration is developed in the P_1 pyroclastic sequence which underlies Paradise Ridge and in the D_1, D_2 and D_3 dikes which are intrusive into the pyroclastic rocks. Detailed alteration mineralogy of these units is described by McGowan (1985). Alteration is distributed relative to the northeast-trending No. 5 structure (Fig. 7). This structure is believed to represent the high-level expression of a large quartz vein at depth, and consists of discontinuous stringers of sulfide-rich quartz in a clay matrix.

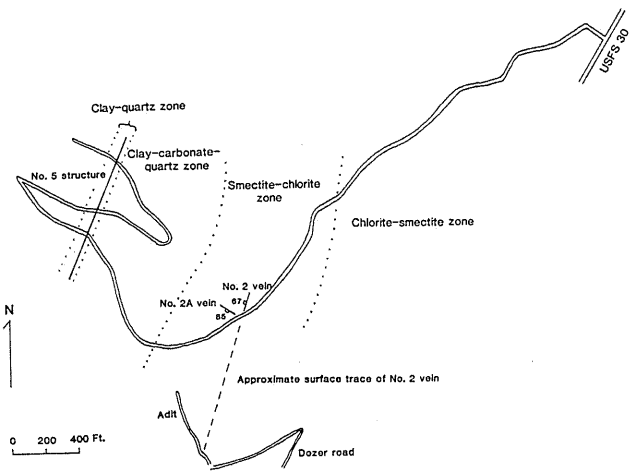

Fig. 7. Map of the exploratory roadcut and zoning of alteration about the No. 5 structure.

The most intense alteration is found in a narrow clay-quartz zone that is 16 to 31 m wide and centered on the No. 5 structure. In this zone, all primary phases are altered to illite, kaolinite, and quartz. This zone grades outward to a carbonate-clay-quartz zone containing calcite, Fe-carbonate, illite, kaolinite, and quartz. Calcite content in rocks of this zone ranges up to approximately 20%. K-feldspar and albite are present as replacement of primary plagioclase. This zone is 155 to 185 m wide on the footwall side of the No. 5 structure, and may be wider on the hanging wall.

Smectite replaces illite as the dominant clay mineral in the smectite-chlorite zone, although illite and some chlorite are also present. Quartz, albite, and calcite are other important alteration minerals. This zone lacks the heavily carbonate-dominated signature of the previous zone, and is about 245 m wide. Beyond this zone, alteration assemblages contain a higher proportion of chlorite. Yellow-brown smectite clays, quartz, albite, and zeolites are present and the alteration merges with the regional propylitic alteration.

VEINS

The prospect contains at least four mineralized quartz veins which range from 15 cm to about 2 m in width, strike north to northeast, and have dips ranging from steeply to the west to near vertical. Veins range from milky white quartz to chalcedonic, and are commonly banded to vuggy. Pyrite, although sparse, is the main visible sulfide mineral of the veins. Traces of malachite indicate the presence of copper sulfides, primarily chalcopyrite, in the No. 2 vein at the adit level. Pyrite is locally abundant in the wallrocks of the vein.

At the adit level, the No. 2 vein consists of thick, banded, milky white quartz. Calcite is intergrown with the quartz in bands, but is not evenly distributed over the length of the vein. Zones where the vein is narrow contain less calcite than wider parts of the vein. Vuggy bands in the vein are common, but bladed cavities are developed only locally.

The No. 2 vein pinches and swells several times along its length. Parts of the vein show quartz-cemented breccia 'pods' rather than a definite vein. Quartz-cemented breccias are present along both the hanging wall and footwall margins of much of the vein. These breccias grade outward to quartz-stockworked andesite or to sheared andesite zones. Wallrocks are altered to quartz, chlorite, and calcite to the extent that primary texture can rarely be distinguished.

At the level of the exploratory roadcut, the large quartz veins show development of bladed cavities lined with drusy quartz. Smaller veins consisting of chalcedonic quartz with open-space textures also crop out on the roadcut. Veins along the roadcut are often observed to be emplaced between the margins of a dike and the pyroclastic rocks into which it is intrusive.

FLUID INCLUSIONS

Primary fluid inclusions from the No. 2 vein at the adit level gave homogenization temperatures in the range of 220°C to 259°C, and freezing temperatures in the range of −0.6°C to −1.0°C. No daughter minerals were observed in the inclusions.

Comparison of the homogenization ranges with depth vs boiling temperature curves of Haas (1971) gives minimum depths of formation of 300 to 600 m for the system. The freezing ranges indicate salinities of less than 1 equivalent weight % NaCl.

TRACE METAL CONCENTRATIONS

Trace metal data for the Wind River prospect were determined by instrumental neutron activation analysis (INAA). Data for the No. 2 vein in the adit and for the No. 5 structure along the exploratory roadcut are listed in Table 1. Standards containing Ag, Hg, and/or W were not included in the INAA runs, and values for these elements in ppm are not available.

In the No. 5 structure, Au, Ag, Hg, and W were confined to the structure, and did not form detectable haloes in the wallrocks. Sb and As were found in both the structure and its wallrocks. W was detected only in the No. 5 structure.

In the No. 2 vein, Au, Ag, Hg, and Sb are concentrated in the vein. Highest Ag content appears to occur in those samples containing the most Au. Arsenic increases toward the veins, but concentrations are lowest within the veins. Quartz-cemented breccias contain less As than breccias or shears with little quartz. Sb concentrations increase toward the veins and are highest in the veins. Highest Au concentration is in the quartz veins. Quartz-cemented breccias nearest the vein contain less Au than andesite breccias at greater distance from the vein.

DISCUSSION AND CONCLUSIONS

The Wind River prospect shows a complex interplay between volcanic, hydrothermal, and structural activity. Structural trends in the Wind River area that parallel regional trends and which appear to be the most important in terms of providing foci for the flow of hydrothermal fluids are the north-northeast trend, and to a lesser extent, the northwest trend.

North-south structures in the Wind River area appear to have been the main focus for movement of hydrothermal fluids. These structures parallel the trend of the Straight Creek Fault, but any extension of the Straight Creek Fault south of the juncture with the Olympic-Wallowa lineament is apparently covered by middle to late Tertiary volcanic rocks. Davis (1977) and Schreiber (1981) suggest that the Straight Creek Fault may have extended further south during pre-Tertiary times. Reconstruction of dextral slip along the trend of the fault would place Mesozoic basement rocks as far south as the town of Stevenson, Washington (R. Miller, 1984, pers. comm.), well to the south of the Wind River area.

Much of the Quaternary volcanic activity in southern Washington is believed to have occurred on north-south-trending fissure zones, indicating that north-south structures have been active until quite recently. Whether north-south structures in the Wind River area are related to reactivation of buried southern portions of the Straight Creek Fault or to other causes acting to produce similar trends is a matter of conjecture. The possible presence of older basement rocks beneath the Wind River area might be an important factor in the development of a precious metal hydrothermal system as a source for the gold.

Alteration mineralogy of the Ohanapecosh Formation in the Wind River area was extensively studied by Wise (1961), who worked mainly in the pyroclastic and volcaniclastic sequences to the south of the present study area. He found zeolites, quartz, chlorite, calcite, celadonite, and a smectite tentatively identified as griffithite to be the most common alteration minerals. Unlike the type section at Mt. Rainier, conditions apparently did not reach the stability of wairakite or epidote in the regional alteration.

The hydrothermal alteration found in the Types 1, 2, and 3 alteration zones in the vicinity of the prospect has been superimposed on the regional zeolite-grade alteration. This alteration extends up through the A_1 and A_2 lava flow sequences and widens upward. The three types of alteration are interpreted as representing effects of the hydrothermal system at different lateral and vertical distances from major upflow channels.

Type 1 alteration represents areas where hydrothermal activity was not of sufficient duration or intensity to produce all the features associated with the main system. Intergrowth of calcite plates with quartz in Type 1 breccias and local development of bladed cavities in the quartz are textures similar to those found in the large quartz veins at the prospect. Evidence for multiple episodes of brecciation in these zones is lacking, and alteration of wallrocks and clasts is weak to moderate. Although Sb was transported into the 'rootless zones', they were not subject to extended hydrothermal activity.

The widespread Type 2 alteration found along the crest of Paradise Ridge is laterally extensive. Alteration mineralogies

Table 1. Trace metal data for the No. 2 vein and No. 5 structure.

	No. 2 vein				No. 5 structure
		marginal breccias			
	vein	quartz	andesite	wallrocks	
Au	0.07 - 26	0.01 - 1.2	0.03 - 0.5	n.d.	n.d. - 0.07
As	n.d. - 2.3	14 - 45	21 - 130	6 - 46	4 - 49
Sb	7 - 46	4 - 15	3 - 7	0.6 - 5	2 - 18
Ag	yes	—	—	—	yes
Hg	yes	—	—	—	yes
W	—	—	—	—	yes

Values in ppm. Elements which were detected, but for which concentrations in ppm are not available are designated 'yes'.

are similar to those found in intensely altered zones at the prospect but lack carbonate. Minerals typical of advanced argillic alteration such as alunite or jarosite were not detected. Trace metal anomalies of As and Sb are found in rocks from Type 2 zones, including lavas that mineralogically are not strongly altered. Similar lavas from the North Butte-Middle Butte areas do not contain these metals in detectable concentrations.

The regional Types 1 and 2 alteration are probably structurally controlled, although field evidence for this control is not evident due to poor exposures. Type 1 alteration zones were produced in response to restricted 'leaks' from the main hydrothermal system at the prospect. Host structures did not become major channels for fluid flow and did not develop into large veins. Fluid flow was not prolonged enough to produce more intense alteration of clasts and wallrocks.

Type 2 alteration is more intense, pervasive, and uniform in tuffs intercalated in the lava flow groups due to greater permeability and a higher proportion of more reactive components. The less reactive lavas would be more readily altered in proximity to structures, where greater fracture permeability allowed more interaction of the hydrothermal fluids with the rocks.

Zoned alteration at the prospect was controlled by the No. 5 structure. Intensity of alteration and concentrations of alteration metals decrease outward from the structure, which contains anomalous concentrations of Au, As, and Sb. Gold values, however, are low. The large quartz veins cutting the zoned alteration have produced haloes of As and Sb that are superimposed on the effects of the No. 5 structure.

The quartz veins at the prospect are structurally controlled, and are frequently emplaced along the same zones of weakness as the dikes. The No. 2 vein in the adit shows shearing of wallrocks parallel to vein margins, pinch and swell along its length, and vein-margin breccias. These features suggest this vein fills a fault, and that movement has occurred along the fault during the course of vein deposition.

Alteration mineralogies developed about the No. 5 structure are consistent with the model developed by Giggenbach (1981, 1984) for geothermal systems of the Broadlands type. This model is summarized diagrammatically in Fig. 8. The system is divided into a lower, magmatic-volcanic system in which CO_2 is produced, and an upper, geothermal system in which CO_2 is consumed. Major upflow zones where solutions ascend and cool such as the No. 5 structure, are characterized by silicification and K-metasomatism, resulting in alteration assemblages rich in K-clays, K-micas, or K-feldspar plus quartz. Illite is the most abundant K mineral at the Wind River prospect in and near the No. 5 structure. K-feldspar is found as a replacement mineral in the carbonate-clay-quartz zone of alteration, and K-feldspar and quartz form fracture coatings in the smectite-chlorite zone.

At increasing lateral distances from the major upflow zones, H-metasomatism is caused by attack of CO_2 on Ca-Al silicates, leading to formation of Al-enriched alteration assemblages which may contain clay minerals, micas, calcite, and quartz. Micas are not found in the Wind River alteration assemblages, but various clay minerals, calcite, and quartz are abundant. At increasing distances from the No. 5 structure, illite is replaced by smectite, then by chlorite + smectite. The scarcity of zeolites except at distances from the system may be due to a high CO_2 content favoring formation of calcite + clay minerals.

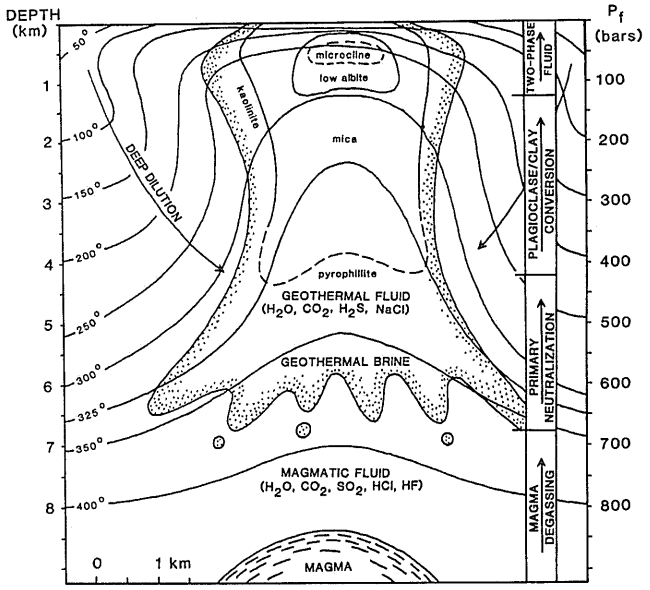

Fig. 8. Schematic cross-section of a geothermal system of the Broadlands type (from Giggenbach, 1981).

Several models for fluid flow in epithermal precious metal systems are presented by Berger and Eimon (1982). The Wind River system seems to best fit the stacked-cell convection model of open vein disposition. This model requires the presence of a stratigraphic barrier of limited permeability, impermeable enough to restrict upward movement of hot fluids, but open in places to permit mixing with higher, cooler waters and allow hydrostatic boiling at depth at temperatures of 200° to 300°C. Hot fluids are mostly confined to large, throughgoing structures, resulting in broad lateral and vertical patterns of metal zoning, and laterally extensive alteration beneath the barrier. These features are produced by a combination of fluid mixing, hydrostatic boiling, and flash boiling in overpressured systems.

The operation of this model and the evolution of the Wind River hydrothermal system with time is summarized diagrammatically in Fig. 9a-c. The A_1 and A_2 lava flow groups acted as the limited permeability barrier. Thermal fluids rose along structures until encountering the barrier. Throughgoing faults or fractures vented fluids to the surface and allowed mixing with fluids of cooler, overlying aquifers. Intermittent boiling may have taken place along the barrier due to structural breaks or incomplete sealing of the system. Major mixing or boiling activity took place where structurally produced breaks in the flow sequences allowed contact between hot thermal fluids and cooler, shallower groundwater. Violent boiling may have occurred in the upper, more fractured parts of the system. Flashing of water to steam during periods of slow recharge to open fractures would increase the amount of acid-leach alteration occurring in this part to the system. This mechanism of acid-leaching is most likely to have occurred in areas where the system was sealed and became overpressured. Boiling levels in the system may fluctuate due to intermittent sealing and overpressuring of the system.

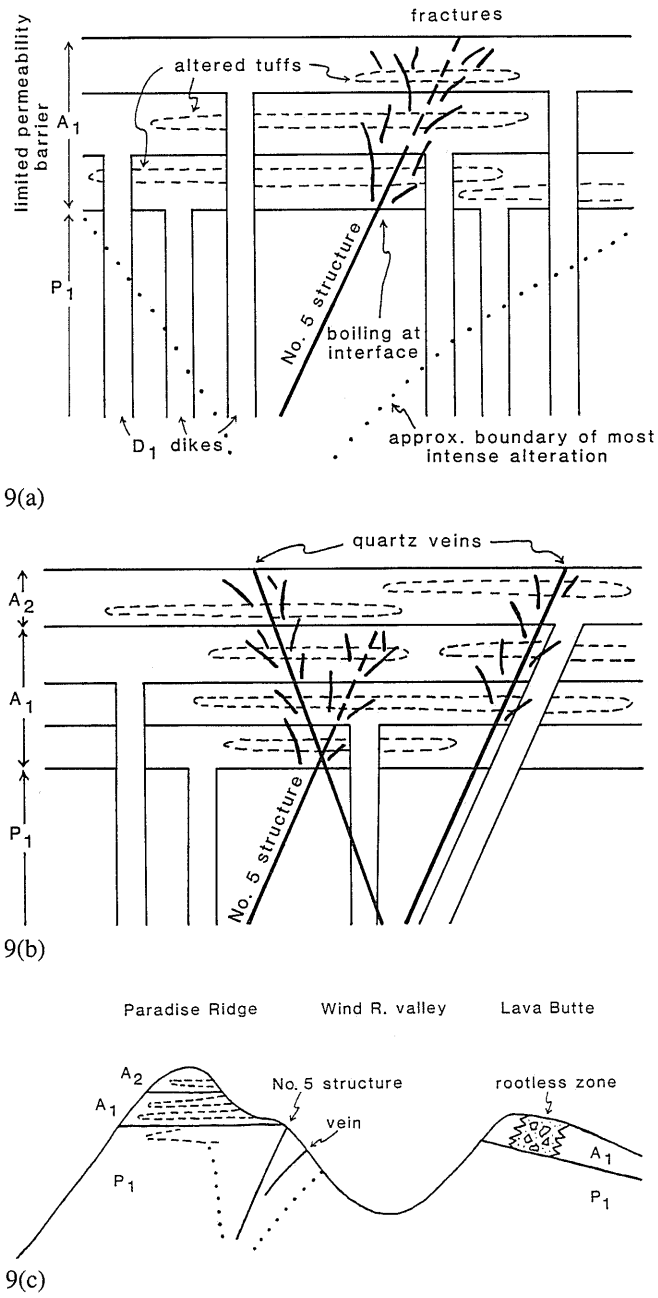

Fig. 9. (a) Flows of the A_1 group begin to be erupted and are deposited on the P_1 pyroclastic rocks. At some time during the deposition of the A_1 flows, the hydrothermal system begins to develop and is focused by structures which vent fluids to the surface. The overlying lava flows act as a barrier to the system. Differing mechanical properties cause the flows to break differently under stress than the pyroclastic rocks. Rising fluids boil in zones of fracturing of the limited permeability barrier. Release of CO_2 and H_2S forms acid condensate which produces strong alteration in the more permeable and more reactive tuffs intercalated with the flows and below the flow groups as a whole. Flashing to steam in these zones may cause pervasive alteration. Repeated, explosive rupture in zones of overpressuring below the water table produces sulfide-rich, quartz-cemented breccias. Eruption of flows continued during the life of the hydrothermal system. Strongly altered D_1 dikes represent feeders for the oldest A_1 flows. D_1 dikes of lesser alteration represent waning of the system. The hydrothermal system becomes buried by the growing volcanic pile.

(b) A_2 flows are deposited. Feeder dikes are emplaced along zones of structural weakness. Renewed hydrothermal activity produces the large quartz veins, which are frequently emplaced along zones of weakness previously intruded by dikes. Locus of boiling shifts upward relative to earlier activity, perhaps in response to changing fluid flow, water table, and paleosurface. Alteration envelopes associated with this later phase of activity overprint previous alteration in higher parts of the system which have since been removed by erosion.

(c) Higher parts of the system over the prospect are removed by erosion. Type 2 alteration on Paradise Ridge indicates previous lateral extent of erosion. 'Rootless zones' represent restricted 'leaks' from the system.

Gold distribution in the No. 2 vein suggests there may have been more than one episode of mineralization. An early pulse of weak mineralization in the structure hosting the No. 2 vein was followed by formation of quartz-cemented breccias along this structure by solutions that were barren of Au. The traces of Au in the quartz-cemented breccias can be accounted for if mineralized wallrock fragments from the previous episode of mineralization were included in the breccias. Subsequently, the structure was active during the main episode of mineralization which produced the No. 2 vein.

The Wind River prospect is spatially located between the Silver Star stock of the Washougal district and the Mt. Margaret, Goat Mt., and Camp Creek stocks of the St. Helens district. These stocks are all intrusive into the Ohanapecosh Formation and represent typical examples of southern Washington porphyry copper systems at current levels of erosion. Comparison of geochemical and fluid inclusion data for the Wind River prospect with that of the St. Helens and Washougal districts indicates that the Wind River prospect represents a shallower, cooler type of system than the south to north progression of Field and Power (1985) would allow for the part of the Cascades in which it occurs. Gold mineralization at the prospect is related to a different episode of mineralization than that responsible for the Cascade porphyry copper systems.

The thick, laterally extensive sequences of lava flows found in the study area are anomalous for the Ohanapecosh Formation as described elsewhere in Washington by other workers. The Ohanapecosh Formation in the area studied by Wise (1961, 1970), which includes the present study area, consists mainly of volcaniclastic sediments and pyroclastic rocks with minor intercalated lava flows. Wise (1961, 1970) interpreted this concentration of lava flows as representing the core of an Ohanapecosh volcano. However, there is some belief by more recent workers in the southern Washington Cascades that the massive andesite flows of the study area are not part of the Ohanapecosh Formation, but are younger and of possible Miocene age (B. Phillips, 1985, pers. comm.). The flows have not been dated.

Since the Wind River hydrothermal system postdates and may overlap deposition of the flows (McGowan, 1985), it would then be Miocene or later in age, and is different from the Cascade porphyry systems because it is related to a different volcanic-plutonic episode. Other epithermal precious metal systems may be related to this later metallogenic episode in other parts of the Cascades.

Acknowledgements — The work reported above represents part of the author's MS thesis at Portland State University in Portland, Oregon. I would like to thank the Washington Department of Natural Resources Division of Geology and Earth Resources and Mr. Milton Mitchek of the Wind River Mining Co. for partial funding of field studies of this project, and the Wind River Mining Co., and subsequently Youngquist Mining Co. for access to the property.

Thanks are due to M. Mestrovich, R. Swanson, J. Dernbach, J. Bull, K. Wilson, B. Lill, C. Burke, and D. Pierson for assistance with various aspects of the project. Valuable discussions have been had with M. Beeson, M. Cummings, P. Hammond, R. Miller, B. Phillips, and R. VanAtta. M. Beeson, M. Cummings, and A. Johnson provided helpful reviews of the original thesis.

REFERENCES

Beeson, M. H., Moran, M. R., Anderson, J. L., and Vogt, B. F., 1982, The relationship of the Columbia River Basalt Group to the geothermal potential of the Mt. Hood area, *in* Priest, G. R. and Vogt, B. F. (editors), Geology and geothermal resources of the Mt. Hood area, Oregon: Oreg. Dept. Geol. Miner. Ind., Spec. Pap. 14, p. 43-46.

Berger, B. R. and Eimon, P. I., 1982, Conceptual models of epithermal precious metal deposits: Soc. Min. Eng. AIME preprint 82-13, 14 p.

Davis, G. A., Monger, J. W. H., and Burchfiel, B. C., 1978, Mesozoic construction of the Cordilleran "collage", central British Columbia to central California, *in* Mesozoic paleogeography of the western United States, Pacific Coast Paleogeography Symposium 2, Soc. Econ. Paleontol. Mineral. Spec. Publ., p. 33-70.

Field, C. W. and Power, S. G., 1985, Metallization in the Western Cascades, Oregon and southern Washington: Geol. Soc. Am. Abstr., v. 17, p. 218.

Fiske, R. S., Hopson, C. A., and Waters, A. C., 1963, Geology of Mt. Rainier National Park: U.S. Geol. Surv. Prof. Pap. 444, 93 p.

Giggenbach, W. F., 1984, Mass transfer in hydrothermal systems — a conceptual approach: Geochim. Cosmochim. Acta, v. 48, p. 2693-2711.

Giggenbach, W. F., 1981, Geothermal mineral equilibria: Geochim. Cosmochim. Acta, v. 45, p. 393-410.

Grant, A. R., 1982, Summary of economic geology data for the Glacier Peak Wilderness, Chelan, Snohomish, and Skagit Counties, Washington: U.S. Geol. Surv., Open File Rep. 82-0408, 41 p.

Grant, A. R., 1969, Chemical and physical controls for base metal deposition in the Cascade Range of Washington: Wash. Dept. Nat. Res. Bull., v. 58, 107 p.

Haas, J. L., 1971, The effect of salinity on the maximum thermal gradient of a hydrothermal system at hydrostatic pressure: Econ. Geol., v. 66, p. 940-946.

Hammond, P. E., Reconnaisance geologic map and cross-sections of the southern Washington Cascade Range, lat. 45°30′-47°15′ N, long. 120°45′-122°22.5′ W: Portland State Univ. Dept. Earth Sci., 31 p.

Hammond, P. E., 1979, A tectonic model for the evolution of the Cascade Range, *in* Armentrout, J. M., Cole, M. R., and Terbest, H. Jr. (editors), Cenozoic paleogeography of the western United States, Pacific Coast Paleogeography Symposium 3, Soc. Econ. Paleontol. Mineral., Spec. Publ., p. 219-237.

Hammond, P. E., 1974, Regional extent of the Stevens Ridge Formation in the southern Cascade Range, Washington: Geol. Soc. Am., Abstr., v. 6, p. 188.

Hammond, P. E., Bentley, R. D., Brown, J. C., Ellingson, J. A., and Swanson, D. A., 1977, Volcanic stratigraphy and structure of the southern Cascade Range, Washington, *in* Brown, E. H., and Ellis, R. C. (editors), Geological excursions in the Pacific Northwest: Geol. Soc. Am. 1977 Ann. Mtg., field trip no. 4, p. 127-169.

McGowan, K. I., 1985, Geochemistry of alteration and mineralization of the Wind River gold prospect, Skamania County, Washington: MS thesis, Portland State Univ., Portland, OR, 136 p.

Misch, P., 1977, Dextral displacements at some major strike faults in the North Cascades: Geol. Assoc. Can., Progr. with Abstr., v. 2, p. 37.

Moen, W. S., 1977, St. Helens and Washougal mining districts of the southern Cascades of Washington: Wash. Dept. Nat. Res., Info. Circ. 60, 71 p.

Newcomb, R. C., 1970, Tectonic structure of the main part of the basalt of the Columbia River Group, Washington, Oregon, and Idaho: U.S. Geol. Surv., Misc. Geol. Invest. Map I-587.

Peck, D. L., Griggs, A. B., Schlicker, A. G., Wells, F. G., and Dole, H. M., 1964, Geology of the central and northern parts of the western Cascade Range in Oregon: U.S. Geol. Surv., Prof. Pap. 449, 56 p.

Schreiber, S. A., 1981, Geology of the Nelson Butte area, south-central Cascade Range, Washington: MS thesis, Univ. of Wash., Seattle, WA, 80 p.

Shepard, R. J., 1979, Geology and mineralization of the southern Silver Star stock, Washougal mining district, Skamania County, Washington: MS thesis, Oregon State Univ., Corvallis, OR, 113 p.

Tabor, R. W., Frizzell, V. A., Vance, J. A., and Naeser, C. W., 1984, Ages and stratigraphy of Lower and Middle Tertiary sedimentary and volcanic rocks of the central Cascades, Washington-application to the tectonic history of the Straight Creek Fault: Geol. Soc. Am. Bull., v. 95, p. 26-44.

Wise, W. S., 1970, Cenozoic volcanism in the Cascade Mountains of southern Washington: Wash. Div. Mines Geol., Bull. 60, 45 p.

Wise, W. S., 1961, The geology and mineralogy of the Wind River area, Washington, and the stability relations of celadonite: PhD dissertation, The Johns Hopkins Univ., Baltimore, MD, 258 p.

Geology and Soil Geochemistry of the Quesnel River Gold Deposit, British Columbia

P. E. Fox
Fox Geological Consultants Ltd., 1409 - 409 Granville Street, Vancouver, B.C. V6C 1T8

R. S. Cameron
Fox Geological Consultants Ltd., 1409 - 409 Granville Street, Vancouver, B.C. V6C 1T8

and

S. J. Hoffman
B.P. Canada Inc., Selco Division, 700 - 809 West Pender Street, Vancouver, B.C. V6C 1K5

Abstract — The Quesnel River (QR) gold deposit is situated near the eastern edge of the Intermontane Belt of British Columbia in a northwesterly-trending volcanic-plutonic assemblage of Upper Triassic-Lower Jurassic rocks. The QR deposit comprises two separate zones within a series of Triassic-Jurassic basaltic lavas, breccias and tuffs close to a small diorite stock. Host rocks are pyritic and intensely propylitized.

Routine sampling of glacial tills led directly to the discovery of both zones. Two clearly defined dispersion trains were obtained in which down-ice dispersion of gold and pathfinder elements (As, Co, Fe, Sb, Cu, Cd, Pb) are well defined for about one kilometre from bedrock sources.

INTRODUCTION

The QR gold deposit lies in the interior plateau country of central British Columbia some 60 kilometres southeast of Quesnel. The deposit, owned by Dome Exploration (Canada) Limited, was discovered during a regional reconnaissance program in 1977. Considerable exploration and development has been done since that time. Some 6,500 kilograms of gold reserves have been outlined to date. Routine geochemical prospecting of glacial tills led directly to the discovery of two mineralized zones within the property limits.

Fig. 1. Location Map. Quesnel River gold deposit.

REGIONAL GEOLOGY

The QR gold deposit is situated near the eastern edge of the Intermontane Belt in a northwesterly-trending assemblage of Upper Triassic-Lower Jurassic volcanic rocks often referred to as the Quesnel Trough or Quesnel Belt. The Quesnel Trough forms part of a volcanic belt that stretches from the 49th parallel to 57°N comprising rocks of the Nicola, Takla and Stuhini Groups (Preto, 1979). Detailed petrologic and stratigraphic studies were undertaken in the 1970's by Lefebure (1976) and Preto (1979) in the Nicola group and by Morton (1976) and Bailey (1976, 1978) in the Horsefly and Morehead Lake areas.

In the vicinity of the QR gold deposit, a narrow belt of mafic and felsic volcanic rocks, comagmatic dioritic stocks, and a variety of sedimentary rocks form the Quesnel Trough. The belt is crudely symmetrical about a central axis of felsic volcanic rocks flanked to the east and west by mafic volcanics and flyschoid sediments respectively. The eastern margin is complexly deformed and represents a zone of thrusting where the Intermontane Belt has been thrust over the Omineca Crystalline Belt to the east (Rees, 1981). The western margin is in fault contact with the Cache Creek Group, possibly along extensions of the Pinchi fault.

The oldest rocks are basaltic sandstone and conglomerate, minor volcanic breccia, limestone and argillite (Bailey, 1976). These rocks make up much of the eastern flank. Overlying these sediments and comprising much of the volcanic belt are some 5000 metres of mafic volcanic rocks of shoshonitic composition. These rocks are green and maroon autobreccias, pillow breccias, pillow lavas and massive flows all overlain by a thin succession, as much as 300 metres thick, of shelf-like limestone, calcareous argillite, siltstone and calcite-cemented basaltic tuff and breccia.

The sedimentary member is covered by a thick sequence of felsic breccia up to 2500 metres thick in which massive flows and compact monolithologic tuff breccias predominate. These

proximal rocks merge outward from eruptive centres to heterolithic epiclastic breccias and sediments.

A linear belt of alkalic stocks composed of diorite, monzonite and syenite lies within the volcanic strata and marks the eruptive centres of the felsic rocks. These stocks intrude their felsic extrusives and commonly alter the surrounding rocks. The stocks are the hosts for several alkalic suite porphyry style mineral deposits, namely Copper Mountain, Afton, and the Cariboo-Bell deposit ten kilometres south of the QR property.

Rock geochemistry of the volcanic and intrusive rocks of the Quesnel Trough is unique (Bailey, 1976; Morton, 1976). In general the geochemistry can be summarized as being alkalic, total alkalies >5%, TiO_2 <1.0%, and moderately undersaturated with respect to silica. Most rock types have up to 5% normative nepheline. Rocks of this chemical composition in orogenic environments are comparatively rare. The closest analogy to the Quesnel Trough is a narrow chain of recent islands east of New Ireland, Papua New Guinea (Johnson et al., 1976). In this case the tectonic setting of the islands is unclear. No evidence exists for an active subduction zone beneath the islands. Johnson et al. (1976) postulates a model whereby the island chain overlies a unique zone of deep faults related to a zone of isostatic readjustment.

LOCAL GEOLOGY

Local stratigraphy within the vicinity of the QR deposit consists of four main units that strike easterly and dip moderately south. Geological plans are given in Figs. 2 and 3. The lowermost unit (Unit 1) consists of at least 850 metres of monolithologic alkali basalt in which chaotic autobreccias are common. Pillow breccias, pillow basalts, massive flows, and thin interbeds of basaltic wacke are less common. The most common rock is an intergranular porphyritic alkali basalt consisting of 20% euhedral augite phenocrysts and 10% tabular plagioclase phenocrysts enclosed by a fine grained matrix. Olivine and analcite phenocrysts are present in thick mafic-rich flows immediately to the northwest. Flows of hornblende-bearing basalt occur near the top of the basalt formation.

Unit 1 grades upwards into poorly sorted blocky basaltic conglomerate and breccia (Unit 5). Textures are dominantly epiclastic with large framework-supported clasts of basalt in a matrix of fine grained fragments and basaltic debris. The matrix contains grey, sparry calcite and fine grained framboidal and colloform pyrite. This unit varies from less than five metres to over 250 metres thick and locally grades upwards and laterally into calcite-cemented hydroclastic coarse tuffs and lapillistones

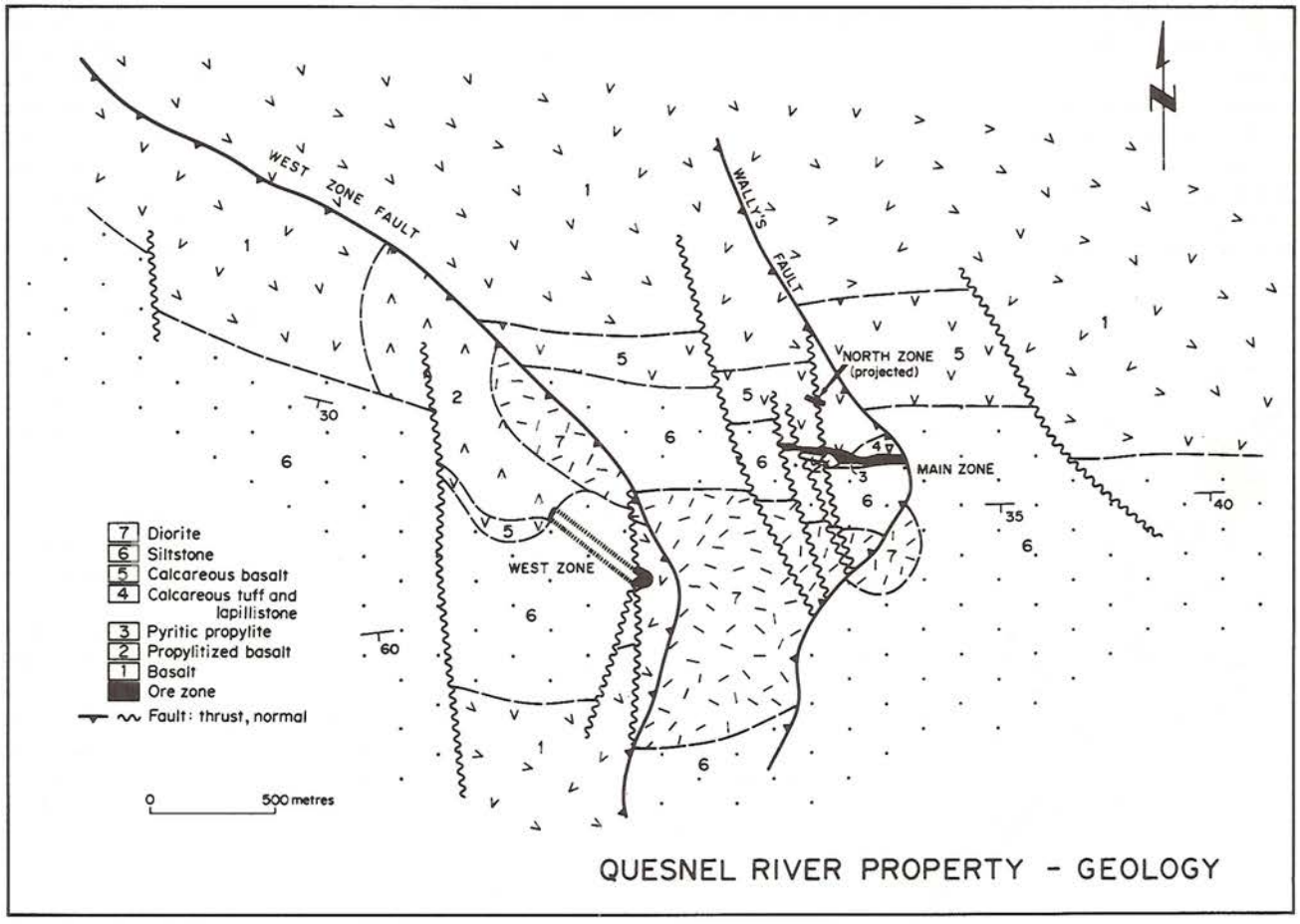

Fig. 2. Surface plan of the Quesnel River gold deposit. Subcropping positions of the ore zones are shown in black. Hach marks at the West zone represent the projected position of the deposit.

(Unit 4). Volcanic textures within the fragments are commonly obscured by intense carbonate alteration (Melling, 1982). Pyrite content varies from 5% to over 20%. Delicate framboidal, colloform and banded textures are common. Ripup clasts of banded pyrite suggest that pyrite deposition was contemporaneous with deposition of the volcanic sediments. This unit varies from four metres to 50 metres in thickness.

A thinly bedded, fissile black argillite and siltstone unit at least 200 metres thick (Unit 6) overlies rocks of Unit 4. The unit is locally calcareous and contains up to 10% fine grained disseminated pyrite and trace amounts of graphite.

The QR stock and related hornblende porphyry dykes and sills intrude and alter the above rocks. The QR stock is a body of medium grained, equigranular diorite measuring 1000 metres by 1500 metres. The stock consists of a diorite margin 100 metres thick enclosing a core of monzodiorite and rare syenite. The intrusive rocks typically consist of 15% augite, 20% biotite, 50% tabular subhedral plagioclase, 10% or less pink K-feldspar and variable amounts of magnetite. A potassium/argon date obtained from biotite collected by A. Panteleyev (personal communication) returned an age of 201 ± 7 Ma.

Surrounding the stock is a halo of altered rock that extends up to 300 metres into the surrounding basalts and sediments. Basaltic rocks are variably propylitized and the siltstone is hornfelsed to a sericitic, bleached, massive, fine grained rock. Gold mineralization is located within the alteration zone in altered equivalents of Units 4 and 5 and in the hornfelsed sediments. These rocks are described in more detail in the following section.

The volcanic rocks and sediments are in most areas undeformed. Penetrative fabrics are absent and fold structures are rare. The main structural element of the deposit is a series of subparallel northwesterly trending, west-dipping normal faults. These faults lower the main basalt-siltstone contact progressively to the west.

The youngest structural features are two low angle faults, Wally's fault and the West zone fault. Wally's fault strikes northwesterly and dips 20° southwest. It is a reverse fault that truncates the main gold zone. The western hanging wall has been displaced about 240 metres to the southeast. The West zone fault is located 1100 metres west of Wally's fault and also strikes northwesterly but is steeper with a 35° dip to the southwest. Absolute displacement has not been determined but movement of the hanging wall is estimated to be at least 500 metres to the northeast, making it dominantly a thrust fault. Both the West zone fault and Wally's fault are composed of anastamosing, foliated, chlorite-rich gouge zones and fracture zones up to a combined thickness of 30 metres. At surface they are the loci of narrow swamps, bogs and shallow depressions.

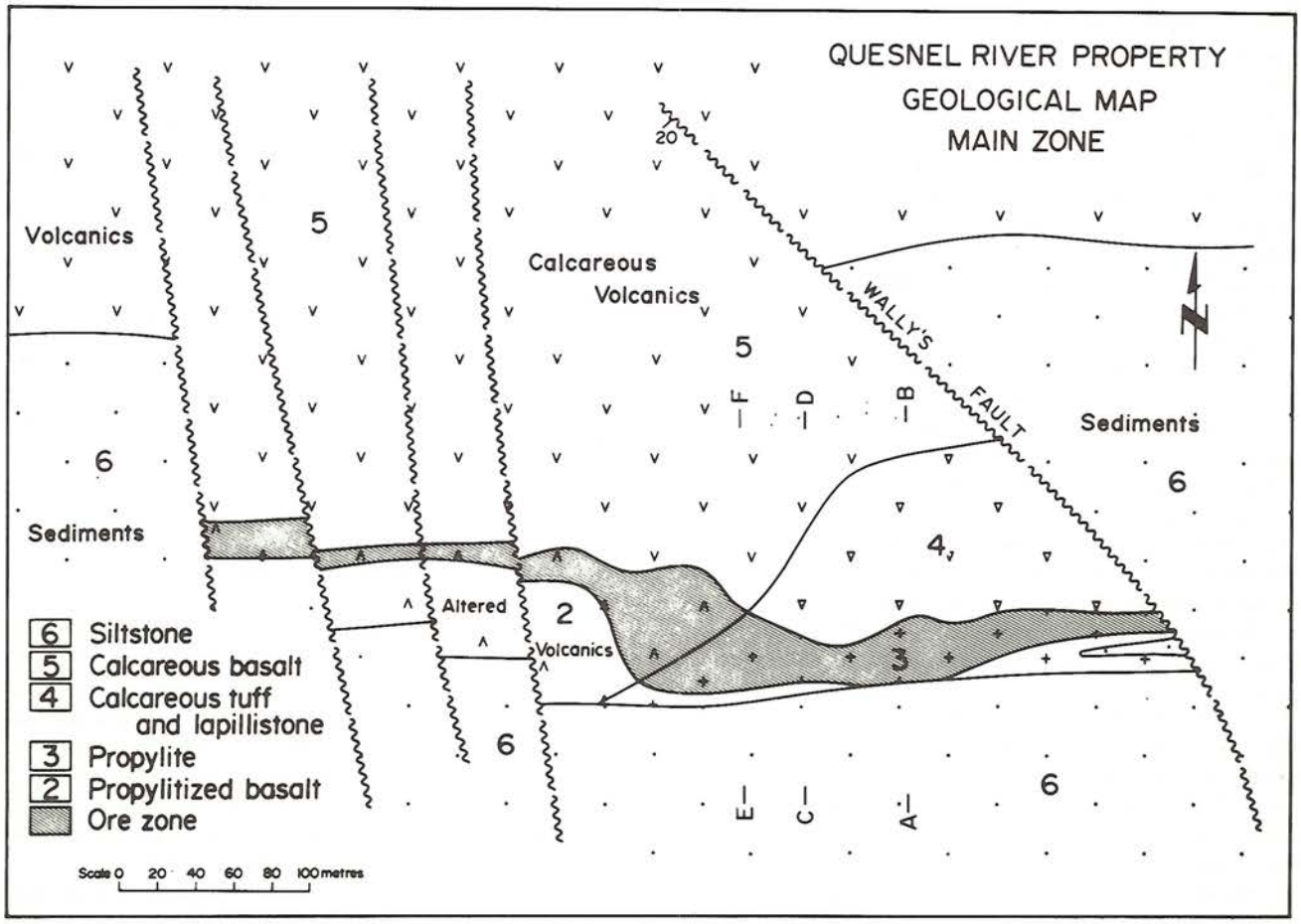

Fig. 3. Geological map of the Main zone deposit. Mineralized zone shown by ruled area. See Fig. 4 for cross sections A-B, C-D, E-F.

ALTERATION AND MINERALIZATION

The QR gold deposit comprises two separate zones: the Main zone, which was the initial discovery in 1977; and the West zone deposit discovered in 1983. Both zones are hosted by propylitically altered equivalents of pyritic, carbonate-altered basaltic rocks lying beneath the siltstone unit.

The Main zone (Figs. 3, 4) is a discordant, north-dipping body approximately 300 metres long. Two ore types are present; pyritic stockworks in propylitized basalts of Unit 2, and disseminated pyrite in massive, propylitized basaltic tuffs of Unit 3. Propylitic basalts of Unit 2 are mottled green, epidote-rich hornblende-augite porphyries that comprise the western part of the mineralized zone. In addition to the basalt mineralogy, these propylitized rocks consist of variable amounts of pyrite, chlorite, fine grained disseminated epidote, epidote-rich selvages on pyrite-carbonate veinlets, and thin pyrite-epidote coatings on fractures. Pyrite is abundant, commonly 2% to 5%, and forms disseminated grains, coarse aggregates and pyrite-rich stringers up to 3mm thick.

Unit 3, which comprises the eastern portion of the mineralized zone, is a massive, epidote-pyrite-carbonate-chlorite rock (propylite) commonly interlayered with altered basalts of Unit 2 to the west. This unit is also interbedded with siltstones and greywackes of Unit 6. Rocks of the propylite unit are typically green, medium grained, massive lapillistone and coarse tuff consisting of equigranular aggregates of epidote, pyrite, carbonate, altered rock particles and lesser amounts of chlorite and andradite. Pyrite content varies from 2% to massive sulphide lenses containing up to 80% pyrite. Granular or clastic textures in which aggregates of epidote and pyrite enclose soft, sericite-rich lithic fragments 2 mm to 5 mm in size, are typical. Large clasts of propylitized basalt are equally common. Pyrite forms irregular aggregates up to 5 mm and occasionally rounded framboids. Chalcopyrite is present in amounts up to 5% but generally occurs as irregularly shaped masses comprising much less than 1% of the rock.

Gold occurs as finely disseminated micron-sized particles along pyrite and chalcopyrite grain boundaries. The gold:silver ratio is 1:1. The best and most consistent gold assays are obtained within 50 metres of the alteration front. Isolated auriferous rocks occur well back of the alteration front and in the overlying sediments where the gold is fracture-related. Such zones, however, are discontinuous and gold tenor is erratic.

The West zone, a tabular body some 400 metres long, lies 800 metres west of the Main zone deposit (Fig. 5). An open syncline brings the deposit to surface at its northern terminus and a normal fault brings a section of it to surface at its southern end. Elsewhere, it lies approximately 50 metres below surface.

The West zone deposit, like the Main zone farther east, lies at the contact between well bedded siltstone and underlying variably altered basalt. Rocks of Unit 4 are three to five metres thick and are composed of pyritic, calcareous basaltic tuff, basaltic wacke, and breccia. The West zone deposit is composed of propylitized basaltic tuff, breccia, interbedded lenses of pyritic siltstone and discontinuous seams of massive sulphide all lying within a zone of propylitic rock surrounding a faulted remnant of the QR stock northeast of the deposit. Sulphides are mostly pyrite with lesser amounts of pyrrhotite, chalcopyrite and traces of arsenopyrite and galena. Coarse gold up to 1 mm in diameter has been observed in drill core. The best gold tenor is located close to the outer edge of the propylitic zone.

Whole rock analyses were done on drill core from two bore holes that straddle the southwestern edge of the zone of propylitic alteration (Table 1). Hole 118 is barren and lies approximately 10 metres outside the propylitic alteration front. Hole 117 has four metres of propylitic basalt and massive propylite rock that grades 6.65 grams per tonne gold. Table 1 compares average whole rock compositions of core from these two holes. The propylite horizon in hole 117 is compared to its unaltered equivalent in hole 118, a calcareous lapillistone. The underlying barren basalts intersected in both holes are also compared. The ore horizon is enriched in total iron, MgO and MnO and strongly depleted in total alkalies compared to the unaltered calcareous lapillistone. Of particular note is the initial low silica and high calcium contents. Rocks from both the West zone and the Main zone are undersaturated in silica and hence quartz is not present.

Table 1: Comparison of equivalent rock types on either side of the alteration Front, West zone, QR property

	Basalt Unit 1 n=6 DDH 117	Basalt Unit 1 n=5 118	Propylite Unit 2 & 3 n=7 117	Tuff Unit 5 n=5 118
SiO_2	45.60	44.89	41.98	41.01
Al_2O_3	15.16	15.78	12.92	14.51
Fe_2O_3	11.60	10.81	15.63	7.22
MgO	6.36	5.72	4.98	2.28
CaO	13.42	11.75	16.77	17.75
Na_2O	1.64	2.90	1.43	3.60
K_2O	1.49	1.59	.82	2.47
TiO	.76	.83	.64	.45
P_2O_5	.53	.58	.36	.30
MnO	.32	.26	.43	.25
Cr_2O_3	.01	.01	.04	.01
LOI	3.10	4.04	3.77	9.62

Hole 118 — Outside the alteration front
Hole 117 — Mineralized

DEPOSIT SUMMARY

Approximately 6500 kg of gold are contained within two zones on the QR property. Both the Main zone and the West zone are stratabound, occurring within a horizon composed of epiclastic, pyritic, calcareous, basaltic rocks. Gold deposition took place within a propylitic alteration halo developed around a zoned alkalic stock with the best gold tenor obtained at the sharp reaction front. Genesis of the deposit is directly related to ongoing evolution of the volcanic pile, the principal features of which are shown in Fig. 6 and summarized below.

(I). Mafic submarine volcanics of shoshonitic composition are deposited from fissure style eruptions. No textural zoning within the basaltic pile is present to indicate any central vol-

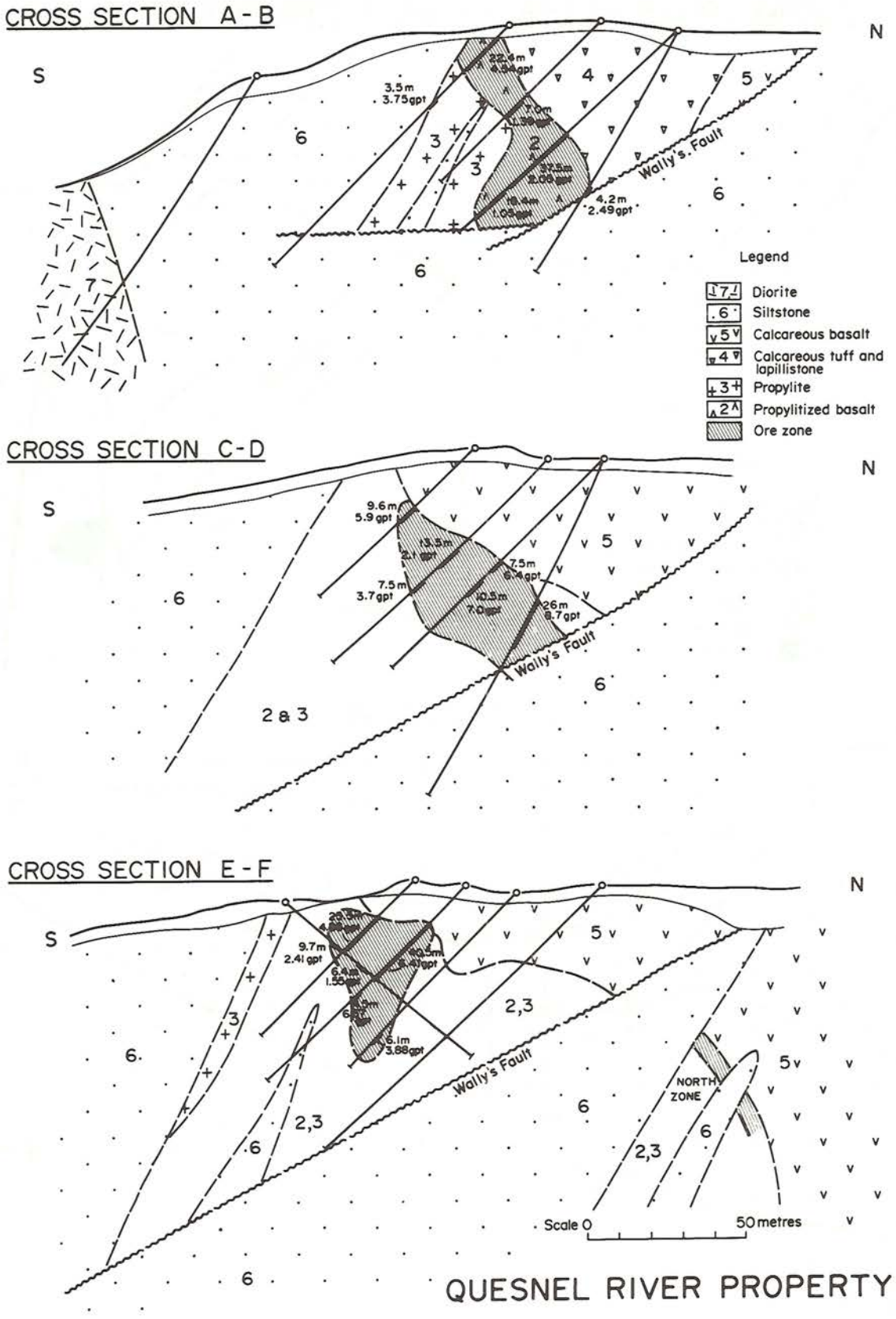

Fig. 4. Cross sections for the Main zone deposit (see Fig. 3 for location). Intercepts in metres and gold content in grams per tonne.

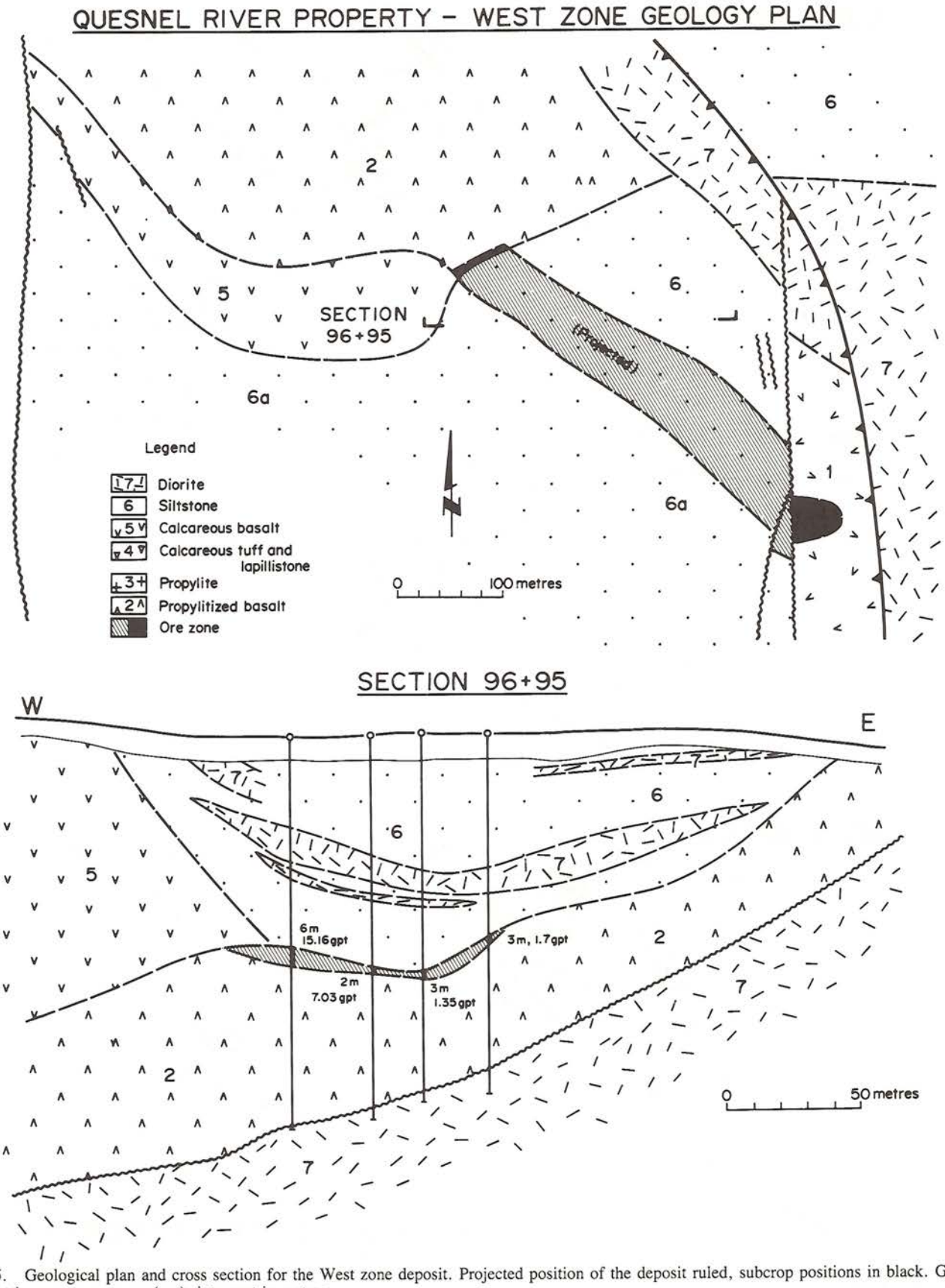

Fig. 5. Geological plan and cross section for the West zone deposit. Projected position of the deposit ruled, subcrop positions in black. Gold content in grams per tonne (gpt), intercept in metres.

canic centres. During the waning stages of the mafic phase, a brief volcanic hiatus allows the development of shelf-like limestones and calcareous sediments. Remnant heat flow from the mafic volcanics or perhaps the initial development of the central volcanic centres present during the subsequent felsic volcanic phase results in local fumarolic activity. This activity results in pyrite-carbonate alteration of basaltic units near the top of the pile. Pyrite precipitates forming fine grained framboidal, colloform masses and bedded textures accompanied by sparry calcite cement. Traces of chalcopyrite in this horizon and local beds of massive pyrite suggest that massive sulphide deposits may have formed at this time. Gold is not present at this stage.

(II). Rapidly rising, differentiating, silica-poor diorite stocks begin to intrude the volcanic pile. Felsic breccias and flows are erupted from central volcanoes. Fragments of the stock and the surrounding basaltic rocks are often taken up in eruptive breccia flows. Felsic rocks quickly grade outward from volcanic centres into distal volcaniclastic and epiclastic equivalents. Possible auriferous exhalative horizons may form at this time within proximal felsic strata.

(III). Eventually the alkalic stock, now strongly differentiated, intrudes its own volcanic extrusives. Possible caldera collapse provides a plumbing system for a convection system of heated, acidic, oxidizing meteoric and/or magmatic fluids. Gold is taken into solution from the surrounding rock mass or contributed directly from magmatic fluids. When gold-laden solutions encounter the pyrite-carbonate horizon, formed in Stage I, the strong pH, Eh barrier precipitates gold from solution at the reaction front forming a QR-type gold deposit. High in the convective system no favourable host rock is present and the system diffuses into a large, low grade porphyry copper deposit.

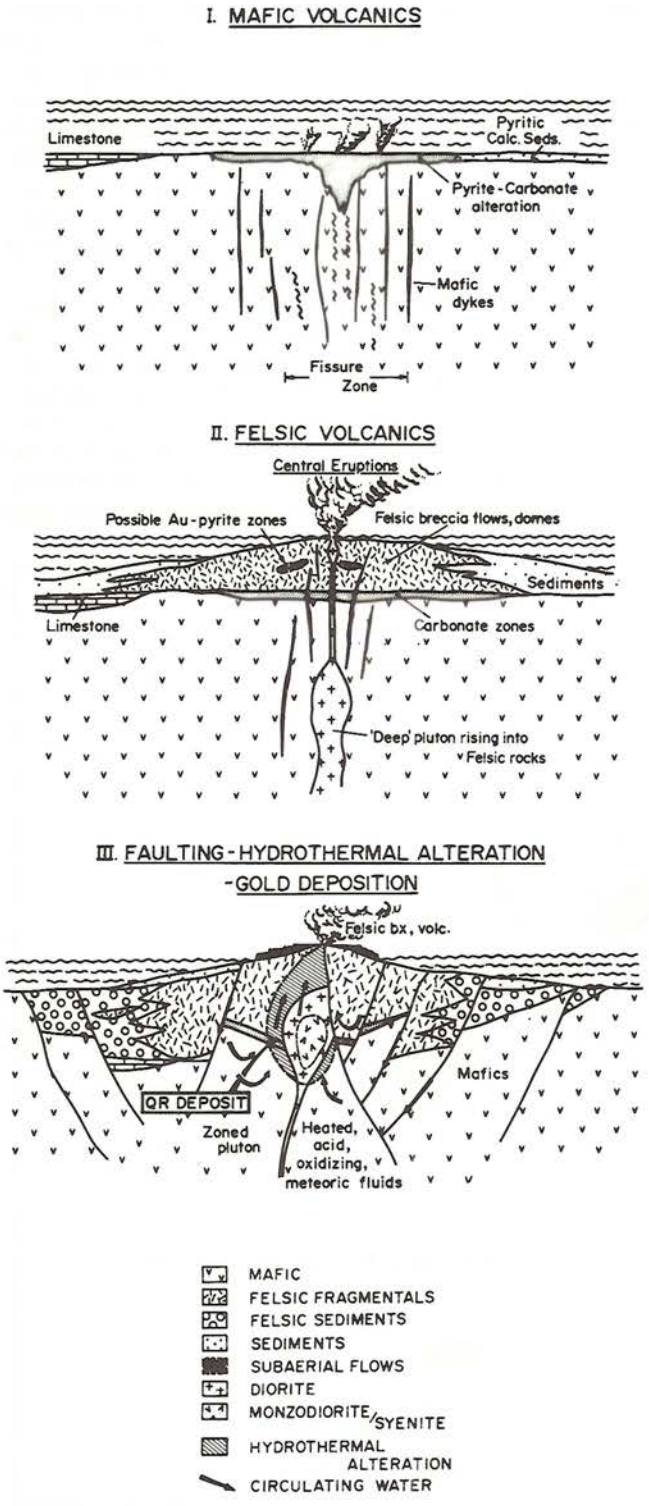

Fig. 6. Geological model depicting the evolution of the QR gold deposit. See text for explanation.

GEOCHEMISTRY

Sampling of glacial tills led directly to the discovery of both mineralized zones within the QR property. Early sampling work, which led to the Main zone discovery, was done on an 80 m x 100 m sampling grid. Later sampling, which led to the West zone discovery, utilized a 40 m x 100 m grid over the critical basalt-siltstone contact. All samples are of surface till material taken 10 cm to 20 cm below a thin layer of organic debris and forest litter. Glacial materials comprise a hard, compact, single stage lodgement till three to five metres thick. The till is extensive, essentially flat, and mantles virtually all of the underlying bedrock except for areas of hilly outcrop east and west of the deposit and on steep, talus-covered slopes on the north side of the Quesnel River. Ice movement based on grooves, bedrock striations and boulder trains is to the northwest. The Quesnel River valley was ice-dammed producing thick lacustrine deposits. Much of this material has been eroded and has now slumped to the valley floor. A thin layer of talus and other colluvial material remains on steep hillsides north of the Quesnel River.

The sampling program comprised 2,700 till samples from which 10-gram subsamples were analyzed for aqua regia leachable metals by ICP, gold being determined separately by atomic absorption following aqua regia digestion. Figs. 7 and 8 are contour maps for gold and arsenic content respectively. Summary maps for Mo, Fe, Co, Sb, Zn, Mg and V are provided in Figs. 9 and 10. Ice direction and the till-talus boundary are noted for each map.

Geochemical patterns in soils surrounding the QR deposit form four major anomalous zones. Two lie within the glacial

environment of the plateau area north of the Quesnel River valley and have a northwesterly trend. Two zones lie within a steeply sloping region of talus fans and colluvium immediately north of the Quesnel River. The four main zones are summarized below:

(1) Main Zone: Down-ice dispersion of 500 metres to 1000 metres is seen for gold, copper (weak), iron, cobalt, and antimony. Accompanying arsenic and vanadium are displaced to the east of the deposit whereas molybdenum lies peripheral on both the east and west margins of the subcropping ore zone. A magnesium feature lies to the north of the deposit whereas a series of calcium anomalies complement the arsenic signature, lying to the east of the ore zone. The anomaly peak of 300 ppb gold coincides with its source area, a tabular body 200 metres long lying at right angles to the regional ice direction.

(2) West Zone: Down-ice dispersion in the order of at least 1000 metres is seen for gold, arsenic, zinc (weak), lead (weak), vanadium, molybdenum and cadmium (weak). The presence of lead, zinc and cadmium and absence of cobalt, antimony, iron and nearby magnesium patterns differentiate the soil expression of the West zone deposit from the Main zone. Bedrock sources additional to the West zone are anticipated to explain the 3 km long gold-arsenic anomaly. In contrast to the Main zone, the gold anomaly peaks are notably displaced down-ice from their bedrock sources.

(3) A large geochemical anomaly southeast of the Main zone deposit is found in a steeply sloping, talus fan-colluvial environment. Anomaly dimensions are approximately in the order of iron = copper = vanadium>cobalt>molybdenum> antimony >bismuth. Metal zonation, whereby the centre of each anomaly shifts eastward, is seen for gold, molybdenum, antimony and bismuth. Arsenic contents are high around the eastern and northeastern margins of the gold zone whereas lead is elevated along the northern and southern boundaries of the metal-rich area. Source rocks are erratically mineralized siltstones east of the QR stock. Preferential erosion of fracture-related gold results in an enhancement of gold in talus fines at the eastern end of the metal-rich area.

(4) A smaller zone similar to (3) above in the same landscape environment lies about 500 metres to the west of the copper-iron outline of (3). The anomaly is described by elevated levels of copper, gold, molybdenum, cobalt, vanadium, iron and lead. Maximum anomaly dimensions are in the order of 200 metres to 400 metres across, and accumulation of one element relative to another is slightly displaced, for example, copper lying upslope of gold. Most outstanding is a very large

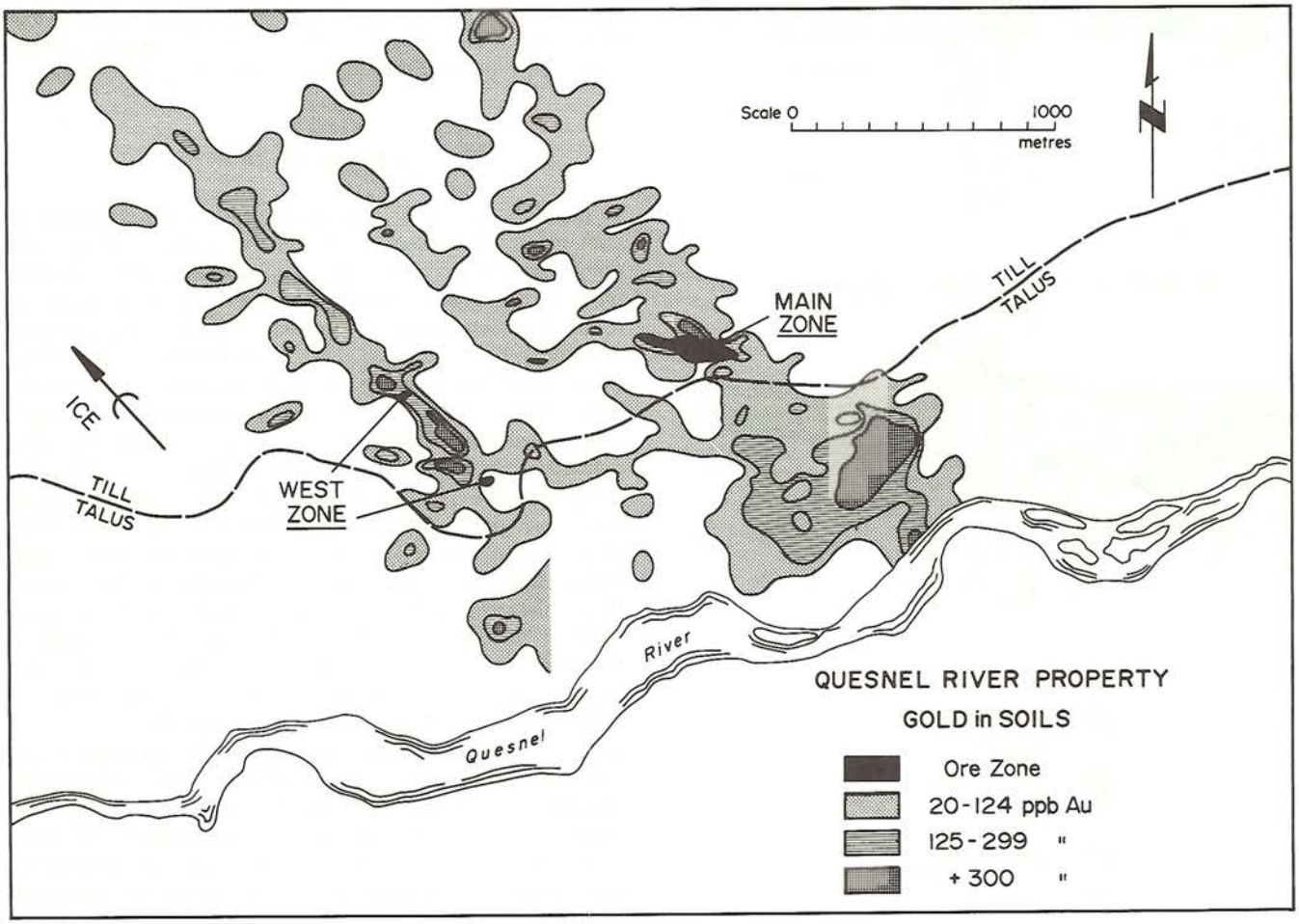

Fig. 7. Contour data for gold content of samples taken from lodgement till over a 40 m x 100 m grid. Subcrop position of mineralized zones in black. Dashed line delimits till-talus boundary. Ice movement to the northwest.

zone of arsenic enhancement some 1200 metres across which encloses the anomalous signatures and extends 500 metres further westward. Bedrock sources for this anomaly are unknown.

All four zones are characterized by a gold, arsenic, vanadium and molybdenum association. Arsenic displays several unusual characteristics whereby the element defines a broad halo around gold associated with the West zone deposit, and can ably fulfull a role as a pathfinder for gold. A similar geochemical relationship between gold and arsenic characterizes the talus fan anomaly to the south. By contrast arsenic is markedly displaced eastward relative to gold associated with the Main zone and the large soil anomaly to the south.

Glaciation on the plateau region is assumed to have been relatively uniform, and disposition of anomalies relative to each other, such as that described for gold and arsenic in the Main and West zones, is believed to reflect similarly-related locations of sources of metal in bedrock. Similarly, anomalies found in the talus fan-colluvial slope environment which are displaced from each other for the various elements, reflect similar displacements in their bedrock sources. Metal zonation in bedrock around the two gold deposits can be proposed based on soil metal distributions. These might suggest lithogeochemical halos which could assist exploration at the diamond drilling stage.

CONCLUSIONS

(1) The QR gold deposit is an epigenetic replacement of calcareous interbeds between massive basalts and a younger series of thin bedded argillites all within a halo of altered and propylitized rocks surrounding a small differentiated stock.

(2) Geochemical sampling of tills proved an effective prospecting tool that lead directly to the discovery of the two deposits. Gold and arsenic are the best pathfinder elements followed by cobalt, iron, antimony, copper (weak), cadmium and lead. Anomaly patterns may reflect primary zoning in bedrock materials in and near the deposits.

(3) Anomaly peaks may be displaced as much as 200 metres from bedrock source areas: resulting down-ice dispersion trains can be as much as three kilometres long.

Acknowledgements — The authors wish to thank Dome Exploration (Canada) Limited for permission to publish much of the material contained in this paper.

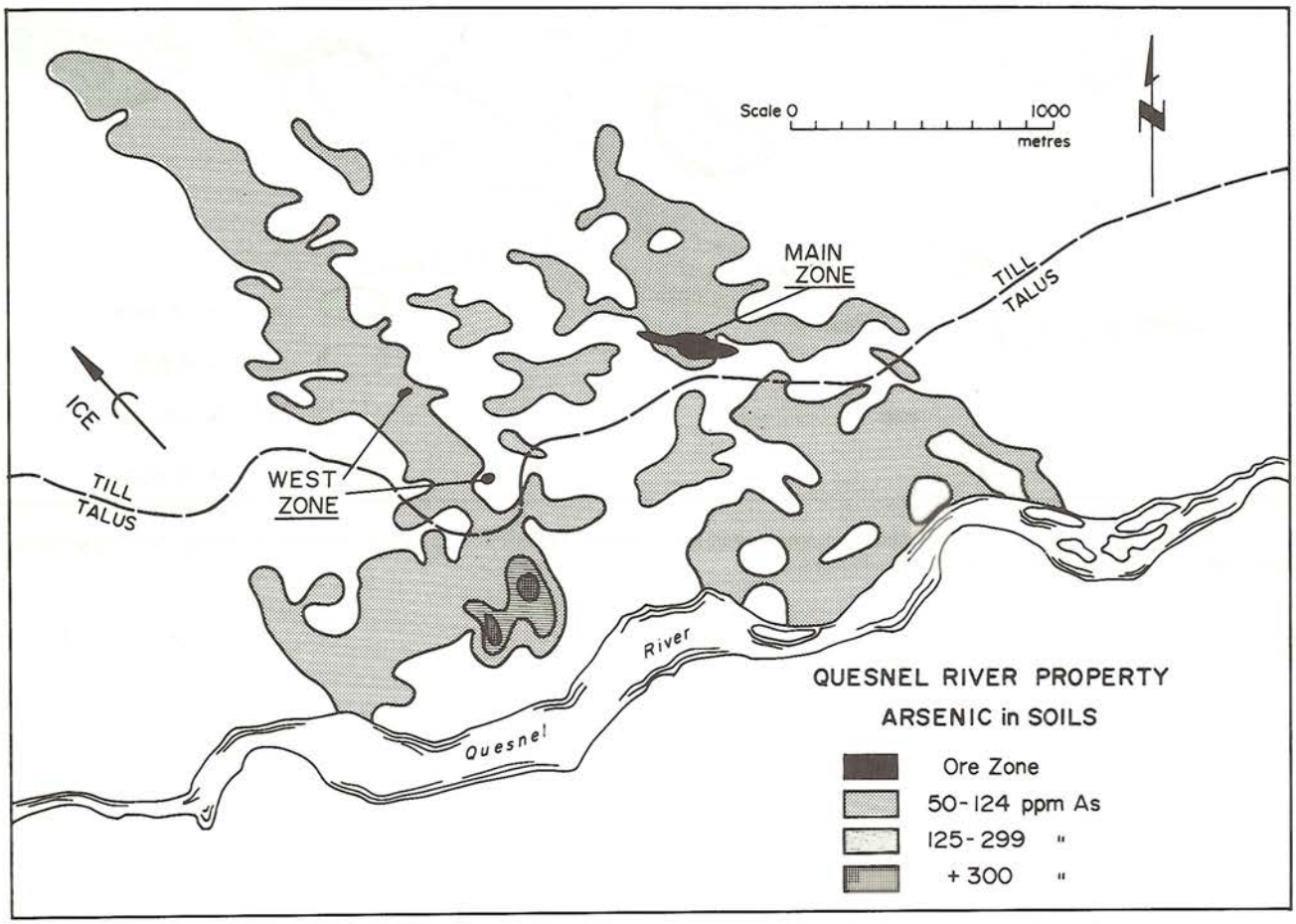

Fig. 8. Contour data for arsenic content of samples taken from lodgement till over a 40 m x 100 m grid. Subcrop position of mineralized zones in black. Dashed line delimits till-talus boundary. Ice movement to the northwest.

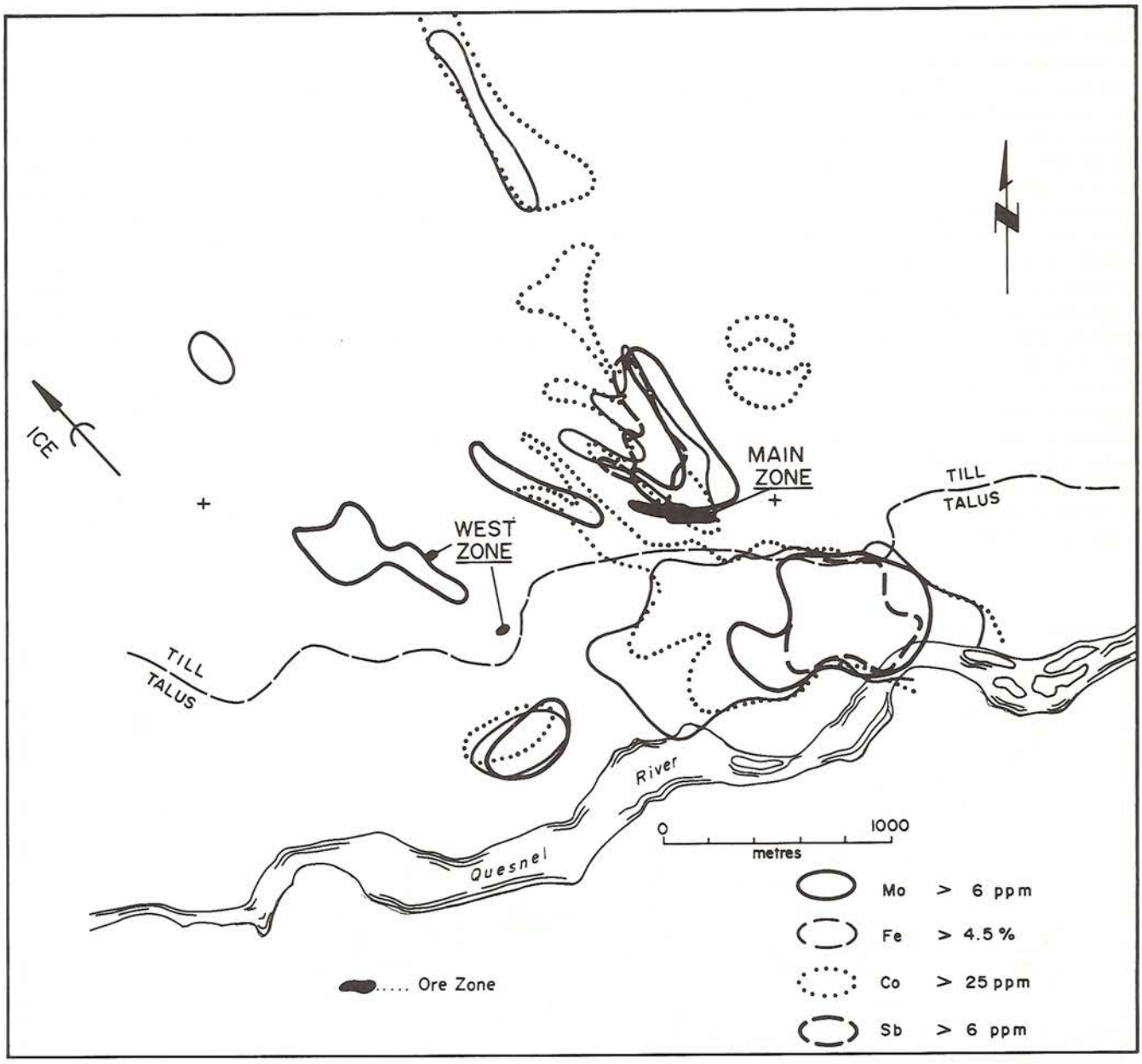

Fig. 9. Summary geochemical map for molybdenum, iron, cobalt and antimony. Dashed line delimits the till-talus boundary. Subcrop positions of mineralized zones shown in black. See text for description.

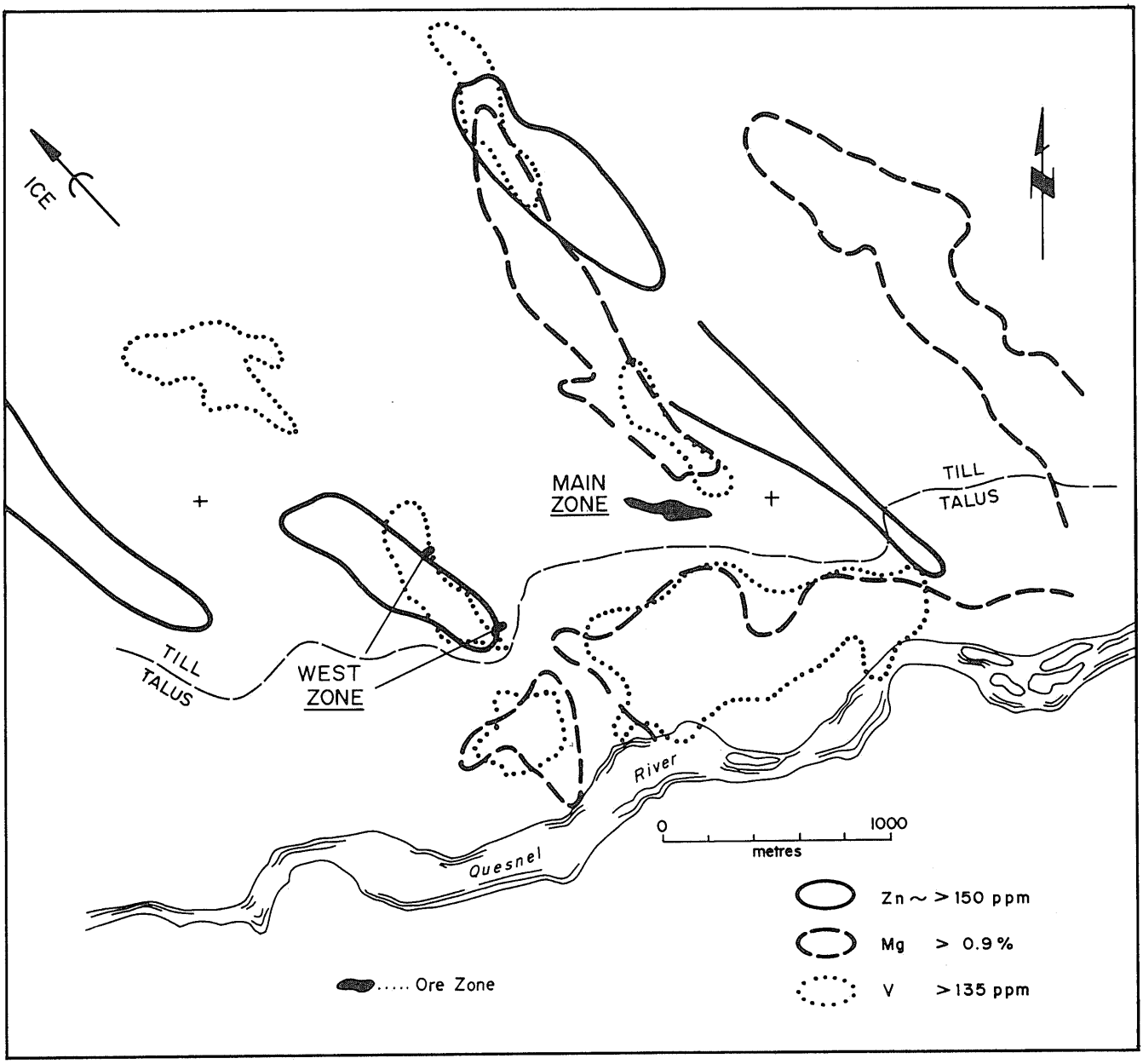

Fig. 10. Summary geochemical map for zinc, magnesium and vanadium. Dashed line delimits the till-talus boundary. Subcrop positions of mineralized zones shown in black. See text for description.

REFERENCES

Bailey, D. G., 1976, Geology of the Morehead Lake area, Central British Columbia; Notes to accompany preliminary Map no. 20; July 1976, 6 p. B.C. Min. Energy Mines Pet. Res., Map 20.

Bailey, D. G., 1978, The Geology of the Morehead Lake area, South Central British Columbia. Ph.D. Thesis, Queens University, 198 p.

Johnson, R. W., Wallace, D. A. and Ellis, G. R., 1976, Feldspathoidal-bearing Potassic Rocks and Associated Types from Volcanic Islands off the West Coast of New Ireland, Papua New Guinea: A Preliminary Account of Geology and Petrology. Volcanism in Australasia, Elsevier, pp. 297-314.

Lefebure, D. V., 1976, Geology of the Nicola Group in the Fairweather Hills, British Columbia. M.Sc. Thesis, Queens University, 178 p.

Melling, D. R., 1982, Carbonate-altered Volcaniclastic Rocks Associated with the Quesnel River Gold Deposit, British Columbia. B.Sc. Thesis, Carleton University, 71 p.

Morton, R. L., 1976, Alkalic Volcanism and Copper Deposits of the Horsefly Area, Central British Columbia. Ph.D. Thesis, Carleton University, 196 p.

Preto, V. A., 1979, Geology of the Nicola Group between Merritt and Princeton. B.C. Min. Energy, Mines, Pet. Res. Bulletin 69, 90 p.

Rees, C. J., 1981, Western Margin of the Omineca Belt at Quesnel Lake, British Columbia. Can. Geol. Surv., Pap. 81-1A: 223-226.

A Multidisciplinary Exploration Case History Of The Shasta Epithermal Gold - Silver Deposit, British Columbia, Canada

B. W. DOWNING
Newmont Exploration of Canada, 900 - 808 West Hastings Street,
Vancouver, B.C. V6C 3A4

and

S. J. HOFFMAN
Selco Division, BP Resources Canada Limited, 700 - 890 West Pender Street
Vancouver, B.C. V6C 1K5

Abstract — The Shasta epithermal, vein-stockwork, Au-Ag deposit is in the Toodoggone gold camp of north central British Columbia. The property has been explored using geochemical and geophysical surveys, geological mapping, and diamond drilling. Two mineralized zones suboutcrop within a 1000 m × 300 m area over an elevation range of 375 metres.

The Shasta deposit is hosted by orange weathering, quartz-eye feldspar crystal tuff in horst block on the flanks of a northwest trending graben. Pyrite, electrum, acanthite and native silver with minor native gold, chalcopyrite, galena and sphalerite, in chalcedony, calcite and quartz fracture fillings, form stockwork vein systems. Best grades are hosted by silicified breccia at the intersection of two or more vein-filled fractures and faults. The Shasta deposit exhibits features common to other Toodoggone camp Au prospects and epithermal deposits from the southwestern US and Mexico.

Known mineralized zones are reflected by Au, Ag, Pb and Zn soil anomalies, Au being dispersed 25 to 100 m eastwards. A potential 3 km strike length of Au-bearing source rocks is indicated by the geochemical soil survey. Multielement studies place the southern limit of the favourable quartz-eye feldspar crystal tuff unit 400 m further northwards than was appreciated previously.

Known mineralized zones have high resistivities reflecting quartz veining and pervasive silicification. Radem VLF anomalies map major fault zones but do not generally correlate with zones of high resistivity. Areas of silicification/Au-Ag occurrence are reflected by low values on a ground magnetometer survey.

The Shasta deposit was found by prospecting. Orientation soil and geophysical surveys have provided anomalies near the discovery prospect which have been followed up successfully.

INTRODUCTION

THE SHASTA epithermal Ag-Au deposit lies 925 km north northwest of Vancouver, British Columbia, Canada, in the Toodoggone gold camp (inset, Fig. 1). Exploration history of the camp has been summarized by Barr (1978). Earliest work was associated with placer Au operations in the 1930s. Activity resumed, with the search for porphyry Cu-Mo deposit types in the 1960s. Follow-up of geochemical anomalies by Kennco Exploration (Western) Ltd. led to discovery of Au and Ag values on Chappelle Creek and culminated in production by Dupont at the 100 tpd Baker Mine, on reserves of 95,000 tonnes averaging 28 gm/t (0.82 oz/ton) Au and 640 gm/t (18.7 oz/ton) Ag. The Lawyers property of Serem Inc. was also identified by the Kennco drainage survey, and has reserves (1985) of 941,000 tonnes averaging 7.2 gm/t (0.21 oz/ton) Au and 268 gm/t (7.82 oz/ton) Ag. The Baker Mine closed in 1983 on depletion of reserves.

The Main zone of the Shasta prospect of International Shasta Resources was found in 1973. Geologic reserves for the most significant of the mineralized zones (from 2,700 m of drilling in 28 holes), the Creek zone found in 1983, based on cut-off grades of 0.7 gm/t (0.02 oz/ton), 1.7 gm/t (0.05 oz/ton) and 3.4 gm/t (0.1 oz/ton) gold equivalent, are estimated at 2.4 million tonnes at an average grade of 2.7 gm/t (0.079 oz/ton), 0.7 million tonnes at an average grade of 5 gm/t (0.145 oz/ton), and 0.52 million tonnes at an average grade of 5.9 gm/t (0.172 oz/ton) gold equivalent, respectively. Gold equivalent grades have been calculated assuming 1 gm of silver to be equivalent to 0.00062 gm of gold (or 1 oz of silver is equivalent to 0.0213 oz of gold - January, 1985). This paper describes the exploration case history.

TOPOGRAPHY/ACCESS

The property occurs in moderately rugged, mountainous terrain, between 1,245 and 1,700 m elevations. Much of the area lies near the bottom of Jock Creek valley which is characterized by secondary forest growth, resulting from the natural reforestation of an old burn dating from 1965. Tributaries of Jock Creek and seepages appear to follow zones of structural weakness or stratigraphy in underlying bedrock.

Access is possible by fixed wing aircraft from Smithers to the Sturdee River all weather airstrip located about five km to the southwest of the property. This is followed by a five minute helicopter trip. Future road access would be relatively easy by following Jock Creek north from the Baker Mine road.

OVERBURDEN

Overburden consists of glacial till which, in areas of known Au prospects, appears to be thin and locally derived. Till thickness on the hillside increases southward, as indicated by the paucity of outcrop. Glacial transport appears to have generally followed the valley of Jock Creek, from west to east. Alluvial deposits are common along Jock Creek.

GEOLOGY

Regional

The Shasta property occurs near the eastern margin of the Intermontane Belt (Sutherland Brown, 1974) in the Cassiar-Omineca mountains (Fig. 1). Oldest rocks in the region are wedges of crystalline limestone correlated with the Permian Asitka Group (Schroeter, 1981), in thrust fault contact with the Middle Triassic Takla Group of andesitic flows and pyroclastic rocks. Takla Group rocks are intruded by the Black Lake granodiorite/quartz monzonite and are overlain by Early to Middle Jurassic Toodoggone volcanics hosting the Shasta Au-Ag occurrences. The Toodoggone volcanics consist of andesitic tuff, flow and pyroclastic breccias, volcanic sediments, and younger grey dacite. They are distinguished by the presence of quartz eyes, particularly in the older andesite tuffs. Toodoggone Group rocks are unconformably overlain by relatively flat lying Late Cretaceous to Tertiary sedimentary rocks of the Sustut Group. The Toodoggone area has undergone several periods of post mineral faulting with minor folding.

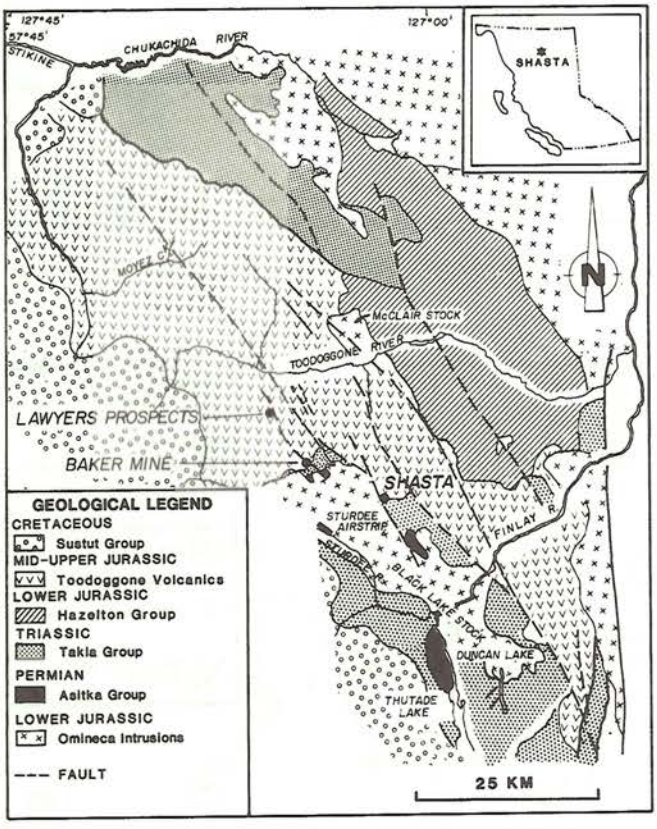

Fig. 1. Location and Regional Geology of the Shasta prospect.

Property

The southeast portion of the map-area (Fig. 2) consists of grey-green to black tuff/tuff breccia, and dacitic flow/breccia of the Takla Formation overlain by the Toodoggone volcanics. The Shasta deposit comprises two main mineralized zones (Main and Creek) within a quartz-eye feldspar crystal tuff (QFT) of the Toodoggone volcanics (Fig. 2). An untested Au prospect (Upper zone of Fig. 2) is hosted by a feldspar crystal tuff (FT). Both units have a characteristic orange weathered surface due to the presence of fine hematite within plagioclase. The QFT and overlying FT are bedded, having a northwesterly strike and westerly dip. Mafic rich lenses (fiamme), ranging from a few millimeters to several cm thick, occur in both units in varying proportions. Quartz eyes decrease in frequency upwards within the QFT and its contact with the overlying FT is gradational. Compared to the QFT, the FT contains more epidote, phlogopite and chlorite, and less indigenous pyrite. Fine-grained, subvertical, northwesterly-trending andesitic dykes up to one meter wide intrude the QFT unit in the Creek zone.

Grey tuff (GT) overlies the QFT and FT. It consists of tuff, tuff breccia and tuff lahar (debris flows), volcanic conglomerate and wackes which range in colour from grey-green (chlorite, epidote) to maroon-purple (hematite-rich). The upper part of the GT is fiamme-rich. Fault contacts obscure relationships between the GT and other rock types. Drill holes indicate that the GT thickens to the west.

Three alteration facies have been identified (Goodall, 1984). These comprise: (1) propylitic to argillic, (2) argillic to advanced phyllic and (3) potassic to silicic. The QFT and FT units are regionally altered, represented by facies (1). Facies (2) and (3) are related to epithermal events. Alteration facies contacts are gradational.

The general structural trend is northerly to northwesterly; however, numerous northeasterly faults trend parallel to Jock Creek. A major fault (Shasta Fault) cuts the QFT and dips at 60 degrees to the west.

Mineralized zones

Faulting, shearing, fracturing and brecciation formed dilatant zones favourable for epithermal mineralization. Two main periods of silica emplacement are recognized. First stage quartz is generally milky, unmineralized and drusy with small quartz crystals infilled by carbonate; the carbonate content (apparently) decreasing with depth. Parallel veins up to 1 cm wide and/or stockworks, are found in sub-parallel zones up to 2 m wide. Wall rock and some of the breccia fragments are weakly to moderately silicified. Second stage grey-brown to translucent (chalcedonic) quartz is found either as a flood of fine veinlets cutting the first stage quartz or as banded chalcedony. Breccia fragments are 80 to 100% silicified/altered, but original textures of the QFT are still recognizable. Greyish chalcedonic quartz is Au-bearing, accompanied by traces of fine grained sulphides. Silicification containing lower grades of Au is pervasive within the host rock a few metres from the mineralized zone. Mineralized zones dip steeply and pinch and swell. The Creek zone consists of several large mineralized breccia zones, some of which have been cut by the Shasta Fault (Fig. 2). The Main zone is also comprised of several areas of quartz vein stockworks and brecciation within the QFT.

Polished section study (Todoruk, personal communication, 1983) identified pyrite, galena, chalcopyrite, sphalerite, acanthite,

native silver, and electrum, with trace amounts of chalcocite and freibergite. Gold occurs as electrum displaying mutual boundaries with acanthite, and as <50 micron sized grains in quartz. Silver is present as acanthite, as rims to and along cleavage planes within galena, as rims to chalcopyrite, and in association with native silver in open spaces.

GEOCHEMICAL SURVEYS

Stream sediment survey

A stream sediment survey over the property did not identify the Shasta gold-silver occurrences. This was not unexpected,

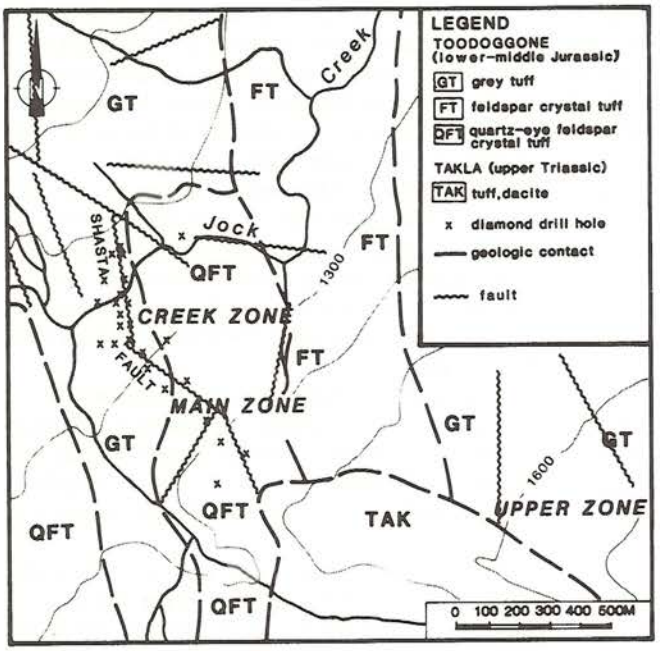

Fig. 2. Property geology — Shasta prospect.

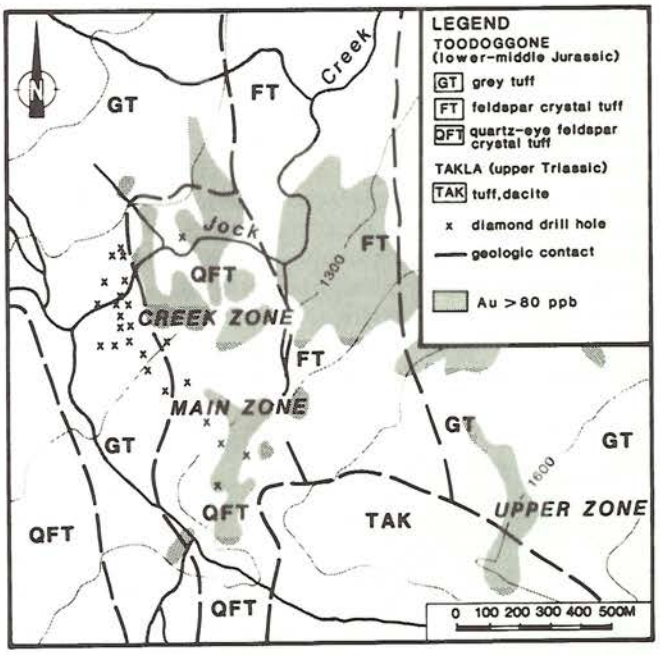

Fig. 3. Shasta prospect gold-in-soil geochemical anomalies exceeding 80 ppb Au.

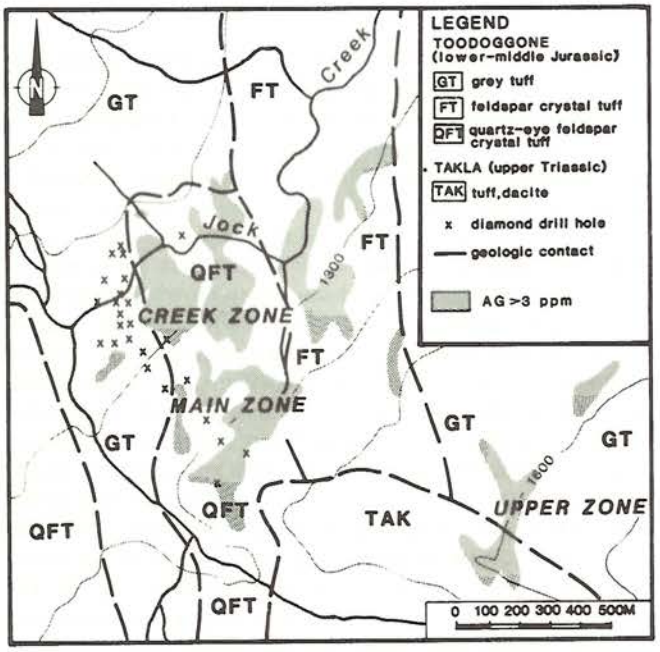

Fig. 4. Shasta prospect silver-in-soil geochemical anomalies exceeding 3 ppm Ag.

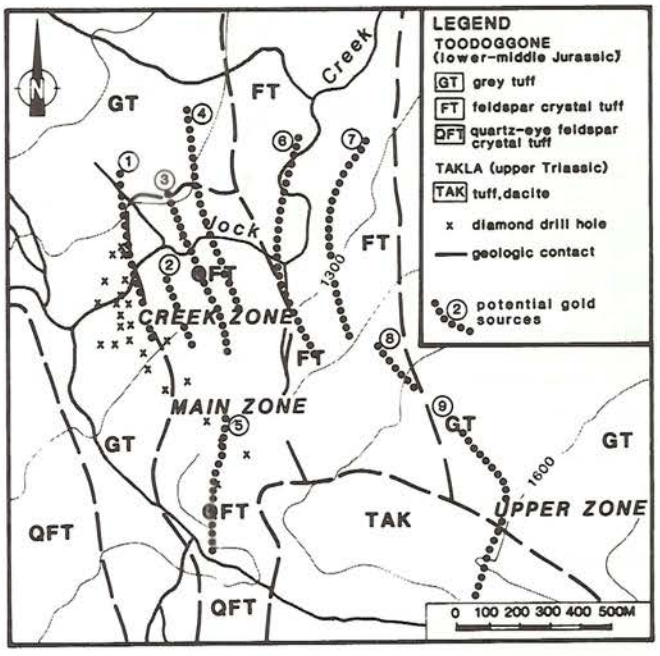

Fig. 5. Geochemical interpretation of the location of gold-in-bedrock sources for the soil anomalies of Fig. 3.

as tributary creeks of Jock Creek are absent in proximity to the known mineralized zones. Maximum stream sediment values on the property are 60 ppb Au and 1.2 ppm Ag.

Soil survey

Soil samples were collected at 25 m or 50 m intervals along lines 50 or 100 m apart. Highest density sampling covers the Creek and Main zones on the west-central portion of the property. Soils are relatively immature. A leaf-humus (LH) layer, is underlain by a variable thickness of humic-rich mineral matter (Ah); the top of the underlying B soil horizon is generally marked by the Bm horizon, a weakly iron-enriched zone, and less frequently by the iron-rich Bf horizon (Clayton et al., 1977). The B horizon was preferentially selected for soil sampling and analysis. Parent material for soil consists of till at 90% of sites and residuum formed from outcrop at 10% of sites. Mineralized boulders were not observed in the till.

Some 1300 samples were collected and then analyzed by Chemex Laboratories of Vancouver for Au (fire assay preconcentration — atomic absorption finish), and for Ag, Pb, Zn, and Cu by atomic absorption following a perchloric/nitric acid digestion. Approximately 1000 sample pulps were reanalyzed by Acme Analytical of Vancouver for a suite of 30 elements by an inductively coupled plasma unit (ICP) following a reverse aqua regia digestion.

Exceptionally high levels of Au (Fig. 3), Ag (Fig. 4) and Pb overlie or lie immediately to the east of the Main and Creek zones. Zn enrichment is somewhat more restricted within the coincident Au-Ag-Pb anomalies. Anomaly thresholds (and maximum values) for Au and Ag are 80 ppb (5,000 ppb) and 3 ppm (50 ppm), respectively.

A steep geochemical gradient marks the western limit of elevated precious and base metal values, a gentler gradient marks the eastern extent. The direction of ice movement inferred from landscape features is from west to east, and the character of the geochemical distribution patterns provides independent evidence that geochemical dispersion is from west to east, with maximum displacement from source in the order of 25 m to 100 m. Nine dispersion trains are recognized (Fig. 5). These suggest up to 3,000 m of strike length for potential bedrock gold sources. Bedrock sources are predicted to underlie the head or western extremity of a geochemically anomalous zone or lie beneath barren material at the up-ice termination of the anomaly following the geochemical model for glacial dispersion proposed by Bradshaw, (1975).

Gold and silver soil anomalies are not accompanied by high concentrations of pathfinder elements such as As, Sb or Bi except at the Main zone where Au-Ag anomalies are flanked by enhanced levels of aqua regia leachable Bi, Mo, As, Fe, P, Ba, Mn, La, Ca, Sb, Al and U. La levels are regionally anomalous, many values exceeding 100 ppm to a maximum of 350 ppm.

The soil survey has identified nine geochemical associations other than those correlated with the base and precious mineralization which, in view of the minimal transport of the glacial till, have been attributed to underlying bedrock lithologies (Fig. 6). The most favourable QFT unit is richest in background levels of Au, Ag, Pb and Cu and can be subdivided into a more metal-rich western member with enhanced levels of aqua regia leachable Mg, Cr, V and Ni. The FT, considered the next most favourable geological unit, is also characterised by soils enhanced in Au, Ag and Pb. Takla Group rocks in the south are associated with elevated levels of aqua regia leachable Cu, Bi, Ni, Co, Mg, Cr, As, Fe, V and Ti. A second smaller area of Takla rocks is predicted to underlie the west central margin of the grid based on a similar geochemical signature (Ni, Co, Mg, Cr). Southern portions of the QFT and FT of Fig. 2 are associated with soils having geochemical signatures typical of Takla tuffs. Background metal variations thus suggest that the area of favourable rock types (QFT, FT) is probably reduced in size from that illustrated on Fig. 2, and that continued exploration of the southermost 400 m of both units on Fig. 2 is likely to be unproductive.

GEOPHYSICAL SURVEYS

The VLF-Resistivity (VLF-R) surveys show that the mineralized zones have high resistivities related to quartz veining and pervasive silicification. The VLF-R survey (Fig. 7) indicates two major resistivity anomalies (Creek and Main) with a possible major east-west break at the south end of the Creek zone and through the Main zone. Northerly-trending resistivity anomalies were also outlined east of the Creek zone. High resistivity areas generally coincide or lie up-ice within 100 m of anomalous Au and Ag values in soils.

A radem-VLF survey detected numerous conductors thought to reflect fault zones, some of which coincide with and are extensions of mapped faults. Radem anomalies do not generally correlate with anomalously high resistivity zones.

The overall magnetic trend is northwest-southeast and appears to correlate with moderately magnetic Takla rocks to the southeast of the map area. Magnetic lows correlate with the areas of silicification/Au-Ag-prospects and probably reflect the destruction of magnetite.

DISCUSSION OF RESULTS

The Creek zone was found by prospecting. Subsequent detailed geological, geochemical and geophysical surveys over the property were conducted to identify signatures associated with the known mineralized zones and define anomalies which could be followed up in the search for additional zones nearby. The geochemical survey results in particular suggest that gold and silver will be found in at least 7 areas additional to the Creek and Main zones. In view of the thin, locally derived till, overburden follow-up is anticipated to be relatively straightforward in searching for the root zones to the surface soil anomalies. Follow-up of soil precious metal anomalies by the VLF-resistivity surveys reported on Fig. 7 was successful. Areas exhibiting coincidence in the interpreted location of a bedrock source for a soil anomaly and a geophysical anomaly were trenched and bedrock gold and silver prospects located. Additional follow-up is needed to evaluate remaining Au anomaly source zones of

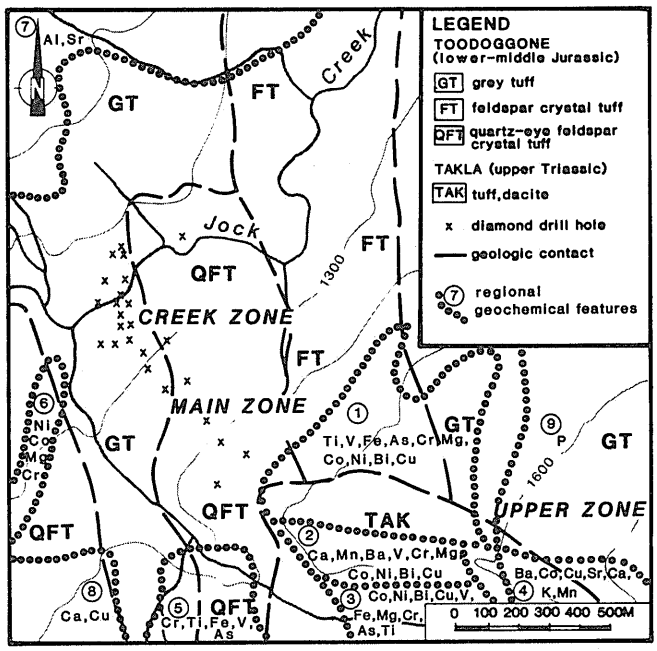

Fig. 6. Element associations in soils believed to reflect significant differences in underlying bedrock as a consequence of minimal glacial dispersion.

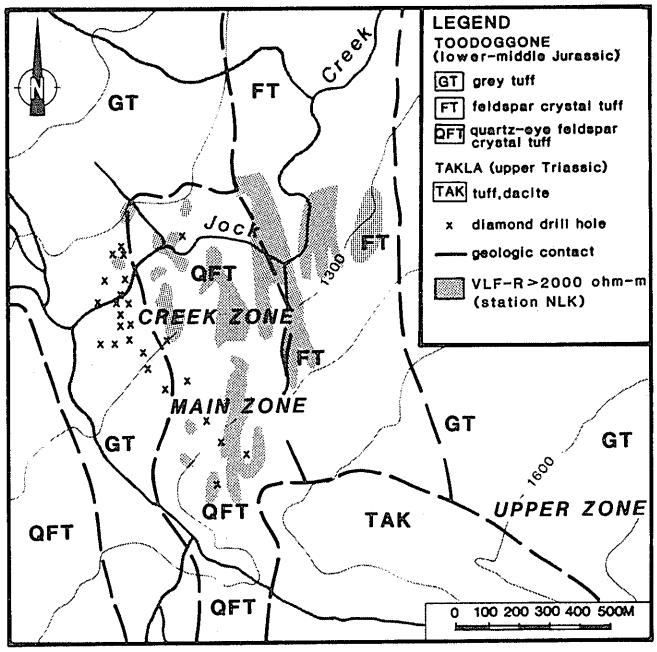

Fig. 7. Shasta prospect VLF-R geophysical anomalies.

Fig. 5, recognizing, from the model of glacial dispersion (Bradshaw, 1975), that a bedrock source containing gold and silver might lie up-ice of a soil anomaly in an area of background gold and silver values.

An understanding of the geology, structural controls, and alteration are important on this property, as they are on most mineral properties. Of great interest as exploration methodologies have been the use of resistivity surveys to highlight silicification and inexpensive multi-element geochemistry to map areas having distinctive geochemical signatures probably related to underlying bedrock. Geochemical distribution maps, for example, have suggested refinements in the geology which downrate the southermost 400 m of FT and QFT of Fig. 2, allowing exploration to be directed towards more favourable geological areas. The multi-element study also suggests some differences between Creek and Main zone prospects which could be of genetic significance.

CONCLUSIONS

The quartz-eye feldspar crystal tuff and feldspar crystal tuff units, regionally anomalous in background gold and silver contents, are associated with some 3 km of north-south trending gold soil anomalies believed to offer exploration potential similar to that documented at the known Creek and Main gold-silver prospects. Follow-up searching for the "root zone" of each significant soil anomaly, at the bedrock-overburden interface, could lead to discovery of bedrock gold sources concealed beneath overburden. The large and widespread zones of alteration suggest an extensive hydrothermal system was active and the potential for discovery of additional Au-Ag reserves is high.

Acknowledgements — The authors wish to thank Newmont Exploration of Canada and International Shasta Resources for permission to publish this paper.

REFERENCES

Barr, D. A., 1978, Chappelle gold-silver deposit, British Columbia: Can. Inst. Mining Metall., v. 71, p. 66-79.

Bradshaw, P. M. D., 1975, Conceptual models in exploration geochemistry. The Canadian Cordillera and Canadian Shield: Assoc. Explor. Geochemists, Spec. Vol. 3, J. Geochem. Explor. v. 4, 213 pp.

Clayton, J. J., Erlich, W. A., Cann, D. B., Day, J. H. and Marshall, I. B., 1977, Soils of Canada, Volume 1, Soils report: Agriculture Canada, 243 pp.

Goodall, G. N., 1984, Alteration of the Toodoggone volcanics, Shasta property: B.Sc. Thesis, Univ. British Columbia, (unpublished).

Schroeter, T. G., 1981, Toodoggone River, B.C.: Ministry of Energy Mines & Petroleum Resources, Geological fieldwork 1980 Paper 1981, p. 124-131.

Sutherland Brown, A., 1974, Aspects of metal abundances and mineral deposits in the Canadian Cordillera: Can. Inst. Mining Metall., Bull., v. 67, p. 48-55.

Soil and Plant Geochemical Orientation Surveys on the Congress Property, Bridge River District, B.C.

B. J. COOKE
Cooke Geological Consultants Ltd., 318 West 23rd Avenue, Vancouver, B.C. V5Y 2H3
and
J. J. BARAKSO
Min-En Laboratories Ltd., 705 West 15th Street, North Vancouver, B.C. V7M 1T2

Abstract — The purpose of this paper is to report on geochemical orientation surveys carried out on the Congress property in 1984 and 1985. In particular, soil and plant samples were collected over two known gold zones in an attempt to identify the optimum sample medium for detecting Au-Ag-As-Sb vein mineralization in the Bridge River district, B.C.

Soil profile studies over the Howard and Extension zones show that well-developed brunisolic soils occur in the Bridge River district, but they contain a volcanic ash layer between the A and B horizons. The B horizon gives pronounced Au, As, Sb, Cd and Tl anomalies over mineralized zones where glacial overburden is thin (‹5 metres). Soil orientation survey lines over the two veins indicate that although the LFH horizon does contain moderate Au and As anomalies and weak Sb anomalies, they are not as strong as the anomalies in the B horizon for Au, Ag, As and Sb.

Plant sample studies over the Howard and Extension zones show that the vegetation is typical, sub-alpine, coniferous forest, dominated by Douglas fir on north slopes and ponderosa pine on south slopes. Douglas fir 1st year growth gave pronounced As and Au anomalies above the mineralized zones. Ponderosa pine produced moderate Au, Sb, Ag and As anomalies, indicating that it too can be sampled in prospecting for gold. Plant orientation survey lines over the two veins suggest that biogeochemical samples do produce significant anomalies that can be ranked as follows: 1) arsenic in Douglas fir › ponderosa pine, 2) gold in Douglas fir › ponderosa pine, 3) antimony in ponderosa pine, › Douglas fir and 4) silver in Douglas fir › ponderosa pine.

Although 1st year stems were the preferred sample medium, it was found that not enough material was available at each sample site due to lack of trees or sparsity of branches. Whole branch sample results were generally lower but more consistent than 1st year growths, so they were used in subsequent biogeochemical surveys.

It was found that low order Au, Sb, Ag and As biogeochemical anomalies were detectable over 10 metres of overburden, up to 100 metres from subcropping gold mineralization, whereas pedogeochemical anomalies were restricted to about 50 metres from source and 5 metres of overburden.

Sampling different trees over the same lines at the same spacings but different times of year (July vs. December), indicated that the same anomalies were identified but the numbers were quite variable from season to season. Since the July survey gave lower numbers than the December survey, there must be more uptake of metals in the relatively wet winters compared to the usually dry summers, contrary to the normal spring-dominant growth cycle of most plants. Therefore, follow-up biogeochemical surveys should be carried out at the same time of year as previous surveys in order for the data to be comparable.

INTRODUCTION

GEOCHEMICAL ORIENTATION surveys were carried out on the Congress property in 1984 and 1985. In particular, soil and plant samples were collected over two known gold zones in an attempt to identify the optimum sample media for detecting Au-Ag-As-Sb vein mineralization in the Bridge River district, B.C.

The Congress property is located approximately 6 kilometres northeast of Goldbridge and 180 kilometres north-northeast of Vancouver in southwestern British Columbia (Fig. 1). It lies immediately west of the old Minto mine and 13 kilometres north of the old Bralorne-Pioneer mine, the largest gold producer in British Columbia.

The claims lie north of Carpenter Lake, near the mouth of Gun Creek, at elevations of 655 metres along the lake to 1,035 metres on top of the hill southwest of the creek. Vegetation is typical, sub-alpine, coniferous forest, dominated by Douglas fir on north slopes and ponderosa pine on south slopes, and the climate is characterized by hot, dry summers and cool, snowy winters.

Placer gold was first discovered in Gun Creek around 1859, as prospectors migrated west up the Bridge River from its confluence with the Fraser River. The Congress vein was located in 1913 and by 1915, a short adit had produced a few tons of antimony-gold ore for metallurgical testing.

Periodic exploration was carried out at the Congress mine until 1960, when the Howard vein was discovered and subsequently explored into the 1980's. The 1984 orientation surveys on the Howard (A) and Extension (D) zones (Fig. 1) prompted follow-up soil sampling and bulldozer trenching that led to the discovery of the Lou zone, and other veins, on the Congress property.

GEOLOGY

The Bridge River district lies at the western margin of the Intermontaine Belt of volcanic and sedimentary rocks, where it abuts against the Coast Plutonic Complex of plutonic and metamorphic rocks. Triassic volcanics and sediments (Cadwallader and Bridge River Groups) are intruded by intermediate plutons (Bralorne intrusions) and faulted against ultramafic intrusions (President intrusions).

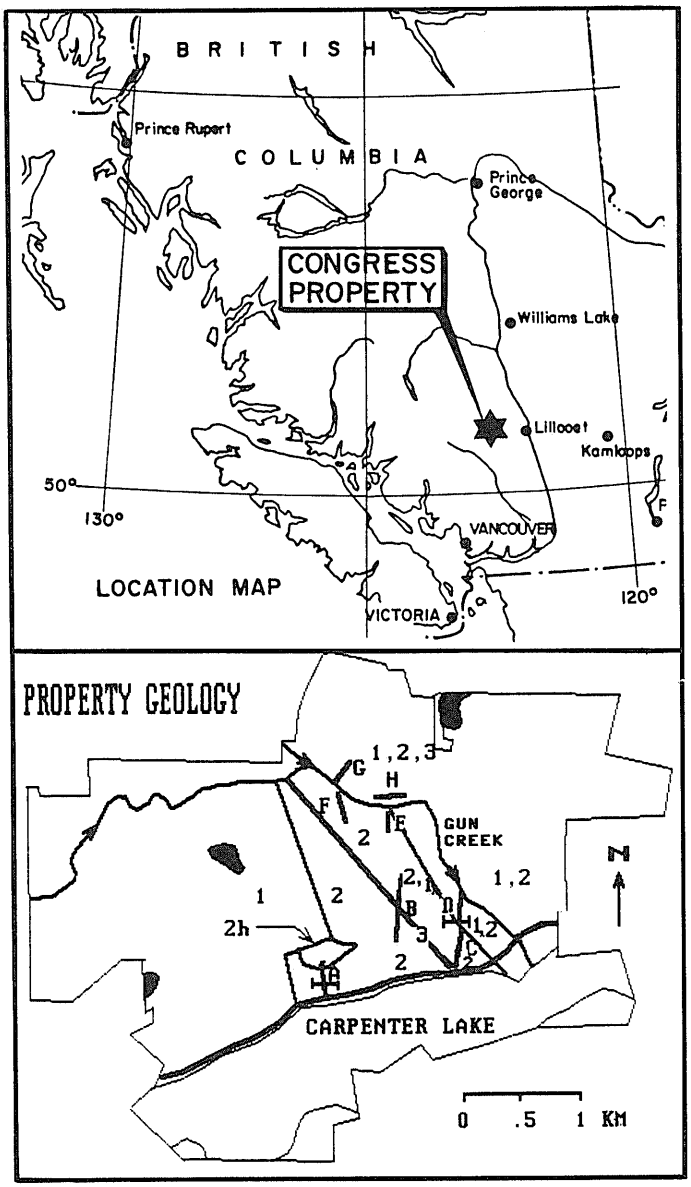

Fig. 1. Congress property is located in the Bridge River district, B.C. (upper diagram). Geology of the Congress property, showing the distribution of four rock types (1 = Bridge River Group (BRG) chert, 2h = BRG gabbro, 2 = BRG basalt, 3 = Tertiary porphyry dikes) and eight mineralized zones (A = Howard, B = Lou, C = Congress, D = Extension, E = Ozone, F = Gun, G = Slide, H = Paul).

Jurassic and Cretaceous basinal sediments and volcanics (unnamed, Taylor Creek and Kingsvale Groups) are sequentially intruded by Cretaceous and Tertiary plutons of felsic composition (Coast, porphyry and Bendor intrusions). Relatively flat-lying Tertiary volcanics (Rexmount porphyry and plateau basalt) cap the lithological sequence.

At Bralorne-Pioneer mine, gold-bearing quartz veins follow two sets of narrow fissures in Pioneer andesite and Bralorne diorite, close to Bralorne granite or albitite dikes and sandwiched by the Fergusson and Cadwallader faults. Many other gold prospects in the region, such as the showings on the Congress property, are gold-bearing sulfide replacements along narrow shears in Bridge River gabbros, basalts and cherts, often near Tertiary porphyry dikes (Fig. 1). On the Congress property, dikes and shears strike northeast to northwest and dip steeply west, commonly following, but locally crosscutting, stratigraphic contacts.

The mineralized shear zones are up to 20 metres wide (average 2 metres), pervasively altered in basalt, gabbro and dike to ankerite-quartz-sericite-kaolinite, and erratically veined by quartz-ankerite-chlorite-graphite-pyrite-arsenopyrite-stibnite-tetrahedrite. Gold and silver grades both run up to 1 oz/ton (average 0.2 oz/ton) and antimony and arsenic values both run as high as 1% (average 0.2%).

PREVIOUS GEOCHEMICAL WORK

Early attempts to prospect for gold in British Columbia using biogeochemistry were successful but tedious and expensive (Warren and Delavault, 1950). Several plants, including Douglas fir, were shown to carry up to 1 ppm Au in ashed samples from the vicinity of gold mineralization.

Later sampling showed that the fresh growth of many plants was more effective in picking up gold (up to 20 ppb in Oregon grape) than older growths. In general, background levels in dried plant matter were less than 2 ppb gold in most plants, 2-10 ppb gold in areas of anomalous gold and more than 10 ppb gold near gold mineralization.

Warren et al., (1964) reported Douglas fir (*Pseudotsuga menziesii*) as a collector of arsenic near gold veins in the Bridge River mining district, British Columbia. They found that 1st year growth gave more pronounced arsenic anomalies than 2nd year growth, which in turn was more anomalous in arsenic than A horizon soils.

Follow-up work showed that 1st year stems collected more arsenic than 1st year needles, so they became the preferred sample medium (Warren et al., 1968). In general, background levels were less than 100 ppm arsenic in ashed Douglas fir stems, 100-500 ppm arsenic where glacial tills picked up arsenic contamination from gold veins, and more than 500 ppm arsenic within 200 feet of subcropping gold-arsenic mineralization.

Recent workers (Girling et al., 1979, Girling and Peterson, 1980, Warren and Barakso, 1982, Dunn, 1986) have confirmed the usefulness of sampling not only Douglas fir for arsenic, but also a wide variety of plants, in different geomorphic environments, for several metals, including gold and silver. Our work at Congress is an attempt to show that although soil surveys are very efficient at locating Au-Ag-Sb-As mineralization beneath thin glacial till, plant sampling increases both the width and depth of metal anomalies and can be effective in detecting gold veins through thicker glacial overburden at a larger sample spacing.

SOIL ORIENTATION SURVEYS

Soil sampling has been used effectively in prospecting for gold in the Bridge River district but only antimony had been analyzed in the limited soil surveys carried out on the Congress

property prior to 1984. As a result, it was decided that soil profile studies would be useful in determining which horizon to sample and what elements to analyze.

Soils are generally well developed brunisols containing LFH, Ah, volcanic ash, Bf and C horizon (Canada Soil Survey Committee, 1970), (Table 1). The dark brown LFH and light brown or grey Ah horizons are quite thin (<10 centimetres) in places, due to the relatively sparse vegetation on steep, south-facing slopes. Light grey Bridge River ash (<100 cm) blanketed the area some 2,440 years BP following an eruption at Plinth Peak about 80 kilometres to the west.

The rusty-brown B horizon is well developed (<150 cm) near gold mineralization where glacial overburden is thin (<5 m) but becomes narrower and less pronounced in other areas, although always present. A light brown C horizon is typically developed on either thin, unsorted glacial drift or thick, bedded fluvial deposits.

Samples were sent to Min-En Laboratories Ltd. in North Vancouver, carefully dried at 95°C and seived to obtain a −80 mesh sample. For gold analysis, a 10 gram sub-sample was pretreated with HNO_3 and $HClO_4$, followed by digestion with aqua regia, volume adjustment with 25% HCl, gold extraction with methyl iso-butyl ketone and determination by atomic absorption spectrophotometry. For trace element analysis, a 1.0 gram sub-sample was digested for 6 hours with HNO_3 and $HClO_4$, diluted to suitable volume and determined by inductively coupled plasma emission spectrophotometry.

Two soil profiles were taken over gold veins in the Howard (A) and Extension zones (D) (Fig. 1). The Howard zone profile was taken immediately over Trench 2 where vein samples assayed 0.32 oz/ton Au, 0.10 oz/ton Ag, 0.037% Sb and 0.44% As over 5.4 metres true width. The LFH and Ah horizons are weakly anomalous in gold, but the Bf horizon, especially the orange-brown Bf3, contains strong Au, As, Sb, Cd, and Tl anomalies (Table 1). The C horizon is enriched in metals as it grades downwards into rusty, oxidized gossan above the gold vein.

CM / PPB	Horizon	Au (ppb)	Ag	As	Sb	Cd	Pb	Tl (ppb)
5	LFH, Ah	15	0.2	38	3	0.4	5	<20
30	Ash	N/A	N/A	N/A	N/A	N/A	N/A	N/A
20	Bf_1	365	0.3	220	49	1.1	12	50
50	Bf_2	1670	0.5	209	45	1.6	12	90
80	Bf_3	810	0.7	710	184	2.2	12	325
30	C	14000	5.3	6550	327	6.9	14	1350

HOWARD ZONE 000W

CM / PPB	Horizon	Au (ppb)	Ag	As	Sb	Cd	Pb	Tl (ppb)
5	LFH, Ah	60	0	84	8	1.4	17	<20
60	Ash	N/A	N/A	N/A	N/A	N/A	N/A	N/A
15	Bf_1	45	0.4	332	52	0.8	17	90
45	Bf_2	140	0.5	234	59	0.7	16	115
30	Bf_3	60	0.1	67	46	1.1	17	120
30	C	5	0.4	29	36	0	12	25

EXTENSION ZONE 012.5W

Table 1. Geochemistry of soil profiles from the Howard and Extension zones, showing metal enrichment in the B horizon relative to the A horizon, and in the Howard zone, enrichment in the C horizon due to subcropping vein mineralization. The volcanic ash was not analyzed (N/A).

The Extension zone profile (Table 1) was sampled about 12.5 metres west of the vein exposed in Trench 16, which yielded 0.10 oz/ton Au, 1.41 oz/ton Ag, 0.93% Sb over 3.0 metres true width. The LFH and Ah horizons are weakly anomalous in Au, the orange-brown Bf2 horizon is strongly anomalous in Au, As, Sb, Cd and Tl, and the C horizon shows background levels in metals as it grades down into unsorted glacial till.

Because the LFH and B horizons are well developed and easily recognized, they were sampled for Au, Ag, As and Sb along soil orientation survey lines over the Howard and Extension zones (Figs. 2 and 3). Other elements were also analyzed as part of a 26 element package but only Pb and Zn showed some correlation with the ore elements.

The LFH soil samples produced moderate anomalies in Au and As, with weak anomalies in Sb and no anomalies in Ag, from the two gold zones. However, B horizon soils gave strong anomalies in all four elements (with one exception — Ag at Howard) with better contrast than the LFH horizon (Figs. 2 and 3). In fact, a 470 ppm antimony anomaly elsewhere on the property led to the discovery of the Lou zone. Consequently, B horizon soils were sampled on the Congress property at 25 metre spacings, and analyzed for Au, Ag, As, Sb, Pb and Zn.

PLANT ORIENTATION SURVEYS

Plant sampling had been tested previously to prospect for gold in the Bridge River district but it had never been used routinely for exploration in the area, probably due to the inconsistency of vegetation and cost of analysis. However, in areas of thick glacial overburden, plants may detect anomalies where soils do not, so it was concluded that orientation sampling studies would be helpful in evaluating which trees to sample (Lyons, 1952), and which elements to analyze.

Vegetation is typical, sub-alpine, coniferous forest, consisting of open-spaced ponderosa pine (*Pinus ponderosa*) on south slopes and densely spaced Douglas fir (*Pseudotsuga menziesii*) on north slopes. Other varieties present are lodgepole pine (*Pinus contorta*) on sandy plateaus, black spruce (*Picea mariana*) in low swamps, yellow cedar (*Chameccyparis nootkatensis*), mountain hemlock (*Tsuga mertensiana*), trembling aspen (*Populus tremuloides*), Oregon grape (*Berberis ssp.*), mountain alder (*Alnus tenuifolia*), and balsam poplar (*Populus balsamifera*).

Plants were sampled over two gold veins on the Congress property, the Howard (A) and Extension (D) zones (Fig. 1). It was found that, although 1st year stems are the preferred medium, there was rarely enough material to sample due to lack of trees or sparsity of branches. Therefore, 1st year stems and needles were taken together, and whole branch (1-3 years growth) stems and needles were also collected, for Douglas fir and ponderosa pine. Whole branch samples were also taken from other species.

Samples were sent to Min-En Laboratories Ltd. in North Vancouver and carefully dried at 85°-95°C and milled to −40 mesh. After mixing and quartering each sample, a 70-80 gram aliquot was ashed at 500°C and then weighed. Approximately 0.5 gram of ash was weighed into beakers and digested in

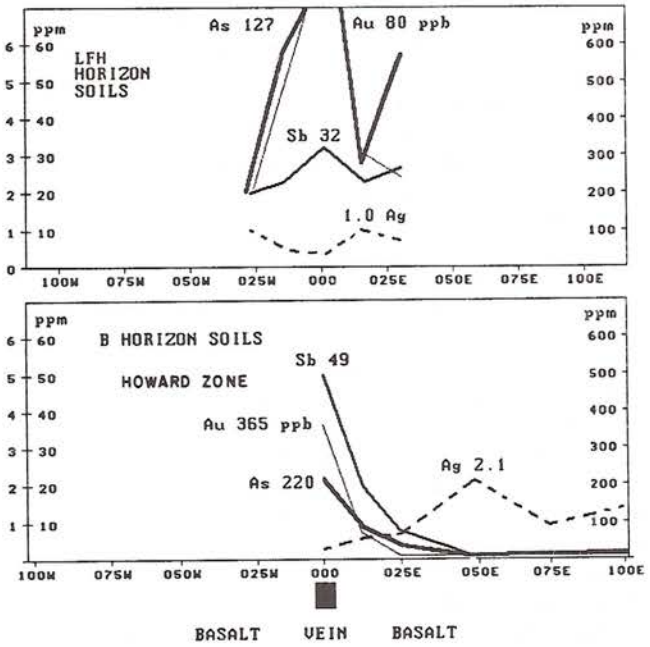

Fig. 2. Geochemistry of orientation line A in the Howard zone, showing the Au-As-Sb anomalies over the vein, stronger in B horizon than in A horizon, and the lack of Ag anomalies.

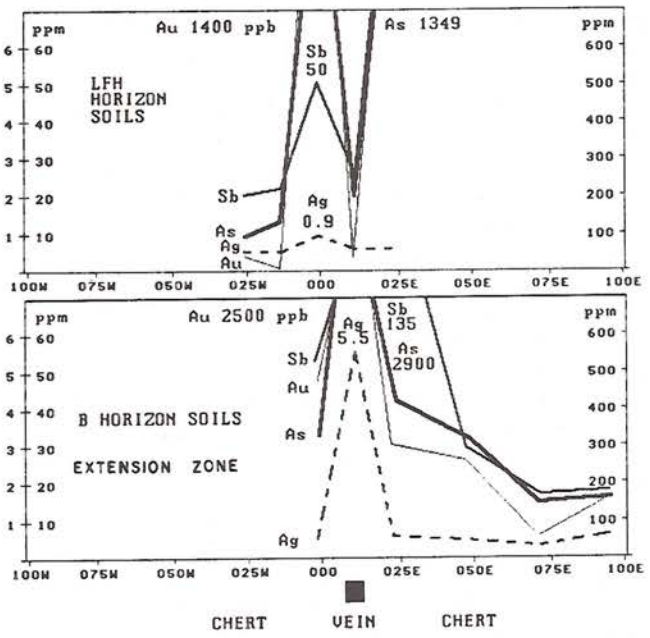

Fig. 3. Geochemistry of orientation line D in the Extension zone, showing the Au-As-Sb-Ag anomalies in the A horizon, offset from the underlying vein, relative to those in the B horizon, located directly over the vein.

HNO_3 and $HClO_4$ for inductively coupled plasma spectrophotometric analysis, and the rest of the ash was used for gold analysis. The gold was determined by aqua-regia dissolution, methyl-iso-butyl-ketone extraction and analysis by atomic absorption spectrophotometry.

In the Howard zone samples, (Fig. 4), both gold and arsenic gave strongly anomalous values (up to 540 ppm As and 541 ppb Au) in Douglas fir 1st year growths. However, moderate metal uptake was also recorded for Ag, Sb, As and Au in ponderosa pine, trembling aspen and Oregon grape.

The Extension zone samples are strongly anomalous for As in Douglas fir (up to 3600 ppm As) and Au in ponderosa pine (up to 230 ppb Au), but moderate metal uptake was also observed for the other metals in Douglas fir, ponderosa pine, mountain alder and balsam poplar (Fig. 4). Ponderosa pine (whole branch > 1st year) gave higher values than the other plants in antimony (up to 19 ppm) and silver (up to 4.1 ppm). Significant gold concentrations (up to 165 ppb) were recorded in four other plants (trembling aspen > balsam poplar > Oregon grape > mountain alder).

Ponderosa pine and Douglas fir provide the most consistent vegetation cover so they were sampled along plant orientation survey lines over the Howard and Extension zones (Figs. 5 and 6). Plant samples were collected by trimming 12 inches of growth from branches around the base of each tree to fill 8″ x 12″ plastic bags (1-2 1).

Results show (Figs. 5 and 6) that the strongest anomalies can be ranked as follows: (1) arsenic in Douglas fir > ponderosa pine, (2) gold in Douglas fir > ponderosa pine, (3) antimony in ponderosa pine > Douglas fir and (4) silver in Douglas fir > ponderosa pine. Silver and antimony values are less variable and give poorer contrast compared to the gold and arsenic numbers.

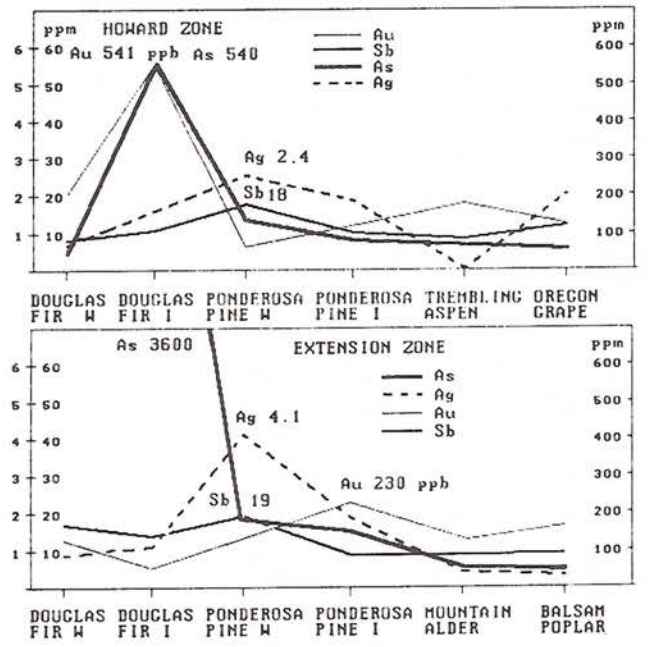

Fig. 4. Geochemistry of plant samples from the Howard and Extension zones, showing strong Au-As enrichment in Douglas fir 1st year growth (I) and weaker Au-Sb-Ag enrichment in ponderosa pine, whole branch samples (W).

Arsenic background levels in Douglas fir and ponderosa pine are quite high (100 to 500 ppm) within 100 metres of a gold zone and peaks run up to 15X background (500 to 6,600 ppm). Gold background values in Douglas fir and ponderosa pine are also high (10 to 100 ppb) with anomalous samples up to 10X background (75 to 940 ppb). Antimony

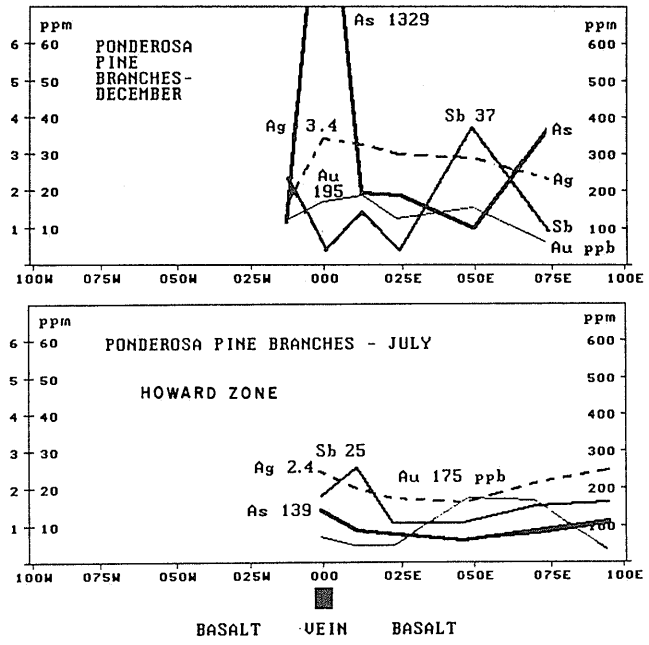

Fig. 5. Geochemistry of orientation line A in the Howard zone, showing higher metal values in ponderosa pine in December relative to July.

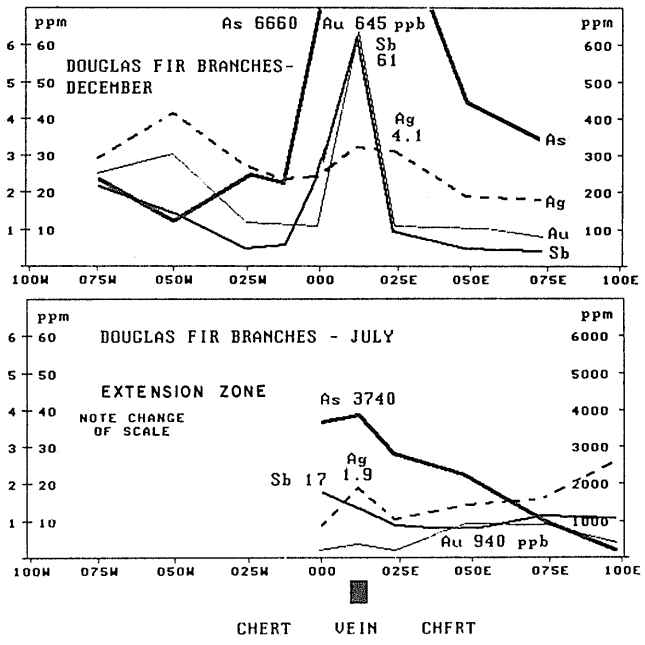

Fig. 6. Geochemistry of orientation line D in the Extension zone, showing strong metal anomalies in Douglas fir from December but weaker metal values from July.

background is 1 to 10 ppm with peaks up to 37 ppm and silver background is 0.5 to 1.5 ppm with peaks up to 6.6 ppm.

Sampling of different trees over the same zones at the same spacings but different times of year (July vs. December), indicated that the same anomalies were identified but the numbers had considerable variability from season to season (Figs. 5 and 6). Since the July survey gives consistently lower values than the December survey, there must be more uptake of metals in the relatively wet winters compared to the normally dry summers, contrary to the normal spring-dominant growth cyle of most plants. Consequently, follow-up biogeochemical surveys should be carried out at the same time of year as previous surveys in order for the data to be comparable.

CONCLUSIONS

1. Soil profile and orientation studies over the Howard and Extension zones show that well developed brunisols occur in the Bridge River district and they contain a volcanic ash layer between the A and B horizons. The B horizon gives pronounced Au, As, and Sb anomalies over the mineralized zones and follow-up trenching of pedogeochemical anomalies was remarkably successful in locating subcropping gold veins.

Plant samples studies over the Howard and Extension zones show that the vegetation is typical, sub-alpine, coniferous forest, dominated by Douglas fir on north slopes and ponderosa pine on south slopes. Plant orientation survey lines over the two veins suggest that biogeochemical samples do produce significant anomalies that can be ranked by intensity as follows: (1) arsenic in Douglas fir > ponderosa pine, (2) gold in Douglas fir > ponderosa pine, (3) antimony in ponderosa pine > Douglas fir and (4) silver in Douglas fir > ponderosa pine. Follow-up trenching of biogeochemical anomalies was in some cases successful in locating buried mineralization.

3. It was found that low order Au, As, Sb and Ag biogeochemical anomalies were detectable over 10 metres of overburden, up to 100 metres from subcropping gold mineralization, whereas pedogeochemical anomalies were restricted to about 50 metres from source and 5 metres of overburden. Sampling different trees over the same lines at the same spacings, but different times of the year (July vs. December), indicate that the same anomalies were identified but the metal levels had considerable variability from season to season.

4. Since the July survey gave lower metal values than the December survey, there must be more uptake of metals in the relatively wet winters compared to the usually dry summers. Therefore, follow-up biogeochemical surveys should be carried out at the same time of year as previous surveys in order for the data to be comparable. If the availability of water influences the uptake of metals, then anomalies located during reconnaissance biogeochemical surveys over areas of thick glacial drift and fluvial beds must be the result of ground waters picking up metals from mineralized zones below the overburden.

Acknowledgments — The writers would like to thank Mr. Louis Wolfin, President of Levon Resources Ltd., and Mr. Lewis Dillman, President of Veronex Resources Ltd., for their faith in carrying out test surveys on the Congress property, and their encouragement in publishing our findings.

REFERENCES

Canada Soil Survey Committee, 1970, The Canadian System of Soil Classification, Canada Dept. Agriculture, Research Branch, 164 pp.

Dunn, C. E., 1986, Biogeochemistry as an aid to exploration for gold, platinum and palladium in the northern forests of Saskatchewan, Canada: J. Geochem. Explor., v. 25, p. 21-40.

Girling, C. A. and Peterson, P. J., 1980, Gold in plants: Gold Bull., v. 13, n. 4, p. 141-157.

Girling, C. A., Peterson, P. J. and Warren, H. V., 1979, Plants as indicators of gold mineralization at Watson Bar, British Columbia, Canada: Econ. Geol., v. 74, p. 902-907.

Lyons, C. P., 1952, Trees, shrubs and flowers to know in British Columbia: J. M. Dent & Sons (Canada) Ltd., Vancouver, 194 pp.

Warren, H. V. and Barakso, J. J., 1982, The development of biogeochemistry as a practical prospecting tool for gold: Western Miner, February, p. 17-31.

Warren, H. V. and Delavault, R. E., 1950, Gold and silver content of some trees and horsetails in British Columbia: Geol. Soc. Amer., Bull., v. 61, p. 123-128.

Warren, H. V., Delavault, R. E. and Barakso, J. J., 1964, The role of arsenic as a pathfinder in biogeochemical prospecting: Econ. Geol., v. 59, p. 1381-1389.

Warren, H. V., Delavault, R. E. and Barakso, J. J., 1968, The arsenic content of Douglas fir as a guide to some gold, silver and base metal deposits: Can. Inst. Min. Metall., Bull., n. 675, p. 1-7.

Comparison of Rock Geochemistry and Mineralogical Alteration as Exploration Guides for Cordilleran Epithermal Precious and Base Metal Vein-Type Deposits in Bolivia and Peru

J. D. APPLETON
British Geological Survey, Keyworth, Nottingham NG12 5GG, England

J. CLAROS
COMIBOL, Casilla 158, Oruro, Bolivia

and

W. RODRIGUEZ
INGEMMET, Pablo Bermudez 211, Apartado 889, Lima, Peru

Abstract — Multielement rock geochemical and mineralogical investigations of the Ag-Pb-Zn vein deposit of San Antonio de Lipez, Bolivia and the Ag-Au vein deposit of Millotingo, Peru illustrate the extent and nature of alteration associated with two contrasting epithermal silver deposits. Alteration patterns are defined by (1) Ag, As, Pb, S, Sb, and Zn, (2) K_2O/Na_2O, K/Rb, and Rb/Sr ratios and (3) mineralogical indicators such as progressive K-feldspathization. Multielement major and trace element rock geochemical information is more rapidly and economically obtained than mineralogical data and appears to be a reliable guide to the identification of mineralized zones.

INTRODUCTION

EXPLORATION for epithermal and mesothermal vein type mineralization in the Andean Cordillera of Bolivia and Peru has been largely directed by the presence of favourable rock types, geological structures and surface expressions of mineralization such as veins and alteration zones (Ahlfeld and Schneider-Scherbina, 1964; Peterson, 1965). Subsequent investigations have nearly always progressed to the drilling stage without the use of geochemical or geophysical techniques. On a mine scale, mineralized structures and alteration, such as zones of silicification, have been used as guides to find ore. In Bolivia, and sometimes in Peru, geochemistry has been used to a limited degree for exploration, usually being restricted to stream sediment and soil geochemistry. When geochemical methods were tried in Bolivia they were only partly successful due to contamination of streams by old mine workings.

To try to develop a cost effective method that would be useful in contaminated areas, the application of rock geochemistry to exploration for precious and base metal vein type deposits was investigated. Many of the deposits of this type in Bolivia and Peru have strong surface expressions, usually in the form of zones of alteration which may extend over 10 km^2. In addition to the alteration zones associated with known mineral deposits, there are many others that are potentially associated with buried mineralization.

Orientation studies of geochemical dispersion around known deposits were carried out in order to provide guidelines for the assessment of such areas of alteration. The main aim of these investigations was to study the application of rock geochemistry but as there is obviously a very close connection between major element chemistry and alteration mineralogy and because alteration mineralogy and zoning have been proposed or used in some areas (JICA, 1984), a comparative study of the relative merits of mineralogical alteration and rock geochemistry as exploration guides was carried out.

Although rock geochemical investigations have been executed in the vicinity of various deposits in Bolivia and Peru (Appleton, in prep.) only those at the contrasting epithermal vein deposits of San Antonio de Lipez in SW Bolivia and Millotingo in central Peru are described here (Fig. 1). The San Antonio de Lipez Ag-Pb-Zn deposit has extensive surface alteration zones whilst the Millotingo Ag-Au deposit has a very limited zone of alteration visible at the surface.

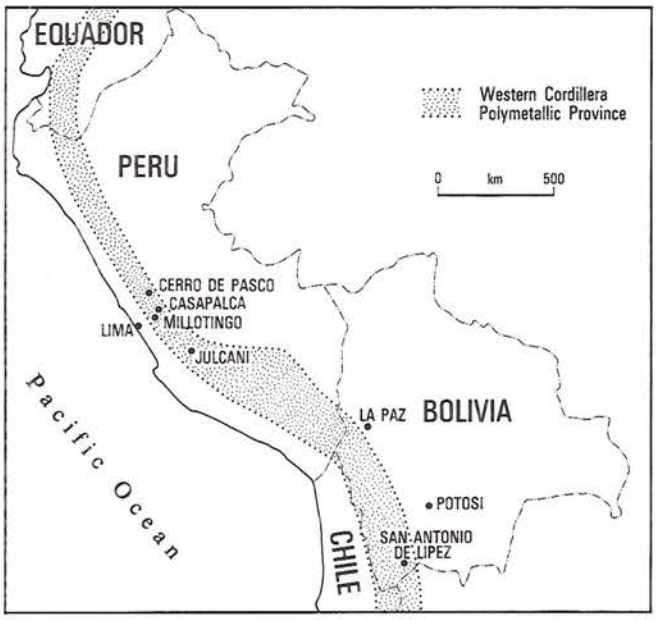

Fig. 1. Location of the San Antonio de Lipez and Millotingo mines within the Western Cordillera polymetallic province.

GEOCHEMICAL TECHNIQUES

Rock samples were collected from surface exposures and in mines by sampling cross-cuts and borehole cores. Cores were sampled by taking approximately ten 100-150 g samples over each 5 or 10 m sampling interval, whilst in the mines, rock chips were taken every 2 m over 10 or 50 m intervals giving aggregate sample weights of approximately 1500 g. The samples were washed, crushed to minus 3 mm and a 100 g split ground to minus 100 microns in a chrome-steel disc mill. SiO_2, Al_2O_3, TiO_2, Total Fe as Fe_2O_3, MgO, CaO, Na_2O, K_2O, MnO, Ag, As, Ba, Cu, Pb, Rb, S, Sb, Sr and Zn were determined by XRF analysis using pressed powder pellets. Hg was determined by flameless AAS and in some cases Ag was determined by AAS following a hot aqua regia digestion. Precision of the XRF analyses based on replicate sample analysis and expressed as the coefficient of variation generally ranges from 12% at 50 ppm to 2% at 1000 ppm.

SAN ANTONIO DE LIPEZ, BOLIVIA

Geology

The Ag-Pb-Zn vein deposit of San Antonio de Lipez, located in SW Bolivia (66°53′W, 21°52′S) within the Western Cordilleran polymetallic province (Ahlfeld, 1967), is emplaced in dacite-rhyodacite lavas and pyroclastics of probable Miocene age (Kussmaul et al., 1977; JICA, 1984). It is one of a group of ten Ag, Pb, Zn, Bi, Au, W, Cu, Sn deposits, exploited for silver during the Spanish Colonial era, that are being reinvestigated by Bolivian state mining organizations. The two main ore zones (I and II; Figs. 2 and 5) extend 600 to 1100 m E-W and 250 to 300 m vertically. They are up to 15 m wide and are formed of a number of smaller parallel veins ranging up to 3 m wide. The veins fill brecciated fissures in altered dacite and contain galena, sphalerite, pyrite, marcasite, chalcopyrite, tetrahedrite, native silver, argentite, pyrargyrite, polybasite, aikinite and greenockite.

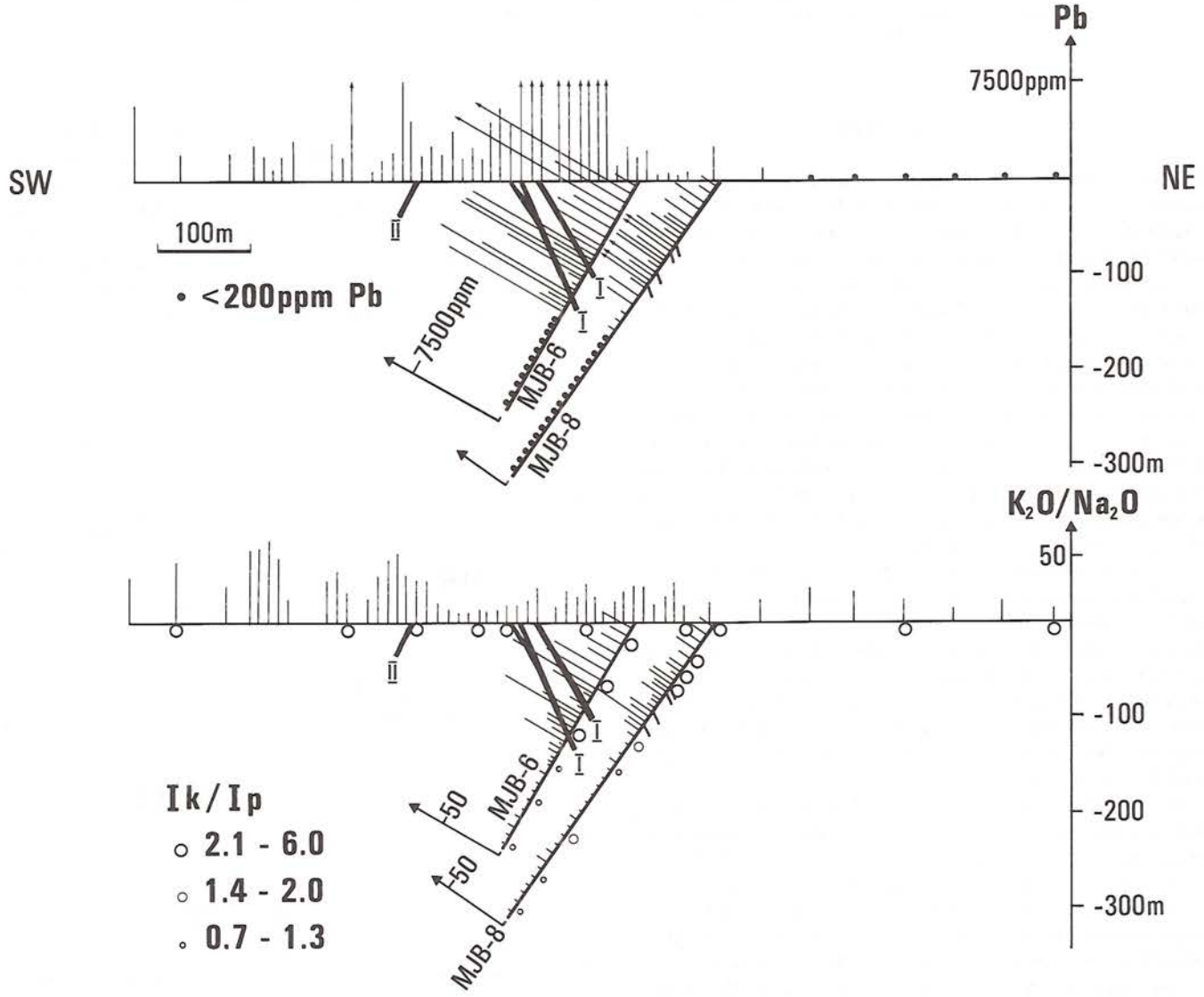

Fig. 2. Pb, K_2O/Na_2O, and Ik/Ip geochemical and mineralogical profiles for the Mesa de Plata adit and boreholes MJB-6 and MJB-8, San Antonio de Lipez, Bolivia. (I = Vein I; II = Vein II; see text for explanation of Ik/Ip).

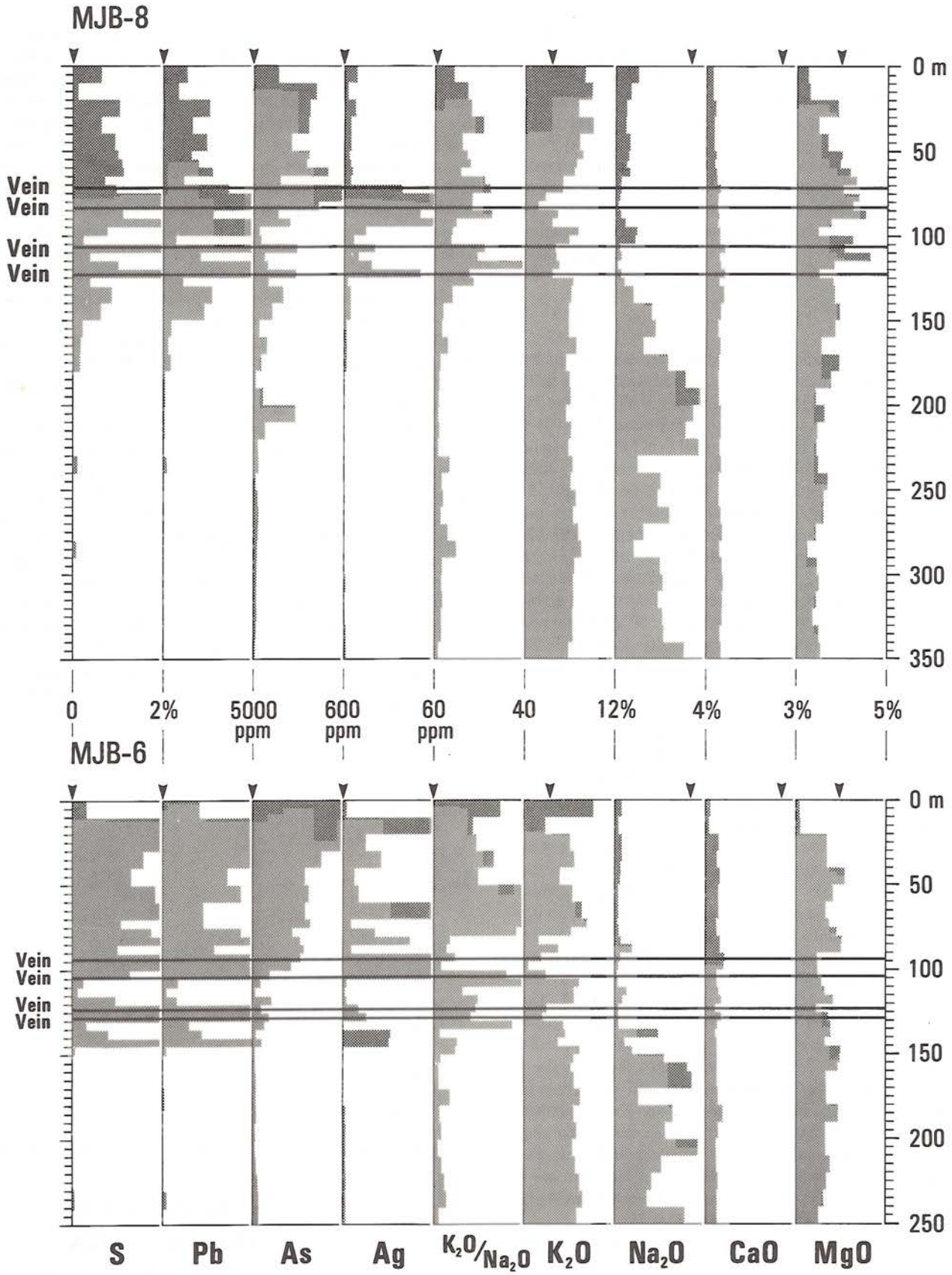

Fig. 3. Geochemical profiles for boreholes MJB-6 and MJB-8, San Antonio de Lipez, Bolivia (arrows indicate unaltered dacite composition; Vein = veins shown on Fig. 2)

Quartz, baryte, and hematite occur as gangue minerals, whilst goethite and covellite are amongst the secondary minerals present. Fluid inclusion studies indicate a temperature of formation of 156-244°C for the early quartz-sulphide mineralization with a lower temperature assumed for the later sulphide-free stage (JICA, 1984). Average grades for veins I and II are 300 g/ton Ag, 1-3% Pb, and 1-3% Zn (JICA, 1984), although the grade is very variable and shoots of higher grade ore are common. Gold values of 9 g/t are reported from silver rich sections of vein I (JICA, 1984). No systematic vertical or lateral variation of base and precious metal values or ratios has been recorded.

Mine Investigations

Mine scale rock geochemical studies were carried out by sampling the only available cross-cut, the Mesa de Plata adit, and two boreholes drilled to locate extensions of Vein I (Fig. 2). The location of the Mesa de Plata adit and boreholes MJB-6 and MJB-8 are shown in Fig. 5. Chemical data for the Mesa de Plata adit exhibit a very strong correlation between the sulphide association ("S") elements (Ag, As, Ba, Cu, Fe, Hg, Pb, S, Sb, Sn and Zn). High "S" element variability reflects the irregular joint/veinlet controlled dispersion associated with the major veins. Relative to unaltered dacite, CaO and Na_2O are strongly depleted and K_2O strongly enriched throughout the 1000 m of the crosscut. K_2O decreases in the immediate vicinity of Veins I and II owing to the influx of "S" elements and advanced argillic alteration. MgO is generally depleted in the altered dacites although close to Veins I and II there is some increase owing to chloritization. The K_2O/Na_2O ratio (Fig. 2) is highly anomalous reaching 64 (mean 21) compared with a normal dacite value of about 1. The K/Rb ratio shows no significant variation, being fairly constant in the range 150 to 180.

Boreholes MJB-6, which intersected Vein I, and MJB-8, which failed to intersect the down-dip extension of Vein I (Fig. 2) have broadly similar geochemical characteristics to the Mesa de Plata adit. Fig. 3 shows that below the vein, Na_2O is not as depleted as above the vein and CaO is depleted throughout the profiles. MgO is generally slightly depleted although in Borehole MJB-8 it is higher in the immediate vicinity of the vein owing to chloritization. K_2O, although enriched throughout the boreholes shows depletion in the immediate vicinity of the vein and slight hanging wall enrichment. Very strong hanging wall "S" element anomalies are illustrated by Ag, As, Pb, and S in Fig. 3. The anomalies extend at least 90 m into the hanging wall whilst in the footwall, both major and trace elements are drastically reduced within only 10-25 m. The rocks below the veins show evidence of hydrothermal alteration and are still anomalous in "S" elements relative to unaltered dacite. As and Pb are enriched by a factor of two and Zn six to ten times. A similar hanging wall/foot wall dispersion pattern has been reported from the Duplex mine in Nevada where the Chief of the Hill vein has a hanging wall anomaly of about 30 m and a footwall anomaly of only about 5 m (Bolter and Al-Shaieb, 1971).

K_2O and Na_2O variation reflects a major difference in mineralogy below and above the vein (Fig. 2). Below Vein I, the andesine-labradorite plagioclase of the unaltered dacite has been converted to a mixture of albite showing relic lamellar twinning and K-feldspar while above Vein I all the plagioclase has been converted to K-feldspar. Alteration of feldspar phenocrysts (both plagioclase and K-feldspar) to hydrous minerals is variable and not strongly reflected in the major oxide chemistry. Kaolinite is generally slightly more abundant than illitic mica-smectite mixed layer clays. Advanced argillic alteration caused by acid leaching is not common although some samples do exhibit this and jarosite is usually the dominant mineral phase. Kaolinite, jarosite and chlorite are the other major alteration minerals in the upper sections of the boreholes which are also characterized by pervasive pyritization. A chlorite rich zone is developed adjacent to Vein I in MJB-8 (Fig. 3) and illitic mica predominates over smectite in the upper sections of the boreholes and also in the Mesa de Plata adit.

The main control over major oxide distribution appears to be the extent of conversion of plagioclase to K-feldspar. Using XRD data, it is possible to illustrate this K-feldspathization by plotting the ratio (Ik/Ip) of the intensity of the K-feldspar 3.24Å peak to that of the plagioclase 3.18Å peak. This technique was originally used to illustrate feldspathization associated with porphyry mineralization (Hausen and Kerr, 1971) but is also applicable to epithermal deposits. The K_2O/Na_2O ratio gives a good estimate of the degree of K-feldspathization (Fig. 4). It should be noted, however, that the Ik/Ip ratio could also be affected by the conversion of plagioclase to clay minerals without a corresponding increase in K-feldspar. The only way to monitor this effectively is to combine XRD and thin-section observations. In the case of boreholes MJB-6 and 8 where the amount of alteration of feldspar (both plagioclase and K-feldspar) to clay minerals is irregular and shows no clear correlation with K_2O/Na_2O, it appears that feldspathization is the main factor controlling Ik/Ip.

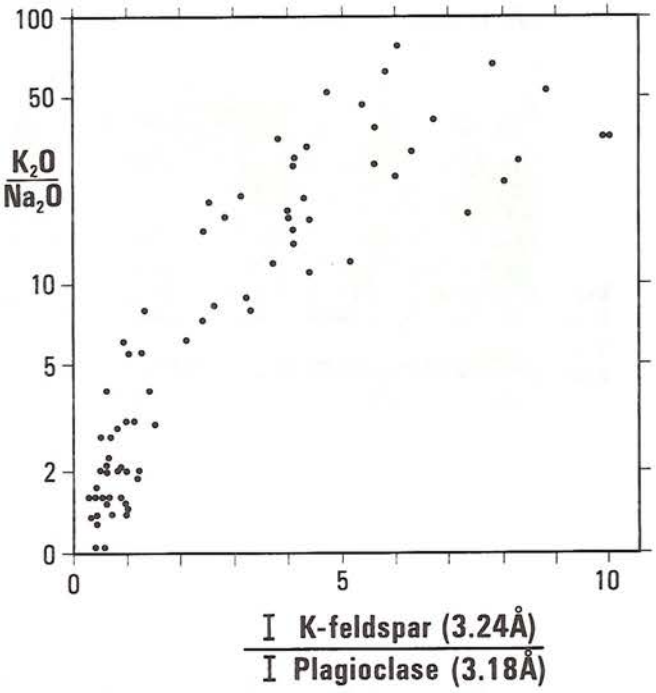

Fig. 4. Relationship between K_2O/Na_2O and K-feldspathisation, indicated by the ratio of the intensities of the K-feldspar (3.24Å) and plagioclase (3.18Å) XRD peaks.

It can be concluded that on a mine scale, constantly or erratically high levels of the "S" elements, K_2O/Na_2O and low K/Rb indicate that there is a relatively high possibility of intersecting major vein mineralization. However, with the type of sampling employed in this study there appears to be no consistent gradual increase towards a major vein. Both "S" element levels and K_2O/Na_2O ratios at the SW end of the Mesa de Plata adit (Fig. 2) suggest that a major vein could exist to the south of the exploited veins (such as a possible eastern extension of an *en echelon* vein cropping out 500 m E. of San Antonio (Fig. 5). After the field work for the present investigations was carried out, drilling intersected significant vein mineralization to the south of the adit showing that rock geochemical and mineralogical indicators can be used as a guide to assist the location of drill holes by providing information that can add weight to structural predictions.

Surface investigations

In surface samples, there are two basic types of alteration which can be detected either chemically or mineralogically. K-feldspathization of the same type noted in the mineralized sections of the boreholes occurs extensively in the old mining area 200-1000 m ENE of San Antonio and also 500 m to the North of San Antonio (Fig. 5). The feldspathized rocks are characterized by Ik/Ip ratios greater than 1 and K_2O/Na_2O ratios in the range 10-60. Jarosite, illitic mica and kaolinite coexist in approximately equal proportions in most of these K-feldspathized rocks. Advanced argillic alteration is developed on a limited scale close to the veins with extreme alteration indicated by the quartz-alunite assemblage. Further away from the main veins (Fig. 5), the alteration is characterized by the partial or total replacement of plagioclase feldspar by calcite and smectite or by a mixture of calcite, smectite and kaolinite. These mildly altered rocks are distinguished by the presence of calcite and low Ik/Ip (<1) and K_2O/Na_2O (<2) ratios. K/Rb ratios are generally high (200-220).

The close association between the "S" elements (Ag, As, Pb, Zn, Sb, Hg) and K_2O/Na_2O noted in the mine and borehole profiles also characterizes the surface samples. This is paralleled by Rb/Sr and MgO/CaO and inversely related to K/Rb which falls to about 150 in the K-feldspathized rocks owing to the preferential enrichment of Rb relative to K.

Strong chemical and mineralogical indicators of mineralization have been identified north of San Antonio where no mineralization has been previously recorded (Fig. 6). More muted chemical and mineralogical anomalies were discovered to the south-east of the known mineralization (Fig. 6). Some of these had strong visible alteration but geochemical data are needed to distinguish them from the low "S", low K_2O/Na_2O, bleached rocks occurring 1 km SSE of the entrance to the Mesa de Plata

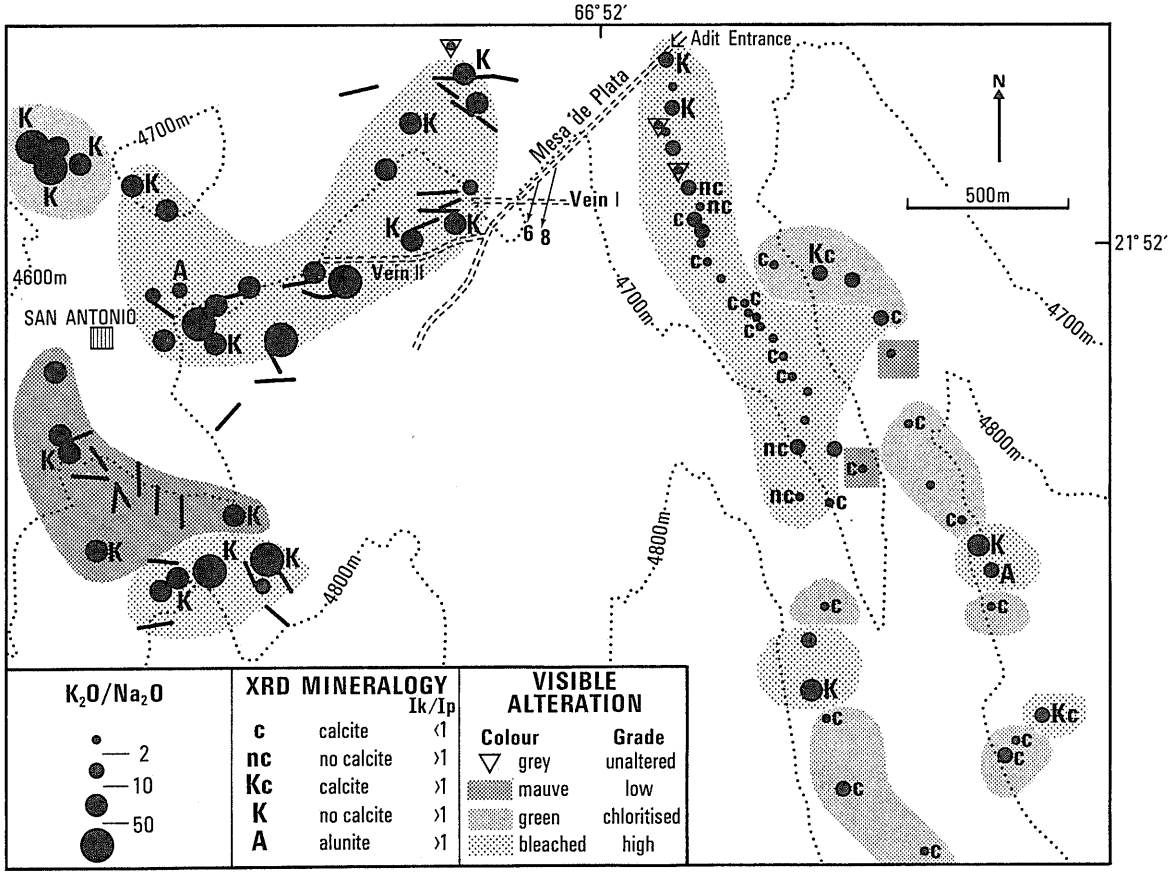

Fig. 5. Relationship between visible alteration, XRD mineralogy and the K_2O/Na_2O ratio in surface samples, San Antonio de Lipez. (arrows 6, 8 = Boreholes MJB-6, -8; dashed lines = surface projection of mine workings; solid line = exposed vein).

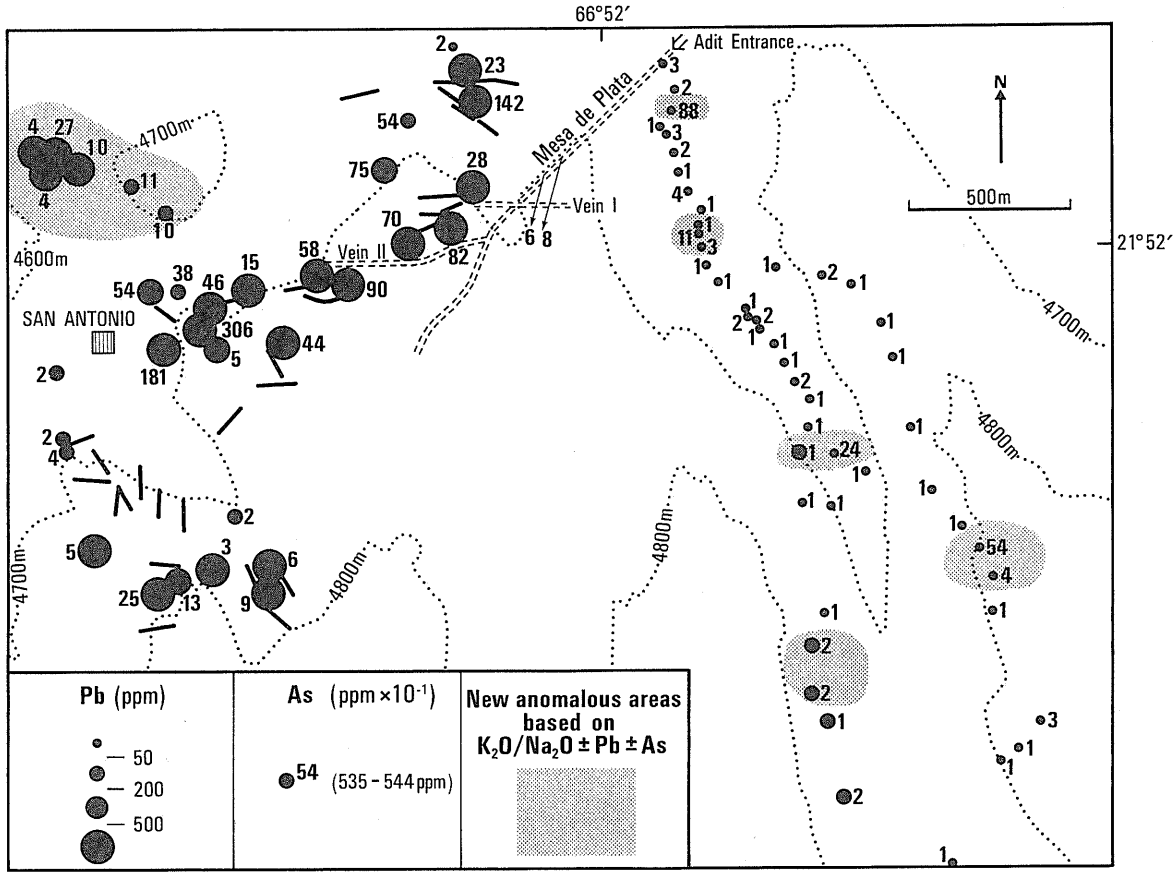

Fig. 6. Pb and As in surface rock samples, San Antonio de Lipez. (Explanation as Fig. 5).

adit. Using the K_2O/Na_2O ratio as an indicator of the strength of hydrothermal alteration, it can be seen from Fig. 5 that the visible alteration characteristics noted in the field are not always a reliable guide to the location of mineralization. Some of the strongly K-feldspathized rocks, such as those 500 m S. of San Antonio (Fig. 5) appear to be weakly altered but their high K_2O/Na_2O and Ik/Ip ratios (Fig. 5) and "tile-texture" K-feldspar (Steiner, 1977) indicate their true alteration state. Conversely, bleached, apparently strongly altered rocks 1000 m SSE of the adit entrance have low K_2O/Na_2O, Ik/Ip, As and Pb (Figs. 5 and 6) indicating weak alteration. This confirms the importance of chemical and mineralogical information when using hydrothermal alteration as an exploration guide.

MILLOTINGO SILVER MINE

Geology

The epithermal silver deposit of Millotingo, located 98 km ENE of Lima (76°14′W, 11°49′S) in the Western Cordillera polymetallic belt of the Andes (Fig. 1), is emplaced in a sequence of Lower to Middle Tertiary lavas, tuffs and pyroclastics of andesite to rhyolite composition (Salazar, 1983). Mineralization occurs in faults 5 to 10 cm wide and as an intense dissemination in minor fractures parallel to the fault producing a mineralized zone over 5 m wide. Polybasite, proustite and pyrargyrite together with traces of galena, sphalerite, and chalcopyrite are the main minerals with quartz and calcite as gangue. The vertical extent of the mineralization is 300-400 m. Galena increases with depth as silver decreases. Grey chalcedonic quartz and pyritization are reported to be the best guides to rich mineralization; white crystalline quartz generally being a negative indicator.

On the surface, the main San Juan vein crops out over 900 m (Fig. 9) and is marked by vein quartz, limonite and silicified rocks. Some kaolinization occurs but the bleaching is generally limited to 1 to 5 m either side of the vein, being much more restricted than in the San Antonio de Lipez area. Annual production is approximately 100,000 tons grading 200 g/t Ag with traces of recoverable Au.

Mine investigations

In the mine, propylitic alteration, incorporating alteration of plagioclase to carbonate, albite and clay minerals accompanied by chloritization of the matrix and some epidotization, affects most of the andesitic rocks. Geochemical profiles for a Level 30 cross-cut (altitude 4135 m, location shown on Fig. 9), illustrate the comparatively restricted, low contrast dispersion

associated with the silver mineralization (Fig. 7a). Pyritization decreases away from the veins as do As, Sb and Ag. Na_2O and CaO gradually decrease towards the veins while K_2O and SiO_2 increase, reflecting the K-feldspathization and silicification that accompanies the mineralization. This hydrothermal alteration can be detected by XRD using Ik/Ip ratios and also microscopically, because "tile texture" K-feldspar (Steiner, 1977) occurs in the strongly altered zone 5-10 m either side of the

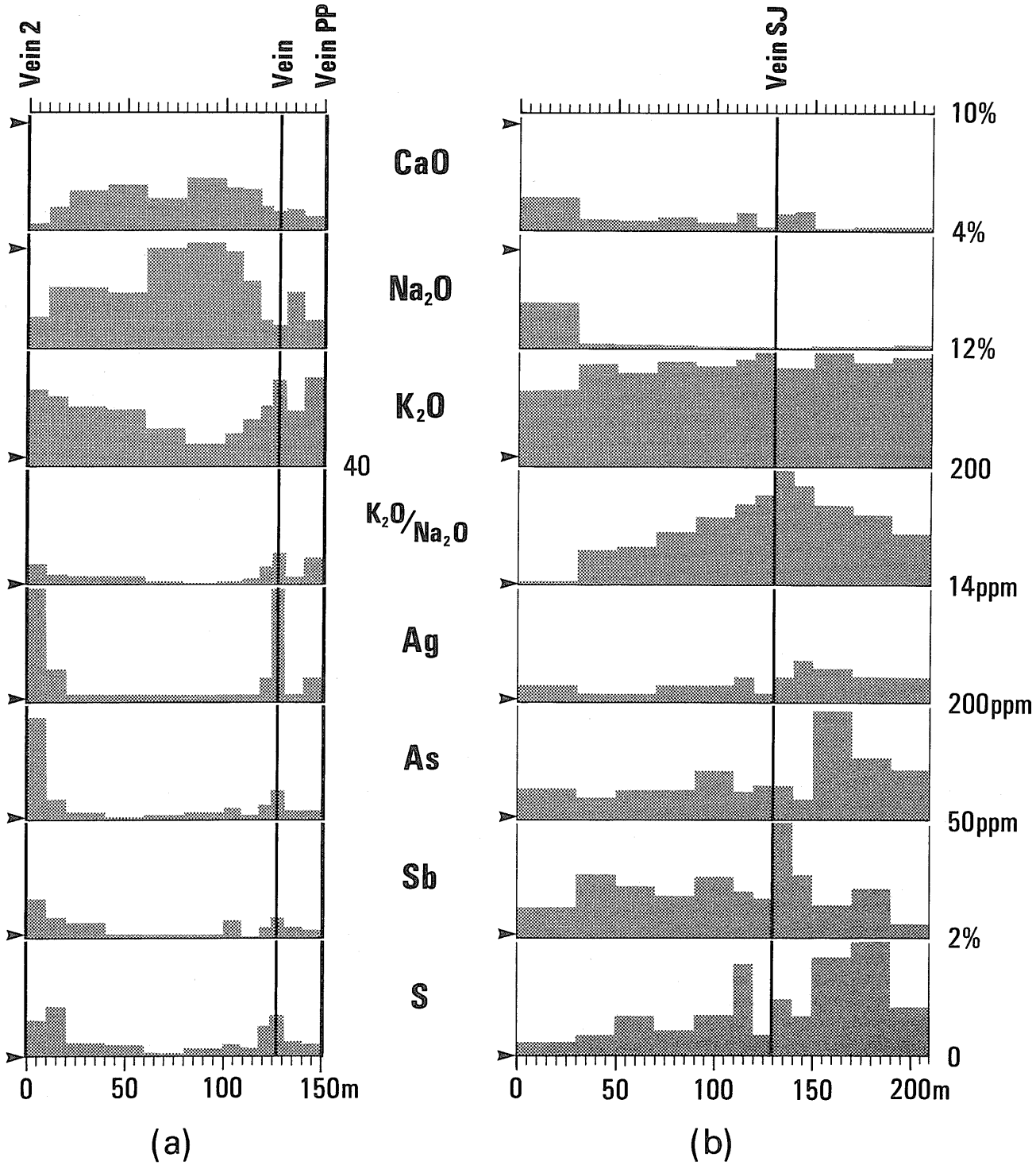

Fig. 7. Geochemical profiles for (a) cross-cut 30N and (b) Level 2 adit entrance cross-section, Millotingo mine, Peru. (arrows indicate unaltered andesite composition; PP = Pozo de Plata; SJ = San Juan; location of cross-cut and section shown on Fig. 9).

major veins. Compared with single element or ratio plots, R-mode factor score plots generally produce smoother and more distinct dispersion profiles, in some cases allowing the detection of a vein from a distance of 50 to 60 m (Fig. 8). For the Level 30 cross-cut (Fig. 8), Factor 1 accounts for 48% of the variance and has loadings of +0.67 to +0.91 for SiO_2, K_2O Ag, As, Ba, Pb, Rb, S, Sb, Rb/Sr, and K_2O/Na_2O and −0.60 to −0.84 for Total Fe, TiO_2, MgO, CaO, Na_2O, Sr and CaO/MgO. Such smooth profiles are not always seen, neither is the dispersion halo always so extensive. For example, in one of the Level 2 cross-cuts (altitude 4165 m), slightly propylitized andesite occurs only 10 m from the major Pozo de Plata vein.

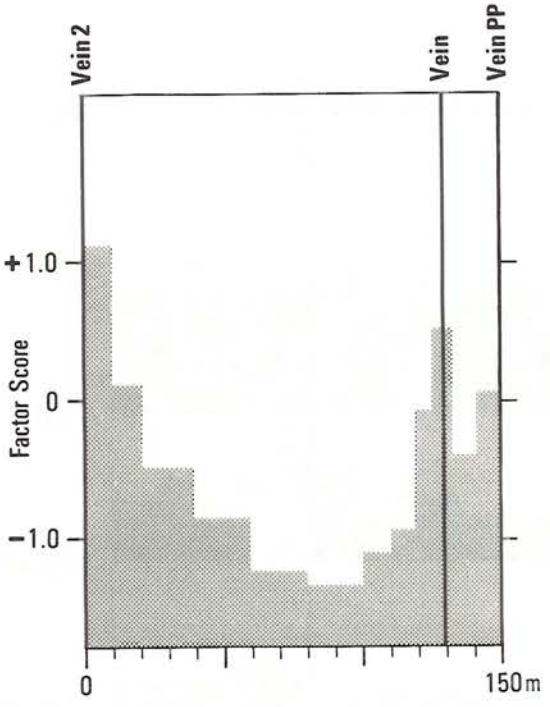

Fig. 8. Factor score profile for cross-cut 30N, Millotingo mine (cf. Fig. 7a; factor loadings given in text.)

At the entrance to the Level 2 adit, 100 m wide sections in andesite either side of the San Juan vein shown strong depletion of CaO and Na_2O while K_2O is correspondingly enriched (Fig. 7b). Although the "S" elements Ag, As, Sb and S are all enriched relative to unaltered andesite, they do not show any gradual increase towards the vein. In this example, it is the major element variation reflecting hydrothermal alteration that gives a smoother dispersion profile. K_2O/Na_2O (Fig. 7b) and SiO_2 increase and TiO_2, Total Fe, and Al_2O_3 decrease systematically towards the vein, illustrating that even in highly altered andesites, the approach to a major vein can, in some cases, be monitored by major element variation over a distance of more than 100 m.

Surface investigations

In surface samples, both alteration mineralogy and rock chemistry provide guides to the location of veins which at the surface usually only exhibit 1 to 2 m wide zones of visible alteration. As in the mine sections there is a close link between mineralogical alteration and major element chemistry (Figs. 9 and 10). The K_2O/Na_2O ratio is a particularly good indicator of the potassic alteration closely associated with the silver mineralization. R-mode factor analysis for the surface samples shows that the first factor, which accounts for 52% of the variation, has strong positive loadings of 0.64 to 0.94 for SiO_2, K_2O, Ag, As, Rb, S, Sb, Rb/Sr, Rb/K, and K_2O/Na_2O while Na_2O, CaO, CaO/MgO, and $(H_2O + CO_2)$ have strong negative loadings of 0.79 to 0.83. This confirms the link between potassic alteration, silicification and the vein mineralization and again illustrates the potential of chemical and mineralogical alteration as exploration guides for this type of mineralization.

In modern geothermal systems (Browne, 1978) rock permeability controls the extent and grade of mineralogical alteration so "S" element dispersion halos should be similarly controlled (cf., Pirie and Nichol, 1981). Although insufficient sampling was carried out to prove this conclusively in the Millotingo area, andesite lava and breccia samples collected 5 m apart about 650 m NNW of the mine entrance (Fig. 9) show that whilst the lava is almost fresh and has normal andesite major and trace element chemistry, the breccia is strongly propylitized and has As and Sb values two to three times above background levels.

DISCUSSION

Comparison of Rock Geochemistry and Mineralogical Alteration as Exploration Guides

Multielement rock geochemical and mineralogical investigations of the Ag-Pb-Zn vein deposit of San Antonio de Lipez, Bolivia and the Ag-Au vein deposit of Millotingo, Peru illustrate the extent and nature of alteration associated with these two contrasting epithermal silver deposits. Although the limited areal extent and strength of geochemical and mineralogical alteration halos at Millotingo contrast with those observed in the San Antonio de Lipez area, alteration patterns in both areas are clearly defined geochemically by Ag, As, Pb, S, Sb, Zn, K_2O/Na_2O, K/Rb, and Rb/Sr and by mineralogical indicators such as progressive K-feldspathization.

Hydrothermal alteration associated with these deposits is reflected by regional propylitization with K-feldspathization, argillic and silica-alunite alteration and silicification being more directly associated with the mineral veins. Although the results of our thin section and XRD studies do not confirm previous investigations in detail (JICA, 1984), it has been shown that mineralogical indicators such as calcite and the Ik/Ip ratio can be used as guides for distinguishing between apparently similar levels of visible alteration on a regional basis and also in borehole cores. The most significant mineralogical indicators of mineralization can be determined using geochemical indicators such as the K_2O/Na_2O ratio with the added advantage that a wide range of elements may be determined simultaneously using multielement analytical techniques such as XRF.

Multielement geochemistry is also more cost effective as XRF determination of the 18 elements used in this study cost

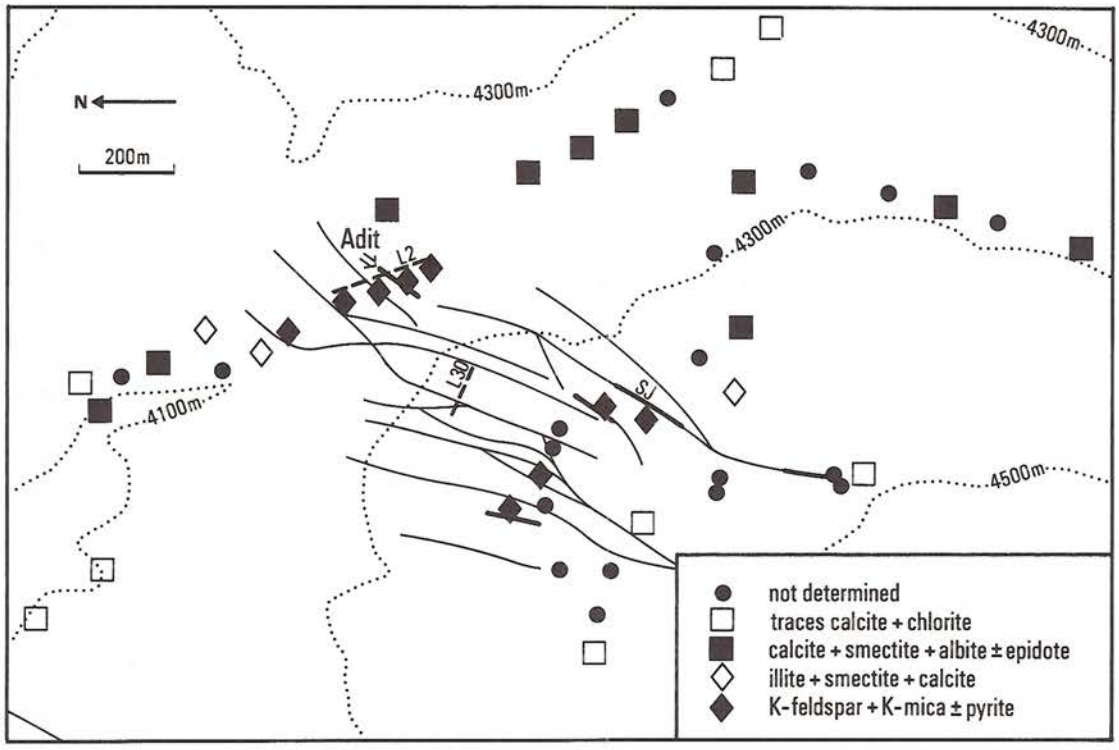

Fig. 9. Mineralogical alteration in surface rock samples from Millotingo, Peru. (thin continuous line = surface projection of underground vein; solid line = surface exposure of vein, SJ = San Juan vein; dashed lines = surface projection of cross-cut 30 (L30) and position of Level 2 adit entrance section (L2) shown in Figs. 7 and 8).

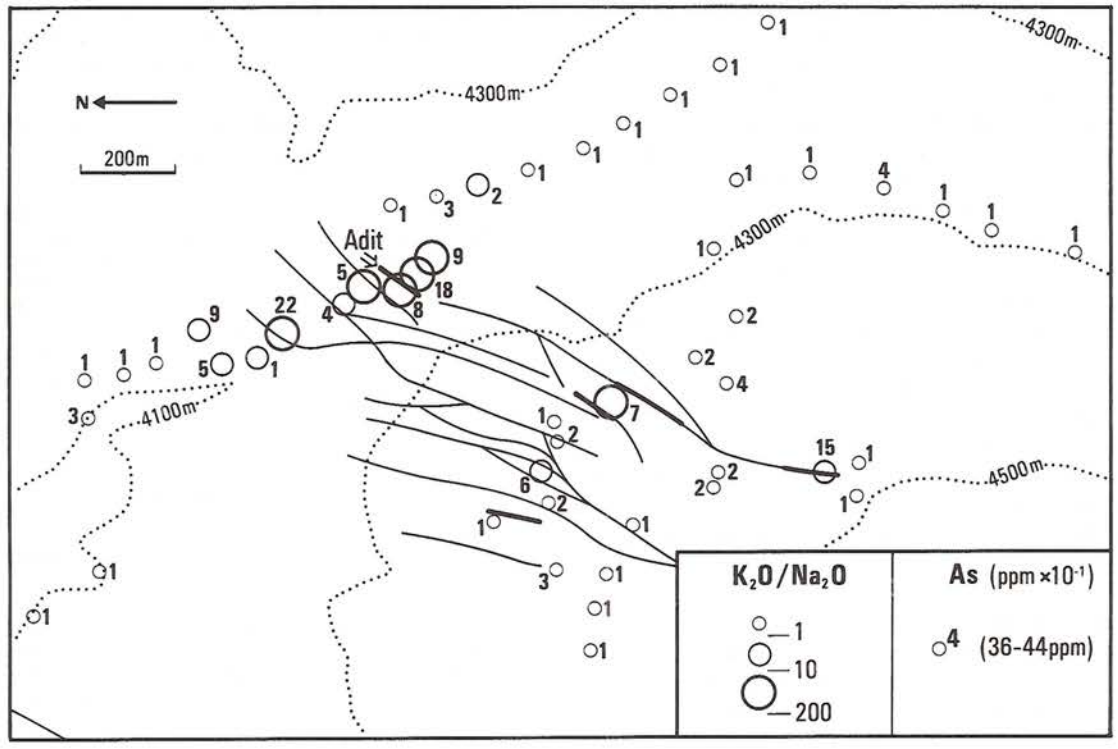

Fig. 10. K_2O/Na_2O ratio and As in surface rock samples, Millotingo, Peru (explanation as Fig. 9.)

U.S. $12 compared with approximately U.S. $20 for an XRD scan with identification of specified minerals or U.S. $140 for an XRD scan with full interpretation and clay mineral speciation. In a developing country where labour costs are relatively low and complex instrumentation inappropriate, the most important elements (Ag, As, K, Na, Pb and Zn) could be determined by a combination of AAS and colorimetry.

The recommended approach is to use multielement rock geochemistry as a guide to both the hydrothermal alteration halos and dispersion of the ore elements accompanied by limited thin section and XRD investigations designed to identify hydrothermal alteration parageneses.

Comparison with Other Cordilleran Epithermal Deposits

The limited amount of rock geochemical data published on other North and South American cordilleran epithermal and mesothermal vein-type deposits such as the Ag-Pb-Zn deposits of Julcani, Peru (Scherkenbach and Noble, 1984 and Fig. 1), Pachuca, Mexico (Dreier, 1982) and the San Juan Mountains, Colorado, USA (Fisher and Leedy, 1973) illustrates that rock geochemistry is generally applicable as an exploration method.

Using only K_2O, Rb and Sr, Scherkenbach and Noble (1984) concluded that K_2O and Rb could be used as guides to mineralization on both regional and mine scales. K_2O and Rb/Sr ratio anomalies extend up to 350 m either side of major veins at Julcani. As at San Antonio de Lipez, narrow zones of K and Rb depletion and Sr enrichment are found adjacent to some veins, presumably reflecting advanced argillic alteration. Mineralogical alteration in the Julcani area is similar to that described in the San Antonio area.

At Pachuca in Mexico, mineralogical alteration and geochemical dispersion appear to be broadly similar to the Millotingo area in Peru, although geochemical profiles were presented for only Ag, Pb and Zn (Dreier, 1982). In mine cross-cuts, significant anomalies were found to extend only 2 to 5m from the veins and it was concluded that Ag, Pb and Zn could be used only for regional prospecting and not as a guide to the detailed location of veins. As, Sb, CaO, K_2O and Na_2O could potentially define more useful alteration patterns.

In the San Juan Mountains area of Colarado, USA, Ag, As, Au, Bi, Pb and Sb are the most useful geochemical guides to breccia pipe mineralization with the highest metal values associated with silicified rocks (Fisher and Leedy, 1973). Burbank and Luedke (1968) working in the same area reported that alteration related to ore mineralization was restricted to a few tens of feet. Although not stated by Fisher and Leedy (1973) it is clear from their data that propylitized lavas and breccias with highly anomalous K/Na ratio in the range 64-70 exist at least 150 m from the intensively silicified and mineralized rocks of the National Belle and Hero Mines. This suggests that the K/Na ratio could provide wider dispersion halos than ore elements such as As and Au.

In the Goldfield mining district of Nevada, USA, Ashley and Keith (1978) concluded that sampling should be restricted to the silicified ledges directly associated with the main ore deposits. In view of the apparent importance of major element ratios such as K/Na it would be interesting to see if the argillic zones surrounding mineralized silicified ledges had more intense major element halos compared with those surrounding non-mineralized ledges, thus perhaps providing more extensive geochemical anomalies than for the ore elements such as Au, Ag and Pb.

CONCLUSIONS

(1). In dacitic volcanic rocks of the San Antonio de Lipez area, constantly or erratically very high levels of "S" elements (Ag, As, Fe, Hg, Pb, S, Sb, and Zn), and the K_2O/Na_2O and Rb/K ratios indicate a relatively high possibility of intersecting major vein minerlization. With the type of sampling employed in this study there appears to be no consistent gradual increase towards a major vein. Strong anomalies extend at least 90 m into the hanging wall and high background levels of the "S" elements together with moderately elevated K_2O/Na_2O, Rb/Sr, Rb/K and MgO/CaO ratios extend at least 300 m from the zone of erratically very high values providing a wide rock geochemical exploration target. K-feldspathization, closely associated with the vein mineralization, can ba determined chemically using the K_2O/Na_2O ratio and by XRD using the Ik/Ip ratio.

(2). Similar but less intense and often less extensive alteration patterns in andesitic volcanic rocks are associated with the Ag-Au epithermal veins at the Millotingo mine in Peru. In some cases using factor score techniques extends the alteration anomaly over 100 m.

(3). Both major element and mineralogical methods can be used to indicate the mineral potential of areas with similar levels of visible alteration. Multielement rock geochemical data is more economically obtained than mineralogical data and permits the detection of "S" element dispersion in addition to ore related hydrothermal alteration thereby making it a more reliable exploration method.

(4). Similarities between the San Antonio and Millotingo vein deposits and epithermal precious and base metal vein deposits in Mexico, Peru and the USA suggest that rock geochemical techniques could be widely applicable in Cordilleran environments of Central and North America.

Acknowledgements — The work described in this paper was largely funded by the Overseas Development Administration of the Foreign and Commonwealth Office, United Kingdom. Logistic support provided by COMIBOL, INGEMMET, and Cia. Minera Millotingo S.A. is gratefully acknowledged as is the assistance with XRD determinations given by R. Merriman and B. Young. For constructive criticism of the manuscript, the authors wish to thank I. L. Elliott, G. E. McKelvey, J. Ridgeway and C. R. Allan. Permission to publish was granted by the Directors of the British Geological Survey (NERC), COMIBOL, Bolivia and INGEMMET, Peru.

REFERENCES

Ahlfeld, F., 1967, Metallogenic epochs and provinces of Bolivia. Min. Deposita, v. 2, p. 291-311.

Ahlfeld, F., and Schneider-Scherbina, A., 1964, Los Yacimientos Minerales y de Hidrocarburos de Bolivia. Ministerio de Minas y Petróleo. La Paz, Bolivia. Bol. No. 5 (Especial) 388 p.

Appleton, J. D. (in prep.), Application of rock geochemistry to mineral exploration. Final Report to Overseas Development Administration, U. K.

Ashley, R. P., and Keith, W. J., 1978, Goldfield mining district, Esmeralda County, Nevada: J. Geochem. Explor., v. 9, p. 204-208.

Bolter, E., and Al-Shaieb, Z., 1971, Trace element anomalies in igneous wallrocks of hydrothermal veins: *in* Boyle R. W. and McGerrigle J. I. (editors), Geochemical Exploration. Can. Inst. Min. Metall., Spec. Vol. 11, p. 289-290.

Browne, P. R. L., 1978, Hydrothermal alteration in active geothermal fields: Annual Review Earth Planet. Sci. v. 6, p. 229-250.

Burbank, W. S., and Luedke, R. G., 1968, Geology and ore deposits of the Western San Juan Mountains, Colorado, *in* Ridge J. D. (editor), Ore deposits of the United States, 1933-1967. The Graton Sales Volume. New York. Am. Inst. Min. Metall. Pet. Eng., p. 714-733.

Dreier, J. E., 1982, Distribution of wall rock alteration and trace elements in the Pachuca-Real Del Monte District, Hildalgo, Mexico: Min. Eng., v. 34, p. 699-704.

Fisher, F. S., and Leedy, W. P., 1973, Geochemical characteristics of mineralized breccia pipes in the Red Mountain district, San Juan Mountains, Colorado: U.S. Geol. Surv. Bull. 1381, 43 p.

Hausen, D. M., and Kerr, P. F., 1971, X-ray diffraction methods of evaluating potassium silicate alteration in porphyry mineralization, *in* Boyle R. W. and McGerrigle J. I. (editors), Geochemical Exploration. Can. Inst. Min. Metall., Spec. Vol. 11, p. 334-340.

JICA (Japan International Cooperation Agency), 1984, Informe de investigación geológica en area de San Antonio de Lipez, República de Bolivia, Fase II: unpublished report, 85 p.

Kussmaul, S., Hornmann, P. K., Ploskonka, E., and Subieta, T., 1977, Volcanism and structure of southwestern Bolivia: J. Volc. Geoth. Res., v. 2, p. 73-111.

Peterson, U. 1965, Regional geology and major ore deposits of Central Peru. Econ. Geol., v. 60, p. 407-476.

Pirie, I. D. and Nichol, I., 1981, Geochemical dispersion in wallrocks associated with the Norbec deposit, Norbec, Quebec: J. Geochem. Explor., v. 15, p. 159-180.

Salazar, H., 1983, Geología de los cuadrangulos de Matucana y Huarochirí: Inst. Geol. Min. Metal. Peru, Serie A, Carta Geológica Nacional, Bol. No. 36, 68 p.

Scherkenbach, D. A., and Noble, D. C., 1984, Potassium and rubidium metasomatism at the Julcani District, Peru: Econ. Geol., v. 79, p. 565-572.

Steiner, A., 1977, The Wairakei geothermal area, North Island, New Zealand: Its subsurface geology and hydrothermal rock alteration: N. Z. Geol. Surv. Bull. 90, 136 p.

Application of R-Mode Factor Analysis to Geochemical Studies in the Eureka Mining District and Vicinity, Eureka and White Pine Counties, Nevada

M. A. CHAFFEE
U.S. Geological Survey, Box 25046, MS 973, Federal Centre, Denver, CO 80225-0046

Abstract — The Eureka mining district, in east-central Nevada, was a major producer of Ag, Au, and Pb, primarily from Paleozoic carbonate formations. A total of 593 <0.063-mm soil samples were analyzed for 31 different elements. After samples thought to be contaminated by smelters were eliminated, 441 samples remained. Of the original 31 elements, enrichments of 15 (Ag, As, Au, Ba, Bi, Cd, Cu, Hg, Mn, Mo, Pb, Sb, Sn, W, and Zn) were deemed to be partly or entirely related to mineralization.

Evaluations of R-mode factor-analysis data and interpretations of factor-score and single-element anomaly maps suggest that:

(1) rocks in antiform structures are better ore hosts than are those in synforms:

(2) some of the formations in the antiforms may be more important ore hosts than has been recognized to date;

(3) two distinct precious-metal-related geochemical associations exist: an Ag-rich base-metal suite (Ag-Cu-Pb-Sb-Zn) and a "Carlin-type" Au suite (As-Hg-Sb);

(4) factor-score distribution maps should be useful as exploration guides; and

(5) information derived from factor analysis may provide a better understanding of the genesis of the Eureka district, as well as that of other areas that may be the result of more than one episode of mineralization.

INTRODUCTION

A GEOCHEMICAL study has been conducted in and around the Eureka mining district, Nevada. The principal objective of the study was to chemically and spatially characterize the mineral deposits present in this area.

Eureka and its associated mining district are in east-central Nevada about 125 km west of Ely (Fig. 1). The most important mine production from the area was between 1870 and 1893 (Nolan and Hunt, 1968), with the most significant mining during this period of oxidized massive-replacement, carbonate rock-hosted Pb-Ag-Au ores. In recent years mining and exploration have been oriented toward sedimentary rock-hosted, disseminated Au deposits.

No district-wide geochemical investigations of the Eureka area have been published to date. A limited study was conducted in the extreme northern part of the Eureka mining district (Miesch and Nolan, 1958), and analyses for samples collected in the vicinity of the Windfall mine have been published (Grove, 1979; Hill et al., 1986). The analyses used for the present study have also been published (Chaffee et al., 1978).

GEOLOGIC SETTING

Regional geologic setting

The Eureka district lies near the margin of a major structural feature, the Roberts Mountains thrust fault. In addition, the boundary between two metallogenic provinces has been postulated to transect the study area (Roberts, 1966; Roberts et al., 1971) (Fig. 1). The eastern margin of the Roberts Mountains thrust fault of Devonian to Mississippian age has been mapped just to the west of the study area (Nolan and Hunt, 1968; Nolan et al., 1971; 1974; Stewart, 1980) (Fig. 1). This major fault moved a sequence of predominantly siliceous clastic and volcanic rocks of the western facies assemblage in Nevada east-

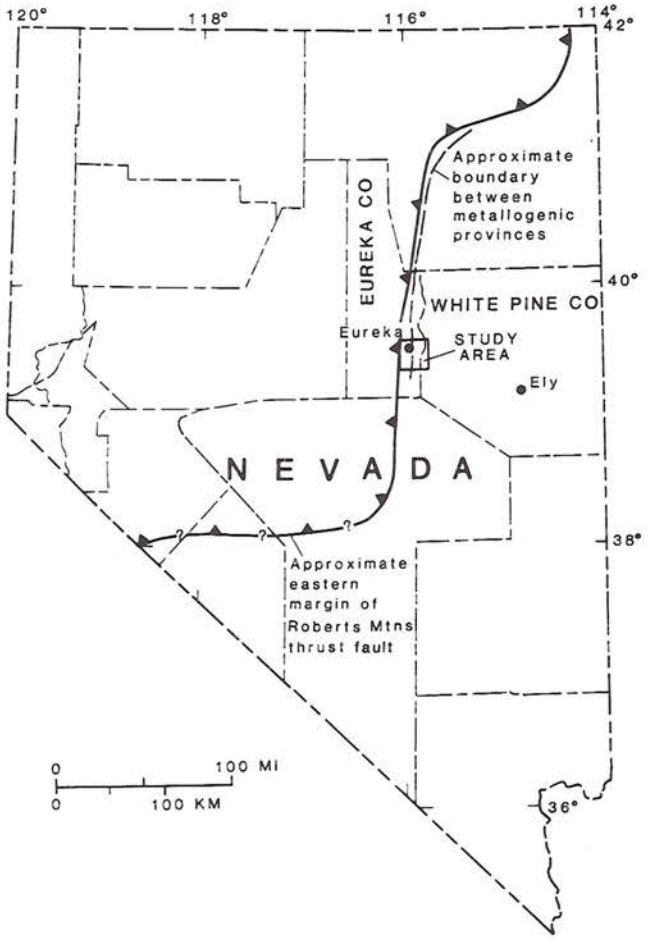

Fig. 1. Map of Nevada showing location of study area. Solid line shows the approximate eastern limit of the Roberts Mountains thrust fault from Stewart (1980). Dashed line shows the approximate location of the boundary between the two major metallogenic provinces defined by Roberts and others (1971).

ward over a sequence containing predominantly marine carbonate rocks of the eastern facies assemblage. Although there is no positive evidence that the upper plate of this fault ever existed in the study area, the area is very near to the margin of the plate, thus presenting an environment analogous to that of many of the sedimentary rock-hosted Au deposits in Nevada that are found in the autochthonous eastern facies rocks where they are exposed through the upper plate rocks.

On the basis of their studies of the chemistry and mineralogy of known mineral deposits in north-central Nevada, Roberts (1966) and Roberts et al. (1971) suggest that this area can be divided into two distinct, major metallogenic provinces. They have placed the boundary between these two just east of the Eureka district (Figs. 1 and 8). Their western province is characterized by As-, Au-, Hg-, and Sb-rich deposits that commonly occur in Paleozoic eugeosynclinal clastic and volcanic rocks of the western facies assemblage, in lithologically similar Mesozoic rocks, and in Tertiary volcanic rocks. Their eastern province is characterized by Pb and Zn deposits, many accompanied by Ag and Au, that commonly occur in Paleozoic miogeosynclinal carbonate rocks of the eastern facies assemblage. Copper, Mo, and W deposits occur in both provinces (Roberts et al., 1971).

Local geologic setting

The geology of the Eureka area is complex and will not be discussed at length. Detailed studies of the local geology, structure,

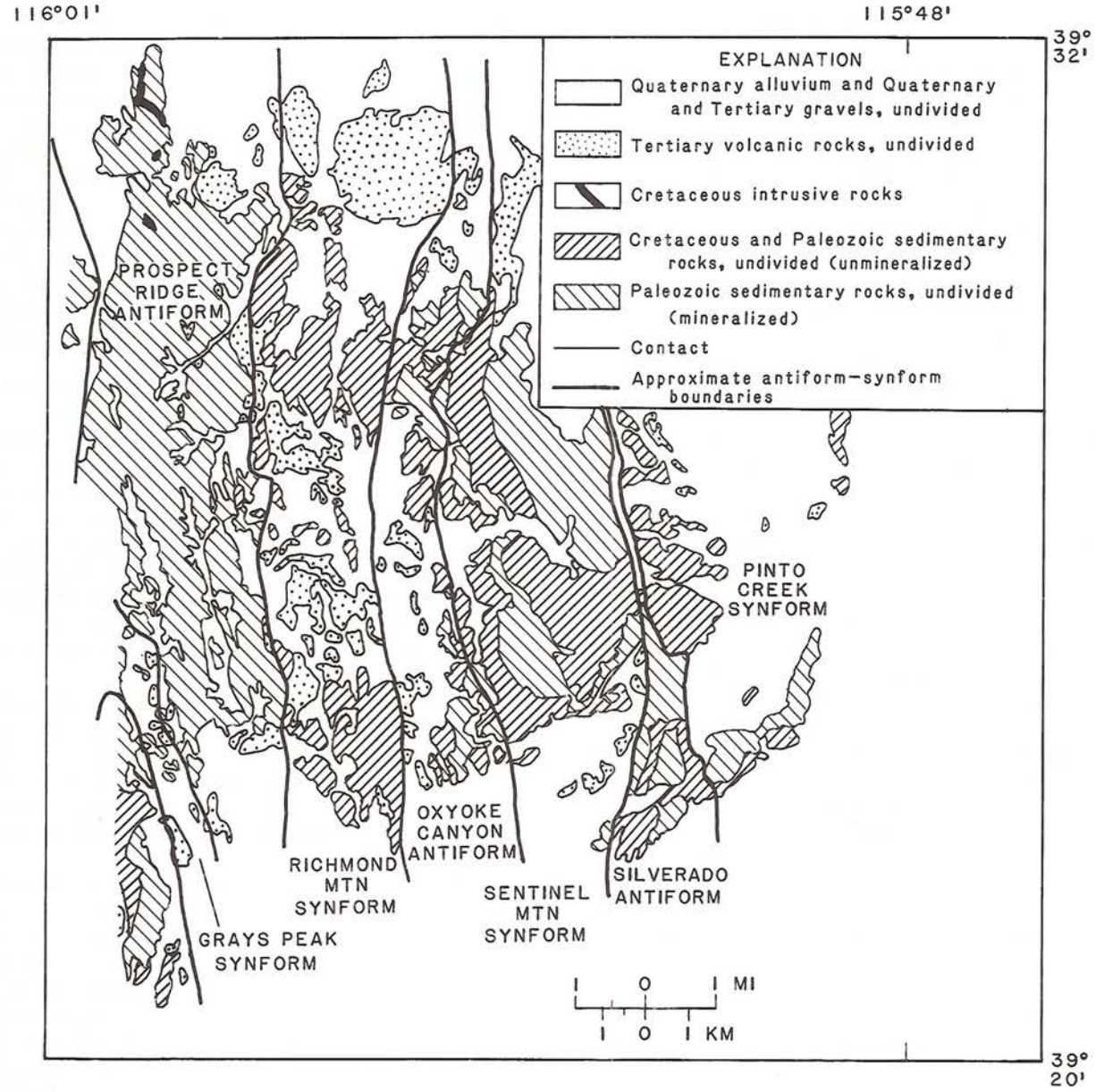

Fig. 2. Generalized geologic map of the Eureka district and vicinity, Eureka and White Pine Counties, Nevada. Geology modified from Nolan et al. (1971; 1974) and Nolan (written communication, 1975).

and mineral deposits have been conducted by Nolan and various co-workers (see, for example, Nolan, 1962; Nolan and Hunt, 1968; Nolan et al., 1956; 1971; 1974) and by Hose et al. (1982). A generalized geologic map of the study area (Fig. 2) has been constructed using information given in these references.

Folding and faulting are well-developed and widespread throughout much of the study area. Many of the resulting structures have served as conduits for mineralizing solutions (Nolan, 1962). On the basis of styles of structure and of stratigraphy, Nolan et al. (1971; 1974) have divided the Eureka area into a series of north-south-trending antiforms and synforms. Their field investigations indicate that mineralization seems to be restricted to the antiforms. The boundaries of these structures are delineated by faults and are shown on Figs. 2 to 8. Localities described below are shown on Fig. 3.

Rocks in the study area range in age from Cambrian to Holocene; most of the outcrops are Paleozoic sedimentary formations. For this report, the recognized geologic formations have been grouped into five units (Fig. 2), based primarily on the past importance of each formation as an ore host. The first unit, labelled "Paleozoic sedimentary rocks, undivided (mineralized)", consists of (1) the Eldorado Dolomite, the Geddes Limestone, the Hamburg Dolomite, the Windfall Formation, the Pogonip Group, the Eureka Quartzite, and the Hanson Creek Formation — all of which crop out only in the Prospect Ridge antiform — and (2) the Devils Gate Limestone, the Beacon Peak Dolomite, the Woodpecker Limestone, the South Hill Sandstone, and the Bay State Dolomite, which crop out in either the Grays Peak synform on the west side of the study area or in the structures east of the Richmond Mountain synform.

The Eldorado Dolomite and the Hamburg Dolomite were the two most important host formations for ores from the mines found along the Prospect Ridge antiform. Mineralization in the other formations in this first geologic unit is known to occur only within the Prospect Ridge and Silverado antiforms and is generally restricted to specific localities within each of these formations.

The second unit, labelled on Fig. 2 "Cretaceous and Paleozoic sedimentary rocks, undivided (unmineralized)", consists of the Prospect Mountain Quartzite, the Pioche Shale, the Secret Canyon Shale, the Dunderberg Shale, the Lone Mountain Dolomite, the Grays Canyon Limestone, the Oxyoke Canyon Sandstone, the Sentinel Mountain Dolomite, the Pilot Shale, the Joana Limestone, the Dale Canyon Formation, the Chainman Shale, the Diamond Peak Formation, the Ely Limestone, the Carbon Ridge Formation, and the Newark Canyon Formation. None of these formations has been identified previously as an ore host in the study area.

The third unit, labelled "Cretaceous intrusive rocks", consists of two major outcrops (Nolan et al., 1971; 1974). The first is a quartz diorite plug, which has been dated at approximately 99 Ma and crops out just south of Ruby Hill (Figs. 2 and 3). This outcrop is the surface expression of a much larger body that has been identified by deep drilling (Nolan and Hunt, 1968) and by a magnetic anomaly (U.S. Geological Survey, 1968). The second outcrop, mapped north of Adams Hill (Figs. 2 and 3), comprises quartz porphyry dike- and sill-like masses, which are thought to be approximately the same age as the plug (Nolan, written communication, 1986).

The fourth unit, labelled "Tertiary volcanic rocks, undivided", consists of volcanic tuffs and flows, which vary in composition from rhyolite to basalt. Most of the outcrops shown on Fig. 2 range in age from approximately 38 Ma to 34 Ma. A few small outcrops in the southeastern part of the map have been dated at about 20 Ma (Nolan et al., 1974). Some relatively small intrusive volcanic dikes are also included in this unit; most of these bodies are too small to be shown on the geologic map.

The fifth unit, shown unpatterned on Fig. 2, consists of Tertiary and Quaternary gravels and Quaternary alluvium.

TYPES OF MINERALIZATION

Several types of ore have been mined in the Eureka area. Most of the production in the district has been oxidized, Ag- and Au-rich Pb ores found as massive-replacement fissure, manto, and pipe-like bodies in the Hamburg Dolomite and the Eldorado Dolomite and, to a lesser extent, in limestones of the Pogonip Group. Most of this production was from mines in the northern part of the Prospect Ridge antiform, particularly from the mines in the Ruby Hill area (Fig. 3) (Nolan, 1962); however, similar ores have been mined at many localities along the Prospect Ridge antiform. Oxidized As, Cu, Mo, and Zn minerals are present locally (Curtis, 1884; Nolan, 1962). Sulfide minerals, including sphalerite, galena, pyrite, arsenopyrite, and molybdenite, are present in the deepest workings in the district and have been seen in core from deep drill holes (Nolan and Hunt, 1968).

A different type of ore was mined underground at the Windfall mine (Fig. 3) in the early 1900's (Nolan and Hunt, 1968). This ore was made up principally of disseminated, microscopic to submicroscopic Au that occurred mostly in fractured and altered Hamburg dolomite. In the past few years Au has been mined in this same area by open-pit methods. Arsenic, Hg, Sb, Te, and Tl are commonly anomalous in this ore (Grove, 1979; Hill et al., 1986); Pb, Zn, and Ag are only rarely enriched. These ores, which are distinctly different in form and trace-element chemistry from the Pb-Ag-Au ores found in other parts of the Eureka district, are similar to "Carlin-type" disseminated Au ores (Bagby and Berger, 1985).

A third type of mineralization is present in the carbonate country rocks just south of the quartz diorite plug (Nolan, 1962) (Fig. 2). Silicated carbonate minerals typical of a contact-metasomatic environment are present; magnetite, pyrite, and pyrrhotite have also been reported. These silicated rocks are known to contain minor occurrences of scheelite and base and precious metals.

Another type of deposit, which consists of argentiferous tetrahedrite and galena in quartz veins and shear zones, occurs at several localities in the Prospect Ridge antiform but mainly in mines and prospects found to the southeast of the Eureka district, at the southern end of the Silverado antiform (Fig. 3). Similar deposits are also known to occur farther north at several localities in the Diamond Mountains (Nolan, 1962; Nolan et al., 1971); these last areas were not examined or sampled for this study. The veins in this type of deposit are characteristically low in Au and locally contain barite and scheelite (Nolan et al., 1971; 1974).

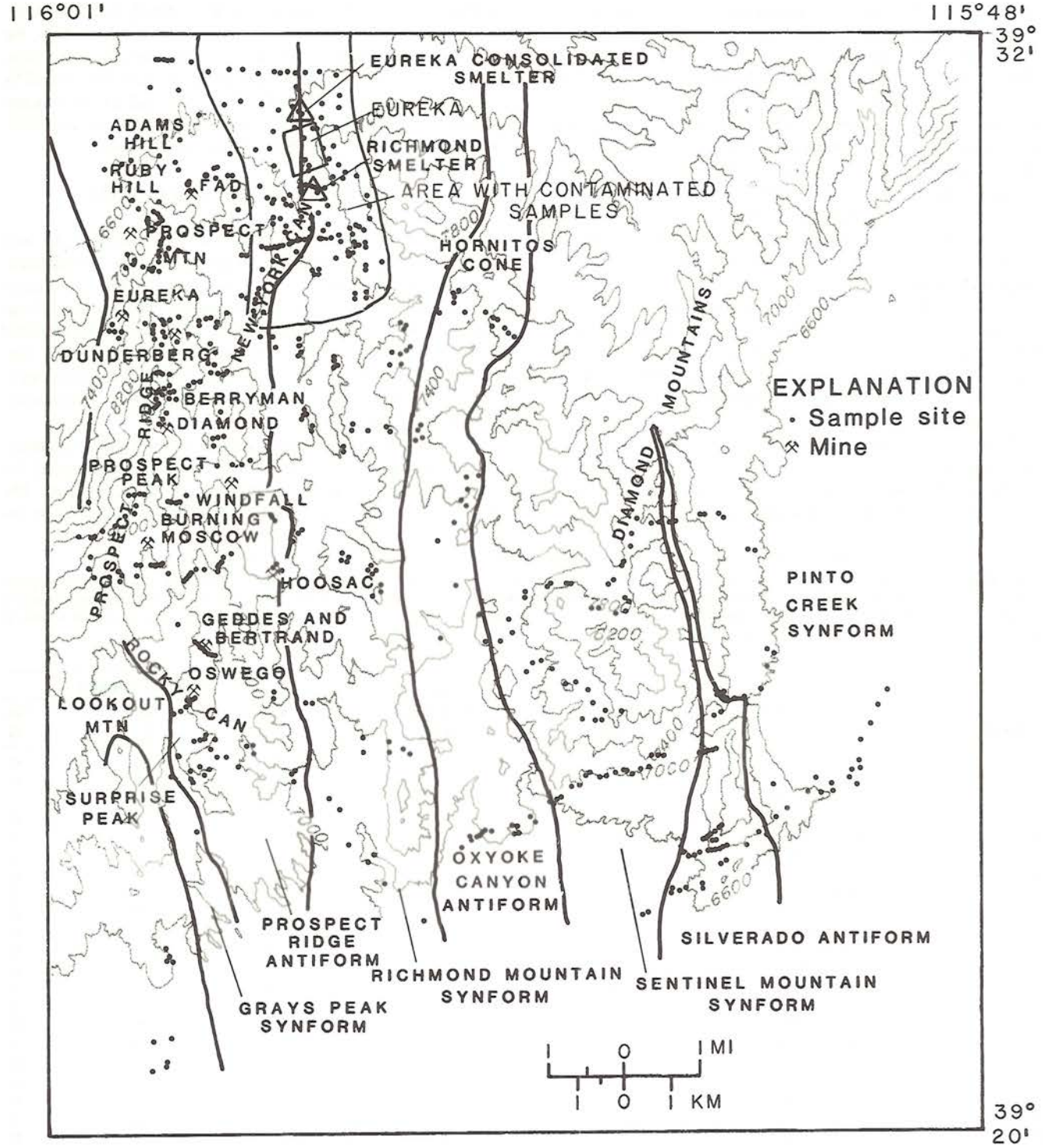

Fig. 3. Map showing place names, sampling sites, and the area of smelter contamination, Eureka district and vicinity, Nevada.

SAMPLE COLLECTION AND CHEMICAL ANALYSIS

A total of 569 rock samples and 593 soil samples were collected for this study. The sites for these samples are shown on Fig. 3. Two contrasting soil fractions were prepared and analyzed for all of the soil samples: a 1- to 2-mm coarse fraction and a <0.063-mm fine fraction. After evaluating these three sample types, the fine-soil fraction was selected as the best sample medium for the detailed interpretation, primarily because this medium had the highest percentage of samples

with values in the detectable ranges for all of the ore-related elements. The remainder of this paper will only be concerned with the fine-soil fraction.

Much of the regional sampling was done on roughly east-west traverses designed to transect the major north-south structural and stratigraphic elements of the study area. More detailed sampling was done in the vicinity of several mineralized structures. The soil samples were composited from material commonly collected at the soil-bedrock interface, at depths of about 10 to 20 cm (4 to 8 in). It is therefore believed that, except for any smelter-related contamination, the material collected for all samples was formed at the sample site and did not include any transported component.

Two major and several smaller smelters operated in the Eureka area during the late 1800s. The sites of the two major smelters, the Richmond and the Eureka Consolidated, are shown on Fig. 3. Because these smelters are known to have emitted particulate effluent, soils collected in and around Eureka were believed to be contaminated.

All samples were analyzed for 30 elements (Ag, As, Au, B, Ba, Be, Bi, Ca, Cd, Co, Cr, Cu, Fe, La, Mg, Mn, Mo, Nb, Ni, Pb, Sb, Sc, Sn, Sr, Ti, V, W, Y, Zn, and Zr) using a six-step semiquantitative emission spectrographic method (Grimes and Marranzino, 1968). Because of the relatively high concentration levels for the respective lower limits of determination, the spectrographic analyses for As, Au, Sb, and Zn were eliminated from the data set and these elements were determined by other more sensitive methods. Gold, Hg, and Zn were determined by atomic-absorption spectrometry (Ward et al., 1969) and As and Sb by colorimetry (Ward et al., 1963).

EVALUATION OF THE SAMPLE DATA

Analyses of obviously mineralized rock samples, as well as soils collected from areas suspected of being mineralized, were compared to analyses of rock and soil samples collected from areas known to be unmineralized. These comparisons indicated that, of the 31 different elements initially determined in the samples (Table 1), a total of 15 elements (Ag, As, Au, Ba, Bi, Cd, Cu, Hg, Mn, Mo, Pb, Sb, Sn, W, and Zn) seem to be enriched due to hydrothermal mineralization in at least some part of the study area.

The fine-soil data set was evaluated by statistical techniques, by examining maps of the distributions of concentrations for the 15 selected elements, and by R-mode factor analysis. The data set was first examined to establish threshold values for

Table 1. Summary of statistical information for 31 elements in 441 <0.063-mm soil samples

[Concentrations for elements Ca, Mg, Fe, and Ti are in percent; concentrations for all other elements are in parts per million. aa, atomic-absorption analysis; cm, colorimetric analysis; all other elements, spectrographic analysis. N, not detected at the lower limit of determination shown in parentheses; L, detected but in a concentration less than that shown in parentheses; G, detected in a concentration greater than that shown in parentheses. Dashes (—), insufficient data to calculate value]

Element	Concentration range	Geometric mean	No. unqualified samples	Qualified samples		
				No. N	No. L	No. G
Ag	N(0.5)-30	1.7	192	215	34	0
As-cm	N(10)-8,000	20	358	16	67	0
Au-aa	N(0.05)-0.35	—	24	234	183	0
B	L(10)-150	34	439	0	2	0
Ba	N(20)-G(5,000)	660	436	1	0	4
Be	N(1)-10	1.6	421	6	14	0
Bi	N(10)-100	—	6	426	9	0
Ca	0.15-G(20)	3.4	439	0	0	2
Cd	N(20)-50	—	5	434	2	0
Co	N(5)-30	9.3	423	10	8	0
Cr	N(10)-300	52	435	3	3	0
Cu	5-500	23	441	0	0	0
Fe	0.15-15	3.0	441	0	0	0
Hg-aa	N(0.02)-G(10)	0.17	438	1	1	1
La	N(20)-100	32	379	37	25	0
Mg	0.20-G(10)	1.9	440	0	0	1
Mn	30-3,000	680	441	0	0	0
Mo	N(5)-30	—	48	378	15	0
Nb	N(20)-50	—	10	274	157	0
Ni	L(5)-100	22	437	0	4	0
Pb	N(10)-10,000	77	439	2	0	0
Sb-cm	L(1)-400	6.2	439	0	2	0
Sc	N(5)-20	9.2	422	13	6	0
Sn	N(10)-200	—	31	392	18	0
Sr	N(100)-1,500	190	422	10	9	0
Ti	0.015-2	0.27	441	0	0	0
V	10-500	86	441	0	0	0
W	N(50)-70	—	8	431	2	0
Y	N(10)-50	18	440	1	0	0
Zn-aa	25-30,000	130	441	0	0	0
Zr	N(10)-700	140	440	1	0	0

each of the 15 selected elements. Once these values were established, the approximate number of anomalous samples in the data set was determined.

For Au, Bi, Cd, Mo, Sn, and W the threshold value was clearly below the lower limit of determination. For these elements, all unqualified values (Table 1) were considered to be anomalous; in some cases the values reported by the analyst as "L" (detected but at a concentration less than the lower limit of determination) (Table 1) were also judged to be anomalous. For the remaining nine elements, preliminary threshold values were established for each element after a study of both percent-frequency histograms and probability plots. The analyses for each of the 15 selected elements were then plotted on a geologic base to verify that the selected threshold values made geologic sense. As a result of an evaluation of these plots, threshold values in several cases were adjusted upward or downward one reporting interval from the preliminary threshold value.

Of the original 15 selected elements, seven (Ag, As, Cu, Hg, Pb, Sb, and Zn) were identified that (1) had an acceptable minimum number of samples with unqualified values (Table 1) and, in addition, (2) were enriched, predominantly as a result of hydrothermal activity. For these seven elements, the number of anomalous samples ranged from 8 to 21 percent, with an average for all seven of 16 percent. Given the highly mineralized nature of the study area, these percentages are considered to be reasonable.

The fine-soil data set was also evaluated by R-mode factor analysis. Factor analysis is a mathematical technique that is used in exploration geochemistry to produce subsets (factors) of the variables (chemical elements) in a data set. Every type of mineral deposit contains a geochemical signature based on a distinct suite of anomalous elements. The factors produced by factor analysis can be studied to see if any of them contain the same group of elements that represent the geochemical signature of a given type of deposit. The relative degree with which a given *element* associates with a given factor is called its *factor loading value*. Within each factor, the relative degree with which each *sample* correlates with the factor is called its *factor score*. Further details concerning factor analysis and its applications to geochemical problems can be found in the literature (See, for example, Davis, 1973; Howarth, 1983).

A preliminary factor analysis was made on the fine-soil data set, using the RRMODE program for R-mode factor analysis written by A. T. Miesch for the U. S. Geological Survey STATPAC system (VanTrump and Miesch, 1977). Elements that were highly censored in the original data set — elements for which more than about 60 percent of the values were qualified with "N" (not detected at the lower limit of determination), "L" (detected at a concentration less than the lower limit of determination, and (or) "G" (detected but at a concentration greater than the upper limit of determination) — were first deleted from the data set. This process eliminated the elements Au, Bi, Cd, Mo, Nb, Sn, and W from the data set used for factor analysis.

Before the factor analysis was run on the remaining elements in the data set, all qualified values were replaced with logical values. Analyses reported as "N" for a given element were replaced by a value equal to one-half of the lower limit of determination. Analyses reported as "L" were replaced by a value equal to seven-tenths of the lower limit of determination. Analyses reported as "G" were replaced by a value equal to the upper limit of determination divided by seven-tenths. All values were transformed to logarithms prior to running factor analysis. A varimax rotation was used.

Maps showing the distributions of the factor scores for the ore-related factors identified in this initial factor analysis indicated that many samples in the vicinity of the town of Eureka were strongly anomalous. Maps showing the distributions of anomalies for many of the individual ore-related elements also indicated that strong anomalies were present and generally centered on the sites of the Richmond and Eureka Consolidated smelters. As a result of these observations, over 150 samples in the area shown on Fig. 3 were classified as being smelter contaminated and were eliminated from the original data set. A statistical summary of the remaining 441 samples is given in Table 1. This table includes data on both the elements included in the factor analysis and those that were deleted prior to running the analysis.

The factor analysis was rerun on the smaller data set. For this new data set, a 5-factor model was selected on the basis of the number of eigenvalues greater than 1. Table 2 shows the factor loading values for this model.

Of the five factors in the data set, two (factors 2 and 5) are thought to be related to mineralization. Of the 15 elements originally considered to be related to mineralization, six (Au, Bi, Cd, Mo, Sn, and W) were deleted from the data set prior to factor analysis because they had too many qualified values. Of the remaining 9 elements, Ba and Mn are known to be more strongly related to lithology than to mineralization, which explains why these two elements are not significantly loaded on the two mineralization-related factors (Table 2). The remaining seven mineralization-related elements are present in the two selected factors.

The first mineralization-related factor, factor 2, contains, in order of highest to lowest loading values of interest, the elements Ag, Pb, Zn, Cu, and Sb. The second is factor 5, which contains, in a similar manner, the elements As, Hg, and Sb. Antimony seems to be loaded equally on both of these factors, whereas, the other elements seem to be clearly loaded on only one of the two factors. Factor 2 is thought to chemically best represent Ag-rich base-metal ores, such as those at Ruby Hill, and is hereafter called the Ag factor. Factor 5 contains the suite of elements most closely identified with "Carlin-type" Au deposits, such as those mined at the Windfall mine, and is hereafter called the Au factor.

The other three factors are thought to be related principally to lithology (Table 2). Factor 3 shows significant loadings for Ca and Mg, the major chemical components of the carbonate-rich sedimentary rock units that are dominant in the study area. The elements with the highest loadings on factor 1 (Be, Co, Fe, La, Mn, Sc, Sr, Ti, Y, and Zr) and factor 4 (B, Ba, Cr, Ni, and V) probably represent the chemistry of accessory minerals in the sedimentary and (or) igneous rocks of the study area.

Although not discussed here, the factor analyses run on the rock and coarse-soil data sets also showed two similar ore-related factors, suggesting that the factors found in the fine-soil fractions are not strictly a function of the size of the soil sample material used or of the type of sample used.

Table 2. Loading values for 5-factor model for 441 <0.063-mm soil samples

[Listed in alphabetical order by element. Underlined values are considered to be significant. aa, atomic-absorption analysis; cm, colorimetric analysis; all other elements, spectrographic analysis]

Element	Factor 1 (Lithology)	Factor 2 (Ag factor)	Factor 3 (Lithology)	Factor 4 (Lithology)	Factor 5 (Au factor)
Ag	-0.06	0.88	0.04	0.08	0.10
As-cm	-0.04	0.14	-0.22	-0.06	0.77
B	0.35	-0.19	-0.11	0.56	0.43
Ba	0.40	-0.03	0.06	0.46	-0.27
Be	0.74	0.07	-0.21	0.01	0.19
Ca	-0.11	0.14	0.93	-0.08	0.01
Co	0.69	0.20	-0.07	0.41	-0.03
Cr	0.32	0.10	-0.06	0.81	-0.02
Cu	0.22	0.76	-0.11	0.29	-0.04
Fe	0.74	0.09	0.12	0.25	-0.14
Hg-aa	-0.07	0.37	0.19	0.04	0.73
La	0.74	-0.10	-0.17	0.28	0.001
Mg	-0.24	0.22	0.85	-0.07	-0.08
Mn	0.55	0.45	0.39	-0.18	0.28
Ni	0.39	0.16	-0.12	0.79	-0.01
Pb	0.16	0.81	0.24	0.04	0.20
Sb-cm	0.09	0.62	0.16	-0.11	0.61
Sc	0.73	0.11	-0.15	0.48	-0.03
Sr	0.66	-0.02	0.12	0.13	-0.05
Ti	0.76	0.14	-0.13	0.27	-0.003
V	0.50	0.32	0.03	0.68	0.01
Y	0.75	0.14	-0.23	0.37	0.02
Zn-aa	0.01	0.79	0.14	0.05	0.18
Zr	0.71	0.08	-0.33	0.26	0.02
Cumulative Variance	0.35	0.54	0.62	0.67	0.72

The factor scores for each of the two mineralization-related factors (Table 2) were arranged in order from the highest positive value to the highest negative value. This ranking was then divided into four groups based on percentiles: (1) the highest 10 percent of the positive values, (2) the next 5 percent of the values, (3) the next 5 percent of the values, and (4) the remaining 80 percent. Based on the percentages of anomalous samples for the seven individual elements that are present in the two mineralization-related factors (Ag, As, Cu, Hg, Pb, Sb, and Zn), the first three factor-score groups, representing the most significant 20 percent of the samples, have been plotted on the accompanying figures.

GEOCHEMICAL MAPS

Five geochemical maps are included in this paper. The first two (Figs. 4 and 5) show the locations of the samples with the highest positive factor scores for the two mineralization-related factors. On these two maps, the three percentile groups of anomalous factor scores are shown. The last three maps (Figs. 6 to 8) show the locations of anomalies for those elements known to be mineralization-related but too highly censored to be included in the factor analysis (Au, Bi, Cd, Mo, Sn, and W). The concentration ranges judged to be anomalous for each element are shown on the respective maps. The areas that are deemed to be the most significant are designated by letters on Figs. 4 to 8 and are described below. All place names mentioned in the discussion are shown on Fig. 3.

Silver-factor map

Fig. 4 shows the distribution of samples with the highest positive factor scores for the Ag factor. Area A is centered on the quartz diorite plug (Fig. 2) and extends from the vicinity of the Fad shaft on the north, through Ruby Hill, to the area south of the plug. Anomalous samples from this area were collected from soils over the limestones of the Pogonip Group near the Fad shaft, the quartz diorite plug, the Eldorado Dolomite at Ruby Hill, and the Geddes Limestone and the Prospect Mountain Quartzite in the southwestern part of Area A. Area B

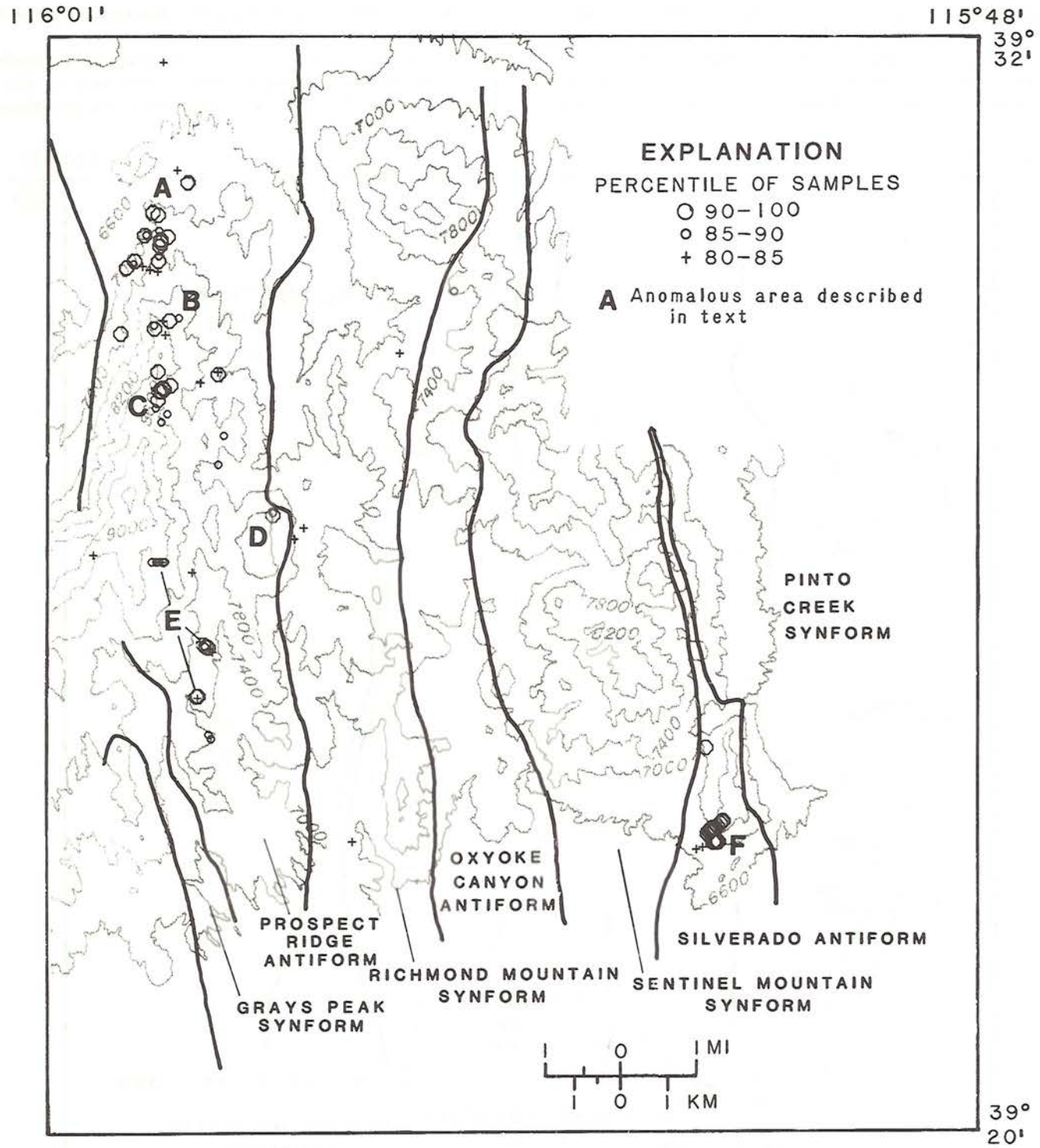

Fig. 4 Map showing sampling sites with anomalous scores for the Ag factor. The large circles locate the strongly anomalous samples; the small circles, the moderately anomalous samples; and the plus symbols (+), the weakly anomalous samples.

comprises a group of samples in the vicinity of the Eureka tunnel. Anomalous samples collected in this area are mainly derived from the Eldorado Dolomite; however, several are derived from the Geddes Limestone, the Secret Canyon Shale, and (or) the Prospect Mountain Quartzite. Area C shows strong clusters of anomalous samples in the vicinity of the Diamond and Berryman tunnels and in the upper part of New York Canyon. Anomalous samples collected in this area are primarily from soils over the Hamburg Dolomite but also include samples collected over the Pogonip Group and the Dunderberg Shale. Area D consists of two samples collected over the Hanson Creek Formation north of the Hoosac mine. Area E includes

samples collected along traverses transecting mineralized structures in the vicinity of (from north to south) the Burning Moscow mine, the Geddes and Bertrand mine, and the Oswego mine. All of these samples were collected from soils over the Eldorado Dolomite. In all three of these traverses, samples collected over formations other than the Eldorado Dolomite did not score high on this factor.

Area F locates samples collected along traverses at the south end of the Silverado antiform. Most of these samples were derived from the Bay State Dolomite; a few of the anomalous

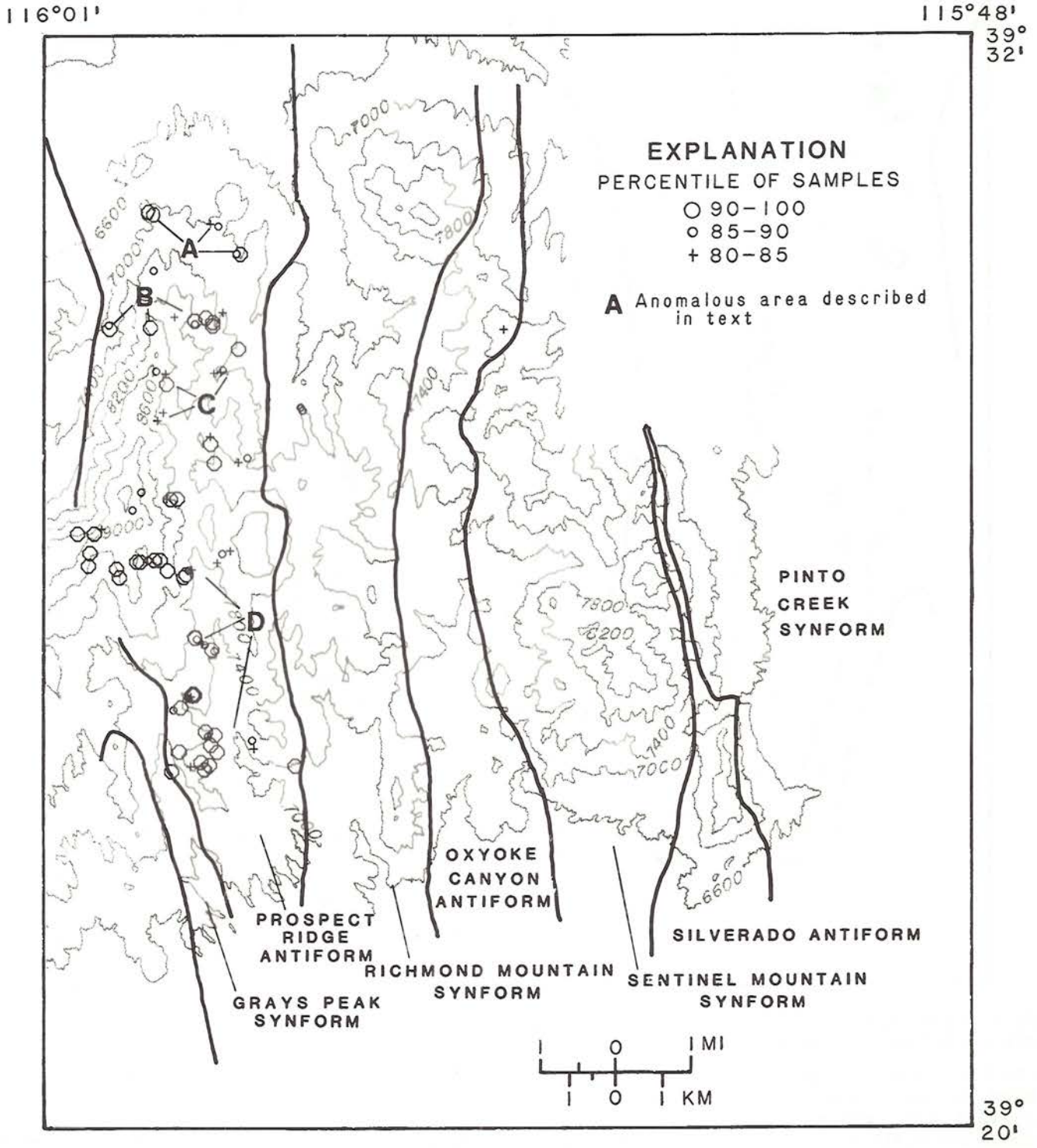

Fig. 5. Map showing sampling sites with anomalous scores for the Au factor. The large circles locate the strongly anomalous samples; the small circles, the moderately anomalous samples; and the plus symbols (+), the weakly anomalous samples.

samples are from the Woodpecker Limestone or the Oxyoke Canyon Sandstone. Of the six areas described for the Ag factor map, Area F contains more of the samples with the highest scores for this factor than does any other area.

Gold-factor map

Fig. 5 shows the distribution of samples with the highest positive factor scores for the Au factor. Area A consists of three clusters of anomalous samples. The four samples in the two clusters to the east of Prospect Ridge are all of soils collected over rocks of the Pogonip Group. The anomalous cluster to the west is on Ruby Hill and is based on samples of soil collected over the Eldorado Dolomite. This last locality was also anomalous for the Ag factor, corroborating the high Ag and Au content of the ores mined in the Ruby Hill area. None of the four soil samples collected over the quartz diorite plug was anomalous for the Au factor. Area B includes two clusters of anomalous samples on either side of Prospect Ridge. Samples from this area were collected from a number of formations, including the Hamburg Dolomite, the Eldorado Dolomite, the Windfall Formation, the Pogonip Group, and the Prospect Mountain Quartzite.

Area C includes three clusters of anomalous samples collected in the vicinity of the Diamond and Berryman tunnels and in the upper part of New York Canyon. Anomalous samples come from the Hamburg Dolomite, the Pogonip Group, the Windfall Formation, and the Dunderberg Shale. These anomalies generally overlap those for the Ag factor in this area. Area D is a large, discontinuous zone that consists of three clusters of anomalous samples and extends from the area surrounding the Windfall mine south-westward across Prospect Peak and the area of the Burning Moscow mine to the head of Rocky Canyon and then southward past the Geddes and Bertrand and Oswego mines to the area south of Surprise Peak. The sample distribution is such that it is not possible to determine the areal extents of these three clusters but they may be part of a single large anomalous area. Exploration for "Carlin-type" Au deposits has been conducted in recent years by several companies in the area just to the west of Area D, near Lookout Mountain (Fig. 3). Anomalous samples in area D are mostly from soils collected over the Eldorado Dolomite and the Pogonip Group; a few are also from soils over the Hamburg Dolomite, the Geddes Limestone, the Hanson Creek Formation, and the Prospect Mountain Quartzite.

Element maps

Fig. 6 shows the distributions of the 24 samples of the fine soil containing anomalous Au ($\geq$0.05 ppm). With the exception of the lone sample southeast of Hornitos Cone (labelled A on the map), all of the anomalous Au samples fall within the Prospect Ridge antiform. This one isolated sample, which is also present on the Au factor map, was found to be at the low end of the anomalous concentration range for Au (0.05 ppm) and contained only weakly anomalous or background concentrations of any of the other mineralization-related elements; thus, the area labelled "A" is not thought to represent significant mineralization.

Samples at sites B to E are anomalous for the element Au but not necessarily for the Au factor. Some of these Au anomalies instead correlate with anomalies for the Ag factor, suggesting that elemental Au may at times be associated with both mineralization-related factors. Anomalies for Au in the soil samples seems to be spatially associated somewhat more with anomalies of the Ag factor in the northern part of the Prospect Ridge antiform and more with anomalies of the Au factor in the southern part. It must be cautioned, however, that these observations are based on only 24 samples and thus may not be a truly accurate picture of the distribution of Au.

The lack of a strong spatial correlation between the elemental Au anomalies and the Au-factor anomalies was not entirely unexpected from a sampling standpoint. Orientation studies of replicate samples analyzed for the 15 selected elements demonstrated that Au concentrations were not always reproducible, whereas those for many of the other selected elements — including the three elements in the Au factor — generally were reproducible. This problem of reproducing Au values is well known to geochemists and is usually thought to be related to the erratic manner of occurrence of Au in relation to the size of an individual sample. The Au-related pathfinder elements (As, Hg, and Sb) are thus thought to be a more reliable indicator of "Carlin-type" Au mineralization in the study area than is the element Au alone.

Fig. 7 shows the distribution of anomalous Mo ($\geq$5 ppm) in the fine-soil samples. Although wulfenite has been reported as a common constituent of the ores in the Eureka district (Curtis, 1884), the concentration levels seen in the soil samples collected for this study do not seem to reflect the presence of this mineral; the maximum concentration reported for Mo is 30 ppm (Table 1). Nearly all of the samples with anomalous Mo are, however, associated with samples that are enriched in one or more of the elements in either the Ag factor or the Au factor, corroborating the association of Mo with known mineralization in both the Prospect Ridge and Silverado antiforms. Area A (Fig. 7) extends from the exposure of the quartz diorite plug southward along the west flank of Prospect Ridge and includes much of the contact-metasomatic zone south of the plug. Anomalous samples were primarily from soils collected over the plug and the Hamburg Dolomite but were also collected from soils over the Secret Canyon Shale and the Geddes Limestone. Area B is near the top of Prospect Ridge in the vicinity of the Eureka tunnel and several other old mines. Anomalous samples are from soils over the Secret Canyon Shale and the Geddes Limestone.

Area C is along the eastern flank of Prospect Ridge west of the Windfall mine. Anomalous samples here were also collected over the Secret Canyon Shale and the Geddes Limestone. Area D is also along the east flank of Prospect Ridge. Anomalous samples are from soils collected over the Eldorado Dolomite and the Geddes Limestone. Area E includes samples collected along both ends of the Geddes and Bertrand mine traverse. Anomalous samples are from soils collected over the Eldorado Dolomite to the northwest and the Geddes Limestone to the southeast. Area F includes two samples from the vicinity of Surprise Peak. One was collected over Geddes Limestone and

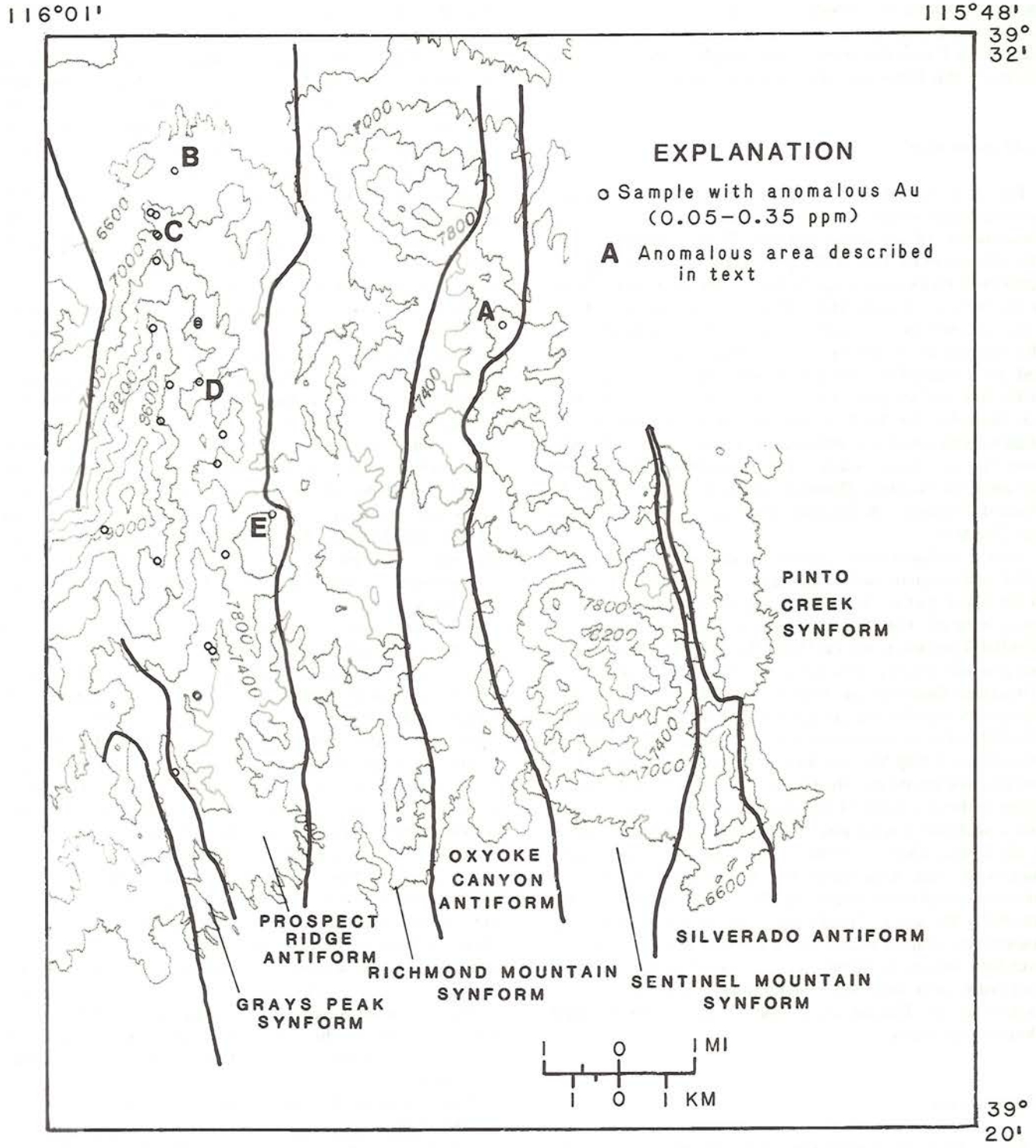

Fig. 6. Map showing sampling sites with anomalous concentrations of Au.

the other over Hamburg Dolomite. Area G includes samples collected at the southern end of the Silverado antiform primarily from soils over rocks of the Bay State Dolomite.

The scattered samples that are anomalous in the Richmond Mountain synform are almost all confined to the Diamond Peak Formation or the Carbon Ridge Formation. The significance, if any, of these anomalous samples is not known. Fig. 8 shows the distributions of anomalous concentrations of Bi (<10-100 ppm), Cd (<20-50 ppm), Sn (10-200 ppm), and W (<50-70 ppm). Of particular interest are anomalies of: (1) Sn at Ruby Hill (letter A); (2) Bi, Cd, and W in the contact-metasomatic zone south of the quartz diorite plug (B); (3) Bi and Sn in the vicin-

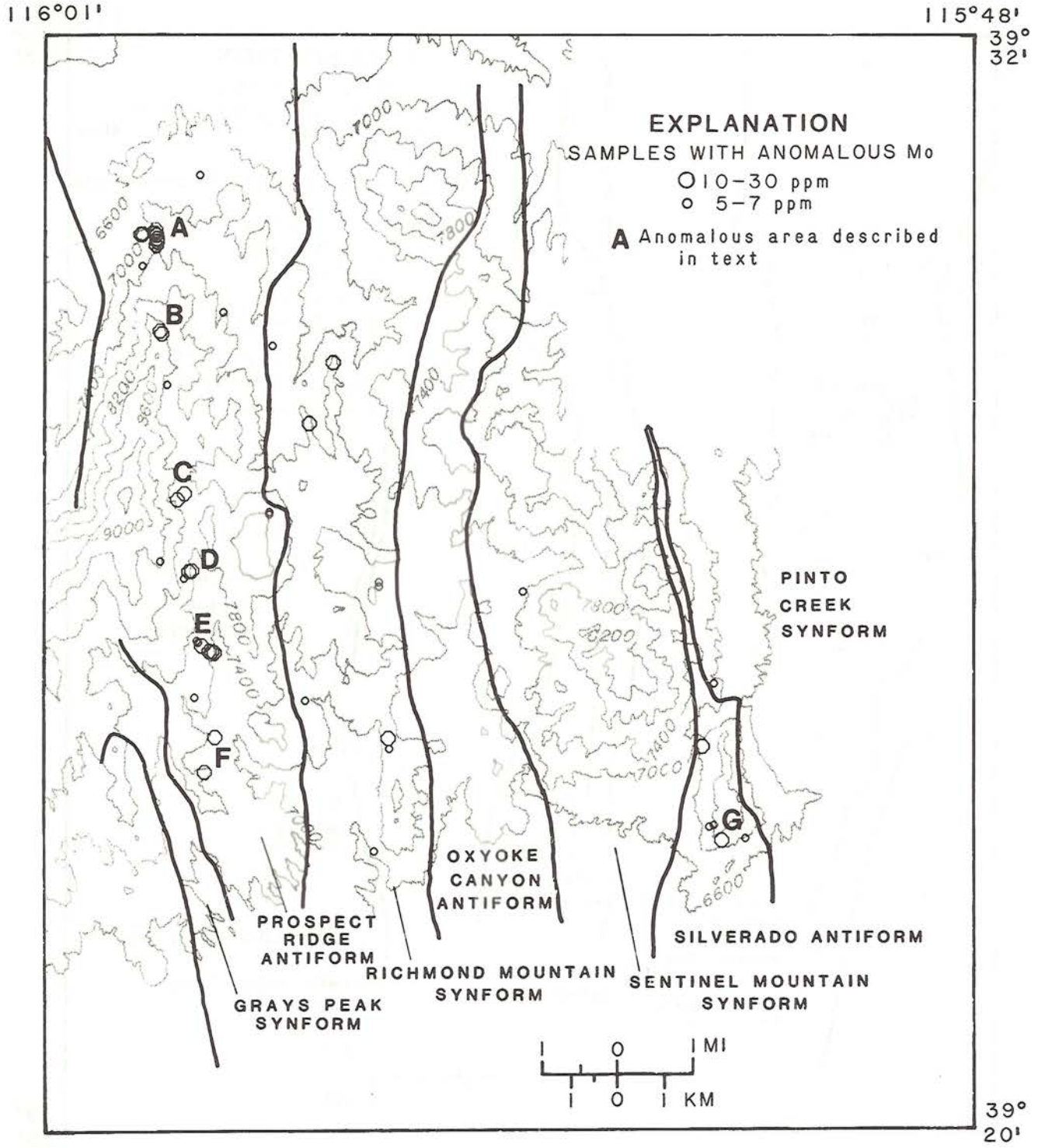

Fig. 7. Map showing sampling sites with anomalous concentrations of Mo.

ity of the Diamond and Berryman tunnels (C); (4) Bi north of the Hoosac mine (D); (5) Sn in the Geddes and Bertrand mine area (E); and (6) Sn and W in the Silverado area (F). A comparison of the distributions of the anomalies for these four elements with anomalies on the two factor maps (Figs. 4 and 5) indicates that there is a closer spatial association of these anomalies with those of the Ag factor than with those of the Au factor, suggesting that Bi, Cd, Sn, and W are more likely to be associated with the element suite in the Ag factor (Ag, Cu, Pb, Sb, and Zn) than with the suite in the Au factor (As, Hg, and Sb).

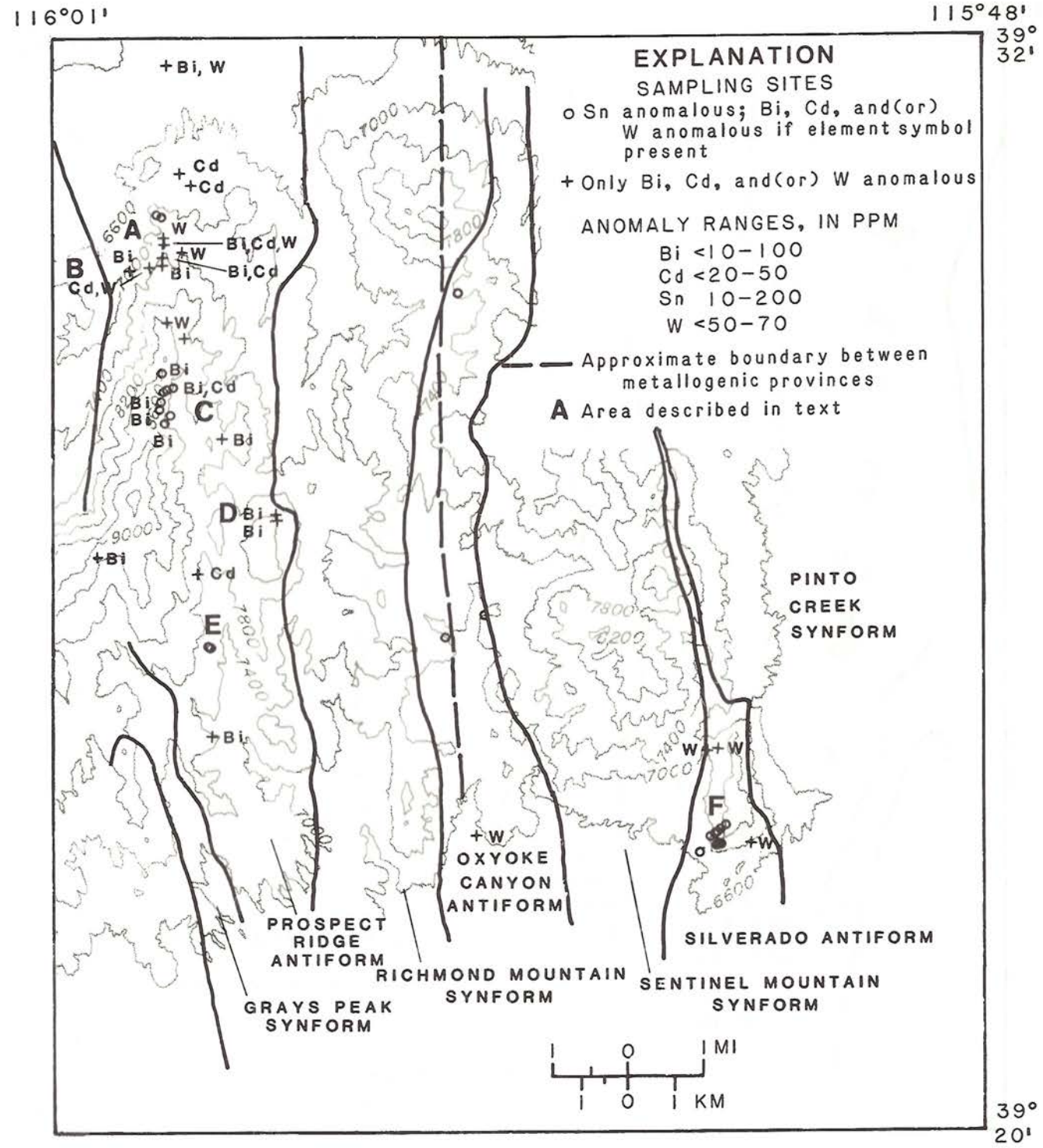

Fig. 8. Map showing sampling sites with anomalous concentrations of Bi. Cd, Sn, and W. Dashed line shows the approximate location of the boundary between the two metallogenic provinces defined by Roberts and others (1971).

DISCUSSION

The two factor maps are thought to indicate the sites and areas with the best potential for Ag-rich base-metal deposits and "Carlin-type" Au deposits in the study area. In the northern part of the Prospect Ridge antiform, samples with high scores for the Ag factor may delineate areas that are favorable for massive-replacement Ag- and base metal-rich deposits in carbonate-rich host rocks and may also identify a Mo-rich porphyry stock. Because of the common spatial associations of

(1) the anomalies associated with the Ag factor (including the elements Ag, Cu, Pb, Sb, and Zn), (2) the anomalies of the other elements thought to be related to that factor (Bi, Cd, Mo, Sn, and W), and (3) the quartz diorite plug south of Ruby Hill, it is speculated that this plug might in fact constitute a Mo porphyry-type deposit at depth. This speculation seems to be corroborated to some extent by published reports that (1) identify wulfenite as a common constituent of the nearby Ruby Hill ores (Curtis, 1884), (2) describe molybdenite in the bottom of the shaft of the deep Richmond mine near Ruby Hill (Curtis, 1884), and (3) note that deep drilling in the quartz diorite plug has penetrated molybdenite associated with quartz veins (Nolan and Hunt, 1968). The identification of a Mo porphyry-type deposit at Mt. Hope, about 35 km northwest of Eureka (Erickson et al., 1983), is further evidence that this part of Nevada presents a favorable environment for Mo deposits.

Prior to this study it was generally believed that most or all of the significant mineralization in the Eureka district was related to a single episode that was associated with intrusion of the quartz diorite plug and associated quartz-porphyry masses. The identification of two distinct mineralization-related factors in the study area suggests either (1) that one episode of mineralization with at least two chemically different ore-fluid phases has occurred or (2) that at least two periods of mineralization separated in time and differing in chemistry have occurred. If the former case holds true, then the quartz diorite plug south of Ruby Hill, and any associated apophyses, are the most likely source of all of the mineralization in the Eureka district and perhaps also that in the Silverado antiform.

If the latter case holds true, then it is thought that the quartz diorite plug may only be the source of the mineralization associated with the suite of elements that probably includes Ag, Bi, Cd, Cu, Mo, Pb, Sb, Sn, W, and Zn. The age and source of the mineralization associated with the suite of elements that probably includes As, Au, Hg, and Sb may, in this situation, be different than that of any other mineralization. Other than the quartz diorite plug, the only obvious source (or sources) of the ore fluid for this second suite of elements would seem to be the Tertiary volcanic rocks themselves or possibly deeply circulating waters related to the Tertiary volcanic activity.

To date no mineralization has been unequivocally proved to be genetically associated with any of the Tertiary volcanic rocks; however, Au mineralization has been reported as being spatially associated with andesite dikes at the Windfall mine (Grove, 1979). This andesite, which is probably the Ratto Spring Rhyodacite of Nolan et al. (1974), appears to be hydrothermally altered locally and is cut by a few Au- and As-bearing fractures. Nolan (written communication, 1986) indicates that the close areal relationship of the Windfall, Geddes and Bertrand, and Oswego mines — as well as the area that has been prospected at Lookout Mountain — with outcrops of the rhyodacite is quite significant, especially because these same localities also contain, to a greater or lesser degree, arsenic in the form of realgar and orpiment rather than scorodite, which was abundant at Ruby Hill.

Whether the Au ores at these mineralized localities are genetically associated with these volcanic rocks or have only been remobilized by intrusion of the dikes has not been established. Other Tertiary dikes have been mapped near several other mines along Prospect Ridge between the Dunderberg mine on the north and the Geddes and Bertrand mine on the south (Nolan et al., 1971; 1974). Hague (1892) described the intimate association of intrusive rhyolite and andesite with mineral deposits at the Hoosac and the Geddes and Bertrand mines; these mines are no longer accessible for examination. It is thus possible that a detailed study of the volcanic rocks in the Eureka area might be rewarding. Clearly, additional research is needed before spatial and age relationships of the two element suites defined here, as well as the source of their associated fluids, can be firmly established.

CONCLUSIONS

Evaluations of the factor-analysis data, of factor-score maps for the two mineralization-related factors, and of maps showing the distributions of anomalies for the six ore-related elements (Au, Bi, Cd, Mo, Sn, and W) that were not included in the factor analysis, allow some conclusions to be made.

The distributions of the anomalies for the 13 ore-related elements discussed (omitting Ba and Mn, which have a significant lithologic component) tend to confirm observations by Nolan et al. (1971) that mineralization is restricted to the Prospect Ridge and Silverado antiforms. Neither the Oxyoke Canyon antiform nor any of the synforms is known to contain any mineral deposits. A broad structural control restricting mineralization to certain antiforms thus seems to exist.

A stratigraphic control for mineralization has been recognized in the past in the Eureka district, with most of the ores mined to date coming from the Eldorado Dolomite or the Hamburg Dolomite. Many of the other formations within the antiforms have been identified in the past as being, at least locally, favorable hosts for ore. The results of this study suggest that some of these latter formations (the Geddes Limestone, the Windfall Formation, the Pogonip Group, the Eureka Quartzite, and the Hanson Creek Formation) may be more important hosts than has been recognized to date.

R-mode factor analysis has identified two distinct mineralization-related suites of elements, suites that could not, on the basis of a study of individual element maps alone, be readily split out of the entire group of elements evaluated. The identification of these two factors is significant in terms of the Eureka area and also, perhaps, of the broader region of northern Nevada. The first suite contains Ag, Cu, Pb, Sb, and Zn (and possibly also Bi, Cd, Mo, Sn, and W) and is thought to represent the Ag- and Pb-rich mineralization that was the source of most of the ores mined in the Eureka district. The second suite contains As, Hg, and Sb (and probably Au) and is thought to represent mineralization similar to that found at the Windfall mine and at many sedimentary rock-hosted Au deposits in Nevada. These two mineralization-related factors also suggest that more than one episode of mineralization and (or) more than one ore fluid may be responsible for the mineralization present in the Eureka district.

In a regional context, samples with high scores for the two precious-metal factors may chemically define the two metallogenic provinces identified by Roberts et al. (1971), although the boundary they show between the two does not seem to exist, at

least not as originally located (Figs. 1 and 8). From a chemical standpoint, the two provinces must overlap in the study area.

In a local context, samples with high scores for the Au factor may delineate areas where sedimentary rock-hosted Au deposits like that at the Windfall mine might occur. The distribution of samples with anomalous scores for this factor suggests that the area of the Prospect Ridge antiform south of the vicinity of the Windfall mine should be the most favorable for this type of Au deposit.

The results of this study emphasize the value of using as many elements as practicable in geochemical exploration surveys. The information derived from the use of R-mode factor analysis at Eureka indicates that this technique may assist both in defining anomalous areas and in providing a better understanding of the genesis of mineral deposits in areas that may contain overlapping phases of mineralization.

Acknowledgements — Many individuals have provided assistance for this project. D.L. Fey, R.H. Hill, and K.E. Kulp assisted in collecting the samples, R.N. Babcock, G.L. Crenshaw, C.A. Curtis, J.V. Desmond, M.S. Erickson, D.L. Fey, C.L. Forn, J.G. Frisken, C.W. Gale, J.R. Hassemer, R.H. Hill, J.D. Hoffman, R.T. Hopkins, Jr., R.F. Kolarich, R.L. Miller, E.L. Mosier, J.M. Nishi, R.M. O'Leary, D.F. Siems, C.D. Smith, Jr., R.L. Turner, and E.P. Welsch assisted with the sample preparation and (or) analysis. The author gratefully acknowledges T.B. Nolan for suggesting and encouraging this study and for his help in the field in clarifying many complex geologic relationships for the author.

REFERENCES

Bagby, W. C., and Berger, B. R., 1985, Geologic characteristics of sediment-hosted, disseminated precious-metal deposits in the western United States, *in* Berger, B. R., and Bethke, P. M. (editors), Geology and Geochemistry of Epithermal Systems: Soc. of Econ. Geol., Reviews in Econ. Geol., v. 2, p. 169-202.

Chaffee, M. A., Forn, C. L., Hassemer, J. R., Hoffman, J. D., Mosier, E. L., Nishi, J. M., O'Leary, R. M., Siems, D. F., Turner, R. L., Welsch, E. P., and VanTrump, G., Jr., 1978, Geochemical analyses of rock and soil samples, Eureka mining district and vicinity, Eureka and White Pine Counties, Nevada: U.S. Geol. Surv. Open-File Rep. 78-790, 94 pp., 2 plates.

Curtis, J. S., 1884, Silver-lead deposits of Eureka, Nevada: U.S. Geol. Surv., Monogr. VII, 200 pp.

Davis, J. C., 1973, Statistics and data analysis in geology. New York, John Wiley & Sons, 550 pp.

Erickson, A. J., Jr., Schwarz, F. P., Jr., and Moore, S. C., 1983, Geology, mineralization, and resources of the Mt. Hope stockwork molybdenum deposit, Nevada (abstr.): Am. Inst. Min. Metall. Eng., Program with Abstracts, Annual Meeting, Atlanta, p. 101.

Grimes, D. J., and Marranzino, A. P., 1968, Direct-current arc and alternating-current spark emission spectrographic field methods for the semiquantitative analysis of geological materials: U.S. Geol. Surv., Circ. 591, 6 pp.

Grove, G. R., 1979, A study of the fine-grained disseminated gold ore of the Windfall mine, Eureka County, Nevada: M.S. Thesis, Univ. of Calif., Santa Barbara, 98 pp. (unpubl.).

Hague, Arnold, 1892, Geology of the Eureka district, Nevada: U.S. Geol. Surv., Monogr. XX, 419 pp.

Hill, R. H., Adrian, B. M., Bagby, W. C., Bailey, E. A., Goldfarb, R. J., and Pickthorn W. J., 1986, Geochemical data for rock samples collected from sediment-hosted disseminated precious-metal deposits in Nevada: U.S. Geol. Surv., Open-File Rep. 86-107, 30 pp.

Hose, R. K., Armstrong, A. K., Harris, A. G. and Mamet, B. L., 1982, Devonian and Mississippian rocks of the northern Antelope Range, Eureka County, Nevada: U.S. Geol. Surv., Prof. Pap. 1182, 19 pp.

Howarth, R. J., 1983, Statistics and data analysis in geochemical prospecting. Handbook of Exploration Geochemistry. New York, Elsevier Scientific Pub. Co., v. 2, 437 pp.

Miesch, A. T., and Nolan, T. B., 1958, Geochemical prospecting studies in the Bullwacker mine area, Eureka district, Nevada: U.S. Geol. Surv. Bull., 1000-H, p. 397-408.

Nolan, T. B., 1962, The Eureka mining district, Nevada: U.S. Geol. Surv., Prof. Pap. 406, 78 pp.

Nolan, T. B., and Hunt, R. N., 1968, The Eureka mining district, *in* Ridge, J.D. (editor), Ore Deposits of the United States, 1933-1967: Am. Inst. Min. Metall. Eng., v. 1, p. 966-991.

Nolan, T. B., Merriam, C. W., and Williams, J. S., 1956, The stratigraphic section in the vicinity of Eureka, Nevada: U.S. Geol. Surv., Prof. Pap. 276, 77 pp.

Nolan, T. B., Merriam, C. W., and Brew, D. A., 1971, Geologic map of the Eureka quadrangle, Eureka and White Pine Counties, Nevada: U.S. Geol. Surv., Misc. Geol. Invest. Map I-612, scale 1:31,680.

Nolan, T. B., Merriam, C. W., and Blake, M. C., Jr., 1974, Geologic map of the Pinto Summit quadrangle, Eureka and White Pine Counties, Nevada: U.S. Geol. Surv., Misc. Geol. Invest. Map I-793, scale 1:31,680.

Roberts, R. J., 1966, Metallogenic provinces and mineral belts in Nevada: Nevada Bur. Mines, Rep. 13, pt. A, p. 47-72.

Roberts, R. J., Radke, A. S., and Coats, R. R., 1971, Gold-bearing deposits in north-central Nevada and southwestern Idaho, *with a section on* Periods of plutonism in north-central Nevada by M. L. Silberman and E. H. McKee: Econ. Geol., v. 66, p. 14-33.

Stewart, J. H., 1980, Geology of Nevada: A discussion to accompany the geologic map of Nevada: Nevada Bur. Mines and Geol., Spec. Pub. 4, 136 pp.

U.S. Geological Survey, 1968, Aeromagnetic map of the Eureka region, Eureka and White Pine Counties, Nevada: U.S. Geol. Surv., Open-File Rep., 1 sheet, scale 1:62,500.

VanTrump, G., Jr., and Miesch, A.T., 1977, The U.S. Geological survey RASS-STATPAC system for management and statistical reduction of geochemical data: Computers and Geosciences, v. 3, p. 475-488.

Ward, F. N., Lakin, H. W., Canney, F. C., et al., 1963, Analytical methods used in geochemical exploration by the U.S. Geological Survey: U.S. Geol. Surv., Bull. 1152, 100 pp.

Ward, F. N., Nakagawa, H. M., Harms, T. F., and VanSickle, G. H., 1969, Atomic-absorption methods of analysis useful in geochemical exploration: U.S. Geol. Surv., Bull. 1289, 45 pp.

Trace-Element Variation in Hydrothermal Tourmalines Associated with Mineralization: El Correo, Sonora, Mexico

S. M. SMITH
U.S. Geological Survey, 5946 McIntyre Street, Golden CO 80403, U.S.A.
L. G. CLOSS
Colorado School of Mines, Golden CO 80401, U.S.A.
and
P. K. THEOBALD
U.S. Geological Survey, 5946 McIntyre Street, Golden CO 80403, U.S.A.

Abstract — Tourmaline is a complex boro-silicate mineral with a large amount of major, minor, and trace-element compositional variation. Because tourmaline associated with ore deposits will scavenge elements from the environment of crystallization and will retain these elements during alteration and weathering, the composition of the tourmaline should reflect the primary dispersion of elements. These factors may make tourmaline uniquely useful in mineral exploration.

Abundant hydrothermal tourmaline was found associated with a large geochemical anomaly, previously located using stream-sediment, vegetation, and soil samples, near El Correo, Sonora, Mexico. Rock samples containing tourmaline were collected along three intersecting traverses cutting regions of known mineralization. Tourmaline was collected from quartz veins, breccias, pegmatites, and as disseminations hosted in metamorphosed, hydrothermally altered, and deeply weathered silicic volcanics, and in metasediments. Clean tourmaline concentrates were analyzed by optical emission spectrography for 30 elements. Single-element plots outline at least two highly anomalous regions. Factor-score plots derived from multi-element *R*-mode factor analysis reveal a large, zoned hydrothermal system characterized by a Cu-Mo-Sn core surrounded by an inner Bi-Ag shell and an outer Pb-Zn-Sr shell.

INTRODUCTION

A STUDY of 142 tourmaline samples collected near El Correo, Sonora, Mexico (Fig. 1) provides the basis for an interpretation of the relationships between the trace-element composition of tourmaline and possible metallic mineralization. Seventeen tourmaline samples from the El Correo region had been analyzed previously during the anomaly validation and follow-up phases of a cooperative resource evaluation project in northern Sonora between the U.S. Geological Survey and Consejo de Recursos Minerales de Mexico (Turner et al., 1980). The large variation in concentrations of trace elements identified during the cooperative project and the suggestion that this variation was related to mineralization prompted the present study.

Many workers have investigated the use of single minerals as sample media. Studies of various mineral separates have shown enhancements of geochemical anomalies as much as an order of magnitude above those observed for more common sample types such as rocks (e.g., Lovering et al., 1970; Graybeal, 1973). The most commonly studied mineral separate has been biotite (Bradshaw and Stoyel, 1968; Lovering et al., 1970; Al-Hashimi and Brownlow, 1970; Darling, 1971; Graybeal, 1973; Jacobs and Parry, 1976; Mason, 1978; and Imeokparia, 1982). Other mineral-separate studies reported in the literature include: magnetite (Fleischer, 1965; Mantei and Brownlow, 1967; and Theobald et al., 1967), pyrite (Auger, 1941; Hawley and Nichol, 1961; Loftus-Hills and Solomon, 1967; Johnson, 1972; and Ryall, 1977), feldspar and muscovite (Bradshaw and Stoyel, 1968), apatite (Tsusue et al., 1981; and Williams and Cesbron, 1977), rutile (Williams and Cesbron, 1977), and tourmaline (Power, 1968; Ethier and Campbell, 1977; Birk, 1980; Taylor and Slack, 1984; Brown and Ayuso, 1985; and Smith, 1985).

Tourmaline has several characteristics which make it a potentially useful mineral for geochemical exploration: (1) Tourmaline crystallizes during the last phases of magmatic differentiation and is concentrated in pegmatites, aplites, and hydrothermal veins (Smith, 1949), and as a hydrothermal alteration mineral. (2) Tourmaline has a complex chemical structure which allows for a large amount of compositional variability. (3) Tourmaline has a tendency to scavenge major, minor, and trace elements from its environment of crystallization; from both the host rock and metasomatic fluids (Black, 1971). Smith (1985) lists 51 major, minor, and trace elements that have been detected in tourmaline (Table 5; p. 50). (4) Tourmaline is directly associated with many ore deposits as a gangue or an alteration mineral, commonly crystallizing nearly simultaneously with ore minerals. (5) Tourmaline is a stable mineral that typically survives weathering (Krynine, 1946) and most alteration events. Taylor and Slack (1984) cite supporting evidence showing that hydrothermal tourmaline may, in some cases, survive high-grade metamorphism and retain its "primary chemical and textural characteristics." The characteristics listed above suggest that hydrothermal tourmaline associated with mineralization may preserve the imprint of primary trace-element dispersion despite later alteration, metamorphism and weathering.

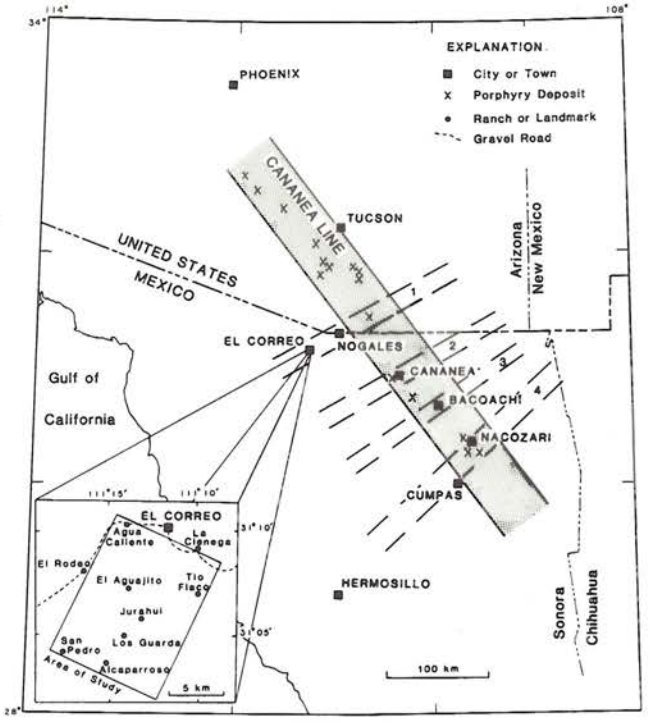

Fig. 1. Location map showing the El Correo study area in relation to the Cananea Line (stippled) and regional northeast-trending lineaments: (1) Nogales Lineament; (2) Cananea Lineament; (3) Bacoachi Lineament; and (4) Cumpas Lineament (modified from Hollister, 1978; and Turner et al., 1982).

PREVIOUS WORK IN EXPLORATION GEOCHEMISTRY: SONORA, MEXICO

A United Nations Development Program in Mexico in the 1960's identified northern Sonora as one of nine zones of high mineral potential and organized an exploration/training program to stimulate development of mineral resources in Mexico. Regional and detailed geochemical, geophysical and geological reconnaissance work identified two areas of major interest near Nacozari (United Nations, 1969). Both of these areas have since been shown to contain porphyry copper deposits (Theodore and Priego de Wit, 1978; Coolbaugh, 1979).

In 1974, a joint multi-disciplinary exploration program designed to evaluate exploration techniques in the arid environment of northern Sonora was established between the U.S. Geological Survey and the Consejo de Recursos Minerales de Mexico under the sponsorship of the National Science Foundation. An integrated regional reconnaissance phase using remote sensing (Raines 1978), geophysics (Kleinkopf et al., 1977), and geochemistry (Turner et al., 1982) identified a series of four northeast-trending lineament zones that are interpreted as "a primary regional control of mineralization in northern Sonora" (Turner et al., 1982). The El Correo region of the Nogales NE-trending lineament zone (Fig. 1) was chosen for an initial detailed reconnaissance study based on high values for lead, molybdenum, zinc, tungsten, copper, silver, boron, manganese, iron and tin in stream sediments and in heavy-mineral-concentrate samples (Turner et al., 1982).

Intermediate-scale (1:50,000) studies of the El Correo region used LANDSAT photo-imagery, photogeology, geophysics and geochemistry to identify areas of interest (Turner et al., 1980). The geochemical patterns obtained in the El Correo region defined a large, zoned hydrothermal system centered near Tio Flaco (Fig. 1) with a radius of about nine kilometres and several smaller subsidiary centers of mineralization near Los Guarda (Theobald, 1981), Agua Caliente (Turner and Eppinger, 1984), Alcaparroso and El Aguajito. A large gravel-filled graben, La Cienega valley, truncates the zoning on the northeast. Fig. 2 shows the lead zone of the El Correo system and the locations of these subsidiary anomalies.

A hypogene model for this hydrothermal system was proposed as consisting of a Cu-Mo core surrounded by successive zones of zinc, lead, silver, etc. The actual geochemical patterns revealed that the hypogene system had undergone extreme supergene redistribution, especially with respect to molybdenum (Fig. 3). The highest concentrations of molybdenum (up

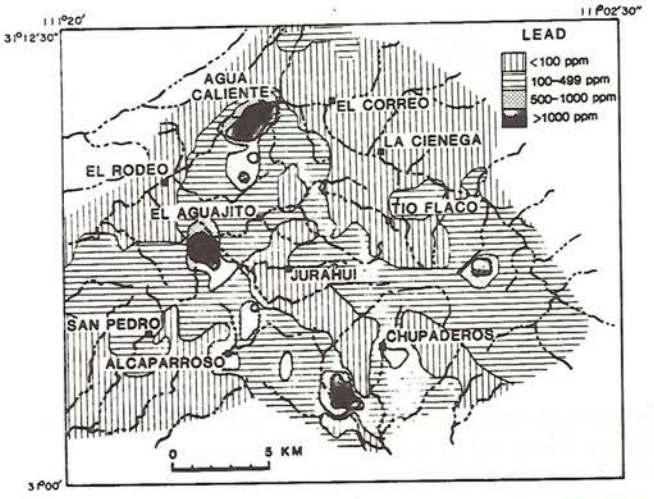

Fig. 2. Lead content of minus 30-mesh stream sediments, El Correo, Sonora, Mexico (from Theobald, 1981).

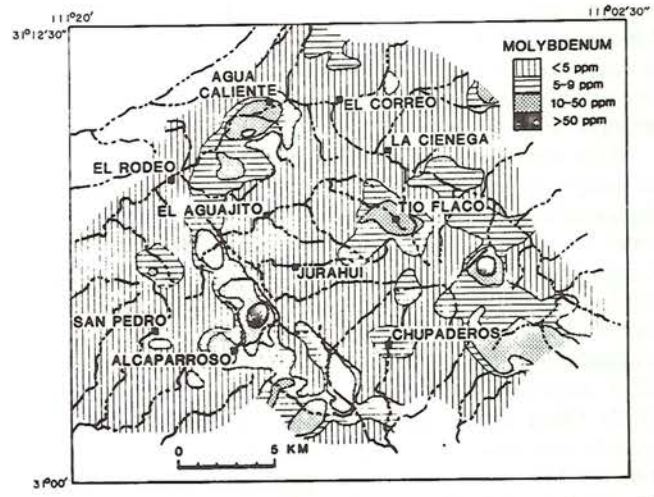

Fig. 3. Molybdenum content of minus 30-mesh stream sediments, El Correo, Sonora, Mexico (from Theobald, 1981).

to 6% in raw stream sediments) were found as placer accumulations of wulfenite in the lead zone (Figs. 2 and 3). Further studies and minor trenching revealed that the primary lead zone itself was molybdenum-poor. Therefore, vast quantities of molybdenum must have moved into the lead zone during supergene alteration (Theobald, 1981).

A reconnaissance study of the El Correo hydrothermal system using tourmaline mineral separates was initiated in order to ascertain whether tourmaline was a viable exploration tool in regions of intense supergene alteration, and to provide an indication of the character of the hypogene trace-element distribution around the Tio Flaco core.

GEOLOGIC SETTING

The El Correo study area is dominated by a structurally complex horst defined by major NNW-trending Basin-and-Range-type normal faults on the east and west. The north end of the horst is truncated by NNE-trending normal faults. Two smaller NNW-trending normal faults form an axial graben near Jurahui. In general, the large normal faults are masked by Tertiary gravel which partially fills the grabens (Fig. 4).

The lithologies of the El Correo study area are typical of the "southern Papago terrane" as defined by Haxel et al. (1984). Stratigraphic relationships, combined with a single unpublished age determination, suggest that the oldest exposed rocks are Jurassic. These are composed of a series of interlayered volcanic flows and volcaniclastic units of quartz latitic composition. The volcanic stratigraphy is not well defined because most geologic contacts are faults or shear zones. Overlying the volcanics in the western part of the study area is a sequence of layered sediments (Jms; Fig. 4) that were metamorphosed to quartz-hornblende-biotite schists and calc-silicate gneisses, probably during a Late Cretaceous regional metamorphic event like that described by Haxel et al. (1984) in southern Arizona. Although the metamorphic grade is difficult to determine owing to the quartzofeldspathic composition of the rocks, an upper greenschist to lower amphibolite grade is assumed. This correlates with the metamorphic grade determined in southern Arizona by Haxel et al. (1984).

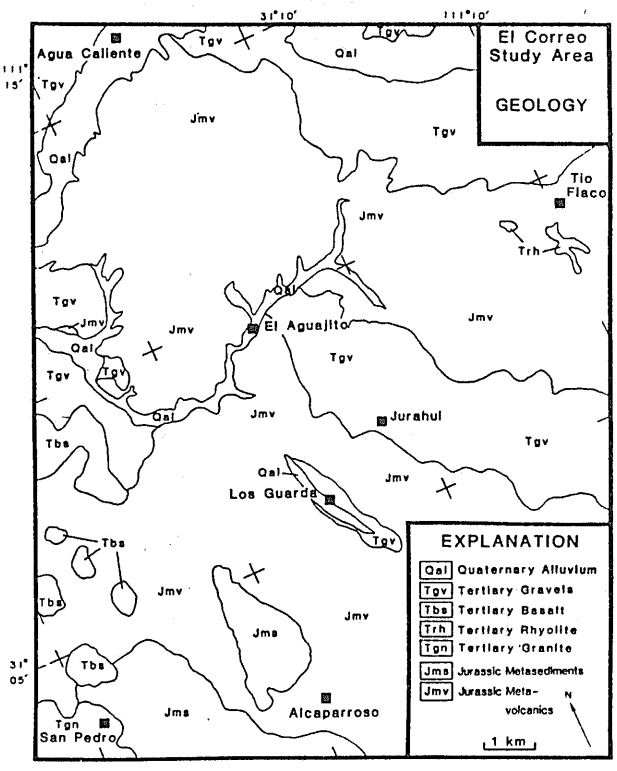

Fig. 4. Generalized geologic map of the El Correo study area. Compiled and modified from unpublished regional air photo interpretations by the Consejo de Recursos Minerales de Mexico and unpublished geologic mapping by the U.S. Geological Survey.

Bimodal Tertiary volcanics form intrusive bodies of rhyolite near Tio Flaco and dikes, sills and flows of basalt along the western part of the study area. The basalt often crosscuts or is interlayered with the consolidated Tertiary gravels.

No mines have been developed within the El Correo study area, although small gold placer workings are numerous around Tio Flaco. Secondary copper stains are found on many rocks throughout the area and chrysocolla is exposed in prospects within the Tio Flaco and Alcaparroso regions. In the vicinity of Agua Caliente, several lead-silver and manganese-silver prospects follow quartz veins. A wulfenite/vanadinite placer was also found near Los Guarda during regional geochemical reconnaissance studies (Turner et al., 1980).

OCCURRENCE OF EL CORREO TOURMALINE

Tourmaline is found in four principal modes of occurrence in the El Correo study area, each with variations. The principal modes are:

(1) Tourmaline breccias and breccia veins: Massive fine-grained tourmaline cementing large breccia zones, occasionally with smaller to micro-breccia veins and associated tourmaline veinlets.

(2) Quartz-tourmaline or tourmaline-quartz veins: Small veins (commonly <15 mm in width) composed predominantly of gray quartz and tourmaline. The veins crosscut the breccias and commonly show a striped appearance owing to the segregation of tourmaline and quartz into parallel bands.

(3) Large bull quartz pods, pegmatites and veins: These are younger than the previous types. Tourmaline concentrations vary from nonexistent in barren quartz pods to predominant as crystal clusters several feet in diameter within quartz. These pods commonly contain minor amounts of mica (usually muscovite), microline and epidote.

(4) Disseminated tourmaline within host rocks: Disseminated tourmaline is defined as that tourmaline which forms radiating "sunburst" clusters, clots, or randomly oriented single crystals within massive rock or along foliation planes. The age relationships of these occurrences vary from site to site. Thin-section petrography shows that some disseminated occurrences are caused by hydrothermal alteration, with tourmaline growing at the expense of the original silicates.

Table 1. Cations which occupy X, Y, and Z structural sites in naturally occurring and hypothetical tourmaline end members of the general composition $XY_3Z_6B_3Si_6O_{27}(0,0H,F)_4$.

End Member	X	Y	Z	References
Buergerite	Na	Fe^{3+}_3	Al_6	Donnay et al. (1966)
Chromdravite	Na	Mg_3	Cr_5Fe^{3+}	Dietrich (1985)
Dravite	Na	Mg_3	Al_6	Deer et al. (1962)
Elbaite	Na	$(Al,Li)_3$	Al_6	Deer et al. (1962)
Ferridravite	Na	Mg_3	Fe^{3+}_6	Walenta and Dunn (1979)
Liddicoatite	Ca	$(Li,Al)_3$	Al_6	Dunn et al. (1977a)
Schorl	Na	Fe^{2+}_3	Al_6	Deer et al. (1962)
Tsilaisite	Na	Mn_3	Al_6	Sahama et al. (1979)
Uvite	Ca	Mg_3	Al_5Mg	Dunn et al. (1977b)
----*	Ca	Fe^{2+}_3	$(Al,Fe^{2+})_6$	Sahama et al. (1979)
				Taylor and Terrell (1967)
----*	Ca	Mn_3	$(Al,Mn)_6$	Sahama et al. (1979)
				Taylor and Terrell (1967)
----*	□	$(Mg,Al)_3$	Al_6	Werding and Schreyer (1984)
----*	□	$(Fe^{2+},Al)_3$	Al_6	Werding and Schreyer (1984)
				Taylor and Terrell (1967)
----*	Li	Fe^{2+}_3	Al_6	Taylor and Terrell (1967)
----*	K	Fe^{2+}_3	Al_6	Taylor and Terrell (1967)
----*	Na	Co_3	Al_6	Taylor and Terrell (1967)
----*	K	Co_3	Al_6	Taylor and Terrell (1967)
----*	Na	Ni_3	Al_6	Taylor and Terrell (1967)
----*	Ca	Ni_3	Al_6	Taylor and Terrell (1967)
----*	Li	Ni_3	Al_6	Taylor and Terrell (1967)
----*	K	Ni_3	Al_6	Taylor and Terrell (1967)
----*	Na	Cu_3	Al_6	Taylor and Terrell (1967)
----*	Na	Zn_3	Al_6	Taylor and Terrell (1967)
----*	K	Mn_3	Al_6	Taylor and Terrell (1967)
----*	Na	Cr_3	Al_6	Taylor and Terrell (1967)
----*	Na	V_3	Al_6	Taylor and Terrell (1967)
----*	Li	Mg_3	Al_6	Taylor and Terrell (1967)

* - Synthetically produced tourmalines, □ - crystal vacancy.

The modes of tourmaline occurrence characterize different regions within the study area. Tourmaline breccias occur primarily in the Tio Flaco region. Tourmaline-quartz veins are found almost everywhere, but are most common in the area immediately west of the Tio Flaco region. Large bull quartz pods, pegmatites and veins are almost totally restricted to the western half of the southernmost traverse from Tio Flaco to Alcaparroso and San Pedro. Disseminated tourmaline occurs sporadically throughout the study area.

Tourmaline from the El Correo area is black in outcrop or hand specimen. It occurs as separate striated prismatic crystals, fibrous aggregates of intergrown prismatic needles, and/or granular aggregates of anhedral microcrystalline material, ranging from less than 0.1 mm up to 10 mm in length. When observed microscopically in reflected light, the prismatic tourmaline is generally brown to black in color, whereas the aggregate tourmaline is gray to black.

These variations in crystal morphology cannot be correlated with any spatial relationships or chemical compositions. Black prismatic and aggregate grains occur throughout the region and in each mode of occurrence. Although the breccias are typically cemented by granular aggregates of anhedral tourmaline, this crystal habit is also common in veins, pegmatites, and disseminations.

MINERALOGY AND CLASSIFICATION OF EL CORREO TOURMALINE

Tourmaline is a complex boro-silicate mineral with a wide compositional variation. The compositional formula is usually given as $XY_3Z_6B_3Si_6O_{27}(O, OH, F)_4$, where X, Y, and Z represent univalent, divalent and trivalent crystal structure sites, respectively. Table 1 lists known and synthetic end-member tourmaline compositions as reported in the literature. The actual compositions of natural tourmalines form solid-solution series between several end members; empirical studies have revealed a continuous isomorphous series between dravite and schorl and between elbaite and schorl, whereas a miscibility gap separates dravite and elbaite (Deer et al., 1962).

Isomorphism in tourmaline is also accomplished by coupled substitutions of cations within the crystal structure. Foit and Rosenberg (1977) proposed two coupled substitutions of major importance which explain most of the variance from stoichiometry in the chemical analyses of tourmaline. Defining a schorl/dravite end member as $R^+R_3^{2+}R_6^{3+}(BO_3)_3Si_6O_{18}(OH)_4$, differing compositions can be explained by two competing substitutions:

$$(OH)^- + R^{2+} = R^{3+} + O^{2-}. \quad (1)$$

$$R^+ + R^{2+} = R^{3+} + \square. \quad (2)$$

(R represents a cation and $\square$ is a crystal vacancy). Fig. 5 illustrates the results of these substitutions. Substitution (1) forms a proton-deficient tourmaline, $R^+R_3^{3+}R_6^{3+}(BO_3)_3Si_6O_{18}O_3(OH)$, analogous to the ferric tourmaline, buergerite (Table 1), whereas substitution (2) forms a solid-solution series with a theoretical alkali-deficient $[\square(R_2^{2+}R^{3+})R_6^{3+}(BO_3)_3Si_6O_{18}(OH)_4]$ end member (Fig. 5). On the basis of statistical analysis, Foit and Rosenberg (1977) stated that substitution (1) accounts for about 75% of the compositional variability due to a $(R^+, H^+)+R^{2+} = R^{3+}$ type substitution (Fig. 5). They also observed that in the alkali-deficient tourmaline, $\square R_3^{3+}R_6^{3+}(BO_3)_3Si_6O_{18}(OH)_2$, the defect site may actually host divalent cations such as Mg^{2+}, Fe^{2+}, or Mn^{2+}.

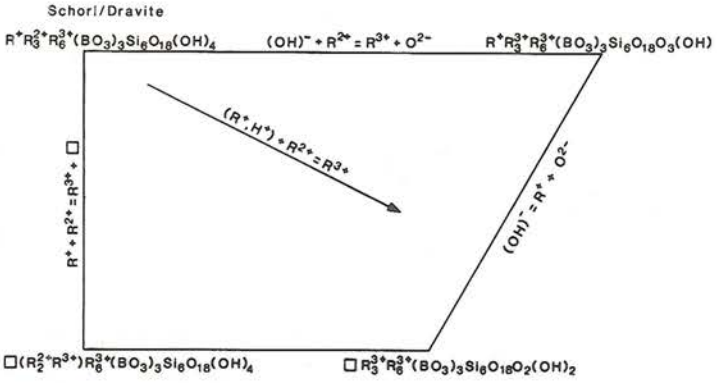

Fig. 5. Diagram showing the relationship between coupled substitutions and tourmaline end members (from Foit and Rosenberg, 1977).

The loose crystal structure of tourmaline also allows trace elements present in the environment of crystallization to be adsorbed or substituted into the crystal lattice. A large number of trace elements have been reported in tourmaline in published analyses (Dietrich, 1985).

The ranges of major element oxides for six tourmaline grains from the El Correo region, determined by microprobe analysis, are 18.6-24.6% total Fe as FeO, 1.9-3.6% MgO, 1.2-2.9% CaO, 0.3-1.1% TiO_2, 18.3-22.9% Al_2O_3, and 32.4-37.4% SiO_2 (J. M. Nishi, written commun., 1986) using average values of 10.0% B_2O_3, 2.0% Na_2O, and 3.0% H_2O for stoichiometric calculations. The tourmalines used in this study are iron-rich and aluminum-poor when compared to the common tourmaline species (Deer et al., 1962).

Tourmaline unit cell parameters *a* and *c* were calculated and plotted for 139 of the tourmaline samples collected in the El Correo region (Fig. 6). El Correo tourmaline tends to follow a trend where the *c*/*a* ratio is 0.45. This trend may reflect a solid substitution series between an alkali-free tourmaline and some dravite/schorl end member as suggested in Fig. 5. Another speculation is that the high trace-element contents of the El Correo tourmalines may be responsible for some of the scatter. In addition, concentrations of F, Cl, and/or OH (not analyzed for in this study) may also affect the unit cell parameters of tourmaline.

Six samples were analyzed by Mossbauer spectroscopy for ferrous/ferric iron ratios. Five of the six tourmalines give Fe^{2+}: Fe^{3+} ratios of approximately 80:20 while a single sample has a ratio of 43:57 (J. D. Brown, written commun., 1983). Whether the Fe^{3+} in these samples is present in the Y or Z structural positions is not known.

In summary, the tourmalines from El Correo are iron-rich and are tentatively classified as schorl. Unit cell parameters, Fe^{2+}: Fe^{3+} ratios, and low alumina contents suggest that these tourmalines also have an alkali-free component and a buergerite or ferridravite component (Table 1).

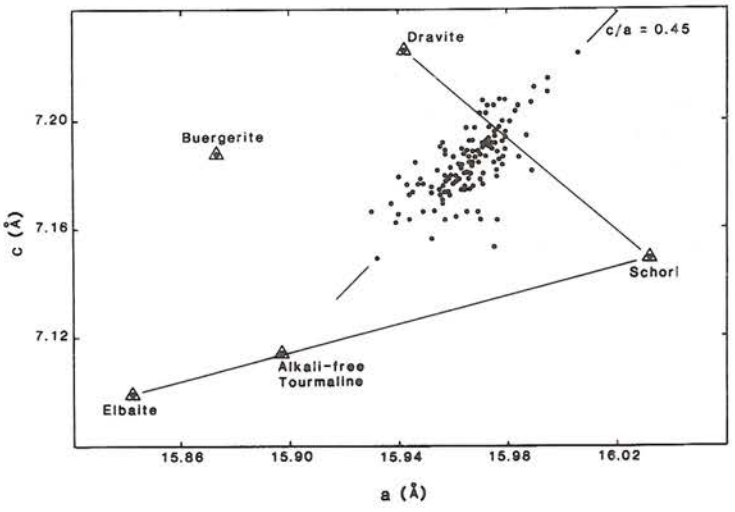

Fig. 6. Unit cell parameters for 139 El Correo tourmalines. (Data points: dravite, schorl, elbaite—Epprecht, 1953; buergerite—Donnay et al., 1966; alkali-free tourmalines—Werding and Schreyer, 1984.)

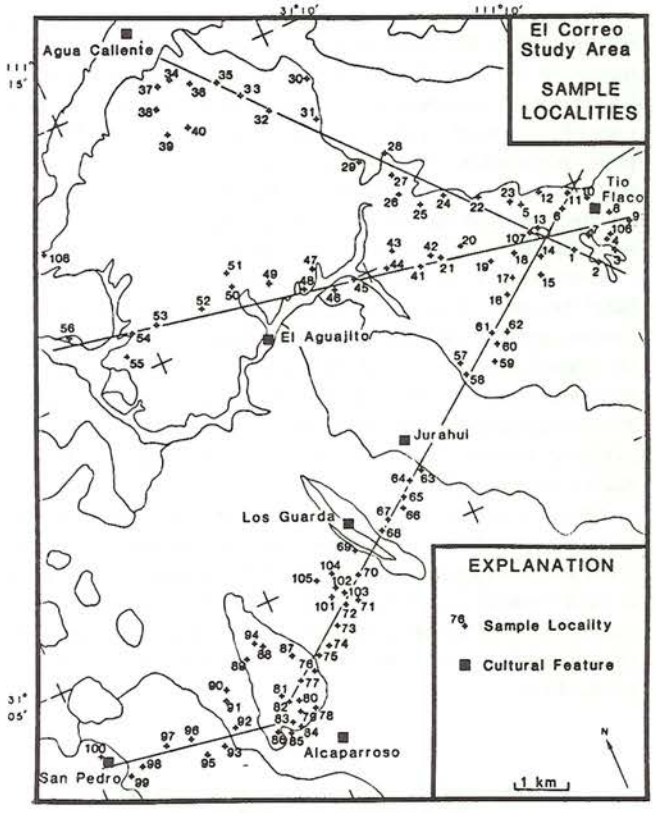

Fig. 7. Distribution of sample localities along three traverse lines and in areas of mineralization, El Correo, Sonora, Mexico. Geologic units (unpatterned) from Figure 4.

SAMPLE COLLECTION, PREPARATION, AND ANALYSES

Rock samples containing tourmaline were collected along three traverses at a density of approximately one site per ½ kilometre, with additional sites in the following areas of known mineralization: Tio Flaco (Cu, Au), Alcaparroso (Cu), Agua Caliente (Pb, Ag), and Los Guarda (Pb, Mo, Ag) (Fig. 7). A duplicate sample was collected at or about every tenth site as a check on sampling and analytical precision. When more than one recognizable generation of tourmaline was present at a single locality, samples were collected to represent each generation. Each of the 142 samples, collected from a total of 108 sites, consisted of 1-5 kilograms of rock chips selected to characterize an occurrence and provide sufficient tourmaline for chemical analysis.

Each sample was crushed and pulverized to approximately ½ mm chips and then sieved using 20-, 35-, 60-, 80-, and 120-mesh stainless steel sieves. Each fraction was visually examined to determine the optimum size fraction(s) for producing clean tourmaline grains. The heavy minerals, including tourmaline (specific gravity 3.00 +), were extracted from these fractions using bromoform (specific gravity 2.85) heavy-liquid separation techniques.

Tourmaline was extracted from the heavy-mineral concentrate using a Frantz Isodynamic Magnetic Separator[1] equipped with an aluminum track set at a slope of 5° and a tilt of 20°. Most tourmaline grains were separated from the sample within a range of 0.4-0.8 amperes. Following the magnetic separation, each sample was hand cleaned to greater than 95% estimated purity under a binocular microscope. The most common contaminant was quartz adhering to the surface of tourmaline grains. Some samples containing large amounts of epidote, which has paramagnetic characteristics close to those of tourmaline, were separated using methylene iodide (specific gravity 3.32). Tourmaline was extracted from the light fraction. Samples with very heavy coatings of iron and manganese oxides were also treated with concentrated HCl.

Samples were hand ground in an agate mortar. Seven samples were split into duplicates to check analytical precision. Ten milligrams from each sample were analyzed in a 1.5-metre Bausch and Lomb DC-arc source optical emission spectrograph for the following 30 elements: Fe, Mg, Ca, Ti, Mn, Ag, As, Au, B, Ba, Be, Bi, Cd, Co, Cr, Cu, La, Mo, Nb, Ni, Pb, Sb, Sc, Sn, Sr, V, W, Y, Zn and Zr. The six-step semiquantitative method outlined by Grimes and Marranzino (1968) was employed. The spectra were recorded on glass plates and visually compared with standards. Values are reported as the approximate geometric midpoints: 0.15, 0.2, 0.3, 0.5, 0.7, 1.0 (or multiples of 10) of ranges whose respective boundaries are: 0.12, 0.18, 0.22, 0.38, 0.56, 0.83, 1.2 (or multiples of 10). The reported precision is plus or minus one step at the 83% confidence level, or plus or minus two steps at the 96% confidence level (Motooka and Grimes, 1976). Duplicate analyses from this study were within these limits (Smith, 1985). Samples were analyzed in a random order to prevent systematic analytical bias. Sample preparation and analytical procedures are illustrated in Fig. 8.

[1] The use of trade names is for descriptive purposes only and does not imply endorsement by the U.S. Geological Survey.

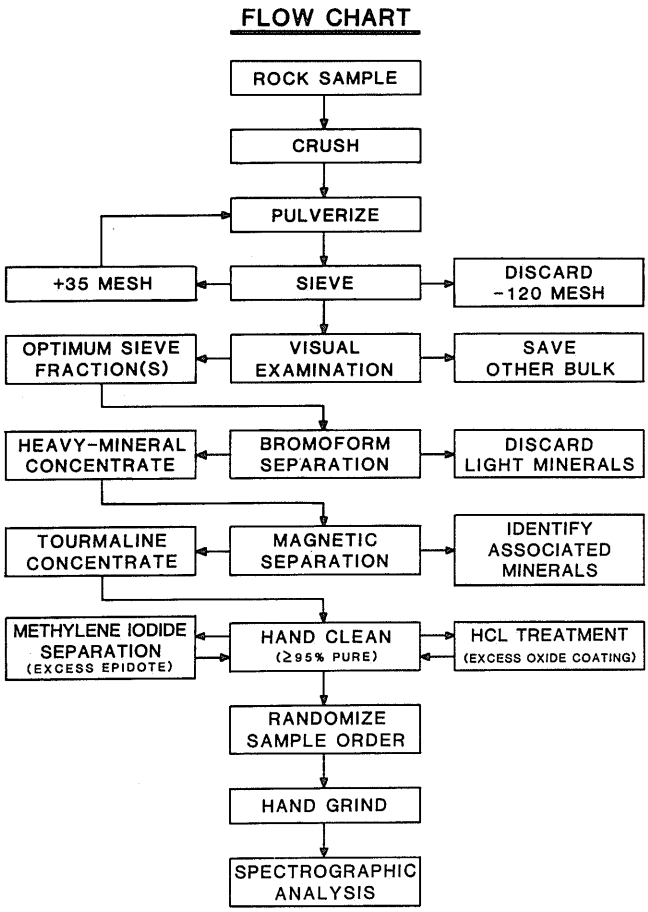

Fig. 8. Sequential steps used in the sample preparation and analysis of tourmaline-mineral separates.

DATA TREATMENT AND RESULTS

Table 2 summarizes the analytical results for single elements in tourmaline from El Correo. Ranges of values for Ba, Co, Cu, Pb, Y and Zr show two or more orders of magnitude while Ag, Bi, Cr, La, Ni, Sc, Sn, Sr, V and Zn have ranges of at least one order of magnitude. The El Correo tourmalines contain high mean values of Mn (2990 ppm), Ag (2.4 ppm), Co (63 ppm), Cr (26 ppm), Cu (199 ppm), Mo (16 ppm), Ni (49 ppm), Pb (728 ppm), Sn (53 ppm), Sr (1465 ppm), V (353 ppm), Zn (1938 ppm) and Zr (185 ppm). Most of these values are higher than the average trace-element contents of tourmaline associated with massive sulfide deposits reported by Taylor and Slack (1984): Cr (78 ppm), Cu (77 ppm), Pb (114 ppm), Sr (98 ppm) and V (195 ppm).

Gold and cadmium were the only elements not detected out of the 30 elements that were determined. Arsenic and tungsten were detected in one sample each and only trace amounts of antimony, lower than the analytical determination limit (100 ppm), were noted. Concentrations of boron were greater than the upper limit of determination (2000 ppm) in every sample; tourmaline normally contains about 10% B_2O_3 (Deer et al., 1962). These elements (Au, Cd, As, W, Sb and B) were removed from further statistical consideration. Niobium data, which only contain 16 unqualified values, were not removed even though they are a statistically invalid population.

The results for three single elements, Cu, Ag and Pb, are presented in this report. Histograms for each element are shown in Fig. 9. Threshold values were determined on the basis of breaks observed within the histograms.

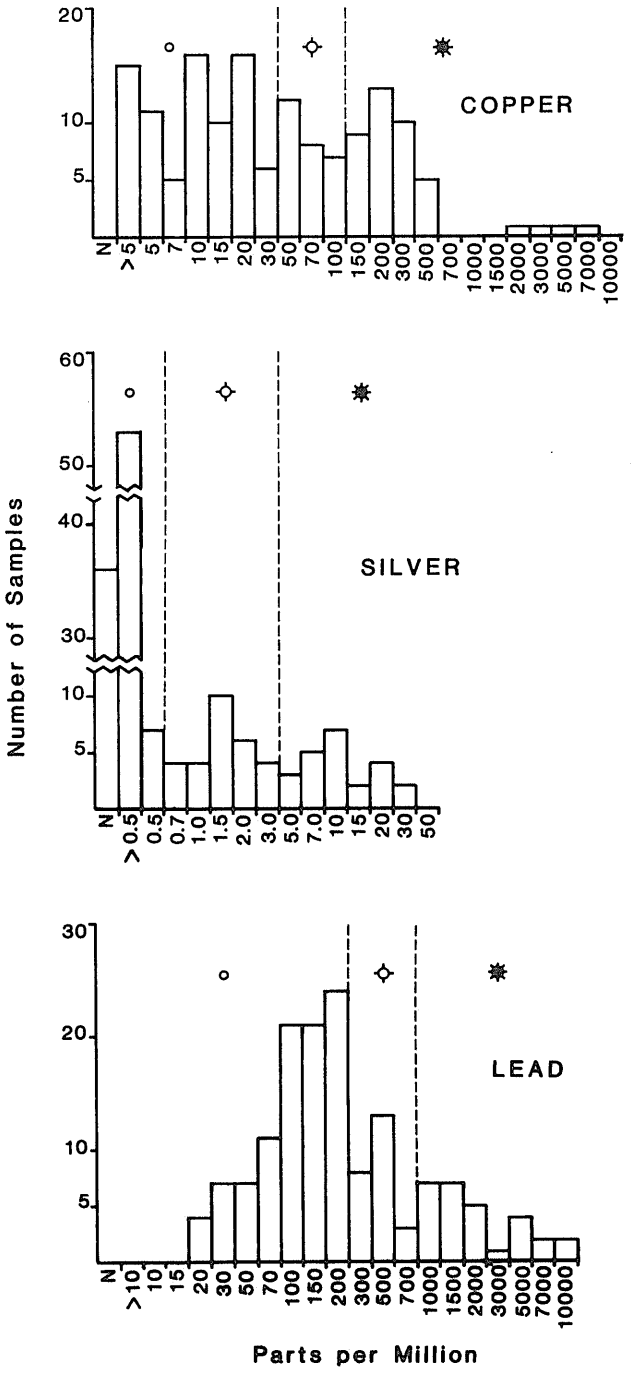

Fig. 9. Histograms of copper, silver, and lead contents in El Correo tourmalines. The three symbols (○, ✧, and ✱) represent ranges of values plotted in Figures 10-12.

Table 2. Univariate statistics for trace-element data for tourmalines from El Correo, Sonora, Mexico.

Element[1] (LDL)	Minimum Value	Maximum Value	Arithmetic[3] Mean	Standard[3] Deviation	Valid Values	Qualified Values[2] L	N	G
Fe% (.05%)	15	30	20.102	1.599	147	0	0	0
Mg% (.02%)	2	10	5.694	1.658	147	0	0	0
Ca% (.05%)	0.15	3	1.238	0.657	147	0	0	0
Ti% (.002%)	0.15	1.5	0.554	0.200	147	0	0	0
Mn (10)	700	5000	2990.476	1848.003	134	0	0	13
Ag (.5)	0.5	30	2.417	5.302	58	53	36	0
As (200)	1000	1000	---	---	1	0	146	0
Au (10)	---	---	---	---	0	0	147	0
B (10)	---	---	---	---	0	0	0	147
Ba (20)	20	2000	247.109	286.092	133	9	5	0
Be (1)	1	20	4.224	3.279	136	1	10	0
Bi (10)	10	300	9.435	26.204	37	36	74	0
Cd (20)	---	---	---	---	0	0	147	0
Co (5)	5	500	62.748	61.280	143	0	4	0
Cr (10)	10	300	26.000	53.175	70	18	59	0
Cu (5)	5	7000	198.912	759.469	132	15	0	0
La (20)	20	1000	47.755	108.562	60	37	50	0
Mo (5)	5	150	16.078	27.672	97	29	21	0
Nb (20)	20	70	11.626	12.440	16	44	87	0
Ni (5)	5	300	48.881	52.393	145	1	1	0
Pb (10)	20	10000	727.619	1611.359	147	0	0	0
Sb (100)	---	---	---	---	0	7	140	0
Sc (5)	5	100	48.034	34.680	139	3	2	3
Sn (10)	10	700	53.163	85.018	146	1	0	0
Sr (100)	100	5000	1465.034	1401.423	145	0	2	0
V (10)	30	1500	352.517	265.951	147	0	0	0
W (50)	50	50	---	---	1	0	146	0
Y (10)	10	1000	63.626	125.742	108	3	36	0
Zn (200)	200	10000	1938.095	1597.186	147	0	0	0
Zr (10)	10	1000	185.361	222.824	133	8	6	0

All elements are reported in parts per million except where otherwise noted. (1) LDL - Lower Determination Limit (value in parentheses). (2) L - noted in the analyses but below the lower determination limit; N - not detected; G - detected at a concentration greater than the upper determination limit. (3) Arithmetic mean and standard deviation values were calculated using a value 2 steps below the LDL for an 'L' and 3 steps below the LDL for an 'N'. Analyses by S. M. Smith.

Tourmaline from El Correo has a wide range of copper contents. Copper concentrations greater than 100 ppm are considered anomalous whereas those from 50 to 100 ppm are classified as probably anomalous (Fig. 9). A map of the Cu distribution (Fig. 10) outlines two strong anomalies located near Tio Flaco and Agua Caliente, and two weaker anomalies near Alcaparroso and Los Guarda.

These anomalies are related to four areas of known mineralization. The Tio Flaco area contains several Cu-stained outcrops and two localities where chrysocolla is associated with tourmaline (Site 1; Cu = 7000 ppm: and Site 6; Cu = 2000 ppm: Fig. 7). Chrysocolla was also associated with tourmaline in two sample localities in the Alcaparroso anomaly (Site 85; Cu = 3000 ppm: and Site 94; Cu = 5000 ppm: Fig. 7). The Agua Caliente anomaly contains argentiferous galena prospects and supergene wulfenite. Covellite was noted in two samples from this area but, in each case, insufficient tourmaline was present for analysis (Sites 35 and 39; Fig. 7). The anomaly at Los Guarda outlines the placer wulfenite/vanadinite occurrence. The four highest values of Cu found in El Correo tourmalines are from sites containing tourmaline intimately associated with secondary copper minerals. The high values may reflect solid inclusions of copper minerals within the tourmaline crystals or minor amounts of copper oxides in fractures or adhering to the surface of the grains.

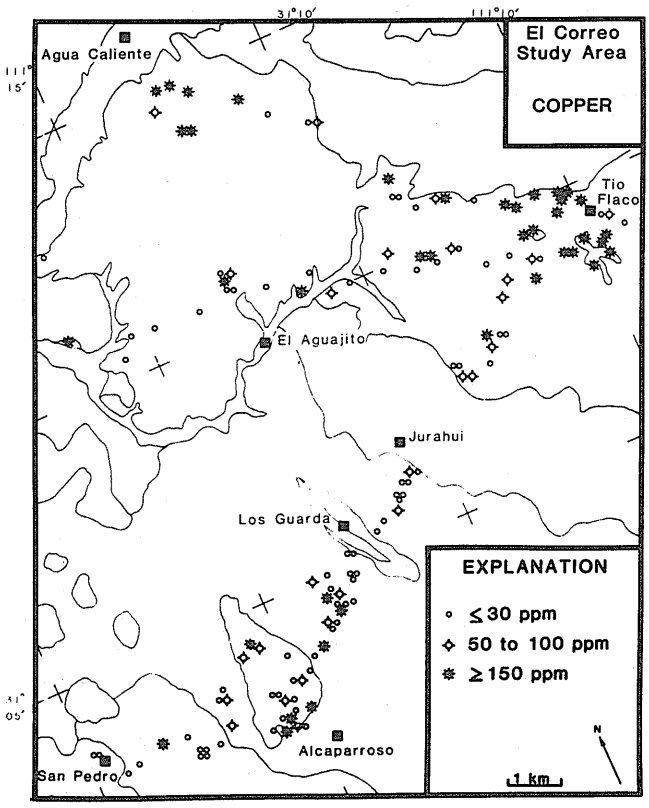

Fig. 10. Spatial distribution of copper in El Correo tourmalines. Geologic units (unpatterned) from Figure 4.

The distribution of molybdenum is similar to the distribution of copper within the study area, with the exception of the Los Guarda area which is conspicuously molybdenum-poor. High values of Mo occur in the Tio Flaco, the Agua Caliente and the Alcaparroso areas. In addition to Mo, Sn, Sc and Y are anomalously high in the Tio Flaco area (Smith, 1985).

Silver contents in tourmaline fall into three populations: (1) a truncated population covering the range "not detected" (N) to 3.0 ppm, (2) a second distribution from about 0.7 to 3.0 ppm, and (3) a third distribution from 5 to 30 ppm (Fig. 9). Anomalous amounts of Ag are found near Tio Flaco and Agua Caliente and, to a lesser extent, near Alcaparroso and El Aguajito (Fig. 11). The Tio Flaco Ag anomaly appears to be offset slightly to the west of the Cu, Mo, Sn, and Sc anomalies. Argentiferous galena was found associated with tourmaline in the Agua Caliente area.

The histogram for lead shows a positively skewed distribution (Fig. 9). The spatial distribution map (Fig. 12) reveals that Pb-enriched tourmaline is found near Agua Caliente and on the west side of the Tio Flaco. The Tio Flaco region is conspicuously barren with respect to Pb in tourmalines. Zinc, strontium and vanadium are similarly depleted in the Tio Flaco area. The Los Guarda region has a few high Pb values but not as many as might be expected with the proximity of placer wulfenite. Site 103 (Fig. 7) in this region has wulfenite/pyromorphite associated with tourmaline, and is located near a small prospect shaft which has produced minor argentiferous galena.

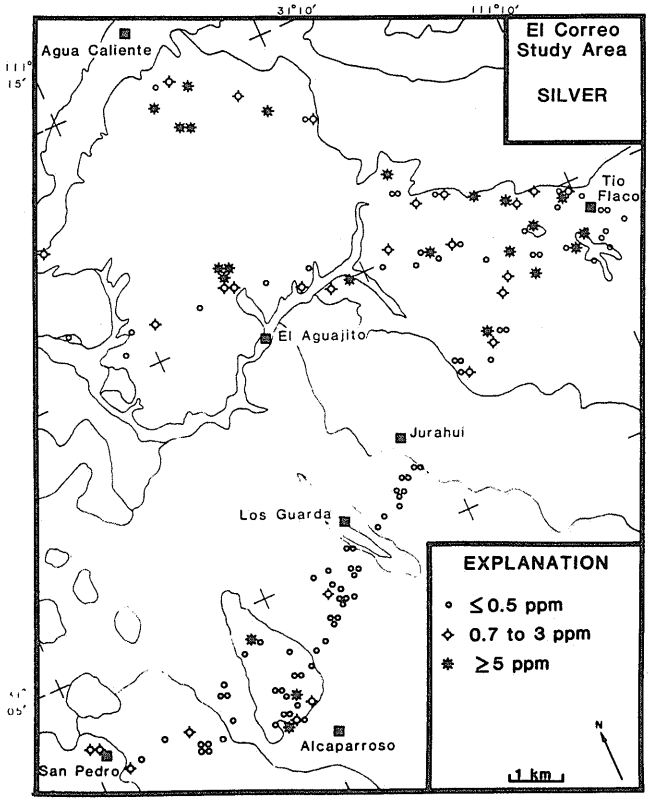

Fig. 11. Spatial distribution of silver in El Correo tourmalines. Geologic units (unpatterned) from Figure 4.

The observation that several elements appear to correlate spatially with different anomalous areas suggests that the tourmaline-depositing fluids were of different compositions. Each separate fluid or phase of an evolving hydrothermal fluid

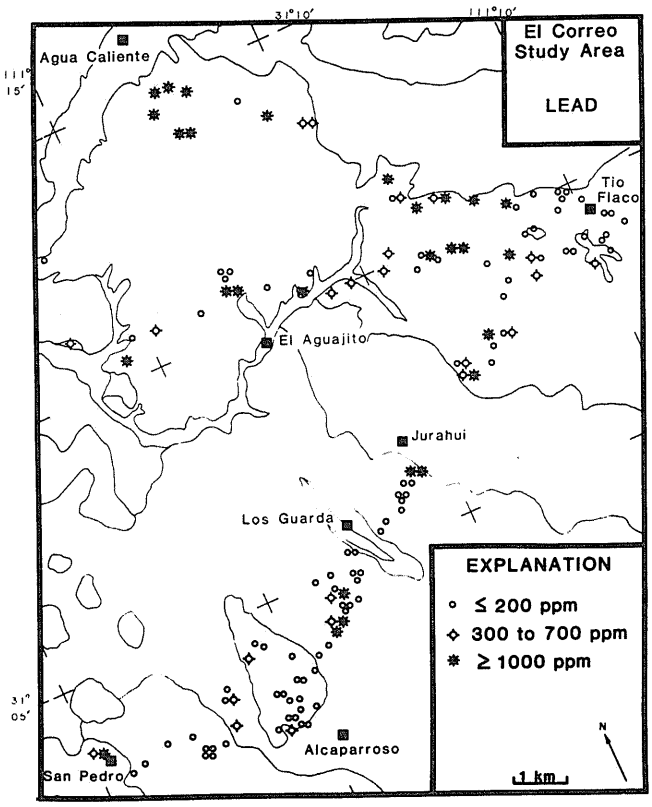

Fig. 12. Spatial distribution of lead in El Correo tourmalines. Geologic units (unpatterned) from Figure 4.

would have a characteristic suite of elements scavenged by the crystallizing tourmalines. If these element associations could be recognized, then different types of mineralization or zones of a mineralizing system may be distinguishable.

R-mode factor analysis is a multivariate technique for grouping variables, such as trace elements, into a few principal associations based upon linear correlation coefficients, while maintaining the individuality of each sample. The relative strength of each factor, or element assemblage, for each individual sample is expressed as a factor score that can be plotted on a distribution map (Closs and Nichol, 1975).

Multivariate statistical analysis techniques such as factor analysis require a data set without qualified values. In order to use all of the information available within the tourmaline data set, qualified values were assigned numerical values. Elements that were noted as being present in the analyses, but at a concentration below the limit of determination (denoted by an "L" in Table 2), were assigned a value two steps below the determination limit value (for example, L(0.5 ppm) = 0.2 ppm). Elements that were not detected in a given sample (denoted by an "N") were assigned a value 3 steps below the determination limit value. When an element concentration was reported as greater than the upper limit of determination ('G'), the assigned value was 1 step above the limiting value.

Eight models consisting of from 2 to 9 factors were developed for the tourmaline geochemical data from El Correo and are discussed in detail by Smith (1985). The selection of the most appropriate model is based upon the recognition of interpretable element associations related to geologic processes. Processes which could potentially influence element associations for this study include: (1) the reaction between host rocks and hydrothermal fluids, (2) the differentiation of hydrothermal fluids, (3) the effects of hydrothermal alteration upon preexisting tourmaline crystals and (4) the preferential partitioning of metals into the crystallizing fluid and/or metallic mineralization.

The six-factor model, representing metal associations most easily related to the geology of the area, is summarized in Table 3. High positive factor scores for factor 1, a ferride-metal association, correlate spatially with the distribution of Jurassic metasediments west of Alcaparroso. These metasediments are interlayered with volcanics of quartz latite composition. High positive factor scores for factor 2, a felsic-metal association, correlate broadly with the spatial distribution of granitic intrusives. Spatial distribution plots of factor scores for factors 1 and 2 are given by Smith (1985; Figs. 49 and 50; Plate 3).

Factors 3, 4, and 6 of the 6-factor model are interpreted as mineralization-related factors. A strong Cu-Mo-Sn-[Be] association (Factor 4; Fig 13) occurs in the Tio Flaco area. (Elements enclosed by brackets have factor loadings between |0.4| and |0.6| and represent weaker members of the elemental assemblages.) Two other areas are also defined by this association; the Agua Caliente region and a small area between Tio Flaco and El Aguajito. The traverse between Jurahui and San Pedro is markedly depleted in the Cu-Mo-Sn-[Be] association in spite of the Cu mineralization noted near Alcaparroso. This observation suggests that the mineralization in the Alcaparroso region is related to a different system (or process) than that in the Tio Flaco and Agua Caliente vicinities.

The spatial distribution pattern of factor 3 (Zn-Pb-Sr-[Mn-Ti]) is illustrated in Fig. 14. The Tio Flaco area is strongly depleted with respect to this base-metal association. Peripheral to the Tio Flaco region, factor 3 scores show a scattered enrichment which becomes increasingly focused approaching the Agua Caliente area. This zoning is best seen on the northernmost traverse and to a lesser extent on the El Aguajito traverse. Again, as in factor 4, the traverse between Jurahui and San Pedro has a different character in spite of the presence of Pb mineralization near Los Guarda.

Another zone is illustrated by a Ag-Bi-[Pb-Mn-Ca] association on the factor 6 map (Fig. 15). This group of metals is enriched in tourmaline found on the west side of the Tio Flaco area. Due to the limited number of samples collected that contain detectable Ag and/or detectable Bi, this factor may not be statistically valid. However, the single-element maps for Ag (Fig. 11) and Bi (Smith, 1985; Fig. 31) show that the anomaly at Tio Flaco has shifted to the west. This observation supports the idea of an element zonation centered about Tio Flaco.

Factor 5 appears to be a second-ferride factor (Fe-[Co-Mg]). This association did not show any spatial relationships on a factor score plot, nor was any common characteristic identified between samples having like factor score values.

In summary, the three mineralization factors define a zoning pattern for the hydrothermal system centered in the Tio Flaco area (Fig. 16). The center of the system is defined by an assemblage of metals in tourmaline which are normally associated with a high-temperature hydrothermal system (Cu-Mo-

Table 3. Summary of results and the interpretation of an *R*-mode factor analysis of the trace-element data for El Correo tourmaline (from Smith, 1985).

Six-Factor Model		
Factor	Element(*) Assemblage	Interpretation
1	Cr-Ni-V-[Ca-Mg-Ti]	Lithologic influence (Metasedimentary rocks)
2	Y-La-Nb-Zr-[Ti-Sc-Ba]	Lithologic influence (Felsic intrusives ± volcanics)
3	Zn-Pb-Sr-[Mn-Ti]	Low-temperature base-metal mineralization
4	Cu-Mo-Sn-[Be]	High-temperature base-metal mineralization
5	Fe-[Co-Mg]	Unknown lithologic(?) influence
6	Ag-Bi-[Pb-Mn-Ca]	Precious-metal mineralization

*Elements within brackets ([Pb]) have factor loadings between |0.4| and |0.6| and represent weaker members of the elemental assemblages.

Sn-[Be]). Peripheral to this high-temperature assemblage is a Ag-Bi-[Pb-Mn-Ca] shell which is, in turn, surrounded by a lower temperature base-metal shell (Zn-Pb-Sr-[Mn-Ti]).

Although the zoned hydrothermal event explains much of the variation in the trace-element content of tourmalines, additional information suggests that other events are also recorded. Overprints of other events can be recorded in tourmaline samples because each sample is a composite of several small tourmaline grains, and each grain may be zoned by successive stages of growth during different events.

The Agua Caliente area appears to have undergone a similar, though smaller, hydrothermal event to that seen near Tio Flaco. This event is recorded by the enrichment of the high-temperature assemblage, the low-temperature assemblage and the high silver contents in tourmalines of the Agua Caliente area.

The southernmost traverse between Jurahui and San Pedro does not record the effects of the Tio Flaco system as expressed by the factor analysis assemblages (Fig. 16). However, data from stream-sediment and heavy-mineral-concentrate geochemical surveys imply that the region dominantly reflects the Tio Flaco system, with the possibility of a smaller peripheral system developed at Alcaparroso (Figs. 2 and 3). Three possible interpretations are given here to explain this apparent contradiction:

(1) The tourmaline trace-element data reflect the presence of two different primary systems, Tio Flaco and Alcaparroso, respectively, whose trace-element signatures, as detected in stream sediment analyses, have been rearranged by secondary processes.
(2) Tourmaline from the Tio Flaco system is lacking in the region between Jurahui and San Pedro.
(3) Trace-element signatures in the Tio Flaco-system tourmalines have been swamped by the influx of a later generation tourmaline of a different source.

Some combination of these interpretations is probably responsible for the difference noted between the tourmaline results and the earlier geochemical surveys.

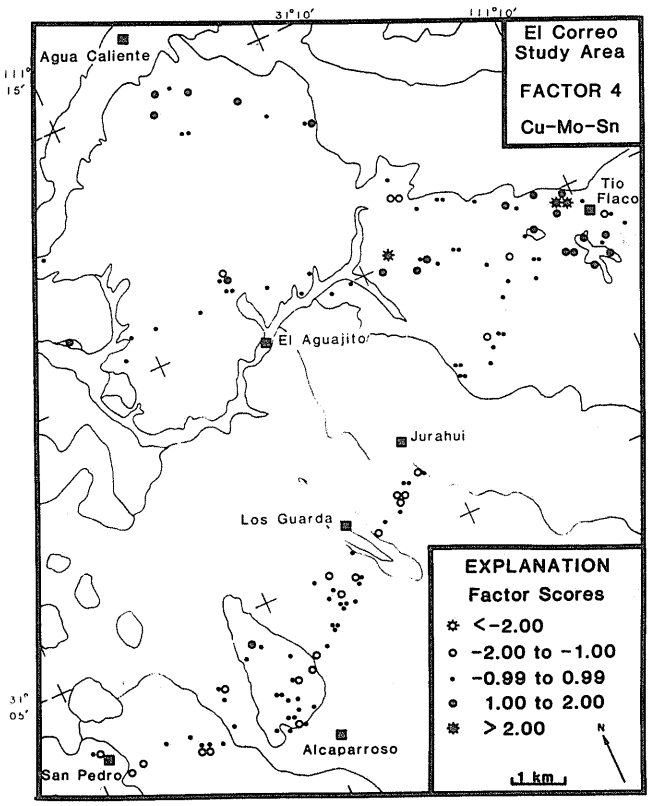

Fig. 13. Spatial distribution of *R*-mode factor scores for factor 4, Cu-Mo-Sn-[Be]. Geologic units (unpatterned) from Figure 4.

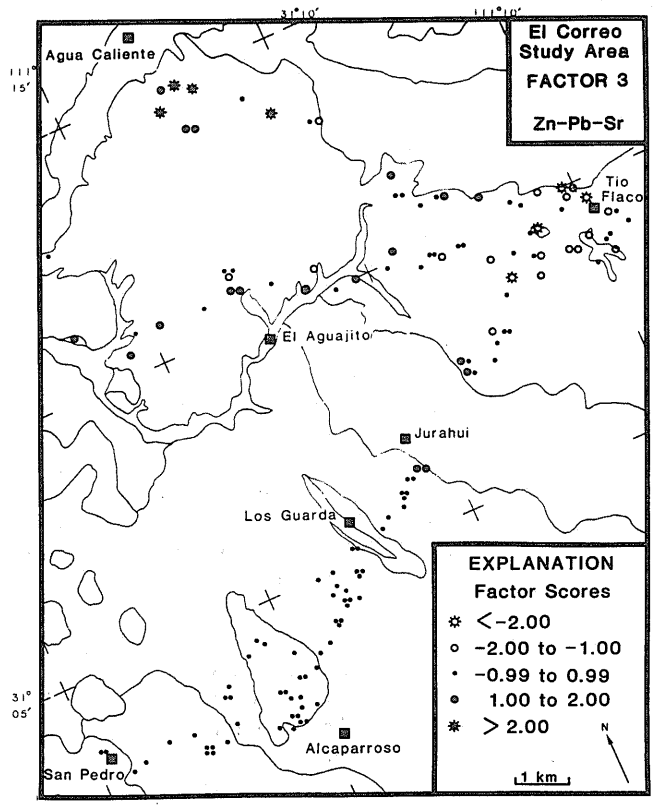

Fig. 14. Spatial distribution of *R*-mode factor scores for factor 3, Zn-Pb-Sr-[Mn-Ti]. Geologic units (unpatterned) from Figure 4.

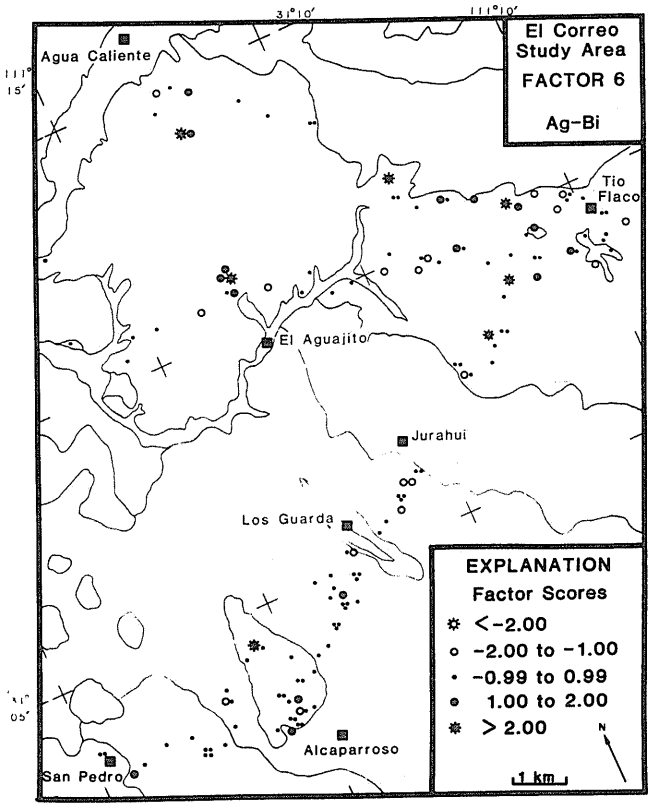

Fig. 15. Spatial distribution of *R*-mode factor scores for factor 6, Ag-Bi-[Pb-Mn-Ca]. Geologic units (unpatterned) from Figure 4.

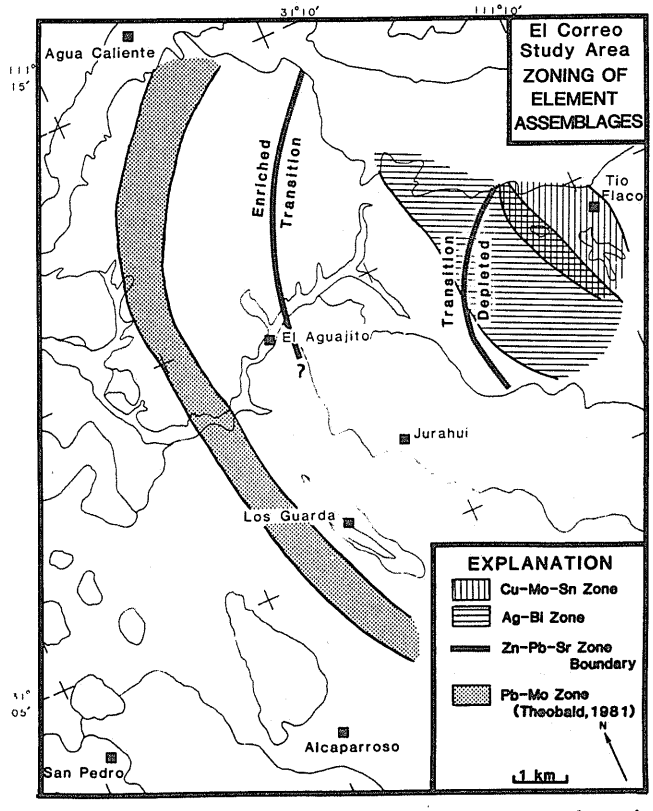

Fig. 16. Composite zonation of the Tio Flaco system as shown by the trace-element assemblages derived from *R*-mode factor analysis of El Correo tourmalines and compared with the Pb-Mo zone (Figs. 2 and 3) of Theobald (1981).

DISCUSSION

Several assumptions were made at the onset of this study. Those assumptions that could most affect the soundness of the conclusions drawn are as follows:

(1) Tourmalines from the El Correo study area are hydrothermal in origin (as opposed to magmatic) and, as such, are spatially and temporally associated with ore minerals deposited by the same hydrothermal event.
(2) Tourmaline is a stable mineral that resists chemical change during alteration and weathering events that postdate the original crystallization.
(3) Tourmaline is an effective scavenger of trace elements that can accommodate large quantities of trace metals within its crystal structure.
(4) The trace-element content of hydrothermal tourmaline reflects the general composition of the crystallizing fluid, and thus may partially reflect the composition of syn-depositional mineralization.

The following discussion will consider the validity of these suppositions.

Two variables were studied to determine the hydrothermal character of the El Correo tourmalines. First, each tourmaline locality was described with respect to the mode of occurrence of tourmaline crystals. Tourmaline is primarily found in quartz veins and as breccia cements which are interpreted as having a hydrothermal origin. Tourmaline-bearing pegmatites and pods are quartz dominant, with little or no microcline feldspar, and commonly contain very fine-grained muscovite, epidote, and tourmaline in varying amounts. This mode of occurrence is tentatively interpreted as having a hydrothermal origin. Where tourmaline is disseminated within the host rock, determining whether the origin is magmatic or hydrothermal is difficult unless a clear association with proximal veining or brecciation can be demonstrated.

Secondly, the Sr:Ca ratio from each tourmaline sample was calculated and compared with the results of a study by Power (1966). All of the El Correo tourmalines, with the exception of two in which Sr was not detected, plot in the region defined as hydrothermal (Fig. 17).

The assumption that tourmaline remained stable and chemically unchanged through subsequent alteration and weathering was not specifically addressed during the course of this study. Observations made from the sample descriptions and from limited petrographic work indicate that the tourmaline crystals are typically euhedral and rarely show evidence of corrosion. The presence of color zoning in tourmaline suggests that the chemistry of the original crystal(s) may have been overprinted by later generations of tourmaline.

Taylor and Slack (1984) noted that some hydrothermal tourmalines associated with massive sulfide deposits retain original, delicate growth structures through subsequent metamorphism. In addition, their study suggested that only minor chemical or isotopic exchange occurred along the rims of the tourmaline grains that are in contact with matrix (commonly sulfide) minerals.

Although tourmaline is known to be stable during weathering and in many cases appears to remain largely unchanged through metamorphism, the effects of retrograde hydrothermal alteration on tourmaline are not completely known. Therefore, the El Correo tourmalines may have been altered or chemically overprinted by later fluids. However, the results from the trace-element analyses of these tourmalines suggest that the compositions reflect a pattern that is close to (if not) the original pattern of primary dispersion of metals imprinted by the hydrothermal system.

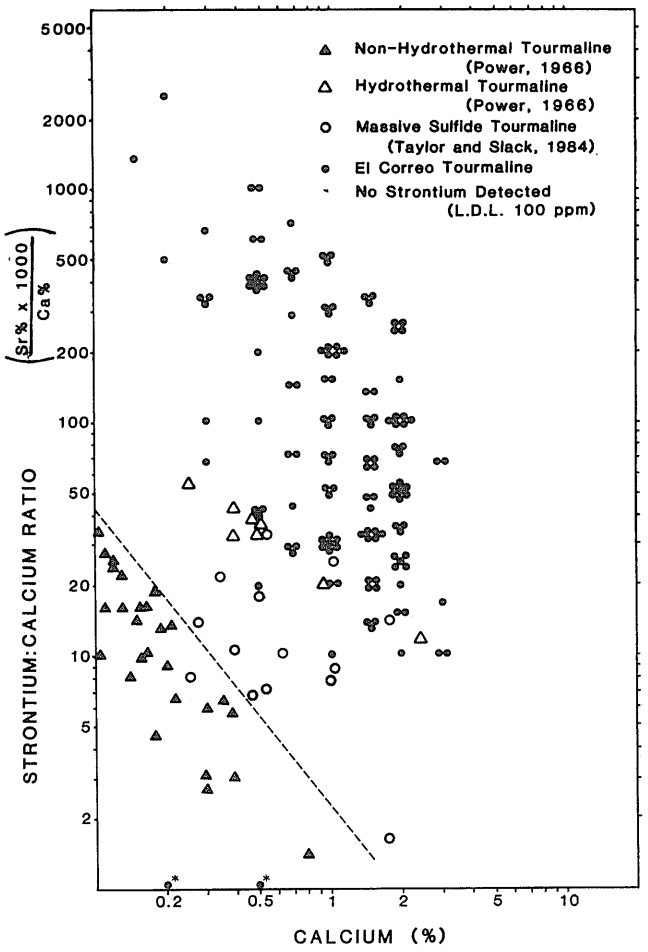

Fig. 17. Strontium-calcium ratios of tourmalines compared with data from Power (1966) and Taylor and Slack (1984). Proposed dividing line between hydrothermal and magmatic tourmaline fields empirically based on plotted data.

The assumption that tourmaline is an effective trace-element scavenger is substantiated by the number of different trace elements found in tourmaline. This scavenging property is also reflected by the large range of trace elements that have been found in tourmaline from the El Correo area (Table 2). Some of the excessive trace-element concentrations may be due to the inclusion of minute, foreign mineral grains. Even if this is the case, the association of trace metals in tourmaline with mineralization is still obtained.

The correlation between high trace-element contents in tourmaline and the occurrence of ore and ore-related minerals suggests that the fourth assumption is valid. Smith (1985) was able to show correlation between trace-element contents and the presence or absence of associated pyrite and ore minerals. Taylor and Slack (1984) also noted a similar correlation between

Table 4. Average trace-element compositions of tourmalines collected from different environments (modified after Taylor and Slack, 1984).

Element	Massive[1] Sulfides	Portugese[2] Granites	English[3] Granites	Breccia Pipes[4] Barren	Breccia Pipes[4] Cu-bearing	El Correo[5] Area
Co	<5	12	22	225	288	63
Cr	78	10	17	128	74	26
Cu	77	22	7	15	52	199
Mn	382	1579	2535	123	154	2990
Ni	<5	4	23	75	98	49
Pb	114	6	--	<10	<10	728
Sc	47	5	41	--	--	48
Sn	21	3	21	--	--	53
Sr	98	6	16	75	112	1465
V	195	4	28	887	722	353
Zn	387	517	--	<50	<50	1938

All values are reported in parts per million. -- = not analyzed. (1) Taylor and Slack (1984); (2) Neiva (1974); (3) Power (1968); (4) Birk (1980); (5) Table 2, this study.

the composition of tourmaline and the nature of coexisting ore minerals. These studies demonstrate that tourmaline scavenges available elements from its environment of crystallization, thus allowing it to reflect the general composition of the crystallizing hydrothermal fluid.

Tourmaline studies of other environments

The total trace-element content of tourmaline from El Correo is very high when compared to tourmalines analyzed from other environments (Table 4). Compared to tourmalines from granites, pegmatites, and aplites, those from El Correo are characterized by enriched Cu, Pb, Sn, Sr and Zn whereas tourmalines from massive sulfide deposits are high in Cr, Cu, Pb and Sr (Taylor and Slack, 1984). An enrichment in Cr, Sr and V appears to characteristic of tourmaline from hydrothermal environments (i.e. massive sulfide, breccia pipe, and from El Correo; Table 4). Enrichment in Cu, Pb and Sr appears in tourmaline most closely associated with known mineralization.

Slack (1980; 1982) proposed that Mg-rich tourmaline (dravite) is a useful prospecting guide for massive sulfide deposits, whereas Fe-rich tourmaline (schorl) generally reflects felsic plutonic environments. One prominent exception to this pattern, however, has been recently documented for the large Kidd Creek massive sulfide in Canada, where the tourmalines are predominantly iron rich (Slack and Coad, 1986). In addition to this correlation between major elements (Mg and Fe) in tourmaline and mineralization environments, the results from this present study suggest that the trace-element content of any hydrothermal tourmaline will also characterize environments of mineralization.

PRACTICAL APPLICATIONS FOR TOURMALINE GEOCHEMISTRY

This trace-element geochemical study of tourmaline was successful in outlining areas of mineralization related to hydrothermal activity. The trace-element zoning sequence in tourmaline

collected from the Tio Flaco area was different from zoning patterns produced by stream sediment and heavy-mineral-concentrate geochemical surveys and suggests that tourmaline preserves primary dispersion patterns through subsequent alteration and weathering. Therefore, tourmaline trace-element geochemistry is another viable tool in exploration for hydrothermal mineral deposits. However, two factors affect the practical application of this exploration technique: (1) the availability of associated tourmaline; and (2) economic constraints.

Tourmaline has been found associated with several known deposits and consequently may be used to locate similar unknown deposits. Unfortunately, this association does not occur in all deposits of a given type. Many porphyry copper deposits in Mexico contain tourmaline (Sillitoe, 1976), whereas those in the southwestern U.S. generally lack tourmaline. Therefore, tourmaline trace-element geochemistry can only be used in certain districts, belts and provinces. Potential regions for using this technique in exploration include the Bolivian tin province (Sillitoe et al., 1975); the Mexican porphyry copper belt (Sillitoe, 1976); breccia pipes in Chile (Sillitoe and Sawkins, 1971) and in the Inguaran District of Michaocan, Mexico (Sawkins, 1979); metasediment-hosted massive sulfides in the Appalachian and Caledonian mountain belts (Taylor and Slack, 1984); and the Proterozoic sediment-hosted massive sulfide province of the Belt Supergroup in British Columbia, Canada (Ethier and Campbell, 1977), and western Montana and northern Idaho.

Economic considerations are an important factor in the utility of tourmaline-mineral-separates geochemistry, as with all exploration techniques. The sample preparation procedures for almost any mineral separate are time consuming and expensive. Due to a lack of demand, few commercial laboratories offer mineral extraction services. Still, expenses can be minimized for tourmaline trace-element geochemistry.

The analysis of tourmaline by the use of semiquantitative optical emission spectrography is adequate, usually cheaper than other analytical techniques and requires only 10 mg of material. Laser spectrographic methods have the ability to analyze even small single crystals and may eventually save time and money by reducing the amount of sample preparation. The analysis of single coarse crystals of tourmaline (where available) also saves time over the preparation of composite fine-grained tourmaline samples. An exploration geochemist may elect to analyze rock chips of veins and breccia cements that contain abundant tourmaline and where the major dilutant is quartz, instead of obtaining pure tourmaline mineral separates.

Tourmaline geochemistry would not be practical for a large, regional reconnaissance study where stream-sediment samples and/or heavy-mineral-concentrate samples are able to delineate anomalies. However, this technique may become useful in areas of intense alteration and/or weathering where secondary dispersion has reduced the chances for a reasonable interpretation from traditional sampling programs. Preliminary tourmaline samples from such areas may be obtained simply and cheaply by physical extraction from previously collected rock and/or heavy-mineral-concentrate samples.

Smith (1985) suggests that although tourmaline may contain large amounts of different trace elements, the suite of Cu, Pb, Sn, Sr, Zn, Mo, Ag, Bi and Cr is sufficient to outline the tourmaline geochemical anomalies associated with mineralization in the El Correo region. This suite is probably sufficient for any exploration program using tourmaline. Although the use of *R*-mode factor analysis enhances the interpretation of hydrothermal zoning in the El Correo study area, such multivariate statistical techniques may not be needed in every tourmaline geochemistry program.

SUMMARY AND CONCLUSIONS

Several conclusions have been drawn based upon field observations, sample descriptions, trace-element distributions and statistical results:

(1) This study confirms the results of a preliminary study of 17 tourmaline samples that suggested anomalous trace-element contents and distribution in hydrothermal tourmaline near El Correo.

(2) Tourmaline from the El Correo area is probably iron-rich schorl with a buergerite or ferridravite component and also an alkali-free tourmaline component.

(3) Owing to the association of enriched trace-element contents in tourmaline coexisting with ore minerals, we can assume that the tourmaline crystallized from the same or similar fluids as the ore minerals and that the trace-element contents of the tourmaline reflect the composition of the original fluids.

(4) The geographic distribution of single-element data revealed the following element associations in tourmaline:
   (a) Tio Flaco — enrichment in Cu, Mo, Sn, Sc and Y, with a corresponding depletion in Pb, Zn, Sr and V.
   (b) Tio Flaco periphery — enrichment in Ag and Bi.
   (c) Agua Caliente — enriched concentrations of Pb, Ag, Cu, Zn and Mo.
   (d) Los Guarda — moderate enrichment in Cu and Pb.
   (e) Alcaparroso — enriched Cu, Ag and Mo.

(5) *R*-mode factor analysis reveals at least two element assemblages associated with lithology and three assemblages associated with mineralization.

(6) The distribution of *R*-mode-factor-analysis-derived element assemblages associated with mineralization outlines a large zoned hydrothermal system centered near Tio Flaco.

(7) The primary hypogene trace-element distribution of the Tio Flaco hydrothermal system as reflected in tourmaline has a Cu-Mo-Sn-[Be] core surrounded successively by an inner Ag-Bi-[Pb-Mn-Ca] shell and an outer Zn-Pb-Sr-[Mn-Ti] shell.

(8) The distribution of element assemblages derived from *R*-mode factor analysis suggests that mineralization in the region between Jurahui and San Pedro may be due to another system, distinct from that centered near Tio Flaco.

(9) The use of tourmaline-mineral-separates geochemistry has been shown to be a useful exploration tool for hydrothermal deposits in regions of intense supergene alteration.

Acknowledgements — This study was part of a cooperative project between the U.S. Geological Survey and the Consejo de Recursos Minerales de Mexico. Additional support was provided by the Colorado School of Mines. We wish to thank R. G. Eppinger for his help, companionship, and fluency in Spanish during the field season in

Sonora; T. Botinelly for assistance in the X-ray diffraction lab; D. Wesson for assistance in the preparation of this manuscript; and M. Queen for assistance and advice in drafting. Discussion with T. Botinelly, R. G. Eppinger, and R. L. Turner, as well as access to their unpublished notes and maps, greatly aided this research. We also wish to thank T. Botinelly, R. G. Eppinger, J. F. Slack, M. Parrish, and one anonymous reviewer whose constructive comments were incorporated in the final manuscript.

REFERENCES

Al-Hashimi, A. R. K. and Brownlow, A. H., 1970, Copper content of biotites from the Boulder Batholith, Montana: Econ. Geol., v. 65, p. 985-992.

Auger, P.R., 1941, Zoning and district variations of the minor elements in pyrite of Canadian gold deposits: Econ. Geol., v. 36, p. 401-423.

Birk, R. H., 1980, The petrology, petrography, and geochemistry of the Black Jack breccia pipe, Silver Star Plutonic Complex, Skamania County, Washington: Unpubl. M.S. thesis, Western Washington University, 107 p.

Black, P. M., 1971, Tourmalines from Cuvier Island, New Zealand: Miner. Mag., v. 38, p. 374-376.

Bradshaw, P. M. D. and Stoyel, A. J., 1968, Exploration for blind ore bodies in southwest England by the use of geochemistry and fluid inclusions: Inst. Min. Metall., Trans., Sect. B, v. 77, p. B144-B152.

Brown, C. E. and Ayuso, R. A., 1985, Significance of tourmaline-rich rocks in the Grenville Province of St. Lawrence County, New York: U.S. Geol. Surv., Bull. 1626-C, 33 pp.

Closs, L. G. and Nichol, I., 1975, The role of factor and regression analysis in the interpretation of geochemical reconnaissance data: Can. J. Earth Sci., v. 12(8), p. 1316-1330.

Coolbaugh, D. F., 1979, Geophysics and geochemistry in the discovery and development of the La Caridad porphyry deposit, Sonora, Mexico, *in* Hood, P. J. (editor), Geophysics and Geochemistry in the Search for Metallic Ores: Geol. Surv. Can., Econ. Geol. Rep., 31, p. 721-726.

Darling, R., 1971, Preliminary study of the distribution of minor and trace elements in biotite from quartz monzonite associated with contact-metasomatic tungsten-molybdenum-copper ore, California, U.S.A. *in* Boyle, R. W. and McGerrigle, J. I. (editors), Geochemical Exploration: Can. Inst. Min. Metall., Spec. Vol. 11, p. 315-322.

Deer, W. A., Howie, R. A. and Zussman, J., 1962, Rock-forming minerals: Vol. 1, Ortho- and Ring Silicates: New York, N.Y., Wiley & Sons, p. 300-319.

Dietrich, R. V., 1985, The tourmaline group: New York, N.Y., Van Nostrand Reinhold Co., 300 pp.

Donnay, G., Ingamells, C. O. and Mason, B., 1966, Buergerite, a new species of tourmaline: Amer. Min. v. 51, p. 198-199.

Dunn, P. J., Appleman, D. E. and Nelen, J. E., 1977a, Liddicoatite, a new calcium end-member of the tourmaline group: Amer. Min., v. 62, p. 1121-1124.

Dunn, P. J., Appleman, D. E., Nelen, J. E. and Norbery, J., 1977b, Uvite, a new (old) common member of the tourmaline group and its implications for collectors: Mineral. Rec., v. 8, p. 100-108.

Epprecht, W., 1953, Die Gitterkonstanton der Turmalin: Schweiz. Mineral. Petrogr. Mitt., v. 33, p. 481-505.

Ethier, V. G. and Campbell, F. A., 1977, Tourmaline concentrations in Proterozoic sediments of the southern Cordillera of Canada and their economic significance: Can. J. Earth Sci., v. 14, p. 2348-2363.

Fleischer, M., 1965, Composition of magnetite as related to type of occurrence: U.S. Geol. Surv. Prof. Pap. 525-D, p. 82-84.

Foit, F. F., Jr. and Rosenberg, P. E., 1977, Coupled substitutions in the tourmaline group: Contrib. Mineral Petrol., v. 62, p. 109-127.

Graybeal, F. T., 1973, Copper, manganese, and zinc in coexisting mafic minerals from Laramide intrusive rocks in Arizona: Econ. Geol., v. 68, p. 785-798.

Grimes, D. J. and Marranzino, A. P., 1968, Direct-current arc and alternating-current spark emission spectographic field method for the semiquantitative analysis of geologic materials: U.S. Geol. Surv., Cir. 591, 6 pp.

Hawley, J. E. and Nichol, I., 1961, Trace elements in pyrite, pyrrhotite and chalcopyrite of different ores: Econ. Geol., v. 56, p. 467-487.

Haxel, G. B., Tosdal, R. M., May, D. J. and Wright, J. E., 1984, Latest Cretaceous and early Tertiary orogenesis in south-central Arizona: Thrust faulting, regional metamorphism, and granitic plutonism: Geol. Soc. Amer., Bull., v. 95, p. 631-653.

Hollister, V. F., 1978, Geology of the porphyry copper deposits of the Western Hemisphere: Soc. Min. Eng. — Am. Inst. Min. Met. Petr. Eng., Inc., New York, 124 pp.

Imeokparia, E. G., 1982, Tin contents of biotites from the Afu Younger Granite Complex, Central Nigeria: Econ. Geol., 77, p. 1710-1724.

Jacobs, D. C. and Parry, W. T., 1976, A comparison of the geochemistry of biotite from some Basin and Range stocks: Econ. Geol., v. 71, p. 1029-1035.

Johnson, A. E., 1972, Origin of Cyprus pyrite deposits: Int. Geol. Congress, 24th, Montreal, Sec. 4, p. 291-298.

Kleinkopf, M. D., de la Fuente-Duch, M. F., Raines, G. L. and Peterson, D. L., 1977, Geophysical studies of mineral resources, Sonora, Mexico [abs.]: Geol. Soc. Am. Abs. with Pgms., v. 9(1), p. 30.

Krynine, P. D., 1946, The tourmaline group in sediments: Jour. Geol., v. 54, p. 65-87.

Loftus-Hills, G. and Solomon, M., 1967, Cobalt, nickel, and selenium in sulphides as indicators of ore genesis: Miner. Deposita, v. 2, p. 228-242.

Lovering, T. G., Cooper, J. R., Drewes, H. and Cone, G. C., 1970, Copper in biotites from igneous rocks in southern Arizona as an ore indicator: U.S. Geol. Surv., Prof. Pap. 700-B, p. 1-8.

Mantei, E. J. and Brownlow, A. H., 1967, Variation in gold content of minerals of the Marysville quartz diorite stock, Montana: Geochim. Cosmochim. Acta, v. 31, p. 225-235.

Mason, D. R., 1978, Compositional variations in ferromagnesian minerals from porphyry copper-generating and barren intrusions of the Western Highlands, Papua, New Guinea: Econ. Geol., v. 73, p. 878-890.

Motooka, J. M. and Grimes, D. J., 1976, Analytical precision of one-sixth order semiquantitative spectrographic analysis: U.S. Geol. Surv., Circ. 738, 25 pp.

Neiva, A. M. R., 1974, Geochemistry of tourmaline (schorlite) from granites, aplites, and pegmatites from northern Portugal: Geochim. Cosmochim. Acta, v. 38, p. 1307-1317.

Power, G. M., 1966, Strontium:calcium ratio in tourmalines from southwest England: Nature, v. 211, p. 1072-1073.

Power, G. M., 1968, Chemical variation in tourmalines from southwest England: Mineral Mag. & J. Mineral Soc. London, v. 36(284), p. 1078-1089.

Raines, G. L., 1978, A porphyry copper exploration model for northern Sonora, Mexico: U.S. Geol. Surv., J. Res., v. 6(1), p. 51-58.

Ryall, W. R., 1977, Anomalous trace elements in pyrite in the vicinity of mineralized zones at Woodlawn, N.S.W., Australia: J. Geochem. Explor., v. 8(1/2), p. 73-84.

Sahama, T. G., Knorring, O. V. and Tornroos, R., 1979, On tourmaline: Lithos, v. 12, p. 109-114.

Sawkins, F. J., 1979, Fluid inclusion studies of the Inguaran copper-bearing breccia pipes, Michaocan, Mexico: Econ. Geol., v. 74, p. 924-927.

Sillitoe, R. H., 1976, A reconnaissance of the Mexican porphyry copper belt: Inst. Min. Metall., Trans., Sect. B, v. 85, B170-B189.

Sillitoe, R. H. and Sawkins, F. J., 1971, Geologic, mineralogic, and fluid inclusion studies relating to the origin of copper-bearing tourmaline breccia pipes, Chile: Econ. Geol., v. 66, p. 1028-1041.

Sillitoe, R. H., Halls, C. and Grant, J. N., 1975, Porphyry tin deposits in Bolivia: Econ. Geol., v. 70, p. 913-927.

Slack, J. F., 1980, Tourmaline — A prospecting guide for massive base-metal sulfide deposits in the Penobscot Bay area, Maine: Maine Geol. Survey, Spec. Econ. Stud. Ser., 8, 25 p.

Slack, J. F., 1982, Tourmaline in Appalachian—Caledonian massive sulphide deposits and their exploration significance: Inst. Min. Metall. Trans., Sec. B, v. 91, p. B81-B89.

Slack, J. F. and Coad, P. R., 1986, Iron-rich tourmalines from Kidd Creek, Ontario [abs.]: Geol. Assoc. Canada - Mineral. Assoc., Canada, Pgms. with Abs., v. 11, p. 128.

Smith F. G., 1949, Transport and deposition of the non-sulphide vein minerals: IV. Tourmaline: Econ. Geol, v. 44, p. 186-192.

Smith, S. M., 1985, Trace element variation in hydrothermal tourmalines associated with mineralization: El Correo, Sonora, Mexico: Unpubl. M.S. thesis, Colorado School of Mines, T-2896, 171 pp.

Taylor, A. M. and Terrell, B. C., 1967, Synthetic tourmalines containing elements of the first transition series: J. Cryst. Growth, v. 1, p. 238-244.

Taylor, B. E. and Slack, J. F., 1984, Tourmalines from Appalachian-Caledonian massive sulfide deposits: Textural, chemical, and isotopic relationships: Econ. Geol., v. 79, p. 1703-1726.

Theobald, P. K., Jr., 1981, Association of Exploration Geochemists Presidential Address: One man's view of a research gap: J. Geochem. Explor., v. 15, p. 1-20.

Theobald, P. K., Jr., Overstreet, W. C. and Thomson, C. E., 1967, Minor elements in alluvial magnetite from the Inner Piedmont Belt, North and South Carolina: U.S. Geol. Surv., Prof. Pap. 554-A, 34 pp.

Theodore, T. G. and Priego de Wit, M., 1978, Porphyry-type metallization and alteration at La Florida de Nacozari, Sonora, Mexico: U.S. Geol. Surv. J. Res., 6(1), p. 59-72.

Tsusue, A., Nedachi, M. and Hashimoto, K., 1981, Geochemistry of apatites in the granitic rocks of the molybdenum, tungsten and barren provinces of southwest Japan, *in* Rose, A. W. and Gundlach, H. (editors), Geochemical Exploration 1980: J. Geochem. Explor., v. 15, p. 285-294.

Turner, R. L., and Eppinger, R. G., III, 1984, Analytical results and sample locality maps of stream sediment, panned-concentrate, soil and drill core samples from the Agua Caliente study area, El Correo quadrangle, northern Sonora, Mexico: U.S. Geol. Surv., Open-File Rept. 84-335, 101 pp.

Turner, R. L., Raines, G. L., Kleinkopf, M. D., and Lee-Moreno, J. L., 1982, Regional northeast-trending structural control of mineralization, northern Sonora, Mexico: Econ. Geol., v. 77, p. 25-37.

Turner, R. L., Theobald, P. K., Jr., Perez, G., and Ortiz, A., 1980, The role of the small-scale geochemical exploration venture: A test case in northern Sonora, Mexico, *in* Meyer, R. F. and Carmen, J. S. (editors), The Future of Small Scale Mining: Unitar, McGraw Hill, New York, N.Y., p. 63-70.

United Nations, 1969, Survey of the metallic mineral deposits in Mexico: U.N. Development Pgm. Rept. DP/SF/UN/19-Mexico, United Nations, New York, 72 pp.

Walenta, K., and Dunn, P. J., 1979, Ferridravite, a new mineral of the tourmaline group from Bolivia: Amer. Min., v. 64, p. 945-945.

Werding, G., and Schreyer, W., 1984, Alkali-free tourmaline in the system MgO-Al_2O_3-B_2O_3-SiO_2-H_2O: Geochim. Cosmochim. Acta, v. 48, p. 1331-1344.

Williams, S. A., and Cesbron, F. P., 1977, Rutile and apatite — Useful prospecting guides for porphyry copper deposits: Mineral. Mag., v. 41(318), p. 288-292.

Stream-Sediment Geochemistry of Two Mineral Provinces in the Healy Quadrangle, Alaska

T. D. LIGHT, R. B. TRIPP and H. D. KING
U.S. Geological Survey, Box 25046, MS 973, Federal Centre,
Denver, CO 80225-0046

Abstract — The concentration, distribution, and association of minerals and trace elements in reconnaissance drainage-basin samples define geochemically anomalous areas within the Healy quadrangle, Alaska. Consolidation of anomalous areas with similar geochemical signatures defines two mineralized provinces in the quadrangle. In the northeastern part of the quadrangle, anomalous concentrations of Ag, As, Au, Ba, Cu, Pb, and Zn reflect volcanogenic massive sulfide occurrences. In the southwestern portion of the quadrangle, high contents of Sn (>1000 ppm) in heavy-mineral-concentrate samples associated with or near anomalous concentrations of base and precious metals characterize a region of possible tin-bearing greisen mineralization in highly evolved siliceous granites.

INTRODUCTION

THE U.S. Geological Survey conducted a multidisciplinary reconnaissance study of the Healy quadrangle in southern Alaska to help evaluate the mineral resource potential of the area. The Healy quadrangle, 63° to 64° N and 147° to 150° W, comprises approximately 16,600 sq. km in the central Alaska Range, and lies 90 km south of Fairbanks, Alaska, and 180 km north of Anchorage, Alaska (Fig. 1). The objective of this study was to use an already existing data set to define the geochemical expressions indicating the most favorable areas for possible occurrences of volcanogenic massive sulfides in the Yukon-Tanana terrane, and of tin-bearing greisens in the McKinley sequence granites.

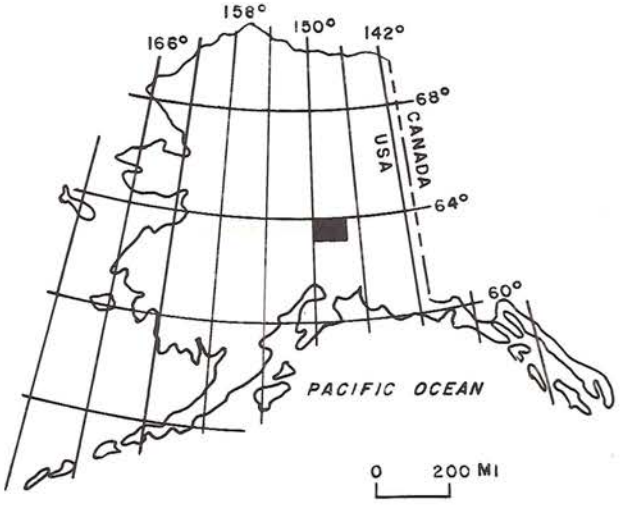

Fig. 1. Index map showing location of the Healy quadrangle, Alaska.

The Healy quadrangle is a geologically complex and diverse area along the accretionary margin of North America. The McKinley and Hines Creek strands of the Denali fault system (Beikman et al., 1977; Beikman, 1978) strike nearly east and traverse the quadrangle (Fig. 2). The Talkeetna thrust strikes northeasterly across the southeastern corner of the quadrangle. These and other major faults in the area have been used to subdivide the Healy quadrangle into as many as 13 separate tectonostratigraphic terranes (Coney et al. 1980; Jones et al. 1981, 1983; Silberling and Jones, 1984). On the basis of correlative geologic units and metamorphic isograds on both sides of the McKinley fault, Csejtey et al. (1982) suggest that the McKinley fault is not a tectonostratigraphic terrane boundary in this area. They also define the Hines Creek fault as a dip-slip fault that developed within the Yukon-Tanana terrane. Using these interpretations as well as other stratigraphic, structural, and lithologic evidence, Csejtey et al. distinguish as few as five tectonostratigraphic terranes in addition to the Jurassic-Cretaceous flysch unit (Bela Csejtey, USGS, written commun., 1985).

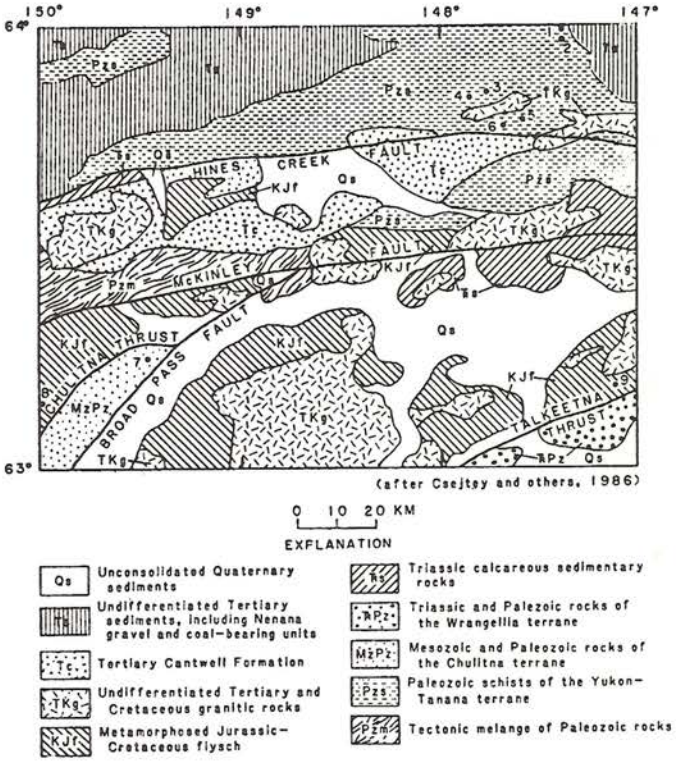

Fig. 2. Generalized geologic map of the Healy quadrangle, Alaska. [Mineral deposits: 1 - Snow Mtn. Gulch; 2 - Red Mtn.; 3 - Virginia Crk.; 4 - Anderson Mtn.; 5 - West Fork; 6 - Cirque; 7 - Golden Zone; 8 - Ohio Crk.; 9 - Valdez Crk.]

The Wrangellia terrane, south of the Talkeetna thrust, was accreted onto the continental margin of North America probably during middle Cretaceous time (Csejtey et al. 1980). The collision of Wrangellia with the Yukon-Tanana terrane to the north caused intense deformation and greenschist to amphibolite facies metamorphism of the flysch and turbidite sediments that were deposited in an oceanic arc basin between the converging terranes (Csejtey et al., 1982).

The Yukon-Tanana terrane, which comprises all the rocks north of the Hines Creek fault and the rocks in the eastern one-half of the quadrangle between the Hines Creek and McKinley faults, consists predominantly of quartz-sericite, carbonaceous and pelitic schists or phyllites, and metavolcanic rocks of Precambrian(?) and Paleozoic age; calcareous sedimentary rocks of Triassic age; and clastic sedimentary and coal-bearing units of Tertiary age (Wahrhaftig, 1968, 1970a-d; Csejtey et al., 1986). The oldest rocks in this part of the quadrangle are pelitic quartz sericite and muscovite schists of presumed Late Precambrian(?) or Paleozoic age that have been previously correlated with the Birch Creek Schist, a term that has been abandoned, and the overlying Keevy Peak Formation (Wahrhaftig, 1970 a-d). Stratigraphically above the Keevy Peak Formation is a series of Paleozoic phyllites, schists, and metavolcanic rocks. A thick sequence of highly deformed Triassic marine calcareous sedimentary rocks occurs in scattered outcrops south of the Hines Creek fault. This unit is most predominant in the east-central portion of the quadrangle. Tertiary age rocks in the Yukon-Tanana terrane are the Cantwell Formation, several undifferentiated coal-bearing units, and the Nenana Gravel. With the exception of small isolated outcrops, these units occur extensively to the north of the McKinley fault.

Rocks in the southern part of the Healy quadrangle are dominantly Jurassic-Cretaceous flysch, Cretaceous granites, and Tertiary granitic and volcanic rocks (Csejtey et al., 1986). Outcrops of Triassic calcareous sedimentary rocks occur in several localities. Rocks in the Wrangellia terrane are the Triassic Nikolai Greenstone and older Pennsylvanian to Triassic sequences of metavolcanic and metasedimentary rocks (Csejtey et al., 1986). The Chulitna terrane, between the Broad Pass and Chulitna faults, comprises several distinct lithologic units, from mid-Paleozoic to Mesozoic age; this terrane consists of sedimentary, volcanic, and plutonic rocks that have been tectonically juxtaposed (Jones et al., 1980), and subsequently intruded by Upper Cretaceous and Tertiary granitic to granodioritic rocks.

MINERAL OCCURRENCES

Mineral deposits in the Upper Chilitna district, northwest of the Broad Pass fault, have been described by Ross (1933a), Hawley and Clark (1968, 1973, 1974), and Hawley et al., (1969) as epigenetic vein-disseminated, vein, breccia-pipe, and contact-metamorphic deposits containing gold, silver, copper, and lead (see Table 1 and Fig. 3 for locations). The Golden zone mine, the largest producer in the quadrangle, was developed in a breccia zone above a quartz diorite porphyry, and produced 1,600 oz Au, 9,000 oz Ag, 21 tons of Cu, and 1.5 tons of Zn (Hawley and Clark, 1974). A tin-bearing greisen in a small granitic stock in Ohio Creek was described by Hawley and Clark (1974). Tin occurrences associated with the McKinley sequence of highly evolved 55-60 Ma granites (Reed and Lanphere, 1973; Lanphere and Reed, 1985) were described by Reed et al., (1978) in the Talkeetna quadrangle, adjacent to the southwest corner of the Healy quadrangle.

The Valdez Creek mining district (Ross, 1933b; Tuck, 1938; Kaufman, 1964; Smith, 1981) comprises placer gold and lode copper and gold deposits in the southeastern corner of the Healy quadrangle. The Denali basalt-copper deposit, which also occurs in this area, contains chalcopyrite, pyrite, and sphalerite, and has been described by Stevens (1972) and Seraphim (1975).

The Yukon-Tanana terrane in the eastern half of the Healy quadrangle contains several occurrences of volcanogenic massive sulfides not previously described. One of these, the Red Mountain deposit (also called the Dry Creek deposit), is a rhyolite-hosted volcanogenic massive sulfide deposit in the Mississippian(?) Mystic Creek Member of the Totatlanika schist in the northeastern corner of the quadrangle.

SAMPLING AND ANALYTICAL PROCEDURES

Stream-sediment samples were collected during the summers of 1980, 1981, and 1982 at 1,064 sites; heavy-mineral-concentrate samples were collected at 1,045 of these sites. The stream-sediment samples consist of active alluvium collected primarily from first-order and second-order streams, dried, and sieved to minus 80 mesh. The heavy-mineral-concentrate samples also consist of active alluvium, screened (2 mm) to eliminate the coarse fraction and panned to eliminate the rock-forming minerals. The heavy minerals were separated using bromoform (specific gravity 2.8), and the magnetic and paramagnetic minerals were removed using an electromagnet. The stream-sediment samples and the nonmagnetic fraction of the heavy-mineral concentrates were analyzed for 31 elements using a semiquantitative, direct-current arc emission spectrography (Grimes and Marranzino, 1968). Most stream-sediment samples were also analyzed by atomic absorption for Au and Zn (O'Leary and Meier, 1984). Analytical data for the stream-sediment and heavy-mineral-concentrate samples were reported by O'Leary et al. (1984). A preliminary interpretation of factor analysis of these data was reported by Light (1985).

GEOCHEMICALLY ANOMALOUS AREAS

In the Healy quadrangle, concentrations and associations of elements and ore-related minerals were used to define 17 separate geochemically anomalous areas. Fig. 3 shows the distribution of geochemically anomalous areas in the Healy quadrangle, and a summary of geochemical data is given in Table 1. Geochemically anomalous areas were defined by the associations of base and precious metals and related elements with concentrations at or above the 95th percentile levels listed in Table 2. Areas containing similar or related geologic and geochemical parameters are grouped to define two major mineralized provinces within the Healy quadrangle.

Table 1. Summary of data for geochemically anomalous areas in the Healy quadrangle

[Elements and minerals in parentheses indicate scattered or isolated anomalies]

No. on Fig. 3	Area	Anomalous elements in stream sediments	Anomalous elements in panned concentrates	Mineralogy of heavy-mineral concentrates[1]	Geologic setting	
					Bedrock[2]	Terrane
1	Big Grizzly Creek area	Ag, Ba, (Cu), Fe, Mo, (Zn)	(As), (Cd), (Mo)	ars, cpy, gal, sch, (sph)	Tc, TKg, Ts, Pzs	Yukon-Tanana terrane
2	Edmonds Creek area	(Cu), Sn, Zn	(Ag), (As), Bi, Sn	ars, cass, cpy, gal, (gold), sch	TKg, KJf, Ts	Jurassic-Cretaceous flysch basin
3	Honolulu area	Ag, (Au), (B), (Cd), Co, Pb, Sn, Zn	Ag, (As), (Au), Bi, Cu, (Mo), Pb, Sb, Sn, W	ars, cass, cpy, flu, (gal), gold, pow, sch, sph	TKr KJf	Jurassic-Cretaceous flysch basin
4	Nenana Mountain area	(Ag), (Cd), (Cu), Mo, (Zn)	As, (Au), (Bi), (Cu), (Pb), (Sb), (Sn), (W), (Zn)	ars, (cass), cpy, gal, (gold), sch, sph	KJf, TKg Ts, Pzs	Jurassic-Cretaceous flysch basin
5	Polychrome Glacier area	--	Cd, (Fe), (Pb), (Sb), Zn	ars, (cass), cinn, cpy, flu, gal, sph	Tc TKg	Jurassic-Cretaceous flysch basin
6	Reindeer Hills--Pyramid Peak area	(Ag), (As), (Au), Sn, (W)	(Ag), (As), Au, Bi, Cd, Sb, Sn, W, Zn	ars, cass, flu, (gal), gold, sch	TKg Pzm Ts	Tectonic-melange Yukon-Tanana terrane(?)
7	Tertiary Nenana Gravel and coal-bearing units	Au	Au, (Mo)	cass, gold, sch	Ts	Yukon-Tanana terrane
8	Upper Chulitna district	Ag, As, Au, (B), (Be), (Cd), (Cr), Cu, (Fe), Ni, (Pb), Sn, W	Ag, As, Au, Bi, Co, (Cr), Cu, Fe, Ni, Pb, Sb, Sn, W, (Zn)	ars, cass, (cinn), cpy, gal, gold, sch, sph, (stib)	TKg, KJf, MzPz	Chulitna terrane
9	Upper Jack River area	Ag, Au, (Cd), (Pb), (Sn)	Ag, (As), (Au), (Bi), Cd, (Cu), Mo, (Sb), (Sn), (W), Zn	ars, cass, (cinn), cpy, flu, (gal), gold, sch, sph	TKg KJf	Jurassic-Cretaceous flysch basin
10	Upper Revine Creek	Ag, As, B, Ba, Co, Cu, Mo, W, Zn	Cu, Mo, (Sb), (Sn), W, (Zn)	ars, cass, cinn, cpy, (gal), pow, sch, sph	Tc, KJf, Pzs TKg	Jurassic-Cretaceous flysch basin
11	Valdez area	(Ag), Au, Cu	(Ag), (Au), (Bi), (Mo), (W)	ars, cpy, (gal), gold, sch	TKg KJf	Jurassic-Cretaceous flysch basin
12	West McKinley fault	As, (Au), (B), (Cr), (Pb), (Sn), (Zn)	Ag, (As), (Au), Cd, Co, Cr, Cu, Fe, Pb, Ni, Sb, (Sn), Zn	ars, (cass), (cinn), cpy, gal, (gold), (sch), sph, (stib)	Tc, TKg, Pmz, KJf	Jurassic-Cretaceous flysch basin and tectonic melange
13	West Fork Glacier area	Ag, (As), Au, Ba, (Cu), (Co), (Cr), Mo	(Ag), (Au)	ars, cpy, (gal), (gold), sch	TKg Ts	Yukon-Tanana terrane
14	Wrangellia terrane	(As), Au, Co, Cr, Cu, Fe, Ni	(Au), (Cu)	(ars), (cinn), cpy, sch	TrPz	Wrangellia terrane of Talkeetna superterrane
15	Wyoming Hills	(Ag), Ba, Pb, Zn	--	sch	Ts, TKg	Yukon-Tanana terrane
16	Yanert Glacier area	Ag, (Ba), (Cu), Mo, W, (Zn)	(As), Cu, (Mo)	ars, cpy, (gal), sch, sph,	TKg, KJf, Ts, Pzs	Yukon-Tanana terrane
17	Yukon-Tanana area	Ag, Au, B, Ba, Co, (Mo), Pb, (W), Zn	Ag, As, (Au), (Bi), Co, (Cu), Fe, Mo, Ni, Pb, (Sb), W	ars, cpy, gal, gold, pow, sch, sph	TKg, Pzs	Yukon-Tanana terrane

[1]Mineral abbreviations: ars, arsenopyrite (FeAsS); cass, cassiterite (SnO_2); cinn, cinnabar (HgS); cpy, chalcopyrite ($CuFeS_2$); flu, fluorite (CaF_2); gal, galena (PbS); pow, powellite ($Ca(Mo,W)O_4$); sch, scheelite ($CaWO_4$); sph, sphalerite (ZnS); stib, stibnite (Sb_2S_3)

[2]See figure 2 for explanation of rock units

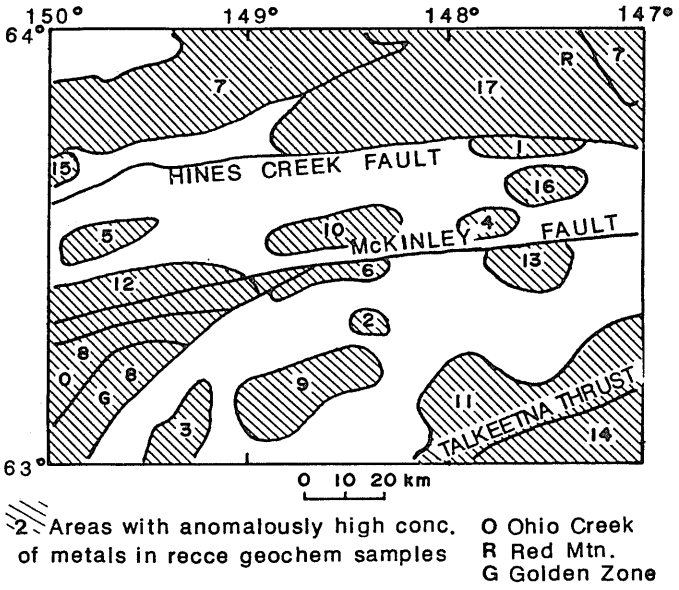

Fig. 3. Geochemically anomalous areas in the Healy quadrangle. [See Table 1 for description of numbered areas.]

Table 2. Element concentrations used to define geochemically anomalous areas

[All data by semiquantative emission spectrographic analysis except where indicated, — = none detected; NA = not analyzed; AA = atomic absorption analyses. Fe given in percent, all other values in parts per million]

Element	Stream sediments	Heavy-mineral-concentrate
Fe(%)	7.0	30
Ag (ppm)	1.5	50
As	200[1]	5000
Au	10[1]	20[1]
B	150	700
Ba	2000	>5000[2]
Be	3	2[1]
Bi	10[1]	70
Cd	20[1]	50[1]
Co	50	200
Cr	500	1500
Cu	150	1000
Mo	10	15
Ni	150	500
Pb	70	2000
Sb	—	200[1]
Sn	10[1]	>1000[2]
W	50[1]	300
Zn	300	1500
Au-AA	0.3	NA
Zn-AA	300	NA

[1] Lower determination limit
[2] Upper determination limit

Petrographic determination of the occurrence and distribution of ore-related minerals in the nonmagnetic fraction of the heavy-mineral concentrates helps define anomalous areas. Because of the intensity of mineralization in the Healy quadrangle, barite, chalcopyrite, and scheelite are ubiquitous, and unreliable as locators of specific deposits. Gold is present in nearly 10 percent of the heavy-mineral-concentrate samples scattered throughout the Healy quadrangle. Galena and sphalerite are abundant in the southwestern and northeastern portions of the quadrangle. Cassiterite and fluorite are restricted to the southwestern portion of the quadrangle.

Volcanogenic massive sulfide belt

Paleozoic schists in the Yukon-Tanana terrane, north of the Hines Creek fault, are metamorphosed marine, volcaniclastic and clastic schists, argillites, and phyllites including the Mississippian(?) Totatlanika Schist, a pelitic quartz-sericite schist (previously correlated with the Birch Creek Schist), and an unnamed metabasalt and metasedimentary unit. At least six volcanogenic massive sulfide occurrences have been reported in these units north of the Hines Creek fault and in the eastern one-third of the quadrangle (Church et al., 1986). The occurrence of anomalously high concentrations of base and precious metals in sediment and concentrate samples, and the distribution of galena, sphalerite, and arsenopyrite in heavy-mineral-concentrate samples from the northern Healy quadrangle indicate that the Yukon-Tanana terrane in the eastern half of the Healy quadrangle is favorable for additional volcanogenic massive sulfide mineralization.

The areas most favorable for massive sulfide occurrences in the Yukon-Tanana terrane were defined by those drainage basins with samples containing: (1) >1,400 ppm Pb (90th percentile) in heavy-mineral-concentrate samples or; (2) drainage basins adja-

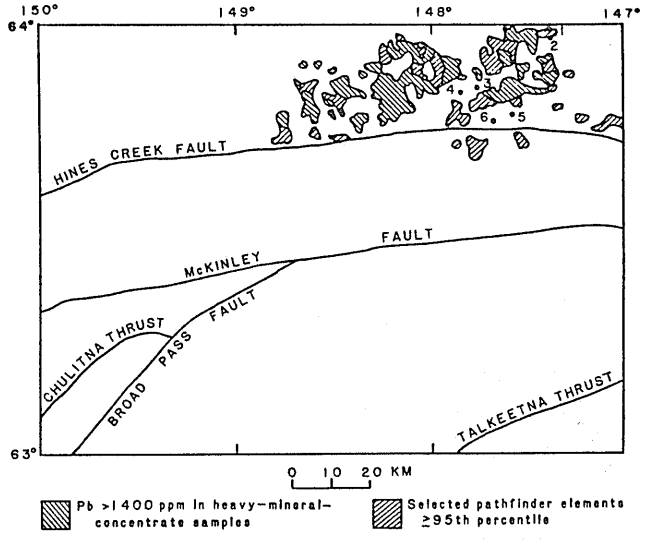

Fig. 4. Drainage basins in the Yukon Tanana terrane containing anomalous concentrations of metals associated with possible massive sulfide mineralization. [Volcanogenetic massive sulfide deposits: 1 - Snow Mtn. Gulch; 2 - Red Mtn.; 3 - Virginia Crk.; 4 - Anderson Mtn.; 5 - West Fork; 6 - Cirque.]

cent to or nearby areas identified in #1, and containing at least several elements at the 95th percentile level or higher from the element suite Ag, As, Au, Ba, Cu, and Zn. Fig. 4 illustrates the distribution of drainage basins meeting these criteria, and defines what are considered to be the most favorable areas for volcanogenic massive sulfide mineralization. These areas form a belt in the eastern one-half of the quadrangle and concentrated north of the Hines Creek fault.

Tin-greisen belt

Highly evolved siliceous granites of the 55-60 Ma McKinley sequence (Reed and Lanphere, 1973) have been described in the Talkeetna quadrangle, adjacent to the southwest corner of the Healy quadrangle (Reed et al., 1978). Tin-bearing greisens associated with McKinley sequence granites occur in the Ohio Creek area, in the southwest corner of the Healy quadrangle (Hawley and Clark, 1974), and near Coal Creek, about 25 km southeast of the Ohio Creek occurrence.

Although epigenetic veins and breccia pipes also occur in the southwest portion of the quadrangle, and signatures may be overprinted, these deposit types contain much less Sn than the greisens. Because cassiterite resists erosion and transportation, high concentrations of Sn in heavy-mineral-concentrate samples may be an indicator of greisen mineralization. Fig. 5 shows those drainage basins with >1,000 ppm Sn in concentrate samples, and nearby drainages containing at least four or more elements of the suite Ag, As, Au, Be, Bi, Cu, Mo, Pb, Sb, W, and Zn at or above the 95 percentile level. The drainages with high Sn concentrations are usually accompanied by several elements in the suite Ag, Bi, Cu, Sb, and W. The drainage basins illustrated in Fig. 5 represent the most favorable areas for tin-bearing greisens or veins.

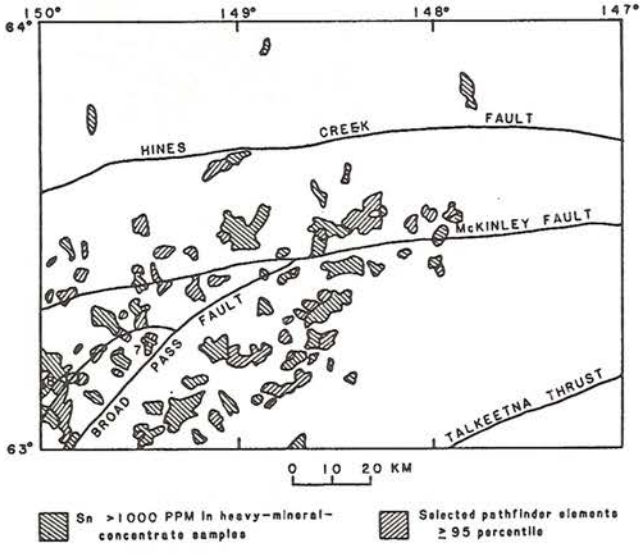

Fig. 5. Drainage basins containing anomalous concentrations of metals associated with possible tin-greisen mineralization. [Mineral deposits: 7 - Golden Zone; 8 - Ohio Crk.]

CONCLUSIONS

Several mineral occurrence types are present in the Healy quadrangle. Where epigenetic veins, breccia pipes, greisens, or volcanogenic massive sulfides occur in close proximity, overlapping or overprinting mineralogical and trace-element signatures are expected. The most prominent and widespread deposit types, as indicated by the mineralogical and semiquantitative spectrographic data, are volcanogenic massive sulfides and tin-bearing greisens. The concentration, distribution, and association of base and precious metals and ore-related minerals in reconnaissance drainage-basin samples define a broad northeasterly trending area favored for tin-bearing greisen mineralization in the southwestern portion of the quadrangle, and an east-trending belt of possible volcanogenic massive sulfide mineralization in the northeastern portion of the quadrangle.

REFERENCES

Beikman, H. M., 1978, Preliminary geologic map of Alaska: U.S. Geol. Surv., 2 sheets, scale 1:2,500,000.

Beikman, H. M., Holloway, C. D. and MacKevett, E. M., Jr., 1977, Generalized geologic map of the eastern part of southern Alaska: U.S. Geol. Surv., O.F. Rep. 77-169B, scale 1:1,000,000.

Church, S. E., Gray, J. E. and Delevaux, M. H., 1986, Use of Pb-isotopic signatures for geochemical exploration in the Healy quadrangle, eastern Alaska Range, *in* Bartsch-Winkler, S. and Reed, K. M. (editors), Geologic studies in Alaska by the U.S. Geological Survey during 1985: U.S. Geol. Surv., Circ. 985, p. 38-41.

Coney, P. J., Jones, D. L. and Monger, J. W. H., 1980, Cordilleran suspect terranes: Nature, v. 288, p. 329-333.

Csejtey, B., Jr., Cox, D. P., Evarts, R. C., Stricker, G. D. and Foster, H. L., 1982, The Cenozoic Denali fault system and the Cretaceous accretionary development of southern Alaska: J. Geophys. Res., v. 87, p. 3741-3754.

Csejtey, B., Jr., Foster, H. L. and Nockleberg, W. J., 1980, Cretaceous accretion of the Talkeetna superterrane and subsequent development of the Denali fault in south-central and eastern Alaska: Geol. Soc. Am., Abst., v. 12, p. 409.

Csejtey, B., Jr., Mullen, M. W., Cox, D. P., Gilbert, W. G., Yeend, W. E., Smith, T. E., Turner, D. L., Wahrhaftig, C., Craddock, C., Brewer, W. M., Sherwood, K. W., Hickman, R. G., Stricker, G. D., St. Aubin, D. R. and Goerz, D. J., III, 1986, Geology and Geochronology of the Healy quadrangle, Alaska: U.S. Geol. Surv., O.F. Rep. 86-396, 92 pp.

Grimes, D. J. and Marranzino, A. P., 1968, Direct-current arc and alternating-current spark emission spectrographic field methods for the semiquantitative analysis of geologic materials: U.S. Geol. Surv., Circ. 591, 6 pp.

Hawley, C. C. and Clark, A. L., 1968, Occurrences of gold and other metals in the Upper Chulitna district, Alaska: U.S. Geol. Surv., Circ. 564, 21 p.

Hawley, C. C. and Clark, A. L., 1973, Geology and mineral deposits of the Chulitna-Yentna mineral belt, Alaska: U.S. Geol. Surv., Prof. Pap. 758-A, 10 pp.

Hawley, C. C. and Clark, A. L., 1974, Geology and mineral deposits of the Upper Chulitna district, Alaska: U.S. Geol. Surv., Prof. Pap. 758-B, 47 pp.

Hawley, C. C., Clark, A. L., Hendrick, M. A. and Clark, S. H. B., 1969, Results of geological and geochemical investigations in an area northwest of the Chulitna River, Central Alaska Range: U.S. Geol. Surv., Circ. 617, 19 pp.

Jones, D. L., Silberling, N. J., Berg, H. C. and Plafker, G., 1981, Map showing tectonostratigraphic terranes of Alaska, columnar

sections, and summary descriptions of terranes: U.S. Geol. Surv., O.F. Rep. 81-792, 20 pp.

Jones, D. L., Silberling, N. J. and Coney, P. J., 1983, Tectonostratigraphic map of the Mount McKinley region: U.S. Geol. Surv., O.F. Rep. 83-11, scale 1:250,000.

Jones, D. L., Silberling, N. J., Gilbert, W. G. and Coney, P. J., 1980, Age, character, and distribution of accreted terranes in the central Alaska Range, south-central Alaska (abstract): EOS (Am. Geophys. Union Trans.), v. 61, p. 1114.

Kaufman, M. A., 1964, Geology and mineral deposits of the Denali-Maclaren River area, Alaska: Alaska Div. Mines Min., Geol. Rep. 4, 15 pp.

Lanphere, M. A. and Reed, B. L., 1985, The McKinley sequence of granitic rocks: A key element in the accretionary history of southern Alaska: Jour. Geophys. Res., v. 90, p. 11,413-11,430.

Light, T. D., 1985, Preliminary interpretation of factor analysis of geochemical data from the Healy quadrangle, Alaska, *in* Bartsch-Winkler, S. (editor), The U.S. Geological Survey in Alaska — Accomplishments during 1984: U.S. Geol. Surv., Circ. 967, p. 64-66.

Light, T. D., Tripp, R. B. and King, H. D., in press, Interpretation of reconnaissance geochemical data from the Healy quadrangle, Alaska: U.S. Geol. Surv., Bull.

O'Leary, R. M., Hoffman, J. D., Sutley, S. J. and King, H. D., 1984, Analytical results and sample locality map of stream-sediment and heavy-mineral concentrate samples from the Healy quadrangle, Alaska: U.S. Geol. Surv., O.F. Rep. 84-104, 151 pp.

O'Leary, R. M. and Meier, A. L., 1984, Analytical methods used in geochemical exploration: U.S. Geol. Surv., Circ. 948, 120 pp.

Reed, B. L. and Lanphere, M. A., 1973, Alaska-Aleutian Range batholith: Geochronology, chemistry, and relation to circum-Pacific plutonism: Geol. Soc. Am. Bull., v. 84, p. 2583-2610.

Reed, B. L., Nelson, S. W., Curtin, G. C. and Singer, D. A., 1978, Mineral resources map of the Talkeetna quadrangle, Alaska: U.S. Geol. Surv., Misc. Field Studies Map MF-870-D.

Ross, C. P., 1933a, Mineral deposits near the west fork of the Chulitna River, Alaska: U.S. Geol. Surv., Bull. 849-E, p. 289-332.

Ross, C. P., 1933b, The Valdez Creek mining district, Alaska: U.S. Geol. Surv., Bull. 849-H, p. 425-468.

Seraphim, R. H., 1975, Denali — A nonmetamorphosed stratiform sulfide deposit: Econ. Geol., v. 70, p. 949-959.

Silberling, N. L. and Jones, D. L., 1984, Lithotectonic terrane maps of the North American Cordillera: U.S. Geol. Surv., O.F. Rep 84-523, 100 pp., 4 sheets, scale 1:2,500,000.

Smith, T. E., 1981, Geology of the Clearwater Mountains, south-central Alaska: Alaska Div. Geol. Geophys. Surv., Geol. Rep. 60, 72 pp.

Stevens, D. L., 1972, Geology and geochemistry of the Denali prospect, Alaska: Am. Inst. Min. Met. Pet. Eng., Ann. Mtg., San Francisco, Reprint 72-I-29, 31 pp.

Tuck, R., 1938, The Valdez Creek mining district, Alaska, in 1936: U.S. Geol. Surv., Bull. 897-B, p. 109-131.

Wahrhaftig, C., 1968, Schists of the central Alaska Range: U.S. Geol. Surv., Bull. 1254-E, 22 pp.

Wahrhaftig, C., 1970a, Geologic map of the Healy D-2 quadrangle: U.S. Geol. Surv., Geol. Quadrangle Map GQ-804, scale 1:63,360.

Wahrhaftig, C., 1970b, Geologic map of the Healy D-3 quadrangle: U.S. Geol. Surv., Geol. Quadrangle Map GQ-805, scale 1:63,360.

Wahrhaftig, C., 1970c, Geologic map of the Healy D-4 quadrangle: U.S. Geol. Surv., Geol. Quadrangle Map GQ-806, scale 1:63,360.

Wahrhaftig, C., 1970d, Geologic map of the Healy D-5 quadrangle: U.S. Geol. Surv., Geol. Quadrangle Map GQ-807, scale 1:63,360.

Pb-Isotope Signatures of Devonian-Mississippian Massive Sulphide Deposits in Alaska and their Significance to Mineral Exploration

S. E. CHURCH, J. E. GRAY
U.S. Geological Survey, Branch of Geochemistry, MS 973, P.O. Box 25046
Denver, CO 80225

M. H. DELEVAUX
U.S. Geological Survey, Branch of Isotope Geology, MS 963, P.O. Box 25046
Denver, CO 80225

and

A. P. LEHURAY
Lamont-Doherty Geological Observatory, Palisades, NY 10964

Abstract — Pb-isotope studies of stratiform massive sulfides and of skarn and magmatothermal vein deposits spatially associated with plutons of Late Devonian age in the western Brooks Range establish a reference point on the sediment-Pb growth curve at 350 ± 25 Ma. These data are used to define a Pb-isotope growth curve for the Brooks Range establishing a local frame of reference for Pb-isotope model ages in that province. Likewise, Pb-isotope studies of volcanogenic massive sulfides of Late Devonian to Early Mississippian age from the Mt. Hayes and Healy quadrangles in the eastern Alaska Range have defined a very different sediment-Pb growth curve reflecting the sedimentary province in which they formed. The deposits have Pb-isotope compositions that are very similar to those of the same age from the Selwyn Basin of the Canadian Cordillera. They record an enrichment of $^{238}U/^{204}Pb$ at about 2.0 Ga suggesting tectonic dismemberment of a once continuous sedimentary basin that received sediments from the Canadian Shield. These distinctive Pb-isotope compositions differ markedly from the Pb-isotope signature found in magmatothermal veins associated with Cretaceous igneous activity in the Bonnifield district and have been used to "fingerprint" geochemical anomalies where the pattern of mineralization is complex.

INTRODUCTION

PB-ISOTOPE MEASUREMENTS made on several types of ore deposits examined during the Alaskan Mineral Resource Appraisal Program (AMRAP) demonstrate that there are major, significant variations among deposits throughout Alaska. Deposits of the same type and age that occur within a given stratigraphic section, particularly the sediment-hosted base-metal (SHBM) and volcanogenic massive sulfide (VMS) deposits, generally have very similar Pb-isotope compositions within a given district. We have defined three basic objectives for our studies: 1) to relate geochemical and Pb-isotope data for specific deposit types to ore-forming processes, 2) to use the Pb-isotope compositions associated with geochemical anomalies to identify the type and probable age of concealed deposits in areas where the geology and mineralization is very complex or the rocks are poorly exposed, and 3) to evaluate the potential use of Pb-isotope signatures of deposits to correlate tectonostratigraphic terranes. In this paper, we explore these objectives using the Pb-isotope signatures of Devonian-Mississippian deposits in the Brooks Range and the eastern Alaska Range.

The isotopic composition of Pb changes systematically through time because of the radiogenic growth of ^{206}Pb, ^{207}Pb and ^{208}Pb from ^{238}U, ^{235}U and ^{232}Th, respectively. When an ore deposit is formed, galena and other Pb-rich minerals represent a chemical separation process that "freezes" the Pb-isotope composition by isolating Pb from its parent isotopes. In theory, measurement of the Pb-isotope composition should provide a measurement of the time of formation of the mineral and, therefore, the deposit. In reality, the history of the Pb that was incorporated into the deposit was probably complex, and the model ages derived are very dependent on the assumed behavior of U and Pb in the pre-galena history of the Pb.

Early isotopic studies of Pb in stratiform ores were used to define the Holmes-Houtermans closed-system Pb-isotope growth curve. They utilized the Holmes-Houtermans whole-earth growth curve to date ore deposits. However, subsequent work often revealed systematic discrepancies between the model ages, derived from the Holmes-Houtermans model, and the geologic age of the deposit. Attempts to refine growth curves for Pb-isotope evolution have been made by a number of workers, but the two most commonly applied to ore deposits are those of Stacey and Kramers (1975) and of Cummings and Richards (1975). Stacey and Kramers utilized a two-stage, closed-system model, in which enrichment of the $^{238}U/^{204}Pb$ occurred in the continental crust at 3.7 Ga, to minimize the age discrepancies for many of the stratiform ores. Cummings and Richards proposed an open-system model where U was preferentially enriched relative to Pb in the crust with time.

Other workers have modeled the evolution of Pb in rocks and ores using complex geologic processes. Armstrong (1968, 1981; Armstrong and Hein, 1973) proposed a dynamic-earth model where sediment-Pb was recycled into the mantle through subduction. Doe and Zartman (1979) and Zartman and Doe (1981) developed a model that partitions Pb, based on the incongruent behavior of U, Th, and Pb, into three reservoirs within the earth: the mantle, the upper continental crust, and the lower continental crust. Doe and Zartman (1979) examined the isotopic variation of Pb in Phanerozoic ore deposits in terms of mixing of Pb between these crustal reservoirs and

argued that most modern Pb could be approximated by the "orogene" curve, that is by processes of mixing Pb from the upper crust with Pb from the other two reservoirs during orogenic cycles.

There are, however, still difficulties in obtaining Pb-isotope model ages that are consistent with the geologic ages for some ore deposits using any of the above Pb-isotope evolution models. This discrepancy may arise because the sediments in ocean basins do not represent a completely homogeneous and well-mixed average of the upper crust. Perhaps the best documented example of the discrepancy between model ages and the geologic age of the deposits can be seen in the Pb-isotope data from ore deposits, mostly of Paleozoic age, in the Canadian Cordillera (Godwin and Sinclair, 1982; Godwin et al., 1982). By systematically examining the Pb-isotope signature of a group of stratiform deposits of similar type and age, they were able to define the Pb-isotope growth curve for sediments derived from the western part of the Canadian Shield (Godwin and Sinclair, 1982). In effect, they refined the orogene model to show that, during the formation of stratiform ore deposits, hydrothermal convection leached Pb from a *specific* or *restricted* upper crustal reservoir. These lower Paleozoic sediments had been derived directly from the old basement rocks of the western part of the Canadian Shield and were deposited in the Selwyn Basin. Furthermore, the sediments containing some of these deposits have not been tectonically displaced from their site of deposition on the western margin of the Canadian Shield.

The heterogeneity of Pb-isotopes in the earth's crust is also evident in studies of rock-Pb from Holocene calc-alkaline volcanic arcs (Fig. 1). These Pb-isotope studies have shown that Pb at the radiogenic end of the mixing arrays is best approximated by sediment Pb. Mixing lines, defined by the average Pb-isotope compositions from the most and least radiogenic extremes of the arrays from volcanic-arc settings, demonstrate that sediments being shed into different parts of oceanic basins preserve a record of the heterogeneous nature of the crust. Mixing arrays are characterized by the steep slopes of the arrays indicating mixing between crustal Pb and mantle Pb represented by the MORB array. When mixing of Pb from the mantle and upper continental crust reservoirs occurs during igneous processes, this record of crustal heterogeneity may be preserved. Whereas the orogene curve or the Stacey-Kramers two-stage model may be a good approximation of the growth of Pb found in calc-alkaline rocks from New Zealand (Z), the Cascades (C), or the Aleutian (A) volcanic-arcs, both growth curves fail to model the behavior of Pb in the upper crustal reservoir for the island-arc rocks from Japan (J) or the Lesser Antilles (O). Pb-isotope growth for the upper end-member of both groups of calc-alkaline rocks should be modeled so that they plot on the Pb-isotope growth curve for oceanic sediments at 0.0 Ga. A *locally defined* sediment-Pb growth curve is needed to approximate Pb-isotope evolution of the Asian and Brazilian cratons because the source areas for sediments derived from the cratons are dominated by old granitic rocks rather than by multi-cycle sediments from active orogenic belts.

Studies of Pb-isotopes from young sulfide deposits demonstrate that the ore-forming processes reflect the same mixing events defined by the study of Pb-isotopes from volcanic-arc rocks. The Pb-isotope signature of volcanogenic massive sulfides from Juan de Fuca, that form on mid-ocean ridges where there is no sediment to be leached, plot near the mantle regression line and reflect Pb from the mantle reservoir (Fig. 1). In contrast, Pb-isotope data from manganiferous, metal-rich sediments from the Guaymas Basin plot above the mantle regression line and reflect leaching of Pb from the sediments in the basin (Chen et al., 1986). Pb from Kuroko-type VMS deposits (K-VMS) reflects the composition of Pb in the volcanic rocks and sediments leached by the hydrothermal cell that formed

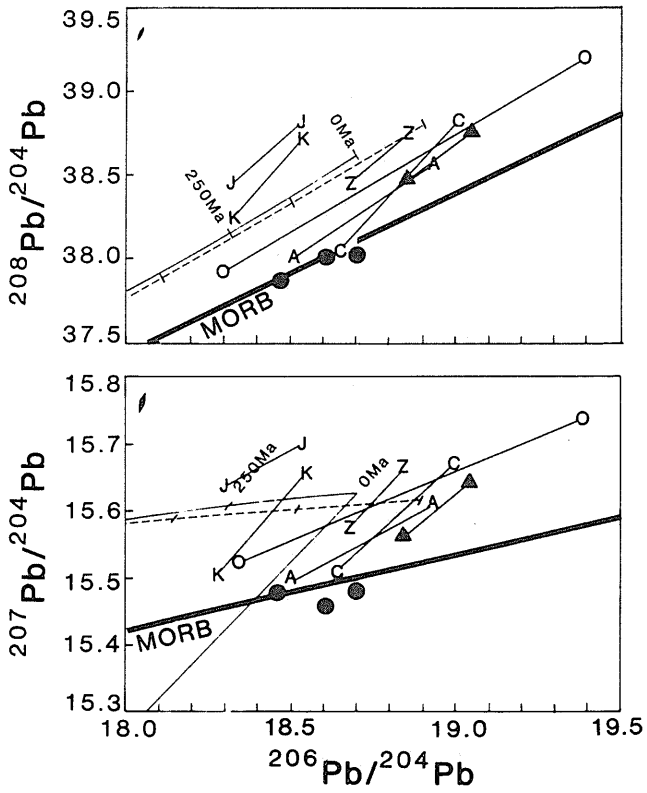

Fig. 1. Pb-isotope diagrams showing the variation of modern Pb-isotope arrays from some volcanic-arcs: J — the tholeiitic series from Japan (Tatsumoto, 1969; Tatsumoto and Knight, 1969); Z — the calc-alkaline andesites from North Island, New Zealand (Armstrong and Cooper, 1971); C — the calc-alkaline suite from the Cascade Range (Church and Tilton, 1973; Church, 1976); A — the calc-alkaline volcanic rocks from the Aleutians (Kay et al., 1978); and O — the Pb-isotope data from the volcanic ore in the Lesser Antilles (Armstrong and Cooper, 1971). The upper ends of the arrays approximate the regional Pb-isotope value for the upper crust whereas the lower value is the least radiogenic Pb-isotope value measured in that volcanic arc. Compare the lower values of each array with the MORB line defined by the regression through the Pb-isotope data from the mid-ocean ridge basalts from the Juan de Fuca and Gorda ridges (Church and Tatsumoto, 1975). The composition of Pb found in three VMS deposits dredged from the Juan de Fuca ridge are shown by dots near the MORB regression line(● — A. P. LeHuray, unpubl. data). Both the Stacey-Kramers growth curve (solid line) and the orogene growth curve (dashed line) are shown for comparison with the spread in Pb-isotopes from modern volcanic-arc rocks. Isochron intercepts are shown on both curves at 250 Ma intervals. The isotopic composition of Pb from the Kuroko deposits in Japan are shown by the K-array (Fehn et al., 1983); the Pb-isotope signature of the porphyry deposits from the Cascade Range is indicated by the triangles (▲ — Church et al., 1986a). Analytical error and fractionation trends are shown in the upper left corner of each diagram.

them (Fehn et al., 1983). Furthermore, the Pb in the Miocene K-VMS deposits in Japan (Fig. 1) have average values that are remarkably similar to the Pb-isotope signature of the tholeiitic volcanic-arc rocks of Japan (Tatsumoto, 1969; Tatsumoto and Knight, 1969), although the Pb in the K-VMS deposits is slightly more enriched in ^{206}Pb. Pb from the K-VMS deposits can also best be modeled by a *locally defined* sediment-Pb growth curve.

Studies of the Pb-isotope signature from young magmatothermal vein and porphyry systems associated with calc-alkaline plutons in the Cascade Range (Church et al., 1986a) have demonstrated that the Pb-isotope signature of calc-alkaline porphyry deposits reflects the Pb-isotope composition of the magma. The Pb-isotope array defined by the porphyry systems from the Cascade Range lies within and along the radiogenic side of the Pb-isotope array defined by studies of the Cascade volcanic arc (Fig. 1). A detailed study was made of five deposits associated with the Miocene Cloudy Pass pluton. The pluton intrudes rocks ranging in age from Miocene to Precambrian(?). Most of the deposits studied are wholly contained within the pluton, but one of them is a low-Pb breccia pipe that is emplaced largely within the overlying Swakane Biotite Gneiss. Pb-isotope studies indicated that little Pb was leached from the overlying Precambrian(?) Swakane Biotite Gneiss during emplacement. Thus, Pb-isotope signatures from galenas from porphyry systems also appear to reflect the mixing process defined by modern calc-alkaline volcanic-arc rocks.

DEVONIAN-MISSISSIPPIAN ORE-Pb FROM THE BROOKS RANGE

All of the Brooks Range sulfides considered here occur in Paleozoic rocks (Table 1). For the purpose of defining a point on the sediment-Pb growth curve for the Brooks Range, we are restricted to the Pb-isotope signature of three groups of deposits: the Lower Devonian K-VMS deposits of the schist belt, the sediment-hosted base-metal (Zn, Pb, ± Ag) and vein deposits (SHBM) of Late Devonian-Early Mississippian or Pennsylvanian age in the western Brooks Range, and the skarn and magmatothermal veins (HV) associated with Devonian plutons in the Survey Pass quadrangle.

Numerous studies have been made of the K-VMS deposits in the schist belt. Hitzman et al. (1982) summarize detailed geologic studies of deposits in the Ambler district. They concluded that these deposits were formed along an active continental margin. Bimodal volcanism is documented within the Ambler district and the VMS deposits are associated with felsic volcanic rocks. $^{207}Pb/^{206}Pb$ ages from zircons separated from metavolcanic rocks from the Ambler district give an age of 365 ± 15 Ma (Dillon et al., 1980). Pb-isotope data from the K-VMS deposits (Table 1) should characterize Pb-isotopic compositions from the "copper belt" on the southern flank of the Brooks Range (Marsh and Cathrall, 1981).

Comparison of the Pb-isotope signature of the K-VMS deposits of the Brooks Range with the Pb-isotope signature from Devonian VMS deposits from the West Shasta district in the eastern Klamath Mountains demonstrates the extent of regional variation and mixing between crustal and mantle Pb in Devonian time (Fig. 2). Doe et al. (1985) argue that the Pb-isotope signature of the West Shasta district represents an enriched-mantle Pb-isotope composition. Pb-isotope data from both groups of K-VMS deposits may approximate mixing arrays between the Devonian mantle and crustal Pb-isotope growth curves appropriate for deposits now found in oceanic terranes of the North American Cordillera.

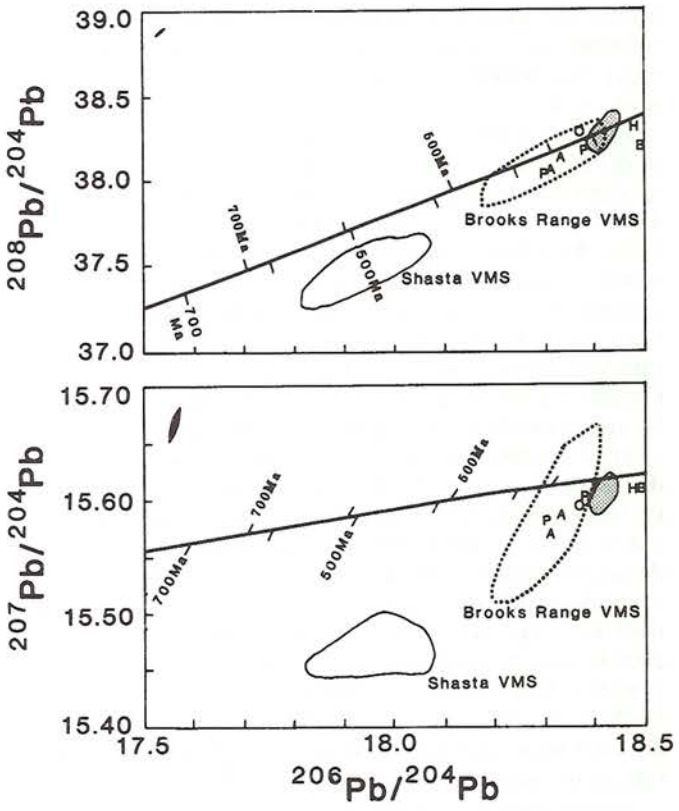

Fig. 2. Pb-isotope data from Devonian-Mississippian SHBM occurrences (Table 1) plot in the small stippled field ($^{206}Pb/^{204}Pb$ — $^{207}Pb/^{204}Pb$ slope = 0.1996 which gives an age of 2.82 Ga ± 590 Ma). The Pb-isotope data from the Arctic VMS deposit (A) from this study is shown within the Brooks Range VMS field (Hitzman et al., 1982). Isochron ages on both the SKGC (below curve) and the BRGC for sediment-Pb (above curve) are shown. Model ages for the BRGC give an age of about 350 Ma for the SHBM deposits whereas the intercept on the SKGC would be about 180 Ma. Data from the skarn and magmatothermal veins associated with the 365 Ma plutons in Survey Pass and shown by a P, O, and B (metamorphosed hydrothermal vein). Analytical error and fractionation trends are shown in the upper left corner of each diagram.

Geologic investigations have also defined a Zn-Pb-Ag, sediment-hosted base-metal (SHBM) province of mineralization north and west of the K-VMS belt in the Brooks Range. The stratiform Red Dog, Lik and Drenchwater deposits occur in an oceanic black shale and chert sequence, the Kuna Formation, of Mississippian and Pennsylvanian age (Lange et al., 1985; Sterne et al., 1984). Lange et al. suggest that these sulfide deposits formed in a starved basin setting. Sulfur-isotope studies indicate precipitation of sulfides during mixing of hydrothermal solutions with seawater (Lange et al., 1985). Nokleberg and Winkler (1982) reported a K-Ar age of 330 ± 17 Ma (Mississippian) from a biotite separate from a pyroxene andesite within the section at the Drenchwater Creek.

Table 1. Pb-Isotope data from sulfides from the Brooks Range, Alaska

Deposit Name	Sample No.	Age* or Host	Deposit Type	Latitude	Longitude	$\frac{^{206}Pb}{^{204}Pb}$	$\frac{^{207}Pb}{^{204}Pb}$	$\frac{^{208}Pb}{^{204}Pb}$	Ref.	Ore** Mineralogy
Smucker	I-1	D	K-VMS	67 18	157 09	18.397	15.661	38.202	1	gal
Dead Creek	I-2	D	K-VMS	67 13	156 32	18.347	15.558	38.218	1	gal
Arctic	AT12-38	D	K-VMS	67 12	156 25	18.308	15.569	38.061		gal
Arctic	AT39-14	D	K-VMS	67 12	156 25	18.330	15.587	38.140		cpy, py, gal
Arctic	I-3	D	K-VMS	67 12	156 25	18.340	15.560	38.146	1	gal
BT	I-4	D	K-VMS	67 07	155 51	18.393	15.651	38.270	1	gal
Sun-10	I-5	D	K-VMS	67 05	155 02	18.244	15.561	37.975	1	gal
Sun-12	I-6	D	K-VMS	67 05	155 02	18.200	15.517	37.904	1	gal
Arrigetch Crk	78AMH110D	D	skarn	67 26	154 03	18.300	15.579	38.050		sph, gal
Akabiuak Pass	78ADG202E	D	HV	67 28	154 41	18.377	15.601	38.177		gal, sph, cpy, aspy
Beaver Creek	77AGK325C	D	mV	67 07	155 24	18.497	15.609	38.206		gal, sph
U. Alatna area	77ADG340D	D	HV	67 50	155 15	18.364	15.591	38.274		gal, cpy, sph
Red Dog	RD-63B	M	SHBM	68 04	162 50	18.409	15.598	38.238	2	gal
Red Dog	78ARD-1	M	SHBM	68 04	162 50	18.414	15.602	38.254	2	gal
Red Dog	LL26-18	M	SHBM	68 04	162 50	18.404	15.590	38.228	3	gal
Red Dog	LL4-14	M	SHBM	68 04	162 50	18.413	15.604	38.197	3	gal, bar
Red Dog	LL26-6B	M	SHBM	68 04	162 50	18.403	15.602	38.254	3	sph, gal, py
Lik	Lik	M	SHBM	68 12	162 58	18.422	15.614	38.298		gal
Husky	HD-1	D	HV	68 04	162 32	18.475	15.608	38.309		gal
Ginny Creek	78Ek127A	D	HV	68 17	161 16	18.395	15.592	38.236	3	gal, sph
Drenchwater	78PM-052	M	SHBM	68 35	158 43	18.406	15.592	38.270	3	gal
Drenchwater	77ANK-13H	M	SHBM	68 35	158 43	18.428	15.609	38.351		gal
Story Creek	79Md194B	M	HV	68 23	157 58	18.404	15.595	38.224	3	gal, sph
Story Creek	STA B-0	M	HV	68 23	157 58	18.415	15.606	38.288		sph, gal, py
Story Creek	STA 1.77	M	HV	68 23	157 58	18.427	15.599	38.272		sph, gal, py
Whoopee Creek	WHC-3	D	HV	68 14	157 50	18.398	15.595	38.253		sph
Whoopee Creek	WHC-10A	D	HV	68 14	157 50	18.406	15.600	38.265		sph, gal

*D = Devonian, M = Mississippian.

**gal = galena, sph = sphalerite, py = pyrite, cpy = chalcopyrite, bar = barite, aspy = arsenopyrite.
References: 1 = Hitzman et al. (1982), 2 = Lange et al. (1985), 3 = Lueck (1986).

Other deposits within the SHBM province appear to be stratabound, although not stratiform, and are characterized by the same simple sulfide mineralogy as the stratiform deposits: sphalerite and galena with minor pyrite. The Ginny Creek occurrence is described as a disseminated deposit that occurs in the Noatak Sandstone of Late Devonian to Early Mississippian age (Mayfield et al., 1979). The Story Creek occurrence contains mineralization in cross-cutting veins and shale-chip breccias. It occurs in the Stuver Member of the Upper Devonian Kanayut Conglomerate and in the Lower Mississippian Kayak Shale (Ellersieck et al., 1982). The Whoopee Creek occurrence is in a fracture zone just below a thrust, located about 17 km south of the Story Creek deposit. Mineralization occurs in both cross-cutting veins and brecciated siltstone (Ellersieck et al., 1982). The Husky deposit is a large vein that cuts Upper Devonian shale (J. Hammitt, pers. comm., 1986). No definitive age relations have been established for these four deposits, although the 330 ± 17 Ma biotite K-Ar age from the pyroxene andesite at the Drenchwater deposit may provide a lower limit. We tentatively identify these occurrences as epigenetic veins within the same overall system as the stratiform ores, analogous to other sediment-hosted Zn-Pb districts such as McArthur River (Muir, 1983), central Ireland (LeHuray et al., 1987), and the Canadian Cordillera (MacIntyre, 1983).

Pb-isotope data from the SHBM deposits form a remarkably homogeneous suite (Table 1 and Fig. 2). The Pb-isotope composition of the Husky vein differs only slightly from the others and is somewhat more radiogenic. The upper end of the K-VMS data array has a very similar Pb-isotope composition. The Pb-isotope data, if interpreted in the light of modern analogues described above, establish a point on the sediment-Pb growth curve for the Brooks Range at about 370-330 Ma. These data require that sediments in the basin be derived from a more radiogenic crust than that defined by either the Stacey-Kramers (SKGC) or the orogene sediment-Pb growth curve (OGC). We have used a three-stage Pb-isotope evolution model to approximate mixing and sedimentation from a source that will match this point on the growth curve. The Brooks Range growth curve (BRGC) shown in Fig. 2 was calculated from the Stacey-Kramers growth curve assuming a $^{238}U/^{204}Pb$ of 12 with the third stage starting at 1.0 Ga.

Skarns and magmatothermal veins are associated with either exposed or buried plutons in the Survey Pass quadrangle, Brooks Range. Both U/Pb and Rb/Sr studies of the Arrigetch Peaks and Mount Igikpak plutons give crystallization ages of 365 ± 15 Ma (Dillon et al., 1980) and 373 ± 25 Ma (Silberman et al., 1979), respectively. Whole-rock Rb/Sr isochron gives an initial Sr intercept of 0.714 ± 0.003 indicating substantial involvement of old crustal material in the magma (Silberman et al., 1979). Galena-bearing veins at Arrigetch Creek, Akabiuak Pass (Grybeck and Nelson, 1980), and in the upper Alatna area (Grybeck et al., 1985) occur in unmetamorphosed to slightly metamorphosed rocks, whereas the rocks at Beaver Creek have been raised to amphibolite grade (Nelson and Grybeck, 1981). Pb-isotope data from three galenas, taken from sulfide occurrences associated with the plutons, indicates a Devonian hydrothermal event, consistent with the BRGC model ages. Pb-isotope data from Beaver Creek in the southwest corner of the Survey Pass quadrangle suggest that the galena picked up radiogenic Pb during subsequent metamorphism to amphibolite grade.

DEVONIAN-MISSISSIPPIAN ORE-Pb FROM THE EASTERN ALASKA RANGE

Studies of the geology and mineral deposits in the Mt. Hayes (Nauman and Duke, 1984; Nokleberg and Lange, 1985) and Healy quadrangles (Light et al., 1987; Csejtey et al., 1986) have defined a belt of VMS deposits north of the Denali Fault in the eastern Alaska Range within the Jarvis Creek Glacier terrane (Nokleberg and Aleinikoff, 1985). We have measured the isotopic composition of Pb in deposits from the Delta, Hayes Glacier and McGinnis Glacier districts in the Mt. Hayes quadrangle, and from the Bonnifield district in the Healy quadrangle (Table 2). The VMS deposits in the Delta district occur

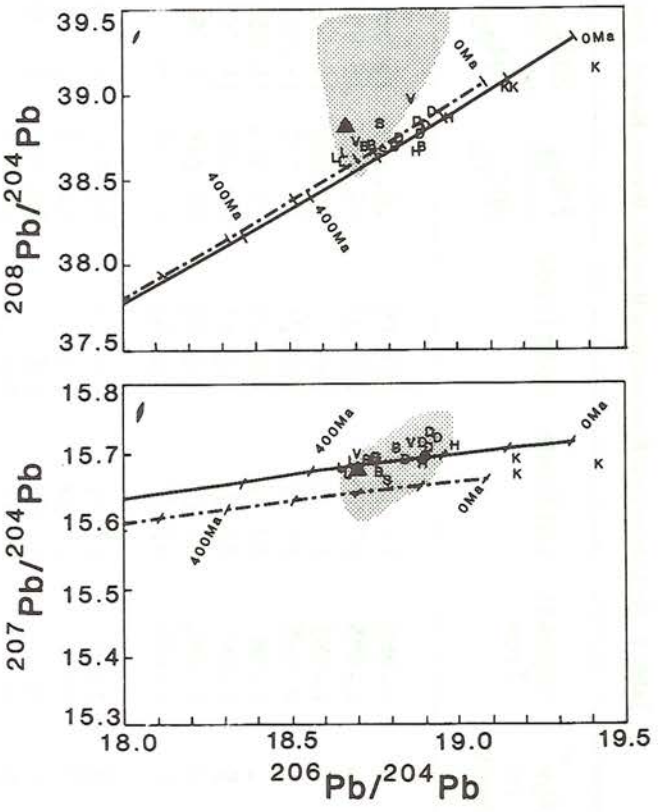

Fig. 3. Pb-isotope diagrams showing the composition of Pb from the VMS deposits from the Delta (D — Cu-rich, L — Pb-rich), Hayes Glacier and McGinnis Glacier (H), and Bonnifield (B, S, V) districts in the Mount Hayes and Healy quadrangles (Table 2). The data from the skarn deposit in the Bonnifield district is shown by the triangle (▲). These data are similar to the Pb-isotope data from SHBM deposits of Devonian age from the Selwyn Basin of the Canadian Cordillera (stippled field; Godwin and Sinclair, 1982). The Pb-isotope signature of the Devonian VMS deposits from the Alaska Range is very different from that of the Brooks Range (Fig. 2). The Brooks Range sediment-Pb growth curve (dashed) and the Canadian Cordillera growth curve (solid) are shown with isochron age intercepts are indicated every 100 Ma. Studies of the later magmatothermal vein mineralization in the Bonnifield district (K) shows that mineralization of a different age can readily be distinguished using Pb-isotope surveys. Analytical error and fractionation trends are shown in the upper left corner of each diagram.

Table 2. Pb-Isotope data from the Devonian-Mississippian VMS deposits of the eastern Alaska Range

Deposit Name	Sample No.	District	Deposit Type	Latitude	Longitude	$\frac{^{206}Pb}{^{204}Pb}$	$\frac{^{207}Pb}{^{204}Pb}$	$\frac{^{208}Pb}{^{204}Pb}$	Ore* Minerals
Dry Creek	DC-9	Bonnefield	VMS	63 55 25	147 23 15	18.765	15.675	38.824	cpy, py
W. Fork L. Delta River	WF-1	Bonnefield	VMS	63 48 10	147 29 40	18.728	15.688	38.699	cpy, py
Cirque	C-3	Bonnefield	VMS	63 47 00	147 38 00	18.742	15.690	38.706	py, cpy
Virginia Creek	VC-2	Bonnefield	VMS	63 49 35	147 48 00	18.821	15.695	38.709	cpy, py
Anderson Mtn	AM-3	Bonnefield	VMS	63 48 35	147 55 50	18.884	15.699	38.709	gal
Snow Mtn Gulch	SMG-1	Bonnefield	VMS	64 00 00	147 25 00	18.680	15.678	38.845	gal
Sheep Creek	81CX17	Bonnefield	VMS	63 55 10	148 16 50	18.858	15.706	38.985	gal
Healy Creek	HC-2	Bonnefield	VMS	63 49 05	148 16 15	18.692	15.687	38.718	gal
West Fork Glacier	79CQ48	Bonnefield	skarn	63 28 24	147 35 15	18.779	15.663	38.667	cpy
Kansas Creek	81CX21	Bonnefield	HV	63 51 30	147 30 00	19.166	15.692	39.044	stib
Glory Creek	GC-1	Bonnefield	HV	63 50 35	147 30 35	19.407	15.683	39.157	gal
Flume Creek	FC-1	Bonnefield	HV	64 00 50	147 17 30	19.168	15.669	39.058	gal
Trio	81AIL140AZ	Delta	VMS	63 15 53	144 02 18	18.834	15.692	38.748	gal
DDY	81AIL162A	Delta	VMS	63 15 32	144 14 20	18.896	15.716	38.779	gal
LP-PP2	81AIL184B	Delta	VMS	63 14 22	144 07 00	18.931	15.726	38.899	gal
Trio	81AIL126A	Delta	VMS	63 15 53	144 02 18	18.886	15.719	38.839	gal
DDN	80AIL028A	Delta	VMS	63 16 31	144 16 23	18.911	15.729	38.828	gal
Rumble Creek	RC	Delta	VMS	63 14 22	144 10 00	18.672	15.690	38.663	cpy, py, gal
Lam. Zn. N. Cirque	LZ-U	Delta	VMS	63 10 46	144 08 55	18.645	15.681	38.630	gal, sph, cpy
Discovery Zn-PPD	PPD	Delta	VMS	63 08 30	144 02 36	18.666	15.674	38.600	gal, sph, cpy
Roberts deposit	82AIL044A	McGinnis Glacier	VMS	63 35 59	146 14 48	18.889	15.691	38.670	cpy
Unnamed occurrence	82AIL052A	Hayes Glacier	VMS	63 41 24	146 39 30	18.985	15.716	38.872	cpy

*gal = galena, sph = sphalerite, py = pyrite, cpy = chalcopyrite, stib = stibnite.

in pelitic and metavolcanic schists containing meta-quartz keratophyre, meta-andesite and meta-dacite (LeHuray et al., 1985). Deposits from the Hayes Glacier and McGinnis Glacier districts are also associated with quartz-rich meta-keratophyre, meta-andesite and meta-dacite (Nokleberg and Lange, 1985). VMS deposits from the Bonnifield district contain deposits associated with both felsic and calc-alkaline volcanic rocks (J. M. Kelley, pers. comm., 1985). Dioritic and gabbroic dykes and sills that crosscut the metamorphic foliation in the metavolcanic units found in the Delta district (Lange and Nokleberg, 1984) may record a subsequent rifting event.

The Pb-isotope data from VMS deposits from the Alaska Range plot in two clusters (Fig. 3). One group of data from pyrite- and chalcopyrite-rich VMS deposits has a more radiogenic Pb-isotope signature (i.e. higher $^{206}Pb/^{204}Pb$ ratios) than the second group from Pb-rich VMS deposits. In the Delta district, the Pb-rich VMS deposits lie south of the pyrite- and chalcopyrite-rich VMS deposits, closer to the Denali Fault. The Snow Mountain Gulch deposit from the Bonnifield district, a distal-VMS deposit hosted in the Mystic Creek Member of the Totatlanika Schist of Mississippian(?) age (D. A. Mako, pers. comm., 1985), also plots within the field of data defined by the less radiogenic group.

Studies of the isotopic composition of Pb from ore deposits may be utilized to evaluate the potential of a given geochemical anomaly for a particular type of mineralization. Studies of many districts by Gulson and his colleagues in Australia (Gulson, 1986) have demonstrated the application of a target Pb-isotope ratio for a particular type of mineralization within a given region. Similar applications can be made in the Canadian Cordillera utilizing the data base of Godwin et al. (1982). Detailed studies of the Pb-isotope composition of geochemically anomalous areas within the Bonnifield district were made to evaluate the regional signature of overlapping VMS and hydrothermal vein mineralization in the Healy quadrangle (Church et al., 1986b). The Pb-isotope signatures of different deposit types obtained from these studies, along with analysis of the chemical data from exploration studies (Light et al., 1987), allowed us to discriminate between VMS mineralization in the Healy and Sheep Creek areas and later hydrothermal vein mineralization (K — Fig. 3) on Flume, Kansas, and Glory Creeks (Table 2). Geologic observations of the hydrothermal vein mineralization in the Bonnifield district at Glory Creek show that mineralization is associated with granitic intrusive rocks mapped as Cretaceous by Csejtey et al. (1986).

APPLICATION OF Pb ISOTOPES FROM ORE DEPOSITS TO REGIONAL TECTONICS

Comparison of the Pb-isotope data from the two groups of VMS deposits from the eastern Alaska Range with those from the Brooks Range demonstrates that a single sediment-Pb growth curve for stratiform deposits from Alaska would be inappropriate. In fact, the different Pb-isotope signatures of Devonian-Mississippian VMS deposits from the two provinces can be used to define the source terranes for sediments that provide the metals found in the deposits themselves. The Pb-isotope data (Fig. 3) from the pyrite- and chalcopyrite-rich deposits from the eastern Alaska Range matches very well with that from the SHBM deposits of Devonian age from the Gataga district in northern British Columbia (Godwin and Sinclair, 1982; MacIntyre, 1983). U-Pb ages of zircon separates from metavolcanic rocks associated with the VMS deposits in the Jarvis Creek Glacier terrane in the Hayes Glacier district are 364 ± 9 Ma (Late Devonian), and upper intercepts on the concordia diagram indicate inherited zircon from an Early Proterozoic source (2.0 - 2.3 Ga; Aleinikoff and Nokleberg, 1985). Detailed studies of ages of metavolcanic rocks and augen gneisses within the Yukon-Tanana terrane indicate a large area of old crustal rocks that have experienced a very similar metamorphic history (Dusel-Bacon and Aleinikoff, 1985; Aleinikoff et al., 1986). Comparison of the common-Pb data from sulfides from the eastern Alaska Range with the three-stage model defined for SHBM deposits from the Canadian Cordillera gives model-Pb ages of about 370 Ma (Godwin and Sinclair, 1982; we have modified the model slightly using 2.0 Ga as the final growth stage). The agreement with the 364 Ma U-Pb age from zircons is remarkably good. We suggest that the Canadian Cordillera sediment-Pb growth curve (CCGC) can be applied to the entire Yukon-Tanana uplands, at least for Pb-isotopes from stratiform deposits that occur in Paleozoic rocks. In contrast, the sediment-Pb growth curve for the Brooks Range does not reflect the old crustal component of the Canadian shield and the relationship with the sediment-Pb growth curve for the West Shasta district defined earlier suggests that the source of sediments for the Selwyn Basin may reflect a rift-basin whereas the sediment-Pb growth curve for the Brooks Range may reflect an open-oceanic or more active continental margin environment, perhaps not very different from that modeled by the orogene growth curve.

Studies of tectonic dismemberment of the Canadian Cordillera have shown that there has been about 900 km of displacement of the Devonian shale-carbonate facies boundary along the Tintina Fault (Fig. 4), with about 420 km of displacement taking place prior to Middle Jurassic time (Gabrielse, 1985). Displacement of a similar magnitude may have taken place along the Denali Fault, however, the amount of offset is much more difficult to document. Nauman and Duke (1984) suggest that the VMS deposits of the Delta district were formed as a result of rifting, resulting in the emplacement of numerous tholeiitic sills in the Devonian sediments to set up hydrothermal cells that formed the VMS deposits. Lange and Nokleberg (1984) argue that the VMS deposits from the Hayes Glacier and McGinnis Glacier districts were formed in a submarine island arc environment.

The Pb-isotope data and the regional synthesis of the geologic data both suggest a genetic relationship between the VMS deposits of the Jarvis Creek Glacier terrane and the rocks of the Canadian Cordillera. However, defining the exact nature and magnitude of the displacement of the deposits in the eastern Alaska Range from other VMS deposits having equivalent Pb-isotope compositions on the margin of the Canadian shield has proven difficult. Whereas Gabrielse (1985) has described oceanic volcanic rocks of late Paleozoic age from the general area west of the Cassiar Mountains (e.g. the Cache Creek terrane), none of the allochthonous terranes appear to match the stratigraphy described in the Delta district by Nauman and Duke (1984). The model developed by MacIntyre (1983) for

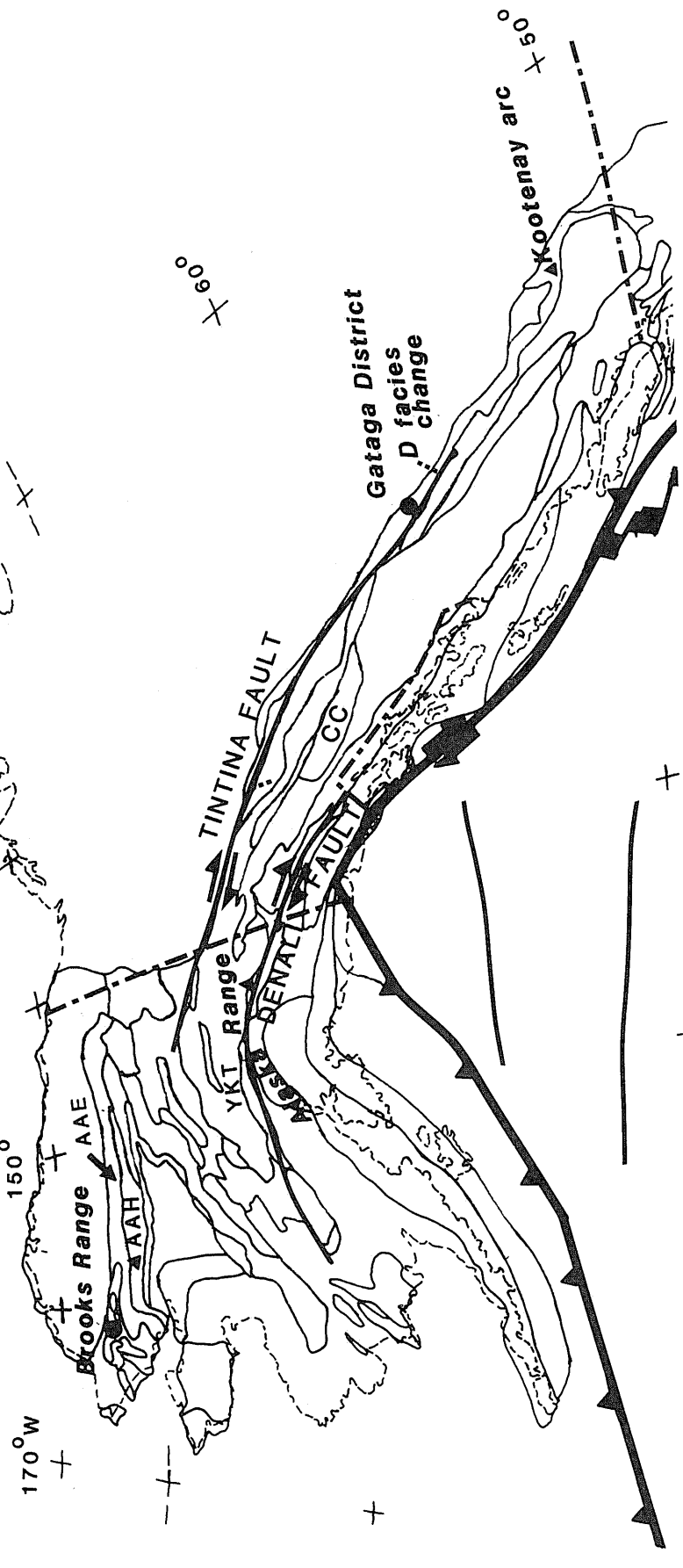

Fig. 4. Map showing major faults and terranes in the Alaska and the Canadian Cordillera discussed in this paper (after Howell et al., 1985). Tectonostratigraphic terranes used in this construction (AAE — Endicott Mountains subterrane of the Arctic Alaska terrane, AAH — Hammond subterrane of Arctic Alaska terrane, YKT — Yukon Tanana terrane) are from Jones et al. (1984). The Jarvis Creek Glacier terrane lies between YKT and the Denali Fault in the eastern Alaska Range, but cannot be shown at this scale. Districts are shown schematically on the map (▲ — VMS deposits, ● — sediment-hosted deposits). The 900 km offset the Devonian shale-carbonate facies on the Tintina Fault is shown by the two short dashed lines (Gabrielse, 1985). Possible correlative allochthonous terranes, such as the oceanic Cache Creek (CC) terrane west of the Cassiar Mountains in northern British Columbia and the Kootenay arc in southern British Columbia are from Monger and Berg (1984).

the SHBM deposits of the Gataga district calls upon basin faulting to provide conduits for ore-forming fluids. No volcanic rocks are present in any of the sediments either within the Gataga district or in the various tectonostratigraphic terranes to the west (Gabrielse, 1985). Perhaps the rocks and deposits found in the Delta district in the eastern Alaska Range represent a direct offset of deposits that were formed outboard of the Gataga district at about 57°N latitude (present position). Alternatively, they may have formed even further to the south and have been displaced by transform movement along numerous faults in western British Columbia similar to that for the Cache Creek terrane documented by Gabrielse (1985).

Monger (1975) describes five areas within the Canadian Cordillera where upper Paleozoic volcanic rocks occur, including the Kootenay arc of southern British Columbia. Rock geochemistry (Souther, 1977) suggests that both tholeiitic and calc-alkaline rocks of Late Devonian age occur in the Kootenay arc. Pb-isotope studies of metamorphosed VMS deposits from the Adams Plateau area of the Kootenay arc are very similar to those from the eastern Alaska Range (F. Gautier and C. I. Godwin, pers. comm., 1986). The somewhat less radiogenic signature of the Pb-rich VMS deposits of the Delta district in the Alaska Range reflects mixing of sediment from a somewhat younger source terrane. Further work is needed to evaluate the possible match of these two ore districts. However, if this match is correct, then the two districts have been offset more than 2 000 km since the beginning of rifting (circa 365 Ma) and the docking of the Jarvis Creek Glacier terrane (circa 110 Ma). Evaluation of the offset of the Jarvis Creek Glacier terrane from the possible source in the Canadian Cordillera would appear to be an important geologic and economic problem, not only because of the obvious importance to the understanding of North American geology and tectonic processes, but also because of its potential importance in the discovery of a new base- and precious-metal-rich VMS district in the North American Cordillera.

Acknowledgements — We thank B. L. Gulson and C. I. Godwin for their thoughtful reviews of the manuscript. Special thanks are extended to F. Gautier and C. I. Godwin for permission to reference their unpublished Pb-isotope work in the Kootenay arc, Finally, we thank all those geologists who have provided us with ore samples and information on the field relations of these deposits.

REFERENCES

Aleinikoff, J. N. and Nokleberg, W. J., 1985, Age of Devonian igneous-arc terranes in the northern Mount Hayes quadrangle, eastern Alaska Range, *in* Bartsch-Winkler, S. (editor), The United States Geological Survey in Alaska: Accomplishments during 1984. U.S. Geol. Surv., Circ. 967, p. 44-49.

Aleinikoff, J. N., Dusel-Bacon, C. and Foster, H. L., 1986, Geochronology of augen gneiss and related rocks, Yukon-Tanana terrane, east-central Alaska: Bull. Geol. Soc. Am., v. 97, p. 626-637.

Armstrong, R. L., 1968, A model for Sr and Pb evolution in a dynamic earth: Rev. Geophys., v. 6, p. 175-199.

Armstrong, R. L., 1981, Radiogenic isotopes: the case for crustal recycling on a near-steady-state no-continental-growth Earth: Phil. Trans. R. Soc. London, A 301, p. 443-472.

Armstrong, R. L. and Cooper, J., 1971, Lead-isotopes in island arcs: Bull. Volcanol., v. 35, p. 27-63.

Armstrong, R. L. and Hein, S. M., 1973, Computer simulation of Pb and Sr isotope evolution of the Earth's crust and upper mantle: Geochim. Cosmochim. Acta, v. 37, p. 1-18.

Chen, J. H., Wasserburg, G. J., Von Damm, K. L. and Edmond, J. M., 1986, The U-Th-Pb systematics in hot springs on the East Pacific Rise at 21°N and Guaymas Basin: Geochim. Cosmochim. Acta, v. 50, p. 2467-2479.

Church, S. E., 1976, The Cascade Mountains revisited: A re-evaluation in light of new lead isotopic data: Earth Planet. Sci. Letters, v. 29, p. 175-188.

Church, S. E. and Tatsumoto, M., 1975, Lead isotope relations in oceanic ridge basalts from the Juan de Fuca-Gorda Ridge area, N.E. Pacific Ocean: Contrib. Mineral. Petrol., v. 53, p. 253-279.

Church, S. E. and Tilton, G. R., 1973, Lead and strontium isotopic studies in the Cascade Mountains: bearing on andesite genesis: Bull. Geol. Soc. Am., v. 84, p. 431-454.

Church, S. E., LeHuray, A. P., Grant, A. R., Delevaux, M. H. and Gray, J. E., 1986a, Lead-isotopic data from sulfide minerals from the Cascade Range, Oregon and Washington: Geochim. Cosmochim. Acta, v. 50, p. 317-328.

Church, S. E., Gray, J. E. and Delevaux, M. H., 1986b, Use of Pb-isotopic signatures for geochemical exploration in the Healy quadrangle, eastern Alaska Range, *in* Bartsch-Winkler, S. and Reed, K. M. (editors), Geologic studies in Alaska by the United States Geological Survey during 1985. U.S. Geol. Surv., Circ. 978, p. 38-41.

Csejtey, B., Jr., Mullen, M. W., Cox, D. P., Gilbert, W. G., Yeend, W. E., Smith, T. E., Wahrhaftig, C., Craddock, C., Brewer, W. M., Sherwood, K. W., Hickman, R. G., Stricker, G. D., St. Aubin, D. R. and Goerz, D. J., III, 1986, Geology and geochronology of the Healy quadrangle, Alaska: U.S. Geol. Surv., Open-File Report 86-396, 92 p., scale 1:250,000, 4 sheets.

Cumming, G. L. and Richards, J. R., 1975, Ore lead isotope ratios in a continuously changing Earth: Earth Planet. Sci. Letters, v. 28, p. 155-171.

Dillon, J. T., Pessel, G. H., Chen, J. H. and Veach, N. C., 1980, Middle Paleozoic magmatism and orogenesis in the Brooks Range, Alaska: Geology, v. 8, p. 338-343.

Doe, B. R., and Zartmen, R. E., 1979, Plumbotectonics, the Phanerozoic, *in* Barnes, H. L. (editor), Geochemistry of Hydrothermal Ore Deposits, 2nd ed., Wiley and Sons, New York, p. 22-70.

Doe B. R., Delevaux, M. H. and Albers, J. P., 1985, The plumbotectonics of the West Shasta Mining District, eastern Klamath Mountains, California: Econ. Geol., v. 80, p. 2136-2148.

Dusel-Bacon, C. and Aleinikoff, J. N., 1985, Petrology and tectonic significance of augen gneiss from a belt of Mississippian granitoids in the Yukon-Tanana terrane, east-central Alaska: Bull. Geol. Soc. Am., v. 96, p. 411-425.

Ellersieck, I. F., Jansons, U., Mayfield, C. F. and Tallier, I. L., 1982, The Story Creek and Whoopee Creek lead-zinc-silver occurrences, western Brooks Range, Alaska, *in* Coonrad, W. L. (editor), The United States Geological Survey in Alaska: Accomplishments during 1980. U.S. Geol. Surv., Circ. 844, p. 35-38.

Fehn, U., Doe, B. R. and Delevaux, M. H., 1983, The distribution of lead isotopes and the origin of Kuroko ore deposits in the Hokuroku District, Japan, *in* Ohmoto, H. and Skinner, B. J. (editors), The Kuroko and Related Volcanogenic Massive Sulfide Deposits, Economic Geology Publ. Co., Austin, Tx., p. 488-506.

Gabrielse, H., 1985, Major dextral transcurrent displacements along the Northern Rocky Mountain Trench and related lineaments in north-central British Columbia: Bull. Geol. Soc. Am., v. 96, p. 1-14.

Godwin, C. I. and Sinclair, A. J., 1982, Average lead isotope growth curves for shale-hosted zinc-lead deposits, Canadian Cordillera: Econ. Geol., v. 77, p. 675-690.

Godwin, C. I., Sinclair, A. J. and Ryan, B. D., 1982, Lead isotope models for the genesis of carbonate-hosted Zn-Pb, shale-hosted Ba-Zn-Pb, and silver-rich deposits in the northern Canadian Cordillera: Econ. Geol., v. 77, p. 82-94.

Grybeck, D. J. and Nelson, S. W., 1980, Geologic map of the Survey Pass quadrangle, Brooks Range, Alaska: U.S. Geol. Surv., Misc. Field Studies Map MF-1176-A, scale 1:250,000, 2 sheets.

Grybeck, D. J., Cathrall, J. B., LeCompte, J. R. and Cady, J. W., 1985, Buried felsic plutons in Upper Devonian redbeds, central

Brooks Range, *in* Bartsch-Winkler, S. and Reed, K. M. (editors), The United States Geological Survey in Alaska: Accomplishments during 1983. U.S. Geol. Surv., Circ. 945, p. 8-10.

Gulson, B. L., 1986, Lead isotopes in mineral exploration: Elsevier, New York, 245 p.

Hitzman, M. W., Smith, T. E. and Proffett, J. M., 1982, Bedrock geology of the Ambler district, southwestern Brooks Range, Alaska: Alaska Div. Geol. Geophys. Surv., Geologic Report 75, scale 1:125,000, 2 sheets.

Howell, D. G., Schermer, E. R., Jones, D. L., Ben-Avraham, Z. and Scheibner, E., (Compilers), 1985; Preliminary tectonostratigraphic terrane map of the circum-Pacific region: Am. Assoc. Petrol. Geol., Tulsa, Ok., scale 1:17,000,000.

Jones, D. L., Siberling, N. J., Coney, P. J. and Plafker, G., 1984, Part A — Lithotectonic terrane map of Alaska (west of the 141st meridian), *in* Siberling, N. J. and Jones, D. L. (editors), Lithotectonic terrane maps of the North American Cordillera. U.S. Geol. Surv. Open-File Report 84-523, p. A1-A12, scale 1:2,500,000, 4 sheets.

Kay, R. W., Sun, S. -S. and Lee-Hu, C. -N., 1978, Pb and Sr isotopes in volcanic rocks from Aleutian Islands and Pribilof Islands, Alaska: Geochim. Cosmochim. Acta, v. 42, p. 263-273.

Lange, I. M. and Nokleberg, W. J., 1984, Massive sulfide deposits of the Jarvis Creek Glacier terrane, Mount Hayes quadrangle, eastern Alaska Range: Geol. Soc. Am., Abstracts with Programs, v. 16, p. 294.

Lange, I. M., Nokleberg, W. J., Plahuta, J. T., Krouse, H. R. and Doe, B. R., 1985, Geologic setting, petrology, and geochemistry of stratiform sphalerite-galena-barite deposits, Red Dog Creek, Drenchwater Creek areas, northwestern Brooks Range, Alaska: Econ. Geol., v. 80, p. 1896-1926.

LeHuray, A. P., Church, S. E. and Nokleberg, W. J., 1985, Lead isotopes in sulfide deposits from the Jarvis Creek Glacier and Wrangellia terranes, Mount Hayes quadrangle, eastern Alaska Range, *in* Bartsch-Winkler, S. and Reed, K. M. (editors), The United States Geological Survey in Alaska: Accomplishments during 1983. U.S. Geol. Surv., Circ. 945, p. 72-73.

LeHuray, A. P., Caulfield, J. B. D., Rye, D. M. and Dixon, P. R., 1987, Basement controls on sediment-hosted Zn-Pb deposits: A Pb isotope study of Carboniferous mineralization in central Ireland: Econ. Geol., in press.

Light, T. D., Tripp, R. B. and King, H. D., 1987, Geochemical characterization of two mineral provinces in the Healy quadrangle, Alaska: This volume.

Lueck, L. L., 1986, Petrologic and geochemical characterization of the Red Dog and other base-metal sulfide and barite deposits in the DeLong Mountains, western Brooks Range, Alaska: Min. Industries Res. Lab., Fairbanks, Ak., MIRL Report 71, 105 p.

MacIntyre, D. G., 1983, Geology and stratiform Barite-sulphide deposits of the Gataga District, northeast British Columbia, *in* Sangster, D. F. (editor), Short Course in Sediment-hosted Stratiform Lead-Zinc Deposits. Can. Miner. Assoc. Handbook, V. 8, Victoria, B.C., p. 85-119.

Marsh, S. P. and Cathrall, J. B., 1981, Geochemical evidence for a Brooks Range mineral belt, Alaska, *in* Rose, A. W. and Gundlach, H. (editors), Geochemical Exploration 1980. J. Geochem. Explor., v. 15, p. 367-380.

Mayfield, C. F., Curtis, S. M., Ellersieck, I. F. and Tallier, I. F., 1979, Reconnaissance geology of the Ginny Creek zinc-lead-silver and Nimiuktuk barite deposits, north-western Brooks Range, Alaska: U.S. Geol. Surv., Open-File Report 79-1092, 20 p., scale 1:63,360.

Monger, J. W. H., 1975, Correlation of eugeosynclinal tectonostratigraphic belts in the North American Cordillera: Geosci. Canada, v. 2, p. 4-10.

Monger, J. W. H. and Berg, H. C., 1984, Part B — Lithotectonic terrane map of western Canada and southeastern Alaska, in Siberling, N. J. and Jones, D. L. (editors), Lithotectonic terrane maps of the North American Cordillera. U.S. Geol. Surv. Open-File Report 84-523, p. B1-B31, scale 1:2,500,000, 4 sheets.

Muir, M. D., 1983, Depositional environments of host rocks to Northern Australian lead-zinc deposits, with special reference to McArthur River, *in* Sangster, D. F. (editor), Short Course in Sediment-hosted Stratiform Lead-Zinc Deposits. Can. Miner. Assoc. Handbook, v. 8, Victoria, B.C., p. 141-174.

Nauman, C. R. and Duke, N. A., 1984, Alteration accompanying massive sulfide mineralization in the Delta District, east central Alaska: Implications for exploration: J. Geochem. Explor., v. 25, p. 254 (abst).

Nelson, S. W. and Grybeck, D. J., 1981, Map showing the distribution of metamorphic rocks in the Survey Pass quadrangle, Brooks Range, Alaska: U.S. Geol. Surv., Misc. Field Studies Map MF-1176-C, scale 1:250,000, 1 sheet.

Nokleberg, W. J. and Aleinikoff, J. N., 1985, Summary of stratigraphy, structure, and metamorphism of Devonian igneous-arc terranes, northeastern Mount Hayes quadrangle, eastern Alaskan Range, *in* Bartsch-Winkler, S., (editor), The United States Geological Survey in Alaska: Accomplishments during 1984. U.S. Geol. Surv., Circ. 967, p. 66-71.

Nokleberg, W. J. and Lange, I. M., 1985, Volcanogenic massive sulfide occurrences, Jarvis Creek Glacier terrane, western Mount Hayes quadrangle, eastern Alaskan Range, *in* Bartsch-Winkler, S. and Reed, K. M. (editors), The United States Geological Survey in Alaska: Accomplishments during 1983. U.S. Geol. Surv., Circ. 945, p. 77-80.

Nokleberg, W. J. and Winkler, G. R., 1982, Stratiform zinc-lead deposits in the Drenchwater Creek area Howard Pass quadrangle, western Brooks Range, Alaska: U.S. Geol. Surv. Prof. Paper 1209, 22 p.

Silberman, M. L., Brookins, D. G., Nelson, S. W. and Grybeck, D. J., 1979, Rubidium-strontium and potassium-argon dating of emplacement and metamorphism of the Arrigetch Peaks and Mount Igikpak plutons, Survey Pass quadrangle, Alaska, *in* Johnson, K. M. and Williams, J. R. (editors), The United States Geological Survey in Alaska: Accomplishments during 1978. U. S. Geol. Surv., Circ. 804-B, p. B18-B19.

Souther, J. G., 1977, Volcanism and tectonic environments in the Canadian Cordillera — a second look; *in* Barager, W. R. A., Coleman, L. C. and Hall, J. M. (editors), Volcanic regimes in Canada, Geol. Assoc. Can., Spec. Paper 16, p. 3-24.

Stacey, J. S. and Kramers, J. D., 1975, Approximation of terrestrial lead isotope evolution by a two stage model: Earth Planet. Sci. Letters, v. 26, p. 207-221.

Sterne, E. J., Zantop, H. and Reynolds, R. C., 1984, Clay mineralogy and carbon-nitrogen geochemistry of the Lik and Competition Creek zinc-lead-silver prospects, DeLong Mountains, Alaska: Econ. Geol., v. 79, p. 1406-1411.

Tatsumoto, M., 1969, Lead isotopes in volcanic rocks and possible ocean-floor thrusting beneath island arcs: Earth Plant. Sci. Letters, v. 6, p. 369-376.

Tatsumoto, M. and Knight, R. J., 1969, Isotopic composition of lead in volcanic rocks from central Honshu — with regard to basalt genesis: Geochem. J., v. 3, p. 53-86.

Zartman, R. E. and Doe, B. R., 1981, Plumbotectonics — the model, *in* Zartman, R. E. and Taylor, S. R. (editors), Evolution of the Upper Mantle. Tectonophysics, v. 75, p. 135-162.

Analysis of Fluid Inclusion Gases in Jasperoid as an Exploration Method for Micron Gold Deposits

P. S. HAYNES and S. E. KESLER
Department of Geological Sciences, University of Michigan, Ann Arbor, MI 48109

Abstract — We have evaluated the possibility that analysis of gases released from fluid inclusions in jasperoid might be used to guide exploration for sediment-hosted, micron gold deposits. Orientation studies were carried out over the Pinson, Carlin, Rain, Dee and Standard deposits, the Taylor silver district and the Willow Creek and Gilbert prospects, and included both upper and lower plate jasperoid. These surveys indicate that the average content of CO and N_2 in jasperoids from mineralized systems is greater than that in jasperoids from barren areas, apparently reflecting the anticipated contribution of these gases to mineralizing fluids from rock-water reactions in the hydrothermal systems. Within individual deposits, fluid inclusions in jasperoid at the center of mineralized systems have relatively low mole fractions of CO_2 and CO in comparison to peripheral parts of the mineralized system, possibly because greater fluid flow in the central part of the system removes these gases more effectively. Although these surveys indicate that systematic patterns in fluid inclusion gas abundances are present in jasperoid associated with micron gold deposits, these patterns are not strong enough or consistent enough to be used as a first-order guide in exploration for these deposits, but might prove useful in conjunction with other lithogeochemical exploration methods in locating centers of widely altered zones.

INTRODUCTION

SEDIMENT-HOSTED MICRON gold deposits have been a major exploration target in the western U.S. since the discovery of the Carlin deposit in the early 1960's. Geochemical exploration for these deposits has included analysis of rocks (Akright et al., 1969; Crone et al., 1984), soils (Wargo and Powers, 1978; Bagby et al., 1986) and Hg gas (Brooks and Berger, 1978) with varying degrees of success. In most such surveys, jasperoid is the first material to be collected and analyzed because it forms the most prominent outcrops. Jasperoid itself can be volumetrically important as ore, as in the Pinson A-zone orebody (Jackson, 1982), or it can be along faults or strata peripheral to ore, as at Carlin and Jerritt Canyon (Noble and Radtke, 1978, Birak and Hawkins, 1985). In addition, however, many areas of jasperoid appear to be barren of gold mineralization (Lovering, 1972), and considerable time can be consumed in evaluating such areas.

This study was undertaken in order to determine whether analysis of bulk fluid inclusion gases released from jasperoid by thermal decrepitation could be used to guide exploration for these deposits. We wished to determine:

(1) whether jasperoids associated with sediment-hosted gold mineralization (either mineralized themselves or barren but close to ore) could be distinguished on the basis of their fluid inclusion gas contents from jasperoids not associated with mineralization, and

(2) whether variations in the compositions of fluid inclusion gases from jasperoid in individual mineralized areas exhibited zoning patterns that could guide exploration.

The attraction of using fluid inclusion gases for such a test is that they will be widespread throughout the hydrothermal system and might reflect the chemistry of the mineralizing system. Although they have sampling problems of their own, as discussed below, fluid inclusions should not suffer from the spotty distribution common for gold in most geological samples.

In order to carry out these tests, we collected (in 1983) approximately 200 samples from eight properties in Nevada (Fig. 1), including two operating mines (Pinson and Carlin)

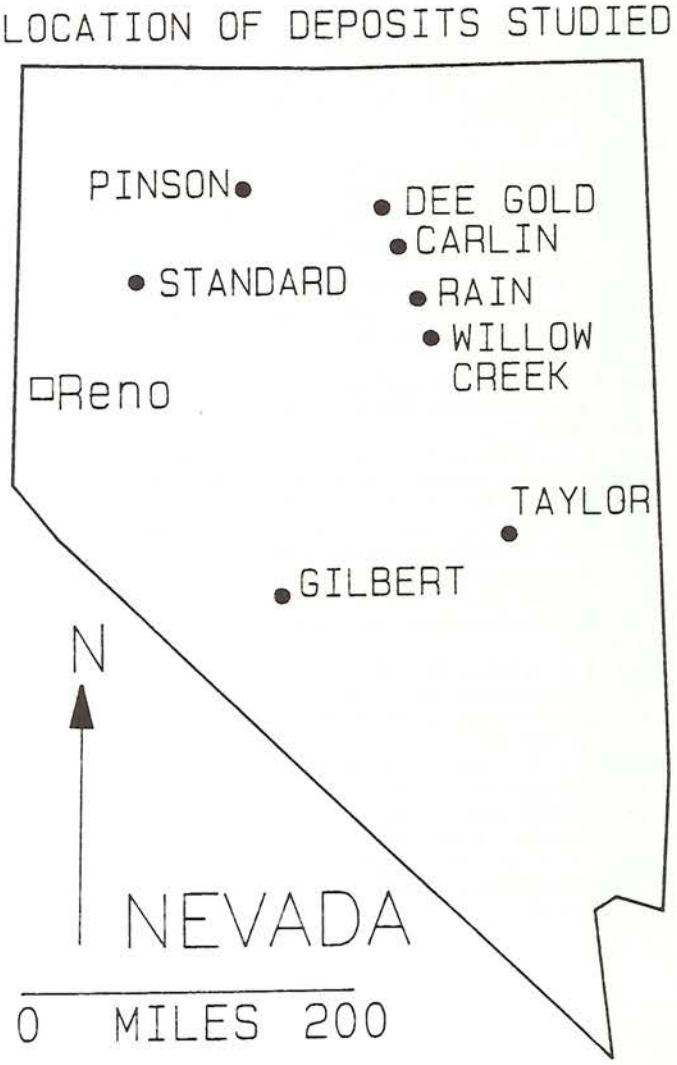

Fig. 1. Location of sediment-hosted, micron gold deposits included in this study.

and two deposits undergoing development at the time (Rain and Dee). Jasperoid known to be associated with mineralization was also collected from the old Standard Mine, a gold producer in the 1940's, as well as from the Taylor mining district, which produced Ag intermittently from 1872 to 1982. Jasperoid potentially associated with mineralization was collected at the Gilbert property. Barren jasperoid was collected from the upper plate at Carlin and Dee, and at the Willow Creek locality. For further information on the sample distribution and geology of these localities, please consult Haynes (1984) and Radtke (1985).

SAMPLE PREPARATION AND ANALYSIS

Gas analyses were performed on samples of jasperoid that were pulverized to −18+60 mesh, a size fraction that was determined to yield the largest amount of gases. Prior to analysis, this material was boiled in aqua regia for 40 to 60 minutes to remove carbonate and sulfide minerals, rinsed thoroughly with distilled, deionized water, and dried at 100°C. The cooled material was then soaked in acetonitrile (CH_3CN) for two days to remove any foreign organic material, and the rinsing and drying were repeated. For actual inclusion gas analyses, 1 g of this pulverized, cleaned jasperoid was placed in a Vycor glass tube and heated at 110°C in a stream of He for 10 minutes to remove adsorbed water. The Vycor glass tube was then closed off and the sample was heated in an He atmosphere to 350°C (about 5 minutes) and left at this temperature for another 15 minutes. The gases in the Vycor glass tube were then switched into an He gas carrier stream and injected onto a 6-foot Chromosorb 102 (Supelco, Bellefonte, PA) column in a Tracor 560 gas chromatograph that was temperature programmed from room temperature to 80°C. Gases exiting this column were detected by a thermal conductivity detector (TCD), then passed through a cold trap at −78°C, and onto a second, 3-foot column of the same type, and finally back through the TCD (Smith et al., 1984; Haynes, 1984). Gases that were analyzed included H_2O, CO_2, CO, CH_4 and N_2 and results were reported as both gas yield (in micromoles/gram of sample) or mole percent (assuming that all important gas phases were analyzed).

Standardization for H_2O was obtained from dehydration of $BaCl_2 \cdot 2H_2O$ and a mixed gas standard from Scott Specialty Gases served for all other gases. Reproducibility of jasperoid analyses was ±15% for CO_2 and ±20% for H_2O, but about ±50% for the gases present in smaller amounts.

CHARACTERISTICS OF FLUID INCLUSIONS IN JASPEROID

A basic assumption of this study was that a sample of the fluid that formed the jasperoid was contained in the fluid inclusions and could be released for analysis by heating the jasperoid to the decrepitation temperature of these inclusions. Numerous polished plates of the jasperoids that we analyzed were examined for fluid inclusions that could be studied by conventional optical methods. Very few such inclusions were observed and none of them provided homogenization or freezing data, a common problem with jasperoid. Studies of fluid inclusions at Carlin, largely in coarser-grained material than we analyzed, have demonstrated the presence of H_2O-rich fluids with a range of salinities extending as high as about 17 equivalent wt.% NaCl, CO_2-rich fluids, and CH_4-rich fluids (Nash, 1972; Radtke et al., 1980; Kuehn and Gize, 1985; Pasteris et al., 1986). The relation of these fluid types to mineralization at Carlin is not yet clear, although at least some of the C-bearing fluids are thought to reflect the metagenesis of organic matter at near lithostatic conditions (Kuehn and Gize, 1985). A significantly larger addition of gas would probably come from the replacement of limestone and organic material by jasperoid, which would liberate CO_2 and possibly CO and N_2. Although the samples that we analyzed in this study probably contained a mixture of these different inclusion populations, we suspect that the gases that were analyzed came largely from H_2O-rich fluid inclusions, because these inclusions would decrepitate at lower temperatures than would the gas-rich CO_2 or CH_4-bearing inclusions (Roedder, 1984).

Further information on the type of fluid inclusions in the jasperoid was obtained by step-heat tests in which analyses were made on gases evolved from samples at 100° intervals between 100 and 800°C. Tests were also carried out on chert to test the possibility that the gases released by heating the jasperoid came from atomic-scale interstitial sites along grain boundaries rather than from typical fluid inclusions. Thermogravimetric analysis (TGA) to 1000°C performed on several jasperoid and chert samples showed generally similar weight loss patterns, with essentially no loss above 800°C. Similar results for flint and diatomite have been reported by Weymouth and Williamson (1951) and Knauth and Epstein (1982), respectively. Step heating tests to temperatures as high as 800°C showed that the CH_4+CO_2+CO/H_2O ratio of the evolved gases peaked at 300 to 400°C for most jasperoids, whereas it increased steadily with increasing temperature for most cherts. The H_2O yield for both jasperoid and chert also showed a strong peak between 500 and 700°C. We have interpreted these results to indicate that considerable grain boundary water is released from both chert and jasperoid during heating, but that an additional C-rich fluid is released by decrepitation of fluid inclusions in jasperoid between 300 and 400° and by opening of inclusions in jasperoid and release of grain boundary water in chert during the alpha-beta transition in quartz at about 573°C. The 300-400°C temperature of release of the C-rich fluid exceeds observed homogenization temperatures of fluid inclusions in jasperoids sufficiently to permit decrepitation of the inclusions (Leroy, 1979), and the elevated content of C in this fluid suggests that it has a different source from C-poor fluids released at other temperatures. Accordingly, a temperature of 350°C was used for decrepitation of all jasperoid samples analysed in this study.

RESULTS OF SURVEYS AROUND SEDIMENT-HOSTED, MICRON GOLD DEPOSITS

Absolute abundances and geochemical relations

The average total gas yield from the jasperoids included in this study was about 20 micrograms/gram of sample (Table 1).

Table 1. Summary of gas compositions in jasperoid from sediment-hosted, micron gold deposits and barren systems in Nevada. Analytical data on individual samples can be found in Haynes (1984).

Name of Area	H_2O Avg.	Range	CO_2 Avg.	Range	CO Avg.	Range	N_2 Avg.	Range	Number of Samples Containing Detectable CH_4
Gas Yield in Micromoles/Gram of Sample									
Pinson	35.3	15- 71	0.43	0.20-0.90	0.27	0.03-1.40	0.25	0.08-0.53	0 of 23 samples
Dee	25.0	9-125	0.27	0.04-2.10	0.09	0.00-0.28	0.17	0.00-0.46	15 of 35 samples
Standard	14.1	3- 31	0.33	0.06-1.00	0.04	0.01-0.07	0.13	0.02-0.32	1 of 35 samples
Willow Creek	16.5	2- 35	0.20	0.04-0.36	0.04	0.02-0.10	0.11	0.05-0.22	0 of 9 samples
Carlin	24.0	4-100	0.65	0.10-2.20	0.08	0.02-0.20	0.09	0.03-0.55	2 of 22 samples
Rain	12.3	2- 40	0.36	0.07-0.85	0.05	0.01-0.09	0.22	0.10-0.56	0 of 12 samples
Gilbert	11.7	3- 83	0.16	0.03-0.60	0.03	0.01-0.06	0.13	0.06-0.45	3 of 32 samples
Taylor	13.7	2- 35	0.60	0.00-1.60	0.07	0.01-0.18	0.21	0.06-0.40	1 of 17 samples

Mole Percent									Jasperoid Hosting Unit	Age of Unit
Pinson	97.2	93- 99	1.35	0.4- 2.6	0.71	0.02-2.50	0.76	0.20-2.50	Comus	Ordovician
Dee	98.0	94- 99	1.02	0.1- 4.1	0.39	0.00-1.00	0.64	0.00-1.40	Popovich	Devonian
Standard	96.0	90- 99	2.63	0.7- 7.6	0.33	0.14-1.30	1.07	0.20-3.70	Prida/Natchez Pass	Triassic
Willow Creek	97.3	94- 98	1.42	0.9- 2.3	0.36	0.16-0.95	0.93	0.50-2.20	Nevada/Devils Gate	Devonian
Carlin	95.5	76- 99	3.72	0.4-20.0	0.47	0.20-1.80	0.41	0.00-1.20	Roberts Mtn/Popovich	Devonian
Rain	94.4	91- 97	2.89	1.2- 5.9	0.53	0.10-1.50	2.26	1.00-5.50	Webb	Mississippian
Gilbert	95.8	87- 99	1.90	0.2- 3.6	1.79	0.06-1.00	0.44	0.20-4.30	Palmetto	Ordovician
Taylor	93.4	84- 98	4.41	0.0-14.1	0.61	0.10-1.00	1.54	0.25-3.90	various	Dev/Perm

	H_2O-CO_2-CO Ternary			H_2O-(CO_2 + CO)-N_2 Ternary			CO_2-CO-N_2 Ternary		
	H_2O	CO_2	CO	H_2O	CO_2 + CO	N_2	CO_2	CO	N_2
Pinson	0.979	0.014	0.007	0.972	0.021	0.008	0.479	0.252	0.270
Dee	0.986	0.010	0.004	0.980	0.014	0.006	0.498	0.190	0.312
Standard	0.970	0.027	0.003	0.960	0.030	0.011	0.653	0.082	0.266
Willow Creek	0.982	0.014	0.004	0.973	0.018	0.009	0.524	0.133	0.343
Carlin	0.958	0.037	0.005	0.954	0.042	0.004	0.809	0.102	0.089
Rain	0.965	0.030	0.005	0.943	0.034	0.023	0.509	0.093	0.398
Gilbert	0.963	0.019	0.018	0.959	0.037	0.004	0.460	0.433	0.107
Taylor									

This amount of fluid could be produced from fluid inclusions making up about 0.01 volume percent of the sample, slightly less than the volume of fluid inclusions in average crystals estimated by Roedder (1979). H_2O makes up at least 90 mole percent of most gas samples, with CO_2 comprising most of the remainder. CO and N_2 rarely exceed 3 mole percent of the gas and are commonly lower than 1 mole percent. Other gases, particularly CH_4, C_2H_4 and H_2S, were present in the fluid inclusions at levels of 0.001 to 0.1 mole percent, although these gases were not detected in enough samples to test their usefulness as exploration guides.

Thermodynamic calculations show that CO_2 and CO in these fluids are not in equilibrium with one another at temperatures of less than about 500°C, which are geologically unreasonable. CO_2 and CH_4 do appear to be in equilibrium, however, and indicate an fO_2 of approximately 10^{-35} for the jasperoid-forming fluid (if our analyses represent a single fluid). Recalculation of the C-H-O-N gas equilibria assuming constant total C, O and N, equilibrium with graphite, and an open system with respect to H_2 indicates equilibrium at temperatures of 270 to 290°C and an increase in the fraction of H in the C-O-H-N gases. A possible explanation for this result is the former presence of NH_3, possibly derived from decomposition of organic material, that has oxidized to N_2 with accompanying diffusive loss of H_2 (Haynes et al., 1984; Smith et al., 1984).

The inclusion gas compositions exhibit significant differences between deposits. For instance, the total gas yield from fluid inclusions was much higher for the Carlin, Pinson and Dee properties than for the other properties (Table 1). This group includes all important deposits in the survey group except Rain. CH_4 was detected in a larger proportion of samples at Dee than at any other location, and appears to decrease along the trend that extends southwest from Dee, through Carlin, to Rain and Willow Creek (Fig. 1). Mole percent N_2 is unusually high at Rain, but there is not a close correlation between deposit size and N_2 abundance for all deposits.

Barren versus mineralized jasperoid

In an effort to determine whether gas analyses could be used to distinguish jasperoid samples from mineralized and barren areas, we compared the data for 34 ore and 31 barren samples that could be assigned to their respective populations with a high level of confidence. The ore group included samples from Pinson, Dee and Carlin, and the barren group included samples from the upper plate at Dee and Carlin, as well as barren material from Willow Creek and Gilbert. As can be seen in Table 2, yields of all gases are greater for the ore samples. Most of the increased gas yield is due to CO and N_2 (Fig. 2). Approximately 70% of the barren jasperoids yield 0.04 micromoles/gm CO or less, in contrast to about 10% of the ore samples. Similarly, about 25% of the ore-related jasperoids have N_2 yields greater than 0.03 micromoles/gm, whereas none of the barren jasperoids exceed this value.

Table 2. Summary of gas compositions in jasperoid from barren and mineralized jasperoid. See Haynes (1984) for complete data.

Type of Jasperoid	H_2O Avg.	Range	CO_2 Avg.	Range	CO Avg.	Range	N_2 Avg.	Range
Gas Yield in Micromoles/Gram of Sample								
Mineralized	29.7	7-71	0.37	0.06-1.53	0.18	0.03-1.42	0.19	0.02-0.53
Barren	17.4	3-61	0.19	0.04-0.74	0.04	0.01-0.13	0.10	0.03-0.28
Mole Percent								
Mineralized	97.3	86-99	1.56	0.42-12.4	0.58	0.02-2.51	0.64	0.10-2.08
Barren	97.5	92-99	1.27	0.31- 4.1	0.32	0.08-0.95	0.99	0.13-4.12

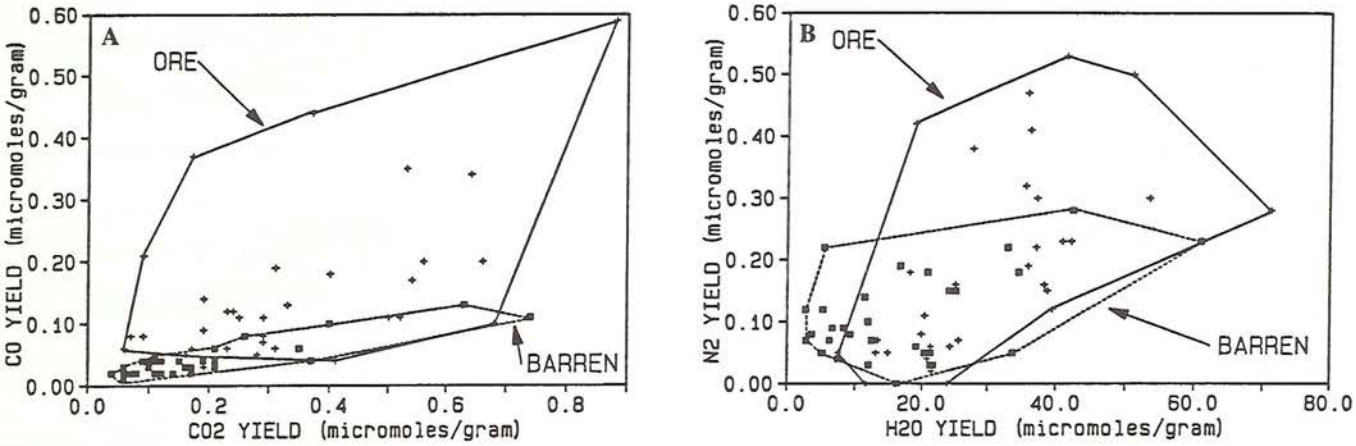

Fig. 2A. Relation between CO_2 and CO yields from ore and barren jasperoid populations discussed in the text showing that ore jasperoids contain significantly more CO. 2B. Relation between H_2O and N_2 yields for ore and barren jasperoids showing that ore jasperoids contain more N_2.

The increased gas yield from ore-related jasperoids probably reflects the more intense hydrothermal activity in the ore zones and the resulting higher probability of trapping more fluid inclusions. As noted earlier, the increased level of CO and N_2 could be due to post-entrapment compositional changes operating on inclusion gases resulting from replacement of limestone and organic material.

Zoning of fluid inclusion gas compositions in individual deposits

Tests for zoning in individual deposits were hampered by the distribution of jasperoid outcrops and intersections in drill holes with respect to mineralization, which caused coverage to differ in its extent and completeness. At Pinson, for instance, we were able to obtain a set of samples along a longitudinal section through mineralization at the A-zone, but which did not extend far beyond mineralization. Similar but less detailed coverage was obtained at Rain. The samples from Dee, Carlin and Standard covered larger areas, but included jasperoids from upper and lower plate sites, making direct comparison of all values difficult.

Patterns are evident in several deposits, however. The section through the Pinson A-zone (Fig. 3) shows well defined lows in gas yields for all gases coinciding with the central part of the mineralized zone in this section. Mole percent values show a high for H_2O over the central zone and lows for CO_2, CO and N_2. The limited sample coverage at Rain indicated a generally similar pattern with relatively low mole percent CO_2 values at the center of the linear mineralized zone (Haynes, 1984). Jasperoid beyond the ore zone at Rain yielded even less CO_2 than the central ore-related jasperoid. Samples from the Dee mineralized zone could not be plotted on a single map or section, but were divided into those from above, below and within the ore zone (Fig. 4). Although there is significant overlap among the three populations, there appears to be an increase in both CO and N_2 contents of the inclusion gases upward from the below ore, through the ore, to the above ore populations. Note, also, that both gas yields and mole fraction values for all samples from within and around the ore zone are higher than samples from jasperoids from the upper plate in the Dee area (Fig. 4).

Regional variations at Carlin are depicted in Fig. 5, which shows that upper plate (Vinini Formation) jasperoids have much lower CO_2, CO and N_2 yields, and lower mole fractions of CO_2 and CO, than lower plate (Roberts Mountain Formation) jasperoids. Within the lower plate itself, jasperoids in the ore zone show highest mole fraction H_2O and slightly depleted CO_2 and CO yields. The pattern at Standard (Fig. 6) shows high H_2O yields and mole percent around the ore zones and in a mineralized zone on the west side of the property (Ronkos, 1986). CO_2 values, either as gas yield or as mole percent, are lowest in and around the pits in the Standard area, and CO and N_2 values vary. At the Gilbert prospect insufficient data were available at the time of our survey to delineate any central mineralized zone. Nevertheless, elevated yields of H_2O, CO_2

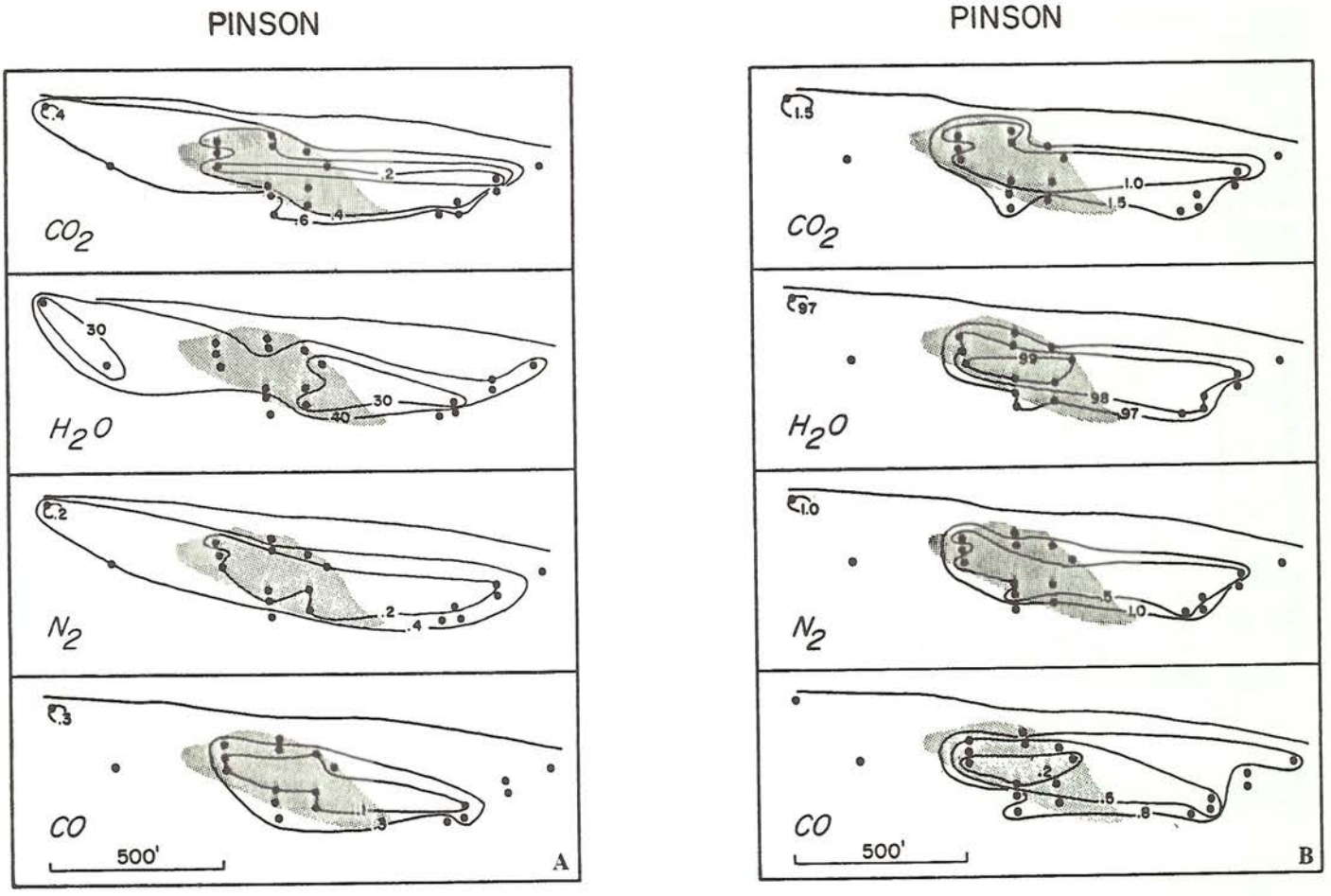

Fig. 3A. Absolute yields of CO_2, H_2O, N_2 and CO (in micromoles/gram) from the Pinson A-zone orebody. Central high-grade ore zone (stippled) and trace of original surface are shown for reference. 3B. Mole percent gas compositions from jasperoids in the Pinson A-zone.

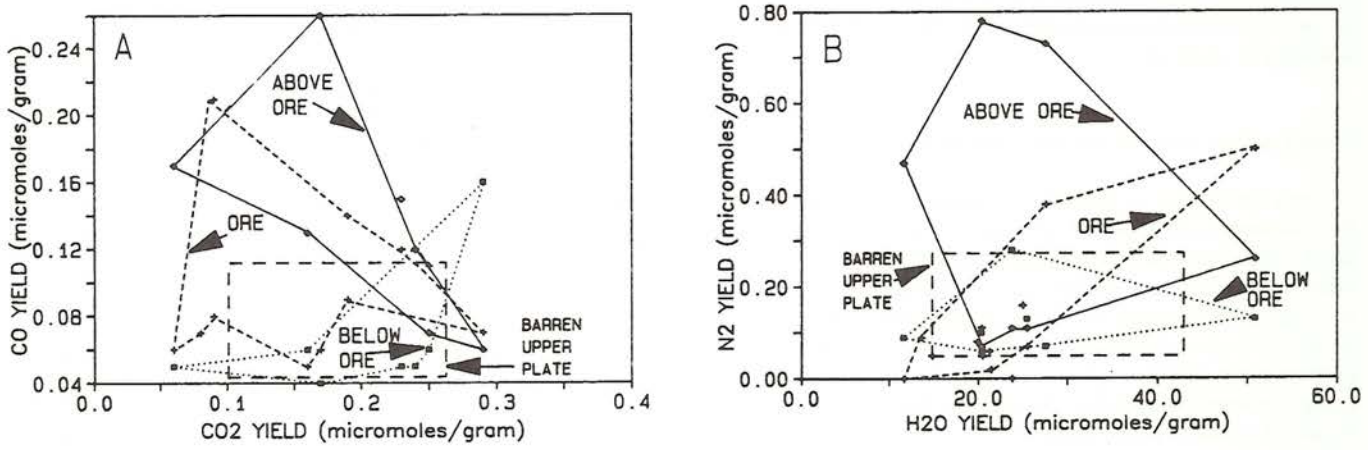

Fig. 4. Gas yield plots for samples from ore, above ore and below ore in the lower plate Popovich Formation at the Dee deposit. Compositional range for barren jasperoid samples from the upper plate is shown in each diagram by the rectangle.

and CO were observed in the central part of the area (Haynes, 1984).

The only other area for which regional variations in inclusion gas composition were related to mineralization was the Taylor mining district (Fig. 7). In a study of jasperoid in the Taylor district, Lovering and Heyl (1974), showed that the color, grain size of matrix quartz, number of vugs and Cu/Cr ratio in jasperoid increased toward the center of mineralization. Our sample coverage was limited to the southeast part of the area (Fig. 7) due to access problems, but even these samples

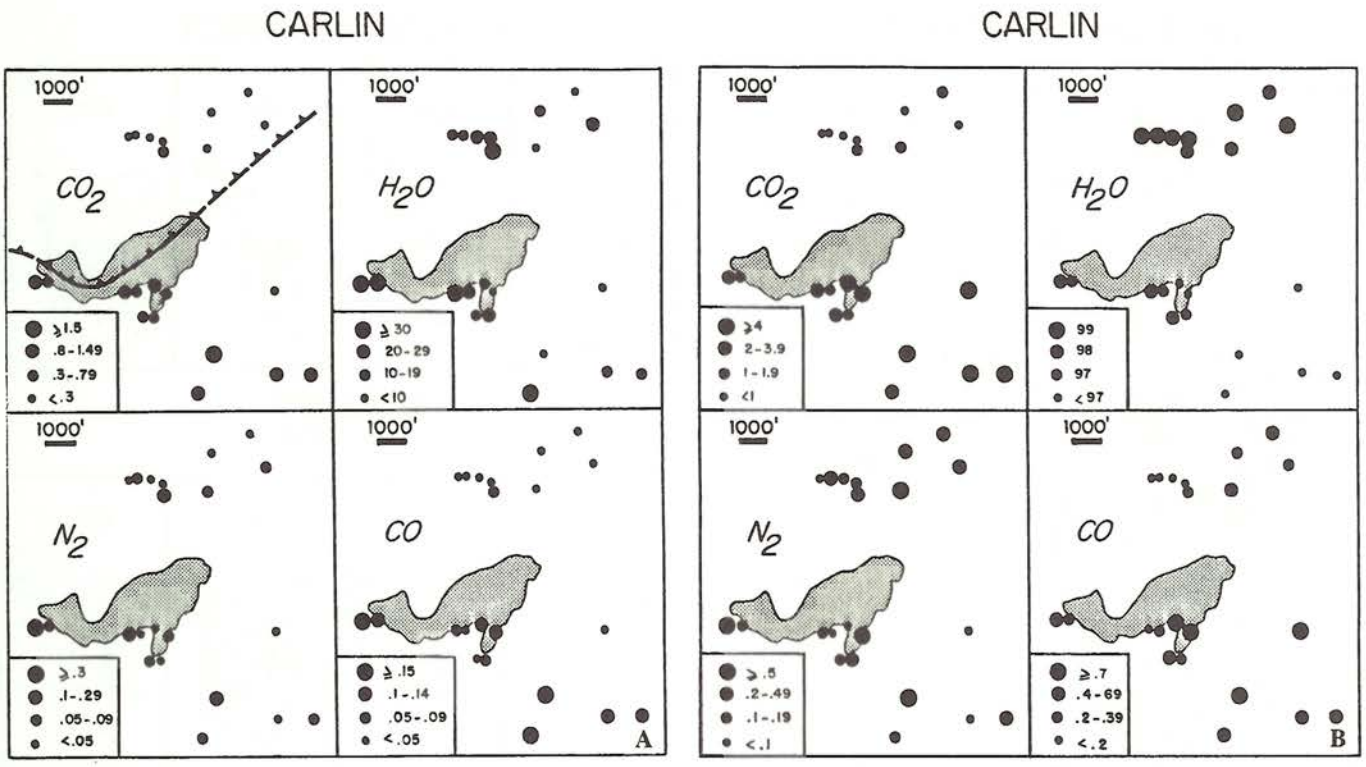

Fig. 5A. Absolute yields of CO_2, H_2O, N_2 and CO (in micromoles/gram of sample) for jasperoids in the Carlin area. Pit area and approximate trace of thrust fault are shown for reference. Note that this map covers a considerably larger area than that shown in Fig. 4. 5B. Mole percent gas compositions from jasperoids in the Carlin area.

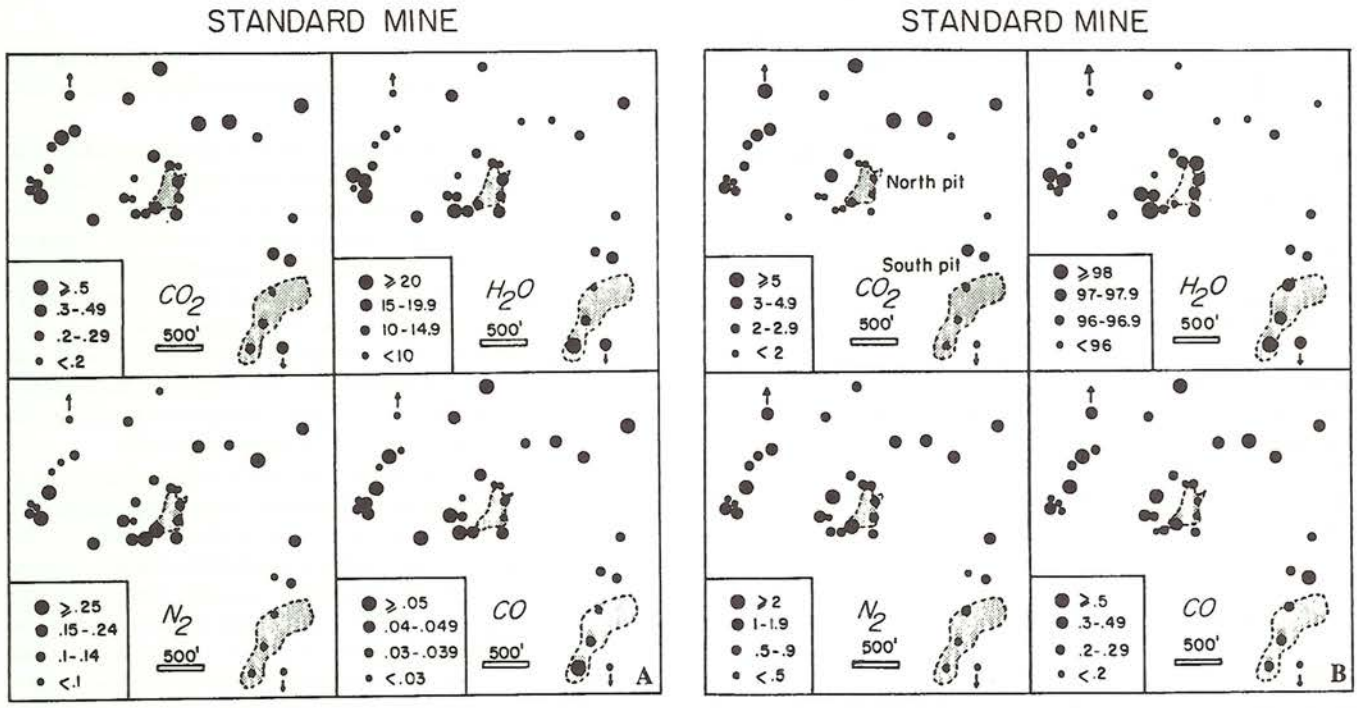

Fig. 6A. Absolute yields of CO_2, H_2O, N_2 and CO (in micromoles/gram of sample) for jasperoids in the Standard mine area. Outlines of the north and south pits are shown for reference. 6B. Mole percent gas compositions from jasperoids in the Standard mine area. The high values on the western edge of the map area are not known to be related to mineralization.

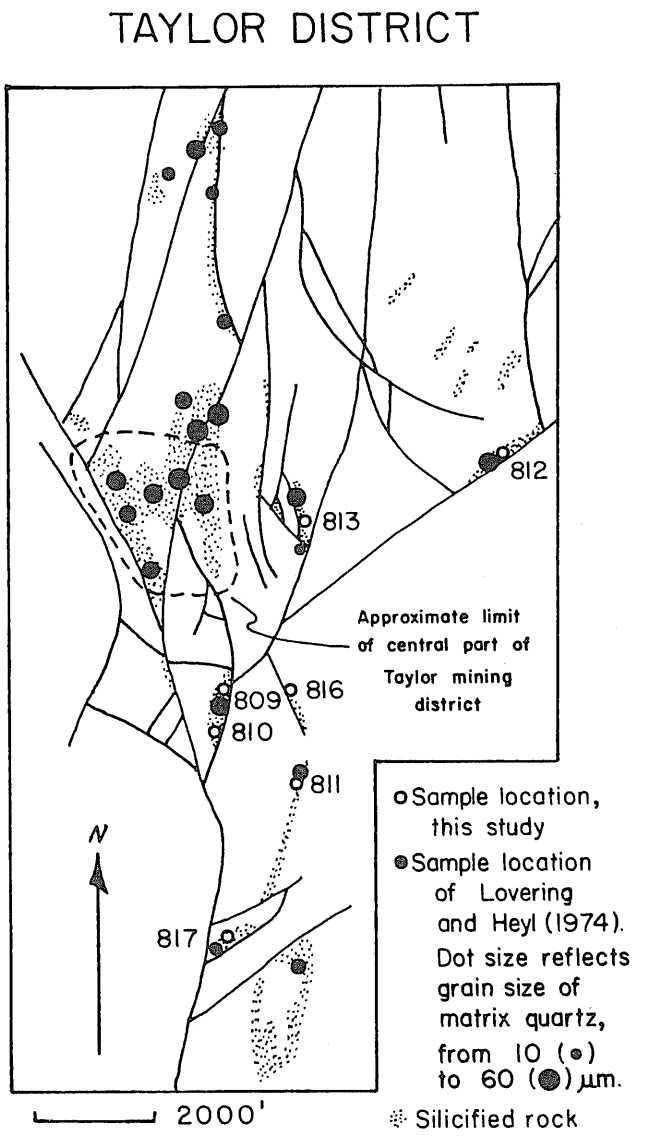

Fig. 7. Taylor mining district showing sample locations for the Lovering and Heyl (1974) study and for this study. Also shown are the location of the central part of the district and the variation of grain size of jasperoid (from Lovering and Heyl, 1974).

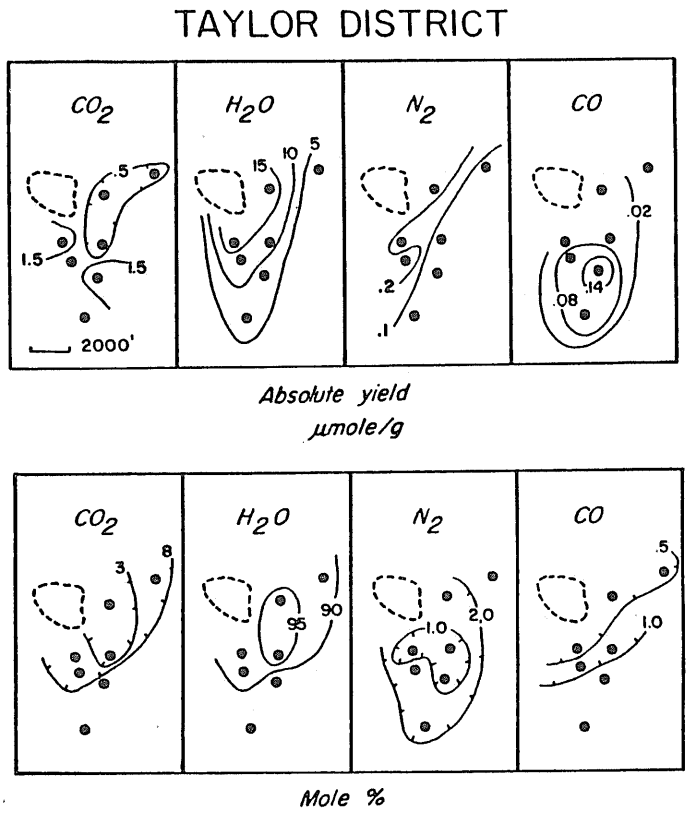

Fig. 8. Composition of gases released from jasperoid samples in the Taylor mining district. Outline of central part of the district is shown for reference to Fig. 7.

show that systematic variations exist in the gas chemistry. As can be seen in Fig. 8, the best patterns are shown by H_2O yield and mole fraction H_2O, both of which are high near the center of the district. The pattern for most other gases is difficult to interpret, but appears to indicate peripheral highs and central lows.

CONCLUSIONS AND APPLICATION TO EXPLORATION

The results of our analyses of fluid inclusion gases in sediment-hosted micron gold deposits indicate that:

1) fluid inclusion gases in jasperoid related to mineralization are characterized by elevated CO and N_2 values with respect to jasperoid in barren systems, and

2) within individual deposits, CO_2, CO, and N_2 values are commonly low relative to the peripheral part of the hydrothermal system.

The first of these observations agrees with the prediction that gases generated by water-rock reactions would be more abundant in these hydrothermal systems than in barren jasperoids. The second observation, which was not predicted, suggests that the central part of the mineralized hydrothermal systems is more permeable than peripheral parts and is flushed more effectively of newly generated gases during mineralization. Such a process would enhance jasperoid formation and possibly ore deposition because accumulation of these gases in the mineralizing fluid would limit the progress of reactions involving the replacement of carbonate rock by silica (jasperoid).

The most reliable application of these results appears to be in distinguishing potentially mineralized from barren jasperoids in newly discovered areas. Even here however, the barren and mineralized populations exhibit considerable overlap. Zoning patterns seen in individual deposits, although fairly consistent with low central $CO_2 \pm CO$, are also not robust enough to be used in early stages of exploration. Thus, it appears that fluid inclusion gas analysis of jasperoid cannot be used as a first-order guide to exploration for sediment-hosted micron gold deposits, although they might prove useful in conjunction with other lithogeochemical methods in efforts to delineate centers of mineralization within areas of widespread alteration.

Acknowledgements — We are grateful to the Anaconda Minerals Company for support for this study and former Anaconda employees, Allan Ried, Jay Raney, Anthony Kuhn and Mark Zdepski for the insights and geologic information that they provided during this work. We are grateful to Cordex Exploration and Newmont Mining Co. for permitting access to their properties and to Cordex geologists Andrew Wallace, Charles Ronkos, Ray Wittkopp and Frank Bergwall and Newmont geologists Charles Eckberg and Gale Knutsen for valuable guidance in sampling of their deposits. Further field assistance was provided by Thomas Schnorr and Harry Stokely. Assistance with fluid inclusion analyses was provided by T. J. Smith, and insights into the chemistry of the systems was gained from discussions with P. L. Cloke and R. E. Beane. The manuscript was improved by the efforts of two anonymous reviewers.

REFERENCES

Akright, R. L., Radtke, A. S. and Frimes, D. J., 1969, Minor elements as guides to gold in Roberts Mountain formation, Carlin gold mines, Eureka County, Nevada: Colo. Sch. Mines, Quarterly, v. 6, p. 49.66.

Bagby, W. C., Pickthorn, W. J., Goldfarb, R. and Hill, R. A., 1984, Application of rank rum analysis to soil geochemistry of the Dee gold mine, Elko County, Nevada (abs.): J. Geochem. Explor., v. 25, p. 245.

Birak, D. J. and Hawkins, R. J., 1985, The geology of the Enfield Bell mine and Jerritt Canyon district, Elko County, Nevada: U.S. Geol. Surv., Bull. 1646, p. 95-106.

Brooks, R. A. and Berger, B. R., 1978, Relationship of soil-mercury values to soil type and disseminated gold mineralization, Getchell Mine area, Humboldt County, Nevada, *in* Lovering, T. G. and McCarthy, J. H., Jr. (editors), Conceptual models in exploration geochemistry, the Basin and Range Province of the Western U.S. and Northern Mexico: J. Geochem. Explor., v. 9, p. 186-194.

Crone, W., Larson, L. T., Carpenter, R. H., Chao, T. T. and Sanzalone, R. F., 1984, A comparison of iron oxide-rich joint coating and rock chips as geochemical sampling media in exploration for disseminated gold deposits: J. Geochem. Explor., v. 20, p. 161-178.

Haynes, P. S., 1984, Application of fluid inclusion analysis of jasperoid to exploration for micron gold deposits: M.Sc. thesis, Univ. of Michigan, 91 p.

Jackson, D., 1982, Pinson gold: Eng. Min. J., v. 183, 8, p. 65-68.

Kuehn, C. A. and Gize, A. P., 1985, Textural and P-T-X characteristics of the hydrocarbon-bearing stages of the paragenesis at Carlin, NV: Geol. Soc. Am., Abstr. v. 17, no. 7, p. 635.

Leroy, J., 1970, Contribution à l'étalonnage de la pression interne des inclusions fluides lors de leur décrépitation: Bull. Mineral., v. 102, p. 584-593.

Lovering, T. G., 1972, Jasperoid in the United States — its characteristics, origin and significance: U.S. Geol. Surv., Prof, Pap. 710, 64 p.

Lovering, T. G. and Heyl, A. V., 1974, Jasperoid as a guide to mineralization in the Taylor mining district and vicinity near Ely, Nevada: Econ. Geol., v. 69, p. 48-58.

Nash, J. T., 1972, Fluid inclusion studies of some gold deposits in Nevada: U.S. Geol. Surv., Prof. Pap. 800-C: C15-C19.

Noble, L. L. and Radtke, A. S., 1978, Geology of the Carlin disseminated gold deposit, Nevada: Nev. Bur. Mines Geology., Rept. 32, p. 40-44.

O'Neil, J. R. and Bailey, G. B., 1979, Stable isotope investigation of gold-bearing jasperoid in the central Drum Mountains, Utah: Econ. Geol., v. 74, p. 852-859.

Pasteris, J. D., Kuehn, C. A. and Bodnar, R. J., 1986, Application of the laser Raman microprobe RAMANCORE U-1000 to hydrothermal ore deposits: Carlin as an example: Econ. Geol., v. 81, p. 915-930.

Radtke, A. S., Rye, R. O. and Dickson, F. W., 1980, Geology and stable isotope studies of the Carlin gold deposit, Nevada: Econ. Geol., v. 75, p. 641-672.

Radtke, A. S., 1985, Geology of the Carlin gold deposit, Nevada: U.S. Geological Survey Prof. Paper 1267, 124 p.

Roedder, E., 1979, Fluid inclusions as samples of ore fluids, *in* Barnes, H. L., Geochemistry of hydrothermal ore deposits, 2nd ed., Wiley-Interscience, New York, p. 684-737.

Ronkos, C. J., 1986, Geology and interpretation of geochemistry at the Standard mine, Humboldt County, Nevada: J. Geochem. Explor., v. 25, p. 129-138.

Schnorr, P. H., Kesler, S. E. and Cloke, P. L., 1984, Micron gold-associated jasperoid: fluid inclusion chemistry and geothermometry (abs.): J. Geochem. Explor., v. 25, p. 247.

Smith, T. J., Cloke, P. L. and Kesler, S. E., 1984, Geochemistry of fluid inclusions from the McIntyre-Hollinger gold deposit, Timmins, Ontario, Canada: Econ. Geol., v. 79, p. 1265-1285.

Wargo, J. G. and Powers, H. A., 1978, Disseminated gold in Saddle Prospect, Lander County, Nevada *in* Lovering, T. G. and McCarthy, J. H., Jr. (editors), Conceptual models in exploration geochemistry, the Basin and Range province of the western U.S. and northern Mexico: J. Geochem. Explor., v. 9, p. 186-194.

Fluid Inclusion Constraints on the Genesis of the Alaska-Juneau Gold Deposit

D. L. LEACH, R. J. GOLDFARB AND T. D. LIGHT
U.S. Geological Survey, P.O. Box 25046, MS 912, Denver, Colorado 80225, U.S.A.

Abstract — The largest lode-gold deposit in Alaska, the Alaska-Juneau deposit, lies along the western flank of the Coast Range batholith and near the center of the 200 km long Juneau gold belt. The Alaska-Juneau ore bodies are confined to a 5.5 km long by 100 m wide zone of intense quartz veining hosted by phyllite and slate. The productive lodes are spatially associated with small, strongly altered greenstone and metagabbro bodies within the metasedimentary rocks.

Microthermometric and Raman spectrographic analysis of fluid inclusions in the vein quartz show the ore forming fluid can be characterized by the H_2O-CO_2-NaCl ($\pm N_2$, CH_4) system. These hydrothermal fluids are believed to have originated during deep-seated prograde metamorphism and to have migrated upward along major structural zones. Ore was deposited from a boiling system at temperatures in excess of 200°C, pressures of at least 1.5 kb, depths of at least 5 km, and was accompanied by intense hydrofracturing of the host rocks. Loss of volatiles during boiling produced dramatic shifts in oxygen and sulfur fugacity and pH, and resulted in ore deposition.

INTRODUCTION

THE JUNEAU gold belt extends for approximately 200 km (Fig. 1) along the southwestern flank of the Coast Range batholith in southeastern Alaska. All of the deposits within the belt lie within 5 km of a prominent linear depression termed the Coast Range megalineament by Brew and Ford (1978). (Also referred to as the Work Channel lineament in British Columbia by Crawford and Hollister, 1982.) From northwest to southeast the gold districts include Berners Bay, Eagle River, Juneau, and Windham Bay, and are hosted in slate, phyllite, diorite, and greenstone.

The Alaska-Juneau and Treadwell systems (Fig.2) within the Juneau district are the most significant deposits along the gold belt. These two systems lie about 6 km apart, on opposite sides of the Coast Range megalineament, near the city of Juneau. Together they have produced about 75 percent of Alaska's total lode gold. Alaska-Juneau produced 3.52 million ounces of gold (Bundtzen et al., 1984), plus 2 million ounces of silver and 40 million pounds of lead (Twenhofel, 1952), from 88.5 million tons of ore between 1893 and 1944. An additional 2.9 million ounces of gold was recovered at Treadwell between 1885 and 1922 (Bundtzen et al., 1984). Combined production from the other mines within the gold belt was slightly less than 150,000 ounces of gold.

Spencer (1906), Wayland (1939, 1960), and Twenhofel (1952) provide detailed descriptions of the geology of the Alaska-Juneau system. The geological setting, vein mineralogy, and intense carbonate alteration halos at Alaska-Juneau are similar to the California Mother Lode, which historically led workers to suggest that the Alaska-Juneau deposit was a "Mother Lode" type system. This study represents an initial fluid inclusion investigation to determine the nature of the ore fluids and the environment of ore deposition at the Alaska-Juneau deposit.

REGIONAL GEOLOGY

Southeastern Alaska is composed of a number of discrete tectonostratigraphic terranes (Fig. 1) accreted onto the North American craton mainly within Cretaceous and Tertiary time. Much of this region consists of the Alexander, Wrangellia, and

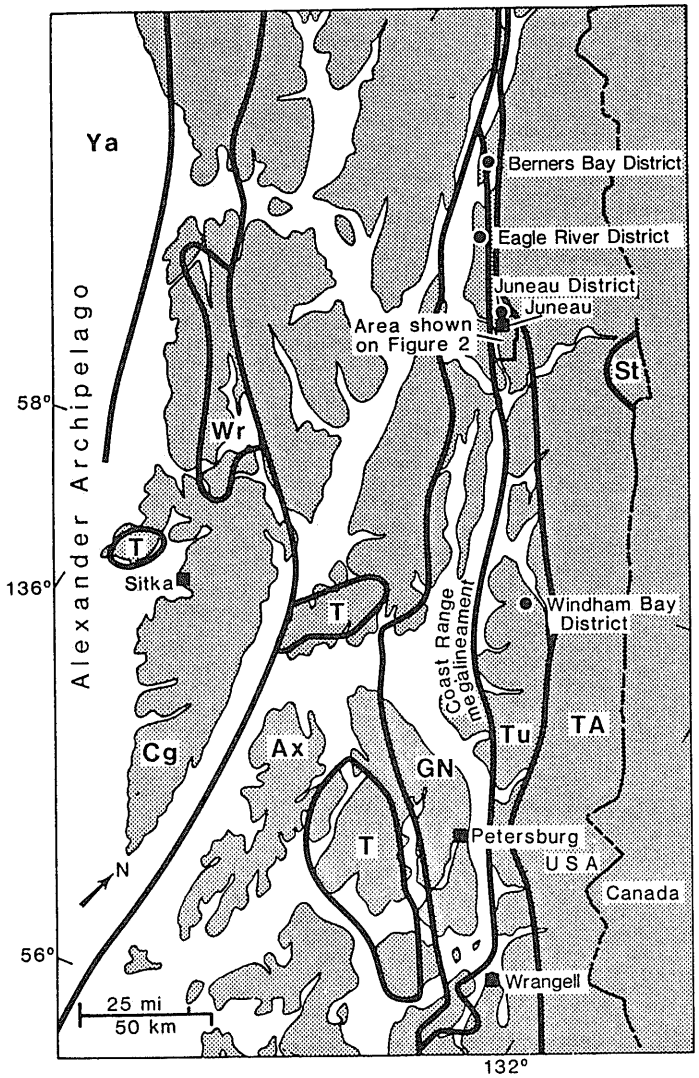

Fig. 1. Generalized tectonostratigraphic terrane map of southeastern Alaska. Terranes as follows: Ax-Alexander, Cg-Chugach, GN-Gravina-Nutzotin, St-Stikinia, T-Tertiary cover, TA-Tracy Arm, Tu-Taku, Wr-Wrangellia, Ya-Yakutat. Generalized from Silberling and Jones (1984). Major gold districts of the Alaska gold belt include Eagle River, Berners Bay, Juneau, and Windham Bay.

Gravina-Nutzotin terranes that were amalgamated into Greater Wrangellia by the Late Jurassic and accreted in the Cretaceous (Coney and Jones, 1985). Alexander is dominated by Precambrian (?) and Paleozoic volcanic and metasedimentary sequences, and Mesozoic volcanics, limestones, and clastic units. Wrangellia contains Upper Paleozoic island arc volcanic rocks, overlain by limestones, clastics, cherts, and Mesozoic basalts. Gravina-Nutzotin represents a Late Jurassic to mid-Cretaceous flysch overlap assemblage between Wrangellia and Alexander (Silberling and Jones, 1984).

To the west, greywacke, argillite, and slate of the Chugach terrane were accreted onto and subducted below Greater Wrangellia during the Late Cretaceous and (or) Early Tertiary. To the east, Greater Wrangellia was accreted onto the Stikinian superterrane of Saleeby (1983), largely making up western British Columbia.

The Taku and Tracy Arm terranes, hosting the Treadwell and Alaska-Juneau deposits respectively, fill the suture between Greater Wrangellia and the Stikinian superterrane. Taku contains Permian marble, phyllite, and bimodal volcanics, and Triassic limestone, slate, and pillow basalt, all deformed between the two larger superterranes. Tracy Arm, immediately east of Taku, is dominantly composed of the Coast Range batholith, a Cretaceous to Eocene continental-margin or Andean-type magmatic arc (Barker and Arth, 1984), plus adjacent metasedimentary units. Coney and Jones (1985) hypothesize that Tracy Arm may represent either a separate tectonostratigraphic terrane, the deeper roots of the Stikinian superterrane, or just a simple metaplutonic overprint. Brew and Ford (1985a) suggest that both the Taku and Tracy Arm terranes are merely metamorphosed portions of the Alexander terrane.

Two important regional crustal structures, both trending northwest-southeast, are aligned with the Juneau gold belt. The 3 to 25 km wide tonalite sill belt of 60 to 70 Ma foliated intrusives, was emplaced along some kind of major structural discontinuity that extends across the length of southeastern Alaska (Brew and Ford, 1981; Brew and Ford 1985b). These biotite-hornblende tonalite bodies within the Tracy Arm terrane comprise one of the younger intrusive events associated with the development of the Coast Range batholith (Barker and Arth, 1984). In the Juneau region, the sill passes approximately 5 km to the east of the Alaska-Juneau ore bodies.

The Coast Range megalineament, running down the center of the gold belt, separates the Alaska-Juneau and Treadwell ore bodies, as well as the hypothesized Taku and Tracy Arm terranes. Brew and Ford (1978) have speculated the megalineament to be the prominent surface expression of the contact between the intrusives and associated high-grade metamorphic rocks of the Coast Range batholith complex with the lower-grade schists to the west. Crawford and Crawford (1986), studying the same structural feature in southernmost Alaska and adjacent British Columbia, suggest it to be a vertical shear zone separating rocks of contrasting thermal histories.

GEOLOGY OF THE ALASKA-JUNEAU DEPOSIT

The Alaska-Juneau ore bodies are hosted by the Perseverance slate, consisting largely of carbonaceous and graphitic phyllite and slate (Wayland, 1960) and lying between the Coast Range megalineament and the tonalite sill belt. The metasediments are believed to represent Lower Permian, Upper Triassic, and possibly Jura-Cretaceous fine-grained clastic units and interbedded tuffs or volcanogenic sediments (Brew and Ford, 1985c). The rocks, generally metamorphosed in the Late Cretaceous or earliest Tertiary to greenschist grades, lack any original sedimentary textures.

Small bodies of metagabbro (originally gabbro and (or) diorite) and greenstone (metamorphosed intermediate to mafic volcanic protoliths) occur throughout the phyllite and slate. These now schistose bodies have been largely metamorphosed to green hornblende-andesine-rich rocks (Wayland, 1960). All of the ore bodies at Alaska-Juneau are spatially associated with these intrusive and extrusive rocks; gold-bearing vein networks lie within the slate and phyllite near the metagabbro or greenstone especially where the metasediments are interfingered with these bodies. Most of the gold-bearing veins in the Alaska-Juneau deposit strike parallel to the long dimension of adjacent metagabbro or greenstone bodies, and crosscut bedding and cleavage. Extensive veining does not occur in the metasediments where there are no such intrusive or extrusive bodies or within the larger, isolated such bodies (Twenhofel, 1952).

The Alaska-Juneau lode system, discovered in 1880, consists of four main ore bodies. These include, from north to south, the Ebner mine, North ore body, South ore body, and Perseverance mine (Fig. 2). Over 85 percent of the gold production came from the North and South ore bodies (Twenhofel, 1952). The lode system consists of a dense network of veins 10 cm to 1 m wide and up to several tens to about 100 m in length. Similar quartz veins with roughly the same gold grades occur along the entire length of the Juneau gold belt; however, the high density of veining in the Juneau region led to its becoming the most productive portion of the belt (Twenhofel, 1952).

The dominant gangue mineral is quartz with subordinate amounts of ankerite. Sulfides comprise one to two percent of the vein (Twenhofel, 1952). Pyrrhotite, galena, and sphalerite are the most common sulfide minerals with local occurrences of pyrite, chalcopyrite, arsenopyrite, and tetrahedrite. Gold appears to be paragenetically late and commonly occurs as a replacement of ankerite or sulfides, especially sphalerite. Most, if not all, of the gold occurs as free gold, and the silver occurs within both gold and galena (Twenhofel, 1952).

Wall rocks adjacent to the gold-bearing veins are conspicuously altered to biotite- and ankerite-rich assemblages, especially within the metagabbros and greenstones. Alteration minerals in the slate include biotite, ankerite, muscovite, quartz, phlogopite, and rare albite and pyrrhotite. The intrusive and extrusive bodies have been extensively altered to minerals including biotite, ankerite, feldspar, pyrrhotite, chlorite, sericite, muscovite, and albite. Alteration reactions are consistent with an overall increase in K_2O and CO_2 (Spencer, 1906; Wayland, 1960).

The age of the Alaska-Juneau system is still unknown. Deformation and associated regional metamorphism occurred up until 60 Ma in the Juneau area (Brew and Ford, 1984). Since the veins at Alaska-Juneau cut the metamorphic foliation, gold mineralization must be at least post-Cretaceous. Several basal-

tic dikes within the Alaska-Juneau ore bodies offset a major east-west fault which in turn offsets the ore bodies (Twenhofel, 1952). Thus the gold mineralization is older than the dikes. While the dikes near Juneau have yet to be dated, possibly similar mafic dikes further south near Ketchikan, related to Cenozoic extensional tectonism throughout southeastern Alaska, are Late Oligocene to Early Miocene in age (Hudson et al., 1979).

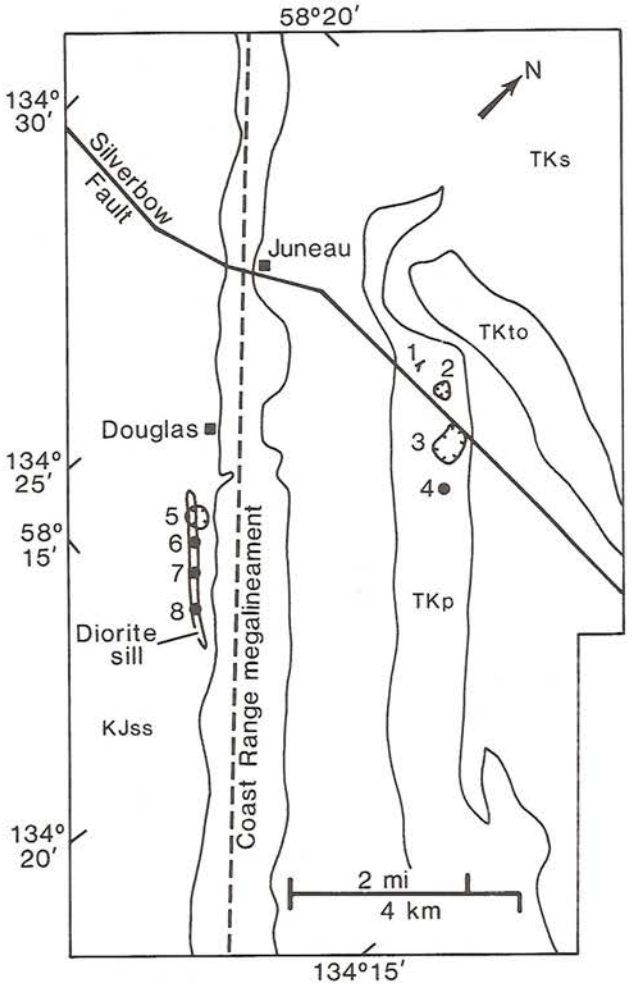

EXPLANATION

Rock units (after Brew and Ford, 1985c)

TKto	Tonolite sill
TKp	Perseverance Slate
TKs	Undivided schist
KJss	Cretaceous–Jurassic turbidites

Mines

1	Ebner
2	Alaska-Juneau North Pit
3	Alaska-Juneau South Pit
4	Perseverance
5	Treadwell
6	700 Foot
7	Mexican
8	Ready Bullion

Fig. 2. Location of the Alaska-Juneau and Treadwell systems.

FLUID INCLUSION INVESTIGATIONS

Samples of vein quartz containing sulfides and gold were collected from throughout the South ore body of the Alaska-Juneau deposit. Examination of numerous polished sections, believed to be representative of the main stage of gold deposition, showed similar fluid inclusion characteristics for veins from all sampled portions of the ore body. With the exception of one sample of sphalerite analyzed by mass spectrometry, all fluid inclusion studies were made on quartz closely associated with gold. Heating and freezing studies were made on a U.S. Geological Survey gas flow microscope stage (Werre et al., 1979). Accuracy of the measurements are within ±0.2°C in the range 0°C to −60°C and within ±5°C up to 400°C. In addition to microthermometry and mass spectrometry, volatiles in the fluid inclusions were analyzed with a laser Raman microprobe.

Most of the fluid inclusions studied were secondary or pseudosecondary in origin, trapped along fractures that subsequently healed (Fig. 3a). Inclusions that could be classified as primary with little ambiguity were rare. Isolated fluid inclusions trapped along growth imperfections in the quartz near sulfide grain boundaries are believed to be primary in origin. Near the base of many quartz crystals, a three-dimensional network of fluid inclusions can be found that may contain primary fluids trapped during rapid crystal growth (Fig. 3d). Although the majority of our data are from secondary and pseudosecondary inclusions, they are consistent with the few data from primary inclusions. Fluid inclusions in sphalerite have similar gas/liquid ratios to the inclusions in quartz; however, the dark color of the sphalerite prevented microthermometric studies. As discussed later, mass spectrometric analysis shows that the fluid inclusions in sphalerite have similar volatile compositions to those in quartz which strengthens our belief that fluids analyzed from within the quartz do characterize the ore fluids.

Gold presents a particularly difficult problem in that definitive petrographic evidence is absent to link any of the fluid inclusion data to gold deposition. As discussed earlier, gold was deposited late in the paragenesis in fractures within quartz and is closely associated with sulfides; therefore, it is likely that some of the secondary and pseudosecondary inclusion fluids contain samples of the gold depositing ore fluids. In addition, gold deposition was accompanied by intense carbonatization of the host rocks which is consistent with the high CO_2 content of the fluid inclusions in quartz.

Description of fluid inclusions

A remarkable feature of all samples studied is the wide variation of CO_2/H_2O ratios between different generations of fluid inclusions. Within a plane of inclusions, the CO_2/H_2O ratios are generally uniform (Fig. 3a, b, c, e, f). Some planes of fluid inclusions contain H_2O with no detectable CO_2 and other planes contain CO_2 with no optically visible H_2O (Fig. 3c). Most planes of inclusions contain mixed CO_2-H_2O fluids with uniform ratios (Fig. 3a, b, e, f). The healed fractures in the quartz have trapped fluids spanning the entire range of CO_2-H_2O compositions. The only temporal relationship that

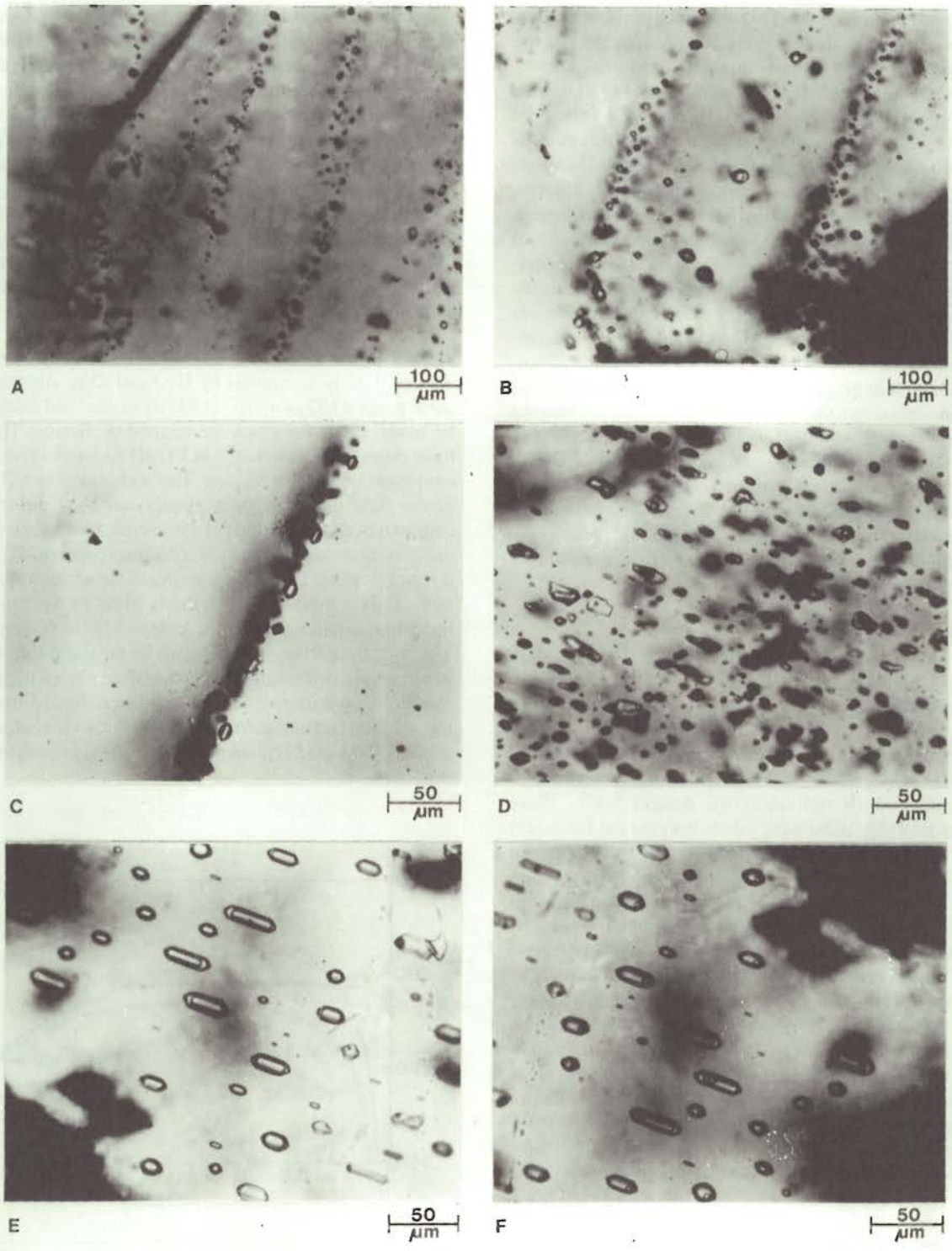

Fig. 3. Fluid inclusions in samples of quartz from the Alaska-Juneau deposit.
(A) Typical trails of secondary fluid inclusions in quartz.
(B) Trails of secondary fluid inclusions of mixed CO_2-H_2O liquids with uniform CO_2/H_2O ratios within each trail of inclusion.
(C) Trail of dense CO_2-rich fluid inclusions with no optically visible H_2O. Th(CO_2) is -13.4°C corresponding to a density of -1.0 gm/cm^3.
(D) A three-dimensional array of mixed CO_2-H_2O inclusions with highly variable CO_2/H_2O ratios. These inclusions, located at the base of a quartz crystal, are believed to have trapped a heterogeneous mixture of immiscible CO_2-rich and H_2O-rich fluids.
(E) Plane of secondary inclusions in quartz with about 85 vol % liquid CO_2 (~60 mole % CO_2) together with liquid H_2O, observed at 25°C.
(F) Plane of secondary inclusions as in (e) but observed at around 0°C: inclusions contain liquid H_2O and a small vapor bubble of CO_2 gas. Density of the liquid CO_2 is close to 0.9 gm/cm^3.

we have observed is that some H_2O-dominant fluid inclusions with the lowest homogenization temperatures appear to be the youngest fluids, possibly representing post-ore fluids.

The generally uniform CO_2/H_2O ratios in many planes of inclusions suggest the fractures in the quartz trapped a homogeneous fluid. However, the wide variation of the CO_2 content from plane to plane clearly indicates that the ore fluid experienced large volatile fluctuations. Although most planes of inclusions have uniform CO_2/H_2O ratios, some planes of inclusions have variable ratios. Some of the variability is certainly due to necking down of fluid inclusions after trapping. However, evidence for the presence of two immiscible fluids can be demonstrated in some healed fractures. For example, some fractures contain every conceivable CO_2/H_2O ratio in such an arrangement that would be difficult to account for by necking down. At the base of many quartz crystals, three dimensional arrays of fluid inclusions occur that are believed to have been trapped during rapid crystallization and which contain highly variable liquid ratios of heterogeneously trapped CO_2- and H_2O-rich fluids (Fig. 3d). The evidence for immiscibility in the CO_2-H_2O system together with the highly variable CO_2/H_2O ratios between planes of inclusions, clearly suggests that episodic phase separation (boiling) was a common phenomenon in the Alaska-Juneau ore deposit.

Microthermometry

Ice Temperatures: Melting of ice in H_2O-dominant (Table 1) inclusions range from -1.2°C to -6.5°C, corresponding to salinities of about 2 to 10 equivalent wt. percent NaCl. These salinities are probably maximum values because the formation of undetected gas clathrates may have occurred and removed H_2O from the residual fluid in the inclusion, giving erroneously low melting temperatures. In addition, the separation of immiscible CO_2- and H_2O-rich fluids during mineralization preferentially partitions the dissolved salts into the H_2O-rich fluid which will lead to erroneously high estimates of the salinity of the parent ore fluid. Although the actual salinity of the bulk ore fluid is uncertain, it is probably low, perhaps less than 5 equivalent wt. percent NaCl.

Melting of CO_2-clathrate: Clathrates were observed in some of the mixed CO_2-H_2O fluid inclusions (Table 1). The absence of clathrate melting at temperatures substantially below 10°C in CO_2-rich fluids is consistent with low salinities (Collins, 1979; Burruss, 1981). From the clathrate melting observed in our samples salinities are estimated to be less than 5 equivalent weight percent NaCl.

Melting temperatures of solid CO_2: The triple point of CO_2(-56.6°C) is depressed from a few tenths of a degree to as much as 4.5°C (Table 1), indicating the presence of other volatiles such as CH_4 or N_2.

Homogenization temperatures of CO_2-vapor with CO_2-liquid: CO_2 homogenizations to the liquid phase range in temperature from 25°C to -13.3°C (Table 1). The majority of the $T_h(CO_2)$ temperatures lie within the range of 5°C to 10°C, corresponding to densities near 0.9 gm/cm^3.

Homogenization temperatures of H_2O- and CO_2-rich fluid inclusions. The homogenization temperatures for both the H_2O-and CO_2-rich fluid inclusions (Table 1) are between 150°C and 295°C, with the majority in the 200°C to 270°C range. Many of the fluid inclusions were probably trapped above the solvus for their composition: therefore, some pressure correction of uncertain magnitude must be added to the observed homogenization temperatures to obtain true trapping temperatures. Many of the CO_2-rich fluid inclusions decrepitated prior to homogenization, indicating high internal pressures. We did not recognize any distinct correlation between the homogenization temperatures and the relative CO_2 content for the mixed CO_2-H_2O fluid inclusions.

Bulk fluid compositions: Microthermometry studies show the ore fluid is dominated by H_2O and CO_2. Estimates of the mole percent CO_2 (or H_2O, table 1) in the fluid inclusions can be made using the graphical method of Burruss (1981). We have observed a wide range in CO_2/H_2O ratios between different planes of fluid inclusions. The wide range of CO_2 contents in the fluid inclusions may simply represent the trapping of end-member compositions of immiscible fluids separated under different pressure-temperature conditions (see Fig. 4). However, it is not possible to precisely estimate the actual bulk composition of the unmixed parent fluid. Most of the studied fluid inclusions contain CO_2 in the range of 30 to 60 mole percent which, if trapped above the solvus of the ore fluid, may represent the bulk composition of the ore fluid during trapping. This range of CO_2 content is similar to those estimated from averaging all the fluid inclusions in the field of view of a group of mixed CO_2-H_2O inclusions that trapped a heterogenous fluid (Fig. 3d).

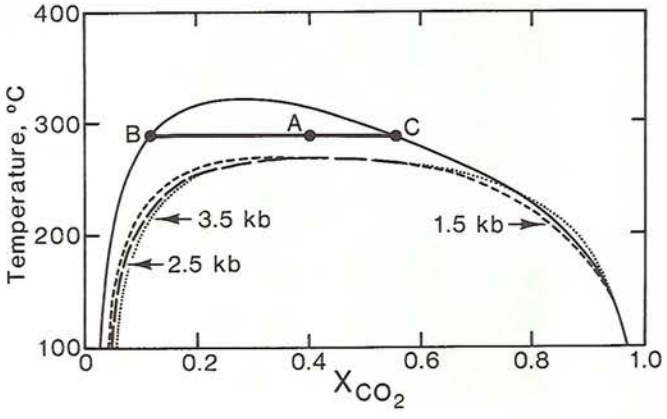

Fig. 4. Selected solvi in the CO_2-H_2O system at various pressures from Todheide and Franck (1963). Below the solvus, two immiscible fluids coexist and above the solvus, a single homogeneous fluid is present. The addition of salts and other volatiles such as N_2 greatly expands the two-phase field. At 290°C and pressures greater than 1.5 kb, a single homogeneous fluid with 40 mole percent CO_2 is present at point A. Reduction in the confining pressure to 0.5 kb results in fluid immiscibility with end member compositions at points B and C. Reduction in confining pressure on the fluid can be achieved by a variety of processes, including uplift and erosion, structural dilation of the fracture by tectonic activity and hydrofracturing.

Table 1. Melting and homogenization temperatures of mixed CO_2-H_2O inclusions from gold-bearing quartz veins

Sample No.	$Tm(CO_2)$[1]	$Tm(H_2O)$[2]	Tm(clathrate)[3]	$Th(CO_2)$[4]	Th(final)[5]	$X(H_2O)$[6]
AJ2a		-4.9			7	1.00
	-58.0			5.8		0.60
	-61.8			-13.3		0.56
	-57.2			8.7	175±25	0.49
	-59.4			7.8		0.40
	-58.1			17.2		0.07
				-6.7		0.04
AJ2b				-4.0	215[8]	0.37
				6.8	285	0.17
				-4.1		0.03
AJ4a	-58.2			6.5		0.02
	-57.8			9.6		0.04
	-58.6			-4.3		0.01
	-57.6		10.0	10.8		0.95
	-57.8			-12.4		0.63
	-57.3			-1.9		0.05
	-56.8		7.8			
			8.4	12.6		0.92
			8.5	13.9		0.77
AJ4b	-56.9			10.3		0.12
	-56.9		10.2	9.4		0.42
	-57.3			7.4	264[8]	0.20
	-56.7		8.5	10.3		0.49
					272	
AJ4c	-57.0			12.1	243[8]	0.21
		-1.2			145	1.00
		-6.5			171	1.00
		-6.2			158	1.00
				25.0	256	
					290	
					226	
					216	
					264	
					194	
AJ4d					250[8]	
				5.4		0.03
				15.8	220[8]	0.81
				4.6	295	0.17
				8.4	285	0.49
				6.2	235	0.19
				9.4	215[8]	0.91
				6.4	256	0.63
				5.0	224	0.92
				5.1	264[8]	0.88
AJ6a	-57.1			15.5		0.01
	-57.0			15.4		0.02
	-57.4		9.6	17.0		0.52
	-57.4		9.5	17.6		0.38
	-57.4		9.5	17.2		0.41
		-1.3				1.00
	-57.6			20.0		0.01

[1]$Tm(CO_2)$, melting temperature of solid CO_2.
[2]$Tm(H_2O)$, melting temperature of solid H_2O.
[3]Tm(clathrate), melting temperature of clathrate.
[4]$Th(CO_2)$, homogenization of CO_2 liquid with CO_2 gas.
[5]Th(final), final liquid-liquid homogenization.
[6]Mole fraction H_2O, calculated using graphical method of Burruss (1981).
[7]All inclusions within section homogenized between 150°C and 200°C.
[8]Tempertures of decrepitation prior to homogenization.

Mass spectrometry and Raman spectroscopy

A high-performance quadrupole mass spectrometer system (Landis, 1985) was used to analyze the composition of gases in the fluid inclusions. Table 2 shows the analytical results for volatiles, excluding water, extracted from approximately 200 mg samples of quartz and sphalerite. Gases trapped within both samples are dominated by CO_2, with N_2 and CH_4 being minor components. Data from just two samples are not adequate to define a representative bulk composition; however, the similar data from quartz and sphalerite support our belief that the fluid inclusions in the quartz samples represent the ore fluid.

A laser Raman microprobe was used to obtain semiquantitative data on the relative volatile contents of individual inclusions. Randomly selected fluid inclusions from different planes of inclusions showed small variations in the relative proportions of CO_2, N_2, and CH_4. In all the analyzed fluid inclusions, the volatiles, excluding water, consisted of about 95 to 98 mole percent CO_2, 2 to 3 mole percent N_2, and less than 1 mole percent CH_4.

Table 2. Mole percent volatiles without water, determined by mass spectrometry

	CO_2	N_2	CH_4
Quartz	97	1.5	1.5
Sphalerite	90	6.5	3.5

Pressure and temperature conditions of ore disposition

Petrographic evidence for the coexistence of immiscible CO_2-and H_2O-rich fluids, documented for several samples, provides some constraints on the pressure of ore deposition. The pressure estimates are limited by our uncertainty of the bulk composition of the ore fluid and the paucity of high temperature-pressure experimental data for the complex fluids. As discussed earlier, the highly variable CO_2/H_2O ratios between different planes of fluid inclusions may represent trapping above the solvus of an ore fluid with variable volatile contents or they may be end-member compositions of unmixed CO_2-H_2O fluids. In any case, estimates of minimum trapping conditions can be obtained from the phase relations at 25°C using calculated phase ratios for the pure CO_2-H_2O system from Bodnar (1982; *in* Roedder, p. 288). Bodnar's diagram for a fluid with 40 mole percent CO_2 (Fig. 5) is appropriate for many fluid inclusions in the samples from the Alaska-Juneau deposit. The addition of salts and other volatiles such as N_2 shifts the position of the solvus to higher P-T conditions.

The estimated densities of the CO_2-rich fluid inclusions for most Alaska-Juneau samples lie within the range of 0.85 to 0.95 g/cm^3, with some as high as 1.0 g/cm^3. At 25°C, the fluid inclusions appear as 2-phase liquid CO_2 + liquid H_2O (inclusions a, b, c and d in Fig. 3). Considering the uncertainty in the bulk CO_2 content of the Alaska-Juneau ore fluid, the homogenization temperatures and the CO_2 densities of the fluid inclusions we studied agree quite well with the high pressure portion of the solvus in Fig 5. Therefore, trapping pressures were likely to be at least 1.5 kb and may be at least 3 kb for most fluid inclusions. If trapping of these fluid inclusions were above the solvus, actual pressure and temperature conditions would be higher, lying along the appropriate isochore. Pressures of 1.5 kb to 3.0 kb correspond to a minimum depth of mineralization of 5.5 to 10.0 km for lithostatic conditions. If there was a significant hydrostatic component to the fluid pressure, then depths of mineralization would be significantly greater.

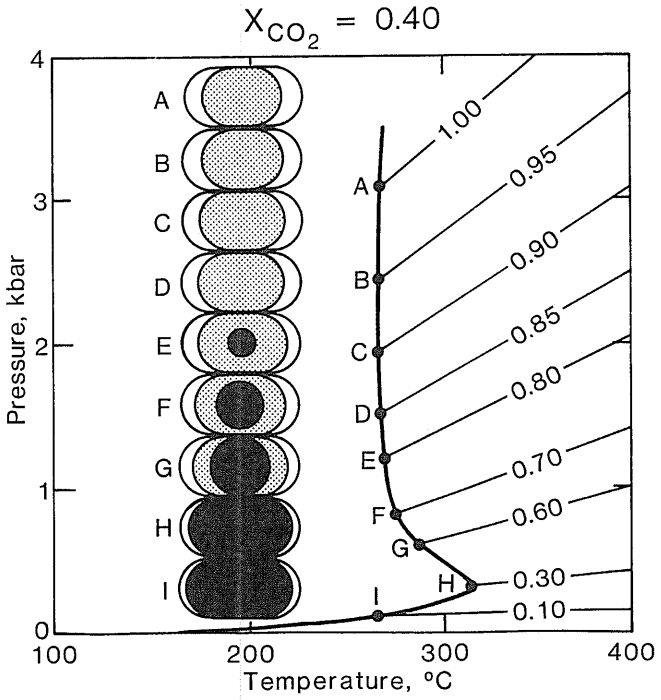

Fig. 5. Diagram from Bodnar (1982; in Roedder, 1984) showing phase relations at 25°C for fluid inclusions with different temperatures and pressures of homogenization for a fluid of 40 mole percent CO_2. The black area represents liquid H_2O, the shaded area represents liquid CO_2 vapor. Most samples from the Alaska-Juneau deposit contain fluid inclusions that appear as inclusions A through D at 25°C, and have CO_2 densities in the range of 0.85 to 1.0 gm/cm^3.

DISCUSSION

The low to moderate salinity, CO_2-rich fluid inclusions; the extensive carbonate alteration; and the mineralogy of the gold veins at the Alaska-Juneau deposit are characteristics common to many world-class gold deposits in North America. Knopf (1929) described the widespread carbonatization associated with the California Mother Lode deposits; Kerrich and Fyfe (1981) discussed the gold-carbonate association with the Archean Canadian lode bodies. Kerrich and Fyfe relate the characteristic alteration pattern of these gold deposits to reactions between CO_2-rich hydrothermal solutions and Ca-, Fe-, and Mg-bearing silicates within mafic host rocks.

The tapping of a deep, prograding metamorphic fluid is consistent with the high bulk CO_2 content, perhaps in the range of 30 to 60 mole percent CO_2, for the Alaska-Juneau system. Crawford (1981) summarized the work of numerous workers in the Alps and discussed the gradual shift of fluid inclusion compositions from hydrocarbon-rich at low metamorphic grades,

to H_2O-dominant with roughly 10 mole percent CO_2 at medium grades, to fluids containing 60 mole percent CO_2 produced during metamorphic reactions near the staurolite isograd. Crawford concluded that the CO_2 content of fluid inclusions within a sedimentary sequence was more a function of metamorphic grade than host lithology. Touret (1981) suggested high density, carbonic fluids are ubiquitous in high grade metamorphic rocks and granulites. However under granulite conditions, H_2O remains within the magmatic melt and a relatively pure CO_2 phase exists within the volatile phase. Therefore, the CO_2-rich fluids at Alaska-Juneau are suggestive of fluid compositions produced during high grade metamorphism, perhaps under amphibolite facies P-T conditions.

The mineralized veins at Alaska-Juneau definitely postdate the Late Cretaceous-earliest Tertiary Barrovian metamorphism of the host sediments. However, in the Early Tertiary, compressional tectonics and underthrusting of the Chugach terrane below the Alexander terrane, and probably more easterly terranes, was still occurring. The dehydration of the underthrusted plate (Fig. 6), undoubtedly expelled large volumes of fluids into shear zones extending upward into the already metamorphosed upper plates. Such a flow event, where deep crustal fluids have migrated upward from prograde metamorphic reaction zones, has also been suggested as a possible mechanism for the genesis of the California Mother Lode system where the Franciscan complex underplated metamorphic belts to the east (Bohlke and Kistler, 1986). Metamorphic devolatilization at higher crustal levels within the subducted Chugach slab may also have led to formation of the gold deposits hosted to the west and northwest by the Chugach terrane itself. These gold deposits in south-central Alaska (Goldfarb et al., 1987) and on Chichagof Island in southeastern Alaska (Goldfarb, unpublished data) contain H_2O-dominant ore fluids with CO_2 contents between 5 and 10 mole percent.

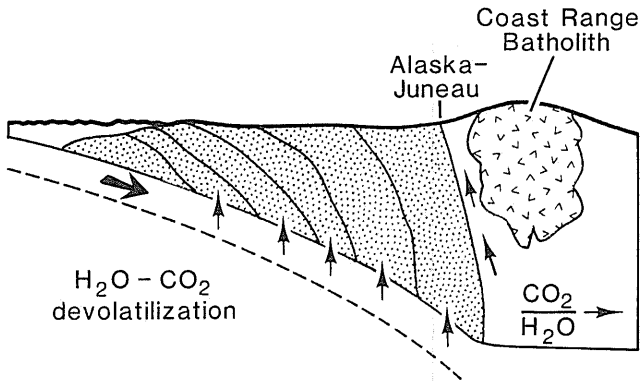

Fig. 6. Diagrammatic illustration showing underplating and subsequent prograde metamorphism. Volatiles released from metamorphism of the subducted slab migrate toward the surface along major structural zones and may have formed lode-gold deposits such as the Alaska-Juneau deposit. The CO_2/H_2O ratios of the prograding metamorphic fluids increase with the increasing metamorphic grade.

A gradual shift from compressional to transform motion occurred in southeastern Alaska between 56 Ma and 37 Ma (Engebretson et al., 1985). Within this time span, subduction beneath the Juneau region ceased and the underthrusted slab slowly attained thermal equilibrium. The thermal gradient in the subducted package probably increased from about 10°C/km to about 30°C/km and was accompanied by the release of an enormous volume of fluid (Fyfe and Kerrich, 1985). Such an event may have allowed deep crustal fluids to infiltrate upward along crustal flaws leading to the Alaska-Juneau deposit. Partially overlapping with cessation of subduction, the overlying Tracy Arm terrane may have been uplifted a total of as much as 35 km between 65 Ma and 45 Ma (Hollister, 1982). This rapid uplift would have dilated major crustal flaws, including the Coast Range megalineament, and possibly tapped CO_2-rich fluids deep in the crust.

Brew and Ford (1985c) report that the Coast Range batholith near Juneau is composed of three distinct intrusive pulses: (1) Upper Cretaceous and (or) Paleocene tonalite, quartz diorite, and minor granodiorite, (2) Paleocene granodiorite and tonalite, and (3) Eocene granodiorite, quartz monzonite, monzodiorite, and granodiorite. Because the first two sets of intrusives have been metamorphosed, whereas the Alaska-Juneau veins cross-cut metamorphic foliation, gold mineralization must postdate the two oldest intrusive episodes. The youngest intrusive episode, though containing nonfoliated to poorly foliated plutons, is not recognized within the vicinity of the Juneau gold belt. The closest exposure of any Eocene intrusive body to Alaska-Juneau has been mapped roughly 17 km to the east (Brew and Ford, 1985c). Thus, if the CO_2-rich fluids were produced in response to local heating of sediments by an intrusive body it must be at depth and is as yet unrecognized.

Light and others (1987) report $\delta^{18}O$ values ranging from +17.1 to +18.1 per mil for 4 samples of vein quartz afrom the Alaska-Juneau deposit. Whole rock $\delta^{18}O$ analysis of the auriferous, silicified dike from the Mexican mine within the nearby Treadwell ore system yielded a value of +20.8 per mil (Roger Ashley, written communication, 1986). Isotopic analysis of a hydrothermal mica from one of the gold-bearing veins at the Alaska-Juneau deposit indicates an ore fluid δD of roughly −20 per mil (Pickthorn et al., 1987). The isotope data would be difficult to attribute to deeply circulating meteoric waters that reacted with metasedimentary rocks. Rather, stable isotope data suggest that isotopically heavy fluids were produced during devolatilization of medium and high grade metamorphic rocks. The exceptionally heavy oxygen values, especially that of the Mexican mine, indicate that decarbonation of chemical sediments within the dominantly pelitic metamorphosed pile could be important. Brew and Ford (1985c) report thin, intercalated, metamorphosed limestone units interbedded within the phyllites and slates of the Coast Plutonic Complex near Juneau.

Regardless of the source of the hydrothermal solutions, these deep crustal fluids probably were focused along major fault zones. Abrupt hydraulic fracturing at the leading edge of such a system could induce fluid flow into an extensive dilation zone. Phillips (1986) points out that orientation of the dilations is often controlled by the anisotropic strength of the host. This is consistent with the parallel orientation of the Alaska-Juneau veins to the small metagabbro and greenstone bodies within the Perseverance slate.

The boiling hydrothermal fluids were focused within these dilation networks. The loss of volatile phases undoubtably produced dramatic shifts in oxygen fugacity, sulfur fugacity, and pH, and probably led to gold deposition. Drummond and Ohmoto

(1985) have described how the loss of CO_2 from an ore fluid accompanied by an abrupt increase in pH can result in the deposition of gold. They showed that metal precipitation is most favourable between 200°C and 300°C for a boiling system, with gold characteristically late in the ore paragenesis. The results of our studies of the Alaska-Juneau system are consistent with these experimental predictions of a boiling hydrothermal system.

SUMMARY

Fluid inclusion studies show that ore deposition at the Alaska-Juneau gold deposit occurred at temperatures probably greater than 200°C, pressures in excess of 1.5 kb, and depths of at least 5 km. The veins formed from a dense, CO_2-rich fluid with a salinity of less than 5 equivalent weight percent NaCl. Petrographic studies have shown that episodic fluid immiscibility occurred with the main ore zone.

Geologic, fluid inclusion, and preliminary stable isotope data tend to favor the generation of the ore-forming solutions along prograding metamorphic paths deep within the crust. The fluids may have been produced during progressive metamorphism of pelitic sequences and (or) may have received a contribution of CO_2 from thinly interbedded carbonate units. The timing of fluid migration and its relationship to the regional tectonics is still uncertain. Veining obviously is no older than latest Paleocene. Fluids may have been generated at depth and trapped along impermeable boundaries until fluid pressure exceeded lithostatic pressure during subsequent regional uplift as suggested by Norris and Henley (1976). Alternatively, if uplift of the rocks presently exposed in the Juneau region was already occurring at the time of fluid formation, fluids from an actively dehydrating subducted slab could immediately flow up dilated conduits as proposed by Fyfe and Kerrich (1985).

Acknowledgments — We thank Al Hofstra and Jim Saunders for their especially constructive criticism of the manuscript. The assistance of Jill Pasteris and Brigitte Wopenka with the laser Raman microprobe and of Al Hofstra and Gary Landis with the mass spectrometer is appreciated. The manuscript also benefited from important discussions with Dave Brew and Bill Pickthorn concerning many aspects of the study. Tim Curry and Scott Rose are thanked for their help in preparation of samples.

REFERENCES

Barker, F., and Arth, J. G., 1984, Preliminary results, Central Gneiss Complex of the Coast Range batholith, southeastern Alaska — the roots of a high-K, calc-alkaline arc?: Phys. Earth Planet. Sci., v. 35, p. 191-198.

Bodnar, R. J., 1982, Fluid inclusions in porphyry-type deposits: Course notes, Mineral Deposits Research Review for Industry, Penn State U., April 6-9, RB1-RB25.

Bohlke, J. K., and Kistler, R. W., 1986, Rb-Sr, K-Ar, and stable isotope evidence for the ages and sources of fluid components of gold-bearing quartz veins in the northern Sierra Nevada foothills metamorphic belt, California: Econ. Geol., v. 81, p. 296-322.

Brew, D. A., and Ford, A. B., 1978, Megalineament in southeastern Alaska marks southwest edge of Coast Range batholithic complex: Can. J. Earth Sci., v. 15, no. 11, p. 1763-1772.

Brew, D. A., and Ford, A. B., 1981, The Coast Plutonic Complex sill, southeastern Alaska, *in* Albert, N. R. D., and Hudson, Travis, eds., The U. S. Geological Survey in Alaska: Accomplishments during 1979: U. S. Geol. Surv., Circ. 823B, B96-B99.

Brew, D. A., and Ford, A. B., 1984, Timing of metamorphism and deformation in the Coast Plutonic-Metamorphic Complex, near Juneau, Alaska: Geol. Soc. Amer., Cord. Sect., Abs. with Prog., v. 16, no. 5, p. 272.

Brew, D. A., and Ford, A. B., 1985a, Southeastern Alaska tectonostratigraphic terranes revisited: Prog. and Abs., 60th Ann. Meeting, AAPG-SEPM-SEG, Pac. Sect., Anchorage, p. 57.

Brew, D. A., and Ford, A. B., 1985b, Southeastern Alaska coincident zone, *in* Bartsch-Winkler, S. (editor), The U.S. Geological Survey in Alaska: Accomplishments during 1984: U. S. Geol. Surv., Circ. 967, p. 82-86.

Brew, D. A., and Ford, A. B., 1985c, Preliminary reconnaissance geologic map of the Juneau, Taku River, Atlin, and part of the Skagway 1:250,000 quadrangles, southeastern Alaska: U. S. Geol. Surv., of Rep. 85-395, 23 p., 2 sheets.

Bundtzen, T. K., Eakins, G. R., Clough, J. G., Lueck, L. L., Green, C. B., Robinson, M. S., and Coleman, D. A., 1984, Alaska's mineral industry 1983: Ak. Div. Geol. Geophys. Surv., Spec. Rep. 33, 56 p.

Burruss, R. C., 1981, Analysis of phase equilibria in C-O-H-S fluid inclusions, *in* Hollister, L. S., and Crawford, M. L. (editors), Fluid Inclusions: Applications to Petrology: Mineral. Assoc. Can., Short Course Handbook, v. 6, p. 39-74.

Collins, P. L. F., 1979, Gas hydrates in CO_2-bearing fluid inclusions and the use of freezing data for estimation of salinity: Econ. Geol., v. 74, p. 1435-1444.

Coney, P. J., and Jones, D. L., 1985, Accretion tectonics and crustal structure in Alaska: Tectonophysics, v. 119, p. 265-283.

Crawford, M. L., 1981, Fluid inclusions in metamorphic rocks — low and medium grade, *in* Hollister, L. S., and Crawford, M. L. (editors), Fluid Inclusions: Applications to Petrology: Mineral. Assoc. Can., Short Course Handbook, v. 6, p. 157-181.

Crawford, M. L., and Crawford, W., A., 1986, Formation of tectonic sutures, southeasternmost Alaska: Geol. Soc. Amer., Cord. Sect., Abs. with Prog., v. 18, p. 97.

Crawford, M. L., and Hollister, L. S., 1982, Contrast metamorphic and structural histories across the Work Channel Lineament, Coast Plutonic Complex, British Columbia: J. Geophys. Res., v. 87, p. 3849-3860.

Drumond, S. E., and Ohmoto, H., 1985, Chemical evolution and mineral deposition in boiling hydrothermal systems: Econ. Geol., v. 80, p. 126-147.

Engebretson, D. C., Cox, Allan, and Gordon, R. G., 1985, Relative motions between oceanic and continental plates in the Pacific basin: Geol. Soc. Amer., Spec. Pap. 206, 59 p.

Fyfe, W. F., and Kerrich, R., 1985, Fluids and thrusting: Chem. Geol., v. 49, p. 353-362.

Goldfarb, R. J., Leach, D. L., Miller, M. L., and Pickthorn, W. J., 1987, Geology, metamorphic setting, and genetic constraints of epigenetic lode-gold mineralization within the Cretaceous Valdez Group, south-central Alaska, *in* Keppie, J. D. Boyle, R. W., and Haynes, S. J. (editors), Turbidite-Hosted Gold Deposits: Geol. Assoc. Can., Spec. Pap. 32, p. 87-105.

Hollister, L. S., 1982, Metamorphic evidence for rapid (2 mm/yr) uplift of a portion of the Central Gneiss Complex, Coast Mountains, B. C.: Can. Min., v. 20, p. 319-332.

Hudson, Travis, Smith, J. G., and Elliot, R. L., 1979, Petrology, composition and age of intrusive rocks associated with the Quartz Hill molybdenum deposit, southeastern Alaska: Can. J. Earth Sci., V. 16, p. 1805-1822.

Kerrich, R., and Fyfe, W. S., 1981, The gold-carbonate association: Source of CO_2, and CO_2 fixation reactions in Archaean lode deposits: Chem. Geol., v. 33, p. 265-294.

Knopf, Adolph, 1929, The Mother Lode system of California: U. S. Geol. Surv., Prof. Pap. 157, 88 p.

Landis, G. P., 1985, Gas analysis of ore-forming fluids, in Krafft, K., ed., U. S. Geol. Surv. Research on Mineral Resources — 1985 Programs and Abstracts: U. S. Geol. Surv., Circ. 949, 28.

Light, T. D., Brew, D. A., and Ashley, R. P., 1987, The Alaska-Juneau and Treadwell lode systems, southeastern Alaska, in Shawe, D., World-class gold deposits: U. S. Geol. Surv., Prof. Pap., in press.

Norris, R. J., and Henley, R. W., 1976, The dewatering of a metamorphic pile: Geology, v. 4, p. 333-336.

Phillips, W. J., 1986, Hydraulic fracturing effects in the formation of mineral deposits: Trans. Inst. Mining Metall., Sect. B, v. 95, p. B17-B24.

Pickthorn, W. J., Goldfarb, R. J., and Leach, D. B., 1987, Response to "Dual Origin of Lode Gold Deposits in the Canadian Cordillera": Geology, in press.

Roedder, Edwin, 1984, Fluid inclusions: Mineral. Soc. Amer., Reviews in Mineralogy, v. 12, 644 p.

Saleeby, J. B., 1983, Accretionary tectonics of the North American Cordillera: Ann. Rev. Earth Planet. Sci., v. 15, p. 45-73.

Silberling, N. J., and Jones, D. L. (editors), 1984, Lithotectonic terrane maps of the North American Cordillera: U. S. Geol. Surv., OF Rep. 84-523, 4 sheets.

Spencer, A. C., 1906, The Juneau gold belt, Alaska: U. S. Geol. Surv., Bull. 287, 161 p.

Todheide K., and Franck, E. V. 1963, Das Zweiphasengebeit und die Kritische Kurve im System Kohlendioxid-Wasser bis zu Drucken von 3500 bar: Z. Phys. Chemie., new ser., v. 37, p. 387-401.

Touret, J. L. R., 1981, Fluid inclusions in high grade metamorphic rocks, *in,* Hollister, L. S., and Crawford, M. L. (editors), Fluid Inclusions: Applications to Petrology: Mineral. Assoc. Can., Short Course Handbook, v. 6, p. 182-208.

Twenhofel, W. S., 1952, Geology of the Alaska-Juneau lode system, Alaska: U. S. Geol. Surv., OF Rep. 60, 170 p.

Wayland, R. G., 1939, Geology of the Juneau region, Alaska, with special reference to the Alaska Juneau ore body: Unpub. Ph.D. thesis, U. Minnesota.

Wayland, R. G., 1960, The Alaska Juneau gold ore body: Neues Jahrb. Mineralogie Abh., v. 94, p. 267-279.

Werre, R. W., Jr., Bodnar, R. J., Bethke, P. M., and Barton, P. B., Jr., 1979, A novel gas-flow fluid inclusion heating/freezing stage: Geol. Soc. Amer., Abs. with Prog., v. 11, p. 539.

Nature of Ore Fluids in the Coquihalla Gold Belt, British Columbia

J. B. MUROWCHICK, K. MUEHLENBACHS AND B. E. NESBITT
Department of Geology, The University of Alberta, Edmonton, Alberta T6G 2E3

Abstract — More than 120 isotopic analyses of O, C, and H from vein quartz, fluid inclusions, serpentine, carbonates, and whole rock samples from the Coquihalla gold belt indicate that the fluids responsible for mineralization were highly evolved (^{18}O-enriched), locally-derived meteoric waters. Fluid inclusion analyses indicate that the fluids had low salinities (*ca.* 2 wt. % NaCl equiv.) and high CO_2 contents (up to 60 vol. % liquid CO_2 in some inclusions). Homogenization temperatures (uncorrected for pressure) average 290±10°C for inclusions related to the mineralizing event. The trapping temperatures are about 380°C, leading to a 750-1250 bar trapping pressure, equivalent to a depth of 3-5 km. As a genetic model, we envisage meteoric waters percolating downward to a decollement at the brittle/ductile transition (ca. 350-400°C at 5-10 km depth), exchanging oxygen and leaching Au from the country rocks. Ascent along fractures adjacent to a transcurrent fault zone focused the fluids and led to Au mineralization via episodic effervescence and/or cooling.

INTRODUCTION

THE GOLD occurrences and deposits of the Coquihalla gold belt (located approximately 20 km northeast of Hope, B.C.) are in many ways representative of mesothermal lode gold mineralization in the Canadian Cordillera (Nesbitt et al., 1986). Five past gold producers and 19 gold occurrences make up the belt; the most recently operating property was the Carolin Mine, which operated from 1982 to 1984.

Isotopic and fluid inclusion studies of the mineralization and host rocks in the belt were undertaken to determine the nature and source of the mineralizing fluids. The results were interpreted in light of associated studies on similar deposits elsewhere in the Canadian Cordillera.

GEOLOGY

The Coquihalla gold belt (Fig. 1) is located in the northern Cascade Mountains of Southern British Columbia along the western margin (defined by the Hozameen Fault system) of the Pasayten Trough (Coates, 1970). The region contains a variety of rock types, including the serpentinites and gabbros of the Coquihalla serpentinite, (Cairnes, 1929; Ray, 1986), spilitized basalts of the Spider Peak Formation (Ray, 1986), cherts and limestones of the Hozameen Group (Haugeraud, 1985), coarse to fine clastics of the Ladner and Dewdney Creek Groups (Cairnes, 1924), and granitoids of the Needle Peak Pluton (Monger, 1970). Several large transcurrent faults are present in this area, including the Fraser and Hozameen fault systems. The geology of the Hozameen fault system, Coquihalla serpentine belt, and the Coquihalla gold belt has been described in detail by Ray (1986) and Ray et al. (1986).

The gold mineralization is, for the most part, hosted by clastic sediments of the Lower to Upper Jurassic Ladner Group. The Ladner Group succession comprises an upper unit of dark pyritic argillites, a middle unit of bedded siltstones with minor argillites, and a lower unit of coarse clastics (greywackes and conglomerates). Most of the gold occurrences are hosted by this lower unit.

The Ladner Group rests unconformably on spilitized subalkaline submarine basalts of the Early Triassic Spider Peak Formation (Ray, 1986). These rocks form the basement of the Pasayten

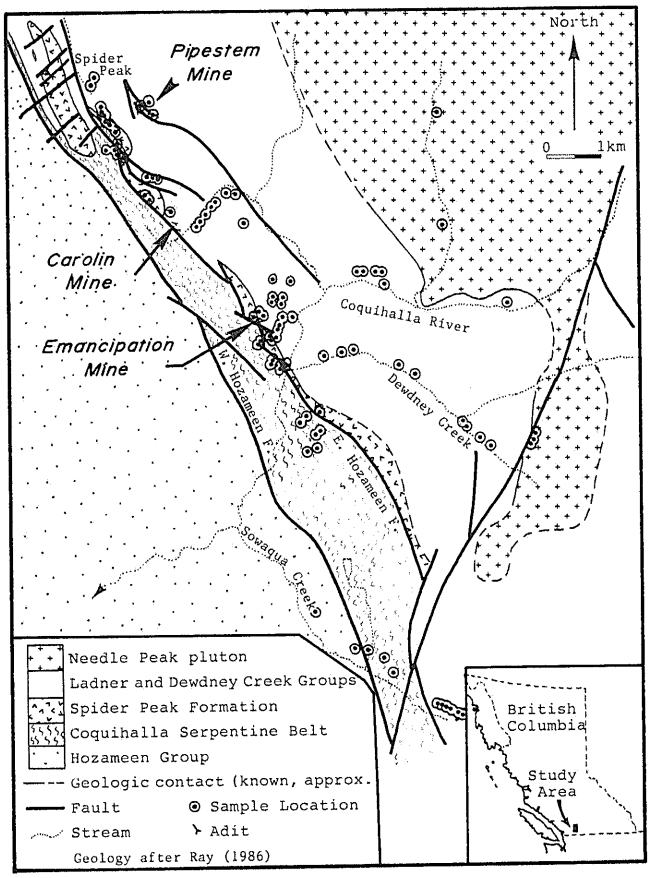

Fig. 1. Geology of the Coquihalla gold belt and vicinity. Sample locations in the Carolin Mine area have been omitted for clarity.

Trough and form a discontinuous strip up to 500 m thick and 15 km long between the Ladner Group to the east and the Coquihalla serpentine belt to the west. Major and trace element analyses (Ray, 1986) indicate they formed in a spreading ridge environment in a back-arc basin.

The rocks of the Ladner Group and Spider Peak Formation are in fault contact with the Coquihalla serpentine belt and Hozameen Group. The serpentine belt is up to two kilometres wide and has a discontinuous length of more than 50 km. The

serpentinite is dominantly composed of massive to sheared antigorite and lizardite, and contains magnetite, pyrrhotite, pentlandite, millerite, and locally, talc. The belt is entirely contained between the East and West Hozameen faults (Fig. 1). West of the serpentine belt lies the Permian to Early Jurassic Hozameen Group (Haugeraud, 1985), composed of cherts, limestones, pelites, basic volcanics, and ultramafic rocks. These, with the Petch Creek serpentinite near Boston Bar, are thought by Ray (1986) to represent a dismembered ophiolite sequence.

A variety of intrusive rocks occur in the vicinity of the Coquihalla gold belt. Pod-like gabbroic intrusions occur in the serpentinite, and about six kilometres east of the serpentinite is the Needle Peak pluton (Monger, 1970) a 200-km^2 granite, granodiorite, and quartz monzonite stock. A 0.5 to 1 kilometre wide contact aureole containing andalusite porphyroblasts is present along the west side of the intrusion; this aureole overprints the earlier regional lower greenschist facies metamorphism.

Spatially related to the Needle Peak pluton are numerous sodic felsic dykes and sills that cut the metasediments between the Needle Peak stock and the East Hozameen fault. These dykes are not found west of the Hozameen fault system, presumably due to post-intrusion transcurrent movement along the fault zone.

Gold occurs in at least three different types of mineralization in the Coquihalla gold belt, including sulphide-poor, gold-bearing quartz veins (e.g. Emancipation, Pipestem, and Monument mines, and most of the showings); sulphide and albite-rich ore (e.g. Carolin mine and the McMaster zone); and gold in talc shears (e.g. Aurum mine). Most of our samples were collected from the sulphide-poor gold-bearing quartz veins and from barren quartz veins associated with, but closely post-dating sulphide and albite-rich gold mineralization.

At Carolin Mine, the ore forms several saddle reef-like replacement ore bodies in the hinge zone of an antiformal fold (Shearer and Neils, 1983). Numerous N- to NW-trending, high-angle normal and reverse faults are localized in the fold hinge zones and cut the ore bodies. The quartz veins, for the most part, appear to immediately post-date the gold deposition at Carolin Mine, but nevertheless are regarded to form part of the overall mineralizing event (Ray, 1986). Younger, easterly-striking and northerly-dipping faults truncate the N- NW-striking faults and the Carolin Mine deposit.

Alteration at Carolin Mine has been described in detail by Ray et al. (1986); it consists mainly of sulphide deposition, albitization, silicification, and late carbonate veining. A sodium enrichment and potassium depletion halo extends for several hundred meters from the Carolin Mine deposit.

ANALYTICAL METHODS

Stable isotopes

Oxygen was extracted from 20-25 mg mineral separates and whole rock samples by BrF_5 digestion and converted to CO_2 for mass spectrometric analysis for ^{18}O according to the technique described by Clayton and Mayeda (1963). Waters collected for deuterium analysis were extracted from 0.5 g samples of hydrous minerals by dehydration under vacuum at 1100°C. Waters from fluid inclusions were extracted from selected vein quartz samples (10 g) that were crushed to medium sand size, outgassed at 250°C under vacuum (decrepitating late secondary inclusions) for 10 to 24 hrs, followed by heating at 1100°C for 4 hrs to decrepitate the remaining inclusions. The waters were converted to hydrogen gas by reducing them with hot (870°C) uranium metal. The H_2 thus produced was then mass spectrometrically analyzed. Carbon and oxygen were extracted from carbonate minerals by H_3PO_4 digestion at 25°C (McRae, 1950). The CO_2 was then analyzed for ^{13}C and ^{18}O by mass spectrometry. Isotopic data are reported in permil (‰) relative to Standard Mean Ocean Water (SMOW) for $\delta^{18}O$ and δD, and to Pee Dee Belemnite (PDB) for $\delta^{13}C$. The uncertainty of the analyses was ± 0.05‰ for $\delta^{18}O$, ± 0.03‰ for $\delta^{13}C$, and ± 3‰ for δD. $\delta^{18}O$ NBS-28 was 9.39‰.

Fluid inclusions

Fluid inclusion analyses were conducted using a U.S.G.S. -Fluid Inc. gas-flow heating/freezing stage modified at the University of Alberta. The stage was calibrated using pure CO_2 inclusions in quartz from Calandra, Grisons, Switzerland (Poty et al., 1976), the triple point of water, and a variety of melting point standards. Reproducibility of Tm was ± 0.2°C below $+10$°C, and Th reproducibility was usually better than ± 1°C. Accuracy is estimated at ± 3°C for Th around 300°C and ± 0.3°C for Tm. Inclusions were crushed under an alkaline $BaCl_2$ solution to test for the presence of CO_2 or other gases in selected two-phase inclusions.

RESULTS

Isotopes

Stable isotope analyses for ^{18}O, ^{13}C, and/or D of 69 vein quartz, 16 carbonate, 14 serpentine and other minerals, 43 whole rock, and 13 meteoric water, fluid inclusion, and hydrous mineral samples were conducted with the results shown in Figs. 2 and 3.

Whole-rock analyses of metasedimentary rocks of the Ladner Group gave $\delta^{18}O$ values of $+13.1$ to 19.6‰ for upper unit argillites, ($+8.1$ to 14.3‰ for argillites from the contact aureole of the Needle Peak pluton), $+12.3$ to 14.8‰ for middle Ladner Group bedded siltstones in the Carolin Mine area, and $+9.4$ to 13.4‰ for the lower Ladner Group coarse clastics in the mine area. Argillite samples from the Dewdney Creek area displayed a steady decrease in $\delta^{18}O$ values approaching the EHF (Fig. 4a), and a similar trend was observed for whole rock samples in the mine area (Fig. 4b).

$\delta^{18}O$ values for vein quartz samples fell into two groups (Fig. 4c): one group ranging from $+15$ to 17‰ and the other ranging from about $+18$ to 20‰. The lower-^{18}O samples are found nearer the East Hozameen Fault (EHF) while the

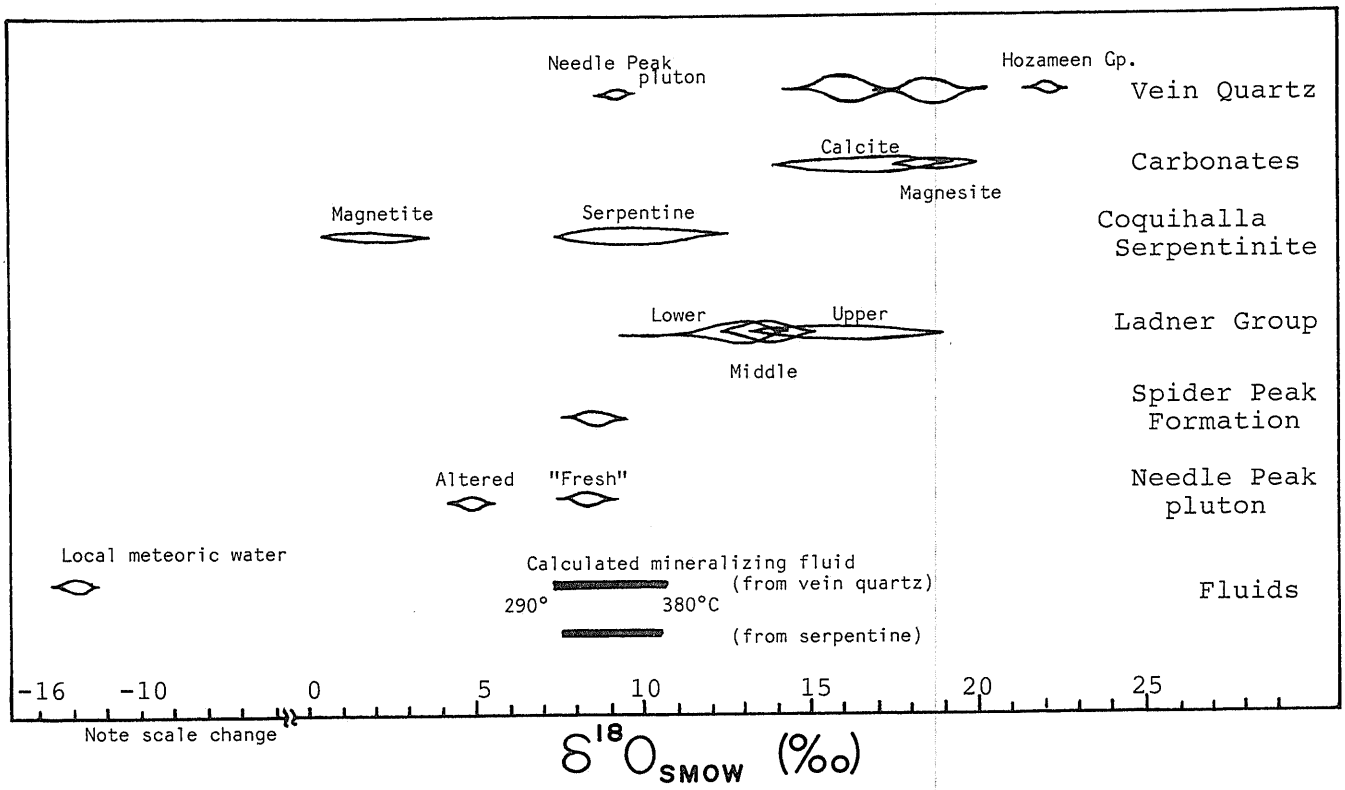

Fig. 2. Measured $\delta^{18}O_{SMOW}$ for various sample materials from the Coquihalla gold belt. Vein quartz in mineralized zones falls in the +14 to +16‰ range in the group of samples within 400 m of the East Hozameen Fault. The Hozameen Group quartz veins reflect the very high $\delta^{18}O$ signatures of the cherts they are associated with regardless of their proximity to the West Hozameen Fault. The calculated $\delta^{18}O$ of the mineralizing fluid (Clayton et al., 1972, and Wenner and Taylor, 1971) is given at the bottom, along with those of the local meteoric waters.

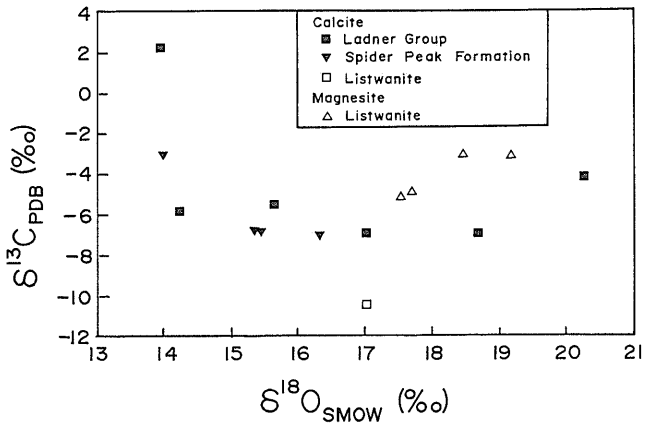

Fig. 3. $\delta^{18}O_{SMOW}$ vs. $\delta^{13}C_{PDB}$ for carbonate samples. The carbon is believed to be derived in part from organic material in the metasediments.

^{18}O-enriched samples occur further east (Fig. 4c). $\delta^{18}O$ contours wrap around the mineralized Idaho Zone (Fig. 5), indicating focused flow through that area. The contours reflect the decreasing water/rock ratio, and possibly decreasing temperature, away from the EHF. A similar gradient occurs in the serpentinite, with $\delta^{18}O$ values decreasing to the west away from the EHF (Murowchick et al., 1986).

Carbonate $\delta^{18}O$ values range from +14.0 to +18.7‰ for vein calcites and +17.5 to 19.3‰ for magnesites from listwanites (Fig. 3). Clustering of the data points was not observed. $\delta^{13}C_{PDB}$ was determined for carbonate samples giving values between −10.4 and +2.1‰ (averaging −5.48‰) for vein calcites, and −5.1 to −5.2‰ for magnesite samples collected from east of Spider Peak.

The $\delta^{18}O$ values for serpentinites of the Coquihalla serpentine belt are notably enriched in $\delta^{18}O$ compared to serpentinites elsewhere in North America, which are normally +2 to 6‰ (Wenner and Taylor, 1974): +7.4 to 8.2‰ for serpentines and +0.4 to 3.5‰ for magnetite separates. The serpentine and serpentinite values become increasingly enriched in $\delta^{18}O$ toward the EHF (Murowchick et al., 1986). Two magnetite/serpentine pairs yielded isotopic temperatures (Wenner and Taylor, 1971) of about 380°C, and a third gave 230°C. The serpentinite yielding the lower temperature appeared to be altered (pale in colour, some chrysotile) whereas the high-T serpentinites were massive dark green antigorite.

Local meteoric waters were sampled from drill holes or seeps in workings between 1,450 and 4,000 feet elevation. The measured $\delta^{18}O$ values (Fig. 2) of these meteoric waters ranged from −12.9 to −14.8‰, whereas the calculated δD values (calculated using the equation $\delta D = 8\delta^{18}O + 10$ of Craig, 1961) ranged from −108‰ at the McMaster Zone to −98‰ at the Emancipation Mine and nearby Coquihalla Valley seeps. δD analyses of five serpentinite samples ranged from −106 to −151‰ with a mean value of −128‰ and a standard deviation of 31‰. The δD of the serpentinizing fluids would have been in the range −103 to

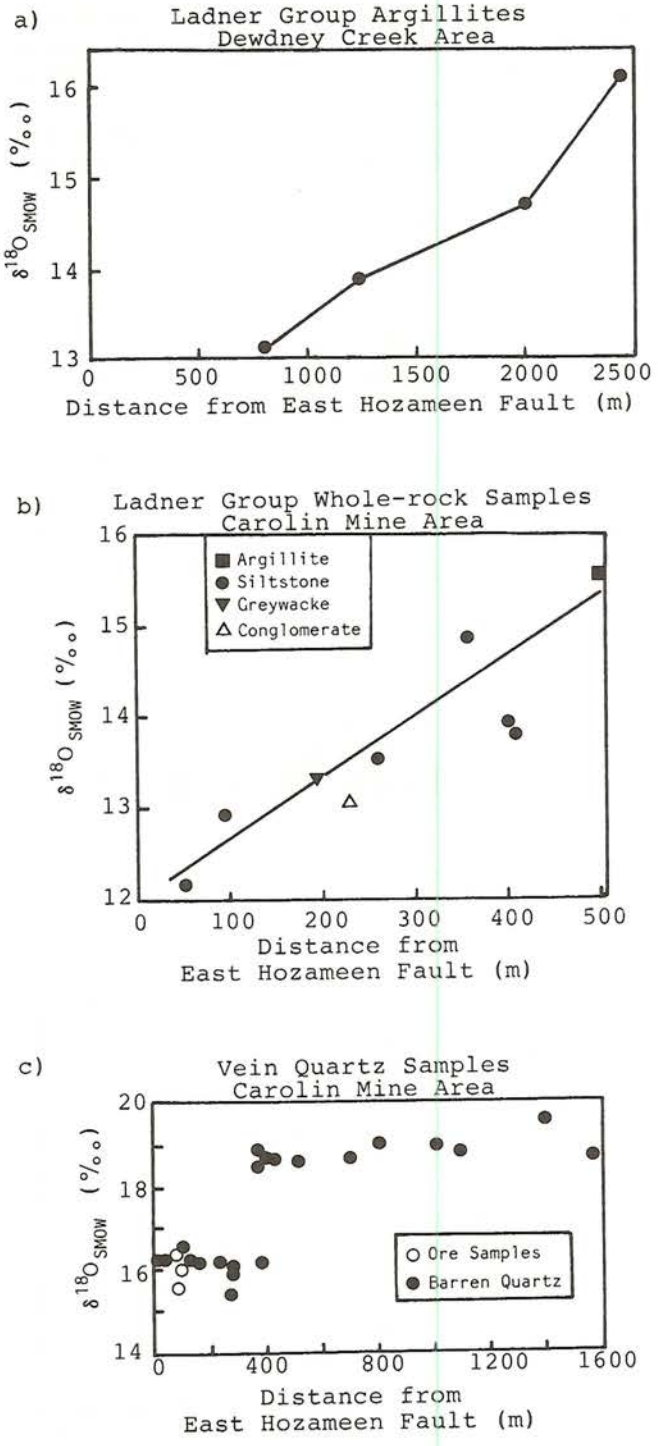

Fig 4. (a) $\delta^{18}O$ of Ladner Group slaty argillites vs. distance from the East Hozameen Fault along Dewdney Creek. The monotonous lithology of the rocks here permits the increase in $\delta^{18}O$ to be clearly seen. (b) $\delta^{18}O$ of Ladner Group metasediments vs. distance from the East Hozameen Fault in the Carolin Mine area. The increase in $\delta^{18}O$ is probably due to temperature gradients and decreasing water/rock ratios away from the fault. (c) $\delta^{18}O$ of vein quartz vs. distance from the East Hozameen Fault. The sharpness of the break at 400 m may be an artifact of the projection of sample locations onto a section normal to the fault trace. The actual profile may be less abrupt (as in a and b).

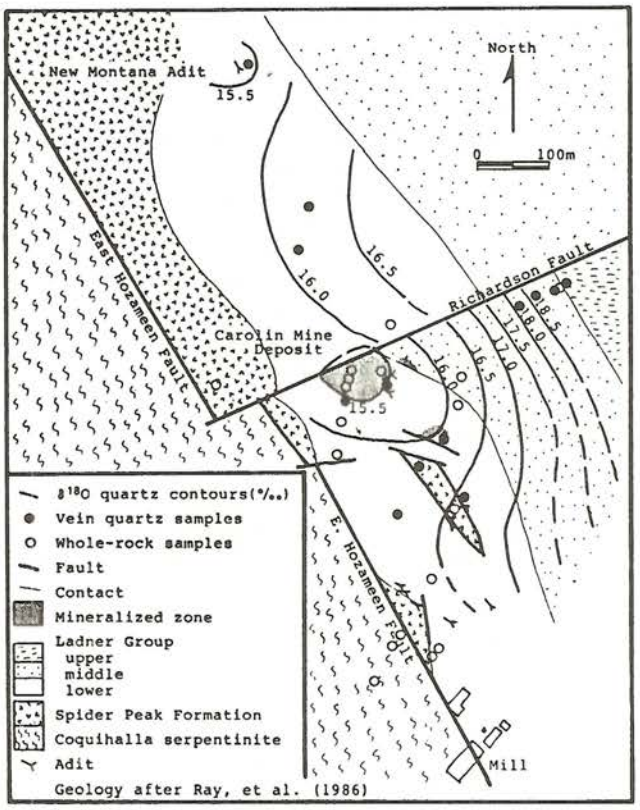

Fig. 5. $\delta^{18}O$ contours in the Carolin Mine area. The contours indicate that fluids came up the East Hozameen Fault and moved outwards. The gradients may be due to decreasing water/rock ratios and/or decreasing temperatures, though the former is likely to be more important in the Coquihalla gold belt.

−107‰ (serpentine-water, 1000 ln α = 21‰ at 380° to 25‰ at 300°C). δD of water extracted from fluid inclusions in quartz ranged from −68 to −123‰ with a mean of −102 and a standard deviation of 20‰.

Fluid inclusions

More than 160 inclusions in 17 samples of vein quartz from the Pipestem Mine in the north to Dewdney Creek in the south were analyzed. Three main types of inclusions were observed. These include relatively large (up to 40μm), stellate inclusions occasionally aligned along growth zones (Type I). Evidence of necking down and possible previous decrepitation is common. Most of these inclusions contain three phases at room temperature: $H_2O(L)$, $CO_2(L)$, and $CO_2(V)$, with roughly 35-60 vol. % CO_2. Though these inclusions appear to be primary, they were likely reset by later tectonic and hydrothermal activity, and are now very similar in composition and thermal behaviour to younger inclusions.

Type II are the most abundant and volumetrically most important inclusions and appear to be pseudosecondary. They are mostly three-phase, but may also be two-phase ($H_2O(L)$ and $CO_2(V)$). Two-phase and three-phase CO_2-rich and CO_2-poor inclusions can be found among inclusions in the same inclusion train or cluster; trapping of a two-phase fluid might produce

such inclusions, but the thermometric and compositional data have not proven that such is the case. A possible source of these inclusions is the development of two immiscible fluids during episodic hydrofracting of the veins by successive fluid influx, as suggested by Leach et al., (1986) for similar inclusions in the Alaska-Juneau deposit, Alaska.

Type III inclusions contained only H_2O(L and V) and are clearly secondary, forming well-defined trains that cut both types of earlier inclusions as well as sulphides and other minerals associated with the gold mineralization. These inclusions are generally quite small (1 to 10μm) and, though they may occasionally be numerous, account for only a small volumetric fraction of the total fluids included in the sample.

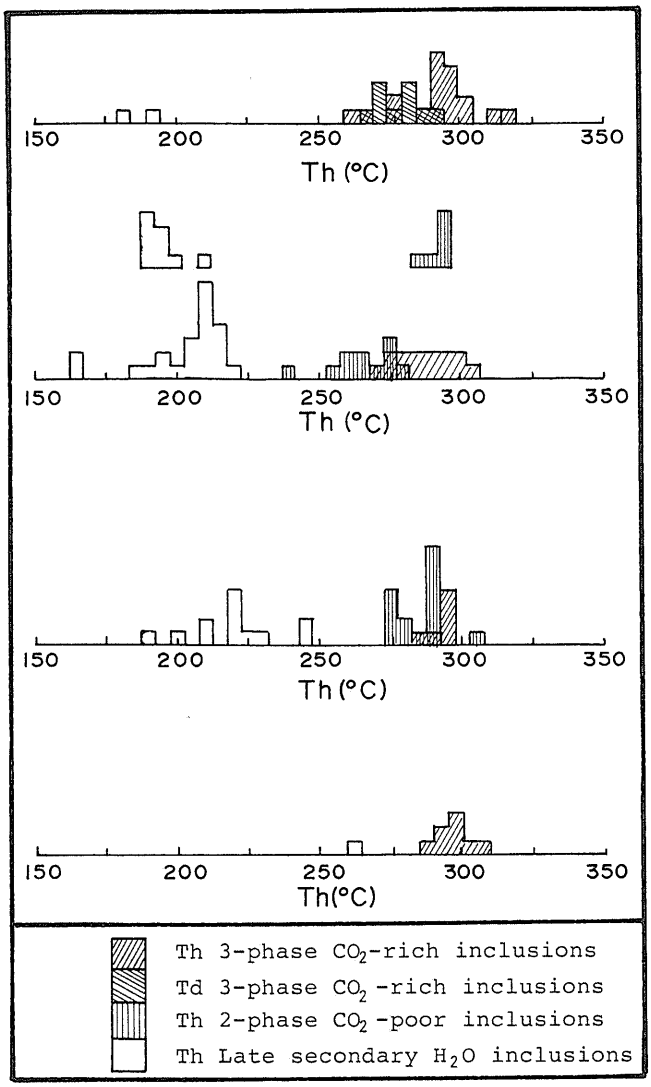

Fig. 6. Frequency distribution of total homogenization temperatures Th. The northernmost sample location (Pipestem Mine, elev. 1,231 m) is at the top, the southernmost (Dewdney Creek, elev. 462 m) is at the bottom of the diagram. Other elevations are: New Montana Mine, 1,230 m; Emancipation Mine, 785 m; and Coquihalla Valley, 455 m. Note the shift in Th with elevation for the late secondary inclusions, but little variation in Th among the CO_2 inclusions over the belt.

Homogenization temperatures (Th) of Type I and II inclusions cluster around 290 to 300°C regardless of location or elevation, but Th of Type III inclusions varies from 180° to about 250°C, decreasing with elevation (Fig. 6).

Salinities were determined from melting temperatures (Tm) of ice or clathrate. Salinities from Tm ice (Fig. 7a) of two-

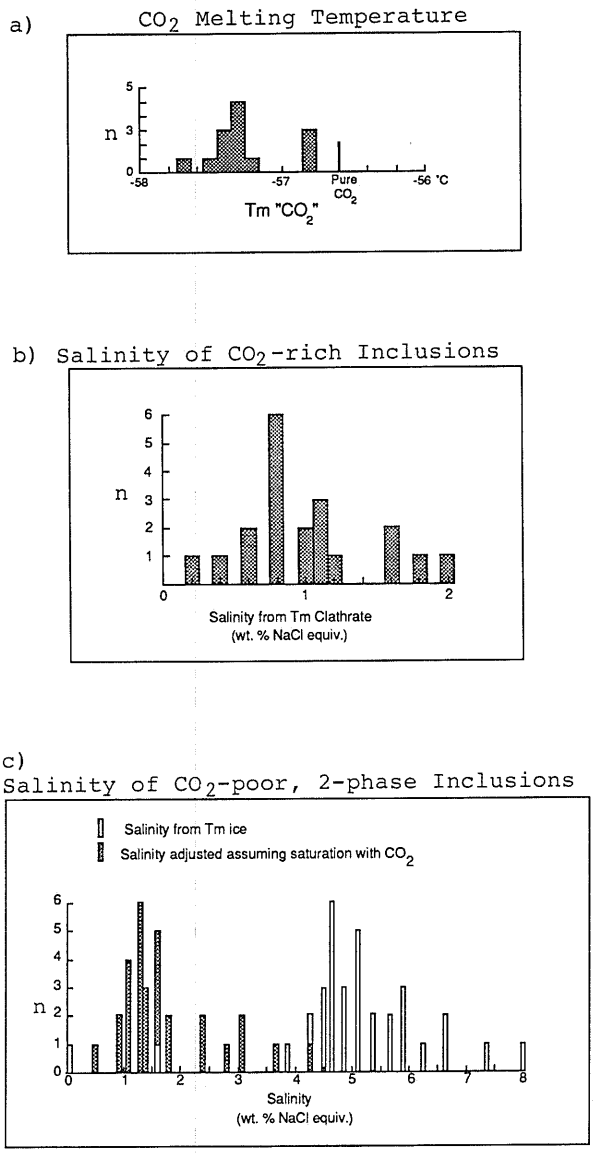

Fig. 7. (a) Salinities calculated from Tm ice. The open bars represent salinities derived directly from the observed Tm ice. The shaded bars represent salinities derived from Tm ice + 1.8°C. This adjustment was made to correct for the presence of CO_2 (assumed to be just below saturation at room temperature) in the two-phase CO_2-poor inclusions. CO_2 was detected by crushing tests. The shaded set thus represents minimum salinities whereas the unshaded set represents maximum salinities. (b) Salinities calculated from Tm clathrate. Note the similarity of these salinities with the lower set in Fig. 7a. The salinities calculated from Tm clathrate are also minimum salinities because of the presence of a small amount of (?)CH_4. (c) Frequency distribution of Tm CO_2. The melting point of pure CO_2 is indicated at −56.6°C. The observed Tm values were slightly lower, indicating the presence of an additional phase (less than 1 mole % CH_4).

phase inclusions that contained CO_2(V) (determined by crushing) were "adjusted" by assuming that the aqueous phase was just undersaturated with respect to CO_2 at room temperature, adding 1.8°C to the observed Tm, and then calculating the salinity from the adjusted Tm. Mean maximum and minimum salinities are 4.8 and 1.4 wt.% NaCl equivalent, derived from the nonadjusted and adjusted Tm values, respectively. Salinities determined from Tm clathrate (Fig. 7b) ranged from 0.2 to 2.0 wt.% NaCl equiv., with a mean of 0.9 wt.%. The mean Tm CO_2 (Fig. 7c) of −57.5°C suggests that less than 1 mole % CH_4, N_2, or other noncondensable gas is present, causing the salinity indicated by Tm clathrate to be slightly lower than the true salinity. At any rate, the salinities in all the inclusion types are low, probably between 1 and 3 wt.% NaCl equivalent.

DISCUSSION

The nature of the mineralizing fluids in the Coquihalla gold belt is partially revealed by the stable isotope and fluid inclusion results. The isotopic data indicate that the fluid in equilibrium with the vein quartz had a $\delta^{18}O$ of +11.2 to 13.6‰ at 380°C

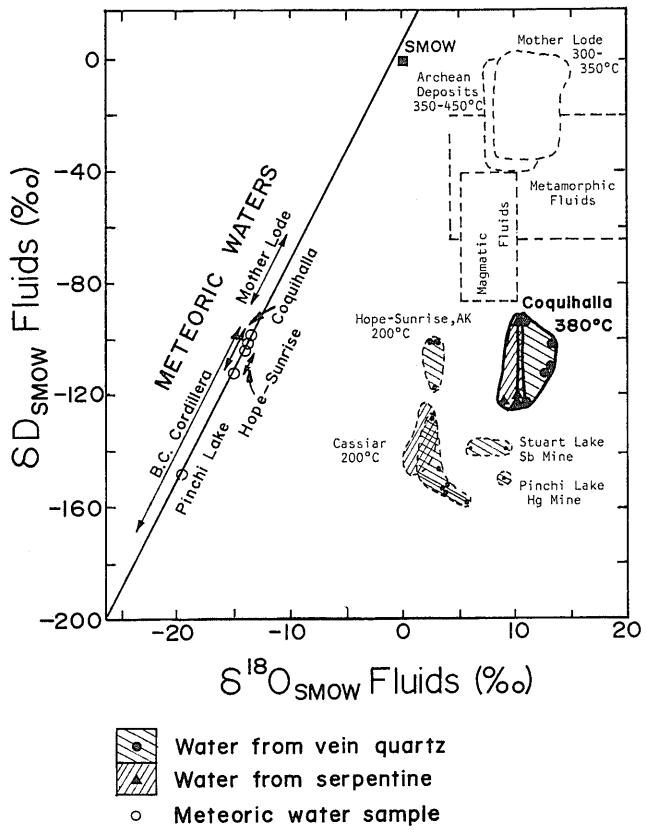

Fig. 8. δD vs. $\delta^{18}O$ for mineralizing fluids from various "mesothermal" lode gold deposits. Note the variation of δD with latitude according to Fig. 9. Sources of data are: Mother Lode — Böhlke and Kistler (1986), Weir and Kerrick (1984), and Rosenbaum and Taylor (1984); Hope-Sunrise, AK — Mitchell et al. (1981); Cassiar serpentinites (recalculated to 200°C) — Wenner and Taylor (1974); Archean gold deposits — Colvine et al. (1984).

(Clayton et al., 1972), with the lower values in the mine area, and an average δD (from inclusion fluids) of −102‰. The fluids in equilibrium with the serpentinites had calculated $\delta^{18}O$ of +8.6 to 10.5‰ (Wenner and Taylor, 1971) and an average calculated δD of −108‰. The similarity of the isotopic results from the vein quartz and the serpentinites suggests that both of those materials were in equilibrium with the same fluid. This is further supported by noting that the accessory mineralogy of the serpentinite (magnetite, pyrrhotite, pentlandite, millerite, magnesite, and talc) is consistent with the f_{O_2} of a CO_2-rich fluid, rather than a more reduced medium (Frost, 1985).

The δD values are quite close to those of the local meteoric waters, but the calculated $\delta^{18}O$ of the mineralizing fluid is about 25‰ heavier than the local meteoric waters. The metasediments in the area have abundant exchangeable oxygen, but little exchangeable hydrogen. Thus, a fluid equilibrating with such rocks would be expected to undergo large enrichments in ^{18}O but only small shifts in δD as long as the water/rock ratio is small. The peculiar isotopic signatures of the Coquihalla mineralizing fluids are not unique. Other "mesothermal" lode gold deposits in the Canadian Cordillera (and genetically related Hg and Sb occurrences) show similar isotopic signatures (Fig. 8): high $\delta^{18}O$ but δD similar to that of the local meteoric waters (Nesbitt et al., 1986) which varies with latitude (Fig. 9).

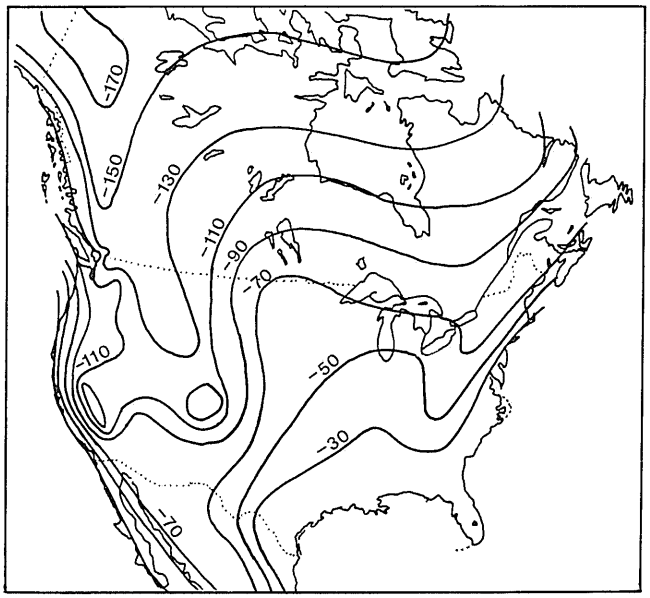

Fig. 9. Variation of δD of modern North American meteoric waters (after Taylor, 1979). Cretaceous to mid-Tertiary meteoric waters display the same trends in the Cordillera, but the paleowaters may have been enriched in D by about 20‰ (Magaritz and Taylor, 1986).

The $\delta^{13}C$ results were not very distinctive, but are believed to reflect the derivation of carbon from organic material in the metasediments. Oxidation of that material is a likely source of the abundant CO_2 found in the fluid inclusions.

Some authors (e.g., Kerrich, R., 1983; Marshall and Taylor, 1980) have called upon metamorphic fluids as the mineralizing agents in gold deposits of this type (a lateral secretion model)

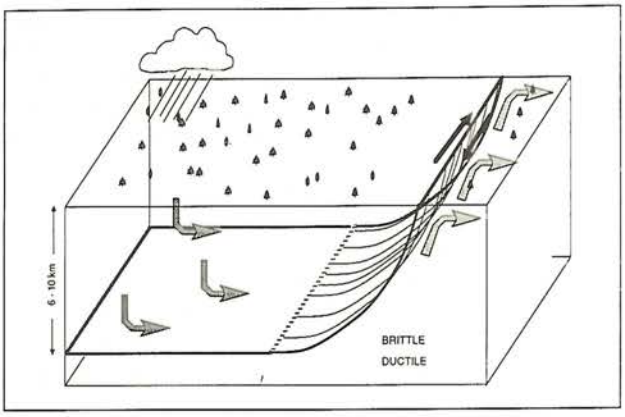

Fig. 10. Schematic block diagram of deep circulation model. Local meteoric waters deeply circulate through the sediment pile, possibly to the brittle-ductile transition, where decollements may occur. Oxygen is exchanged and gold is presumably leached from the sediment pile during this process. The fluids are focussed along fractures, such as the East Hozameen Fault, ascending and spreading into subsidiary fractures and more permeable zones at higher elevations along the fault, precipitating gold and quartz in the process.

based on the high $\delta^{18}O$ values, which are similar to those of metamorphic fluids. However, such a model does not explain the low δD values that vary with latitude among deposits in the Canadian Cordillera. An alternative model (Nesbitt et al., 1986) shown in Fig. 10 calls upon deep circulation of meteoric waters through the sediment pile (enriching the fluids in ^{18}O and CO_2, but not appreciably changing the δD) to a decollement at the brittle-ductile transition (350-400°C at 6-10 km depth). The heated and evolving fluids are focussed into the fault zone, ascending along subsidiary fractures, cooling as they spread out into permeable zones (e.g., the coarse clastics of the lower Ladner Group). Cooling may be important for quartz deposition, but the mechanism of ore deposition is enigmatic; effervescence and accompanying pH changes and volatile loss may be important, but hard evidence has yet to be found.

A key argument for our model is the low δD values. One might argue that these represent contributions from irrelevant late secondary inclusions. However, samples for fluid inclusion extraction were chosen so as to minimize the contribution from late secondary inclusions. Samples were given a preheating to selectively decrepitate the late secondaries before intense heating was commenced to liberate older fluids. In all extracted samples, the volume of the early inclusions decrepitating at high temperature greatly exceeded that of the late secondaries bursting during the pre-treat, further decreasing the possibility of contamination. Fluids of serpentinization of antigorite-rich serpentinite were similar to the fluids extracted from quartz samples; contamination by late secondary inclusions could not be a problem in the serpentine samples. The isotopic signatures of antigorites are less easily reset than those of chrysotiles (Wenner and Taylor, 1974), so the signatures obtained from the serpentinites are considered reliable. Furthermore, the $\delta^{18}O$ gradients imply that the fluids came from near the East Hozameen Fault, spreading outwards to the east and west.

CONCLUSIONS

Based on isotopic and fluid inclusion evidence, the fluids responsible for mineralization in the Coquihalla gold belt were determined to be highly evolved local meteoric waters that were greatly enriched in ^{18}O during deep circulation. During the evolution of these fluids, CO_2 was added from organic material in the host metasediments. Focusing of the fluids along a decollement at the brittle/ductile transition at depths of 6 to 10 km and subsequent ascent along subsidiary fractures adjacent to the Hozameen Fault Zone led to deposition of abundant vein quartz and gold mineralization at temperatures of 350 to 380°C, pressures of 750 to 1250 bars, at a depth of 1 to 3 km.

Acknowledgements — We would like to gratefully acknowledge the assistance of Carolin Mines and Aquarius Resources, Ltd., especially Dr. P. W. Richardson for permission to collect samples at the mine and publish our results, and R. J. E. Neils, for assistance while on the mine property. We would also like to thank Dr. G. E. Ray of the B.C. Ministry of Mines, Energy, and Petroleum Resources for his many discussions and assistance in the field. R. St. Louis and Pam Murowchick assisted in the field and laboratory. This work was funded by a NSERC Strategic Grant No. G1107 to Muehlenbachs and Nesbitt.

REFERENCES

Böhlke, J. K. and Kistler, R. W., 1986, Rb-Sr, K-Ar, and stable isotope evidence for the ages and sources of fluid components of gold-bearing quartz veins in the northern Sierra Nevada Foothills metamorphic belt: Econ. Geol., v. 81, p. 296-322.

Cairnes, C. E., 1924, Coquihalla area, British Columbia: Geol. Surv. of Can., Mem. 139, 187 p.

Cairnes, C. E., 1929, The Serpentine Belt of Coquihalla region, Yale district, British Columbia: Geol. Surv. of Can., Summary Report, part A, p. 144-197.

Clayton, R. N. and Mayeda, T. K., 1963, The use of bromine pentafluoride in the extraction of oxygen from oxides and silicates for isotopic analysis: Geochim. Cosmochim. Acta, v. 27, p. 43-52.

Clayton, R. N., O'Neil, J. R. and Mayeda, T. K., 1972, Oxygen isotope exchange between quartz and water: J. Geophys. Res., v. 77, p. 3057-3066.

Coates, J. A., 1970, Stratigraphy and structure of Manning Park area, Cascade Mountains, British Columbia, *in* Structure of the Southern Canadian Cordillera. Wheeler, J. O. (editor), Geol. Soc. Can., Sp. Pap. 6, p. 149-154.

Craig, H., 1961, Isotopic variations in meteoric waters: Science, v. 133, p. 1702-1703.

Colvine, A. C., Cherry, M. E., Durocher, M. E., Fyon, A. J., Lavigne, M. J., Jr., MacDonald, A. J., Marmont, S., Poulsen, K. H., Springer, J. S. and Troup, D. G., 1984, An integrated model for the origin of Archean lode gold deposits: Ont. Geol. Surv., O.F. Rep. 5524, 98 p.

Frost, B. R., 1985, On the stability of sulfides, oxides, and native metals in serpentinite: J. Petrology, v. 26, p. 31-63.

Haugerud, R., 1985, The geology of the Hozameen Group and Ross Lake shear zone, Maselpanik area, northern Cascades, southwestern British Columbia: Ph.D. Thesis, University of Washington, Seattle, WA.

Kerrich, R., 1983, Geochemistry of gold deposits in the Abitibi greenstone belt: Can. Inst. Mining Metall., Sp. Vol. 27, 75 p.

Leach, D. L., Light, T. D. and Goldfarb, R. J., 1986, Fluid-inclusion constraints on the genesis of the Alaska-Juneau gold deposit: G.A.C. Cordilleran Section, Assoc. Expl. Geochem. Symposium: Exploration in the North American Cordillera. Program and Abstracts, p. 53-54.

Magaritz, M. and Taylor, H. P., 1986, Oxygen 18/Oxygen 16 and D/H studies of plutonic and metamorphic rocks across the Cordilleran batholiths of southern British Columbia: J. Geophys. Res., v. 91, p. 2193-2217.

Marshall, B. and Taylor, B. E., 1980, Origin of hydrothermal fluids responsible for gold deposition, Alleghany district, Sierra County, California: Geol. Soc. Am., Abstracts with Programs, v. 12, p. 118.

McRae, J. M., 1950, On the isotopic chemistry of carbonates and a paleotemperature scale: J. Chem. Phys., v. 18, p. 849-857.

Mitchell, P. A., Silberman, M. L. and O'Neil, J. R., 1981, Genesis of gold vein mineralization in an upper Cretaceous turbidite sequence, Hope-Sunrise District, Alaska, *in* Silberman, M. L., Field, C. W. and Berry, A. L. (editors), Proceedings of the Symposium on Mineral Deposits of the Pacific Northwest. U.S. Geol. Surv., O.F. Rep. 81-355, p. 34-39.

Monger, J. W. H., 1970, Hope map-area, west half (92 H W 1/2), British Columbia: Geol. Surv. Can., Pap. 69-47, 75 p.

Murowchick, J. B., Muehlenbachs, K. and Nesbitt, B. E., 1986, Isotopic gradients around gold mineralization, Coquihalla gold belt, southern B.C.: Geol. Soc. Am., Abstracts with Programs, v. 18, p. 701.

Nesbitt, B. E., Murowchick, J. B. and Muehlenbachs, K., 1986, Dual origins of lode gold deposits in the Canadian Cordillera: Geology, v. 14, p. 506-509.

Poty, B., Leroy, J. and Jachimowicz, L., 1976, Un nouvel appareil pour la mesure de températures sous le microscope: l'installation de micro thermométrie Chaixmeca: Soc. Fr. Mineral. Cristallogr. Bull., v. 99, p. 182-186.

Ray, G. E., 1986, The Hozameen Fault system and related Coquihalla serpentine belt of southwestern British Columbia: Can. J. Earth Sci., v. 23, p. 1022-1041.

Ray, G. E., Shearer, J. T. and Neils, R. J. E., 1986, The Geology and Geochemistry of the Carolin Gold Deposit, Southwestern British Columbia, Canada: Gold '86 Proceedings Volume, Ed. A. James Macdonald, p. 470-487.

Rosenbaum, S. and Taylor, B. E., 1984, Sources and temperatures of ore fluids in the northern Mother Lode, California (Alleghany District): Oxygen and carbon isotope evidence: Geol. Soc. Am., Abstracts with Program, v. 16, p. 639.

Shearer, J. T. and Neils, R. J. E., 1983, Carolin Mines: A geological update: Western Miner, November, p. 21-24.

Taylor, H. P., Jr., 1979, Oxygen and hydrogen isotope relationships in hydrothermal mineral deposits, *in* Barnes, H. L. (editor), Geochemistry of Hydrothermal Ore Deposits, 2nd ed. John Wiley and Sons, New York, p. 243.

Weir, R. H., Jr. and Kerrick, D. M., 1984, Mineralogic and stable isotopic relationships in gold-quartz veins in the southern Mother Lode, California: Geol. Soc. Am., Abstracts with Program, v. 16, p. 688.

Wenner, D. B. and Taylor, H. P., Jr., 1971, Temperatures of serpentinization of ultramafic rocks based on $^{18}O/^{16}O$ fractionation between coexisting serpentine and magnetite: Contrib. Mineral. Petrol., v. 32, p. 165-185.

Wenner, D. B. and Taylor, H. P., Jr., 1974, D/H and $^{18}O/^{16}O$ studies of serpentinization of ultramafic rocks: Geochim. Cosmochim. Acta, v. 38, p. 1225-1286.

Diamond Exploration Geochemistry in the North American Cordillera

H. T. DUMMETT
Westmont Mining Inc., 2341 S. Friebus, Tucson, Arizona 85713

C. E. FIPKE
C. F. Minerals Research, 263 Lake Avenue, Kelowna, B.C. V1Y 5W6

and

S. L. BLUSSON
Pioneer Metals Corporation, 1730 - 401 W. Georgia Street, Vancouver, B.C. V6B 5A1

Abstract — Over the past ten years a significant number of diamond-bearing diatremes have been discovered in the North American Cordillera. By far the largest proportion of these have been discovered as a direct result of heavy mineral, stream geochemical exploration.

The most common hosts for diamond are kimberlites and related ultrabasic intrusions that are similar in composition to kimberlite and lamproite. All of these rock types contain some or all of a distinctive, mantle-derived suite of xenocrysts and phenocrysts as silicates and/or oxides. The most common members of the suite are pyrope garnet, chrome diopside, picroilmenite and chromite. Diamond is certainly the most important mineral in the kimberlite and lamproite families. However, its exploration use in North America, unlike that in Western Australia, is severely restricted because its concentrations are orders of magnitude less than those of the other minerals mentioned above.

The oxide-silicate mineral suite associated with diamond lends itself well to geochemical exploration, in particular, heavy mineral stream sediment sampling. All of the minerals have relatively high specific gravities, they are all much more durable in glacio-fluvial regimes than associated minerals, they have distinctive surface textures and two in particular have unique colors. These attributes make it possible to concentrate and identify whichever member(s) of the suite is present in the sampled materials.

There is also an expanding body of evidence that suggests that parts of the compositions of these distinctive minerals can be factored in such a way as to yield a unique sub-assemblage of minerals that are strongly indicative of a paragenesis similar to that of diamond. Such factors are presently derived from relatively uncomplicated arithmetic manipulations of microprobe analyses. The disadvantage of this approach is that it applies at present to only one group of diamond-bearing rocks, out of a possible three or four.

The following paper will discuss diamond exploration in the Cordillera on a case study basis and describe non-proprietary data that are parts of a number of recent diamond discoveries. These discoveries will emphasize the Sloan group in Colorado, Jack in British Columbia, and the Mountain Diatreme in the Northwest Territories.

One of the principal objectives of the paper is to review diamond exploration in the W. Cordillera from the explorationist's point of view, i.e., the treatment will be descriptive in many instances without providing, or even attempting to provide, all the answers. The case studies have been chosen so that they are illustrative and representative of the scale and distribution of kimberlitic anomalies in a particular terrain.

INTRODUCTION

SINCE 1976 a number of companies have explored the W. Cordillera of N. America for diamondiferous kimberlite and lamproite. These are not the only known hosts of diamond, but in the case of N. America they are probably the most important. In general, the exploration techniques used by each company are alike, however, in detail these techniques can be significantly dissimilar.

Most of the techniques are constructed in the anticipation that the diamond host will be a "typical" kimberlite, despite the fact that it is becoming increasingly difficult to satisfactorily define this rock type. An example of this problem is the recent recognition of diamondiferous lamproite in Arkansas that, for decades, was described as kimberlite and/or peridotite (Scott-Smith and Skinner, 1984; Waldman et al., 1986).

Kimberlite most often contains a somewhat unique suite of silicates and oxides in concentrations that usually vary between about 0.5% and 10% of the rock by volume for each mineral. Each of these minerals is a member of the so-called heavy mineral suite, i.e., S.G. >2.9. The silicates also have very distinctive colors and the silicates and oxides have compositions that are, in general, restricted to occurrences in kimberlite. These characteristics have meant that these minerals lend themselves readily to discovery by heavy mineral geochemical exploration.

It is appropriate to note that the most diagnostic mineral that could be utilized in these programs is diamond, however, it occurs in concentrations in the host that are so low that its utility is severely restricted. It has been used very effectively in parts of Australia but this use is somewhat unique.

The following discussion will deal with kimberlite as the most common diamond host in the Cordillera. The recent recognition of lamproite as another important source rock has meant that the explorer need be aware that the differences from kimberlite are significant only to the extent that some of the kimberlitic minerals may not be as abundant in lamproite and that other non-"kimberlitic" minerals may be additionally useful in the exploration for diamondiferous lamproite.

This discussion will describe the results of geochemical programs carried out in three sub-areas in the Cordillera. In each case the geochemical techniques used for discovery were some-

what different as were the target kimberlites and the overall geological setting. Other factors such as climate, topography and drainage were also different and had a major impact on the design and execution of the subsequent exploration programs for each sub-area. The three areas to be discussed are in the foothills of the Colorado Rockies, the Main Ranges of the British Columbia Rockies and in the MacKenzie Mountains of the Northwest Territories. Refer to Fig. 1 for general locations of each of the areas.

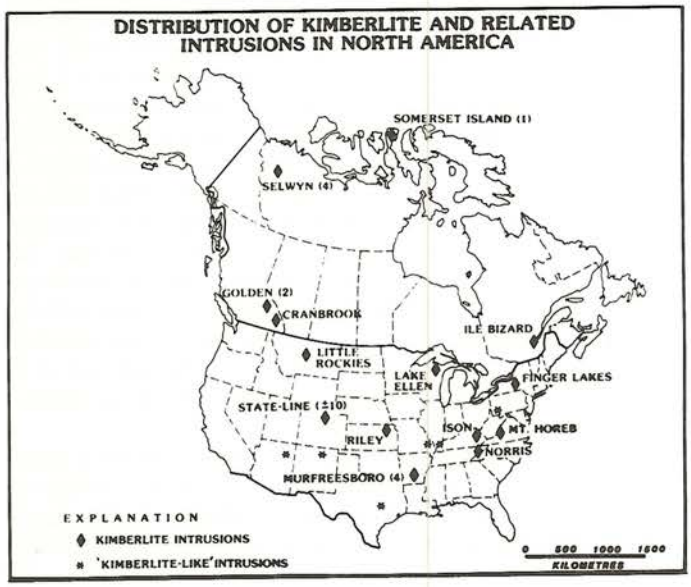

Fig. 1. Locations of the important kimberlite provinces in North America. Numbers in parentheses after the district name are for the number of known diamondiferous pipes in the district. The Sloan pipe is part of the State-line group, Jack is part of the Golden Group, and the Mountain Diatreme is part of the Selwyn group.

SAMPLING TECHNIQUES

Common to all the areas that were explored is a topography of moderate to extreme relief produced by a well-developed drainage system of intermittent and perennial streams and rivers. Because of this, it was assumed that detritus from an eroding kimberlite would probably be transported from its source to the nearest drainage(s). This transport would be accomplished largely by mechanical agencies, principally soil creep and run-off accompanying rainfall and snow melt. The three case studies discussed here were therefore part of exploration programs that were designed assuming that discovery would be effected in large part by mineral anomalies in stream silts.

Although this assumption is self evident to most explorationists working in the Cordillera, this type of diamond exploration is significantly different from that practiced in other parts of the world. For example, much emphasis is placed on soil and loam sampling in southern Africa and South America because of the poorly developed drainage systems and/or a topography of little relief that does not promote effective dispersion of kimberlitic detritus.

Initially, therefore, for all three areas, a "guesstimate" was made that a sample interval of about 1.5 km along all the major drainages would probably be sufficient to locate heavy mineral anomalies derived from kimberlites in the drainage basin. This sampling interval proved in most cases to be appropriate for discovery, although in many cases much follow-up sampling and reconnaissance mapping was necessary before such discovery was made.

To the extent that it was possible, i.e., dictated by the sample site and/or the medium being sampled, approximately 10 to 15 kg of minus 6 mesh sample was gathered at each site. Samples were invariably taken at those sites that were judged most likely to have concentrated the heavy fraction of the stream load. All samples were sent to the C.F. Minerals laboratory in Kelowna, British Columbia for initial processing, that is, the recovery and classification of the heavy mineral fraction.

This processing consists of three main stages: washing, screening and drying; heavy liquid separation (TBE and methylene iodide); and classification of the "heavies" into four categories using Frantz isomagnetic separators. These latter categories provide separates for each of the most easily recognizable kimberlitic minerals, viz., pyrope, chrome diopside, ilmenite and diamond.

Subsequent examination of the magnetic separates was usually carried out at the project offices or at a laboratory in Superior Oil Company's Tucson office. The objective of this examination was to label and describe the anomalous samples and extract from them a representative selection of the kimberlitic population for mounting prior to microprobe analysis.

Microprobe analysis was carried out at Superior's Geoscience Lab in Houston, Texas, or at the probe facility of the University of Cape Town's Geology Department. The importance of microprobe/SEM analysis will be discussed as a separate part of this paper. It is relevant to note here that it significantly contributes to the explorer's ability to rank anomalous drainages and, in so doing, shorten the time between anomaly recognition and diamond discovery.

COLORADO

The Sloan kimberlites

This group of at least six Siluro-Devonian kimberlite pipes and an unknown number of dikes are located in Larimer County in north-central Colorado about 65 kms northwest of Ft. Collins (Fig. 1). They are included in a larger group informally known as the "State-line pipes" because the other pipes in the group define an area which straddles the state boundary shared by Colorado and Wyoming. All of the subsequent discussion will describe the geochemical exploration associated with the pipes and will refer to the dikes only where necessary.

The topography in the vicinity of the pipes consists of rolling hills with a relief of about 185 meters. The two principal drainages, Rabbit Creek and Meadow Creek are perennial, while their tributaries flow after heavy rains or during the spring thaw.

The hillsides and upland plateaus are covered by mixed aspen and coniferous forest while the valleys are predominantly grassland. It is important to note that the kimberlites are also usually covered by grasses for the most part. This phenomenon has not been studied in detail but it appears to be due to an

aversion of the arboreal species to clay-rich soils in this part of Colorado and Wyoming.

The Sloan pipes are hosted by Precambrian crystalline and metamorphic rocks (Silver Plume Granite and its equivalents). Each pipe is quite different in shape, size and the nature of the various kimberlite intrusions that occupy the respective diatremes (Table 1). All of these bodies, including Sloan 1 and 2, are small compared to pipes that are commonly mined and which have surface areas that are typically larger than ±12 hectares.

Table 1. Physical characteristics of the Sloan kimberlites

Pipe #	Pipe Shape	Pipe Area (Ha)	Elevation (m amsl)	# of kimberlites within diatreme
1	Elongate	7	2200	8
2	Dike-like	3	2200	3
3	Irregular	<1	2300	?1
4	Irregular	1	2200	?1
5	Irregular	3	2300	3
6	Oval	2	2300	3

Sloan 1 and 2 are in fact parts of the same highly irregular-shaped diatreme. The eastern part of this diatreme, a 30 meter wide, dike-like extension, is known as Sloan 2. Sloan 1 is also rather complex in that it contains at least eight discrete kimberlite intrusions while Sloan 2 probably contains no more than three. Although Sloan 5 and 6 occur very close to each other, they are not known to be contiguous.

A limited number of absolute age dates have been reported for the pipes in the Colorado Rockies. Most recently, Smith (1983), obtained two ages from Iron Mountain in Wyoming, 308 ± 32 Ma and 395 ± 15 Ma, and one age from the Estes Park dike, 394 ± 45 Ma. The last two of these dates support a fission track age of 380 Ma reported by Naeser and McCallum (1977) from an unidentified pipe in the State-line group.

At the outset of exploration in Colorado, it was decided to sample all perennial and intermittent drainages at a three kilometer spacing. This distance was somewhat arbitrarily selected and the spacing was intended to be modified if circumstances dictated. In the case of Rabbit Creek a spacing of about 0.8 km was initially selected because the presence of a number of kimberlites was suspected. In the case of Meadow Creek, the initial spacing of three kilometers was shortened to 0.8 km after the anomalous nature of the drainage had been established.

The geochemical dispersion patterns associated with the Sloan pipes is very much a reflection of their primary mineralogies. Sloan 1 and 2, for example, contain some kimberlites that are rich in pyrope and chrome diopside, i.e. these two minerals occur in concentrations of up to 5% by volume of the rock. At least two of the major phases at Sloan 1 do not, however, contain mesoscopic chrome diopside and pyrope. Much of the Sloan 2 diatreme is occupied by a single intrusion that contains megacrystic pyrope, chrome diopside and ilmenite and it is possibly this phase that dominates the kimberlitic detritus downstream from that pipe as well as Sloan 1.

The diamond population at Sloan 1 and 2 contains a spectrum of shapes from those that are well preserved octahedra to types that are highly resorbed tetrahexahedra. Colors range from those that are near D or E to some that are very dark

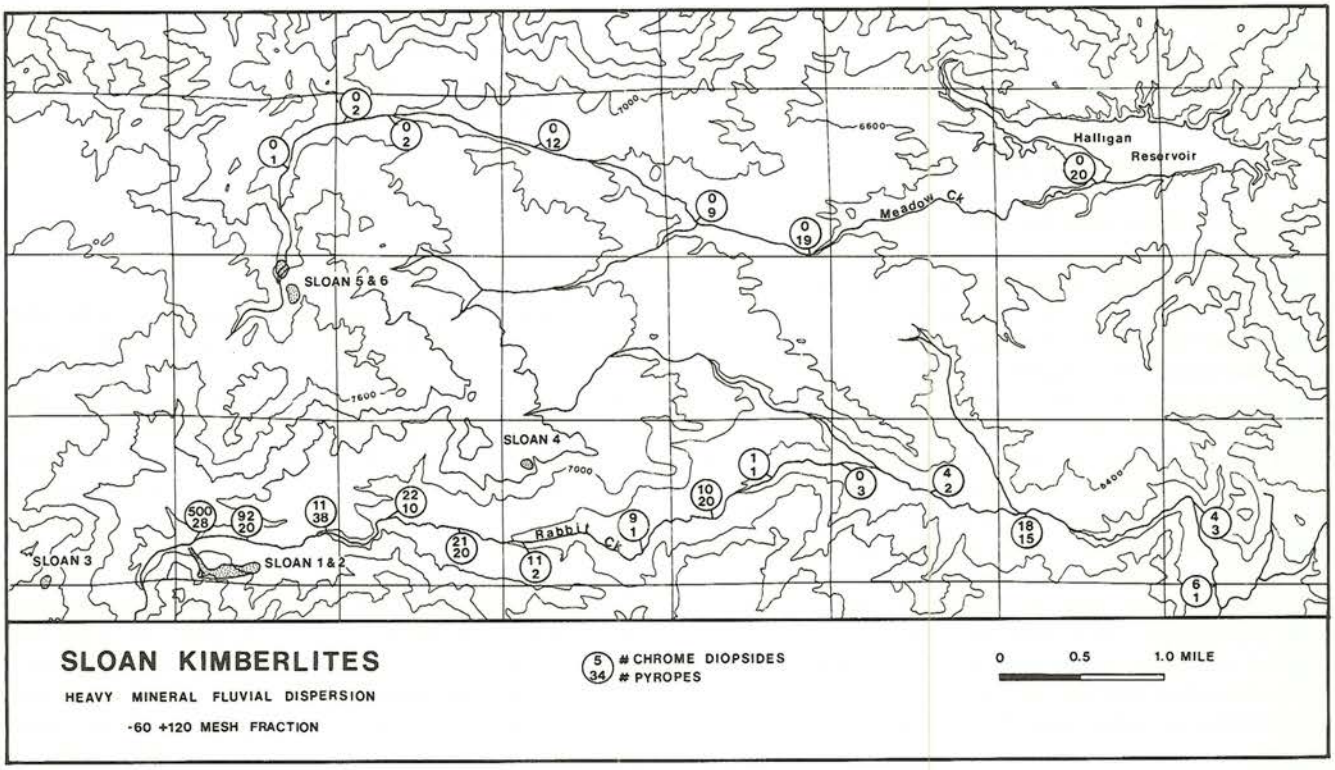

Fig. 2. Dispersion of pyrope and chrome diopside in the Sloan district drainages.

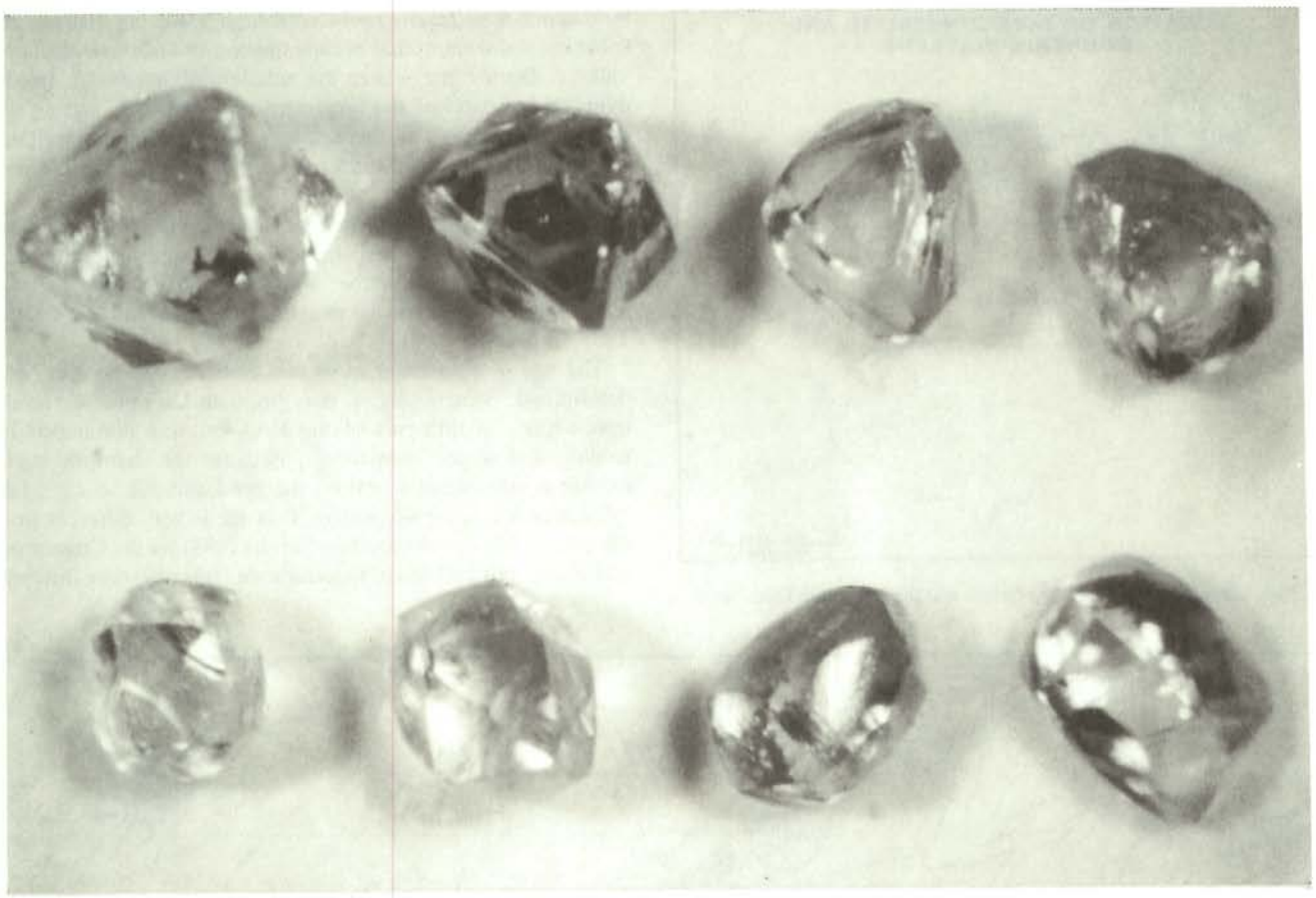

Fig. 3. A selection of gem diamonds from Sloan 1 and 2. The stones each weigh about 0.10 carats and also show the range in shape from well preserved octahedron to resorbed tetrahexahedron.

brown — yellow stones are very rare. A typical selection of gem diamond shapes is shown in Fig. 3.

The distribution and mode of the anomalous samples in Rabbit Creek is shown in Fig. 2 at fourteen sites. This diagram details only the results for mineral abundances in the −60 to +120 mesh fraction. Chrome diopside at each of the sample sites usually occurs as angular to subangular grains because it seems to disintegrate readily into progressively smaller pieces as a function of a very well developed cleavage and distance from source. Pyrope on the other hand, is commonly rounded to subrounded, although angular grains are present in some of the samples.

The number of mineral grains occurring at each site exhibits a general decrease with increasing distance from the source kimberlites. However, there are a number of sites at which there is a significant increase in the number of minerals relative to the site immediately on the upstream side. This phenomenon is true for both minerals sampled. Once it was established that this was not due to the ingress of "new" kimberlitic detritus from an additional source, it was concluded that the site(s) probably represented more favorable conditions for the concentration of heavy minerals.

The dispersion of kimberlitic minerals from Sloan 5 and 6 in Meadow Creek is also shown in Fig. 2. Notice that the stream load does not contain chrome diopside because most of the source kimberlites, like some of those at Sloan 1, are chrome diopside poor. These kimberlites do, however, contain pyrope but the dispersion pattern for this mineral is unusual in that its relative abundance shows an increase with distance from source. In the case of this particular creek it is unlikely that this phenomenon is an artifact of site specific concentrating conditions. Alternatively, it could be due to a progressive change in the gradient of the stream, which becomes flatter towards its point of entry into Halligan Reservoir. This would imply that as the gradient flattened, more and more of the sediment load would be deposited.

BRITISH COLUMBIA

Jack Diatreme

The Jack is the larger of at least two diatremes in a group that occurs about 35 km northwest of Golden in east-central British Columbia (Fig. 4). These two pipes are at the northwestern end of a kimberlitic province that is approximately 50 km long (NW-SE) and 8 km wide and is parallel to the regional tectonic fabric.

Topography in the area of the diatreme is extreme — relief is on the order of 1800 metres. The drainage pattern is dominated

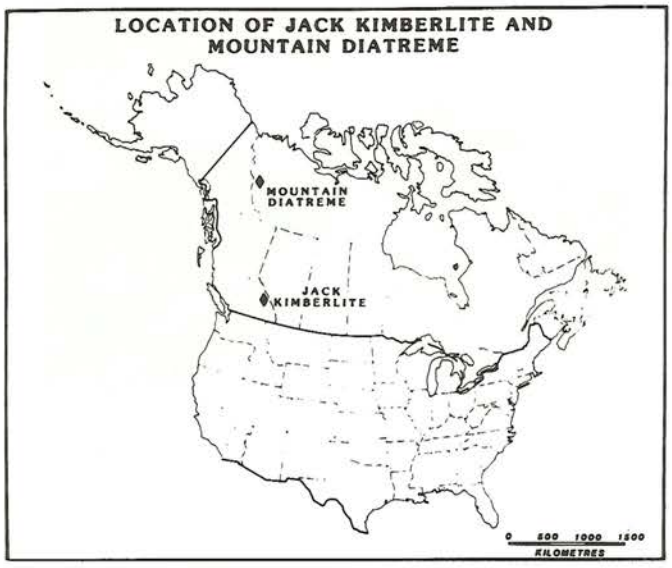

Fig. 4. Location of the Jack kimberlite and the Mountain Diatreme.

by a number of small creeks with high gradients that are the tributaries of streams that occupy the bottoms of large glaciated valleys. During the winter the smaller tributaries are frozen over, as are parts of the larger streams, however, during the spring thaw flow in all these drainages is torrential. Mechanical dispersion of detritus under these fluvial conditions is therefore very efficient.

The diatreme is hosted by Late Cambrian to Ordovician and ?Silurian carbonates which form part of the east dipping limb of the Cockscomb anticline, which in turn is thrust easterly over the U. Devonian on the west dipping Mons fault (Northcote, 1983; Wheeler, 1962).

The age of emplacement of this diatreme has not yet been determined. Structurally, it may pre-date Laramide deformation which, in this part of the Rockies, was dominated by folding and major imbrication. Because the diatreme rocks exhibit a very weak foliation, the pre-Laramide or even late syn-Laramide age is suggested. This age is very different from the 241 ± Ma age obtained by Smith (1983) for the Cross pipe, which is about 250 km to the southeast. It is also very different

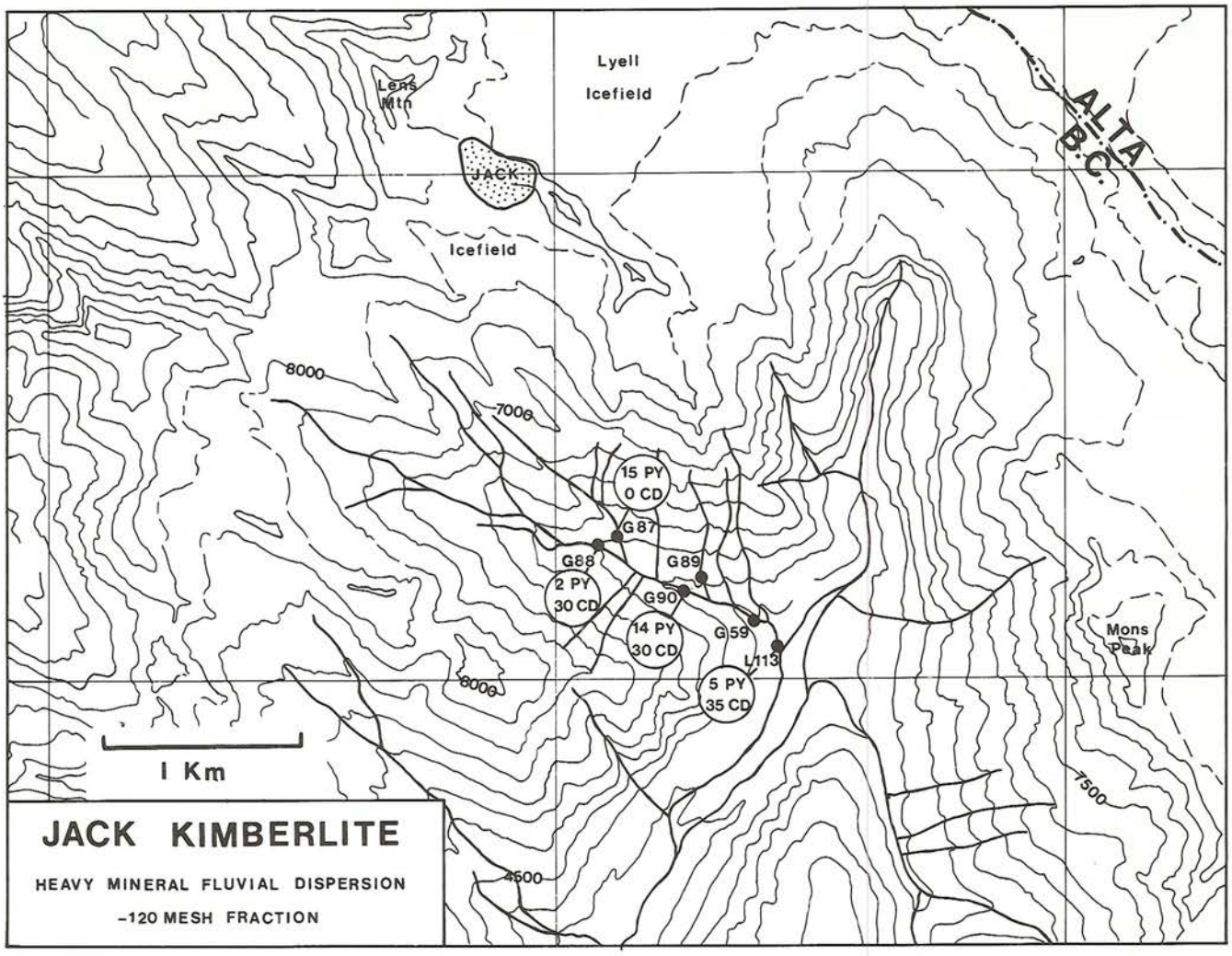

Fig. 5. Fluvial dispersion of pyrope and chrome diopside from the Jack kimberlite.

from the 408 ± 15 Ma date obtained by Wanless et al. (1965) from a small pipe about 30 km to the south of the Jack.

The dimensions of the Jack can best be approximated by outcrops of kimberlitic marl and tuff occurring along a ridge which strikes southeast from Lens Mountain and separates the Lyell icefield from a smaller icefield to the southwest (Fig. 5). One large outcrop of marl is located within the smaller icefield. Together, these limited outcrops define a pipe that measures at least 1.20 km by 0.50 km for an aggregate surface area of about 58 hectares, making this one of the larger kimberlitic pipes in the world. The marls that make up at least 75% of the outcrop are epiclastic, i.e., they accumulated as back-wash sediments in the crater created by the explosive emplacement of the diatreme.

The dispersion pattern for kimberlitic detritis from the Jack is shown in Fig. 5. During initial sample investigation only the −60 to +120 mesh fraction was examined. Of all the samples examined, only one (L113) contained a single grain of chrome diopside. Subsequent examination of the −120 mesh fraction of these same samples yielded a number of samples containing both chrome diopside *and* pyrope. Furthermore, the results of the sampling indicated that there are at least two sources of kimberlitic detritus in the headwaters of the drainage sampled by sample L113.

Sample G87 contains detritus that is probably derived from the Jack, while sample G88 probably contains detritus from another kimberlite. This interpretation is possible because the character of the two samples is so different; whereas G87 is pyrope-rich and contains no chrome diopside, G88 is chrome diopside-rich but contains subordinate pyrope. It is possible, though, that this difference in the make-up of the two samples is an artifact of the sampling procedure. Downstream from these two sites the drainage contains minerals derived from both sources.

NORTHWEST TERRITORIES

The Moutain Diatreme

This large diatreme is one of a small group, numbering perhaps three or four, that occur in the Sayunei Range of the

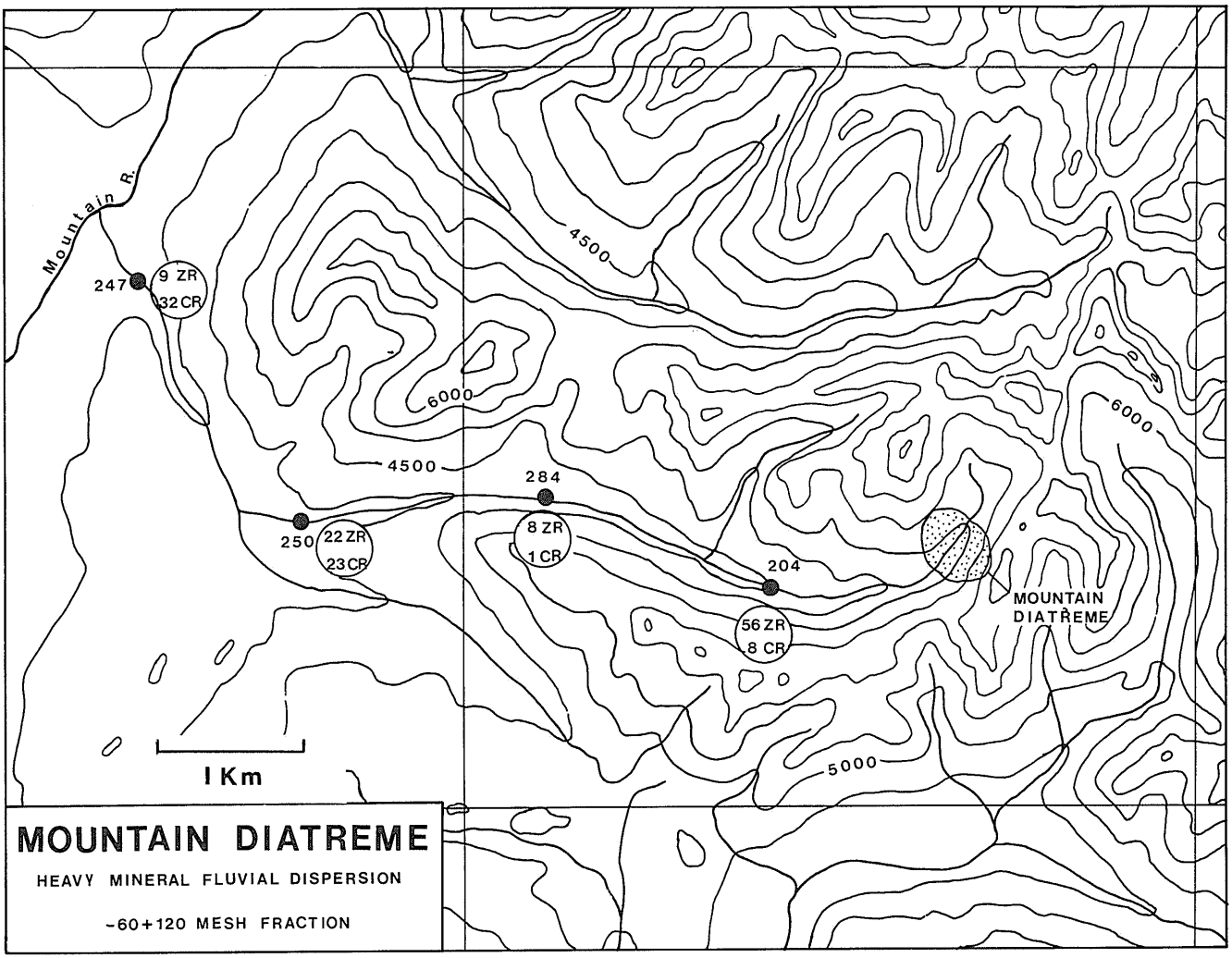

Fig. 6. Dispersion of kimberlitic zircon and kimberlitic chromite from the Mountain Diatreme.

western NWT. The Sayunei Range is part of the northern Mackenzie Mountains. The diatreme is about 195 kms southwest of Norman Wells, a settlement on the Mackenzie River.

Topography in the area consists of mountains that are commonly between 1980 and 2100 metres high, incised by broad valleys that have elevations between 1200 and 1500 metres. The valleys are occupied by streams and rivers that flow only during the short summer season. Dispersion of kimberlite detritus has been very efficient as in the case of the Jack.

The Mountain Diatreme has been emplaced into unnamed Early Cambrian to Middle Ordovician carbonates and Early Ordovician to Early Silurian Mt. Kindle carbonates. The Mountain, as well as some of the satellite diatremes, occurs at or near the edge of the carbonate platform of the Mackenzie Mountains (Godwin and Price, 1986). The same authors report radiometric dating (K-Ar and Rb-Sr on phlogopite) that has yielded two Silurian ages for emplacement, i.e., 445 ± 17 Ma and 427 Ma.

The diatreme measures approximately 850 metres by 450 metres and has a surface area of about 9 hectares. It is geologically simple in that it is occupied by only two major kimberlitic phases, a central green breccia and a marginal rusty weathering breccia. Godwin and Price (1986) have mapped three other phases that are volumetrically minor. One of these phases, the epiclastic reworked tuff, is important because it indicates that the diatreme is exposed very near its original surface of emplacement and has undergone minimal erosion since that time. This is analogous to the level of exposure of the Jack. Unlike the Jack however, the Mountain Diatreme was preserved by deposition of younger sediments very soon after its emplacement and it is only recently that it has been exhumed (post-Eocene).

This exploration example affords a good illustration of the necessity of adapting geochemical techniques to a very specific target. The detritus downstream from the diatreme is dominated by kimberlitic zircon and kimberlitic chromite, whereas chrome diopside, pyrope and picroilmenite are very minor constituents.

Dispersion of this detritus is illustrated in Fig. 6 for results from the −60 to +120 mesh fractions. The mineral train is considerable, i.e. at least 10 kms and to some extent this is a function of geography. Because of the high latitude, oxidation of kimberlitic rocks is minimal and has resulted in the unusual occurrence of large (± 1 metre diam.), ice-rafted boulders of the diatreme rocks at least 5 kms downstream from their source. In addition many smaller kimberlitic boulders have been transported downstream for at least 3 kms by run-off. Both of these phenomena mean that there are sources for detritus, that are a considerable distance from the diatreme and which contribute to the drainage being sampled. It is very rare to find kimberlitic rocks as part of the boulder train at lower latitudes, e.g. in Colorado.

The behavior of the geochemical anomalies is also unusual inasmuch as zircon exhibits a pattern of decreasing abundance with distance from source, whereas the pattern for chromite is just the opposite. Admittedly, this conclusion is based on a small number of sample points, nonetheless it is difficult to explain this phenomenon as it relates to two minerals with similar densities.

MICROPROBE GEOCHEMISTRY

The compositions of some members of the pyrope family have made it possible to devise a target-ranking technique that significantly improves the explorer's ability to discover diamond-bearing kimberlite. The technique described below refers, thus far, only to pyrope derived from diamondiferous, peridotitic kimberlite. At least two other ultrabasic rocks contain diamond, namely eclogitic kimberlite and lamproite. The basis for the technique is the hypothesis that mantle peridotite contains an assemblage of minerals, especially diamond and pyrope, that become part of a kimberlite melt by disaggregation of such entrained peridotite as the melt rises to the earth's surface.

The pyropes, Group 10 of Dawson and Stephens (1976), that are so useful in this respect have been described and discussed by Sobolev et al., (1973), Boyd and Gurney (1982) and Gurney (1984). Shown in Fig. 7 are binary plots of pyrope compositions from the matrices of a number of kimberlites, from those that are barren or very low-grade to two pipes that are currently being mined. These plots are a modification of those as used by Sobolev (1974). Note: these "Sobolev diagrams" are not, by implication, a more useful way of illustrating the data than those used by Gurney (1984).

The plots are derived from SEM analyses carried out at Superior Oil's Geoscience Lab in Houston and/or at the probe facility of the Geology Department at the University of Cape Town. Also included are some data from the literature, although these comprise less than 10% of the points shown. Each of the plots is subdivided into four rectangular areas. The most important of these is in the lower left corner and defines the field of compositions similar to pyropes that are most typically found as diamond inclusions. The upper right area usually includes the majority of pyrope compositions for peridotitic kimberlite that correspond to Group 9 of Dawson and Stephens (1976).

The first two plots shown include no compositions in the "diamond inclusion" (DI) field and are representative of pipes that are very low grade or barren, i.e. Jack and Lovedale. the Lovedale pipe referred to here is in the Cape Province of South Africa and should not be confused with the diamondiferous pipe of the same name referred to by Wagner (1914) that is in the Orange Free State. The data from the Sloan pipe include very few compositions in the DI field indicative of low average grades, which is indeed the case. The data for the high grade Mir (USSR) and Finsch (South Africa) pipes contain many pyrope compositions in the DI field.

Somewhat predictably, the data set shown leaves the impression that interpretations of probe data are likely to be relatively simple and straightforward as they apply to this particular group of kimberlites and their pyropes. It is well to remember that during the operation of an exploration program the character (peridotitic, eclogitic or lamproitic) of the target will not be known until much exploration data has been generated — it is at that time that interpretations as outlined above can properly be made.

Qualifications that should and can be imposed on the data interpretation are illustrated by the Jack example. At first glance the data from this pipe are, as indicated above, suggestive of very few diamonds in the host. However, this particular data set is small compared to that from the other sites. There are

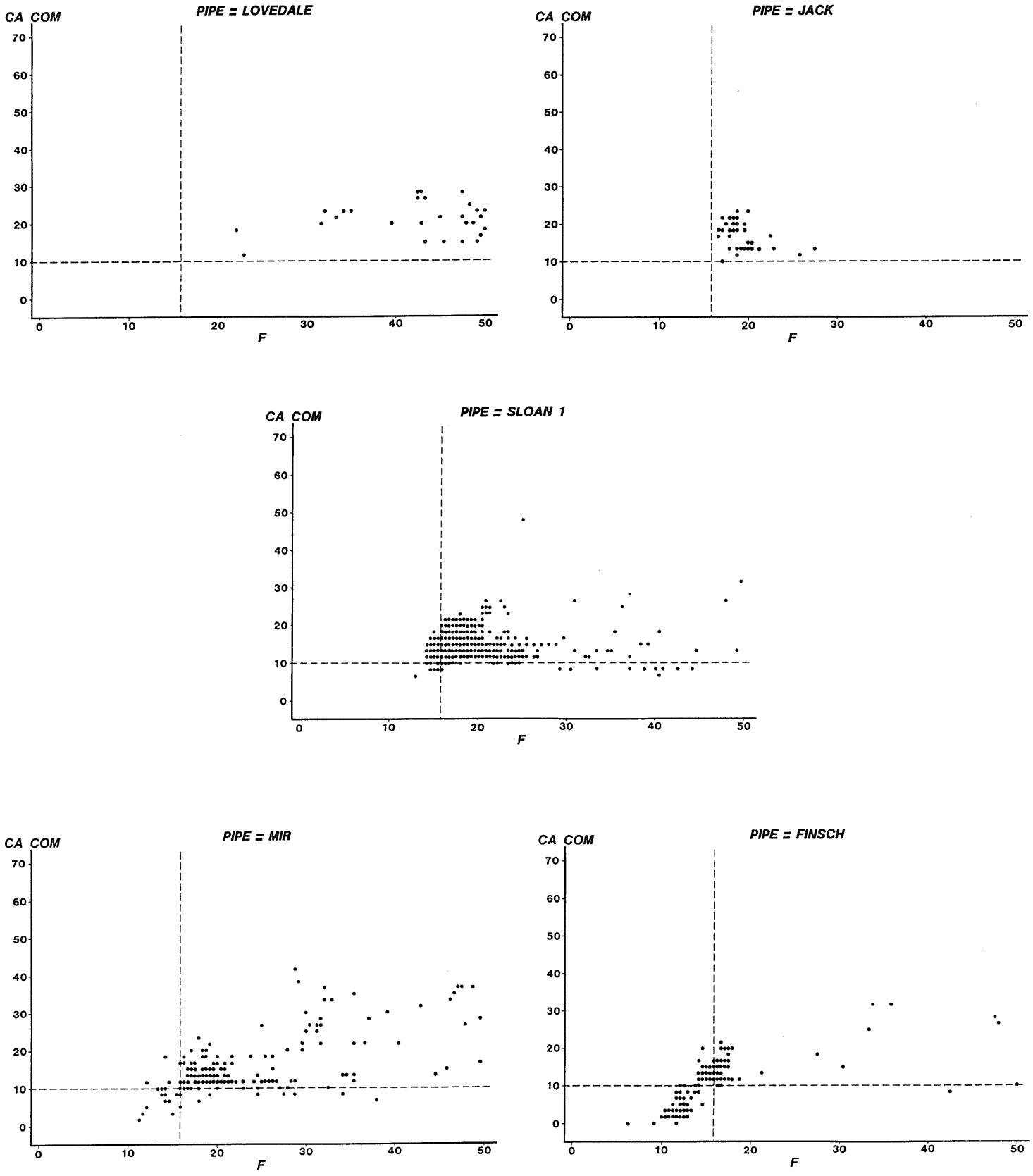

Fig. 7. Plots of pyrope compositions from Lovedale, Jack, Sloan, Mir and Finsch.

also no exposures of kimberlitic breccias, instead the data are from minerals in rocks that include a very dilute (<5%) kimberlitic component. It is possible therefore, that the Jack interpretation will change as more data are generated and the underlying kimberlites are sampled. In the case of Sloan, there is also the added possibility that much of the diamond population has been derived from disaggregated eclogite, as well as peridotite.

In practice therefore, definitive conclusions about the significance of the pyrope compositions require a large data base to serve as a filter to properly label those samples that contain pyropes with a high probability of diamond paragenesis. The diagrams shown above are thus intended to serve as an introduction to the methodology and should be integrated into diamond exploration programs with appropriate caution.

CONCLUSIONS

It is indeed possible to discover diamondiferous kimberlite in the North American Cordillera using comparatively uncomplicated geochemical exploration techniques. Demonstrably, the most effective of these is heavy mineral sampling of stream sediment. This is because the physical characteristics of kimberlitic minerals (color, surface texture and density) enhance their respective abilities to be concentrated in stream silts as well as facilitate their subsequent recovery and recognition.

Each of the studies cited above has readily detectable geochemical signatures that are similar to the extent that the anomalies are made up of one or more members of the kimberlite mineral family. The examples are different in respect of how each member has behaved in the fluviodynamic sense, i.e. it is not yet possible to explain nor predict how effectively one particular mineral will be transported or concentrated in streams and rivers in the Cordillera.

Successful exploration programs are, therefore, those that have maximized similarity of sample treatment from site to site. Specifically, this has meant no pre-concentration in the field (i.e. hand-panning) and, to the extent possible, exactly the same laboratory treatment of all samples over an extended period of time. Given such control it is possible to assign to each kimberlitic mineral anomaly a probability of diamond association and, in so doing, significantly minimize both time and money commitments to the discovery of "ore".

Acknowledgements — We owe a very special debt to our colleagues, the management, geologists, mineralogists, samplers and lab technicians of the Superior Oil Company, Falconbridge Nickel Company of Canada and C.F. Minerals Research, for their essential contribution to the design and execution of a number of very effective and exciting diamond exploration programs. Dr. John Gurney of the University of Cape Town was a very enthusiastic and instructive consultant to all the above programs. The authors would also like to thank Mobil Corporation and Long Lac Minerals (USA) for permission to include data from the Sloan district in this paper.

REFERENCES

Boyd, F. R., and Gurney, J. J., 1982, Low-calcium garnets key to craton structure and diamond crystallization: Yearbook Carnegie Inst., Washington, 81, p. 261-267

Dawson, J. B., and Stephens, W. E., 1976, Statistical classification of garnets from kimberlite and associatied xenoliths: Addendum. J. Geol., v. 84, p. 495-496

Godwin, C. I., and Price, B. J., 1986, Geology of the Mountain Diatreme kimberlite, north-central MacKenzie Mountains, District of MacKenzie, Northwest Territories: Can. Inst. Min. Metall. Bull. (in press)

Gurney, J. J., 1984, A correlation between garnets and diamonds in kimberlites, *in* Glover, J. E. and Harris, P. G., eds., Kimberlite occurrence and origin: a basis for conceptual models in exploration. Univ. of W. Australia. Pub. 8; 143-166

Naeser, C. W. and McCallum, M. E., 1977, Fission-track dating of kimberlitic zircons: Second Int. Kimberlite Conf. Extended Abstracts (Carnegie Inst., Washington, D.C.).

Northcote, K. E., 1983, Report on the Jack claims, Lens Mountain 82N/14E, Golden Mining Division, Lat 51°54'N Long 117°08'W: Brit. Columbia Dept. Mines., Assessment Report.

Scott-Smith, B. H., and Skinner, E. M. W., 1984, A new look at Prairie Creek, Arkansas, *in* Kornprobst, J., ed., Kimberlites III: Annales Sci. L'Universite de Clermont Ferrand, 74; pt.1, 27-36

Smith, C. S., 1983, Rubidium-strontium, uranium-lead and samarium-neodymium isotopic studies of kimberlite and selected mantle-derived xenoliths: Ph.D. thesis, Univ. Witwatersrand, 435 p. (unpubl.).

Sobolev, N. V., Lavrenty'ev, Y. G., Pokhilenko, N. P., and Usova, L. V., 1973, Chrome-rich garnets from the kimberlites of Yakutia and their parageneses: Contrib. Mineral. Petrol., v. 40, p. 29-52

Sobolev, N. V., 1974, Deep-seated inclusions in kimberlites and the problem of composition of the upper mantle: Amer. Geophysical Union, Washington, D.C., 279 p.

Wagner, P. C., 1914, The diamond fields of South Africa: Cape Town, Struik, 355 p.

Waldman, M. R., McCandless, T. E., and Dummett, H. T., 1986, Geology and mineralogy of the Twin Knobs #1 lamproite, Pike County, Arkansas: Geol. Soc. Amer., Special Paper (in press).

Wanless, R. K., Stevens, R. D., Lachance, G. R., and Rimsaite, J. Y. H., 1965, Age determinations and geological studies, K-Ar isotopic ages: Geol. Surv. Can. Paper 65-17, Report 6, p. 19.

Wheeler, J. O., 1963, Rogers Pass Map-Area British Columbia and Alberta: Geol. Surv. Can. Paper 62-32, 1-30.

Behavior of Scheelite in a Cordilleran Stream

D. SAXBY AND W. K. FLETCHER
Department of Geological Sciences, University of British Columbia
Vancouver, B.C., V6T 2B4

Abstract — Erratic distributions are characteristic of drainage surveys for elements dispersed as major constituents of heavy minerals. We have investigated this for scheelite dispersion downstream from a skarn deposit in the McKenzie Mountains of the Yukon Territory. Paired low and high energy sediment samples were collected up to 26 km downstream from the deposit. Heavy mineral concentrates were prepared (SG >3.3) and scheelite grains counted to estimate the W content of five size fractions.

Although significantly higher W concentrations are found at high energy sites, those from low energy sites are much less erratic. Furthermore, both sampling errors and variations in tungsten values on the stream bed decrease with decreasing grain size. The latter is attributed to grain size becoming more important than density in controlling transport of the smaller particles. With respect to exploration, although high energy sites are more sensitive indicators of the presence of scheelite in a drainage basin, low energy sites provide a better guide to its source. Sampling the finer size fractions minimizes hydraulic effects and improves sampling statistics.

INTRODUCTION

STREAM SEDIMENT sampling is based on the premise that a single sediment sample is a natural composite of the products of weathering and erosion upstream from the sample site. However, for elements dispersed as heavy minerals there is substantial evidence that sorting and hydraulic processes can influence concentrations sufficiently to disrupt regular downstream decay of an anomaly away from its source (Gladwell, 1981; Sleath and Fletcher, 1982; Fletcher et al., 1985; Zantop and Nespereira, 1979). In addition, random sampling and subsampling errors can be significant when sampling for rare grains (Clifton et al., 1969; Ingamels, 1974; Day and Fletcher, 1986). Analytical errors also become important if analytical detection limits are approached (Fletcher, 1981) — conditions likely to be encountered in geochemical exploration for elements such as Au, Sn and W. This study attempts to assess and suggest practical methods of minimizing these problems for tungsten dispersed as scheelite.

STUDY AREA

Location and geology

The Clea tungsten property is located at 62°4′ north latitude and 129°52′ west longitude in the Pelly River drainage of the Selwyn Mountains, Yukon Territory, Canada (Fig. 1). Geologically the property lies within the eastern margin of the Selwyn Basin, a northwest trending subprovince of the Canadian Cordillera bounded on the east and west by the coeval McKenzie and Cassiar carbonate platforms, respectively (Gabrielse, 1967).

In the eastern part of the basin Palaeozoic sediments are intruded by Cretaceous quartz monzonite stocks. The Clea deposit is associated with one such stock, 500 m in diameter at the surface, intruded into interbedded argillaceous and calcareous Silurian sediments (Godwin et al., 1980; Gordey, 1981). Dick (1980) describes five skarn zones characterized by wollastonite; pyroxene-garnet-vesuvianite; pyroxene-vesuvianite; amphibole-garnet; and biotite-garnet. Scheelite, the only abundant tungsten mineral, occurs mainly in the amphibole-garnet and biotite-garnet zones in Clea and Omo cirques and on the intervening arête as far as 1 km from exposed quartz monzonite.

Physiography

Alpine glaciation during the Pleistocene has resulted in topographic features ranging from cirques rimmed by jagged horns and arêtes to broad U-shaped valleys and gently rolling hills. Elevations vary from 2,177 m at the head of Clea cirque to 1,000 m on the floor of the main valley which forms the headwaters of the Pelly River and has a catchment area of about 160 km within the study area. Tributary drainages drop steeply from cirques and ridges for an average of 5 km before reaching the main valley. Reaches along the Pelly alternate between steep bedrock falls, meanders in alluvium and rapids in glacial till with an overall gradient of 1.25%.

Climate is relatively dry, alpine continental with an extreme temperature range. The property is snow-free from mid-July to mid-August and summer rain showers are frequent.

METHODS

Sampling

To isolate variations in abundance of scheelite resulting from hydraulic effects, paired sediments were studied at adjoining high and low energy stream environments, distinguished on the basis of sediment texture, at sixteen stations over a distance of 25 km along the Pelly River (Fig. 1). Sediments at high energy sites are all gravels, those at low energy sites range from gravelly sands to gravels. Additionally, duplicate high and low energy samples were collected at ten stations, within 10-50 m of the original pair. A typical sampling plan is shown in Fig. 2. Samples were collected, either from pits dug through uniformly textured sediments or by taking a surface layer if this was necessary to stay within a particular size range (depositional unit), and sieved to minus 2 mm (10-mesh) on-site to give an

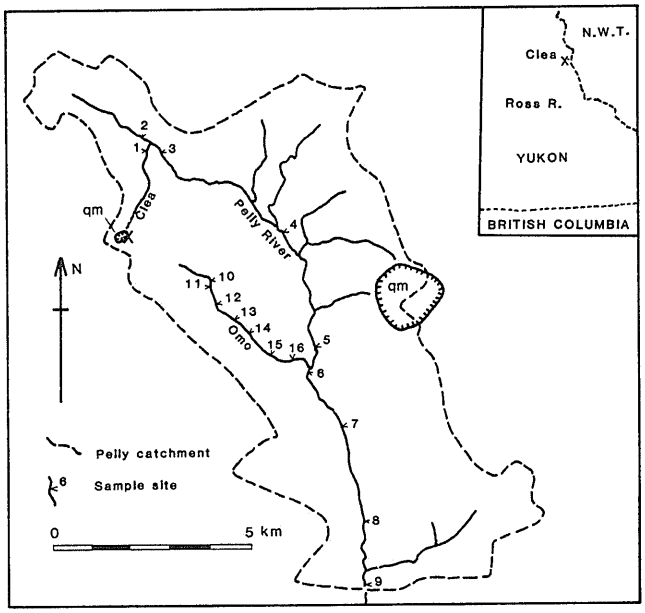

Fig. 1. Sample sites along the Pelly River and its tributaries: qm = quartz monzonite, X = Clea property.

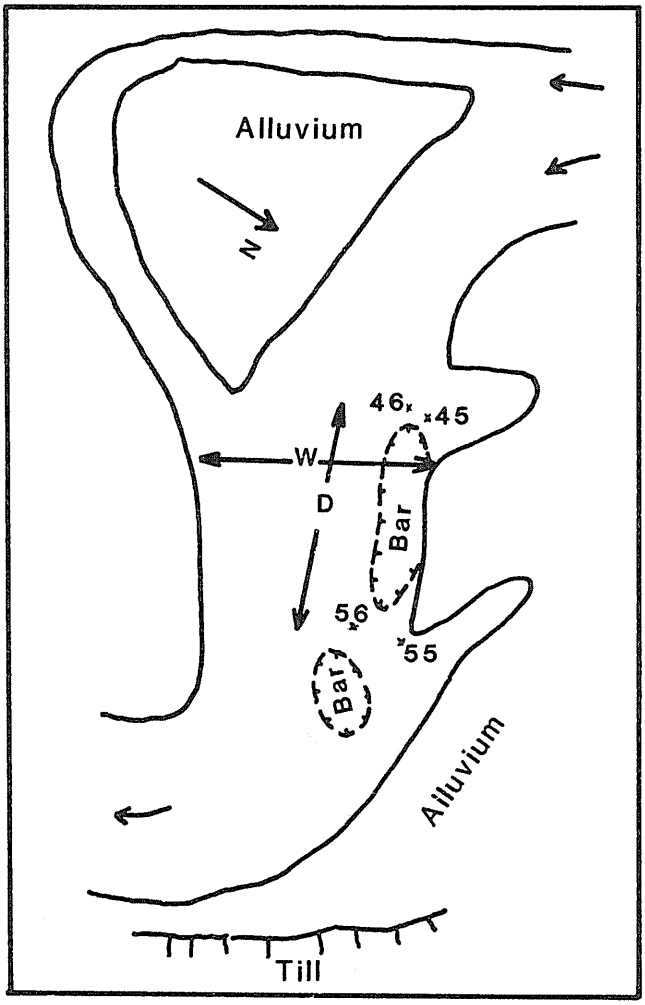

Fig. 2. Sampling plan at station 14. Samples 45 and 55 at low energy sites, 46 and 56 at high energy sites; W = 6.2 m and D = 9.3 m.

average of 14 kg of wet sediment. Each site was sketched and a vertical photograph taken from a height of 1.5 m to cover 1.0 x 0.6 m with a weighted metre stick for scale. The photograph was subsequently used to classify sediment texture according to Folk (1974) with the median grain size being defined such that larger and smaller grains cover equal areas. Stream velocites were measured at half-depth with a propeller driven fish.

Sample preparation and grain counting

The flow sheet for sample preparation is summarized in Fig.3 and described more fully by Saxby (1985). To avoid excessive use of heavy liquids, mineral separations were limited to five size fractions between 45 and 270-mesh. Each fraction was weighed and its tungsten content estimated by counting grains of scheelite under UV-light. Samples containing prohibitively large amounts of scheelite were split and reweighed before counting a subsample containing at least one hundred grains of scheelite. Counting errors were estimated by recounting all five size fractions for ten randomly selected samples: coefficients of variation were better than ±20% for 80% of the samples. Scheelite grain counts were converted to tungsten concentrations (Table 1) using a grain size-concentration calibration based on X-ray fluorescence analysis of the five fractions of a single sample having a high W content.

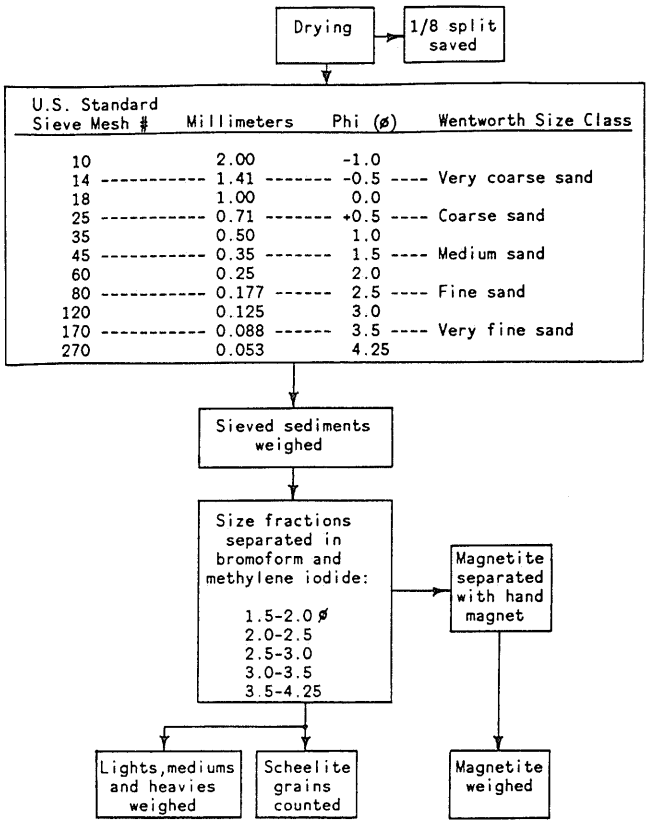

Fig. 3. Flow chart for sample processing.

Table 1. Weights of scheelite grains and corresponding tungsten contents in five size fractions based on X-ray fluorescence analysis.

Grain size ASTM #	W (ppm)	Grains of scheelite per gram	Weight of 1 scheelite grain (ug)	Weight of W in 1 scheelite grain (ug)
−45+60	1436[a]	57[b]	39.4	25.2
−60+80	3327	291	17.9	11.4
−80+120	2427	552	6.89	4.40
−120+170	1861	781	3.74	2.38
−170+270	570	1464	0.610	0.389

a. determined by XRF.
b. based on duplicate grain counts.

RESULTS

Chemical analyses from a heavy mineral sampling programme are usually expressed as concentrations in either the heavy mineral fraction or recalculated to the original sieved sediment weight. It is reasonable to assume, because heavy minerals are closer in density to scheelite than to the light fraction, that the former method will minimize variability caused by hydraulic effects. We have therefore chosen to present data as ppm tungsten in heavies.

Downstream profiles of tungsten concentrations (Fig. 4) show a number of similarities between the different size fractions: thus (1) differences between tungsten content at different stations and between high and low energy samples at a single station are usually greater than between duplicates; (2) in many cases tungsten concentrations in the five size fractions covary between high and low energy environments; and (3) tungsten concentrations are similar in high and low energy environments near stream headwaters but downstream show a relative increase in high energy environments. Except at station 5 on the Pelly River, this trend is most pronounced for the coarsest size fractions and results in up to approximately twentyfold differences in tungsten contents of adjoining samples. Finally, and of obvious concern for exploration, only low energy samples from the Pelly River have their highest tungsten content near their supposed source at the Clea deposit.

Systematic variations related to local hydraulic effects for an individual station are best seen at station 14 (Figs. 2 and 5) where tungsten concentrations, median scheelite grain size and stream velocities are all greater in high than in low energy conditions. Also high: low energy concentration ratios increase with grain size, as observed in the downstream profiles, to give a 20x enhancement of tungsten in the coarsest fraction. However, these observations were fully repeated at only one other station and it is apparent that no simple empirical relationship exists between flow velocities, sediment texture and abundance of scheelite.

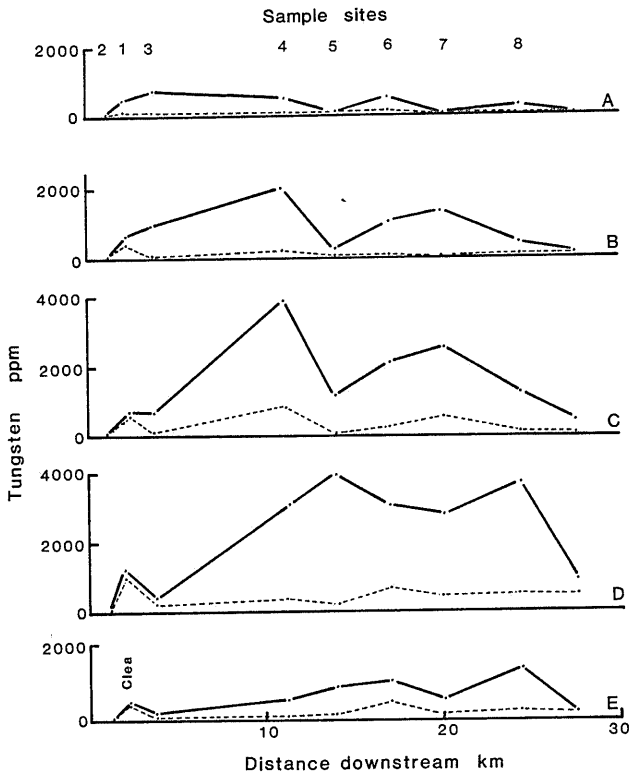

Fig. 4. Variation in tungsten content of heavy mineral concentrates. A = 1.5 - 2.0 phi (45 - 60 mesh); B = 2.0 - 2.5 phi (60-80 mesh); C = 2.5 - 3.0 phi (80 - 120 mesh); D = 3.0 - 3.5 phi (120 - 170 mesh); E = 3.5 - 4.25 phi (170 - 270 mesh): (——) = high energy; (------) = low energy. See Fig. 1 for locations.

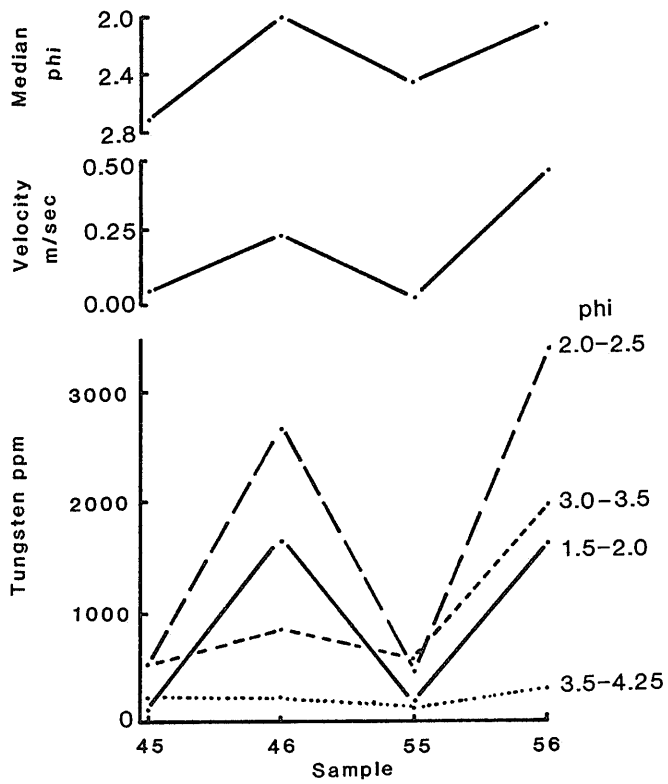

Fig. 5. Variations in tungsten content at sites 45, 46, 55 and 56 in relations to median grain size of sediment and stream velocity.

DISCUSSION

Hydraulic effects

Differences in tungsten content between paired high and low energy environments have been expressed in Table 2 as minimum and maximum concentration ratios (CR's) at each station and also, averaged over all stations, as geometric mean concentration ratios (GMCR's). Concentration ratios and GMCRs were calculated from W content of a given size fraction relative to the total weight of minus 10-mesh sediment: i.e.

$$CRx = \frac{\text{high energy (Wx/Sed)}}{\text{low energy (Wx/Sed)}}$$

and $$GMCRx = \text{antilog}\ \{(\Sigma_1^N \log_{10} CR)/N)\}$$

where Wx is the weight of tungsten in size fraction x, Sed is the total weight of minus 10-mesh sediment in that sample and N is the number of high-low energy pairs. Calculated in this way, enrichment (or depletion) of all size and density fractions can be compared on the same basis without bias (Saxby and Fletcher, 1986). GMCR's of unity indicate either no enrichment (depletion) between paired samples or equal enrichment in both.

Correlations between log concentration ratios are given in Table 3. They are greatest between the same or adjoining size and adjoining density fractions. Better correlations are obtained, for example, between scheelite and magnetite than between scheelite and lights, indicating, as would be anticipated, that grains of more similar density are more likely to behave in the same manner than are dissimilar grains. With respect to grain size, the strongest correlations between scheelite and less dense fractions are with either the same or coarser size fractions. Correlations also improve as the grain size of scheelite decreases so that CR's for the finest scheelite have strong correlations ($r>0.8$) with those of the three next coarsest sizes of magnetite, heavies and lights. These trends are even more clearly shown by the GMCR's (Table 2) which increase with increasing grain size and density, and are most similar and closest to unity for the finest size fraction. Although considerably more variable, maximum CR's follow the same general trend.

Correlations between CR's and trends of GMCR's indicate that: (1) systematic differences in tungsten concentrations between high and low energy sites are closely related to grain size and density, which is consistent with physical (hydraulic) processes being involved, and (2) that these processes become less effective in generating localized differences in tungsten content between adjoining areas of the stream bed as grain size decreases. The latter conclusion was also reached by Fletcher et al. (1985), with respect to behaviour of cassiterite in a mountain stream and is consistent with their interpretation that enrichment of heavy minerals in stream sediments largely results from the selective winnowing away of lighter minerals.

The observation that CR's for scheelite generally correlate best with CR's for coarser sizes of lower density fractions indicates that small grains of a relatively dense mineral behave more like larger grains of lower density minerals. This is consistent with the concept of settling (hydraulic) equivalence of grains as first proposed by Rubey (1933). However, the improved correlations between CR's of scheelite and lights as grain size decreases suggests that for the finer fractions density differences become less important than entrapment of fine particles, irrespective of their density, between much larger bedload grains. This is corroborated by the GMCR's which approach unity for

Table 2. Range of concentration ratios and the geometric mean concentration ratio for four density fractions. Based on concentrations calculated relative to the weight of minus 10-mesh sediment.

Density fraction	Size interval (ASTM) and GMCRs				
	−45+60	−60+80	−80+120	−120+170	−170+270
Scheelite	4.97	6.78	3.36	2.33	1.65
Magnetite	2.06	1.95	1.85	1.35	1.22
Heavies	1.87	1.72	1.34	1.19	1.25
Lights	.87	.94	.93	.88	.83

Table 3. Correlation coefficients for scheelite log concentration ratios versus log concentration ratios of five size fractions of scheelite, magnetite, heavies and lights. Log concentration ratios relative to the total weight of minus 10-mesh sediment: n = 24.

Size and Density Fraction	Scheelite size fraction and r values				
	−45+60	−60+80	−80+120	−120+170	−170+270
Scheelite					
−45+65	1.00	.86	.82	.77	.63
−60+80		1.00	.90	.85	.75
−80+120			1.00	.94	.81
−120+170				1.00	.94
−170+270					1.00
Magnetite					
−45+60	.79	.77	.83	.79	.69
−60+80	.76	.77	.86	.88	.80
−80+120	.67	.72	.83	.87	.85
−120+170	.68	.72	.82	.90	.89
−170+270	.66	.81	.84	.92	.94
Heavies (SG>3.3)					
−45+60	.81	.84	.85	.79	.66
−60+80	.78	.88	.91	.90	.82
−80+120	.72	.82	.87	.90	.87
−120+170	.64	.73	.80	.85	.85
−170+270	.54	.65	.72	.78	.82
Lights (SG=2.65)					
−45+60	.48	.47	.50	.58	.61
−60+80	.57	.63	.73	.83	.83
−80+120	.55	.67	.74	.85	.87
−120+170	.50	.67	.72	.84	.88
−170+270	.33	.55	.56	.72	.85

the finest grain size and indicate little relative enrichment of scheelite versus lights. Grain size as well as density is therefore an important factor in heavy mineral behaviour and enrichment in the streambed. This relationship between heavy mineral accumulation and grain size is of fundamental significance insofar as it suggests that entrainment, rather than settling, processes are principally responsible for the accumulations. Similar conclusions have been reached by Slingerland (1984) with respect to the origin of placer deposits.

Varying concentrations of tungsten in relation to hydraulic conditions will also influence sampling reproducibility. Table 4, based on sediments from the six lowest stations on the Pelly River, gives the number of scheelite grains to be found in approximately 10 kg of sediment together with a theoretical sampling precision from the Poisson distribution calculated as $P_{95\%} = 200/\sqrt{n}$, where n is the number of grains. It is apparent that the minimum sample size required to achieve reasonable reproducibility is considerably in excess of that normally collected during routine geochemical surveys. This problem is least severe for the high energy environments because the sediment has, in effect, been pre-panned by the stream to concentrate the heavies. Results emphasize the need to collect very large samples and field-screen the sediment or pre-concentrate heavy minerals by panning whenever rare grains of a heavy mineral are sought.

Tungsten concentrations in the three coarsest fractions of high energy sediments from station 5 on the Pelly River are notably lower than at neighbouring stations and atypical in that concentration ratios increase from coarse to fine sediment (Fig. 4). These results are also unexpected in view of a subsequent report (Geological Survey of Canada, 1981) of anomalously high tungsten concentrations in a stream joining the Pelly River a short distance upstream of 5 (Fig. 1). This anomaly has been traced to scheelite bearing skarn in float bordering a quartz monzonite stock (pers. comm. I. Thomson). Apparently this tributary stream supplies coarse heavies relatively impoverished in scheelite to the Pelly River. As a result only the two finest fractions of heavy mineral concentrates from station 5 suggest the possible presence of this additional source of tungsten. This situation might arise because coarse grained scheelite is (1) not sufficiently abundant at the source; (2) it is comminuted during transport; or (3) has a shorter dispersion train than fine scheelite — as reported by Fletcher et al. (1985), for cassiterite.

Application to exploration

Zantop and Nespereira (1979) found heavy mineral panning to be more reliable than sediment geochemistry in exploration for tungsten and tin. However, as shown in the present study, local hydraulic conditions can give rise to up to twentyfold variations in the tungsten content of heavy mineral concentrates from adjoining sites and average variability is from 1.7 to 6.8x depending on the size fraction considered (Table 2). In

Table 4. Median number of scheelite grains in 10 kg of minus 10-mesh sediment and precision estimates for numbers of scheelite grains in high and low energy environments in the Pelly River.

Energy environment / Precision	Size interval (ASTM)				
	−45+60	−60+80	−80+120	−120+170	−170+270
High energy					
Md # of grains	35	99	278	352	463
P (%)	33	20	12	11	9
Low energy					
Md # of grains	4	5	21	43	83
P (%)	100	89	44	31	22

Precision estimated at $P_{95} = 200/\sqrt{n}$

addition, sampling reproducibility with very low numbers of scheelite grains, particularly in the coarser size fractions from low energy sites, can give up to 100% errors with 10 kg of minus 10-mesh sediment.

With respect to hydraulic effects, samples from low energy environments are least affected and should give the most regular anomaly decay patterns downstream from a point source (Fig. 4). In contrast, high energy samples have higher tungsten contents but greater between site variability, depending on the efficiency of the winnowing process, in which downstream concentrations can exceed those closer to the source. Because of their greater number of scheelite grains (Table 4), sediments from high energy sites are better indicators of the presence of scheelite in a catchment (for preliminary reconnaissance) whereas low energy sites will provide a more reliable guide to its source providing care is taken to collect sufficient sediment to ensure a representative sample.

Both sampling errors and hydraulic effects are reduced as grain size decreases. For example, in the minus 170+270-mesh fraction estimated sampling errors at low energy sites are 20% (compared to up to 100% for coarse fractions - Table 4) and the GMCR is 1.7 (compared to values up to 6.8 for coarser fractions - Table 2). Use of finer grain sizes may also, on the basis of results from station 5, provide longer dispersion trains. Thus, providing fine scheelite is liberated at source or produced by comminution during transport, use of the finer fractions of the sediment may give the most reliable results.

CONCLUSION

(1) Scheelite in heavy mineral concentrates is susceptible to local hydraulic effects that result in significant concentration differences between adjoining high and low energy environments. These can disrupt the regular decay of an anomalous dispersion train away from its source.

(2) The increased number of scheelite grains in sediments from high energy environments gives better sampling statistics and is a more sensitive indicator of the presence of scheelite within a catchment. However, the less variable results from low energy sites should provide a better guide to its source.

(3) Sampling errors and hydraulic effects decrease as grain size decreases. Use of finer fractions of the sediment may therefore provide the most reliable data.

Acknowledgements — We wish to acknowledge the interest and helpful suggestions that were received throughout this study from Dr. I. Thomson. Placer Development Limited funded the project and provided logistical support for the fieldworks: we are most grateful.

REFERENCES

Clifton, H. E., Hunter, R. E., Swanson, F. J. and Philips, R. L., 1969, Sample size and meaningful gold analysis: U.S. Geol. Surv., Prof. Pap. 625-C, 17 p.

Day, S. and Fletcher, W. K., 1986, Particle size and abundance of gold in stream sediments from southern British Columbia: J. Geochem. Explor., v. 26, p. 203-214.

Dick, L. A., 1980, A comparative study of the geology, mineralogy and conditions of formation of contact metasomatic mineral deposits in the northeastern Canadian Cordillera: Unpub. Ph.D. thesis, Queens University, 473 p.

Fletcher, W. K., 1981, Analytical Methods in Geochemical Prospecting. Elsevier, 255 p.

Fletcher, W. K., Dousset, P. E. and Yussof b. Ismail., 1985, Elimination of hydraulic effects in stream sediment data: behaviour of cassiterite in a Malaysian stream: J. Geochem. Explor., In press.

Folk, R. L., 1974, Petrology of Sedimentary Rocks. Hemphill, 182 p.

Gabrielse, H., 1967, Tectonic evolution of the Northern Canadian Cordillera: Can. J. Earth Sci., v. 4, p. 271-298.

Geological Survey of Canada, 1981, Regional stream sediment and water geochemistry of the Nahanni map area, Yukon and Northwest Territories: Open File Rpt. 868.

Gladwell, D. R., 1981, Research into geochemical exploration techniques for stanniferous mineralization: Unpub. Ph.D. Thesis, Univ. of London, 283 p.

Godwin, C. I., Armstrong, R. L. and Tompson, K. M., 1980, K-Ar and Rb-Sr dating and genesis of tungsten at the Clea tungsten skarn property, Selwyn Mountains, Yukon Territory: Can. Inst. Min. Metall. Bull., v. 73, p. 90-93.

Gordey, S. P., 1981, Geology of the Nahanni map-area (105-I), Yukon Territory and District of Mackenzie: Geol. Surv. Can., Open File Rpt. 780.

Ingamells, C. O., 1974, New approaches to geochemical analysis and sampling: Talanta, v. 21, p. 141-155.

Rubey, W. W., 1933, The size distribution of heavy minerals within a water-laid sandstone: J. Sed. Pet., v. 3, p. 3-29.

Saxby, D. W., 1985, Sampling problems and hydraulic factors related to the dispersion of scheelite in drainage sediments, Clea Property, Yukon Territory: Unpub. MSc. Thesis, Univ. of British Columbia, 152 p.

Slingerland, R., 1984, Role of hydraulic sorting in the origin of fluvial placers: J. Sed. Pet., v. 54, p. 137-150.

Sleath, A. and Fletcher, W. K., 1982, Geochemical dispersion in a glacial stream, Purcell Mountains, B.C., *in* Prospecting in Areas of Glaciated Terrain, Davenport, P. (editor), Can. Inst. Min. Metall., p. 195-203.

Zantop, H. and Nespereira, J., 1979, Heavy mineral panning techniques in exploration for tin and tungsten in north western Spain, *in* Geochemical Exploration 1978, Watterson, J. R. and Theobald, P. K. (editors), Assoc. Explor. Geochem., p. 329-336.

Current Atomic Absorption and Inductively Coupled Plasma Optical Emission Methods for Geochemical Investigations

J. S. KANE AND A. F. DORRZAPF, JR.
U.S. Geological Survey, National Center, Mail Stop 923, Reston VA 22092

Abstract — Atomic absorption (AAS) analyses have played a major role in geochemical investigations for approximately 25 years. The multiple element inductively coupled plasma optical emission (ICP-OES) methods introduced recently will soon be equally important. Both techniques can determine more than 40 elements in widely varied sample types and, for many elements, are completely interchangeable.

This paper reviews current practices in the authors' laboratories for AAS and ICP-OES analyses of geochemical samples, emphasizing changes required in routine igneous silicate rock procedures for other sample types. It also presents a brief discussion of the approaches used to assess the accuracy of the routine or modified procedure.

INTRODUCTION

ATOMIC ABSORPTION spectrometric (AAS) methods have, until recently, been the principal method for the geochemical analysis of samples in solution, with the capacity to determine 40 plus elements, in a single element mode of operation. The method was first introduced using flame atomization in the early 1960's. The alternative of graphite furnace atomization (HGA-AAS) became available in the early 1970's, lowering AAS detection limits 10-100 fold over those obtainable by flame analysis. At about the same time, inductively coupled plasma optical emission (ICP-OES) instruments became available commercially. With the introduction of this method, simultaneous multielement analysis of solutions became a reality. The ICP method is well on its way to supplanting AAS in routine geochemical analyses, though it is not yet as extensively used as AAS in determining recommended values for "standard rock" samples.

This is apparent from a tabulation of method contributions (Rubeska, 1977) to recommended values for the 1976 suite of USGS standard rocks (Flanagan, 1976) and from literature summaries of more recent method contributions to the published standard rock data base (Govindaraju, 1982). Flanagan based 85% of his recommended values on neutron activation analysis (NAA), 48% on d.c. arc optical emission (OES), 31% on X-ray fluorescence (XRF) and isotope dilution mass spectrometry (IDMS), 25% on AAS, and 8% on colorimetric analysis, the total exceeding 100% as many elemental values were based on more than one method. The key points are the extensive reliance on NAA and OES, the important contribution of AAS and the absence of ICP. The 1979-1983 survey of method contributions to the standard rock data base in approximately 50 analytical and geochemical journals totals 100% for each year. The AAS contribution to this period equals or exceeds that in the 1976 derivation of recommended values, averaging 25%, and the growing importance of ICP, at 12% for 1982-1983, is clear. Also apparent is a major decline in reliance on colorimetric and d.c. arc OES methods, both now below 5%.

This paper will briefly summarize the considerations involved in selecting which of the methods, ICP, flame AAS, or furnace AAS, is most appropriate for a given analytical determination. The point of departure in the discussion is the collection of methods for silicate rock analysis used in the authors' laboratories, the optical spectroscopy section of the Geologic Division at the U.S. Geological Survey in Reston, VA. The discussion presented is in many respects, but not all, independent of the particular instruments used for analysis. The authors' analytical experience is with the Jarrell Ash Model 3 Atom Comp direct reader spectrometer* for ICP-OES and with Perkin Elmer Model 603* and Model 5000* spectrometers for AAS. It should be noted that a sizeable proportion of our work is done at crustal abundance or depleted concentration levels, and that our methods are designed to achieve equally good analytical accuracies at those levels as at the enriched concentrations which are perhaps of more interest in exploration work.

SAMPLE DECOMPOSITION AND METHOD DETECTION LIMITS

One of the most obvious and important factors in method selection is the detectability of the analyte at its concentration in solution. Flame AAS and ICP-OES provide very similar detection limits for all elements. The ICP measurement will, however, be slightly better for refractory elements (V, Cr, Ba, Zr, etc.) and flame AAS will offer a small advantage for the heavy metals (Ag, Cd, Zn, etc.).

The analyte concentration in solution is significantly affected by the selection of dissolution procedure. Fundamentally, two dissolution procedures are available - fusion with a suitable flux and acid digestion. While many fluxes are available for fairly specific applications, the one we use most extensively is a mixed lithium metaborate/tetraborate fusion for the determination of major and minor rock forming elements in a modification of the rapid rock procedure of Shapiro and Brannock (1962). Because a 6:1 flux to sample ratio by weight is required for complete sample decomposition, and because AAS sample uptake systems and crossflow nebulizers for the ICP cannot process more than 0.5-1.0% total dissolved solids (TDS) with adequate long-term reproducibility of nebulization and calibration, use of a fusion decomposition results in a solution more dilute than sample by a factor of 1250-2000.

* Trade names are given for identification only and do not imply endorsement of a specific product by the U.S. Geological Survey.

This means that detection, by flame AAS or ICP, of trace elements whose concentration in the solid sample is less than 100 ppm will rarely be possible. The high salts content due to the flux as well as the potentially high analyte blank typically contributed by impurities in the flux will eliminate the possibility of using the HGA-AAS method to improve the detection limit for analytes after fusion in most cases.

Acid digestion procedures can achieve higher sample weight to solution volume ratios than fusions, leading to better detectability of trace analytes, for two reasons. First, there is no contribution to TDS in the solution from the flux, and secondly silica is volatilized almost totally as SiF_4, eliminating the contribution to TDS from a predominant rock-forming constituent. This means, of course, that the acid digestion is unsuitable for whole rock major element analysis. Incomplete dissolution of ilmenite, leading to low Ti analyses, has been noted for amphibolites but not for igneous rocks. Low recovery of Al has also been encountered on occasion, particularly for GXR-1, a geochemical exploration standard. These digestion losses as well as the Si loss make acid decomposition unsuitable for major element determinations in comparison to the fusion preparation. However, many trace element analyses, particularly those in the HGA-AAS method range, which cannot be done using a fusion solution, become possible.

Sealed bomb digestions are not used, despite dissolution of refractories and retention of Si in solution, because the need to buffer the hydrofluoric acid (HF) volume with boric acid results in the same sample weight to solution volume ratio as for the fusion. Many trace elements would again be undeterminable.

While the principal use of the acid digestion is for the determination of trace elements not detectable in a fusion solution, it must be recognized that a number of refractory minerals which concentrate trace elements are incompletely dissolved by acid attack, and that analytical values in their presence will be erroneously low. The magnitude of the error will vary from sample to sample as a function of the ratio of analyte in the silicate lattice to that of the resistant mineral. For example, a comparison of Cr analyses by AAS after acid digestion with recommended values, or with solid sample NAA data, shows complete recovery after digestion for the granite G-2, the granodiorite GSP-1 and the diabase W-2. However results are 15% low for marine mud MAG-1 and basalt BHVO-1 and low by 70-75% for peridotite PCC-1 and dunite DTS-1, due to the increasing percentage of Cr occurring as acid-insoluble chromite. Similarly, zirconium losses are encountered when analyzing granites, granodiorites, and schists by ICP after acid digestion, because of the presence in sample of zircon. No such losses occur when analyzing rhyolites, andesites, diabases or basalts. Barium losses on acid digestion are severe when baryte occurs in the sample. Work in our laboratory on massive sulfides (Philpotts et al., 1986) has shown that Ag, Cd and Pb losses accompany the barium loss in baryte-rich samples, the heavy metals apparently being trapped in the insoluble $BaSO_4$. Numerous other instances of poor dissolution with acid digestion, affecting the accuracy of analysis by any solution method can be cited. Dolezal et al. (1966) present detailed discussions of sample dissolution procedures and the potential errors in each.

PRECISION OF MEASUREMENT

Once a measurement method and a dissolution technique are selected to assure detection of the desired analytes, achievable precision of measurement must be considered. Statistical theory predicts, and experimental data confirms, that imprecision as indicated by percent relative standard deviation (% rsd) will be as much as ± 100% near the detection limit, but will be only ± 1-2% at 100 times that concentration. If several elements to be determined by ICP to take full advantage of its multielement measurement capability, let us say Ni, Cd, Ag in sediments, are all in the poor precision concentration for the method, accurate analytical results will be achieved only by making a large number of replicate analyses ($n > 10$). Where extensive replication is not possible, HGA-AAS should instead be used, since the measured concentrations will be 10-100 times further from the detection limit of this method and ± 2% rsds will be achievable. Assuming a ± 20% rsd for the ICP measurement, 100 replications would be required to provide equal accuracies for the ICP mean value and a single HGA-AAS result. With either a greater ICP rsd or a smaller number of ICP replications, the ± 2% HGA-AAS result will provide superior accuracy. If the ICP method is used with limited replication of measurement, the poor accuracy of the data must be fully recognized.

Illustration of method selection and adaptation as a function of analyte concentration follow first for iron and then for cadmium to point out the differing emphases for major and trace element analyses.

IRON DETERMINATIONS

Iron concentrations (total iron reported as Fe_2O_3) for a number of geologic sample types are shown in Fig. 1. Below these are a number of potential measurement options. Most of these permit analysis over only short concentration ranges, 1½ to 2 orders of magnitude being typical for both flame and furnace AAS. Depending on the ICP instrument being used, a 4-5 order of magnitude calibration range may be possible, as indicated by the extended range ICP method in the figure. This larger calibration range is in many ways as important to the explosive growth in the use of ICP as is the multielement capability of the method. However for analyses of the highest accuracy, illustrated by Rapid Rock ICP in the figure, calibration standards are selected to tightly bracket only a small portion of the potential range. For example, Rapid Rock ICP calibration is from granitic iron (G-2, 2.75% Fe_2O_3) to basaltic iron (BHVO-1, 12.3%) only. With this approach, analytical error (as indicated for standard rock control samples by the deviation between recommended literature value and experimentally measured value) will be considerably less than 0.1% absolute for Fe_2O_3 in the 1-10% range, and less than 1% relative for Fe_2O_3 greater than 10%. Typical errors for AGV-1, DNC-1, GSP-1 are 0.01-0.03% absolute, at Fe_2O_3 concentrations from 3.00% to 6.92%. Use of the broader extended range to encompass all sample concentrations in a single analytical run increases this error somewhat, as control data indicates: STM-1 and P-1 with absolute errors of 0.10-0.13% for Fe_2O_3 at 3.53 to 5.91% and GXR-1 with a relative of 2.4% at 25.3%

Fe_2O_3. Even these errors are quite small, however, in comparison to the widely ranging literature data from which recommended values for standard rocks are derived. Extreme values typically range ± 25% relative to the recommended value, though enough are tightly clustered about the recommended value to provide confidence that it is within 1% of "true" value, permitting use of the standard rocks as calibration standards.

Using both AAS and ICP methods with a single tightly bracketing calibration of about one order of magnitude, different dilutions of the sample fusions could be used for measurement of Fe concentrations of subsets of a group of samples spanning the full iron concentration range of the figure. For example, ICP or flame AAS calibration from 0.01% to 0.10% is ideal for sands and glasses, and could also be used for 1/10 dilutions of feldspars, for 1/100 dilutions of normal silicates and coal ashes, and for 1/1000 dilutions of ore and exploration samples at $Fe_2O_3 > 10\%$. With flame AAS and with a scanning ICP instrument, measurement of subsets at different wavelengths, each with a narrow calibration range, again maintains highest accuracy of analysis. Returning to Fig. 1, flame AAS measurement for 0.10%-1.0% (potash feldspar BCS-376 to Kaolinite KK) could be done using the most sensitive 248.3 nm line, measurement for 0.50-10.0% (granite MA-N to diabase DNC-1) at 252.7 nm, and measurement for >10% (basalt BHVO-1 to iron ore BS-1) at 346.6 or 392.0 nm. Direct reader ICP instruments do not permit similar use of alternate wavelengths, and for many elements, AAS does not have sufficiently well-spaced and numerous alternate lines that the full concentration range can be covered without gaps.

Many geochemical programs do not require the high degree of accuracy provided by the differing dilutions for sample subsets or measurement of the subsets with different analytical lines, as outlined above. These procedures are reserved for the specific applications, such as standard rock certification, and whole rock analysis by the Shapiro and Brannock (1962) method, which require them. The extended range ICP calibration is used in preference whenever possible.

Iron is most frequently encountered at relatively high concentrations, occurring as a major constituent of the sample matrix. Contamination of the sample while exercising normal care during preparation, by acids or the laboratory environment, will be insignificant in relation to the amount of the analyte in the sample. It is one of the dominant matrix elements so that errors due to spectral or physical matrix interferences are not likely to be encountered in its measurement and detection limits will rarely be a concern. Applying the foregoing procedures to Cd adds a new level of complexity to the discussion.

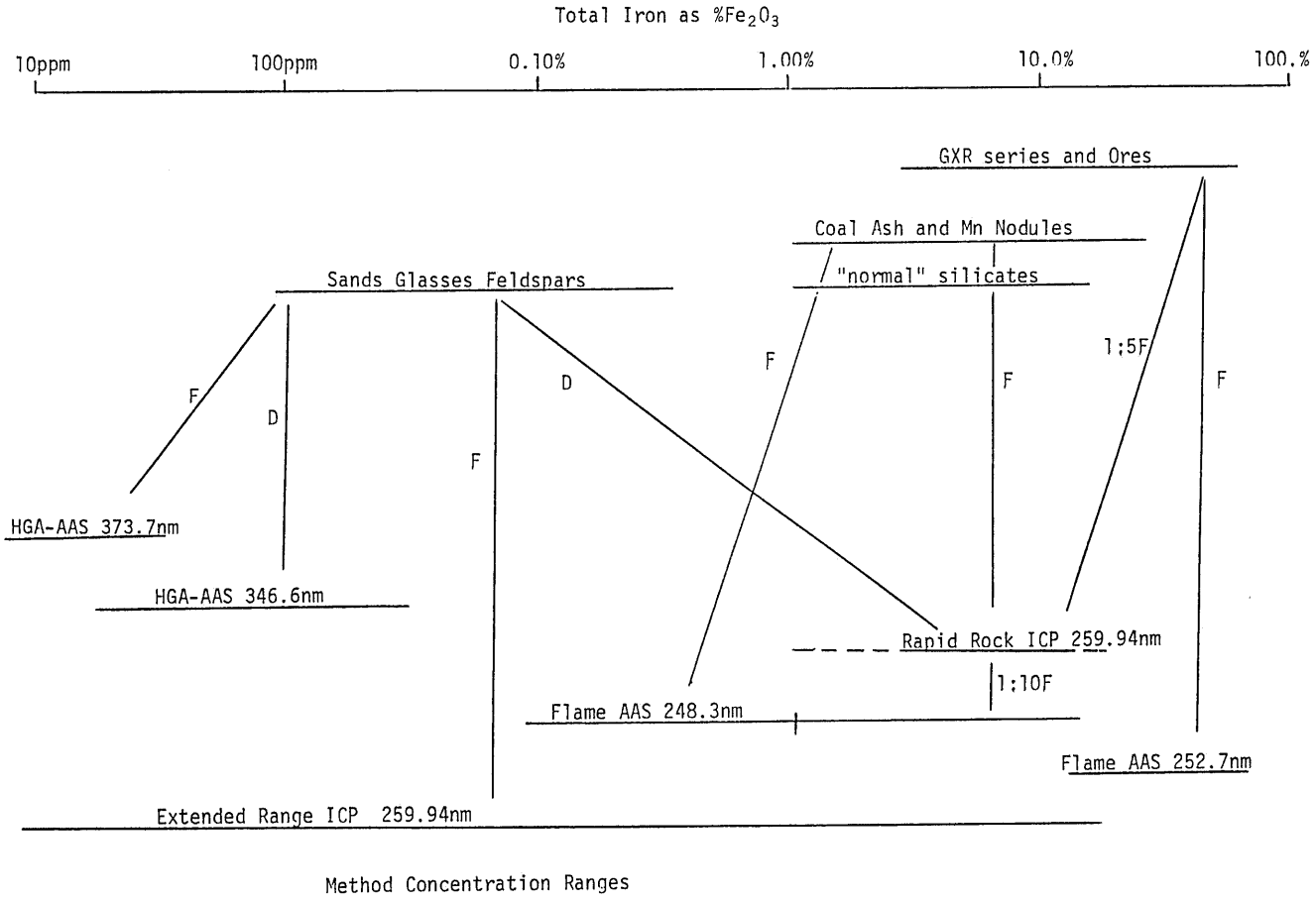

Fig. 1. Iron concentrations as a function of geochemical sample type and calibration ranges for several analytical measurement protocols.

CADMIUM DETERMINATION

For standard silicate analysis, Cd is an ultratrace element. Contamination errors can be large enough to prevent accurate analysis. Neither flame AAS nor ICP methods have sufficiently low detection limits for analysis of average crustal abundances (200 ppb) of the element following acid digestion. Even at ppm and greater concentrations, interferences can affect measurement by both of these methods.

Fig. 2 shows typical Cd concentration ranges for both geochemical samples and methods of analysis.

Graphite furnace AAS measurement, which provides appropriately low determination limits for measurement of Cd at crustal abundance levels, is affected by very high background signals. The background varies markedly with wavelength, and results from non-specific light absorption by the bulk sample matrix. Until recently, deuterium arc background correction was the only available means for background compensation in AAS. This correction is erroneous when the background signal exceeds approximately 0.60 absorbance units. For furnace analysis, particularly at the low UV wavelengths (190-230 nm) this is common, and results in a requirement to chemically separate the analyte from the bulk sample before measurement. Introduction of Zeeman and Smith-Heiftje background correction systems eliminate the need for extraction at least for those samples above 500 ppb Cd. These methods of background correction are accurate for background signals to 2.0 absorbance. The 1/10 to 1/50 dilution required to lower sediment, coal ash, Mn nodule, and GXR standard Cd concentrations to the furnace method calibration range for the 228.8 nm line reduces the background enough for accurate Zeeman (but not for accurate deuterium arc) correction. Larger dilutions permitted the determination of Cd in ore samples and standards by HGA-AAS, using two analytical wavelengths. However for those samples which are too low in Cd concentration for detection after dilution, typically silicate rocks, Zeeman correction for furnace measurement will still be inadequate, and the separation procedure must be retained.

For Cd analysis by AAS, only two analytical lines are available, separated by a factor of 500 in sensitivity. There are, as a result, some concentration gaps between them which can be closed only by varying the dilution factor for analysis. For example, ore samples containing between 2 and 20 ppm in Cd can be measured with flame atomization at 228.8 nm on undiluted digestions, while those whose Cd concentrations are 750 ppm to 3% can be measured at 326.1 nm, again without dilution. However, samples with 20 to 750 ppm Cd will require dilution into the range of the 228.8 nm line. Because flame atomization generates much smaller background signals than those for furnace atomization, deuterium arc background correction is generally adequate for these ore analyses.

While extended range calibration for ICP analysis can provide adequate detection of about 2 ppm Cd in the absence of spectral overlaps, an iron overlap on the 214.438 nm line on our direct reader ICP requires us to use a chemical separation before measurement or an AAS method, except when analyzing ores highly enriched in Cd. Spectral interferences which account for less than 75% of the total spectral signal can be subtracted from the signal accurately. The iron interference which we encounter creates an apparent 1.1 ppm Cd for 1% Fe. Accurate correction, then, for a sample with 10% Fe, can be done only if Cd in sample exceeds approximately 3.5 ppm. For ores with 17.5 - 35% Fe (see Fig. 1), the minimum Cd concentrations for ICP determination increase to 8.75 - 18 ppm. Thus for SU-1 and GXR-1, with <10 ppm Cd and 25% Fe, AAS analysis rather than ICP had to be used in the massive sulfide program (Philpotts et al., 1986).

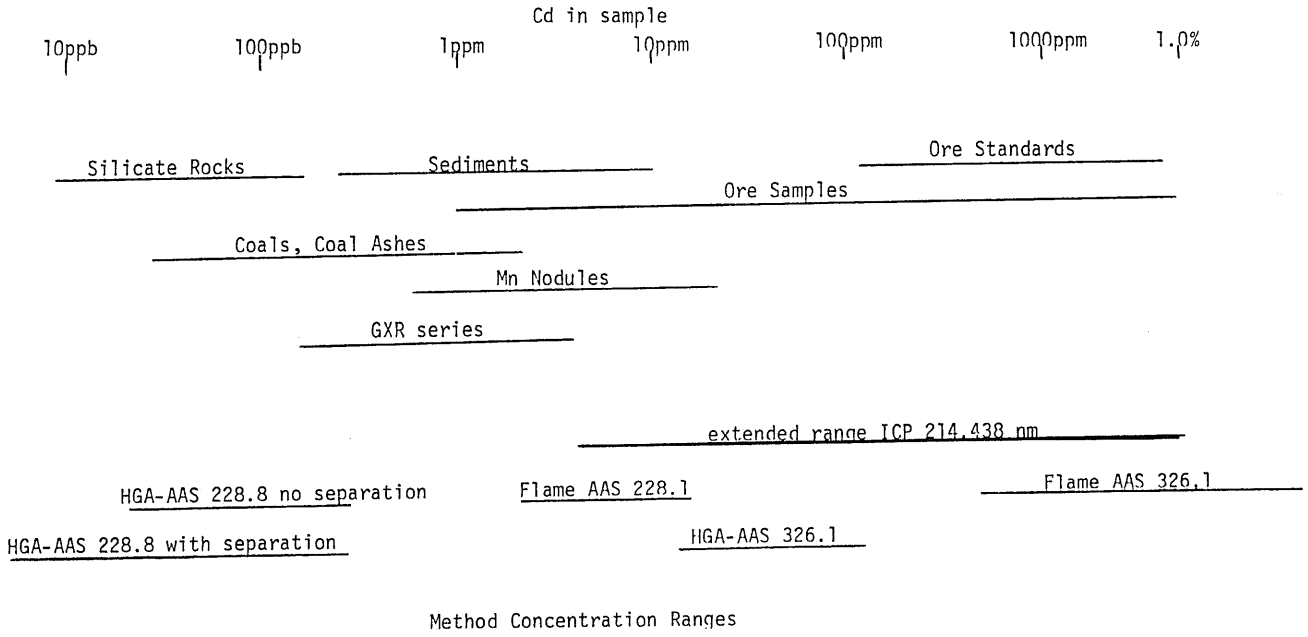

Fig. 2. Cadmium concentrations as a function of geochemical sample type and calibration ranges for several analytical measurement protocols.

CONCLUSIONS: METHOD ACCURACY USING GEOCHEMICAL REFERENCE SAMPLE DATA

For major elements, particularly in the newer suites of international geochemical reference samples, consensus values ("recommended values") (Abbey, 1983; Flanagan, 1976; Govindaraju, 1980, 1982) are assumed to be within approximately 1% of "true" value, despite the diverse collected data from which they are derived. An appropriate subset of these reference samples can be used for instrument calibration and a second subset used as quality control samples. Agreement between the analytical and consensus values for the quality control samples provides a high level of confidence in the overall accuracy of data for all samples analyzed. This approach has been discussed for Fe determinations by the rapid rock method.

For trace element analysis, the situation is very different. The total data base is much more limited, and the reported concentrations for a given analysis from several contributing laboratories can vary as much as three orders of magnitude. In Govindaraju's and Mevelle's words (1983), "It is normally conceded with exasperation that compiled data on trace elements reveal wide analytical dispersions, often of alarming proportions." In these instances, derivation of a consensus or recommended value is not possible, and use of reference samples of known concentration as calibration standards to minimize matrix mismatch between standards and samples cannot be undertaken.

While general confidence exists in the fact that recommended values for the major elements are within 1% of true value, and for minors within 5-10%, perhaps dispersions of 20% are more realistic for trace elements. Still, for many, the recommended values are not known with nearly that degree of certainty. Dispersions of $\pm 100\%$ about the median value are common, and dispersions as great as $\pm 500\%$ sometimes occur. In such instances it is difficult to justify designation of the median, or any other estimation of modal value, as a recommended or "true" value.

Methods contributing to an expansion of the data base must be examined for error sources so that new data improves in this respect. Where reliable geochemical reference standard data are unavailable for this purpose, inter-method comparisons of data from within a single laboratory can prove helpful. In this laboratory, AAS and ICP data are frequently collected for the same elements on single sample preparations to verify that all needed spectral interferences affecting the ICP determination have been identified and that the correction factor is accurately applied. Where the dissolution step is potentially the largest source of error, ICP or AAS data are evaluated against that from a whole-sample technique such as EDXRF or d.c. arc-OES. Discrepancies may persist in trace element data despite these efforts, but these approaches will help to minimize them.

In summary, the ICP-OES and AAS methods routinely used in our laboratory were initially developed for typical silicate rock analysis. The considerations for modification of these basic procedures such that they could be applied accurately to numerous other sample types have been discussed. In a number of instances the two methods can be used interchangeably; in others one is distinctly more suitable than the other. We have attempted to illustrate the two situations with examples of our current analytical methods.

The methods used in our laboratory provide geochemical data of high accuracy on a routine basis; improvements in them can and will be made as changes in state-of-the-art technology permit.

REFERENCES

Abbey, S., 1983, Studies in "standard samples" of silicate rocks and minerals, 1969-1982: Geol. Surv. Canada, Paper 83-15, 114 p.

Dolezal, J., Povondra, P., and Sulcek, Z., 1966, Decomposition techniques in inorganic analysis: New York, Elsevier Publishing Co. Inc., 224 p.

Flanagan, F. J., 1976, Descriptions and analyses of eight new USGS rock standards: U.S. Geol. Surv. Prof. Pap. 840, 192 p.

Govindaraju, K., 1980, Report (1980) on Three GIT-IWG Rock Reference Samples: Anorthosite from Greenland, AN-G, Basalte d'Essey-la-Cote, BE-N; Granite de Beauvoir, MA-N: Geostandards Newsletter, v. 4, p. 49-138.

Govindaraju, K., 1982, Report (1967-1981) on Four ANRT Rock Reference Samples: Diorite DR-N, Serpentine UB-N, Bauxite BX-N, and Disthene DT-N: Geostandards Newsletter, v. 6, p. 91-159.

Govindaraju, K., and Mevelle, G., 1983, Geostandards and geochemical analysis: Spectrochimica Acta, v.38B, p. 1447-1456.

Philpotts, J. A., Dorrzapf, Jr., A. F., Kane, J. S., Kirschenbaum, H., Johnson, R. G., Aruscavage, P. J., Palmer, C. A., Brown, Z. A., Skeen, C. J. and Rait, N., 1986, Comparison of Analytical Techniques Being Used in the U.S. Geological Survey Compositional Study of Massive Sulfides from the Southern Juan de Fuca Ridge, Abstract, Geoexpo 86, Vancouver, May 12-14, 1986.

Rubeska, T., 1977, The state of the art of trace element analysis of geologic samples: Geostandards Newsletter, v. 1, p. 15-20.

Shapiro, L. and Brannock, W. W., 1962, Rapid analysis of silicate, carbonate, and phosphate rocks: U.S. Geol. Surv. Bull. 1144-A, 56 p.

Comparison of Some Multielement Analytical Techniques Applied to Massive Sulfides from the Juan de Fuca Ridge and to Sulfide Standards

J. A. PHILPOTTS, J. S. KANE, R. G. JOHNSON, A. F. DORRZAPF, JR., Z. A. BROWN, J. S. MEE, H. KIRSCHENBAUM, N. RAIT, C. SKEEN, W. CRANDELL, C. PALMER, J. MARINENKO and F. BROWN
U.S. Geological Survey, 923 National Center, Reston, VA 22092, U.S.A.

Abstract — Abundances of S, Zn, Fe, Cu, Pb, Cd, Co, Ag, Sb, Si, Mg, Ca, Ba, Sr, Mn, Al, Na and As have been determined for eight sulfide standards and a suite of massive sulfides from the Juan de Fuca Ridge in order to evaluate the capabilities of seven different analytical techniques. Acid dissolution, particularly of samples bearing insoluble sulfates, did not fully recover Pb, Ba, Sr or Ag. Roasting and fusion decomposition resulted in loss of volatile elements (Cd, Pb, Zn, Cu). The emission spectographic measurement for Ag reached upper limit saturation at only 80 ppm. The high abundances of elements such as Zn, Fe and Cu caused spectral and background interferences that degrade element determination sensitivity for many of the techniques. Inductively coupled plasma (ICP) optical emission spectroscopy appears to be the single most useful multielement technique for the analysis of sulfides.

INTRODUCTION

THE U.S. Geological Survey is involved in a program of study of the Juan de Fuca (JDF) Ridge, an ocean-floor spreading-center lying about 400 km off the coasts of Oregon, Washington, and British Columbia. As part of this program, we have undertaken a geochemical study of massive-sulfide chimneys collected at the JDF Ridge in September-October 1984 using the DSRV *Alvin* submersible. The massive-sulfide chimneys form at hot-springs near the ridge axis from the interaction of seawater and hydrothermal fluid. The geochemical work includes comprehensive chemical analysis of these massive sulfides. The JDF samples are predominantly ZnS with FeS_2 as the other major component. Silica, anhydrite, barite and isocubanite ($CuFe_2S_3$) are major phases in occasional samples.

We have embarked on a systematic program aimed at evaluating and improving analytical techniques applied to sulfides. The present paper discusses results obtained with the multielement techniques that are routinely used in this laboratory for analyzing silicates. These techniques include semiquantitative d.c. arc emission spectrography (SQES), energy dispersive X-ray fluorescence spectroscopy (EDXRF), inductively coupled plasma optical emission spectrometry (ICP), and instrumental neutron activation (INAA). SQES is included as one of the techniques being compared both because it is competitive for some elements and because it appears generally useful in reconnaissance analyses of sulfides. Atomic absorption spectrometry (AA) is also included because it can provide analyses for many of the same elements as the other techniques, although not simultaneously. Omitted from the discussion are those analyses performed by only one technique.

APPROACH TO METHODS COMPARISON

Comparison and evaluation of the analytical methods are based on data obtained for eight sulfide standards and sizable subsets of 56 JDF massive sulfide samples. Accuracy of the techniques was judged both by comparing element determinations for the standards with their certified values and by comparing results from the techniques with each other for both the standard and JDF suites. Unfortunately, certified values are not available for these standards for all the elements we have determined. Also, only Zn, Cu, Pb and Ag are certified for all eight standards. We have obtained only limited numbers of values per technique for most elements to date and hence do not have statistically sound estimates of precision for the standard analyses. For this reason we present results only for single analyses along with certified values in Table 1. Our values should *not* be taken as definitive values for these samples. These were first attempts at analyzing these materials, the techniques were not optimized for determinations of individual elements, and as yet we have not adequately gauged their reproducibility. The results are presented only as an objective measure of the present capabilities of our techniques.

The best idea at present of the precision of the various analytical techniques for sulfides is obtained from the multi-sample two-technique comparisons of the JDF data. All deviations in analytical results represent the combined error from both techniques being compared. However, by comparing multiple techniques, consistency arguments frequently enable at least crude proportioning of both intertechnique bias and precision. At the very least, random error for each technique of any pair is expected to be less than the combined random error.

This evaluation procedure involves correlation rather than regression analysis. It is complicated by features such as nonlinear correlations and random errors that are functions of concentration. Scatter diagrams are the most informative way of presenting this information at a glance. In particular, log-log plots enable ready assessment of changes in relative error with concentration, of the lower limits of measurement, and of constant intertechnique bias. However, inasmuch as space considerations limit the number of scatter diagrams we can present, the JDF results for each element are summarized in Table 2 in terms of inter-technique correlation coefficients (r) and the number of samples involved (n). Rather than present all possible combinations, the data are presented relative to one reference technique (*) for each element. The reference technique was selected to maximize the intersection of data sets presented.

Our JDF data comparisons identified some intertechnique biases, particularly in the cases of SQES, which did not appear optimally calibrated for the concentration ranges occurring in

Table 1. Certified values and single analysis elemental abundances by analytical technique for eight sulfide standards

		CCU-1	CPB-1	CZN-1	KC-1	MP-1a	SU-1	113a	329
S %	CERT		17.8	30.2			12.1	30.6	
	GRAV	35.6	17.9	30.1	27.3	12.8	11.9	30.1	29.7
	LECO	34.2	17.6	29.7	26.8	12.8	12.6		29.1
	EDXRF			31.7	26.1	12.8		30.0	28.8
ZN %	CERT	3.22	4.42	44.74	20.07	19.02	.0294	57.3	45.5
	AFLAA	3.41	4.60	45.5	20.9	16.7		50.2	42.6
	AICP	3.44	4.53	44.0	20.0	19.9	.032	51.1	41.2
	FICP	3.59	4.38	45.4	17.1	16.3		47.1	33.4
	INAA	3.33	4.56	42.5	20.2	18.7	.033	56.1	
	EDXRF			43.1	20.0	20.2		54.4	42.4
	SQES						.043		
FE %	CERT		8.43	10.93				2.08	12.94
	AFLAA	32.9	9.71	11.7	17.8	6.22	24.5		
	AICP	31.2	8.38	11.1	16.2	5.72	23.8	2.12	13.0
	FICP	31.7	8.25	11.1	16.1	5.88	23.8	2.03	12.4
	INAA	30.1	8.47	10.5	15.8	5.87	24.6	1.90	
	EDXRF			11.3	13.5	5.71		2.19	13.4
	SQES		14	11	13	5.7		2.1	11
CU %	CERT	24.71	.254	.144	.112	1.44	.8215	.31	.132
	AFLAA	24.7	.239	.158	.106	1.26	.865		
	AICP	23.9	.237	.141	.111	1.34	.830	.249	.116
	EDXRF			.16	.074	1.66		.32	.14
	SQES		.20	.13	.11			.22	.12
PB %	CERT	.106	64.74	7.45	6.87	4.33	.0249	2.80	6.06
	AFLAA	.105		7.40	6.90	4.45	.024		
	AICP	.094		7.34	6.91	4.19	.019	2.73	6.00
	EDXRF			7.20	6.74	3.86		2.94	5.98
	SQES	.099					.029		
CD ppm	CERT		143	1 320				7 800	1 400
	AGFAA	158	99	1 200	1 200	580	5		
	AICP	115	149	1 300	778	568		7 400	1 400
	EDXRF			1 400	788	634		7 900	1 424
	SQES	190	180	1 100	900	670			1 500
CO ppm	CERT						540		
	AFLAA				22	10	587		
	AICP	23	3	6.5	32		540	730	
	INAA	19	3.1	6.4	26.2	1.5	623	706	
	SQES	18	2.5	6	25	1.7	320	420	4.2
AG ppm	CERT	139	626	93	1 120	69.7	4	467	89
	AGFAA	130	610	100		57	5		
	AICP	176	800	102	1 400	74		380	110
	INAA	137	578	87	1 040	63		418	
	EDXRF			112	1 150	140		534	98
	SQES	58	610	110		85	6.1	160	82
SB ppm	CERT		3 600	520					
	AGFAA			500					
	AICP		2 330	460	162				
	INAA	2.1	3 610	470	243	33.8			
	SQES		4 100	670	310				280
SI %	CERT	1.22	.35						
	FICP	1.20	.33	.51	11.0	19.2	16.4	.70	.29
	EDXRF			.80	11.5			.82	.60
	SQES	3.5	.7	1.4	15	23	22	1	.51
MG %	CERT						2.3	.45	.099
	AICP	.629		.190			2.37	.390	.095
	FICP	.724	.090	.193	.030	.012	2.41	.452	.096
	SQES	1.4	.14	.37	.090	.095	3.3	.60	.095
CA %	CERT						2.9	.85	.06
	AICP	.070	.581	.126	.173	1.32	2.79	.730	.060
	FICP	.079	.608	.143	.200	1.36	2.79	.786	.057
	SQES	.095	.93	.23	.22	2.6	2.9	.770	.062
BA ppm	INAA						230		
	SQES	2.2	5.2	4.5	3.2	1.9	130	2.1	
SR ppm	SQES	1.3	2.4	2.3	3.7	1.9	130	3.5	

Table 1. (continued)

		CCU-1	CPB-1	CZN-1	KC-1	MP-1a	SU-1	113a	329
MN ppm	CERT			2 190			850		
	AFLAA	88	400	2 620	142	560	970		
	AICP	53	396	2 354	135	519	967	84	2 700
	FICP		400	2 200	100	500	930	100	2 600
	SQES	120	680	4 100	150	680	1 400	120	3 700
AL %	CERT	.131	.15	.13			4.9		
	AICP	.133	.156	.141	.766	1.65	4.93	.110	.100
	FICP	.127	.148	.132	.794	3.44	4.97	.085	.085
	SQES	.28	.20	.17	.61	3.2	4.7	.047	.067
NA %	AICP	.054			.178		.809	.080	.090
	FICP	.022	.015	.015	.215	.007	.743	.015	.030
	INAA	.015	.220	.190	.270		.720		
	SQES						.720		
AS ppm	CERT		560	260		8 400	418		
	AGFAA	37	560	240	390	10 000	605		
	AICP	122	562	270	312	7 430	821	98	380
	INAA	38	620	277	283	7 830	483	124	
	SQES	100	740	260	310	9 200	600	120	410

CERT = certified values
GRAV = gravimetric analysis
LECO = LECO sulfur analyzer
AGFAA = acid-dissolution graphite furnace atomic absorption
AFLAA = acid-dissolution flame atomic absorption
AICP = acid-dissolution inductively coupled plasma spectroscopy
FICP = fusion decomposition inductively coupled plasma spectroscopy
INAA = instrumental neutron activation analysis
EDXRF = energy dispersive X-ray fluorescence
SQES = semi-quantitative emission spectroscopy

Certified values for the CCRMP standards CCU-1, CPB-1, CZN-1, KC-1 and MP-1a are from Steger (1983); for the CAAS standard SU-1 from Webber (1965); and for the NBS standards 113a and 329 from the NBS Standard Materials Catalog 1984-85.

the JDF sulfides, and EDXRF, a technique that we are still tuning-up for the analysis of sulfides. We are currently taking steps to reduce these biases. Bias is discussed below only when it appears that it might be of *general* significance in the analysis of sulfides by a specific technique.

ANALYTICAL TECHNIQUE OVERVIEW

A comprehensive report covering analytical methods used in this laboratory is available (Baedecker, 1986). We present here a brief overview of each technique, mentioning modifications and difficulties relating to the analysis of sulfides, and listing elements determined. Tradenames identifying instruments are used in this paper for descriptive purposes only; endorsement by the U.S. Geological Survey is not implied.

Semiquantitative emission spectrography

SQES is a minicomputer-based, graphite-electrode d.c. arc method that determines 64 elements using a scanning microphotometer and an Ebert 3.4 m Mark III spectrometer (Golightly et al., 1986). The technique is semiquantitative because it uses stored coefficients based on previously arced standards. The 15 mg sample size may degrade precision, especially for trace elements, due to sample inhomogeneity.

The major problems encountered in analyzing the JDF samples were the interference and background effects produced by Cu and Zn. Copper contents greater than 0.15% rendered Nd undetectable, necessitated the use of alternate lines for In, Sc and Y, and resulted in degraded detection limits for Ag, Ni, U, V, La, Er, Yb and Pt. Zinc contents greater than 1% rendered Na and Li undetectable, necessitated the use of alternate lines for In, Sb and Sc, and degraded detection for V, La, Eu, Tb, Dy, Er, Yb and Pt. SQES is most valuable for trace element determinations. Upper limits of utility encountered with the JDF samples with our present technique were for Zn 10%, Fe 25%, Cu 1%, Pb 0.1%, and Ag 80 ppm. For Cu, Cd, Co, Si, Al and As, SQES results appear to degrade at the lowest concentrations in the JDF suite. SQES does not appear useful for Zn, Sb or Na. The error quoted with SQES is +50% and −33% of the reported value. For the JDF samples, random errors for some determinations, including those for Cd, Si, and Mn, are smaller than the quoted error.

Energy dispersive X-ray fluorescence spectrometry

EDXRF utilized a Kevex 7000/0700 spectrometer. Primary excitation (Rh anode) was used for Al, Si, and S; a Ge second-

Table 2. Correlation coefficients for seven techniques applied in the analysis of Juan de Fuca massive sulfides.

		AFLAA	AGFAA	AICP	FICP	INAA	EDXRF	SQES
ZN	r	.997		*		.996	.990	
	n	23				31	48	
FE	r	.998		*	.998	.999	.992	.927
	n	33			55	32	48	42
CU	r	.995		*			.994	.919
	n	26					37	20
PB	r	.994		*			.942	.736
	n	32					45	39
CD	r		.992	*		.998	.989	.981
	n		31			32	45	55
CO	r	.998		*		1.000		.946
	n	13				13		29
AG	r		.960	.955		*	.982	.202
	n		30	25			26	32
SB	r		.926			*		
	n		14					
SI	r				*		.993	.987
	n						48	52
MG	r			1.000	*			.994
	n			5				46
CA	r			.999	*	—	.999	.973
	n			21		3	7	43
BA	r					.997	*	.982
	n					14		31
SR	r					*		.960
	n							4
MN	r	*			.990			.985
	n				7			33
AL	r			.681	*		.941	.623
	n			25			4	25
NA	r			.874	*	.936		
	n			38		29		
AS	r		.287	−.223		*		.904
	n		29	15				22

r = correlation coefficient
n = number of samples
* = reference technique

ary target for Fe, Cu and Zn; a Ag target for Pb; and a Gd target was used for Ag, Cd and Ba. Samples were prepared by mixing powdered samples (<100 mesh) with microgranular cellulose, and forming briquettes in a hydraulic press. A method for fusing massive sulfides while retaining sulfur has been developed (Johnson and Rait, 1986), but data for the JDF samples are not yet available.

The major problems encountered in using EDXRF for the analysis of sulfides were the severe absorption and enhancement effects caused by high and varying concentration of heavy elements such as Pb, Zn and Fe. These strong matrix effects required the use of a mathematical matrix correction model. Because of the small number of well-characterized standard reference materials, the correction method chosen employed interelement influence coefficients calculated from fundamental parameters (Johnson and Fleming, 1986) by means of the Rousseau "fundamental algorithm". EDXRF appears useful for determining Zn, Fe, Cu, Cd, Ca, Ba and Al in JDF materials; Pb, Ag and Si results were not quite as good. Sulfur results were poor, owing perhaps to failure of the absorption correction algorithm, to incorrect modelling of the substantial background, or to faulty correction of an unresolved overlapping lead line. For Cu, Pb, Cd, Si, Ca and Al, EDXRF results appear to show distinctly increased random error for the lowest concentrations in the JDF suite.

Atomic absorption and inductively coupled plasma emission spectrometry

A detailed discussion of our atomic absorption and inductively coupled plasma emission methods is given in a companion paper (Kane and Dorrzapf, 1987) and in Lichte and others (1986) and Aruscavage and Crock (1986). Even though ICP calibration ranges for the elements of interest may extend over four or five orders of magnitude we have had to use multiple dilutions of solutions in working with the JDF sulfides; because our ICP instrument is a fixed-slit direct reader (Jarrell Ash Model 1160) high element concentrations cannot be analyzed simply by changing the wavelength of measurement. We have

prepared JDF samples for ICP analysis using both acid (HF-HCl-HNO_3-$HClO_4$) dissolution (AICP) and lithium metaborate -lithium tetraborate fusion (FICP). One risk in using acid is incomplete sample dissolution. This is particularly problematic for samples containing sizable insoluble sulfate and may result in erroneously low results for elements such as Pb, Ba, Sr and Ag. Fusion, on the other hand, runs the risk of loss of some volatile elements (Cd, Pb, Zn, Cu). Fusion also increases the load of total dissolved solids and for many trace elements we therefore have eschewed FICP in favor of AICP. We use twice the proportion of flux to sample that is used for silicates (6:1) in order to preclude adherence of the fusion bead to the graphite crucible in the case of high-Fe (>15%) sulfides. For the JDF samples, FICP has been used to determine Fe, Si, Mg, Ca, Mn, Al and Na abundances. We have used AICP to determine Zn, Fe, Cu, Pb, Cd, Co, Ag, Mg, Ca, Al and Na abundances. For ICP analysis, Fe can cause spectral interferences for Cd, V and Ce; Zn interferes with Mo and Sb.

Atomic absorption analysis suffers less from spectral interference than does ICP. However, unlike the ICP, our AA instruments (PERKIN ELMER: 5000, ZEEMAN and 603) provide data only one element at a time and calibration is linear over only an order of magnitude or two at best. We have used both flame (AFLAA) and graphite furnace (AGFAA) atomic absorption after acid digestion (the same as for AICP) in the analysis of JDF samples. AGFAA offers the potential of better detection limits relative to AFLAA and ICP techniques although this can degrade, depending on matrix. Cadmium, silver, and antimony abundances have been determined in JDF samples by AGFAA. AFLAA was used to determine concentrations of Zn, Fe, Cu, Pb, Co and Mn; Mg, Ca, Al and Na determinations are also quite feasible.

Instrumental neutron activation analysis

INAA of the JDF samples was performed using procedures established for silicate rocks (Baedecker and McKown, 1986) and for coal (Palmer and Baedecker, 1986), although the sulfides presented several problems that are not normally encountered. Sample sizes were kept below 100 mg to minimize neutron self-absorption effects due to high Cd concentrations. The samples were counted further from the Ge (Li) detectors than normal due to the high activity of ^{65}Zn and this worsened the counting statistics for all elements. The high activity of ^{122}Sb in several samples resulted in large interference of the primary line for ^{24}Na. The elements Zn, Fe, Cd, Co, Ag, Sb, Ca, Ba, Sr, Na and As were determined in the JDF samples. Errors (one standard deviation based on counting statistics alone) were at or below 10% for most elements in the JDF samples; Ca, Ba and Sr tended to have higher errors.

DISCUSSION BY ELEMENT

This paper considers analytical results for 17 elements in addition to sulfur. These are about equally divided between elements occurring in sulfides and those in other phases including silicates and sulfates. The elements are treated by group in approximate order of abundance as follows: S; Zn, Fe, Cu, Pb, Cd, Co, Ag, Sb; Si, Mg, Ca, Ba, Sr, Mn, Al, Na; and As.

Sulfur was determined only by EDXRF of the multielement techniques and the results are only semiquantitative. The highest quality results for S are obtained by classical gravimetric analysis. In a companion paper (Kirschenbaum and Philpotts, 1987) we have discussed in detail the procedures for gravimetric determination of total S and its distribution among sulfide and soluble and insoluble sulfate. S results for the eight standard sulfides as determined by gravimetric analysis, LECO Analyzer, and EDXRF are given in Table 1. Determinations using the LECO Sulfur Analyzer are much less time-consuming than gravimetric analysis and the quality appears adequate for most purposes, particularly if the magnesium perchlorate (anhydrone) filter columns, which are used to dry the SO_2 analyte, are changed prior to each analysis session. For the six JDF samples analyzed in common the LECO results gave a correlation coefficient of 0.997, and an average ratio of 0.983 with standard deviation 0.026 relative to the gravimetric determinations. S contents of the JDF suite range from 46% to 24%.

Zinc concentrations in the JDF suite range from about 60% to 1%. We have determined Zn by AFLAA, AICP, EDXRF and INAA. All of these techniques appear to yield quantitative analytical results. Figure 1 shows the good but sinuous correlation for Zn determined by AFLAA and by AICP on the same sample dissolutions. The sinuosity probably derives from nonlinearity and slight mismatch of standards of different dilutions in this particular AFLAA analysis. It serves to underline how small actual random error is for these techniques when Zn is a major element. Determination of Zn by our SQES technique has an upper limit of 10% Zn. Comparison of results with those of other techniques for the three samples in common with less than 10% Zn indicates that this element is poorly determined by SQES at any level in the percentage range.

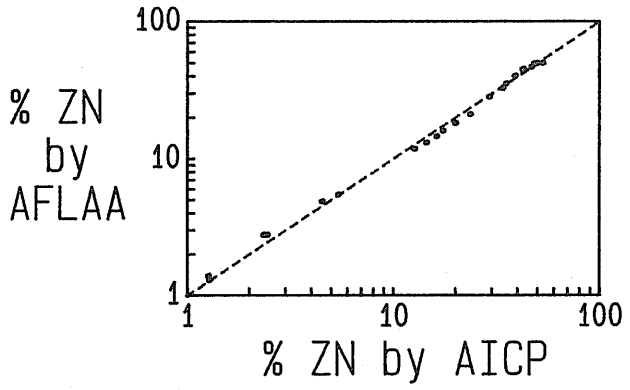

Fig. 1. Log % Zn by AFLAA versus log % Zn by AICP for Juan de Fuca sulfides. Note the sinuosity and small random error.

The average agreement of concentrations determined by AFLAA, AICP, EDXRF and INAA with certified Zn values for the sulfide standards is better than 5% for each technique (Table 1). Good agreement extends to the two values obtained by AICP and INAA for SU-1 which has a certified value of

only 0.0294% Zn, which is much lower than the JDF abundances; the detection limits of these techniques for Zn in sulfides is apparently quite low. Analysis of the sulfide standards by FICP resulted in Zn determinations that were up to 27% lower than certified values; volatile loss of Zn occurred during the roasting step which preceded fusion.

Iron was well-analyzed by more techniques than any other element: AFLAA, AICP, FICP, EDXRF, INAA and SQES (Tables 1 and 2). Fe content in the JDF suite ranges from about 40% to 1%. With the possible exception of AFLAA, none of the techniques show any obvious increase in random error at lower concentrations. The upper limit for our SQES determinations is about 20% FE. Below this, SQES appears to offer useful determinations.

Certified Fe values are available for only four of the standard sulfides (Table 1). Other than AFLAA and SQES, all techniques gave average biases of less than 5% relative to the certified values. For the two cases where comparison is possible, AFLAA results averaged 11% higher than certified. More accurate calibration of AFLAA might be achieved by using a different measurement wavelength. The four standards lacking certified values also show a tight clustering of analytical results (Table 1).

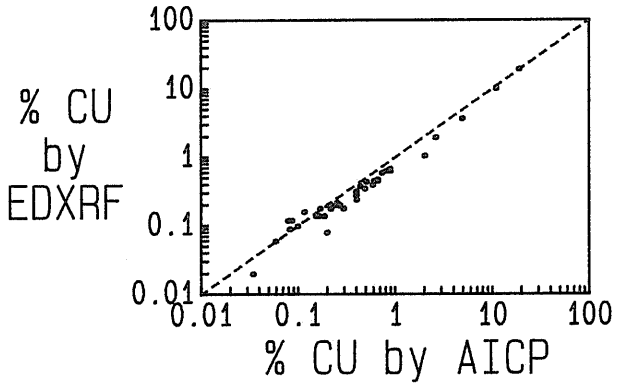

Fig. 2. Log % Cu by EDXRF versus log % Cu by AICP for Juan de Fuca sulfides. Note the curvature.

Copper concentrations in our JDF suite range from about 20% to less than 100 ppm; only four of 56 samples have more than 1% Cu. Cu was analyzed by AFLAA, AICP, EDXRF, and SQES. There appears to be room for analytical improvement in some of these techniques. Correlations of EDXRF results with data from other techniques appears to be non-linear (Fig. 2); presumably adjustments in coefficients used in the EDXRF data reduction should remove such an effect. Above about 3,000 or 4,000 ppm Cu the SQES determinations tend to show large deviations relative to results from other techniques; below this concentration random error attributable to SQES appears to be at least as small as that attributable to EDXRF. The lowest Cu concentration in the JDF suite is about 50 ppm which is reported by AFLAA and SQES; AICP records values down to 100 ppm and EDXRF down to about 200 ppm. There is a suggestion of increased scatter for EDXRF and SQES at these lower limits. The average bias relative to certified values for the sulfide standards is less than 5% for all the techniques except SQES (Table 1). Among other things this agreement indicates that acid digestion is putting all of the Cu into solution.

Lead concentrations range from about 6,000 ppm to 100 ppm in the JDF samples. Pb was determined by AICP, AFLAA, EDXRF and SQES. The only technique not reporting determinations at the lowest concentrations was EDXRF for which the lower limit was about 400 ppm. The AICP and AFLAA determinations correlate well with each other (Table 2). The poorer correlation of EDXRF data with AICP results is in large part due to an anomalous subset of four samples which have much lower Pb by AICP (≈300 ppm.) than by EDXRF (≈700 ppm). The same situation holds for the SQES-AICP correlation (Fig. 3). The anomalous subsets in the EDXRF-AICP and SQES-AICP correlations represent the highest Fe samples in our JDF suites; they are also highest in Ba. There clearly appears to be a matrix compositional effect disturbing these correlations. Because the anomaly occurs in both correlations, the AICP data is suspect. We suggest that during acid dissolution, Pb may be lost to $BaSO_4$ which is high in the anomalous samples.

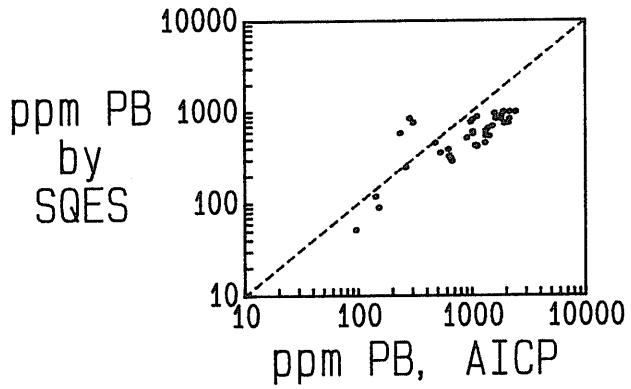

Fig. 3. Log ppm Pb by SQES versus log ppm Pb by AICP for Juan de Fuca sulfides. Note, on the left, the insoluble-sulfate-bearing subgroup.

Pb determinations by AFLAA, AICP, EDXRF, and SQES for standard sulfides agree well with certified values (Table 1). None of the JDF chimney samples have more than 1% Pb and therefore standard CPB-1 (64.74%) was not analyzed for Pb. Such high-Pb samples are not completely dissolved with acid digestion; fusion decomposition gives a considerable improvement in Pb recovery, which nevertheless remains low. However, results for the other sulfide standards, including CZN-1 with 7.45% Pb, give no indication of incomplete Pb recovery and this is not likely to be a general problem for the JDF samples except for the high Ba-Fe subset discussed above.

Cadmium contents range from about 3,000 ppm to 30 ppm in the JDF samples. Cd has been determined by AICP, INAA, EDXRF, AGFAA and SQES. The correlations are unexpectedly good (Table 2). There is no evidence that corrections for an Fe spectral interference have degraded the ICP determinations. All of the good correlations show distinct increase in scatter at lower Cd concentrations (e.g. Fig. 4). EDXRF does not report determinations for the samples having the very lowest Cd contents but other than this, detection limits of the techniques appear adequate to treat the JDF concentrations. Except for an anomalous Cd value for CPB-1 by AGFAA, probably caused by digestion loss of Cd along with the undissolved Pb, there is

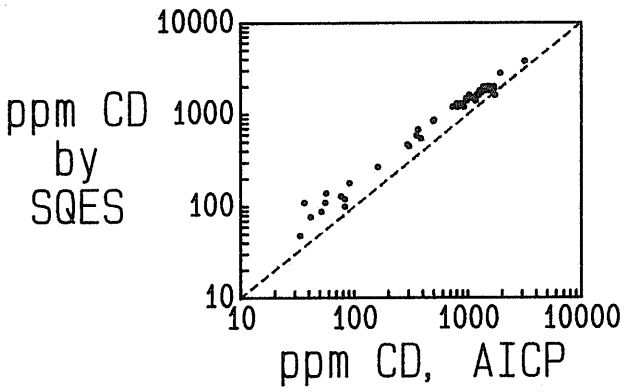

Fig. 4. Log ppm Cd by SQES versus log ppm Cd by AICP for Juan de Fuca sulfides. Note the increase of random errors at low concentrations.

good agreement among the values determined for the standard sulfides (Table 1) and with the certified values.

Cobalt concentrations range over three orders of magnitude in the JDF samples from about 1,700 ppm to 1 ppm. INAA and AICP show excellent correlation (Fig. 5; Table 2). AFLAA determinations also show very good correlation with the AICP results down to about 100 ppm; below this concentration the AFLAA data appear to deviate with negative bias. SQES yields useful semiquantitative determinations over the entire concentration range, with somewhat more scatter at the lower end.

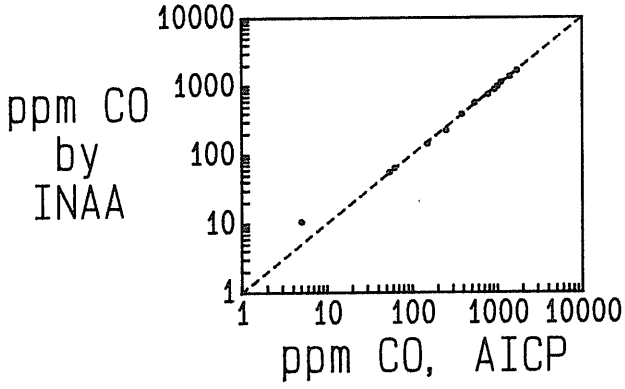

Fig. 5. Log ppm Co by INAA versus log ppm Co by AICP for Juan de Fuca sulfides.

A certified value is given for only one of the standards, SU-1. Determinations by AICP, INAA, and AFLAA are in good agreement with this certified value and with each other for other standards, MP-1a being the only exception. SQES values are also in good agreement for the five standards with Co less than 30 ppm but appear low by about 50% for two standards with 600 ppm and 700 ppm Co. The JDF data suggests similar bias for the SQES results.

Silver concentrations range from about 800 ppm to 10 ppm in the JDF samples. Based on results for the JDF samples and for the standard sulfides (Table 1) INAA appears to be the preferred technique, of those compared, for Ag. EDXRF data show the best correlation with INAA determinations. The poorer correlations for AICP-INAA and AGFAA-INAA are to a large extent due to small anomalous subsets. The relative discrepancy of these subsets is positive for AICP and negative for AGFAA. Background correction errors accompany high Cu in the AICP method and two of the three samples off the curve are Cu-rich. Ag was below the AICP detection limit for the samples with anomalously low AGFAA determinations. Ag might be in residue or precipitate for these acid digestions. The SQES determinations look reasonably good below about 80 ppm Ag which appears to be an effective upper limit, at least for sulfides, for useful determinations for the line-width technique that we have routinely used for Ag at these levels (Fig. 6).

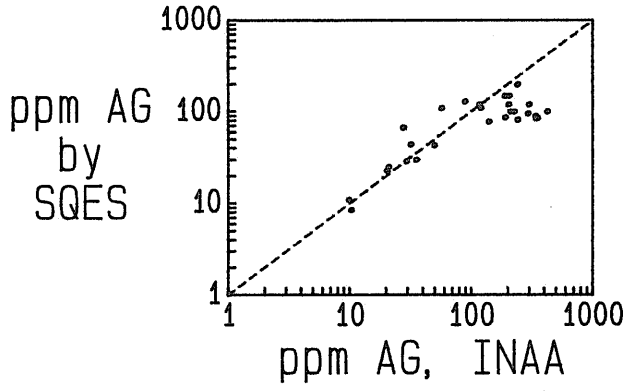

Fig. 6. Log ppm Ag by SQES versus log ppm Ag by INAA for Juan de Fuca sulfides. Note the upper limit saturation of SQES results between 80 and 200 ppm Ag.

All of the sulfide standards have certified Ag values and these range from 1,120 ppm to 4 ppm. INAA determinations agree to better than 10% with the certified values as do four of five AGFAA determinations (Table 1). EDXRF and AICP results do not compare as well. One difficulty for AICP is a large background correction to Ag for Cu in standard CCU-1.

Antimony concentrations in the JDF samples range from about 180 ppm to 2 ppm. Much of this range is below the effective determination limits for AICP and SQES. Comparison of AGFAA and INAA results shows a fair amount of scatter (Table 2). For the sulfide standards (Table 1) INAA and AGFAA values are in good agreement with each other and the two certified values.

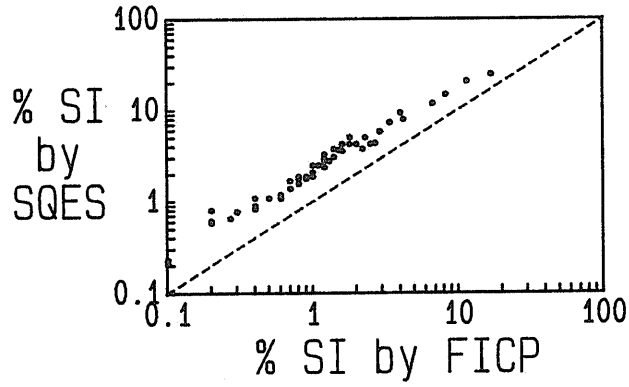

Fig. 7. Log % Si by SQES versus log % Si by FICP for Juan de Fuca sulfides. Note the bias and small random error.

Silicon concentrations range from about 17% to 0.1% in the JDF suite. Si has been determined by FICP, SQES and EDXRF. The acid dissolution techniques are not appropriate inasmuch as Si is lost as the volatile fluoride. Comparison of the SQES values with those by FICP gives about as good a correlation as we have found for SQES data (Table 2; Fig. 7) albeit with considerable inter-technique bias. EDXRF determinations have a higher correlation coefficient but show more scatter relative to the FICP results below about 0.2% Si. The FICP determinations are in excellent agreement with the two certified values for the standards (Table 1).

Magnesium contents of the JDF samples range from 10.1% to 0.01% or lower. The high value is isolated in composition and this tends to inflate correlation coefficients for the suite (Table 2). There is excellent agreement between the values determined by AICP and FICP for the five samples analyzed in common, of which only one sample has less than 0.1% Mg. The SQES-FICP correlation is also good, albeit with increasing scatter below about 0.1% Mg. FICP and AICP results are in good agreement with each other and with the three certified values (Table 1).

Calcium concentrations in the JDF samples range from 10% to less than 0.1%. Both AICP and EDXRF determinations show excellent correlations with FICP values (Table 2). The SQES-FICP correlation shows more scatter but SQES appears entirely satisfactory for semiquantitative determinations. Below about 0.1% Ca all the correlations show significant scatter. INAA values were obtained for the three samples with the highest Ca contents (about 10%). These values appear high by about 30%. In general, INAA does not appear to be a good quantitative technique for Ca in most massive sulfides.

FICP and AICP determinations for the sulfide standards are generally in good agreement with each other and with certified values (Table 1). Whereas SQES values for four of the standards are more or less in agreement with results by other techniques, SQES determinations for CCU-1, CPB-1, CZN-1, and MP-1a are distinctly high.

Barium concentrations range from about 7% to 2 ppm in the JDF samples. INAA and EDXRF determinations show good correlation (Table 2). The lower limit for INAA determinations is about 1 000 ppm. For EDXRF it is about 100 ppm. SQES results are more scattered relative to the EDXRF determinations but show reasonably good correlation. With one exception, all the sulfide standards have considerably less than 100 ppm Ba and we have obtained only SQES data; there are no certified values for Ba in these standards. Because of known severe dissolution losses of Ba for samples containing barite, such as the JDF suite, AICP was not attempted. Analysis for Ba by AICP might be facilitated via a double decomposition or other additional procecural steps. FICP is expected to produce good Ba determinations.

Strontium concentrations in our JDF suite range from about 4,000 ppm to 1 ppm. Determinations were obtained only by INAA and SQES and for only four samples of those analyzed to date. The four samples are among the highest in Sr but they are also all Fe-rich. The detection limit for INAA in the Zn-rich samples is at several thousand ppm and this is above the concentration of Sr in these samples. SQES data indicates that Sr in all the sulfide standards is very low; there are no certified values. Determinations of Sr were not attempted by AICP because, as for Ba, dissolution losses are expected. FICP is expected to produce good Sr determinations.

Manganese concentrations range from about 6,000 ppm to 10 ppm in the JDF suite. Determinations were reported for FICP, AFLAA and SQES. The lower limit for the FICP results was 100 ppm Mn. Only six of the JDF samples analyzed were above this limit and the data values are scattered relative to those by AFLAA. In contrast, both SQES and AFLAA values were obtained to below 10 ppm, the lowest concentrations occurring. The SQES and AFLAA results show a good correlation. All of the standards have Mn concentrations near 100 ppm or higher (Table 1). Only CZN-1 and SU-1 have certified values. Determinations by AFLAA, AICP and FICP are generally in good agreement with each other and with the certified values.

Aluminum determinations on the JDF samples by AICP, FICP, EDXRF and SQES appear to be semiquantitative for the most part. Below about 0.2% Al, both AICP and SQES values scatter widely when compared with FICP results; only about 20% of the samples have aluminum in excess of this concentration. AICP and FICP determinations for the standard sulfides with Al greater than 0.1% generally agree with each other and with certified values to within a few percent, Mp-1a data being an exception (Table 1).

Sodium concentrations in the JDF suite range from about 0.4% to 0.02% with a lone sample having 0.55% Na. Na has been determined via AICP, FICP and INAA. The best correlations holds between INAA and FICP data (Table 2); discrepancies of 50% or more are not uncommon, and are due to the low abundances. Agreement between techniques is also poor, in general, for the sulfide standards (Table 1); there are no certified values for Na in these samples. INAA Na values may be degraded to some extent by interference due to high antimony and reduced sensitivity due to the high Zn in addition to the low abundance of Na.

Arsenic data obtained for the standards appears reasonably consistent (Table 1) although all of the techniques report values higher than certified for SU-1. For the JDF samples, however, there are major discrepancies. INAA determinations range from 700 ppm to 4 ppm As. SQES data shows good correlation (Table 2) with the INAA data although the effective lower limit for SQES appears to be 100-200 ppm As. Results from AGFAA and AICP analyses, however, show little correlation with the INAA values and tend to be low. Volatile loss during acid dissolution or subsequent precipitation may account for this discrepancy but it is curious that the standards showed no such effect.

Other elements: Determinations were attempted on a number of other trace elements. Results are not presented in the tables because of lack of corraborating data or as yet unexplained large discrepancies between techniques. These elements are Cr, Cs, Hf, Hg, Mo, Ni, rare earth elements, Sc, Se, Ta, Th, U, W and Zr. Corroborating results are also not yet available for K, P and Ti although AICP analysis appears to yield acceptable determinations.

CONCLUSIONS AND FURTHER WORK

The As results help to emphasize that there are many problems yet to be solved. This analytical study of sulfides is still very much work in progress. The tables, figures, and discussion do indicate which elements can be readily determined in sulfides using the various multielement techniques. The scatter of data in the correlations and the detection limits are believed to be generally representative of the techniques as applied to sulfides. Of the methods tested SQES, INAA and AGFAA have the highest sensitivity; AFLAA, AICP and FICP are intermediate; and EDXRF has the lowest sensitivity. In terms of numbers of elements determined well, AICP may be the single most useful technique.

In order to obtain better statistics on precision, we are obtaining further data on the standards. We also hope to extend the study to more elements and additional techniques, for example ICP-mass spectrometry and multi-element atomic absorption spectroscopy using continuum source.

Acknowledgements — Internal reviews by Pat Hatcher, John Morgan, and Frank Walthall, all of the U.S. Geological Survey, Reston, are much appreciated. We give special thanks to Carol Popish and Mary Catherine Kiel for typing service above and beyond.

REFERENCES

Aruscavage, P. J. and Crock, J. G., 1986, Atomic absorption methods, *in* Methods for Geochemical Analysis, Baedecker, P. A., (editor), U.S. Geol. Surv., Bull., 1770.

Baedecker, P. A. (editor), 1986, Methods for Geochemical Analysis: U.S. Geol. Surv., Bull., 1770.

Baedecker, P. A. and McKown, D. M., 1986, Instrumental neutron activation analysis of geological samples, *in* Methods for Geochemical Analysis, Baedecker, P. A. (editor), U.S. Geol. Surv., Bull., 1770.

Golightly, D. W., Dorrzapf, A. F., Jr., Mays, R. E., Fries, T. L. and Conklin, N. J., 1986, Analysis of geologic materials by D. C. arc spectrography and spectrometry, *in* Methods for Geochemical Analysis, Baedecker, P. A. (editor), U.S. Geol. Surv. Bull., 1770.

Johnson, R. G. and Fleming, S. L. II, 1986, Energy-dispersive X-ray analysis of massive sulfides with fundamental influence coefficients: X-ray Spect., submitted.

Johnson, R. G. and Rait, N., 1986, Fusion of massive sulfides for X-ray fluorescence analysis: Chem. Geol., submitted.

Kane, J. S. and Dorrzapf, A. F., Jr., 1987, Current atomic absorption and inductively coupled plasma emission methods for geochemical investigations: GEOEXPO/86, Vancouver, B.C., May 12-14, (this volume).

Kirschenbaum, H. and Philpotts, J. A., 1987, Classical chemical analysis of forms of bound sulfur in massive sulfides with an application to chimney samples from the Juan de Fuca Ridge: GEOEXPO/86, Vancouver, B.C., May 12-14, (this volume).

Lichte, F. E., Golightly, D. W. and Lamothe, P. J., 1986, Inductively coupled plasma atomic emission spectrometry, *in* Methods for Geochemical Analysis, Baedecker, P. A. (editor). U.S. Geol. Surv., Bull., 1770.

NBS Standard Reference Materials Catalog 1984-85: Natl. Bur. Stand., Spec. Pub. 260, Washington, D.C.

Palmer, C. A. and Baedecker, P. A., 1986, The determination of 41 elements in whole coal by instrumental neutron activation analysis, *in* Coal Methods Manual, Golightly D. (editor). U.S. Geol. Surv., in press.

Steger, H. F., 1983, Certified Reference Materials: CANMET Report M38-13/834-3E, Canadian Certified Reference Materials Project, Energy, Mines and Resources Canada, 555 Booth Street., Ottawa, Canada K1A 0G1.

Webber, G. R., 1965, Second report of analytical data for CAAS syenite and sulfide standards: Geochim. Cosmochim. Acta, v. 29, p. 229-248.

Classical Chemical Analysis of Forms of Bound Sulfur in Massive Sulfides with an Application to Chimney Samples from the Juan de Fuca Ridge

H. KIRSCHENBAUM and J. A. PHILPOTTS
U.S. Geological Survey, 923 National Center, Reston, VA 22092

Abstract — The assemblage of sulfur-bearing minerals in massive sulfides can provide insight on the formation and subsequent evolution of these deposits. Classical gravimetric chemical analysis provides a tool complementing mineralogical and normative methods of examining sulfide and sulfate abundances in massive sulfides. We have tested and refined classical procedures for accurate determinations of total sulfur and of sulfur in total sulfides, total sulfates, and acid-soluble and insoluble sulfates, using massive sulfide chimney samples from the Juan de Fuca Ridge. The results show convincing internal consistency. The highest soluble sulfate values were found for the Ca-rich rim of a "black smoker" chimney. The highest concentration of acid-insoluble sulfate occurs in a pyritic sample and presumably reflects the occurrence of barite; measured Ba and sulfate values are in good agreement for this sample.

INTRODUCTION

As PART of the U.S. Geological Survey's program on the Juan de Fuca Ridge, a spreading-center off the west coast of North America, we are involved in a geochemical study of massive sulfide chimneys formed at hot-springs on the ocean floor. Factors of importance in the construction and subsequent evolution of the chimney materials include temperature and the operative oxidation conditions. These conditions are reflected in the phase assemblages of the chimneys, including those of the sulfur-bearing minerals, the various sulfides, sulfosalts, and sulfates. Some of the Juan de Fuca chimneys appear to be of the high-temperature "black-smoker" variety. One model for the origin of "black-smoker" chimneys (Haymon, 1983) proposes sulfide deposition within a protective shell of sulfate formed when seawater is heated by hydrothermal fluid. This sulfate is vulnerable to subsequent reaction with the hydrothermal fluid. Sulfates may also be primary precipitates from hydrothermal fluids without immediate seawater interaction. With the waning of the active constructive processes the massive sulfide chimneys are susceptible to reaction with seawater. Sulfates may go back into solution in seawater at low temperature. Sulfides are susceptible to oxidation by seawater unless (at least locally) anoxic conditions prevail or burial occurs. The proportions of sulfides, and soluble and insoluble sulfates provide evidence for unravelling the history of chimney construction and subsequent modification.

The nature and abundances of the sulfur-bearing minerals can be examined via optical, electron beam, and X-ray diffraction techniques and indirectly via calculated mineral norms. They are also amenable to study by bulk chemical determination of the forms of bound sulfur. These complementary chemical techniques identify groups of compounds having similar chemical properties rather than being mineral-specific. However, they can be applied to fine-grained or even imperfectly crystalline samples such as those perhaps formed by rapid precipitation, by alteration, or by the activity of the sulfur processing microorganisms that form the basis of the spectacular ecosystems established in the deep-sea hot-spring environment (Grassle, 1982). In addition the chemical techniques offer a precision and sensitivity not obtainable with normal X-ray diffraction.

Chemical techniques appropriate for determining the various forms of bound-sulfur in silicate rocks are described in the literature. It is not obvious, *a priori*, that these techniques will work well for massive sulfides. The present note discusses their application to Juan de Fuca sulfides. Specifically, this paper reports on analytical methods for determining total sulfur, and its distribution among sulfides and acid-soluble and insoluble sulfates. Detailed step-by-step procedures are available by mail from the authors. It might be noted that whereas the techniques have been studied with massive sulfides as the analytical focus, much of what is covered here might have application in other sulfur-bearing systems. (Any trade names in this publication are used for descriptive purposes only and do not constitute endorsement by the U.S. Geological Survey).

DISCUSSION

The six chimney samples selected for the present study were chosen so as to reflect the compositional diversity of our Juan de Fuca massive sulfide suite collected in October 1984 using the DSRV *Alvin* submersible. The suite is dominated by sphalerite and/or wurtzite. Sample numbers given are the last three digits of our USGS laboratory control numbers W-229_____. Samples 431 (chimney interior) and 978 (whole rock) are characteristic of this Zn-rich material. Sample 979 (whole rock) is predominantly FeS_2; it is also noteworthy for having about 4 percent Ba. Sample 974 is a "black smoker" chimney with a core of isocubanite and a sulfate-rich exterior; the bulk sample has about 11 percent Cu and 8 percent Ca. Sample 427 (core) is of intermediate Zn and Fe content and contains about 5 percent Cu. Sample 416 (surficial) also has intermediate Zn and Fe; it is noteworthy for having 17 percent Si.

Concentrations for the various sulfur-bearing phases are given in Table 1. Total sulfur ranges from 24 to 46 percent. Total sulfur was determined via a Na_2CO_3/Na_2O_2 fusion. The combination of 200 mg of sample, 4 g Na_2CO_3, and 0.3 g Na_2O_2 was found to result in complete decomposition of all sulfides tested (including sphalerite-, galena-, pyrite- and chalcopyrite-rich samples) with oxidation of all sulfur. Results for single determinations of total sulfur in seven sulfide standards are given in Table 2; they range from 12 to 35 percent. Agreement with certified values is within 1 percent relative difference, except in the case of NBS 113a for which it is 1.6 percent.

Table 1 Percent (%) sulfur determined for various phases

Decomposition Procedure Used	Na_2CO_3/Na_2O_2 Fusion	HNO_3/Br_2 Digestion	(1 + 1) HCl Digestion	$CdCl_2/BaCl_2$ Digestion	Impervious to HNO_3/Br_2 Digestion	By Difference	By Difference
	A	B	C	D	E	(B-C)	(D-C)
	% Total Sulfur	%S in sulfides Plus Soluble Sulfate	%S in Soluble Sulfate	%S in Total Sulfate	%S in Insoluble Sulfate	%S in Total Sulfides	%S in Insoluble Sulfate
Sample							
416	23.6	23.4	1.0	nd-due to high SiO_2 content	0.4	22.4	—
427	44.6	44.8	0.6	0.6	nd	44.2	0
431	31.1	31.1	0.01	0.01	nd	31.1	0
974	30.0	29.9	6.1	6.0	nd	23.8	0
978	32.3	32.3	0.05	0.04	nd	32.3	0
979	46.3	45.2	0.5	1.6	1.1	44.7	1.1

nd: not determined

Table 2 Comparison of total sulfur obtained by gravimetric determination and by the LECO SC-132 sulfur analyzer for Juan de Fuca sulfides and standard sulfides

Juan de Fuca Massive Sulfides	% Total S Literature Value	% Total S Gravimetric (X)	% Total S LECO (Y)	% Relative Difference $\left(\frac{Y}{X}-1\right)$
416		23.6	24.3	+3.0
427		44.6	43.8	−1.8
431		31.1	30.7	−1.3
974		30.0	29.4	−2.0
978		32.3	30.6	−5.3
979		46.3	45.2	−2.4
Sulfide Standards				
CCRMP: CZN-1	30.2(a)	30.1	29.7	−1.3
CCRMP: CPB-1	17.8(a)	17.9	17.6	−1.7
CCRMP: MP-1a	12.7(a)	12.8	12.8	0
CCRMP: KC-1	(d)	27.3	26.8	−1.8
CCRMP: CCU-1	35.4(a)	35.4	34.2	−3.4
CAAS: SU-1	12.0(b)	11.9	12.6	+5.9
NBS: 113a	30.6(c)	30.1	—	—
NBS: 329	—	29.7	29.1	−2.0

CCRMP: Canadian Certified Reference Materials Project
CAAS: Canadian Association for Applied Spectroscopy
NBS: National Bureau of Standards
(a) Steger (1984)
(b) Webber (1965)
(c) NBS Special Publication 260, 1985
(d) KC-1, not reported. KC-1a, 27.5% (a)

Fusion of sphalerites (30-60 percent Zn) with Na_2CO_3/Na_2O_2 sometimes produced filtrates which, when diluted, became cloudy with the formation of a white gelatinous precipitate. This precipitate was collected on filter paper and dried. Scanning electron microscope analysis showed only Zn. The precipitate did not contain sulfur. The precipitate was identified as $Zn(OH)_2$ which forms in basic media (Curtman, 1954, p. 170-172) and which dissolved when the solution was acidified.

Gravimetric total sulfur values for both standard and chimney sulfides are compared in Table 2 with total sulfur values obtained using the LECO SC-132 Sulfur Analyzer. The LECO procedure as described by Kirschenbaum (1983) was modified by Norma Rait (U.S.G.S., Reston, VA) to determine the sulfur content of massive sulfides. The LECO values were corrected by using a working curve based on different weights of a standard of known sulfur content (NBS 113a was used). Approximately 40 mg of each massive sulfide sample were mixed with 0.25 g of reagent grade V_2O_5 flux for analysis. Blanks were negligible. Comparing the results from the gravimetric and LECO procedures (Table 2) produces a 3 percent standard deviation with a negative bias for the LECO results.

Total sulfides plus acid-soluble sulfates, were determined by HNO_3/Br_2 acid decomposition and oxidation (Maxwell, 1986; Kolthoff et al., 1969). Although elemental sulfur and organic sulfur are not common, they would also be included in this determination if present. Determination of acid-soluble sulfates by themselves is described by Maxwell (1968); total sulfides are determined by difference.

Our procedure for determining sulfides involves precipitation of $BaSO_4$ from a hot solution. Kolthoff et al. (1969, p. 613-614) state that after acid decomposition and oxidation the interference due to iron is minimized by reducing it to the ferrous state and making the precipitation in a cold dilute solution. We have found no significant difference between precipitates from hot or cold solutions. The advantage of making the precipitation of $BaSO_4$ from hot solution is that it minimizes the tendency of $BaSO_4$ to supersaturate (Maxwell, 1968, p. 237). Precipitation from a hot solution generally causes less occlusion of contaminants than precipitation at room temperature (Rieman et al., 1951, p. 257-258) and $BaSO_4$ precipitated in hot solution forms larger and more perfect crystals thus improving the filterability of the precipitate. Soluble sulfate in the chimney samples is reported as percent sulfur in column C of Table 1. Values range from 0.01 to 6.1 percent S, with the highest value being for the Ca-rich sample 974. If the 7.6 percent Ca in sample 974 is all present as sulfate, it would require 6.1 percent S. It is likely that most of the acid-soluble sulfate in the Juan de Fuca chimney samples is present as calcium sulfate. The chalcopyrite-rich standard, CCU-1, yielded duplicate results for acid-soluble sulfates of 0.22 percent S.

Massive sulfide sample 974 containing 11 percent Cu, 8 percent Ca, 6 percent SiO_2, 23 percent Fe, 0.3 percent Pb, and 4 percent Zn, produced a dark-gray residue after ignition of the $BaSO_4$ precipitate in the determination of acid-soluble sulfate. The ignited residue from this sample was yellow when determining total sulfur. According to Maxwell (1968, p. 440), if the residue is colored it should be fused again. However, since the SEM (scanning electron microscope) analysis of the colored residues from the sulfur and sulfate determination showed only $BaSO_4$ in detectable amounts, the residues were not re-fused and re-precipitated. The internal consistency of the results for sample 974 (Table 1) also shows that calculable coprecipitation did not take place.

In the determination of total sulfates (Vlisidis, 1966) all the available sulfate sulfur is converted to barium sulfate by digesting the sample with an acidified solution of barium chloride in an inert atmosphere to prevent oxidation of any sulfide sulfur. Any insoluble sulfate present remains with the precipitated barium sulfate. Cadmium chloride is added in order to precipitate any sulfide ion that may be liberated in the digestion. This addition insures that no sulfide sulfur is oxidized in the initial filtration. In working with the Vlisidis (1966) procedure it is important to be certain that all excess reagent barium, monitored as insoluble yellow chromate, is removed from the residue during washing, otherwise eroneously high results will ensue (Reagent Chemicals, 1981, p. 172). It is equally important to be certain, for the same reason, that all excess sulfate is later removed; to test for excess sulfate, a $BaCl_2$ solution is added to the last wash (Reagent Chemicals, 1981, p. 29).

Total sulfate in the Juan de Fuca chimney samples is not abundant, ranging from 0.01 to 6.0 percent S (column D, Table 1). All of the sulfate in four of the six chimneys is soluble sulfate. Sample 979 has total sulfate of 1.6 percent S (column D, Table 1) and soluble sulfate of 0.5 percent S (column C, Table 1) indicating an insoluble sulfate of 1.1 percent S (last column, Table 1). Total sulfate could not be determined directly for sample 416 (35% SiO_2) because colloidal SiO_2 precipitated out and filtering proved difficult. Complete recovery of the total sulfate could not be achieved. It was decided, therefore, to make a direct determination of insoluble sulfate in sample 416 and also to check the calculated value for sample 979. The insoluble sulfate content in sample 416, was determined using the insoluble acid residue from the total sulfide procedure (Maxwell, 1968); the residue was fused with Na_2CO_3 and taken through the procedure for total sulfur (Kirschenbaum, 1983). The ignited residues were analyzed by SEM and were found to be exclusively $BaSO_4$. To further check the validity of this procedure, sulfur was determined on the filtrate portion of the sample as in the procedure for determining sulfides (Maxwell, 1968); a value of 23.4 percent sulfur was found, agreeing very well with the previous determination of 23.4 percent (see column B, Table 1) and proving that no loss occurred. A total sulfur determination was also performed on the zinc dust reagent (96.1 percent assay). The zinc dust, which is used to reduce trivalent Fe in the procedure, is a large component of the residue that was fused with Na_2CO_3. Less than 100 ppm sulfur was found. The conclusion is that the portion of sample 416 that was impervious to HNO_3/Br_2 digestion did indeed contain insoluble sulfate. The total sulfate calculated for sample 416 is 1.4 percent as sulfur (soluble sulfate is 1.0 percent, column C, Table 1).

The acid-insoluble sulfate determined by this technique for sample 979 is 1.1 percent S (column E, Table 1). This is in excellent agreement with the value of 1.1 percent S calculated by subtracting soluble sulfate from total sulfate. It also agrees with the somewhat less precise calculation of 1.1 percent S obtained by subtracting the value for sulfides plus soluble sulfate (column B, Table 1) from total sulfur (column A, Table

1). We interpret the acid-insoluble sulfate in the Juan de Fuca samples to be almost entirely barite. Sample 979 has about 4.3 percent Ba, which would contribute 1.0 percent S, in good agreement with the determined and calculated values for insoluble sulfate. The only other chimney sample with significant Ba is sample 416; this is the only other sample showing insoluble sulfate (column E, Table 1).

In general, we conclude that the gravimetric determinations of the various forms of bound sulfur in the Juan de Fuca chimney samples show excellent internal consistency and indicate that the techniques may be used with considerable confidence on other massive sulfide samples.

Acknowledgements — We thank Richard R. Larson (USGS, now retired) for his identification of ignited residues and other precipitates of unknown composition on the scanning electron microscope (SEM). His work removed much uncertainty and allowed us to continue the chemical analysis of forms of sulfur in massive sulfides with renewed confidence. We also thank Norma Rait for the analyses which she performed with the LECO SC-132 Sulfur Analyzer shown in Table 2 under "% Total S LECO".

REFERENCES

Curtman, L. J., 1954, Introduction to Semimicro Qualitative Chemical Analysis, New York, The Macmillan Company, 391 pp.

Grassle, J. F., 1982, The biology of hydrothermal vents: A short summary of recent findings: Marine Tech. Soc. J., v. 16, p. 33-38.

Haymon, R. M., 1983, Growth history of hydrothermal black smoker chimneys: Nature, v. 301, p. 695-698.

Kirschenbaum, H., 1983, The Classical Chemical Analysis of Silicate Rocks — The Old and The New: U.S. Geol. Surv., Bull., 1547, 55 pp.

Kolthoff, I. M., Sandell, E. B., Meehan, E. J. and Bruckenstein, Stanley, 1969, Quantitative Chemical Analysis: London, Macmillan, 1199 pp.

Maxwell, J. A., 1968, Rock and Mineral Analysis: New York, John Wiley and Sons, 584 pp.

NBS Standard Reference Materials Catalog 1984-85, Natl. Bur. of Stand., Spec. Publ., 260, Washington, D. C., p. 71.

Reagent Chemicals, Sixth Edition, American Chemical Society Specifications, 1981: Washington, D.C., American Chemical Society, 612 pp.

Rieman, William, III, Neuss, J. D. and Naiman, Barret, 1951, Quantitative Analysis, A Theoretical Approach: New York, McGraw Hill, 523 pp.

Steger, H. F., 1984, Certified Reference Materials, CANMET Report 84-14E, Canadian Certified Reference Materials Project, Energy, Mines and Resources Canada, 555 Booth Street, Ottawa, Canada K1A 0G1, 41 pp.

Vlisidis, A. C., 1966, The Determination of Sulfate and Sulfide Sulfur in Rocks or Minerals: U.S. Geol. Surv., Bull., 1214-D, 5 pp.

Webber, G. R., 1965, Second report of analytical data for CAAS syenite and sulfide standards: Geochim. Cosmochim. Acta, v. 29, p. 229-248.

Determination of Anions by Ion Chromatography — Application to Pedogeochemical Exploration for Metallic Mineralization

P. J. LECHLER AND M. O. DESILETS
Nevada Bureau of Mines and Geology, University of Nevada-Reno
Reno, Nevada 89557, U.S.A.

Abstract — Ion chromatography is a fast, sensitive, low cost method for the determination of ppm levels of anions. Fluoride, chloride, bromide, sulfate, selenite, arsenate, nitrate, and phosphate may be measured simultaneously in water extracts of soil samples.

Orientation soil surveys were conducted around known Ni-Co-Cu and Au-Ag mineralization in semi-arid environments in Nevada and around Cu-Zn-Au-(Ag) mineralization in a temperate environment in the Sierra Nevada foothills on the Nevada/California border.

Preliminary results indicate that sulfate, chloride, and fluoride are particularly useful for evaluating the validity of metal anomalies, mainly in the semi-arid environments. Sporadically-detectable arsenate values suggest that a more sensitive analytical methodology may result in the production of useful arsenate, and perhaps selenite, data also. Nitrate and phosphate were detected in many of the orientation samples but their interpretation is complicated by the possibility of contamination from grazing livestock.

INTRODUCTION

GEOCHEMICAL EXPLORATION has long been recognized as a viable and effective technique for locating metallic mineral deposits and increasingly-novel sampling, analytical, and data processing methods continue to enhance the effectiveness of the discipline. However, understanding the geochemical topography in any given survey, and especially attempting to correctly classify background and anomalous samples, continues to be the subject of much research. The correct interpretation of geochemical anomalies is of primary importance in exploration programs, and can mean the difference between a successful or unsuccessful, and a cost-effective or expensive, program.

Traditional approaches to conducting a near surface geochemical exploration program begin with sampling the appropriate geologic material, usually on a grid pattern or along stream drainages. Next, the samples are analyzed for one or more metallic target elements (Au, Ag, Cu, Ni, etc.), and increasingly, one or more metallic (Hg, Tl, etc.) or semimetal (As, Sb, etc.) pathfinder elements. The analytical data sets are then usually processed statistically and/or mapped prior to selection of areas of high mineral potential. These target areas are usually defined by samples exhibiting statistically anomalous target metal and/or pathfinder element concentrations. High metal concentrations are not always the result of dispersion from mineral deposits, however, but may be due to other natural or anthropogenic processes or sources (Levinson, 1980). The trend towards multielement analytical programs and sophisticated multivariate statistical data processing is largely aimed at gaining more geochemical/geological insight into the true meaning of the elevated elemental abundances used to define target areas.

One aspect of soil geochemistry that can add significantly to the understanding of metal abundances, but which has been largely neglected, is the distribution of certain anions. For instance, most weathering metallic sulfide mineral deposits which yield high concentrations of metals to the soil profile should also yield sulfate (Lamey, 1966). Because many metal sulfides contain high concentrations of other semi- or nonmetals such as arsenic, selenium, etc. (Vinogradov, 1959), anions such as arsenate and selenite (Bohn et al., 1979) can be expected to concentrate in soil as well. In addition, environments such as rhyolite-hosted precious metal deposits may be identified by anions originating as volcanic gases (HCl, HF, etc.) such as chloride and fluoride.

While much research has in the past addressed the subject of specific anion distributions in particular minerals, rocks, and soils around known ore bodies, there is an apparent paucity of anion data being reported in contemporary surveys. Just as the trend towards multielement (cation) analytical programs necessarily followed the introduction of analytical instrumentation such as atomic absorption, inductively-coupled plasma, and energy-dispersive X-ray, so has the inclusion of anion data in exploration programs been hindered by the lack of suitable (rapid, low cost) instrumentation. Approximately ten years ago, however, a technique called Ion Chromatography was conceived, and has since been developed into a reliable, accurate, relatively low cost method capable of determining most of the anions of geochemical interest simultaneously at ppm levels. The geochemical/geological information gained from the addition of anion data to the normal cation data set removes much of the ambiguity from the classification of samples into background and anomalous subsets. Other methodology, such as that employed by Fuge and Andrews (1986) for the determination of chlorine and iodine may also be suitable for the measurement of individual anion abundances in geochemical exploration. Reliance on cation-anion covariances may allow the enhancement of statistical confidence levels and encourage the follow-up evaluation of weaker anomalies generated by more deeply-buried, blind mineralization.

SAMPLING AND ANALYSIS

Data from three different areas in Nevada are presented. The soils from each area are somewhat different and necessitated different sampling procedures. Soils developed on weathered gabbroic rocks in Cottonwood Canyon are poorly developed aridisols; C-horizon soils were sampled and sieved to

minus 80-mesh. Soils underlying the Nevada Sovereign claim block are much better developed aridisols with pronounced K-horizon development (petrocalcic layer near the top of the B-horizon); B-horizon soils were sampled and sieved to minus 80-mesh. The Verdi Peak area represents an alpine coniferous forest environment underlain by basaltic bedrock. Soils are well developed mollisols; B-horizon material was sampled and also sieved to minus 80-mesh.

'Total' metal digestions were performed by adding 5 ml nitric acid and 10 ml perchloric acid to 2 g of sample and heating to perchloric fumes at approximately 300 degrees C. These solutions were diluted to 100 ml with deionized water and analyzed with a Perkin Elmer model 2380 atomic absorption spectrophotometer. 'Partial' metal digestions involved the addition of 10.0 ml of 0.5 N nitric acid to 1 g of sample in 16 × 125 mm borosilicate test tubes which were then agitated briefly in an ultrasonic bath. The samples were allowed to equilibrate for 24 hours and were then homogenized and centrifuged prior to analysis by atomic absorption spectrophotometry.

Anion sample preparation involved adding 50 ml deionized water to 2 g of sample in 125 ml polypropylene bottles. The bottles were capped and heated in a boiling water bath for one hour. After cooling to room temperature, the solutions were transferred to 16 × 125 mm borosilicate test tubes, centrifuged to clarify the liquids, and anions were determined by ion chromatography. The instrumentation and operational parameters used are listed in Table 1; a sample chromatogram is shown in Fig. 1.

Several weak digestions for anions were investigated, including hot and cold water digestions performed at ambient pressure. The results of these tests are summarized in Table 2. Since conductivity detection is employed in the ion chromatograph, strongly ionized and conductive solutions should be avoided as they may overwhelm the conductivity suppression feature which is a critical aspect of ion chromatography. An attempt to utilize a very weak nitric acid digestion to liberate anions (as oxyanions such as arsenate and selenate, etc.) from reduced mineral species (sulfides) resulted in very broad nitrate peaks and significant nitrate memory between samples, and was abandoned. Hydrogen peroxide was utilized as an oxidizer in a subsequent test to avoid the introduction of exotic anions but the chromatograph began to perform erratically while running these digestions, and this procedure was also reluctantly abandoned. Further evaluation has indicated that erratic performance was caused by particulate clogging of the ion exchange column rather than by any peculiar chemical phenomenon due to the oxidizer, and further research into the usefulness of hydrogen peroxide is underway.

Table 1. Instrumental parameters used for anion determinations.

Instrumentation
Dionex 2000i/SP Ion Chromatograph
Columns: HPIC-AG4A Guard Column HPIC-AS4A Separator Column AMMS-1 Micromembrane Suppressor
Detector: Conductivity
Eluent: 0.75 mM Sodium Bicarbonate/2.0 mM Sodium Carbonate
Regenerant: 0.025N Sulfuric Acid
System Pressure: 6-700 psi
Sample Size: 50 Microlitre

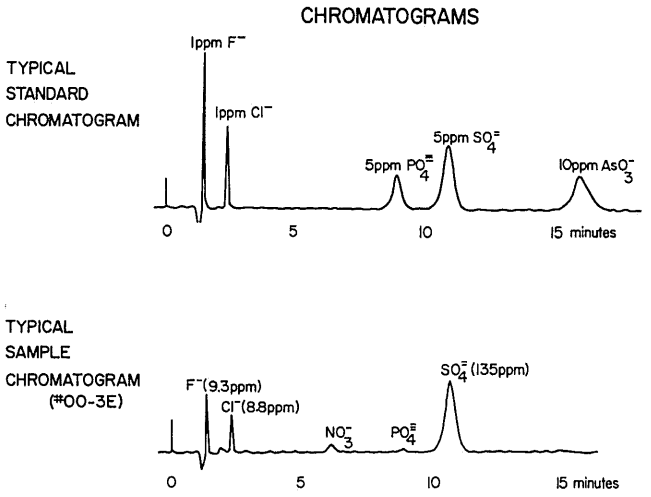

Fig. 1. Representative standard and sample chromatograms run at a chart speed of 1 cm/min. The sample chromatogram reflects a 2 g/50 ml dilution. Sample 00-3E is from the Nevada Sovereign claim block.

Table 2. Summary of the results from alternate digestion techniques. The Cold and Hot digestions were equilibrated at ambient pressure for one hour.

Technique Development

Solvent: Deionized Water Sample: #1-05

Dilution: 2 g/50 ml

	Fluoride	Chloride	Sulfate
Cold:	3.6 ppm	961 ppm	344 ppm
Hot:	12.0	993	452
Bomb: (100C)			
60 min.	11.4	1212	504
120 min.	10.7	—	500
240 min.	11.1	—	492

ELEMENTAL DISTRIBUTIONS

Cottonwood Canyon

The Cottonwood Canyon project area lies in the Table Mountain Mining District, Churchill County, Nevada, approximately 50 km east-southeast of Lovelock (Fig. 2). In this area of the Stillwater Range, Cottonwood Creek cuts deeply into Triassic metasediments and Lower Jurassic rocks of the Humboldt Gabbroid Complex. Faulting has juxtaposed limestones and quartzites against gabbroic rocks, with mineralization of nickel and cobalt sulfides and arsenides occurring in the

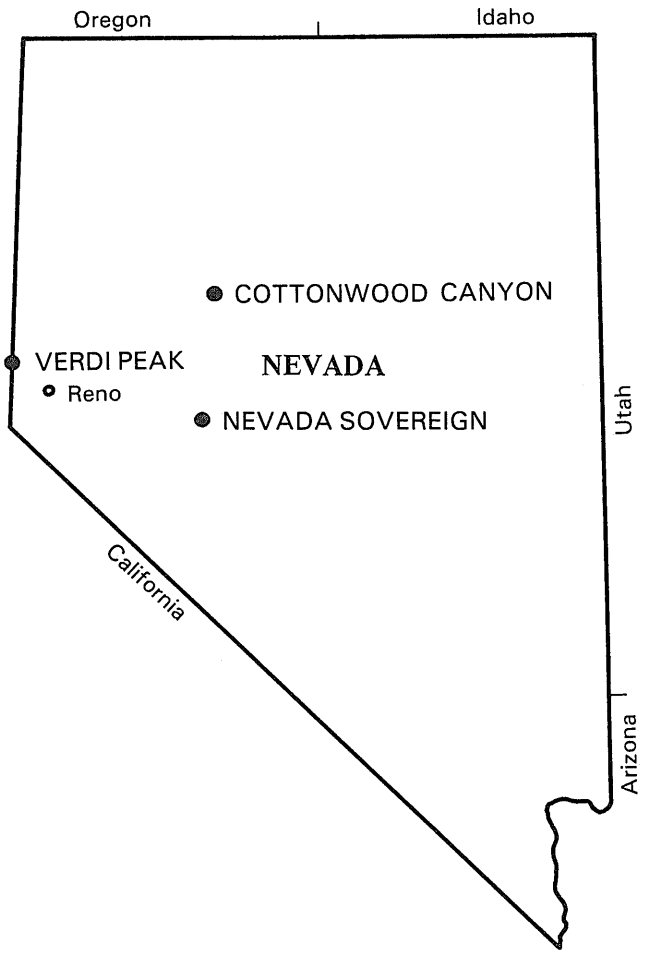

Fig. 2. Map of Nevada showing locations of project areas.

metasedimentary rocks along these zones. Some production of Ni-Co ores from the Nickel and Lovelock mines was reportedly conducted in the late 1800's (Ferguson, 1939).

A small prospect approximately 300 m west of the Lovelock Mine was selected as a suitable area in which to conduct a soil orientation survey. Here a pit had been excavated into intensely altered and hematitized quartzite adjacent to a gabbro/quartzite fault contact. Mineralization is weak but unmistakable with concentrations of 596 ppm Ni, 263 ppm Co and 284 ppm Cu in the altered rock; unaltered quartzite contains 11 ppm Ni, 5 ppm Co and 24 ppm Cu.

Gabbroic rocks composing the hillside to the west of the contact are overlain by variably thin and poorly developed aridisol soil veneers of which the C-horizon was sampled for evaluation of the presence of a secondary dispersion halo of ore-associated elements.

Both 'total' and 'partial' digestions were performed for metal determinations; a hot water leach was the only digestion conducted for anion analysis. However, Andrews, et al., (1984) demonstrated that the correlation between 'partial' and 'total' halogens is significant, and similarly-distributed soil anomalies will result. As can be seen in Fig. 3a, metal variations are small and increases in metal concentrations, as the mineralization is approached, are systematic but weak (sample numbers represent feet from mineralization). Basic statistics describing element distributions are presented in Table 3.

Secondary metal dispersion is limited by the alkaline nature of the desert soils and halo effects extend only 3-10 m laterally into the surrounding soils. The total extraction produced enhanced anomalies for Co and Cu but produced large background variations in Ni concentration, masking the Ni increase towards mineralization. Improved resolution is produced by the partial extraction technique for Ni. The generally good resolution produced by the partial extraction technique (Fig. 3b) in the Cottonwood Canyon soils argues for hydromorphic- rather than clastic- dispersion of the metals and anions. Generally the secondary metal halo is extremely weak, due in part to the weak mineralization at this prospect, and would probably be overlooked in a reconnaissance survey without some supplemental information indicating that the increased metal abundances reflect the presence of abnormal metal concentrations in bedrock. This additional information would be provided by anion data.

The principal anions with which these surveys are concerned are: (a) sulfate produced by the weathering and oxidation of metal sulfides, (b) chloride because of its ubiquitous presence in ore-producing brines (and subsequent release from fluid inclusions upon weathering, Andrews, et al., (1984)), and (c) fluoride because of the possibility of broad haloes being produced by pneumatolytic, fluorine-bearing gases related to volcanic-associated mineral deposits.

Table 3. Mean, standard deviation, and threshold (Levinson, 1974) values for the three project area sample populations.

Basic Statistics			
Cottonwood Canyon	Mean ppm	Std. Dev.	Mean + 2sd
Total Nickel	60.1	9.91	79.9
Total Cobalt	23.9	9.22	42.3
Total Copper	20.8	6.1	33
Partial Nickel	5.6	2.1	9.8
Partial Cobalt	6.8	3.4	13.6
Partial Copper	6.1	1.2	8.5
Fluoride	6.56	2.27	11.1
Chloride	66.7	216	499
Sulfate	57.3	116	289
Nevada Sovereign			
Silver	0.77	0.36	1.49
Copper	15.4	3.68	22.8
Fluoride	6.18	6.44	19.1
Chloride	5.29	15.5	36.3
Sulfate	18.6	41.3	101
Verdi Peak			
Zinc	122	52.2	226
Copper	70.4	49	168
Silver	1.13	0.61	2.35
Fluoride	1.34	1.5	4.34
Chloride	14.1	8.64	31.4
Sulfate	3.51	3.89	11.3

Fig. 4 shows the anion distributions in the Cottonwood Canyon soils. The mineralized quartzite here is strongly enriched in sulfate (4747 ppm versus 35 ppm in unaltered quartzite), slightly enriched in fluoride (19 ppm versus 4.9 ppm), and shows no enrichment, and in fact a slight depletion, in chloride (47 ppm in the mineralized quartzite versus 63 ppm in the unaltered rock). Fluoride soil chemistry exhibits a weak, narrow halo adjacent to mineralization; the chloride halo is also narrow but is strong even though the mineralized rock itself appears slightly depleted in chloride. The sulfate halo is strong and somewhat broader than are those for the halides, extending laterally nearly as far as the metal halo. This indicates that the pH influence imparted to the interstitial soil fluids by sulfuric acid may be the variable which controls secondary dispersion of the metals in the Cottonwood Canyon soils.

There is also a coincident chloride-sulfate peak 95 ft from mineralization, but there is no associated nickel, cobalt, or copper peak in that area. Therefore, the probability is low that the anions are reflecting the presence of nickel, cobalt, or copper mineralization at this site. However, there may be hydrothermally-altered gabbroic bedrock beneath the soils at that location.

In contrast, the sample containing the highest 'total' nickel (75 ft from known mineralization) exhibits no associated anion anomalies, and therefore also has low mineral potential.

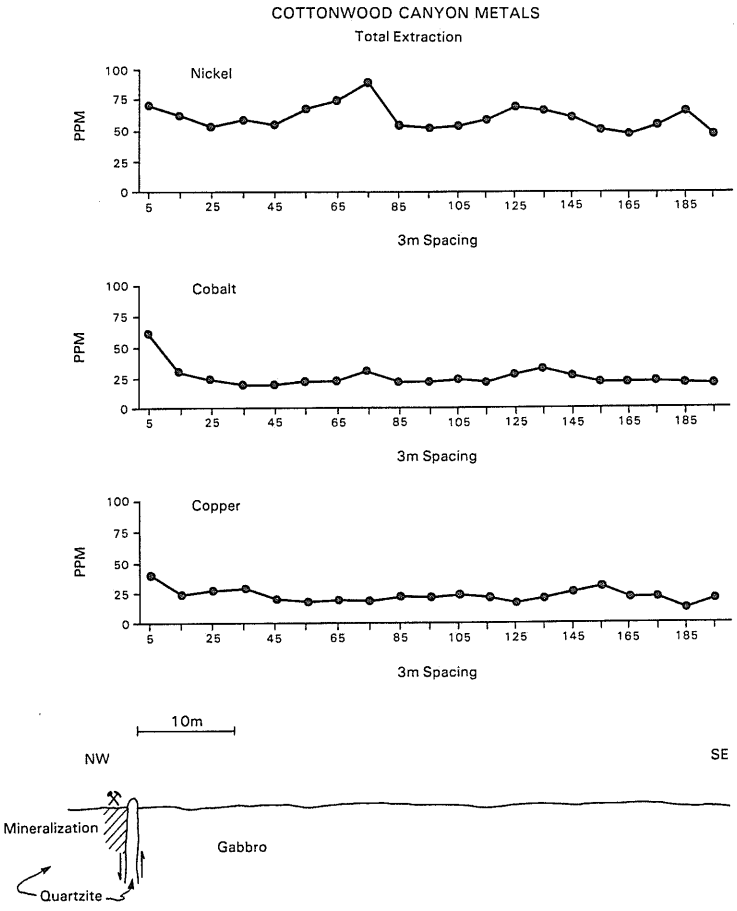

Fig. 3a. Results of total digestions for cobalt, nickel and copper in Cottonwood Canyon soils.

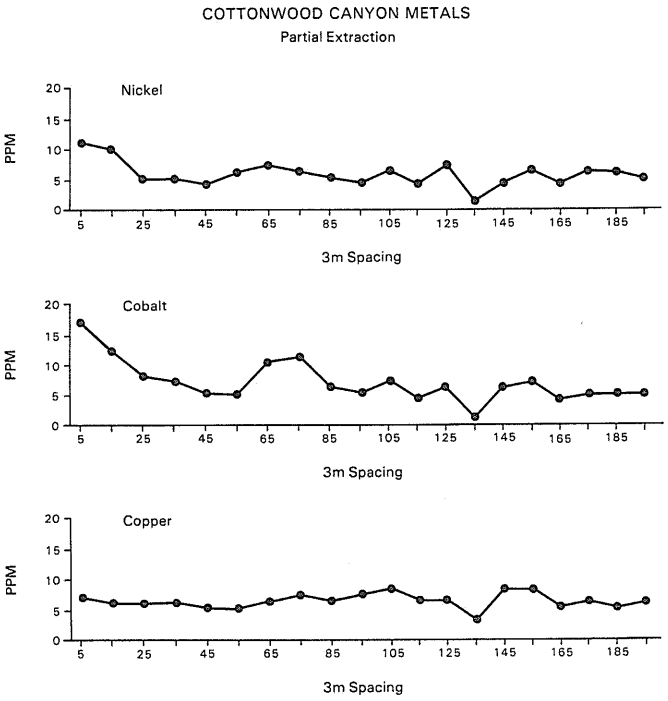

Fig. 3b. Results of partial digestions for cobalt, nickel and copper in Cottonwood Canyon soils.

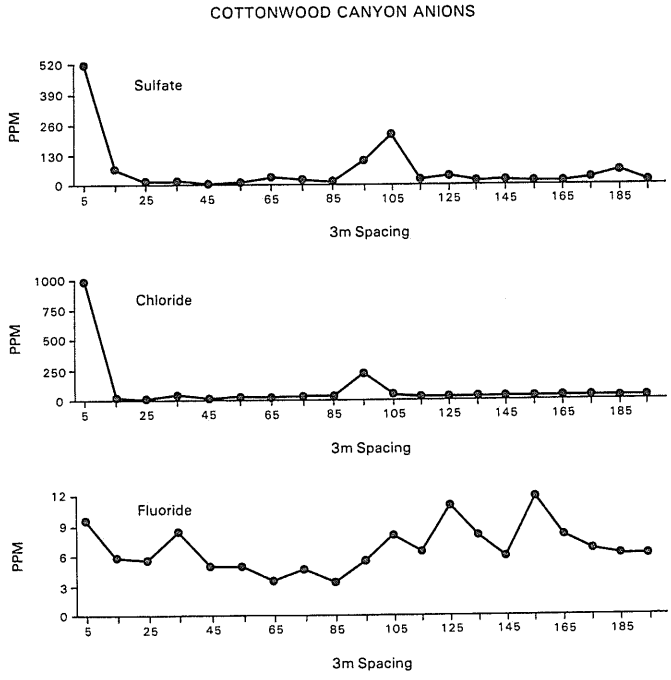

Fig. 4. Anion distributions in Cottonwood Canyon soils.

Nevada Sovereign Claim Block

The Nevada Sovereign Project Area lies approximately 100 km south of Cottonwood Canyon, between the Fairview and Eastgate mining districts, Churchill County, Nevada (Fig. 2). Both dis-

tricts are predominantly gold-silver districts. Nevada Sovereign is an unpatented, undeveloped Au-Ag mining claim.

The project area (claim block) is underlain predominantly by Tertiary rhyolite which is intruded by two Tertiary rhyodacite plugs (Fig. 5). Soils are fairly well-developed aridosols with pronounced, shallow K-horizons below which B-horizon soils were collected along an E-W baseline and two N-S lines. Sample spacing was 33 m.

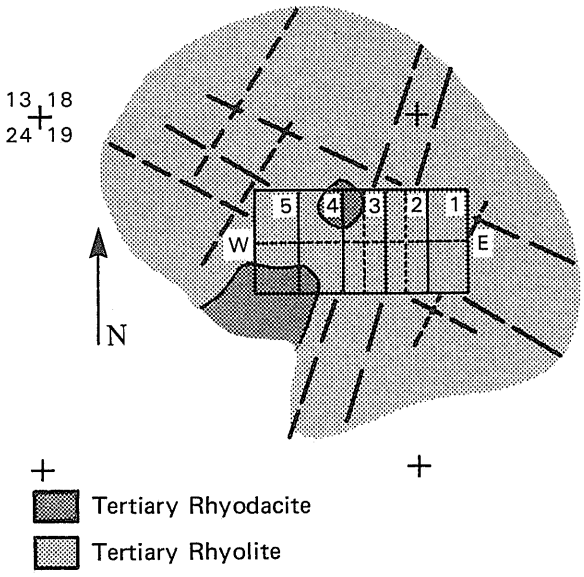

Fig. 5. Generalized geologic map of the Nevada Sovereign claim block. Dotted lines indicate locations of soil sample traverses; heavy dashed lines indicate inferred faults or fractures. E-W line is referred to in text.

Analytical results for metals and anions in samples from the E-W line are presented graphically in Figs. 6 and 7. Silver and copper were determined in solutions prepared by the 'total' digestion technique. Mercury was determined by flameless atomic absorption in dilute nitric acid digestions of the soil pulps.

Several areas of potential interest are apparent upon initial inspection. Sample 00-6E, at the extreme eastern edge of the claim block, exhibits the highest Ag, Cu and Hg abundances, the second highest fluoride concentration and elevated sulfate. It is possible that these values continue to increase to the east, outside the Nevada Sovereign claim block, and may indicate high potential for vein-type or rhyolite-hosted Au-Ag mineralization there. Selected soil gold assays indicate anomalous concentrations in some samples.

Two other areas, 00-4E/00-3E and 00-4W to 00-13W, exhibit high metal and/or anion concentrations in adjacent samples, surrounded by zones of background levels, suggesting genetic relationships between these neighboring metal-anion anomalies. It is possible that these patterns define related zones of alteration-mineralization. The two zones of apparent alteration (strong anion peaks) at 00-5W/6W and 00-12W/13W coincide approximately with possible NNE-trending faults or fractures mapped from topographic- and air photo-lineaments. The high metal values in sample 00-8W may reflect a zone of precious metal

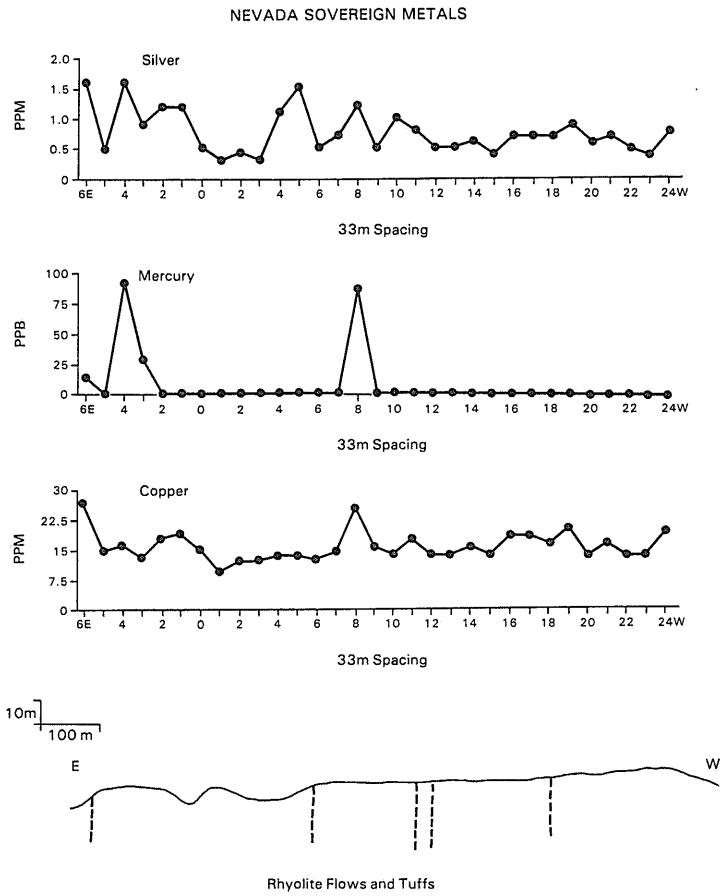

Fig. 6. Graphs showing distribution of metals in Nevada Sovereign soils along E-W traverse. Dashed lines indicate inferred structure.

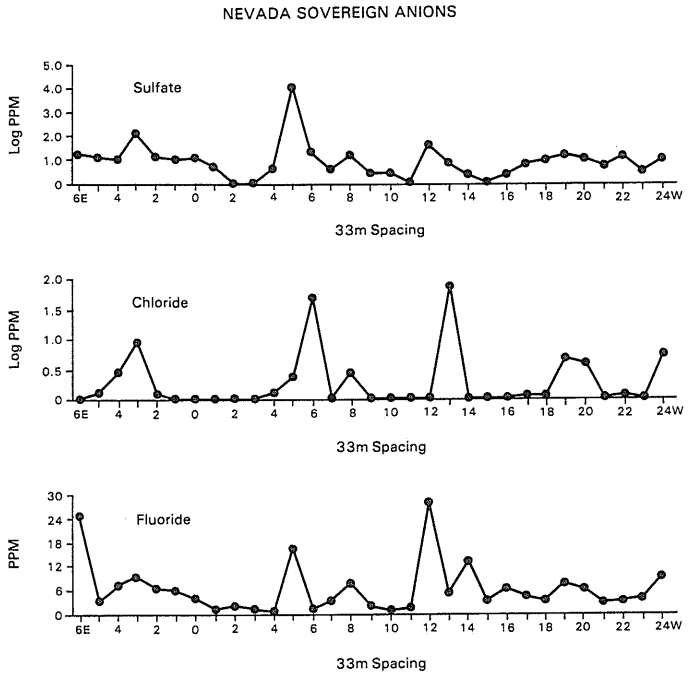

Fig. 7. Graphs showing distributions of anions in Nevada Sovereign soils.

mineralization related to structure and possible bedrock alteration in the adjacent (easterly) samples.

Verdi Peak

The Verdi Peak Project Area lies approximately 20 km west of Reno, Nevada in the coniferous forest of the eastern Sierra Nevada foothills (Fig. 2). Here, a sequence of Jurassic basalts, covered with a mantle of well developed mollisols, has produced a soil geochemical anomaly displaying high copper and zinc concentrations and elevated silver abundances. The discovery of the soil anomaly was fortuitous as there is no surface indication of mineralization or previous prospecting in the immediate area. However, the project is situated approximately 10 km WSW of Peavine Mountain, a district of significant Au-Ag-Cu mineralization. There is a prospected basalt outcrop approximately 1 km SW of the project area exhibiting pronounced copper carbonate staining along fracture surfaces. Select samples from this site carry approximately 5 oz/ton silver. The prospected basalt outcrop and geochemical soil anomaly each lie along NW-trending lineaments (faults?) as defined by aerial photographs. Subsequent to soil sampling in the project area, material from the bottom of a 1 m deep pit near sample #13 was analyzed for gold and copper. Fire assay returned a value of 0.006 oz/ton Au; the copper concentration in the B-horizon soil sample increased from 245 ppm at approximately 0.3 m deep to approximately 500 ppm at 1 m, indicating the probable presence of bedrock mineralization at depth.

Soil chemistry in the project area shows the presence of a Cu-Zn and weak Ag anomalous area from samples #12-14 (Fig. 8). Sample #12 is high in silver, #13 is high in copper, and #14 is high in zinc. The topography slopes steeply towards #12 and the neighboring anomalies described above may reflect either a zoned secondary dispersion halo or some peculiar primary distribution at depth. In the pH range 3-7, this particular elemental distribution may be most suitably explained by the preferential adsorption of zinc over copper on soil montmorillonite (Sposito, 1984). Montmorillonite should be a stable soil constituent developed on basaltic parent material under weakly-acidic conditions (Levinson, 1974). Verdi Peak soils exhibit pH's of approximately 6.0. Thus, the development of a zoned secondary dispersion halo, telescoped downslope, may be a plausible explanation for the observed distributions. The soil sulfate distribution (Fig. 9) is, to a large extent, a mirror image of the zinc pattern and probably indicates bedrock zinc sulfide as a source, and probable supergene mobilization as soluble zinc sulfate.

Chloride is the dominant anion in these soils, although the distribution pattern gives little valuable information and appears random with respect to the metal abundances. Fluoride concentrations are low and provide little useful information.

DISCUSSION

In certain geological/geochemical environments, even where significant mineralization is present, elemental anomalies may not be very pronounced. Under these circumstances qualitative

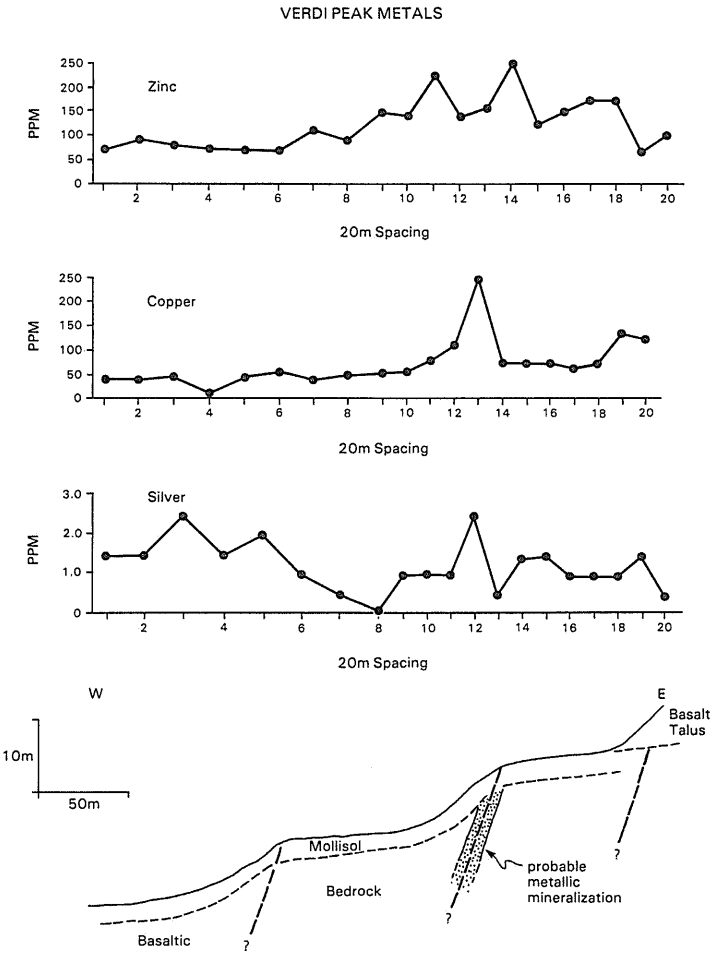

Fig. 8. Distribution of metals in Verdi Peak soils. Heavy dashed lines indicate inferred faults.

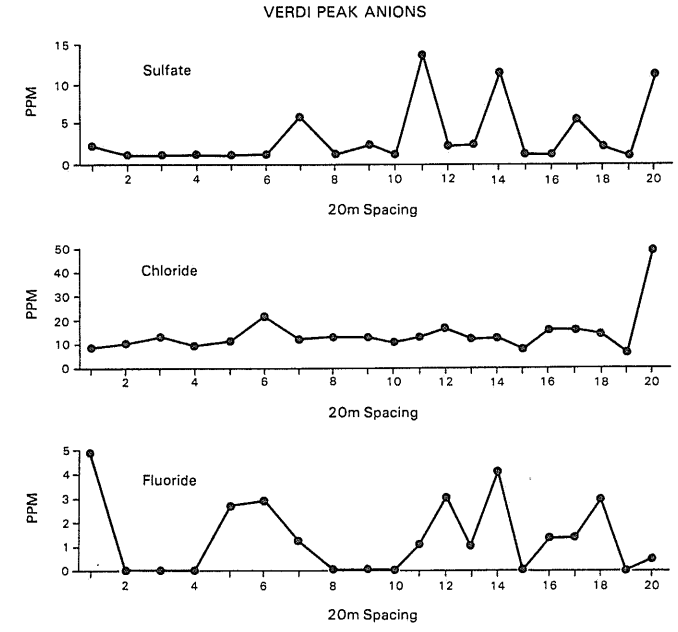

Fig. 9. Distribution of anions in Verdi Peak soils.

assessment of inter-element variations may be more important than quantitative evaluation of individual peak heights. These environments include alkaline soils typical of desert and semi-arid regions as at the Cottonwood Canyon and Nevada Sovereign project areas in this report. Most metals are precipitated rapidly as hydroxides or carbonates in an alkaline supergene environment. Also, deeply buried mineral deposits may present only weakly-anomalous soil metal anomalies regardless of the pH of soil pore waters. In either case, the qualitative nature of the 'complete' soil chemistry at each sample location may be more valuable than absolute abundances.

Intuitively, any weathering mineral deposit containing sulfides should produce a sulfate anomaly along with elevated ore-metal and pathfinder element abundances. All three project areas displayed sulfate peaks along with metal anomalies in areas of known or probable mineralization. Significant fluoride anomalies were present only in the Nevada Sovereign project area soils and probably reflect alteration zones in the underlying rhyolitic rock; they are adjacent to chloride and sulfate anomalies there. Chloride anomalies at Cottonwood Canyon may reflect primary metal transport by chloride-bearing solutions and subsequent secondary dispersion into soils. This may also be the case at Nevada Sovereign, however the ultimate chloride source there may have been volcanic gases, as in the case of fluoride. A clear pattern and demonstrable usefulness for chloride in soils at Verdi Peak is lacking.

Other anions for which there are good fundamental reasons to expect their presence in the soil halo are arsenate and selenite (Bohn et al., 1979). Selenite is detectable by ion chromatography, is present in sulfides at reasonably high concentrations, and should be present in sulfate-rich soil haloes which are related to sulfide mineralization. No selenium oxy-anion was detected in any of the samples from the three project areas in this report. However, sample dilutions were not as concentrated as they might be, and the ion chromatograph was run at only a moderately sensitive setting to keep chloride and sulfate peaks on scale. Further investigations utilizing a high-sensitivity analytical technique will be conducted in an attempt to detect and characterize selenium and arsenic oxy-anion abundances. Weak arsenate peaks were detected in several samples but, as is the case for selenite, further, high-sensitivity testing will be required to assess the usefulness of arsenate.

The majority of samples exhibited significant phosphate and nitrate peaks, but these anions were ignored because of the possibility of soil contamination from grazing livestock. In addition, sample chromatograms occasionally exhibit unidentified peaks, possibly representing complex inorganic or organic anions.

CONCLUSIONS

It is felt that these preliminary investigations, testing both the usefulness of the ion chromatograph and the value of the data which it produces, have demonstrated that the addition of anion data to the routinely-collected cation data can reduce the ambiguity of classifying marginal anomalies and add a measure of confidence that should be worth the additional expense. Hot, deionized water digestions carried out in sealed vessels extracted a significant proportion of the soluble anions without the potential for loss of volatile constituents. Notoriously-insoluble anion complexes such as arsenate may also exhibit relatively poorer sensitivity by ion chromatography than, for instance, the halogens, and are detected in soil samples only occasionally. Arsenate, along with selenite, antimonate, etc. have significant value as pathfinders for certain types of mineralization in modern geochemical surveys, but improved, high sensitivity analytical methods must be developed to enable their detection at lower abundances. Sulfate is valuable as an indicator of the possible proximity of weathering (oxidizing) sulfide minerals. Chloride can be an important indicator of the presence of hydrothermally altered bedrock as it is released to the soil profile upon weathering and destruction of fluid inclusions. Fluoride appears to have greatest use as an indicator of alteration in volcanic (especially rhyolitic) terrain. Due to the high mobility of most anions in the secondary environment, element abundances are greatly depleted in temperate climatic areas with well-flushed soil profiles and collection of meaningful data may be more successful in semi-arid and arid settings (more research is necessary). Anion anomalies may be related either to hydrothermal alteration/mineralization in underlying bedrock or simply to the development of high-alkali soils and are, in themselves, inconclusive indicators of metallic mineralization. They do, however, provide valuable information regarding the origin and validity of metal anomalies.

REFERENCES

Andrews, M. J., Bibby, J. M., Fuge, R. and Johnson, C. C., 1984, The distribution of iodine and chlorine in soils over lead-zinc mineralization, east of Glogfawr, Mid-Wales: J. Geochem. Explor., v. 20, p. 19-32.

Bohn, H. L., McNeal, B. L. and O'Connor, 1979, Soil geochemistry: John Wiley and Sons, New York, 329 pp.

Ferguson, H. G., 1939, Nickel deposits in Cottonwood Canyon, Churchill County, Nevada: Nev. Bur. Mines Geol., Bull. v. 32, 21 pp.

Fuge, R. and Andrews, M. J., 1986, Chlorine and iodine, potential pathfinder elements in exploration geochemistry: Applied Geochem., v. 1, p. 111-116.

Lamey, C. A., 1966, Metallic and industrial mineral deposits: McGraw Hill, New York, 567 pp.

Levinson, A. A., 1980, Introduction to exploration geochemistry (second edition): Applied Publishing Ltd., Wilmette, 614 pp.

Sposito, G., 1984, The surface chemistry of soils: Oxford Univ. Press, New York, 234 pp.

Vinogradov, A. P., 1959, The geochemistry of rare and dispersed chemical elements in soils (in English): Consultants Bureau, Inc., New York, 33 pp.

Gallium: An Overview, Markets, Supplies and Occurrence

R. W. TEKVERK AND J. E. FAY
Faytek Incorporated, 1115 Lambert Lane, P.O. Box 2229, Coeur d'Alene, Idaho 83814

Abstract — Gallium's crustal abundance is similar to that of lead, but its tendency toward geochemical dispersion makes gallium expensive and difficult to produce in large quantities. Expanding use of gallium compounds in integrated circuits and gallium arsenide's potential use as a high efficiency photovoltaic material are increasing demand and production. Traditionally gallium has been recovered as a byproduct of zinc and aluminum processing. Non-traditional sources could provide new supplies of lower cost gallium, prompting increased use especially in photovoltaic applications. Alkaline intrusives, particularly late stage differentiates, contain higher than average amounts of gallium. High concentrations of gallium occur in some gossans and other oxidized zones of low temperature base metal sulfide deposits.

INTRODUCTION

ELECTRONIC devices composed of various gallium compounds have been mentioned in the popular press and media with increasing frequency. Because many people are unaware of the unusual properties which give gallium and gallium compounds so much potential in various electronic uses, this paper will start with background information, including history, current uses and supplies, followed by gallium geology and geochemistry.

HISTORY

In 1871, the Russian chemist Mendeleyev predicted the existence and described the properties of an element he called eka-aluminum because of its position below aluminum in his newly published periodic table. Gallium is the 4th period element in the Boron Group, falling just below aluminum. It shares many properties with aluminum as well as with zinc, indium and germanium with which it often occurs. Four years after Mendeleyev's prediction, Lecoq de Boisbaudran, a French chemist, observed gallium's spectral lines in material from sphalerite samples collected in the Pyrenees. He then isolated the metal and studied its properties. As an interesting historical note, the accuracy of Mendeleyev's description of an as yet undiscovered element convinced scientists of the theoretical soundness of his periodic table. Lecoq de Boisbaudran named the element gallium, a derivative of Gallia, the Latin name for France. Although the element had many unusual and potentially useful properties it was little used except for experimental and research purposes for almost 100 years.

PHYSICAL PROPERTIES

Gallium metal is silvery white and soft enough to be cut with a knife, with a hardness of about two. Superficial oxidation causes it to take on a bluish tinge. It is one of very few metals which can be liquid near room temperature. With a melting point of 29.75°C, and a boiling point of 2,403°C, it has the longest useful liquid range of any element. For comparison, it has six times the liquid range of mercury. It expands upon solidification and supercools readily, remaining a liquid at temperatures as low as 0°C. It has a very low vapor pressure even at high temperatures and thus has been used in high temperature thermometers and manometeres. Gallium wets most surfaces and forms a brilliant mirror when painted on glass. It's high heat conductivity and thermal stability make it useful as a heat exchange medium. Toxicologically, gallium is a safe metal, and its association with other metals sometimes makes them less toxic. In addition, gallium isotopes are used in a number of medical applications. Yet with all these useful characteristics, it was not until the advent of solid state devices in electronics that a significant demand for gallium developed.

CURRENT USES

Gallium compounds such as arsenide, aluminum-arsenide, arsenic phosphate, indium-arsenide and phosphide are used in light emitting diodes, laser diodes, Gunn-effect diodes for microwave applications, switching diodes, light detectors and photoelectric materials. Gallium semiconductor compounds are used in fiber optics and in components for calculators, radio, television, high-fidelity equipment, and other instruments. For example, most laser disk players utilize a gallium arsenide laser. Metallic gallium is also used in the manufacture of solid-state devices.

The first light-emitting diodes were gallium arsenide devices and this is still the largest use of gallium. A light-emitting diode is a semiconductor that emits electromagnetic radiation when activated by a voltage difference. The major use of LED's is in small light-emitting visual display systems such as those in pocket calculators. It is estimated that about 500,000 light-emitting diodes would contain about one kilogram of gallium arsenide. (Petkof, 1985).

The excellent semiconductive properties of various gallium based compounds, particularly gallium arsenide, are responsible for an explosion of research and patents relating to this element. A growing number of applications - many within the military - require a higher performance material than silicon. Gallium arsenide has a variety of advantages over silicon in integrated circuits. Electrons have higher mobility in gallium arsenide than silicon. This property allows gallium arsenide integrated circuits to switch five or six times faster and perform at higher frequencies while consuming less power and generating less heat. Gallium arsenide also has an inherently greater radiation tolerance than silicon. This gives gallium arsenide microprocessors and solar cells a greater survival capability in nuclear and cosmic radiation with obvious implications for military and space based uses. Finally, gallium arsenide inte-

grated circuits have a wider operating temperature range than silicon chips. Gallium arsenide can tolerate temperatures of up to 400°C as opposed to about 200°C for silicon. The use of gallium arsenide in computer chips and high efficiency solar cells could increase dramatically, especially with recent advances in the growth of single crystals of GaAs that have few structural defects. Sumitomo Electric has grown 65 mm diameter crystals with from 0 to 200 dislocations per square centimetre. Conventional GaAs materials had dislocation densities on the order of 5,000 per square centimetre at best, with 40,000 dislocations per square centimetre being common in most commercial materials. High dislocation density, which degrades the efficiency of the semiconductor chip, has been a major barrier to broad acceptance of gallium arsenide crystals by the electronics industry.

Another interesting use of gallium in integrated circuits is in substrates for magnetic domain memories, frequently called bubble memory devices. The material used in this application is single crystal gallium gadolinium garnet (Hirsch & Laurie, 1986.) Bubble memories are more dense (with respect to information contained) than silicon memories or discs and they are nonvolatile. With nonvolatile memory, there is no loss of data after a power failure. Gallium gadolinium bubble memories are also highly reliable and can operate in a wide range of environments.

Finally, an application with tremendous potential is gallium's use in photovoltaic cells. Gallium arsenide is a more efficient generator of electricity than the silicon material used in conventional solar cells. Presently it is also considerably more expensive. The higher cost of gallium arsenide has limited its use in photovoltaic cells to research prototypes and exotic uses such as NASA satellites where the overall cost of the gallium arsenide is negligible compared to the efficiency and performance advantages obtained. Concentrating systems focus the sunlight collected over a larger surface area onto a smaller area of solar cells. By using various concentrating designs, gallium arsenide solar cell efficiency can be increased even further. Again GaAs can operate at higher temperatures which is advantageous in concentrating devices. Gallium arsenide solar cells are also more resistant to radiation damage which is important in space based uses and military applications.

It is our contention that with a decline in the price of gallium and an increase in production the demand for high efficiency gallium arsenide photovoltaic cells could far outweigh all other uses combined. Changes in economic conditions which are conducive to the emergence of a wide spread gallium arsenide photovoltaic industry are already underway and will be discussed later.

TRADITIONAL SOURCES

The first commercial processes for producing gallium recovered the metal from zinc smelter residues. Prior to World War II, most of the world's gallium was produced in Germany. Intermediate products from the processing of the copper - bearing schists of the Mansfeld district were used. Dowa Mining Co. of Japan presently produces about 5,000 kilograms a year from zinc smelter residues. By-product gallium derived from zinc production may be a major source of gallium in the future.

Currently, most gallium is produced in a high state of purity from sodium aluminate liquor obtained in the refining of bauxite by the aluminum industry. Most bauxite contains about 50 ppm gallium, though some may contain up to 100 ppm. In the aluminum refining process, bauxite is dissolved and pure aluminum oxide trihydrate is precipitated by seeding and cooling the aluminate liquor. After repeated dissolutions of bauxite and precipitation of alumina, gallium builds up in the recycled liquor. Finally, the gallium rich solution is electrolysed to obtain metallic gallium which is then purified by various techniques. Total world resources of gallium in bauxite are estimated to exceed one billion kilograms (Petkof, 1985).

Gallium is refined commercially to the 99.99999% purity necessary for most electronic uses. The present price for this grade of gallium is approximately $525.00 (U.S.)/kilogram in lots over 100 kilograms. Figure 1 shows the historical decline in the price of gallium over the last 20 years. This is due to increased recovery efficiency and increased competition. We expect the price of gallium to continue downward, possibly more dramatically as production from nontraditional lower cost sources increases.

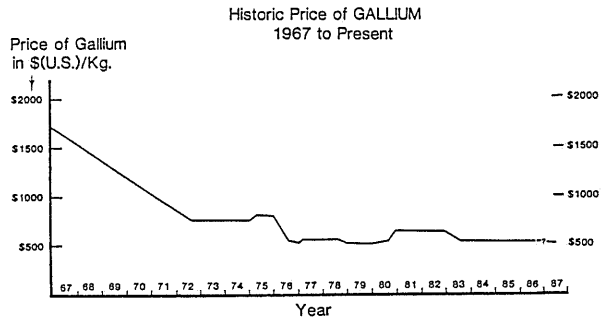

FIG. 1. Historic price of gallium; 1967 to 1987

Figure 2 shows U.S. imports and consumption as well as estimated Japanese consumption and world production. In 1982. Alcoa stopped producing gallium in the United States. This is reflected in the drop in world production in 1983 and the increase in U.S. imports at this time. U.S. demand has been relatively stable and is expected to increase modestly over the next year. Japanese consumption has risen dramatically and this accounts for a recent surge in world production.

FUTURE SOURCES

Many previous studies on the commodity gallium seem to assume the status quo will prevail. Usually, after mentioning some alternate sources, the graphs and charts are constructed based on the premise that most, if not all future gallium supplies will be produced as a byproduct of aluminum refining processes. Several factors cause us to doubt this premise. First, most commercial processes for the extraction of gallium from sodium

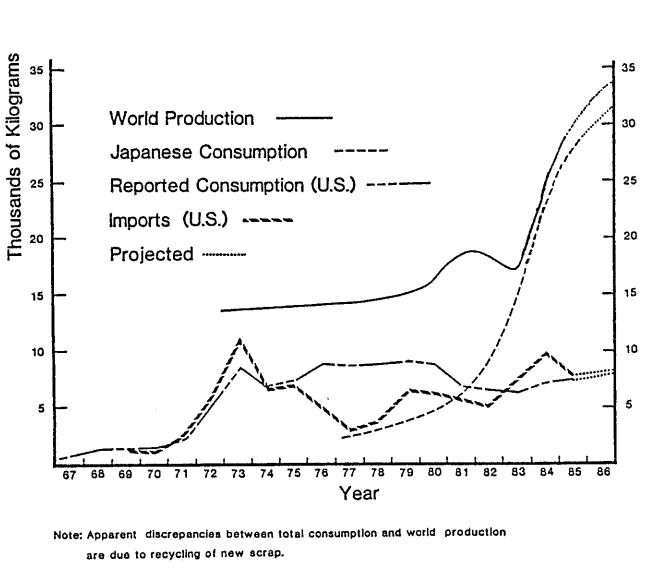

FIG. 2. Gallium production and consumption

aluminate leach liquors are inefficient. Supposedly, ion exchange resins can recover up to 95 to 98 percent with solutions of 200 ppm (Loreth et al., 1986), but this will still be costly. Also, the small scale of the gallium industry does not fit readily into the production plan at major aluminum companies. After producing gallium for many years Alcoa ceased production in 1982. A very small percentage of the world's bauxite production is processed for gallium extraction. Second, most previous gallium studies have ignored, or at least underestimated, the impact of the exploration geologist. Explorationists have just begun to think about the geologic and geochemical processes that could bring about ore-grade primary or secondary concentrations of gallium. A transition from the traditional gallium sources of aluminum and zinc by-products has already begun. Some examples:

The much described and discussed Apex mine in southern Utah is now producing gallium from oxidized ore at a former copper mine. Ultimately the company plans to produce 10,000 kilograms/year. The ore mineral in this case is a gallium rich jarosite. The geology of the Apex Mine is further discussed below.

Highwood Resources, owners of the Thor Lake beryllium, yttrium, rare-earth, tantalum-niobium, gallium deposits in the Northwest Territories have found that "Gallium substitutes for aluminum in albite and microcline in the footwall assemblages of the deposit." (Trueman, 1986) The reported grade is 0.05% gallium trioxide over widths of up to 30 feet for a length of 3,000 feet with a possible depth of 500 feet. Here the gallium mineralization is hosted by a Proterozoic alkaline intrusive. (Trueman, Pers. Comm.)

Renzy Mines of Canada hopes to recover 3,500 pounds per year of gallium oxide from fly ash at its new plant near Edmonton, Alberta.

GALLIUM GEOLOGY AND GEOCHEMISTRY

Gallium has a crustal abundance of about 15 ppm, which is about the same as lead and 10 times the abundance of molybdenum. Though relatively common, gallium does not occur free or as a major constituent of any minerals except for Gallite, ($CuGaS_2$), a rare and economically insignificant copper gallium sulfide mineral which occurs mostly as exsolution lamellae in sphalerites from Tsumeb, Namibia. A very rare gallium hydroxide named Soehngeite ($Ga(OH)_3$) has also been described in rocks from Tsumeb. The highest gallium content in a mineral has been found in Germanite $Cu_3(Ge,Ga,Fe,Zn)\ (S,As)_4$, which contains up to 1.85% gallium again in samples from Tsumeb.

Gallium is very well dispersed throughout the crust and shows a rather uniform abundance in contrasted rock types. Shaw (1957), in a comprehensive review of the geochemistry of gallium reported that the Ga/Al ratio in igneous rocks ranges from about 1: 10,000 to 1: 40,000. There is very little change in the Ga/Al ratio in most igneous series except for a slight Ga enrichment in some late stage differentiates. This enrichment is most notable in well differentiated alkaline intrusives.

Because its ionic size, valence and chemical characteristics are so close to those of aluminum, gallium is essentially always found within the structure of aluminum silicates. Gallium is also very similar to ferric iron and thus can substitute for iron in various minerals such as jarosite.

Pelagic sediments have Ga/Al ratios similar to those in granitic rocks, implying little fractionation of gallium from aluminum during weathering, transport and sedimentation. Gallium is somewhat concentrated in the hydrolysate fraction of sediments. In bauxites, gallium and aluminum are both concentrated with respect to the parent rock. The geochemical consistency of the Ga/Al ratio persists through metamorphism. Metamorphic rocks derived from hydrolysate sediments contain more gallium than do those derived from sandstone and other sediments poor in aluminum.

The abundance of gallium in soils ranges from about 10 to 90 ppm, averaging about 15 ppm or the same as crustal abundance. Carbonaceous chondrites have about 10 ppm gallium and limited data would indicate that this element is well dispersed even in terms of cosmic abundances.

In spite of its impressive dispersion in geological environments it is not impossible to concentrate gallium nor is it impossible to separate gallium from aluminum.

Three different geological processes known to concentrate gallium shed light on some aspects of the geochemical behavior of this element.

1) Gallium concentrations are high in alkaline intrusives. Gallium accumulates towards the end of the magmatic process. The Ga/Al ratio is highest in late stage differentiates indicating that Ga is concentrated in relation to aluminum in the late stages of the magmatic process.

The Thor Lake deposit, mentioned earlier, is a possible example of magmatic differentiation and ensuing alteration leading to a potential gallium ore body.

2) Gallium, like aluminum, is enriched in the products of intense weathering. It is more mobile than aluminum, and the ratio of gallium to aluminum commonly decreases in residual

materials of the weathering process. However, studies on Arkansas bauxites have found the Ga/Al ratio to be increased in the formation of bauxite from nepheline syenites. Gallium concentration ratios for bauxitic materials compared to parent nepheline syenites averaged 4.3 versus a 2.7 concentration ratio for aluminum. (Gordon and Murata 1952) The contrasting trends may be related to the redox conditions in the weathering environment or differences in the amounts of residual materials in which gallium can become incorporated. In many soil profiles the concentration of gallium is positively correlated with the amount of clay. It would be interesting to examine the gallium content of weathering products derived from well differentiated alkaline intrusive complexes. Such weathering could result in bauxitic clays which, though subeconomic with respect to aluminum, could be extremely enriched in gallium.

3) Gallium is mobilized in the oxidizing conditions of the supergene zone. Slight differences in the acid - base properties of gallium and aluminum lead to separation in supergene environments. Evidently, gallium and aluminum separate in both acidic and strongly alkaline environments. Gallium may then be precipitated in various ways, particularly by adsorption into iron hydroxides.

The Apex Mine

The Apex Mine, near the town of St. George in southwest Utah, is the first mine in the world to be operated primarily for co-product germanium and gallium. The ore at the Apex Mine is defined by Bernstein (1986) as a goethite - limonite - hematite zone that contains local concentrations of jarosite, azurite, malachite and other supergene copper, iron, lead and zinc minerals. This zone forms a highly irregular, branching, chimney-like body occurring in dolomitized and silicified breccia, gouge and fissures associated with steeply dipping fault zones within the gently dipping Pennsylvanian Callville limestone. Germanium is concentrated mostly in the goethite, hematite and limonite, whereas gallium is concentrated chiefly in jarosite and in some limonite. Published reserves indicated 243,000 short tons of ore containing 0.032% gallium and 0.064% germanium plus 1.63% copper, 1.58% zinc and 1.21 oz/ton silver. In the richest ore, jarosites contained from 1,100 to 3,500 ppm and averaged 2,860 ppm gallium together with significant amounts of silver and lead. The gallium substitutes for iron in the jarosite structure (Dutrizac, in press.) Not all jarosites in the Apex Mine are gallium rich, but this mineral is the major gallium carrier.

SUMMARY AND CONCLUSIONS

Technological advances utilizing gallium's unique properties are increasing the uses and demand for the metal. Gallium compounds, particularly gallium arsenide, can be used in the fabrication of superior semiconductor and photovoltaic materials. Increased demand has spurred producers to look for lower cost, higher grade sources. With a decrease in the cost of gallium, world consumption (particularly within the photovoltaic industry) could increase dramatically. Traditional sources, such as byproducts from aluminum and zinc processing, have inherently high costs. Non-traditional primary sources may restructure the pricing of gallium. One exploration model suggested by the occurrence of gallium in jarosite - group minerals and limonite at the Apex Mine would indicate that high concentrations of gallium should be looked for in gossans and other oxidized zones of copper rich, arsenic bearing sulfide deposits, particularly those hosted in carbonate rocks. Other exploration targets including well differentiated alkaline intrusive complexes may well prove viable.

REFERENCES

Bernstein, L. R., 1986, Geology and Mineralogy of the Apex germanium - gallium mine, Washington County, Utah: U.S. Geol. Surv., Bull. #1577, 9 pp.

Dutrizac, J. E., Jambor, J. L. and Chen, T. T., in press, Host minerals for the gallium - germanium ores of the Apex mine, Utah: Econ. Geol.

Gordon, M. Jr. and Murata, K. J., 1952, Minor elements in Arkansas bauxite: Econ. Geol., v. 47, p. 169-179.

Hirsch, H. E. and Laurie, G. H., 1978, Some advanced uses of germanium and gallium: Soc. of Mining Eng. Preprint Number 86-89, 7 pp.

Loreth, M. J. et al., 1986, The economics of gallium and germanium: Charles River Associates Report, Boston, Ma. (Paper delivered at AIME 1115th Annual Mtg. March 1986.

Petkof, B., 1985, Gallium: Mineral Facts and Problems, 1985 edition, U.S. Bur. Mines, p. 291-296.

Shaw, D.M., 1957, The geochemistry of gallium, indium, thallium - a review: *in* Physics and Chemistry of the Earth, v. 2, p. 164 - 211. London, Pergamon Press.

Trueman, D.L., 1986, Geological and mineralogical aspects of the Thor Lake beryllium, yttrium, rare-earth, tantalum - niobium, gallium deposits, Northwest Territories: AIME 115th Annual Meeting, March 1986, Tech. Program p. 28.

WORKSHOP REPORTS

Exploration in Desert Environments

P. K. THEOBALD,
U. S. Geological Survey, Golden, CO. 80401

THE DESERT environments of the American west are defined as those areas where evaporation exceeds precipitation, thus excluding Vancouver. More than 20 participants exchanged views and comments on a wide range of topics ably introduced by M. A. Chaffee, W. Gilmore, J. S. Lovell, G. L. Raines, D. B. Smith, and myself. Presentations ranged from theoretical approaches to case histories, and topics ranged from the identification of selected alteration minerals from a satellite to the microscopic examination of "soils" for bacteria.

The great variety of desert environments was recognized from the outset. The climatic change, all within the arid zone, along the Cordillera from Mexico to the Arctic, can be as dramatic as the change from arid to humid. The influence of aeolian sedimentation can vary from pure loess blankets a metre or more thick to bare, rocky pavements almost devoid of fine material. Many of the modern deserts reflect relatively recent climatic change, and the present regime is often superimposed on a previous cycle of more humid weathering and erosion. This superimposition characterizes much of the Cordillera; however, a more extreme example may be represented by the desertification of the humid-tropical, lateritic weathering profile in western Australia. Thus, the climatic history of a given area within the desert environment must be considered if an exploration program in this environment is to be successful.

Nearly all of the geochemical exploration techniques currently in vogue have been tried in the desert. With a few notable exceptions, all of these techniques seem to be at least as useful — often more suitable — for the arid environment than for more humid environments. The prime exception is the use of water. There was no discussion of surface water or true lake sediments as sample media. The variety of evaporites in normally dry playas was considered to be a sump for highly soluble elements from relatively large catchment areas, a source of airborne detritus rich in mobile elements, and a potential resource in and of themselves. The value of groundwater was recognized, as was the infrequency of seeps or wells which often allows only seasonal sampling opportunities.

The second exception to the general utility of surface sample media in many, but not all, desert areas is the dominance of aeolian transport of fine detritus over that contributed by fluvial processes. In the problems areas, the majority, often 90 percent or more, of the fine surface debris is very fine-grained sand and silt of aeolian origin — loess. For most elements, the effect of the loess in a sample is simple dilution. Where the loess blanket is extensive and thick, the dilution is significant enough to mask all but the most extreme anomalies. Two remedies were offered. Gilmore, Smith, and I all emphasized the value of heavy-mineral concentrates to take advantage of hydraulic equivalence to sort long-travelled aeolian silt from more locally derived material. Alternatively, I emphasized the need to shift to coarser fractions of the surface debris — in the medium sand to coarse pebble range — if unconcentrated material is to be used. Success with the latter approach has been reported from loess-blanketed areas in Australia (Carver et al., 1985), Inner Mongolia (Ren et al., 1984), and in Saudi Arabia (Theobald and Allcott, 1973).

Aeolian dilution is not common to all deserts or to all parts of the deserts. In the Cordillera, the problem is not severe enough to require discarding of the fine fractions. Thus, hope remained for those participants who were seeking micron-sized gold. The search for such gold deposits is a problem of a specific deposit type, not a climatic regime. That the dilution was not sufficient to obliterate gold anomalies in Nevada was clearly portrayed by Gilmore, who was able to define discrete, essentially residual gold anomalies in the minus-150-mesh fraction of heavy-mineral concentrates. Similarly, Smith was able to isolate gold-rich rocks in southern California using the indicator elements arsenic and antimony, again in heavy-mineral concentrates. It seems unlikely, however, that these reasonable simple approaches will be effective for very fine-grained gold in the true loess-blanketed deserts. Thus, ample ground for exploration will be available to the imaginative innovator when the readily found deposits of the Cordillera are exhausted.

The desert environment seems particularly well suited to the use of several of the less widely used exploration techniques. Chaffee, for example, reviewed the wide variety of indicator plants that seem to thrive in the vicinity of mineral deposits. These range from the long-known selenium accumulators of the vetch family (Cannon, 1957, 1960) used to locate uranium deposits to the relatively common California poppy, which seems particularly attracted, at least in some areas, to copper-rich soils (Chafee and Gale, 1976). Most of these indicator plants require careful distinction among species, hence, require the expertise of a botanist. Some, such *Erigonum inflatum,* a sulfate indicator, are easily recognized by less specialized people. Biogeochemical techniques are particularly well adapted to the arid environment, where a number of deep-rooted phreatophytes penetrate to the water table. Mesquite, in particular, has been demonstrated to translocate anomalous metals from bedrock through tens of metres of transported overburden (Horsnail and Lovstrom, 1974).

Lovell reviewed the role of soil gas in exploration. The relatively great thickness of unsaturated ground above any existing water table makes this approach particularly attractive in desert environments, though the complexity of poorly understood reactions within the vadose zone relegates the technique, in Lovell's opinion, to a last resort. Rather than the common sulfur gases, H_2O and SO_2, the gases encountered at the surface over an oxidizing sulfide body are more likely to be COS or CS_2 (Taylor et al., 1982). Secondary reactions yield CO_2 and consume oxygen (Lovell et al., 1983). Though it is an indirect approach, soil gases have been readily detected in

anomalous concentrations from the deserts of southwestern U.S., where subjacent sulfide bodies were covered by hundreds of metres of overburden. Thus, in the desert environment both biogeochemical and soil-gas analyses offer potential for three-dimensional geochemical exploration.

The advantages of cloudless skies over a sparsely vegetated terrane were extolled by Raines as the ideal environment for the techniques of remote sensing. He described a statistical method of analysis of the spatial and directional characteristics of linear features that allows definition of significant trends and the lineaments responsible for the trends. These trends were related to geochemical features, known mines, and target areas for mineral exploration (Raines, 1977; Turner et al., 1982). Because of the paucity of vegetation in most desert areas, a large proportion of the reflected energy measured from an aircraft or satellite platform comes directly from the soils and rocks of the desert floor. By using spectrographic analysis of this reflectance one can distinguish absorption bands characteristic of specific chemical bonds. Using these reflection characteristics, Raines displayed synoptic maps of alteration-mineral groups and tickled our imaginations with the potential to produce similar maps for specific alteration minerals.

The tone of the workshop was distinctly positive. This was probably best exemplified by Lovell, who took great pains to use the reciprocal of the oxygen values to display a negative anomaly positively. The desert was not viewed as a hostile environment for exploration, but as an environment in which many techniques can be applied and in which there are many avenues open to future mineral discoveries. Thanks are due to the excellent speakers, the enthusiastic participants, and the overworked organizers, particularly Barry Smee, for a gratifying experience. Hopefully, we will meet again — in the desert.

REFERENCES

Cannon, H. L., 1957. Description of indicator plants and methods of botanical prospecting for uranium deposits on the Colorado Plateau: U.S. Geol. Surv., Bull., 1030-M: 399-516.

Cannon, H. L., 1960. The development of botanical methods of prospecting for uranium on the Colorado Plateau: U.S. Geol. Surv., Bull., 1085-A, 50 pp.

Chaffee, M. A. and Gale, C. W., 1976. The California poppy (*Eschoscholtzia mexicana*) as a copper indicator plant — a new example: J. Geochem. Explor., v. 5. p. 59-63.

Carver, R. N., Chenoweth, L. M. Mazzucchelli, R. H. Oats, C. J. and Robbins, T. W., 1985. "Lag," a geochemical sampling medium for arid regions: (abs.). 11th Int. Geochem. Explor. Sym., Toronto, Prog. and Abstr: 44.

Horsnail, R. F. and Lovstrom, K. A., 1974. A geochemical exploration strategy for porphyry copper deposits in a desert pediment environment: (abs.). Mining Eng., v. 26. p. 78.

Lovell, J. S., Hale, M. and Webb, J. S., 1983. Soil air carbon dioxide and oxygen measurements as a guide to concealed mineralization in semiarid and arid regions: J. Geochem. Explor., v. 19, p. 305-317.

Raines, G. L., 1977. Maps of lineaments, lineament intersections, and hydrothermal alteration in northern Sonora, Mexico: U.S. Geol. Surv., Open-File Rep. 77-78.

Ren, T., Zhao, Y., Zhang, H., Yang, S., et al., 1984. A preliminary study on the utilization of regional geochemical prospecting methods in the arid and desert area of Inner Mongolia: Geophys. and Geochem. Explor., v. 8, p. 284-296 (in Chinese with English abstract).

Taylor, C. H., Kesler, S. E. and Cloke, P. L., 1982. Sulfur gases produced by the decomposition of sulfide minerals: application to geochemical exploration: J. Geochem. Explor., v. 17, p. 165-185.

Theobald, P.K. and Allcott, G. H., 1973. Tungsten anomalies in the Uyaijah ring structure: U.S. Geol. Surv., Saudi Arabian Proj. Rep. 160, Ministry of Petroleum and Mineral Resources, Jiddah, Saudi Arabia, 86 pp.

Turner, R. L., Raines, G. L., Kleinkopf, M. D. and Lee-Moreno, J. L., 1982. Regional northeast-trending structural control of mineralization, Northern Sonora, Mexico: Econ. Geol., v. 77, p. 25-37.

Heavy Mineral Sampling

W. K. FLETCHER

University of British Columbia, Vancouver, B.C. V6T 2B4

APPROXIMATELY thirty geologists and exploration geochemists participated in a lively two-day workshop stimulated by the presentations of eight speakers. Two presentations from eastern Canada focussed on heavy minerals in glacial tills with one (S.A. Averill) illustrating the application of concentrate mineralogy and gold morphology as guides to the type and size of the source. Ian Nichol then described problems associated with conventional procedures, including noisy data and losses of fine gold during reverse circulation drilling and gravity separation, that can result in exploration failures.

The remaining presentations concentrated on applications and behaviour of heavy minerals in drainage sediments. John Barakso also presented case histories dealing with the role of heavy minerals in soils and lithogeochemistry and Bruce Ballantyne gave a beautifully illustrated account of the mineralogy of the Atlin placers.

Chuck Fipke described laboratory methods for separation of the heavy mineral fraction containing the element of interest and several speakers gave their procedures for selecting the sample site and collecting the sample. These ranged from field screening to obtain large (10 kg) samples of minus 20-mesh sediment (C. F. Fipke and W. Gilmour) to use of a portable suction dredge (F. M. Smith). Smith also noted the importance of sampling time and the very weak gold anomalies found in California immediately following the spring run-off. K. Fletcher then attempted to resolve some of the problems associated with heavy minerals on the basis or theoretical models for their transport by streams.

Despite general agreement on the need to collect large samples to ensure sample representivity, there was no consensus on the best locations (or times) for sampling. Similarly there was considerable discussion on how analytical data should be treated or presented. It was noted that these problems will not be resolved without more information on the relative importance of provenance (source lithology) versus process (hydraulic effects) on heavy mineral concentrations on the stream bed. Clearly there is scope for improving heavy mineral techniques and many questions remain for discussion at some future workshop.

Lithogeochemical Sampling

A. DAVIDSON
Corporation Falconbridge Copper Ltd., Vancouver, B.C.

APPROXIMATELY 40 geologists and geochemists took part in this highly successful and topical workshop. Participants hailed from all over Canada and the USA, as well as some from Europe and Australia. The particular interests of the participants were quite varied and ranged from lithogeochemistry as an aid to finding massive sulphide and gold deposits to analytical methods and lithogeochemistry as a guide to rock type.

A. Davidson of Corporation Falconbridge Copper led off the discussions with an introduction to lithogeochemistry and addressed the questions of "What are we looking for?" "What do we want to sample?" "What analytical methods do we use?" "What do we do with all the data?" and finally "Where is the ore?". Lithogeochemistry was seen to be equally applicable in the search for volcanogenic massive sulphides, sedimentary copper deposits, uranium and gold deposits.

Ian Pirie of Corporation Falconbridge Copper looked in more detail at lithogeochemical alteration halos associated with Archean massive sulphide deposits. He showed examples of how these halos and lithogeochemistry could be used at the scale of the greenstone belt, the camp, and the individual deposit. The applicability of some of the major and trace elements was also examined.

Peter Holbeck of Esso Minerals then presented a case history on the lithogeochemistry around the Paleozoic age Kutcho Creek massive sulphide deposite in Northern British Columbia. His study showed that fluorine and manganese were two of the better indicator elements.

Jan Peters of the University of Toronto brought lithogeochemistry to present day deposits by showing the chemical changes occurring in rocks associated with the presently forming massive sulphides in the Guaymas Basin. He also mentioned the buffering effect that the calcareous and other sediments could have on the pH of the circulating fluids and thus on their ability to leach metals from the basement rocks.

R. Edmunds, an independant consultant, uses *R*-mode factor analysis on lithogeochemical samples to try to distinguish between "ore bearing" sedimentary basins and "barren" basins. He showed how this could be done on the basis of very few samples once the Factor Group had been set up. That ended the first day of the workshop.

Dean Toye of Acme Analytical Labs led off the second day and discussed the use of ICP and Mass Spectrometry in lithogeochemical studies. ICP is a cost effective method of geochemical analyses. Linda Bloom, an independant geochemical consultant, discussed fire assay and XRF techniques for gold and semiquantitative lithogeochemistry (XRD). She also discussed the problems of accuracy versus precision and showed us some of the problems to expect from analytical labs.

Stan Hoffman of BP/Selco then proceeded to discuss patterning with respect to ICP analysis and led a discussion on procedural techniques in gold lithogeochemistry.

Ian Thompson of Placer Development presented two lithogeochemical case histories, one from the Belore property in the Timmins gold camp and the other from the McDerrmott Mercury mine in Nevada.

C. Eckburg of Newmont Gold ended the formal presentations with a discussion of the Carlin, Gold Quarry, and Maggie Creek, epithermal deposits in Nevada.

All of the formal presentations were extremely well done and a great deal of discussion was generated.

The workshops continue to be a highlight of AEG meetings.

OTHER PAPERS PRESENTED AT THE SYMPOSIUM

Epithermal Gold Exploration in the Great Basin — Two Decades of Evolutionary Growth
B. R. BERGER and J. V. TINGLEY
U.S. Geological Survey, Golden, Colorado

Man-Made Variables in Applied Geochemistry
L. BLOOM and E. J. BROOKER
X-Ray Assay Laboratories Limited, Don Mills, Ontario

The Cochiti Mining District, Jemez Mountains, New Mexico
S. L. BOLIVAR and L. W. MASSEN
Los Alamos National Laboratory, Los Alamos, New Mexico

Mineralogy and Lithogeochemistry of Advanced Argillic Alteration Related to Epithermal Copper-Gold Mineralization at the Frieda River Prospect, Papua New Guinea
R. BRITTEN
Esso Minerals Canada Ltd., Vancouver, B.C.

Early Jurassic Volcanic Arc Setting of the Silbak Premier Mine, Near Stewart, B.C.
D. BROWN
University of British Columbia, Vancouver, B.C.

Geochemistry of Eureka-Excelsior Gold Deposit, Cracker Creek District, Oregon
C. CALDER and M. IKRAMUDDIN
Eastern Washington University, Cheney, Washington

Toward a Comprehensive Metallogeny of the Canadian Cordillera: Distribution of Metals by Terrane
R. C. CARNE, R. J. CATHRO, W. D. EATON and C. A. MAIN
Archer, Cathro & Associates (1981) Limited, Vancouver, B.C.

Mineral Exploration via Measurements of Soil-Absorbed Sulfur Gases: Two Case Studies
J. E. CHAVEZ and S. O. FARWELL
University of Idaho, Moscow, Idaho

Economic Geology of the Pacific Northwest of the United States
E. S. CHENEY, T. E. DUBE, T. E. GILBERT and J. MARGOLIS
University of Washington, Seattle, Washington

The Distribution and Abundance of Gold in Stream Sediment, Southern British Columbia
S. J. DAY and W. K. FLETCHER
University of British Columbia, Vancouver, British Columbia

Geology and Genesis of the Dolly Varden Silver Camp, Alice Arm Area, Northwestern British Columbia
B. D. DEVLIN and C. I. GODWIN
University of British Columbia, Vancouver, B.C.

The Practical Application of Biogeochemistry to Mineral Exploration in Canada's Forests
C. E. DUNN
Geological Survey of Canada, Ottawa, Ontario

Trace Element Geochemistry Anomalies and Guides to Mineralization: Red Butte, Owyhee Uplands, Oregon
S. C. EVANS and M. L. CUMMINGS
Portland State University, Portland, Oregon

Hydrothermal Alteration and Au-Hg Mineralization Associated with the Devils Mountain Fault Zone, Skagit County, Washington
D. C. GRAHAM
Western Washington University, Bellingham, Washington

Dirt Bagging — A Cost Effective Geochemical Exploration Tool?
J. S. GRAVEL
G. H. S. Geochemical Services Ltd., Vancouver, B.C.
S. J. HOFFMAN
BP Canada Inc., Selco Division, Vancouver, B.C.

Copies of the volume of abstracts for the symposium may be obtained from the Association of Exploration Geochemists, P.O. Box 523, Rexdale, Ontario, Canada, M9W 5L4 at a cost of $Cdn 5.00 postage paid.

Processes of Sulfide Accumulation in Seafloor Polymetallic Sulfide Deposits: Axial Seamount and Southern Explorer Ridge
M. D. HANNINGTON and S. D. SCOTT
University of Toronto, Toronto, Ontario

Lithogeochemistry of Black Range Tin Mineralization, New Mexico
D. B. HARVEY and P. C. GOODELL
University of Texas, El Paso, Texas
C. H. MAXWELL
U.S. Geological Survey, Denver, Colorado

K/T1 Ratios in Various Types of Gold Deposits
M. IKRAMUDDIN
Eastern Washington University, Cheney, Washington

Gold-Silver Geochemistry of the DeLamar Silver Mine, Owyhee Country, Idaho
R. LASMANIS
Department of Natural Resources, Olympia, Washington

A BASIC Computer Program to Aid the Interpretation of Regional Geochemistry: Application to Metallogenic Studies in Intensely-Mineralized Pershing Co., Nevada
P. J. LECHLER
Nevada Bureau of Mines and Geology, Reno, Nevada

Geology of the Mount Skukum Tertiary Epithermal Gold-Silver Vein Deposits, Southwestern Yukon Territory
B. W. R. McDONALD
University of British Columbia
E. B. STEWART
AGIP Canada Ltd., Calgary, Alberta
C. I. GODWIN
University of British Columbia, Vancouver, B.C.

Application of Organic Geochemistry in Base Metal Exploration
R. W. MACQUEEN
Geological Survey of Canada, Calgary, Alberta

Development of Drainage Basin Models Utilizing Regional Sediment Survey Data: A Subtle Anomaly Recognition Approach
P. MATYSEK
Ministry of Mines, Energy and Petroleum Resources, Victoria, B.C.

Secondary Geochemical Dispersion of Ore Elements From Disseminated Gold Deposits, Tonkin Springs, Eureka County, Nevada
M. B. MEHRTENS
U.S. Mineral Exploration Co., Arvada, Colorado

A Comparative Geochemical Study of Barren and Mineralized Carlin-Type Gold Deposits
C. E. NELSON
Mineral Consultant, Denver, Colorado

Use of High-Grade Mineralized Rock-Chip Geochemistry in Resource Evaluation and Generative Exploration Programs
R. L. NIELSON and E. R. LASKOWSKI
Consulting Geologists, Evergreen, Colorado

The Geochemistry of Graben Structure Mineralization, Chiwakum and Methow Grabens, Washington Cascades
P. C. NISBET
Northwest Kaolin Ltd., Sequim, Washington

Hydrothermal Vent Deposits From the Southern Trough of Guaymas Basin, Gulf of California: A Fluid Inclusion, Stable and Radiogenic Isotope Study
J. M. PETER
University of Toronto, Toronto, Ontario
W. C. SHANKS
U.S. Geological Survey, Reston, Virginia
D. KADKO
Oregon State University, Corvallis, Oregon
S. D. SCOTT
University of Toronto, Toronto, Ontario

Regional Lake Sampling Surveys: Geochemical Exploration and Metallogenesis in the Meguma Zone, Southern Nova Scotia
P. J. ROGERS and R. MILLS
Dept. of Mines and Energy, Halifax, Nova Scotia

A Newly Developed Decrepitation Measurement System and Its Application in the Search for Epithermal Precious Metals in Japan
N. SATO and I. TAKATORI
Mitsubishi Metal Corporation, Tokyo, Japan

Explorer Ridge and Tuzo Wilson Seamounts: Update
S. D. SCOTT
University of Toronto, Toronto, Ontario
R. L. CHASE
University of British Columbia, Vancouver, B.C.
P. J. MICHAEL and G.T. SHEA
University of British Columiba, Vancouver, B.C.
T. J. BARRETT, M. GORTON, M. HANNINGTON and J. PETER
University of Toronto, Toronto, Ontario

Explorer Ridge: Co-Occurence of Trace-Element-Enriched Basalts With Sulfide Deposits as a Possible Exploration Tool on Land
G. T. SHEA, P. J. MICHAEL and R. L. CHASE
University of British Columbia, Vancouver, B.C.

Relative Error Analysis of Replicate Geochemical Data: Advantages and Applications
C. R. STANLEY and A. J. SINCLAIR
University of British Columbia, Vancouver, B.C.

Geology of the Alligator Ridge Gold Deposits, Nevada, U.S.A.
A. P. TAYLOR
Amselco Minerals Inc., Denver, Colorado

Application of ICP-MS for the Determination of Trace Elements in Geological Samples
A. VANDER VOET, W. DOHERTY and P. WONG
Ontario Geological Survey, Toronto, Ontario

The Discovery of the Bear-Totem Au, Ag, Deposit at Muddy Lake, Northern B.C.
H. H. WOBER and K. R. SHANNON
Chevron Canada Resources Ltd., Vancouver, B.C.

Geology and Exploration of the Willa Prospect — A Breccia-Hosted Au-Cu-Ag Deposit in Southeastern B.C.
R. H. WONG
BP Canada Inc., Selco Division, Vancouver, B.C.
C. D. SPENCE
Lornex Mining Corporation Ltd.
D. K. MUSTARD
BP Canada Inc., Selco Division, Vancouver, B.C.
L. J. WERNER
Northair Mines Ltd., Vancouver, B.C.

LIST OF CONTRIBUTORS

	Page
Appleton, J. D.	83
Barakso, J. J.	77
Berg, H. C.	19
Berger, B. R.	217
Bloom, L.	217
Blusson, S. C.	168
Britten, R.	217
Bolivar, S. L.	217
Brooker, E. J.	217
Brown, D.	217
Brown, F.	189
Brown, Z. A.	189
Calder, C.	217
Cameron, R. S.	61
Carne, R. C.	217
Cathro, R. J.	217
Chaffee, M. A.	94
Chase, R. L.	219
Chavez, J. E.	217
Cheney, E. S.	217
Church, S. E.	132
Claros, J.	83
Closs, L. G.	109
Cooke, B. J.	77
Crandel, W.	189
Cummings, M. L.	217
Davidson, A.	215
Day, S. J.	217
Delavaux, M. H.	132
Desilets, M. O.	202
Devlin, B. D.	217
Doherty, W.	
Dorrzapf, A. F. Jr.	184, 189
Downing, B. W.	72
Dube, T. E.	217
Dummett, H. T.	168
Dunn, C. E.	217
Eaton, W. D.	217
Evans, S. C.	217
Farwell, S. O.	217
Fay, J.	209
Fipke, C. E.	168
Fletcher, W. K.	177, 214, 217
Fox, P. E.	61
Gilbert, D. J.	217
Godwin, C. I.	217
Goldfarb, R. J.	19, 150
Goodell, P. C.	218
Gorton, P. J.	219
Graham, D. C.	217
Gravel, J. C.	217
Gray, J. E.	132
Hannington, M. D.	218, 219
Harvey, D. B.	218
Haynes, P. S.	142
Hoffman, S. J.	61, 72, 217
Höy, T.	1
Ikramuddin, M.	217, 218
Johnson, R. G.	189
Kadko, D.	218
Kane, J. S.	184, 189
Kesler, S. E.	142
King, H. D.	126
Kirschenbaum, H.	189, 198
Laskowski, E. R.	218
Lasmanis, R.	218
Leach, D. L.	150
Lechler, P. J.	202, 218
LeHuray, A. P.	132
Light, T. D.	19, 126, 150
Main, C. A.	217
Margolis, J.	217
Marinenko, J.	189
Massen, L. W.	217
Matysek, P.	218
Maxwell, C. H.	218
McDonald, B. W. R.	218
McGowan, K. I.	51
McMillan, W. J.	1
McQueen, R. W.	218
Mee, J. S.	189
Mehrtens, M. B.	218
Meuhlenbachs, K.	160
Michaels, P. J.	219
Mills, R.	219
Murowchick, J. B.	160
Mustard, D. K.	219
Nelson, C. E.	218
Nelson, S. W.	19
Nesbitt, B. E.	160
Nielsen, R. L.	218
Nisbet, P. C.	218
Palmer, C. A.	189
Pantaleyev, A.	1
Peter, J. M.	218, 219
Philpotts, J. A.	189, 198
Rait, N.	189
Rodriguez, W.	83
Rogers, P. J.	219
Rota, J.	42
Sato, N.	219
Saxby, D.	177
Scott, S. D.	218, 219
Shannon, K. R.	219
Shea, G. T.	219
Sinclair, A. J.	219
Skeen, C. J.	189
Smith, S. M.	109
Spence, C. D.	219
Stanley, C. R.	219
Stewart, E. B.	218
Takatori, I.	219
Taylor, A. P.	219
Tekverk, R.	209
Theobald, P. K.	109, 213
Tingley, J. V.	217
Tripp, R. B.	126
VanderVoet, A.	219
Werner, L. J.	219
Wober, H. H.	219
Wong, P.	219
Wong, R. H.	219